Deborah D.L. Chung

Engineering Materials and Processes

Composite Materials

Science and Applications

Second Edition

Springer

Engineering Materials and Processes

Series Editor

Professor Brian Derby, Professor of Materials Science
Manchester Materials Science Centre, Grosvenor Street, Manchester, M1 7HS, UK

Other titles published in this series:

Fusion Bonding of Polymer Composites
C. Ageorges and L. Ye

Composite Materials
D.D.L. Chung

Titanium
G. Lütjering and J.C. Williams

Corrosion of Metals
H. Kaesche

Corrosion and Protection
E. Bardal

Intelligent Macromolecules for Smart Devices
L. Dai

Microstructure of Steels and Cast Irons
M. Durand-Charre

Phase Diagrams and Heterogeneous Equilibria
B. Predel, M. Hoch and M. Pool

Computational Mechanics of Composite Materials
M. Kamiñski

Gallium Nitride Processing for Electronics, Sensors and Spintronics
S.J. Pearton, C.R. Abernathy and F. Ren

Materials for Information Technology
E. Zschech, C. Whelan and T. Mikolajick

Fuel Cell Technology
N. Sammes

Casting: An Analytical Approach
A. Reikher and M.R. Barkhudarov

Computational Quantum Mechanics for Materials Engineers
L. Vitos

Modelling of Powder Die Compaction
P.R. Brewin, O. Coube, P. Doremus and J.H. Tweed

Silver Metallization
D. Adams, T.L. Alford and J.W. Mayer
Microbiologically Influenced Corrosion
R. Javaherdashti

Modeling of Metal Forming and Machining Processes
P.M. Dixit and U.S. Dixit

Electromechanical Properties in Composites Based on Ferroelectrics
V.Yu. Topolov and C.R. Bowen

Charged Semiconductor Defects
E.G. Seebauer and M.C. Kratzer

Modelling Stochastic Fibrous Materials with Mathematica®
W.W. Sampson

Ferroelectrics in Microwave Devices, Circuits and Systems
S. Gevorgian

Porous Semiconductors
F. Kochergin and H. Föll

Chemical Vapor Deposition
C.-T. Yan and Y. Xu

Deborah D. L. Chung

Composite Materials

Science and Applications

Second Edition

Springer

Deborah D.L. Chung, PhD
State University of New York, Buffalo
Dept. Mechanical & Aerospace Engineering
318 Jarvis Hall
NY 14260–4400, Buffalo
USA
ddlchung@buffalo.edu

ISSN 1619-0181
ISBN 978-1-84882-830-8 e-ISBN 978-1-84882-831-5
DOI 10.1007/978-1-84882-831-5
Springer London Dordrecht Heidelberg New York

British Library Cataloguing in Publication Data
A catalogue record for this book is available from the British Library

Library of Congress Control Number: 2010920533

Cover design: eStudio Calamar, Figueres/Berlin

Printed on acid-free paper

Springer is part of Springer Science+Business Media (www.springer.com)

In Celebration of the 20th Anniversary of the Composite Materials Research Laboratory, University at Buffalo, State University of New York

With thanksgiving for the past twenty years and excitement for the future, I dedicate this book to the Composite Materials Research Laboratory, which I founded at the University at Buffalo, State University of New York, in 1989. With the highly appreciated involvement of a large number of researchers, including students, postdoctoral associates, visiting scholars, faculty members and industrial participants, the Laboratory has made advances in the science and technology of composite materials, as shown by 400 peer-reviewed journal publications that cover composites with polymer, cement, and metal matrices, including those for aerospace, automotive, civil, electronic, energy and thermal applications. The Laboratory has emphasized material development that is application driven and process oriented, as partly described in this book. Our most notable breakthroughs relate to smart concrete, vibration damping materials, cement-based pn-junctions, thermoelectric materials, multifunctional structural materials, carbon nanofiber applications, electromagnetic interference shielding materials, electronic packaging materials and thermal interface materials. The graduation of over 30 doctoral students is particularly heartwarming. Special appreciation is extended to Mr. Mark A. Lukowski, for twenty years of technical support.

In further celebration of the anniversary, the Laboratory has commissioned Kenneth C.K. Yip (composer) and I (lyrics and narration writer) to write a musical that merges science and music. The piece is entitled *Materials Are Needed to Make Anything*, and is for performance by a chorus and two vocal soloists and percussion accompaniment. This is the first musical work that centers on engineering materials! Choirs interested in performing this 30-minute piece are welcome to contact me.

Deborah D.L. Chung
Director and Professor
Composite Materials Research Laboratory
Buffalo, NY
June 1, 2009

Preface to the Second Edition

The field of composite materials has progressed greatly over the last few decades, as shown by the widespread use of fibrous composite materials for airframes, sporting goods and other lightweight structures. Enabling this technological progress is scientific understanding of the design and mechanics of composite materials that involve continuous fibers as the reinforcement.

Current challenges in the field of composite materials are associated with the extension of the field of composite materials from structural composites to functional and multifunctional composites, the development of composite materials for electrical, thermal and other functional applications that are relevant to current technological needs, and the improvement of composite materials through processing. Examples of functions are joining (e.g., brazing), repair, sensing, actuation, deicing (as needed for aircraft and bridges), energy conversion (as needed to generate clean energy), electrochemical electrodes, electrical connection, thermal contact improvement and heat dissipation (i.e., cooling, as needed for microelectronics and aircraft). Processing includes the use of additives (which may be introduced as liquids or solids), the combined use of fillers (including discontinuous ones) at the micrometer and nanometer scales, the formation of hybrids (such as organic–inorganic hybrids), the modification of the interfaces in a composite, and control over the microstructure. In other words, the development of composite materials for current technological needs must be application driven and process oriented. This is in contrast to the conventional composites engineering approach, which focuses on mechanics and purely structural applications.

The second edition is aimed at providing in an organized manner the concepts and technical details for addressing the challenges mentioned above. Compared to the first edition, the second edition has been greatly expanded (with hundreds of illustrations added), extensively reorganized and almost totally rewritten.

As a part of a comprehensive treatment of composite tailoring methods, numerous examples of methods, in addition to data and micrographs that support their effectiveness, have been added to the second

edition. Topics added to the second edition include vibration damping, degradation, durability, mechanical joining, electrical connection and nanocomposites. Composites with polymer, cement, metal and carbon matrices are covered in terms of the structure, properties, fabrication and applications. Up-to-date information on lightweight structural materials and civil infrastructure materials is provided. Materials for structural, electrical and thermal applications are comprehensively covered with much information that is not in the first edition. The emphasis on process-oriented composite design, application-oriented functional properties and multifunctional structural materials makes this book different from all other books on composite materials.

Due to the large amount of up-to-date and down-to-earth information, the book is also suitable for use as a reference book for students and professionals that are interested in the development of composite materials. Due to the tutorial style, basic concept coverage, example problems and review questions, the book is also suitable for use as a textbook for undergraduate and graduate students that have had a semester of an introductory materials science course. The relevant academic disciplines include materials, chemical, mechanical, aerospace, electrical and civil engineering.

Deborah D.L. Chung
Buffalo, NY
April 16, 2009
http://alum.mit.edu/www/ddlchung

Preface to the First Edition

Books on composite materials are essentially limited to addressing the fabrication and mechanical properties of these materials, because of the dominance of structural applications (such as aerospace applications) for traditional composite materials. However, nonstructural applications are rapidly increasing in importance due to the needs of the electronic, thermal, battery, biomedical and other industries. The scientific concepts that guide the design of functional composites and that of structural composites are quite different, as both the performance and cost requirements are different. Therefore, this book is different from related books in its emphasis on functional composite materials. The functions addressed include structural, thermal, electrical, electromagnetic, thermoelectric, electromechanical, dielectric, magnetic, optical, electrochemical and biomedical functions. The book provides the fundamental concepts behind the ability to provide each function, in addition to covering the fabrication, structure, properties and applications of the relevant composite materials.

Books on composite materials tend to emphasize polymer-matrix composites, though cement-matrix composites are the most widely used structural materials, and metal-matrix, carbon-matrix and ceramic-matrix composites are rising in importance. In contrast, this book covers composite materials with all of the abovementioned matrices.

The most common approach for books on composite materials is to emphasize mechanics issues, due to the relevance of mechanics to structural applications. A less common approach for books on composite materials is to categorize composite materials in terms of their matrices and cover the composites in accordance with their matrix materials. In contrast, this book takes a new approach, namely the functional approach—covering composites in accordance with their functions. The functional approach allows the readers to appreciate how composites are designed for the needs of various industries. Such appreciation is valuable for students who are preparing themselves for industrial positions (most students are) and for professionals working in various industries. Moreover, the functional approach allows

an organized presentation of numerous scientific concepts other than those related to mechanical behavior, thereby enabling a wide scientific scope to be covered.

The book is tutorial in style, but it is up-to-date, and each chapter includes an extensive list of references. The readers need to have taken a course on introductory materials science. They do not need to have taken any prior course on composite materials. Therefore, the book is suitable for use as a textbook for upper-level undergraduate students and for graduate students. It is also suitable for use as a reference book for students, engineers, technicians, technology managers and marketing personnel.

Because of the wide scientific scope enabled by the functional approach, the book is expected to be useful to all kinds of engineers (including electrical, thermal, chemical and industrial engineers). In contrast, the conventional approach that emphasizes mechanical behavior limits the readership to materials, mechanical, aerospace and civil engineers.

Deborah D.L. Chung
Buffalo, NY
April 1, 2002

Contents

1 Composite Material Structure and Processing

1.1 Introduction

Composite materials are multiphase materials obtained through the artificial combination of different materials in order to attain properties that the individual components by themselves cannot attain. They are not multiphase materials in which the different phases are formed naturally by reactions, phase transformations, or other phenomena. An example is carbon fiber reinforced polymer. Composite materials should be distinguished from alloys, which can comprise two more components but are formed naturally through processes such as casting. Composite materials can be tailored for various properties by appropriately choosing their components, their proportions, their distributions, their morphologies, their degrees of crystallinity, their crystallographic textures, as well as the structure and composition of the interface between components. Due to this strong tailorability, composite materials can be designed to satisfy the needs of technologies relating to the aerospace, automobile, electronics, construction, energy, biomedical and other industries. As a result, composite materials constitute most commercial engineering materials.

An example of a composite material is a lightweight structural composite that is obtained by embedding continuous carbon fibers in one or more orientations in a polymer matrix. The fibers provide the strength and stiffness, while the polymer serves as the binder. In particular, carbon fiber polymer-matrix composites have the following attractive properties:

- Low density (lower than aluminum)
- High strength (as strong as high-strength steels)
- High stiffness (stiffer than titanium, yet much lower in density)
- Good fatigue resistance
- Good creep resistance
- Low friction coefficient and good wear resistance
- Toughness and damage tolerance (as enabled by using appropriate fiber orientations)
- Chemical resistance (chemical resistance controlled by the polymer matrix)

- Corrosion resistance
- Dimensional stability (can be designed for zero CTE)
- Vibration damping ability
- Low electrical resistivity
- High electromagnetic interference (EMI) shielding effectiveness
- High thermal conductivity.

Another example of a composite is concrete, which is a structural composite obtained by combining (through mixing) cement (the matrix, i.e., the binder, obtained by a reaction – known as hydration – between cement and water), sand (fine aggregate), gravel (coarse aggregate), and optionally other ingredients that are known as admixtures. Short fibers and silica fume (a fine SiO_2 particulate) are examples of admixtures. In general, composites are classified according to their matrix material. The main classes of composites are polymer-matrix, cement-matrix, metal-matrix, carbon-matrix and ceramic-matrix composites.

Polymer-matrix and cement-matrix composites are the most common, due to the low cost of fabrication. Polymer-matrix composites are used for lightweight structures (aircraft, sporting goods, wheel chairs, etc.), in addition to vibration damping, electronic enclosures, asphalt (composite with pitch, a polymer, as the matrix), solder replacement, etc. Cement-matrix composites in the form of concrete (with fine and coarse aggregates), steel-reinforced concrete, mortar (with fine aggregate, but no coarse aggregate) or cement paste (without any aggregate) are used for civil structures, prefabricated housing, architectural precasts, masonry, landfill cover, thermal insulation, sound absorption, etc.

Carbon-matrix composites are important for lightweight structures (e.g., Space Shuttles) and components (e.g., aircraft brakes) that need to withstand high temperatures, but they are relatively expensive due to the high cost of fabrication. Carbon-matrix composites suffer from their tendency to be oxidized ($2C + O_2 \rightarrow 2CO$), thereby becoming vapor.

Carbon fiber carbon-matrix composites, also called carbon-carbon composites, are the most advanced form of carbon, as the carbon fiber reinforcement makes them stronger, tougher, and more resistant to thermal shock than conventional graphite. With the low density of carbon, the specific strength (strength/density), specific modulus (modulus/density) and specific thermal conductivity (thermal conductivity/density) of carbon-carbon composites are the highest among composites. Furthermore, the coefficient of thermal expansion is near zero.

Ceramic-matrix composites are superior to carbon-matrix composites in terms of oxidation resistance, but they are not as well developed as carbon-matrix composites. Metal-matrix composites with aluminum as the matrix are used for lightweight structures and low-thermal-expansion electronic enclosures, but their applications are limited by the high cost of fabrication and by galvanic corrosion.

Metal-matrix composites are gaining importance because the reinforcement serves to reduce the coefficient of thermal expansion (CTE) and increase the strength and modulus. If a relatively graphitic kind of carbon fiber is used, the thermal conductivity can also be enhanced. The combination of low CTE and high

thermal conductivity makes them very attractive for electronic packaging (e.g., heat sinks). Besides good thermal properties, their low density makes them particularly desirable for aerospace electronics and orbiting space structures; orbiters are thermally cycled by moving through the Earth's shadow.

Compared to the metal itself, a carbon fiber metal-matrix composite is characterized by a higher strength-to-density ratio (i.e., specific strength), a higher modulus-to-density ratio (i.e., specific modulus), better fatigue resistance, better high-temperature mechanical properties (a higher strength and a lower creep rate), a lower CTE, and better wear resistance.

Compared to carbon fiber polymer-matrix composites, a carbon fiber metal-matrix composite is characterized by higher temperature resistance, higher fire resistance, higher transverse strength and modulus, a lack of moisture absorption, a higher thermal conductivity, a lower electrical resistivity, better radiation resistance, and absence of outgassing.

On the other hand, a metal-matrix composite has the following disadvantages compared to the metal itself and the corresponding polymer-matrix composite: higher fabrication cost and limited service experience.

Fibers used for load-bearing metal-matrix composites are mostly in the form of continuous fibers, but short fibers are also used. The matrices used include aluminum, magnesium, copper, nickel, tin alloys, silver-copper, and lead alloys. Aluminum is by far the most widely used matrix metal because of its low density, low melting temperature (which makes composite fabrication and joining relatively convenient), low cost, and good machinability. Magnesium is comparably low in melting temperature, but its density is even lower than aluminum. Applications include structures (aluminum, magnesium), electronic heat sinks and substrates (aluminum, copper), soldering and bearings (tin alloys), brazing (silver-copper), and high-temperature applications (nickel).

Although cement is a ceramic material, ceramic-matrix composites usually refer to those with silicon carbide, silicon nitride, alumina, mullite, glasses and other ceramic matrices that are not cement.

Ceramic-matrix fiber composites are gaining increasing attention because the good oxidation resistance of the ceramic matrix (compared to a carbon matrix) makes the composites attractive for high-temperature applications (e.g., aerospace and engine components). The fibers serve mainly to increase the toughness and strength (tensile and flexural) of the composite due to their tendency to be partially pulled out during the deformation. This pullout absorbs energy, thereby toughening the composite. Although the fiber pullout is advantageous, the bonding between the fibers and the matrix must still be sufficiently strong for the fibers to strengthen the composite effectively. Therefore, control over the bonding between the fibers and the matrix is important for the development of these composites.

When the reinforcement is provided by carbon fibers, the reinforcement has a second function, which is to increase the thermal conductivity of the composite, as the ceramic is mostly thermally insulating whereas carbon fibers are thermally conductive. In electronic, aerospace, and engine components, the enhanced thermal conductivity is attractive for heat dissipation.

A third function of the reinforcement is to decrease the drying shrinkage in the case of ceramic matrices prepared using slurries or slips. In general, the drying shrinkage decreases with increasing solid content in the slurry. Fibers are more effective than particles at decreasing the drying shrinkage. This function is attractive for the dimensional control of parts made from the composites.

Fiber-reinforced glasses are useful for space structural applications, such as mirror back structures and supports, booms and antenna structures. In low Earth orbit, these structures experience a temperature range from –100 to 80°C, so they need an improved thermal conductivity and a reduced coefficient of thermal expansion. In addition, increased toughness, strength and modulus are desirable. Due to the environmental degradation resistance of carbon fiber reinforced glasses, they are also potentially useful for gas turbine engine components. Additional attractions are low friction, high wear resistance, and low density.

The glass matrices used for fiber-reinforced glasses include borosilicate glasses (e.g., Pyrex), aluminosilicate glasses, soda lime glasses and fused quartz. Moreover, a lithia aluminosilicate glass-ceramic and a CaO-MgO-Al_2O_3-SiO_2 glass-ceramic have been used.

1.2 Composite Material Structure

The structure of a composite is commonly such that one of the components is the matrix while the other components are fillers bound by the matrix, which is often called the binder. For example, in carbon fiber reinforced polymer, which is important for lightweight structures, the polymer is the matrix, while the carbon fiber is the filler. In case of a structural composite, the filler usually serves as a reinforcement. For example, carbon fiber is a reinforcement in the polymer-matrix composite.

Composites can be classified according to the matrix material, which can be a polymer, a metal, a carbon, a ceramic or a cement (e.g., Portland cement). They can also be classified according to the shape of the filler. A composite that has particles as the filler is said to be a particulate composite. For example, concrete is a particulate composite in which cement is the matrix and sand and stones are the two types of particles that are present together. A composite with fibers used as the filler is said to be a fibrous composite.

The components in a composite can also take the form of layers. An example is laminate flooring that consists of layers of polymer, paper and fiberboard that are joined together during fabrication.

A composite material can be in bulk or film form. The film form can be such that the composite is a standalone film or a film that is attached to a substrate. Less commonly, a composite material takes the form of particles or fibers; i.e., a single particle or fiber consisting of more than one component.

1.2.1 Continuous Fiber Composites

A fibrous composite involving continuous fibers is particularly attractive as a structural material due to the high strength and modulus of the fibers, which bear most of the load. A continuous carbon fiber polymer-matrix composite is an example. The use of steel reinforcing bars (called "rebars") to reinforce concrete gives steel reinforced concrete, which is another example (even though steel rebars are not referred to as fibers). A fibrous composite is also attractive in that it can be tailored by choosing the orientation of the fibers. A common configuration involves the fibers being in the form of plies. A ply, also known as a lamina, is a sheet that has fibers with the same orientation in the plane of the sheet. Each lamina has thousands of fibers along its thickness because each fiber tow consists of thousands of fibers. The composite is made up of a number of laminae such that the fiber orientations can be different among the laminae. For example, the fibers in the consecutive laminae can be oriented at 0, 90, +45 and –45°, resulting in a two-dimensionally "quasi-isotropic" configuration. A conventional system of notation for describing the lay-up configuration of the laminae is illustrated below.

$[0]_8$ means an eight-lamina composite with all laminae having fibers in the same direction (0°). $[0/90]_{2s}$ (where the subscript "s" means "symmetric") means an eight-lamina composite with the stacking order 0, 90, 0, 90, 90, 0, 90, 0°, where the first four laminae and the remaining four laminae are mirror images and the mirror plane is the center plane of the composite. $[0/45/90/-45]_s$ means an eight-lamina composite with the stacking order 0, 45, 90, –45, –45, 90, 45, 0°, where the first four laminae and the remaining four laminae are mirror images. $[0/45/90/-45]_{2s}$ means a 16-lamina composite with the stacking order 0, 45, 90, –45, 0, 45, 90, –45, –45, 90, 45, 0, –45, 90, 45, 0°, where the first eight laminae and the remaining eight laminae are mirror images. $[0/45/90/-45]_{2s}$ means a 16-lamina composite with the stacking order 0, 45, 90, –45, 0, 45, 90, –45, –45, 90, 45, 0, –45, 90, 45, 0°, where the first eight laminae and the remaining eight laminae are mirror images. $[0/45/90/-45]_{3s}$ means a 24-lamina composite with the stacking order 0, 45, 90, –45, 0, 45, 90, –45, 0, 45, 90, –45, –45, 90, 45, 0, –45, 90, 45, 0, –45, 90, 45, 0°, where the first 12 laminae and the remaining 12 laminae are mirror images.

An optical micrograph of the interlaminar interface between two laminae that are at 90° to one another (i.e., a crossply configuration). The interlaminar interface is the region between the two parallel lines that are separated by 8.7 μm. The fibers above the interface are in the plane of the paper, whereas those below the interface are perpendicular to the paper

The direction perpendicular to the laminae is known as the through-thickness direction. The interface between two adjacent laminae is known as the interlaminar interface, which is the mechanically weak link in the laminate. Figure 1.1 is an optical micrograph of the interlaminar interface between two laminae that are 90° relative to one another (i.e., a crossply configuration). This means that the through-thickness direction is relatively weak mechanically, and delamination (local separation of the laminae from one another) is a common form of damage in these composites. When the fibers are carbon fibers, which are much more conductive electrically than the polymer matrix, the through-thickness direction

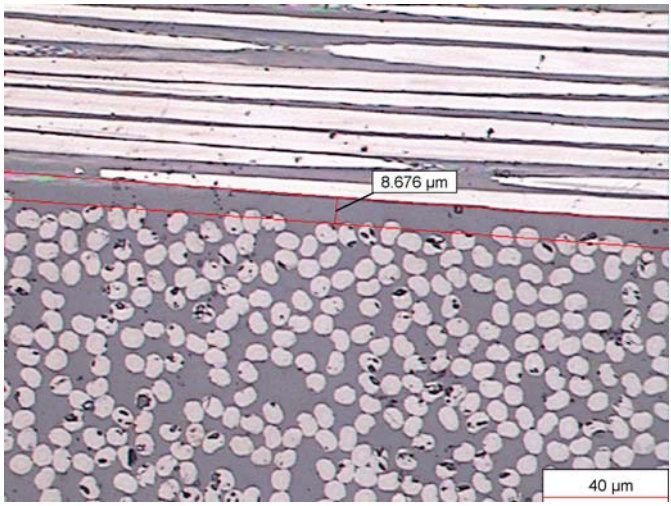

Figure 1.1. An optical micrograph of the interlaminar interface between two laminae that are at 90° to one another (i.e., a crossply configuration). The interlaminar interface is the region between the two parallel lines that are separated by 8.7 µm. The fibers above the interface are in the plane of the paper, whereas those below the interface are perpendicular to the paper

also has a relatively high electrical resistivity (i.e., low electrical conductivity). In other words, the composites are strongly anisotropic (i.e., the properties are different in different directions) both mechanically and electrically.

1.2.2 Carbon–Carbon Composites

The carbon fibers used for carbon–carbon composites are usually continuous and woven. Both two-dimensional and higher-dimensional weaves are used, though the latter has the advantage of enhanced interlaminar shear strength.

The weave pattern of the carbon fabric affects the densification of the carbon–carbon composite during composite fabrication. An 8H satin weave is preferred over a plain weave because of the inhomogeneous matrix distribution around the crossed bundles in the plain weave. Microcracks tend to develop beneath the bundle crossover points.

For two-dimensional carbon–carbon composites containing plain weave fabric reinforcements under tension, the mode of failure of the fiber bundles depends on their curvature. Fiber bundles with small curvatures fail due to tensile stress or due to a combination of tensile and bending stresses. Fiber bundles with large curvatures fail due to shear stresses at the point where the local fiber direction is most inclined to the applied load.

Circular fibers are preferred to irregularly shaped fibers, as the latter leads to stress concentration points in the matrix around the fiber corners. Microcrack initiation occurs at these points, thus resulting in low strength in the carbon–carbon composite.

1.2.3 Cement-Matrix Composites

Cement-matrix composites include concrete, which is a cement-matrix composite with a fine aggregate (sand), a coarse aggregate (gravel) and optionally other additives (called admixtures). Concrete is the most widely used civil structural material. When the coarse aggregate is absent, the composite is known as a mortar, which is used in masonry (for joining bricks) and for filling cracks. When both coarse and fine aggregates are absent, the material is known as cement paste. Cement paste is rigid after curing (the hydration reaction involving cement – a silicate – and water to form a rigid gel).

The admixtures can be a fine particulate such as silica (SiO_2) fume to decrease the porosity in the composite. It can be a polymer (used in either a liquid solution form or a solid dispersion form) such as latex, again to decrease the porosity. It can be short fibers (such as carbon fibers, glass fibers, polymer fibers and steel fibers) to increase the toughness and decrease the drying shrinkage (shrinkage during curing – undesirable, as it can cause cracks to form). Continuous fibers are seldom used because of their high cost and the impossibility of incorporating continuous fibers into a cement mix. Due to the bidding system used for many construction projects, low cost is essential.

Fibrous cement-matrix composites are structural materials that are gaining in importance quite rapidly due to the increasing demand for superior structural and functional properties. Discontinuous fibers used in concrete include steel, glass, polymer and carbon fibers. Among these fibers, carbon and glass fibers are micrometer scale (e.g., 10 μm) in diameter, whereas steel and polymer fibers are usually much larger in diameter (e.g., 100 μm). For the microfibers, the fiber length is typically around 5 mm, as fiber dispersion becomes more difficult as the fiber length increases. Due to the weak bond between fiber and the cement matrix, continuous fibers are much more effective than short fibers at reinforcing concrete. However, continuous fibers cannot be incorporated into a concrete mix, and it is difficult for the concrete mix to penetrate into the space between adjacent fibers, even in the absence of aggregates. The alignment of the continuous fibers in concrete also adds to the implementation difficulty. Therefore, short fibers are typically used.

The effect of short fiber addition on the properties of cement increases with increasing fiber volume fraction unless the fiber volume fraction is so high that the air void content becomes excessively high. (The air void content increases with fiber content, and air voids tend to have a negative effect on many properties, such as the compressive strength.) In addition, the workability of the mix decreases with increasing fiber content. Moreover, the cost increases with increasing fiber content. Therefore, a rather low volume fraction of fibers is desirable. A fiber content as low as 0.2 vol% is effective, although fiber contents exceeding 1 vol% are common. The required fiber volume fraction increases with increasing fiber diameter and increases with increasing particle size of the aggregate.

The improvement in the structural properties due to the addition of discontinuous fibers to cement includes increases in the tensile ductility and flexural toughness and a decrease in the drying shrinkage. A low drying shrinkage is par-

ticularly valuable for large structures, as cracks can form due to the shrinkage and the cracks are wide for the same fractional shrinkage if the structure is large. In the case of the fiber being carbon fiber, improvements in the tensile strength and the flexural strength also occur. Carbon fibers (made from isotropic pitch) are advantageous in their superior ability to increase the tensile strength of cement, even though the tensile strength, modulus and ductility of the isotropic pitch based carbon fibers are low compared to most other fibers. Carbon fibers are also advantageous because of their relative chemical inertness.

In relation to most functional properties, carbon fibers are exceptional compared to the other fiber types. Carbon fibers are electrically conducting, in contrast to glass and polymer fibers, which are not conducting. Steel fibers are conductive, but their typical diameter ($\geq$60 μm) is much larger than the diameter of a typical carbon fiber (10 μm). The combination of electrical conductivity and small diameter makes carbon fibers attractive for use in composite functional property tailoring.

1.3 Processing of Composite Materials

The technology and cost of composite materials depend largely on the processability; i.e., how the components are combined to form a composite material. The processability depends largely on the ability of the components to join, thereby forming a cohesive material. The processing often involves elevated temperatures and/or pressures. The required temperature and pressure, as well as the processing time, are typically dictated by the matrix material. The bonding of the filler with the matrix at an elevated temperature has a disadvantage in that bond weakening or even debonding may occur during the subsequent cooling, due to the difference in the thermal contraction (related to the coefficient of thermal expansion, or CTE) between filler and matrix. The bond weakening will result in the filler being less effective as a reinforcement, thus causing the mechanical properties of the composite to diminish. This problem tends to be particularly serious in metal-matrix composites, due to the relatively high processing temperatures involved.

Fiber composites are most commonly fabricated by the impregnation (or infiltration) of the matrix or matrix precursor in the liquid state into the fiber preform, which can take the form of a woven fabric. In the case of composites in the shape of tubes, the fibers may be impregnated in the form of a continuous bundle (called a tow) from a spool and subsequently the bundles can by wound on a mandrel. Instead of impregnation, the fibers and matrix material may be intermixed in the solid state by commingling reinforcing fibers and matrix fibers, by coating the reinforcing fibers with the matrix material, by sandwiching reinforcing fibers with foils of the matrix material, and in other ways. After impregnation or intermixing, consolidation is carried out, often under heat and pressure.

1.3.1 Polymer-Matrix Composites

Polymer-matrix composites (abbreviated PMC) can be classified according to whether the matrix is a thermoset or a thermoplastic polymer. Thermoset-

matrix composites are traditionally far more common, but thermoplastic-matrix composites are currently the focus of rapid development. The advantages of thermoplastic-matrix composites compared to thermoset-matrix composites include the following:

Lower manufacturing costs:

- No cure
- Unlimited shelf-life
- Reprocessing possible (for repair and recycling)
- Fewer health risks due to chemicals during processing
- Low moisture content
- Thermal shaping possible
- Weldability (fusion bonding possible).

Better performance:

- High toughness (damage tolerance)
- Good hot/wet properties
- High environmental tolerance.

The disadvantages of thermoplastic-matrix composites include the following:

- Limitations in relation to processing methods
- High processing temperatures
- High viscosities
- Prepreg (collection of continuous fibers aligned to form a sheet that has been impregnated with the polymer or polymer precursor) is stiff and dry when a solvent is not used (i.e., not drapeable or tacky)
- Fiber surface treatments less developed.

Fibrous polymer-matrix composites can be classified according to whether the fibers are short or continuous. Continuous fibers have much more effect than short fibers on the composite's mechanical properties, electrical resistivity, thermal conductivity, and on other properties too. However, they give rise to composites that are more anisotropic. Continuous fibers can be utilized in unidirectionally aligned tape or woven fabric form.

Polymer-matrix composites are much easier to fabricate than metal-matrix, carbon-matrix, and ceramic-matrix composites, whether the polymer is a thermoset or a thermoplastic. This is because of the relatively low processing temperatures required to fabricate polymer-matrix composites. For thermosets, such as epoxy, phenolic, and furfuryl resin, the processing temperature typically ranges from room temperature to about 200°C; for thermoplastic polymers, such as polyimide (PI), polyethersulfone (PES), polyetheretherketone (PEEK), polyetherimide

(PEI), and polyphenyl sulfide (PPS), the processing temperature typically ranges from 300 to 400°C.

Thermosets (especially epoxy) have long been used as polymer matrices for carbon fiber composites. During curing, usually performed in the presence of heat and pressure, a thermoset resin hardens gradually due to the completion of polymerization and the associated crosslinking of the polymer molecules. Thermoplastic polymers have recently become important because of their greater ductility and processing speed compared to thermosets, and the recent availability of thermoplastics that can withstand high temperatures. The higher processing speed of thermoplastics arises from the fact that amorphous thermoplastics soften immediately upon heating above the glass transition temperature (T_g), and so the softened material can be shaped easily. Subsequent cooling completes the processing. In contrast, the curing of a thermoset resin is a reaction that occurs gradually.

Short-fiber or particulate composites are usually fabricated by mixing the fibers or particles with a liquid resin to form a slurry, and then molding to form a composite. The liquid resin is the unpolymerized or partially polymerized matrix material in the case of a thermoset; it is the molten polymer or the polymer dissolved in a solvent in the case of a thermoplastic. The molding methods are those conventionally used for polymers by themselves. For thermoplastics, the methods include injection molding (heating above the melting temperature of the thermoplastic and forcing the slurry into a closed die opening through the use of a screw mechanism), extrusion (forcing the slurry through a die opening via a screw mechanism), calendering (pouring the slurry into a set of rollers with a small opening between adjacent rollers to form a thin sheet), and thermoforming (heating above the softening temperature of the thermoplastic and forming over a die using matching dies, a vacuum or air pressure, or without a die using movable rollers). For thermosets, compression molding or matched die molding (applying a high pressure and temperature to the slurry in a die to harden the thermoset) is commonly used. The casting of the slurry into a mold is not usually suitable because the difference in density between the resin and the fibers causes the fibers to float or sink unless the viscosity of the resin is carefully adjusted. To form a composite coating, the fiber-resin or particle-resin slurry can be sprayed instead of molded.

Instead of using a fiber-resin slurry, short fibers in the form of a mat or a continuous spun staple yarn can be impregnated with a resin and shaped using methods commonly used for continuous fiber composites. Yet another method involves using continuous staple yarns in the form of an intimate blend of short carbon fibers and short thermoplastic fibers. The yarns may be woven, if desired. They do not need to be impregnated with a resin to form a composite, as the thermoplastic fibers melt during consolidation under heat and pressure.

One method of forming unidirectional fiber composite parts with a constant cross-section (e.g., round, rectangular, pipe, plate, I-shaped) is pultrusion, in which fibers are drawn from spools, passed through a polymer resin bath for impregnation, and gathered together to produce a particular shape before entering a heated die.

Unidirectional composites suffer from poor mechanical properties in the transverse direction (i.e., perpendicular to the direction of pultrusion). Thus, structural composites are usually not unidirectional. Composites with continuous fibers in various orientations are commonly fabricated by hand lay-up of unidirectional fiber tapes or woven fabrics and impregnation with a resin. The molding, called bag molding, is done by placing the tapes or fabrics in a die and introducing high-pressure gases or a vacuum via a bag to force the individual plies together. Bag molding is widely used to fabricate large composite components for the skins of aircraft.

The fabrication of a high-performance polymer-matrix composite laminate containing continuous fibers commonly involves prepreg sheets. A prepreg is a sheet of continuous oriented fibers that have been impregnated with a polymer or a polymer precursor. An example of a polymer precursor is an epoxy resin, which upon subsequent curing (usually under heat and pressure) forms epoxy polymer, a thermoset. Figure 1.2 shows a scanning electron microscope image of the surface of a carbon fiber epoxy prepreg. The fibers cannot be discerned because they are covered with the resin. An example of a polymer in a prepreg is nylon, which is a thermoplastic polymer. The softening of the thermoplastic polymer upon heating above the glass transition temperature allows the prepreg to be flexible, thus conforming to the desired shape. In the case of an epoxy resin prepreg, the prepreg is flexible and tacky as long as the resin has not been cured. In order to increase the usable period of an epoxy resin prepreg, the prepreg is typically stored in a freezer, as the low temperature in the freezer helps slow down the curing process. Even with storage in a freezer, the usable period of an epoxy resin prepreg is only a few months.

Instead of using unidirectional fibers, one can use a woven fiber fabric. The fabric may be impregnated with the resin or the polymer prior to being stacked

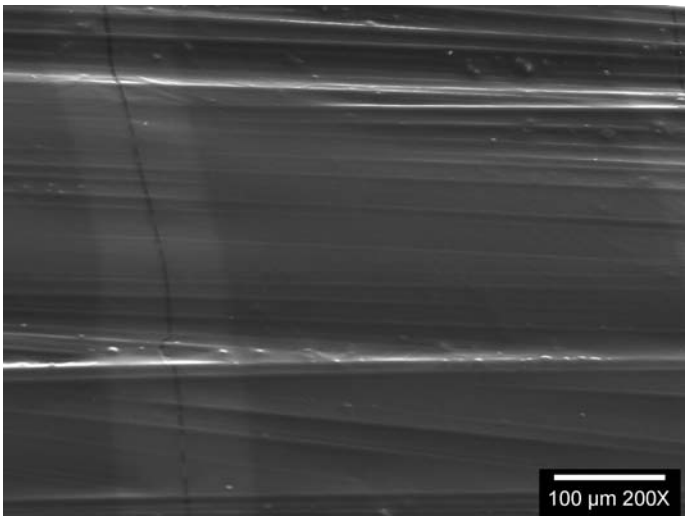

Figure 1.2. A scanning electron microscope image of the surface of a carbon fiber epoxy prepreg. The fibers cannot be discerned due to their being covered with the resin

and consolidated to form a composite. Related to weaving is braiding, which is commonly used to form a composite tubing.

The fabric may be stacked in the absence of a resin and then the resin in infiltrated into the stack – a process known as resin transfer molding (RTM). The advantage of using a fabric is that fabrics are easy to handle. RTM is attractive in that it allows the fabrication of composites of intricate shapes. In RTM, a fiber preform (usually prepared by weaving or braiding and held under compression in a mold) is impregnated with a resin. The resin is admitted at one end of the mold and is forced by pressure through the mold and preform. The resin is subsequently cured. This method is limited to resins of low viscosity, such as epoxy. A problem with this process is the formation of surface voids by the volatilization of dissolved gases in the resin, the partial evaporation of mold releasing agent into the preform, or the mechanical entrapment of gas bubbles.

The weaving of fibers to form a fabric results in the local bending of the fibers in the resulting fabric. The bending occurs where a fiber in one direction crosses that in another direction, as illustrated in Fig. 1.3. Due to this bending, the mechanical properties of a composite made from fabric tend to be inferior to those of a composite made from unidirectional prepregs.

Most of the composite fabrication methods mentioned above involve the impregnation of the fibers with a resin. In the case of a thermoset, the resin is a liquid that has not been polymerized or is partially polymerized. In the case of a thermoplastic, the resin is either the polymer melt or the polymer dissolved in the solvent. After resin application, solid thermoplastic results from solidification in the case of melt impregnation, and from evaporation in the case of solution impregnation. Both amorphous and semicrystalline thermoplastics can be melt processed, but only the amorphous resins can normally be dissolved. Because of the high melt viscosities of semicrystalline thermoplastics (due to their long and rigid macromolecular chains), direct melt impregnation of semicrystalline thermoplastics is difficult. Melt impregnation followed by solidification produces a thermoplastic prepreg that is stiff and lacks tack; solution impregnation usually produces prepregs that are drapeable and tacky, although this character changes as solvent evaporation occurs from the solution. The drapeable and tacky character of thermoplastic prepregs made by solution impregnation is comparable to that of thermoset prepregs. Hence, the main problem with resin impregnation occurs for semicrystalline thermoplastics. Instead of thermoplastic impregnation of fibers by using a melt or a solution of the thermoplastic, solid thermoplastic in the form of powder, fibers, or slurries can be impregnated.

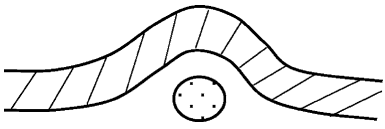

Figure 1.3. The bending of a fiber in a woven fabric. The *circle* represents a fiber that is perpendicular to the paper. The other paper, which is in the plane of the paper, bends around it

An alternative to impregnation is the commingling of continuous reinforcing fibers with continuous thermoplastic fibers. This commingling can be performed on a fabric level, where yarns of different materials are woven together (coweaving); it can be performed on a yarn level, where yarns of different materials are twisted together; or it can be performed on a fiber level, where fibers of different materials are intimately mixed within a unidirectional fiber bundle. During processing (such as compression molding or filament winding), the thermoplastic fibers melt, wet the fibers, and fuse to form the matrix. However, there is a preferred orientation in the thermoplastic fibers due to the spinning process used in their production, and this may be a problem. Furthermore, the thermoplastic fibers have a tendency to form drops during heating. In addition, the availability of high-temperature thermoplastic fibers is limited. PEEK is most commonly used for commingling with carbon fibers. Fiber-matrix adhesion in a commingled system depends on the molding temperature, residence time at the melt temperature, and the cooling rate. This is probably due to several complex mechanisms such as matrix adsorption on the fiber surface, matrix degradation leading to chemical bonding, and interfacial crystallization. On the other hand, prepregs made from commingled fibers are flexible and drapeable, and the use of three-dimensional braiding allows net structural shape formation and enhances damage tolerance due to the lack of delamination. To prevent the ends of the braided preform from unbraiding, the thermoplastic fibers are melted with a soldering gun before cutting, or alternately the ends of the braided preform are wrapped with a polyimide tape and cut through the tape. The fiber commingling makes a uniform polymer distribution possible even when the three-dimensional preform is very large, although the heating time during consolidation needs to be longer for dense three-dimensional commingled fiber network braids than for unidirectional prepregs.

The shaping of thermoplastic-matrix composite laminates can be performed by thermoforming in the form of matched-die forming or die-less forming. However, in addition to shaping, deformations in the form of transverse fiber flow (shear flow perpendicular to the fiber axis) and interply slip commonly occur, while intraply slip is less prevalent. Die-less forming uses an adjustable array of universal, computer-controlled rollers to form an initially flat composite material into a long, singly curved part with one arbitrary cross-sectional shape at one end and another arbitrary shape at the other end. Heating and bending of the material are strictly local processes, occurring only within a small active forming zone at any one instant. The initially flat workpiece is translated back and forth along its length in a number of passes. On successive passes, successive portions of the transverse extent of the workpiece pass through the active forming region. Induction heating is used to provide the local heating in die-less forming, because it enables rapid, noncontact, localized and uniform through-thickness heating.

The schedule for varying the temperature and pressure during the curing and consolidation of prepregs to form a thermoset-matrix composite must be carefully controlled. Curing refers to the polymerization and crosslinking relations that occur upon heating and lead to the polymer, whereas consolidation refers to the application of pressure to obtain proper fiber-matrix bonding, low void content,

and the final shape of the part. Curing and consolidation are usually performed together as one process.

One method of forming continuous fiber composites in the shape of cylinders or related objects is filament winding, which involves wrapping continuous fibers from a spool around a (commonly cylindrical) mandrel. The fibers are wound in various predetermined directions (e.g., 90°) relative to the axis of the mandrel. The winding pattern is a part of the composite design. Since the composite is very strong in the fiber direction, filament winding results in a cylindrical article that resists radial expansion, as needed for pressure vessels. The fibers can be impregnated with a resin before or after winding. Filament winding is used to make pressure tanks. The temperature of the mandrel, the impregnation temperature of the resin, the impregnation time, the tension of the fibers, and the pressure of the fiber winding are processing parameters that need to be controlled.

The processing of polymer-matrix composites typically requires heating. In the case of a thermosetting resin, the heating is to cause the completion of polymerization (cross-linking) of the resin. In the case of a thermoplastic matrix, the heating is done to soften or melt the thermoplastic matrix. (The melting temperature is higher than the softening temperature but it allows more extensive flow.) As the polymerization process is a reaction, it takes time. In contrast, the softening or melting is a phase transition that occurs once the appropriate temperature is reached. As a result, the processing time tends to be considerably longer for a thermoset-matrix composite than a thermoplastic-matrix composite.

1.3.2 Metal-Matrix Composites

The processing of a metal-matrix composite (abbreviated MMC) tends to be much more expensive than that of a polymer-matrix composite due to the high processing temperature required. The fabrication of metal-matrix composites often involves the use of an intermediate, called a preform, in the form of sheets, wires, cylinders, or near-net shapes. The size and shape of the preform are the same as those of the composite article to be made. The preform contains the reinforcement, which is usually held together by a binder that can be a polymer (e.g., acrylic, styrene), a ceramic (e.g., silica, aluminum metaphosphate), or the matrix metal itself. For example, continuous fibers are wound around a drum and bound with a resin, and subsequently the wound fiber cylinder is cut off the drum and stretched out to form a sheet. During subsequent composite fabrication, the organic binder evaporates. As another example, short fibers are combined with a ceramic or polymeric binder and a liquid carrier to form a slurry; this is then filtered under pressure or wet pressed to form a wet "cake," which is subsequently dried to form a preform. When the matrix metal is used as the binder, a continuous fiber bundle is immersed in the molten matrix metal so as to be infiltrated with it, thus forming a wire preform; alternately, fibers placed on a matrix metal foil are covered and fixed in place with a sprayed matrix metal, thus forming a sprayed preform.

A binder is not always needed, although it helps the fibers to stay uniformly distributed during subsequent composite fabrication. Excessive ceramic binder

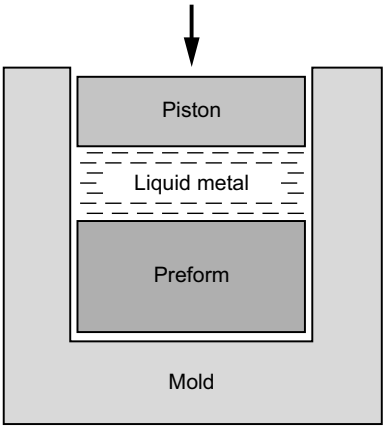

Figure 1.4. Process of liquid metal infiltration for the fabrication of a metal-matrix composite

amounts should be avoided, as they can make the resulting metal-matrix composite more brittle. For ceramic binders, a typical amount ranges from 1 to 5 wt.% of the preform. When woven fabrics are used as reinforcement, a binder is less important, as the weaving itself serves to hold the fibers together in a uniform fashion.

The most popular method of fabricating metal-matrix composites is the infiltration of a preform by a liquid metal, typically under pressure, as illustrated in Fig. 1.4. The temperature needs to be above the solidus temperature (i.e., the temperature above which liquid metal exists, such that the liquid metal coexists with the solid metal unless the temperature is above the liquidus). In order to use a liquid metal infiltration temperature that is not too high, a metal (e.g., aluminum) with a relatively low melting temperature is usually chosen for the matrix.

The low viscosities of liquid metals compared to resins or glasses make infiltration very appropriate for metal-matrix composites. Nevertheless, pressure is usually required because it is difficult for the liquid metal to wet the reinforcement. The pressure can be provided by a gas (e.g., argon) or a piston, as illustrated in Fig. 1.4. When a piston is used, the process can be quite fast and is known as squeeze casting. The lower the pressure, the higher the porosity in the resulting composite, as shown in Fig. 1.5. In addition, the higher the filler volume fraction, the higher the porosity tends to be, as also shown in Fig. 1.5.

One challenge when using liquid metal infiltration to fabricate particulate metal-matrix composites relates to the difficulty involved in making composites with a low volume fraction of the filler due to how difficult it is to make preforms with a low volume fraction of filler. This difficulty stems from the fact that filler particles naturally contact one another in the form. One method of achieving a low filler volume fraction involves using a combustible secondary particulate (e.g., carbon particles) in addition to the noncombustible filler (e.g., silicon carbide particles) in the preform. After preform fabrication, the combustible particulate is removed by oxidation (i.e., burning), thus resulting in a preform with a low filler volume fraction (as low as 18%). Figure 1.6 shows SEM photographs of a preform with

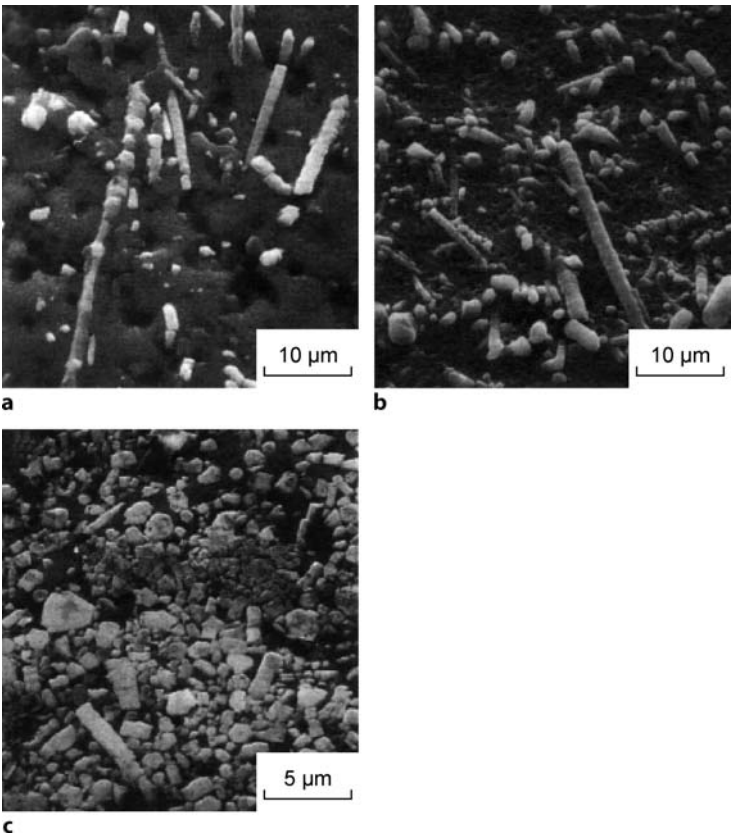

Figure 1.5. Scanning electron microscope photographs of polished sections of aluminum-matrix silicon carbide whisker composites fabricated by liquid metal infiltration. The whiskers have diameter 1.4 μm and length 18.6 μm. **a** 10 vol% SiC whiskers, with infiltration pressure of 1.4 MPa and porosity 5%. **b** 10 vol% SiC whiskers, with infiltration pressure of 13.8 MPa and porosity <0.5%. **c** 31 vol% SiC whiskers, with infiltration pressure of 13.8 MPa and porosity 3%. (From [2])

silicon carbide particles (3–5 μm) used as the reinforcement and carbon particles (activated carbon, equiaxed, 20 μm) as the combustible particulate before and after burning the carbon [1].

The infiltration method can be used to produce near-net shape composites, so that subsequent shaping is not necessary. As infiltration using a gas pressure involves a smaller rate of pressure increase compared to using a piston, infiltration is more suitable than squeeze casting for near-net shape processing. If shaping is necessary, it can be achieved by plastic forming (e.g., extrusion, swaging, forging, and rolling) when short fibers or particles are used as the reinforcement. Plastic forming tends to reduce the porosity and give a preferential orientation to the short fibers. These effects result in improved mechanical properties. For continuous fiber metal-matrix composites, shaping cannot be achieved by plastic forming, and cutting is necessary.

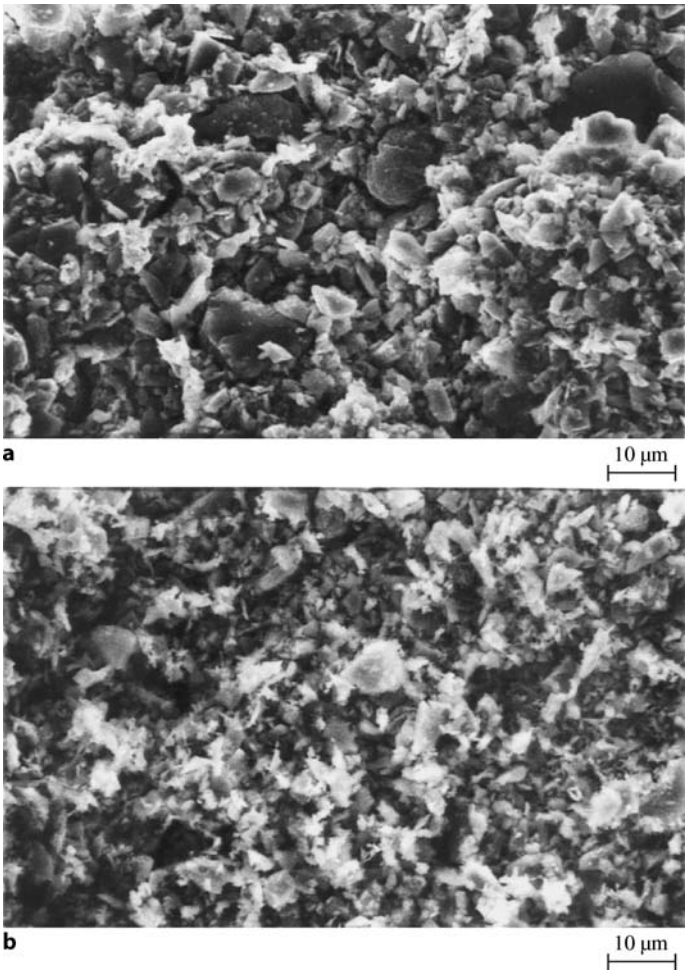

Figure 1.6. SEM photographs of a preform with SiC particles (reinforcement) and carbon particles (combustible particulate), fabricated using an acid phosphate binder. **a** Before burning off the carbon particles (dark large particles). **b** After burning off the carbon particles. (From [1])

A second method for fabricating metal-matrix composites is diffusion bonding. In this method, a stack of alternating layers of fibers and metal foils is hot pressed (at, say, 24 MPa for 20 min) to cause bonding in the solid state. This method is not very suitable for fiber cloths or continuous fiber bundles because it is difficult for the metal to flow into the space between the fibers during diffusion bonding. In contrast, the infiltration method involves melting the metal, so metal flow is relatively easy, making infiltration a more suitable method for fiber cloths or continuous fiber bundles. A variation of diffusion bonding involves the hot pressing of metal-coated fibers without the use of metal foils. In this case, the metal coating provides the metal for the metal-matrix composite. In general, the

diffusion bonding method is complicated by the fact that the surface of the metal foil or metal coating tends to be oxidized and the oxide makes the bonding more difficult. Hence, a vacuum is usually required for diffusion bonding.

A third method of fabricating metal-matrix composites involves hot pressing above the solidus of the matrix metal. This method requires lower pressures than diffusion bonding, but the higher temperature of the pressing tends to cause reinforcement degradation, resulting from the interfacial reaction between the reinforcement and the matrix metal. One way to alleviate this problem is to insert a metal sheet of a lower solidus than the matrix metal alternately between the wire preform layers and then hot press at a temperature between the two solidus temperatures.

A combination of the second and third methods involves first heating fibers laid up with matrix metal sheets between them in vacuum in a sealed metal container above the liquidus of the matrix metal, then immediately hot pressing the container at a temperature below the solidus of the matrix metal.

A fourth method of fabricating metal-matrix composites involves the plasma spraying of the metal onto continuous fibers. As this process usually results in a composite of high porosity, subsequent consolidation (e.g., by hot isostatic pressing) is usually necessary. Compared to the other methods, plasma spraying has the advantage of being able to produce continuous composite parts, though the subsequent consolidation step may limit their size.

Slurry casting, a fifth method, is complicated by the tendency for the carbon fibers (low in density) to float on the metal melt. To overcome this problem, which causes nonuniformity in the fiber distribution, compocasting is necessary. Compocasting (rheocasting) involves vigorously agitating a semi-solid alloy so that the primary phase is nondendritic, thereby giving a fiber-alloy slurry with thixotropic properties.

A sixth method of making a metal-matrix composite is power metallurgy (PM). This process involves the sintering of the metal matrix particles when these particles have been mixed with the filler (Fig. 1.7). The sintering involves solid-state diffusion, which causes the metal particles to join to one another. The joining starts with the formation of a neck between two adjacent particles, as illustrated in Fig. 1.8. As sintering progresses, the necks become wider, so that the porosity in the overall material becomes smaller. Because the diffusion is in the solid state, the temperature is below the melting temperature of the metal. However,

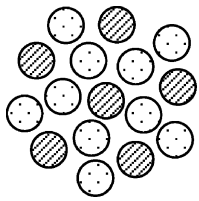

Figure 1.7. A mixture of the filler particles and the metal particles, as used in the admixture method of powder metallurgy for the fabrication of a metal-matrix composite

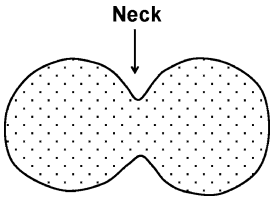

Figure 1.8. The formation of a neck between two metal particles during the fabrication of a metal-matrix composite by powder metallurgy

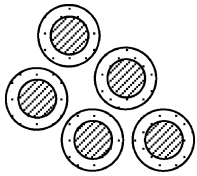

Figure 1.9. Filler particles coated with metal for making a metal-matrix composite by the coated filler method of powder metallurgy

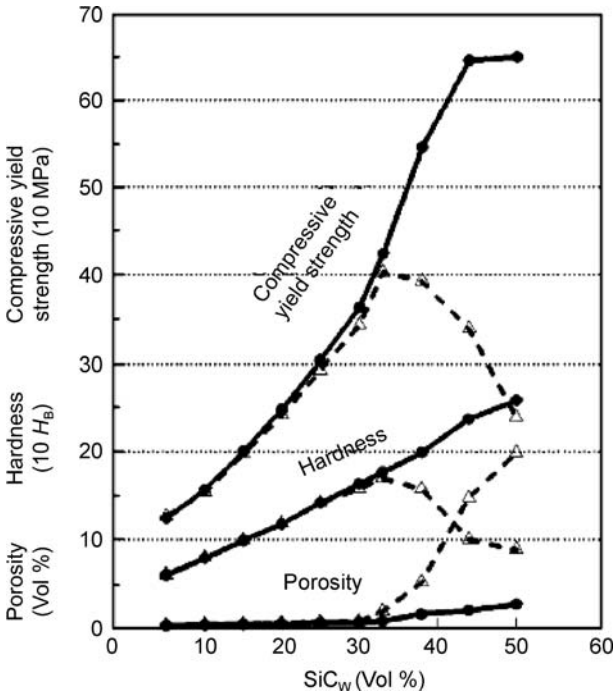

Figure 1.10. Variation in the porosity, hardness and compressive yield strength of silicon carbide whisker copper-matrix composites fabricated by powder metallurgy. *Circles*, coated filler method. *Triangles*, admixture method. (From [3])

the temperature must be adequate for the diffusion to be significant. This process requires not only high temperature but also high pressure, since pressure helps the densification process (i.e., the reduction of the porosity of the article subjected to sintering). The pressure may be applied before or during the sintering. Due to the need for high pressure, an article made by this method is limited in size. Since the melting temperature of the filler is usually much higher than that of the metal matrix, the sintering pertains to the metal particles rather than to the filler. As a result, the volume fraction of filler in the resulting composite is usually low (e.g., 20%); otherwise there is not enough metal matrix to bind the filler particles (or fibers) together to form a composite. To alleviate this problem, the filler particles (or fibers) may be coated with the metal matrix (e.g., by plating) prior to sintering (Fig. 1.9). By using the coated filler, with the use of the metal particles being optional, the filler volume fraction can be greatly increased compared to when the uncoated filler is used. A high filler volume fraction (e.g., 60%) is necessary to achieve a low CTE, as needed for microelectronic heat sinks. Just for mechanical properties, a high filler volume fraction is not necessary.

Figure 1.10 shows that the advantage of the coated filler method over the conventional admixture method is particularly significant when the filler volume fraction is high (e.g., more than 30 vol% when silicon carbide whisker is used as the filler).

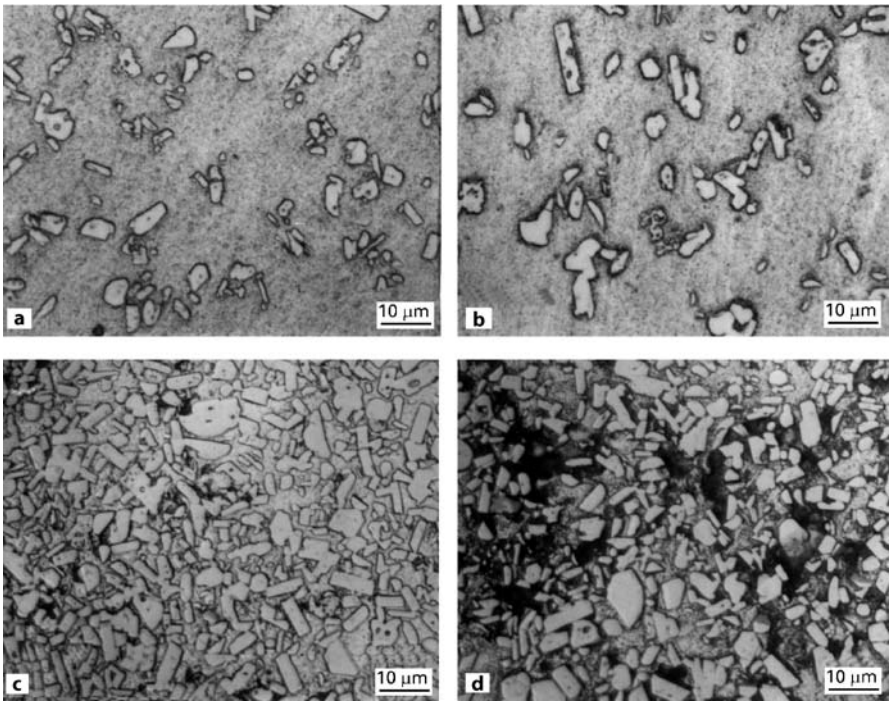

Figure 1.11. Optical microscope photographs of copper-matrix titanium diboride platelet composites fabricated by powder metallurgy. **a** 15 vol% TiB_2, coated filler method; **b** 15 vol% TiB_2, admixture method; **c** 60 vol% TiB_2, coated filler method; **d** 60 vol% TiB_2, admixture method. (From [4])

In the regime of high filler volume fraction, the coated filler method gives lower porosity, higher hardness and higher compressive yield strength. Due to its high modulus and high aspect ratio, silicon carbide whisker is a highly effective reinforcement. Silicon carbide particles are commonly used as an abrasive. Figure 1.11 shows copper-matrix composites made by the two methods and containing 15 vol% titanium diboride (TiB_2) platelets (3–5 μm) have similarly low porosities, but that the composite made using the admixture method has a much higher porosity than that made using the coated filler method when the composite contains 60 vol% TiB_2 platelets. Titanium diboride is a ceramic that is unusual in its high thermal conductivity (about 100 W/m K) and low electrical resistivity (about $20 \times 10^{-6}\,\Omega\,\text{cm}$).

1.3.3 Carbon-Matrix Composites

Carbon-matrix composites are made by the carbonization of the matrix of a polymer-matrix composite. The process of carbonization (also known as pyrolysis) is akin to charring, which involves a chemical reaction that removes essentially all atoms that are not carbon from the polymer (the carbon precursor). The carbonization process is typically conducted in an inert atmosphere at around 650–1,200°C. The atmosphere is usually nitrogen at temperatures up to 1,000°C and is argon at temperatures above 1,000°C. Argon at high temperatures is used because carbon tends to react with nitrogen to form poisonous cyanide compounds above 1,000°C. One common carbon precursor is pitch (a polyaromatic hydrocarbon material derived from petroleum or coal), which is a mixture of thermoplastic polymers. Pitch is attractive because of its relatively high char yield (i.e., the mass of the resulting carbon divided by the mass of the carbon precursor). A high char yield means a smaller amount of porosity in the resulting carbon-matrix composite. There are many grades of pitch. Those with higher molecular weights tend to give higher char yields. Due to the porosity, which is detrimental to the mechanical properties of the composite, the carbon-matrix composite is commonly subjected to impregnation of the carbon precursor and then another round of carbonization. In order to achieve a sufficiently low porosity, multiple cycles of impregnation–carbonization are conducted, thus resulting in a high processing cost. In order to decrease the required number of cycles, the last cycle is commonly followed by a process known as chemical vapor infiltration (CVI), in which the remaining pores are filled with carbon that is deposited from the thermal decomposition of a carbonaceous gas that infiltrates the composite.

A thermoplastic polymer such as pitch melts upon heating. The melting of the matrix is undesirable for the conversion of a polymer-matrix composite to a carbon-matrix composite. Furthermore, during carbonization, pitch tends to bloat due to the evolution of gases generated by pyrolysis. The bloating can cause the expulsion of pitch from the carbon fiber preform during carbonization. Thus, the carbonization process is usually preceded by a process known as stabilization, which involves heating at 200–300°C in the presence of oxygen. In stabilization, oxygen diffuses into the carbon precursor and reacts with it, thus converting it

chemically to a form that does not melt. Hence, the stabilization process is also known as infusibilization.

The fabrication of carbon–carbon composites is carried out using four main methods, namely:

1. liquid phase impregnation (LPI);
2. hot isostatic pressure impregnation carbonization (HIPIC);
3. hot pressing, and;
4. chemical vapor infiltration (CVI).

All of these methods (except, in some cases, CVI) involve the initial preparation of a prepreg by either wet winding continuous carbon fibers with pitch or resin (e.g., phenolic), or wetting woven carbon fiber fabrics with pitch or resin. Unidirectional carbon fiber tapes are not as commonly used as woven fabrics, because fabric lay-ups tend to result in more interlocking between the plies. For highly directional carbon–carbon composites, fabrics that have a greater number of fibers in the warp direction than the fill direction may be used. After prepreg preparation and, in the case of fabrics, fabric lay-up, the pitch or resin needs to be pyrolyzed or carbonized by heating at 350–850°C. Due to the shrinkage of the pitch or resin during carbonization (which is accompanied by the evolution of volatiles), additional pitch or resin is impregnated in the case of LPI and HIPIC, and carbonization is carried out under pressure in the case of hot pressing. In LPI, carbonization and impregnation are carried out as distinct steps; in HIPIC, carbonization and impregnation are performed together as a single step.

The carbon yield (or char yield) from carbonization is around 50 wt.% for ordinary pitch and 80–88 wt.% for mesophase pitch at atmospheric pressure. Mesophase pitch tends to be more viscous than ordinary pitch, making impregnation more difficult. In the case of resins, the carbon yield varies widely from one resin to another. Significant increases in the carbon yield of pitch can be obtained through the use of high pressure during carbonization. Mesophase spheres that exhibit a highly oriented structure similar to liquid crystals and are initially around 0.1 μm in diameter are observed in isotropic liquid pitch above 400°C. Prolonged heating causes the spheres to coalesce, solidify, and form larger regions with lamellar order; this favors graphitization upon subsequent heating to ~2,500°C. The high pressure during carbonization lowers the temperature at which the mesophase forms. At very high pressures (~200 MPa), coalescence of mesophase does not occur. Therefore, an optimum pressure is around 100 MPa. Pressure may or may not be applied during carbonization in LPI, but it is always applied during carbonization in HIPIC.

In LPI, after carbonization, vacuum impregnation is performed with additional pitch or resin in order to densify the composite. Pressure (e.g., 2 MPa) may be applied to help the impregnation. The first carbonization decreases the density from the value of the green composite, so that subsequent impregnation and re-carbonization are necessary. The carbonization–impregnation cycles are repeated several times (typically 3–6) in order to achieve sufficient densification. Both the density and interlaminar shear strength (ILSS) increase with the number of cycles.

The density levels off after a few cycles of impregnation and recarbonization. This is because the repeated densification cycles cause the mouths of the pores to narrow down, making it difficult for the impregnant to enter the pores. As a consequence, impregnant pickup levels off. This problem can be alleviated by intermediate graphitization, where the composites are subjected to heat treatment at 2,200–3,000°C between the carbonization and impregnation steps after the densification cycle when the density levels off. On graphitization, the pore entrances open up due to the rearrangement of the crystallites in the matrix. These opened pores then become accessible during further impregnation, thus leading to a further increase in density. The use of mesophase pitch instead of isotropic pitch for impregnation can cut down on the required number of impregnation cycles.

In HIPIC, an isostatic inert gas pressure of around 100 MPa is applied to impregnate pitch (rather than resins, which suffer from a low carbon yield) into the pores in the sample while the sample is being carbonized at 650–1,000°C. The pressure increases the carbon yield and maintains the more volatile fractions of the pitch in a condensed phase. After this combined step of carbonization and impregnation, graphitization is performed by heating without applied pressure above 2,200°C. HIPIC allows the density to reach a higher value than LPI (with or without intermediate graphitization), and fewer cycles are needed for HIPIC to achieve the high density. However, HIPIC is an expensive technique.

One HIPIC process involves vacuum impregnating a dry fiber preform or porous carbon–carbon laminate with molten pitch by placing it inside a metal container (or can) containing an excess of pitch. The can is then evacuated and sealed (preferably using an electron beam weld) and placed within the work zone of a hot isostatic press (HIP) unit. The temperature is then raised at a programmed rate above the melting point of the pitch, but not high enough to result in weight loss due to the onset of carbonization. The pressure is then increased and maintained at around 100 MPa. The pitch initially melts and expands within the can and is forced by isostatic pressure into the pores in the sample. The sealed container acts like a rubber bag, facilitating the transfer of pressure to the workpiece. After that, the temperature is gradually increased towards that required for pitch carbonization (650–1,000°C). The pressure not only increases the carbon yield but also prevents liquid from being forced out of the pores by pyrolysis products. The optimum carbonization pressure for HIPIC is 100–150 MPa. Lower pressures are insufficient to prevent bloating of the composites due to the evolution of carbonization gases.

HIPIC increases the carbon yield of pitch, especially when the molecular size of the pitch is small. The increase in pressure up to 10 MPa causes the carbon yield to increase significantly for a pitch with a low molecular weight, but only slightly for a pitch with a high molecular weight. This is due to the already high carbon yield of pitch with a high molecular weight when the pressure is low. This improvement can be attributed to the trapping and decomposition of the evolved hydrocarbon gases under high pressure; the decomposition produces carbon and hydrogen. The increase in pressure causes the bulk density to increase, the porosity to decrease, and the flexural strength to increase.

In hot pressing (also called high-temperature consolidation), carbonization is performed at an elevated temperature (1,000°C typically) under uniaxial pressure

(2–3 MPa typically) in an inert or reducing atmosphere or in a vacuum. During hot pressing, graphitization may occur even for thermosetting resins, which are harder to graphitize than pitch. This is known as stress graphitization. Subsequently, further graphitization may be performed by heating without applied pressure at 2,200–3,000°C. No impregnation is performed after the carbonization. Composites made by hot pressing have flattened pores in the carbon matrix, and the part thickness is reduced by about 50%.

In CVI (also called CVD, chemical vapor deposition), gas phase impregnation of a hydrocarbon gas (e.g., methane, propylene) into a carbon fiber preform takes place at 700–2,000°C, so that pyrolytic carbon produced by the cracking of the gas is deposited in the open pores and surface of the preform. The carbon fiber preform can take the form of carbon fabric prepregs that have been carbonized and graphitized, or the form of dry wound carbon fibers. There are three CVI methods, namely the isothermal method, the temperature gradient method, and the pressure gradient method.

In the isothermal method, the gas and sample are kept at a uniform temperature. As carbon growth in the pores will cease when they become blocked, there is a tendency for preferential deposition on the exterior surfaces of the sample. This results in a need for multiple infiltration cycles such that the sample is either skinned by light machining or exposed to high temperatures to reopen the surface pores for more infiltration in subsequent cycles.

In the temperature gradient method, an induction furnace is used. The sample is supported by an inductively heated mandrel (a susceptor) so that the inside surface of the sample is at a higher temperature than the outside surface. The hydrocarbon gas flows along the outside surface of the sample. Due to the temperature gradient, the deposition occurs first at the inside surface of the sample and progresses toward the outside surface, thereby avoiding the crusting problem.

In the pressure gradient method, the hydrocarbon gas impinges on the inside surface of the sample, so the gas pressure is higher at the inside surface than the outside surface. The pressure gradient method is not as widely used as the isothermal method or the temperature gradient method.

Both the temperature gradient method and the pressure gradient method are limited to single samples, whereas the isothermal method can handle several samples at once. However, the isothermal method is limited to thin samples due to the crusting problem.

A drawback of CVI is the low rate of deposition resulting from the use of a low gas pressure (1–150 Torr), which favors a long mean free path for the reactant and decomposed gases; a long mean free path enhances deposition into the center of the sample. A diluent gas (e.g., He, Ar) is usually used to help the infiltration. Hydrogen is often used as a carbon surface detergent.

An attraction of CVI is that CVI carbon is harder than char carbon from pitch or resin, making CVI carbon particularly desirable for carbon–carbon composites used for brakes and friction products.

The fiber-matrix bond strength in carbon–carbon composites must be optimal. If the bond strength is too high, the resulting composite may be extremely brit-

tle and thus exhibit catastrophic failure and poor strength. If it is too low, the composites fail in pure shear, with poor transfer of the load to the fiber.

The main disadvantages of carbon–carbon composites are their high fabrication cost, poor oxidation resistance, poor interlaminar properties (especially for two-dimensionally woven fibers), the difficulty involved in making joints, and the insufficient engineering database.

1.3.4 Ceramic-Matrix Composites

A ceramic-matrix composite (abbreviated to CMC) is commonly made from a polymer-matrix composite by converting the polymer matrix to a ceramic. The process often involves thermal composition and, in this case, it is known as pyrolysis. For example, polycarbosilane (a polymer that has both carbon and silicon atoms) is often used as the precursor of silicon carbide.

The fibers can be short or continuous. In both cases, the composites can be formed by viscous glass consolidation, i.e., either hot pressing a mixture of fibers and glass powder, or by winding glass-impregnated continuous fiber under tension above the annealing temperature of the glass.

Short ($\leq$3 mm) fiber borosilicate glass composites are prepared by hot pressing, in vacuum or argon, using an isopropyl alcohol slurry of fibers and Pyrex powder (<50 μm particle size) at 700–1,000°C (depending on the fiber content, which ranges from 10 to 40 vol%) and 6.9 MPa. Fibers longer than 3 mm are more difficult to disperse in the slurry. The resulting composite has fibers that are randomized two-dimensionally, as some alignment occurs during pressing.

Continuous fiber composites are made by allowing fibers from a spool to pass through a glass powder slurry (containing water and a water-soluble acrylic binder), winding the slurry-impregnated fibers onto the sides of a hexagonal prism (mandrel or take-up drum), cutting up the flat unidirectional tapes from the mandrel, stacking the pieces (plies) in a proper orientation, burning out the stack to remove the binder, and hot pressing the stack at a temperature above the working temperature of the glass. This process is known as slurry infiltration or viscous glass consolidation. During hot pressing, the glass must flow into the space between adjacent fibers. Since glass does not wet carbon, sufficient pressure is necessary.

Viscous glass consolidation can also be carried out without hot pressing. In this case, a glass powder-impregnated continuous fiber tow is wound under tension (e.g., about 15 ksi or 100 MPa) onto a collection mandrel at a temperature above the annealing temperature of the glass.

Other than viscous glass consolidation, another method for forming short or continuous fiber glass-matrix composite is the sol–gel method, i.e., infiltration by a sol and subsequent sintering, using metal alkoxides and/or metal salts as precursors and using an acid or base catalyst to promote hydrolysis and polymerization. Composite fabrication consists of two steps:

1. the preparation of fiber-gel prepregs, and
2. thermal treatment and densification by hot pressing.

In the first step, the sol-impregnated prepregs are allowed to gel, dried at room temperature for a day, dried at 50°C for a day, and then heat-treated at 300–400°C for 3 h. In the second step, hot pressing is performed in a nitrogen atmosphere with a pressure of 10 MPa. In the case of a borosilicate glass, the hot pressing temperature is between 900 and 1,200°C. The sol–gel method is advantageous in that homogenization of the components during impregnation can readily be achieved and sintering temperatures are substantially lowered because of the smaller particle size compared to the slurry infiltration method. The easier impregnation or infiltration decreases the tendency for the particles to damage the fibers. However, the sol–gel method has the disadvantage of excessive shrinkage during subsequent heat treatment.

The slurry infiltration and sol–gel methods can be combined using particle-filled sols. Particle filling helps to reduce the shrinkage.

Yet another method is melt infiltration, which requires that the glass is heated at a temperature much above the softening temperature in order for the glass to infiltrate the fiber preform. This high temperature may lead to a chemical reaction between the fibers and the matrix.

The reaction between SiO_2 and carbon fibers is of the form:

$$3C + SiO_2 \rightarrow SiC + 2CO\ .$$

To reduce the extent of this reaction, SiC-coated carbon fibers are used for SiO_2-matrix composites.

Fibers such as carbon fibers have the following effects on the glass:

1. they increase the toughness (and, in some cases, the strength as well);
2. they decrease the coefficient of thermal expansion, and;
3. they increase the thermal conductivity.

The increase in toughness occurs in glass with short and randomly oriented fibers, as well as glass with continuous fibers. However, the strength is usually decreased by the fibers in the former and is usually increased by the fibers in the latter. Even for continuous fibers, the strengthening is limited by widespread matrix cracking (both transverse and longitudinal).

The high-temperature strength of carbon fiber reinforced glasses in air is limited by the oxidation of the carbon fibers. This oxidation cannot be prevented by the glass matrix. In an inert atmosphere, the high-temperature strength is limited by the softening of the glass matrix.

1.3.5 Cement-Matrix Composites

Cement is basically calcium silicate, where the SiO_4 tetrahedron (with the silicon atom being sp^3 hybridized and located at the body center of the tetrahedron, while the oxygen atoms are located at the four corners of the tetrahedron) is the fundamental building block. The realization of a cement-matrix composite does not require heat or pressure. This is why concrete processing can be performed in the

field (as in road construction) rather than in a factory. The process involves mixing cement particles with water and allowing them to react. This reaction is exothermic (i.e., heat is released during the reaction) and is known as hydration. Here, water enters the cement crystals and forms a gel that is a hydrate, particularly calcium silicate hydrate (abbreviated C-S-H, with the average chemical formula $3CaO \cdot 2SiO_2 \cdot 3H_2O$). Partly because of the difference in volume between the reaction products and the original material, shrinkage (commonly known as drying shrinkage) accompanies the hydration reaction. In order to make sure that there is sufficient water available for the hydration reaction, the reaction is commonly conducted in a moisture chamber that has a high relative humidity (approaching 100%). During the first 24 h of the reaction, the originally fluid cement paste gradually becomes a rigid material that can thus be demolded if desired. This part of the hardening process is known as setting. However, the set material has not completed the hydration reaction, so the strength has not reached the desired high level. Therefore, setting is followed by curing for weeks (typically 28 days in laboratory studies). While curing, the material is exposed to moisture (as in a moisture chamber) for an extended period so as to allow the hydration reaction to approach completion.

Five types of Portland cement are standardized in the US by the American Society for Testing and Materials (ASTM). They are ordinary (Type I, which is the most commonly used type), modified (Type II), high-early-strength (Type III), low-heat (Type IV), and sulfate-resistant (Type V).

Effective use of discontinuous fibers in concrete requires dispersion of the fibers in the mix. The dispersion is particularly challenging when the fiber diameter is small, such as 10 μm. The ease of dispersion increases with decreasing fiber length. The fiber dispersion is enhanced by using silica fume (a fine particulate) as an admixture at the level of, say, 15% by mass of cement. The silica fume is typically used along with a small amount (say 0.4% by mass of cement) of methylcellulose (a water-soluble polymer) to aid the dispersion of the fibers and the workability of the mix. Latex (typically a copolymer of styrene and butadiene in the form of a particulate dispersion, used typically at levels of 15–20% by mass of cement) is much less effective than silica fume at aiding fiber dispersion.

1.4 Composite Design Concepts

The filler can take the form of particles, discontinuous fibers or continuous fibers. The fibers can be oriented in one or more particular directions, or they can be randomly oriented. The combined use of different fillers is possible. For example, concrete is used in combination with sand and stones, which are different in particle size, in order to achieve a high total filler volume fraction. The fine particles fill the space between the large particles (Fig. 1.12), thus resulting in a total filler volume that cannot be achieved through the use of a single type of filler. In another example, carbon fiber and polymer fiber are used together in a polymer-matrix composite in order to achieve a balanced combination of high toughness (provided by the polymer fiber) and high modulus (provided by the carbon fiber). The two

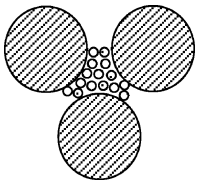

Figure 1.12. Packing of particles of two different sizes to attain a high density of packing

types of fibers can be in the same lamina or in different laminae of the composite. When they are in the same lamina, they can be in the same prepreg sheet or in the same woven fabric.

The matrix can be polymer, cement, metal, carbon, ceramic or a hybrid of multiple types of matrix materials. An example of a hybrid matrix is one consisting of both carbon and silicon carbide, as obtained, for example, by the pyrolysis of a precursor that is a mixture of a carbon precursor and a silicon carbide precursor. A hybrid matrix with carbon and silicon carbide is more oxidation resistant than a carbon matrix.

A special design of a hybrid matrix involves a spatial gradient in the proportion of the two components so that a certain property (e.g., the CTE) of the matrix varies along the composition gradient. Such a matrix is said to be functionally gradient. The functional gradient is made possible by a composition gradient. When the composite is used as an interface layer between article A and article B, such that A and B are different in CTE, it is desirable for the composite to be functionally gradient, so that its CTE in the part of it that is proximate to article A is close to that of A, and its CTE in the part of it that is proximate to article B is close to that of B. Such a CTE gradient helps to enhance the thermal fatigue resistance (i.e., the ability to withstand temperature cycling). An example is the coating of a carbon–carbon composite with silicon carbide for the purpose of oxidation protection, such that the interface layer has a composition gradient, with the side proximate to the carbon–carbon composite being rich in carbon and the side proximate to the silicon carbide being rich in silicon carbide.

In general, the longer the fiber, the greater its ability to reinforce a material. Thus, continuous fibers are dominantly used for polymer-matrix structural composites. However, discontinuous fibers are attractive for composite processing methods that require mixing of the filler and the matrix material to form a dispersion (or a slurry) that is introduced into the composite processing equipment. An example of such a processing method is injection molding, which involves the injection of the dispersion into a mold cavity that dictates the shape and size of the composite article. Injection molding is widely used to make polymer-matrix composite articles of complex shapes (such as telephone receivers). In order for the dispersion to conform to the intricate shape (fine details) of a mold for injection molding, it is advantageous for the filler to be small in size. Thus, nanofillers (nanoparticles or nanofibers) are attractive. Another example is concrete mixing, which results in a slurry that is poured into a mold (called a "form" in fieldwork) that dictates the shape and size of the concrete article (called a "struc-

ture" in fieldwork). Pouring into a mold is a process that is generally known as "casting."

In molding or casting, the fluidity (or workability) of the dispersion is important, particularly if the mold has an intricate shape. The fluidity can be enhanced by increasing the proportion of the liquid in the dispersion. However, the use of excessive liquid is often not desirable, as it may result in increased porosity in the resulting composite. In the case of a cement-matrix composite, the higher the water/cement ratio in the cement mix, the lower the strength of the resulting composite. An alternate method involves the use of a plasticizer, which is a chemical additive used in minor amounts. A plasticizer for cement is adsorbed onto the surfaces of the cement particles, thus causing a negative charge and hence electrostatic repulsion between cement particles. By separating the cement particles, water can reach more of the cement particles, thus causing the water present to be more effectively used for the hydration reaction. Thus, the plasticizer reduces the amount of water required, thus allowing the fluidity to be adequate without having to use a high water/cement ratio. This is why a plasticizer for cement is also known as a water-reducing agent. Examples of plasticizers for cement include lignosulfonates, sulfonated naphthalene condensate, and sulfonated melamine formaldehyde, which are organic polymers. Their long molecules wrap themselves around a cement particle and provide the particle with a negative charge.

Dispersion stability refers to the essential absence of a tendency for the filler in a dispersion to separate from the liquid part of the dispersion. In this context, stability should be distinguished from thermal stability. The liquid part is called the "vehicle" when it is based on a polymer or water. A vehicle based on a polymer or a polymer precursor (a resin) is often used to make a polymer-matrix composite. Vehicles based on water are used in cement-matrix composite fabrication. In metal-matrix composite fabrication, the liquid part is the molten metal.

Instability is usually associated with the filler units sticking to one another and then settling. The greater the difference in density between the filler and the liquid, the higher the tendency for instability. The stability is important for achieving a uniform distribution of the filler in the resulting composite. Matching the density of the filler to that of the liquid is a technique that is used to achieve stability. In general, the density of a liquid can be increased by dissolving an appropriate solid in the liquid. However, this method may not be able to give the required degree of stability, since the density of a liquid can be increased by only a limited degree.

Another method of improving the stability of a dispersion involves the use of a dispersant, which is a chemical additive that makes it more difficult for the filler units to aggregate. Filler aggregation is promoted by a low filler–filler interface energy and a high filler–liquid interface energy. By lowering the energy of the filler–liquid interface or increasing the energy of the filler–filler interface, the tendency for filler aggregation can be reduced. One method of increasing the energy of the filler–filler interface involves providing electrical charge to the filler units, thus resulting in electrostatic repulsion between the filler units. One method of decreasing the energy of the filler–liquid interface involves the use of a surfactant, which is a wetting agent that enhances the wettability of the liquid on the filler.

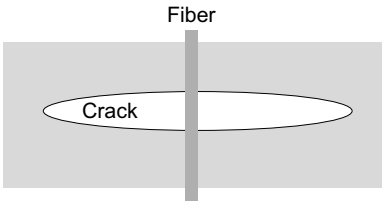

Figure 1.13. Fiber bridging a microcrack; microcracks tend to be present in brittle materials

Good wetting means that the liquid spreads across the surface of the filler. Poor wetting means that the liquid forms droplets on the surface of the filler. Another method of improving the wetting involves treating the surface of the filler by either coating the filler with a material that is more wettable by the liquid or applying chemical functionalization (i.e., the formation of functional groups on the surface of the filler that improve the wettability of the surface).

The ability of a fiber of a chosen length to reinforce a material increases with the strength of the bond between the reinforcement and the matrix. This bond depends on the microstructure and chemistry of the interface. For example, it can be enhanced by fiber surface treatment, such as a treatment that results in certain functional groups on the fiber surface (e.g., carboxyl and carbonyl groups on the surface of a carbon fiber). However, a bond that is too strong is disadvantageous to toughening when the toughening mechanism involves fiber pull-out (the pulling out of a fiber that bridges a microcrack as the microcrack opens, as illustrated in Fig. 1.13). Thus, for brittle-matrix composites, such as those with ceramic, carbon and cement matrices, the bond strength needs to be optimized.

The tailoring of composite interfaces is as important as the tailoring of composite components. Surface modification of a filler is commonly used for interface engineering. For example, this modification can involve the coating of the filler surface with molecules (e.g., a silane coupling agent) that have appropriate functional groups at their ends in order to provide some covalent linkage between the filler and the matrix across the interface. In other words, one end of the molecule attaches itself to the filler while the other end attaches itself to the matrix. There are many types of silane coupling agents that differ in the functional groups at the two ends of the molecule. For example, a molecule ending with a trichloro, trimethoxy or triethoxy functional group attaches to the surface of an oxide filler, whereas a molecule ending with an organofunctional functional group attaches to the polymer matrix. Because silane coupling agents are soluble in water, they are typically applied in the form of aqueous solutions. The use of a coupling agent is essential for glass fiber polymer-matrix composites. Otherwise, moisture attack causes debonding of the glass fiber from the polymer matrix.

1.5 Applications of Composite Materials

Due to their relatively low processing costs, polymer-matrix and cement-matrix composites are the most common types of composite. Polymer-matrix composites

with continuous fiber reinforcement are widely used for lightweight structures, such as airframes. Polymer-matrix composites with metal particles (e.g., silver particles) are used for electrical interconnections. Rubber-matrix composites reinforced with carbon black particles are used for automotive tires. Cement-matrix composites in the form of concrete are widely used for civil infrastructure. Metal-matrix, carbon-matrix and ceramic-matrix composites are less common, though they also have their particular markets.

Metal-matrix composites known as cermets (meaning ceramic-metal combinations) that contain a low volume fraction (e.g., 15%) of ceramic (e.g., tungsten carbide) particles are used in cutting tools such as drills. They are also used in resistors and other electronic components that need to withstand high temperatures. Metal-matrix composites containing ceramic (e.g., SiC) particles at a high volume fraction (e.g., 60 vol%) are used as heat sinks and housing for microelectronics due to their low CTE. A low CTE is needed due to the low CTE of the semiconductor (such as silicon). Metal-matrix composites containing graphite flakes as the filler are also used as self-lubricating piston cylinders for automobile engines due to the lubricity of graphite. Metal-matrix composites containing continuous carbon fibers are used as structural materials, though the reaction of carbon fiber with aluminum forms a brittle compound, Al_4C_3, that lines the fiber–matrix interface. This reaction can be alleviated by coating the fiber with nickel or titanium diboride (TiB_2). However, this structural application faces tough competition from advanced metal alloys that are much less expensive.

Carbon-matrix composites (typically coated with silicon carbide or other ceramics in order to improve their oxidation resistance) are used for high-temperature, lightweight structures, such as the nose cones and leading edges of Space Shuttles and the nose cones of intercontinental ballistic missiles, although they suffer from the tendency of carbon to be oxidized in the presence of oxygen at temperatures above about 700°C. A particularly common type of carbon-matrix composites utilizes carbon fiber as the reinforcement, so that both reinforcement and matrix are carbon and the material is known as a carbon–carbon composite. The market for carbon–carbon composites is mainly related to aerospace: re-entry thermal protection, rocket nozzles and aircraft brakes. Other applications include furnace heating elements, molten materials transfer, spacecraft and aircraft components, and heat exchangers, air-breathing engine components, hypersonic vehicle airframe structures, space structures and prosthetic devices.

Biomedical applications encompass those that pertain to the diagnosis and treatment of conditions, diseases and disabilities, as well as the prevention of diseases and conditions. They include implants (e.g., hips, heart valves, skin and teeth), surgical and diagnostic devices, pacemakers (devices connected by electrical leads to the wall of the heart, enabling electrical control over the heartbeat), electrodes for collecting or sending electrical or optical signals for diagnosis or treatment, wheelchairs, devices for helping the disabled, exercise equipment, pharmaceutical packaging (for controlled release of the drug into the body, or for other purposes) and instrumentation for diagnosis and chemical analysis (such as equipment for analyzing blood and urine). Implants are particularly challenging, as they need to be made of materials that are biocompatible (compatible with fluids such as

blood), corrosion resistant, wear resistant, fatigue resistant, and that are able to maintain these properties over tens of years.

Carbon is a particularly biocompatible material (more so than gold), so carbon–carbon composites are used for implants. Composites with biocompatible polymer matrices are also used for implants. Electrically conducting polymer-matrix composites are used for electrodes for diagnostics. Composites with biodegradable polymer matrices are used for pharmaceutics.

Materials for bone replacement or bone growth support need to have an elastic modulus similar to that of the bone. Tailoring of the modulus can be achieved through composite design, i.e., appropriate choice of the reinforcement and its volume fraction.

Ceramic-matrix composites are more attractive than carbon-matrix composites for high-temperature applications, due to the much lower tendency for ceramics to be oxidized. Examples of ceramic matrices include silicon carbide (SiC) and silicon nitride (Si_3N_4), which can withstand temperatures of up to around 1,700°C in the presence of oxygen. Above 1,700°C, these ceramics can oxidize and become silicon dioxide (SiO_2). Ceramic-matrix composites with ceramic fiber reinforcement are known as ceramic–ceramic composites. It is preferable that the fiber and the matrix are the same in composition so that that there is no CTE mismatch between them, for the sake of thermal fatigue resistance. One example of a ceramic–ceramic composite is a SiC–SiC composite. The ceramic reinforcement serves to toughen the composite. This is because of the tendency for microcracks to occur in the brittle ceramic matrix and the tendency for fiber bridging to occur across a microcrack (Fig. 1.13). The fiber pull-out that accompanies crack opening causes the absorption of energy and hence toughening. However, this mechanism of toughening requires that the bond between the fiber and the matrix is not too strong. Toughening is valuable, due to the inherent brittleness of ceramics. However, the technology of ceramic-matrix composites is not mature enough for implementation, due to both performance and cost issues.

Review Questions

1. Why is aluminum commonly used as the matrix of a metal-matrix composite?
2. Why is magnesium not commonly used as the matrix of a metal-matrix composite?
3. What are the main advantages of thermoplastic-matrix composites compared to thermoset-matrix composites?
4. Why is the pultrusion method of composite fabrication limited to unidirectional composites?
5. What is the main disadvantage of using woven fibers rather than nonwoven fibers as a reinforcement in a composite material?

6. Why is it difficult to use liquid metal infiltration to prepare metal-matrix composites with a low filler volume fraction?
7. What is the main disadvantage of the plasma spray method of metal-matrix composite fabrication?
8. Why is the stabilization step used in the fabrication of a carbon fiber from a pitch fiber?
9. Describe the CVI method of carbon–carbon composite fabrication.
10. What is the main advantage of having fillers of two different particle sizes in the same composite material?
11. Why is fiber bridging attractive for a brittle-matrix composite?

References

[1] Y. Xu and D.D.L. Chung, "Low-Volume-Fraction Particulate Preforms for Making Metal-Matrix Composites by Liquid Metal Infiltration," *J. Mater. Sci.* 33(19), 4707–4710 (1998).
[2] S.-W. Lai and D.D.L. Chung, "Consumption of SiC Whiskers by the Al-SiC Reaction in Aluminum-Matrix SiC Whisker Composites", *J. Mater. Chem.* 6(3), 469–477 (1996).
[3] P. Yih and D.D.L. Chung, "A Comparative Study of the Coated Filler Method and the Admixture Method of Powder Metallurgy for Making Metal-Matrix Composites," *J. Mater. Sci.* 32(11), 2873–2894 (1997).
[4] P. Yih and D.D.L. Chung, "Titanium Diboride Copper-Matrix Composites," *J. Mater. Sci.* 32(7), 1703–1709 (1997).

Further Reading

D.R. Askeland and P.P. Phule, *The Science and Engineering of Materials*, 5th Edition, Thomson, Toronto, 2006, Chaps. 16, 17 and 18.
D.D.L. Chung, "Electromagnetic Interference Shielding Effectiveness of Carbon Materials", *Carbon* 39(2), 279–285 (2001).
D.D.L. Chung, "Composites Get Smart", *Materials Today* Jan. 2002, pp. 30–35.
D.D.L. Chung, "Composites, Intrinsically Smart Structures", *Encyclopedia of Smart Materials*, ed. Mel Schwartz, Wiley, New York, 2002, vol. 1, pp. 223–243.
D.D.L. Chung, "Acid Aluminum Phosphate for the Binding and Coating of Materials", *J. Mater. Sci.* 38(13), 2785–2791 (2003).
D.D.L. Chung, "Functional Composite Materials", *Advances in Condensed Matter and Materials Research*, ed. Francois Gerard, Nova Science Publ., Hauppauge, NY, 2003, pp. 89–147.
D.D.L. Chung, "Carbon-Cement Composites", *World of Carbon 2 (Fibers and Composites)*, ed. Pierre Delhaes, Taylor & Francis, London, 2003, pp. 219–241.
D.D.L. Chung, "Composite Materials", *Kirk–Othmer Encyclopedia of Chemical Technology*, 5th Ed., Wiley, New York, 2004.
D.D.L. Chung, "Multifunctional Polymer-Matrix Structural Composites", *Annual Technical Conference – Society of Plastics Engineers*, 2004, pp. 1410–1414.
D.D.L. Chung, "Composite Materials", *Kirk–Othmer Concise Encyclopedia of Chemical Technology*, 5th Ed., Wiley, New York, 2007.
D.D.L. Chung, G. Song, N. Ma and H. Gu, "Smart Materials and Structures", *High Performance Construction Materials* (Engineering Materials for Technological Needs series, vol. 1), eds. C. Shi and Y.L. Mo, World Scientific Publ., Singapore, 2008.

S.-W. Lai and D.D.L. Chung, "Fabrication of Particulate Aluminum-Matrix Composites by Liquid Metal Infiltration", *J. Mater. Sci.* 29(12), 3128–3150 (1994).
P. Yih and D.D.L. Chung, "Powder Metallurgy Fabrication of Metal Matrix Composites Using Coated Fillers," *Int. J. Powder Metallurgy* 31(4), 335–340 (1995).

2 Carbon Fibers and Nanofillers

2.1 Carbons

Not included in the five categories mentioned in Sect. 1.1 is carbon, which can be found in the form of graphite (its most common form), diamond and fullerenes (a recently discovered form). Note that these are not ceramics, because they are not compounds.

Graphite (a semimetal) consists of carbon atom layers stacked in the *AB* sequence such that the bonding is covalent (due to sp^2 hybridization) and metallic (two-dimensionally delocalized $2p_z$ electrons) within a layer, and van der Waals between the layers. This bonding makes graphite very anisotropic, so it is a good lubricant (due to the ease with which the layers can slide past one another). Graphite is also used in pencils because of this property. Moreover, graphite is an electrical and thermal conductor within the layers but an insulator in the direction perpendicular to the layers. The electrical conductivity is valuable when using graphite for electrochemical electrodes. Graphite is chemically quite inert. However, due to its anisotropic structure, graphite can undergo a reaction (known as intercalation) in which foreign species (called the intercalate) are inserted between the carbon layers. Disordered carbon (called turbostratic carbon) also has a layered structure, but, unlike graphite, it does not have the *AB* stacking order and the layers are bent. Upon heating, disordered carbon becomes more ordered, as the ordered form (graphite) has the lowest energy. Graphitization refers to the ordering process that leads to graphite. Conventional carbon fibers are mostly disordered carbon such that the carbon layers lie preferentially along the fiber axis. A form of graphite called flexible graphite is formed by compressing a collection of intercalated graphite flakes that have been exfoliated (i.e., allowed to expand by over 100 times along the direction perpendicular to the layers, typically through heating after intercalation). The exfoliated flakes are held together by mechanical interlocking, as there is no binder. Flexible graphite is typically generated in the form of sheets that are resilient in the direction perpendicular to the sheet. This resilience allows flexible graphite to be used as a gasket for fluid sealing.

Diamond is a covalent network solid that exhibits the diamond crystal structure due to sp^3 hybridization (akin to silicon). It is used as an abrasive and as a thermal conductor. It has the highest thermal conductivity of any material. However, it is an electrical insulator. Due to its high material cost, diamond is typically used in

the form of powder or thin-film coating. Diamond should be distinguished from diamond-like carbon (DLC), which is amorphous carbon with carbon that is sp^3-hybridized. Diamond-like carbon is mechanically weaker than diamond but also less expensive than it.

Fullerenes are molecules (C_{60}) with covalent bonding within each molecule. Adjacent molecules are held by van der Waals' forces. However, fullerenes are not polymers. Carbon nanotubes are a derivative of the fullerenes, as they are essentially fullerenes with extra carbon atoms at the equator. The extra atoms cause the fullerene to lengthen. For example, ten extra atoms (i.e., one equatorial band of atoms) exist in the molecule C_{70}. Carbon nanotubes can be singlewalled or multiwalled nanotubes, depending on the number of carbon layers in the wall of the nanotube.

2.2 Carbon Fibers

Since carbon fiber composites are important for both structural and functional applications, as covered in this book, this section provides an introduction to carbon fibers. The structural importance of carbon fibers stems from their high strength, high modulus and low density. The functional importance of carbon fibers stems from their high electrical conductivity.

There are three forms of carbon, namely graphite, diamond and fullerene. Carbon fibers belong to the graphite family, although they may not be crystalline. Graphite has a layered crystal structure, with the carbon layers stacked in the *AB* sequence (Fig. 2.1). Within a layer, the chemical bonding is a mixture of covalent bonding and metallic bonding. The covalent bonding, which results from the sp^2 hybridization of each carbon atom, is responsible for the high modulus and strength in the plane of the carbon layers. The metallic bonding, which is due to the delocalized p_z electrons, is responsible for the high electrical conductivity and high thermal conductivity in the plane of the carbon layers. Perpendicular to the carbon layers, the bonding involves van der Waals forces (secondary bonding). Due to the weak interlayer bonding, the carbon layers can easily slide with respect to one another, thus making graphite a good solid lubricant. Due to the difference between the in-plane and out-of-plane bonding, graphite is mechanically much stronger and stiffer and is electrically and thermally much more conductive in the plane of the carbon layers than in the direction perpendicular to them.

A carbon fiber is made from a polymer fiber by converting the polymer into carbon, using a process similar to that used for the fabrication of carbon-matrix composites, as described in Sect. 1.3.3. The diameter of a continuous carbon fiber is commonly around 7 μm. A carbon fiber can have various degrees of crystallinity, as controlled by the process of fabrication. For a given carbon precursor, e.g., pitch and polyacrylonitrile (PAN), the higher the heat treatment temperature, the greater the degree of crystallinity (also known as the degree of graphitization). After carbonization, a carbon fiber is noncrystalline (amorphous) and is said to be turbostratic. In the turbostratic form, there are still carbon layers, but the layers are not very extensive, not very flat and not very parallel, and they do not exhibit

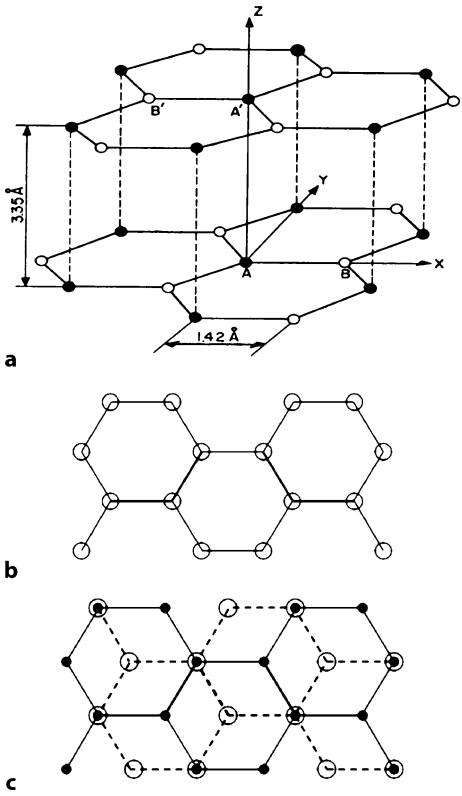

Figure 2.1. Crystal structure of graphite. **a** Three-dimensional view. **b** Two-dimensional view of a single carbon layer. **c** Two-dimensional view of two superimposed adjacent carbon layers. The *A* atoms (*solid circles*) constitute one carbon layer, whereas the *B* atoms (*open circles*) constitute the adjacent carbon layer

the *AB* stacking sequence. This means that turbostratic carbon has short-range order but no long-range order, as in the case of noncrystalline materials in general. In order for the carbon fiber to achieve a degree of crystallinity, the carbonization process needs to be followed by graphitization, which is heat treatment at a higher temperature, such as 2,300–3,000°C. Because the crystalline state is the thermodynamically stable state (i.e., the state of lowest energy), the carbon atoms would automatically move to approach the crystalline state if there was enough thermal energy for them to move. In other words, the crystallization process is spontaneous.

A carbon fiber has the carbon layers preferentially aligned with the fiber axis, even though the layers may not be flat (Fig.2.2). In other words, the layers are not randomly oriented; there is a distribution of orientations such that there is a degree of preference for the orientation parallel to the fiber axis. In general, the preferred orientation is known as the texture (or crystallographic texture). In the case of fibers, the preferred orientation is that in which the direction perpendicular to the carbon layers is preferentially in the cross-sectional plane of the fiber, such that

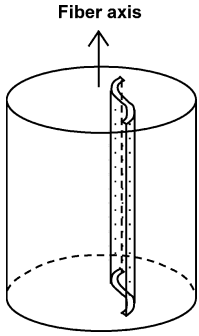

Figure 2.2. Preferential orientation of a carbon layer along the axis of a carbon fiber

this direction is two-dimensionally random in this plane. This is a type of texture known as the fiber texture, which in general refers to a texture involving preferential orientation of a certain crystallographic direction in a particular physical direction such that there is two-dimensional randomness of the crystallographic direction perpendicular to this direction. The fiber texture is a natural consequence of the fiber fabrication, which typically involves flow of the carbon precursor during the formation of the precursor fiber. This texture causes the modulus, strength, electrical conductivity and thermal conductivity of carbon fibers along the fiber axis to be high, in spite of the crystallographic anisotropy. This also means that the properties of a fiber in the transverse direction are inferior to those in the axial direction. Since a composite is typically designed to exploit the axial properties of the fiber (e.g., a composite is designed with the fibers aligned along the direction of the composite that needs to be strong), the inferior transverse properties are usually not an issue.

Carbon fibers are electrically and thermally conductive, in contrast to the non-conducting nature of polymer and ceramic matrices. Therefore, carbon fibers can serve not only as a reinforcement but also as an additive for enhancing the electrical or thermal conductivity. Furthermore, carbon fibers have a near-zero coefficient of thermal expansion, so they can also serve as an additive to lower the thermal expansion. This combination of high thermal conductivity and low thermal expansion makes carbon fiber composites useful for heat sinks in electronics and for space structures that require dimensional stability. As the thermal conductivity of carbon fibers increases with the degree of graphitization, applications requiring a high thermal conductivity should use graphitic fibers such as high-modulus pitch-based fibers and vapor-grown carbon fibers.

Carbon fibers are more cathodic than practically any metal, so in a metal matrix, a galvanic couple is formed with the metal as the anode. This causes corrosion of the metal. The corrosion product tends to be unstable in moisture and causes pitting, which aggravates corrosion. To alleviate this problem, carbon fiber metal-matrix composites are often coated.

The carbon fibers in a carbon-matrix composite (called a carbon–carbon composite) serve to strengthen the composite, as the carbon fibers are much stronger

than the carbon matrix due to the crystallographic texture (preferred crystallographic orientation) in each fiber. Moreover, the carbon fibers serve to toughen the composite, as the debonding between the fibers and the matrix provides a mechanism for energy absorption during mechanical deformation. In addition to having attractive mechanical properties, carbon–carbon composites are more thermally conductive than carbon fiber polymer-matrix composites. However, at elevated temperatures (above 320°C), carbon–carbon composites degrade due to the oxidation of carbon (especially the carbon matrix), which forms CO_2 gas. To alleviate this problem, carbon–carbon composites are coated.

Carbon fiber ceramic-matrix composites are more oxidation resistant than carbon–carbon composites. The most common form of such a composite is carbon fiber reinforced concrete. Although the oxidation of carbon is catalyzed by an alkaline environment and concrete is alkaline, the chemical stability of carbon fibers in concrete is superior to that of competitive fibers, such as polypropylene, glass, and steel. Composites containing carbon fibers in more advanced ceramic matrices (such as SiC) are rapidly being developed.

The conductivity of carbon fiber and the nonconductivity of the polymer matrix enable carbon fiber polymer-matrix composites to be tailored for functional properties. For example, the electrical resistivity of a carbon fiber polymer-matrix composite is sensitive to the damage in the composite, thereby allowing the composite to be a sensor of its own damage. Damage in the form of fiber breakage increases the resistivity in the fiber direction of the composite. Damage in the form of delamination increases the resistivity in the through-thickness direction of the composite, since delamination diminishes the extent of fiber–fiber contact across the interlaminar interface. In other words, the fibers of one lamina cannot contact those of an adjacent lamina in the area where the two laminae are separated by a delamination crack. Damage monitoring, also known as structural health monitoring, is practically important, due to the aging and deterioration of aircraft made of composites.

A high degree of graphitization is attractive due to the resulting high values of modulus, electrical conductivity and thermal conductivity along the fiber axis. Although a high degree of crystallization enhances the modulus, it is detrimental to the strength of the fiber. This is because high crystallinity facilitates the sliding of a carbon layer relative to another layer, thus resulting in easy shear of the layers and hence low strength in the fiber. Therefore, there are two main grades of carbon fiber, namely high-modulus fiber (with a relatively high degree of graphitization, as in the case of a fiber that involves both carbonization and graphitization in its fabrication process) and high-strength fiber (with a relatively low degree of graphitization, as in the case of a fiber that involves carbonization but no graphitization in its fabrication process).

A high degree of graphitization enhances the oxidation resistance of the fiber. The oxidation of carbon refers to the reaction of carbon with oxygen to form carbon monoxide or carbon dioxide gas, which vanishes. This reaction occurs only at an elevated temperature. As a result, carbon fiber cannot withstand a high temperature in the presence of oxygen, although it can withstand extremely high temperatures in the absence of oxygen. This oxidation problem also applies to the

matrix of a carbon-matrix composite. In general, the more crystalline the carbon, the higher the onset temperature for oxidation.

2.3 Nanofillers

Nanocomposites refer to composites with nanometer-scale structure. This structure can relate to the grain size, the filler size, the pore size, etc. A small pore size helps to improve the mechanical strength of a porous material. A small grain size is attractive since it leads to a high yield strength in metals and a high toughness in ceramics. A small filler size provides a large filler–matrix interface area per unit volume. The large area can be advantageous or disadvantageous, depending on the type of property. For example, it may result in a composite of low strength (in spite of the possibly high strength within a single unit of the nanofiller, e.g., within a single nanofiber) due to the mechanical weakness of the interface; it may also result in a composite of high electrical resistivity (in spite of the possibly low electrical resistivity within a single unit of the nanofiller, e.g., within a single nanofiber) due to the electrical resistance associated with the interface. On the other hand, the high interface area may be good for the performance of electrochemical electrodes due to the fact that the electrochemical reaction occurs at the interface between the electrode and the electrolyte, as in a battery; it may also be good for shielding from electromagnetic interference (abbreviated to "EMI") that occurs in the near-surface region of a conductive filler unit, due to the skin effect (the phenomenon in which high-frequency electromagnetic radiation penetrates only the near-surface region of an electrical conductor). Thus, nanocomposites are not necessarily superior to conventional composites.

A nanofiller refers to a filler in the nanometer size range (0.5–500 nm, typically 1–100 nm) along at least one of its dimensions. For example, a nanoplatelet is in the nanometer size range in the direction perpendicular to the plane of the platelet, but

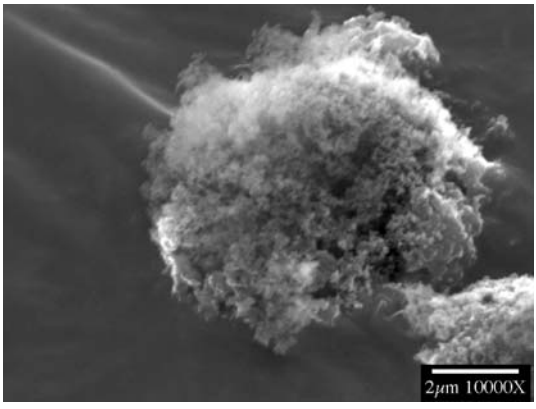

Figure 2.3. A scanning electron microscope photograph of fumed alumina, which takes the form of porous agglomerates of nanoparticles around 13 nm in size

is considerably larger in the plane of the platelet; a nanofiber is in the nanometer size range in its diameter, but is much larger along its length.

Nanofillers take the form of nanoparticles (e.g., carbon particles around 30 nm in size in carbon black, and alumina particles around 13 nm in size in fumed alumina, which is shown in Fig. 2.3), nanofibers (e.g., carbon nanofibers of diameter 150 nm, as shown in Fig. 2.4, with carbon layers oriented like a fishbone, as illustrated in Fig. 2.5), nanotubes (e.g., carbon nanotubes with one or more concentric carbon layers along the tube axis in the wall of the tube, which has a hollow channel at its center), nanoplatelets (e.g., graphite nanoplatelets, as shown in Fig. 2.6, and nanoclay), and other shapes. The porous agglomerate structure of carbon black and fumed alumina (Fig. 2.3) results in squishability (high compressibility), meaning that a small compressive force causes an agglomerate to become a sheet. Figure 2.7 shows carbon black before and after compression. The squishability enables it to conform to the topography of a surface or an interface, thus allowing the filler to be effective for interface or surface nanostructuring. Figure 2.8 illustrates interfacial microstructures corresponding to good and bad conformability of the interfacial filler. Conformability is also helped by the nanometer size of the carbon black particles, as the small particles can fill the small valleys in the surface

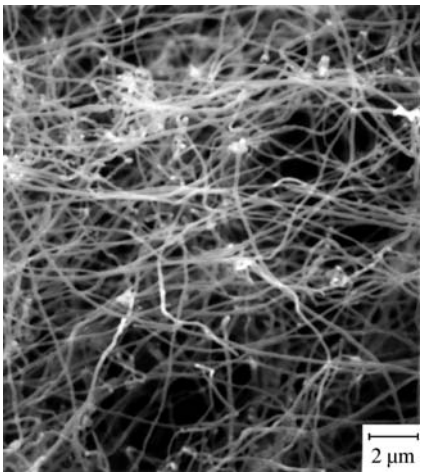

Figure 2.4. A scanning electron micrograph of carbon nanofibers with an intertwined morphology

Figure 2.5. Carbon nanofiber with the carbon layers oriented like a fishbone. The structure is like a stack of ice cream cones with the tip of each cone cut off, thus resulting in a hollow channel at the center

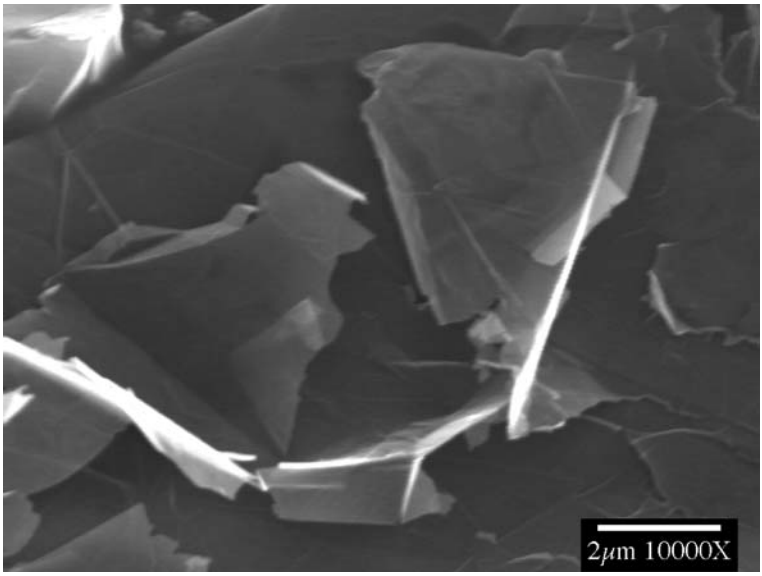

Figure 2.6. A scanning electron micrograph of graphite nanoplatelets

topography. However, conformability is dependent on not only the particle size but also the aggregate size. Each aggregate consists of a number of particles. Figure 2.9 illustrates three types of carbon black, as distinguished by the aggregate size. A small aggregate size tends to facilitate conformability.

Carbon nanotubes are classified according to the number of concentric cylindrical carbon layers within them. They can be single-walled, double-walled or multiwalled, corresponding to nanotubes with one, two and multiple carbon layers, respectively. Carbon nanotubes are also described in terms of their chirality, which relates to the crystallographic direction of the axis of the tube. This direction can be one of numerous directions in the plane of a flat carbon layer (Fig. 2.1b). The electrical behavior of a carbon nanotube depends strongly on the chirality; it may act as a metal or a semiconductor.

Nanofillers are all discontinuous. Although discontinuous carbon nanotubes can be connected (usually with the aid of a small amount of binder) to form a continuous yarn, the nanotubes in the yarn remain discontinuous. This discontinuity contributes to the limited effectiveness of carbon nanotubes when used as a reinforcement. In addition, the degree of alignment of carbon nanotubes is low compared to that of continuous carbon fibers. This poor alignment also contributes to the limited effectiveness of carbon nanotubes when used as a reinforcement. Due to the poor alignment, the maximum volume fraction of carbon nanotubes in a composite is much lower than that of continuous carbon fibers in a composite. For example, the maximum volume fraction of carbon nanotubes is around 10%, whereas that of continuous carbon fibers is around 60%. For these various reasons, it is difficult for carbon nanotubes to compete with continuous carbon fibers as load-bearing components in structural composites.

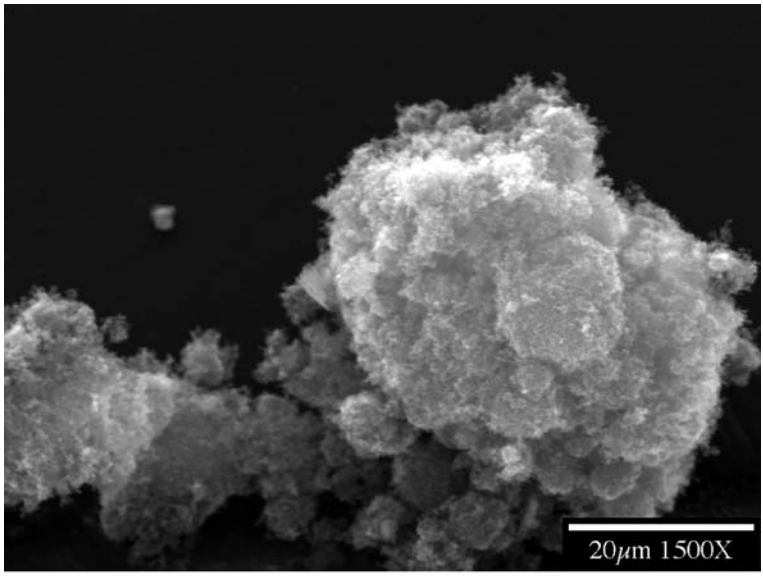

a

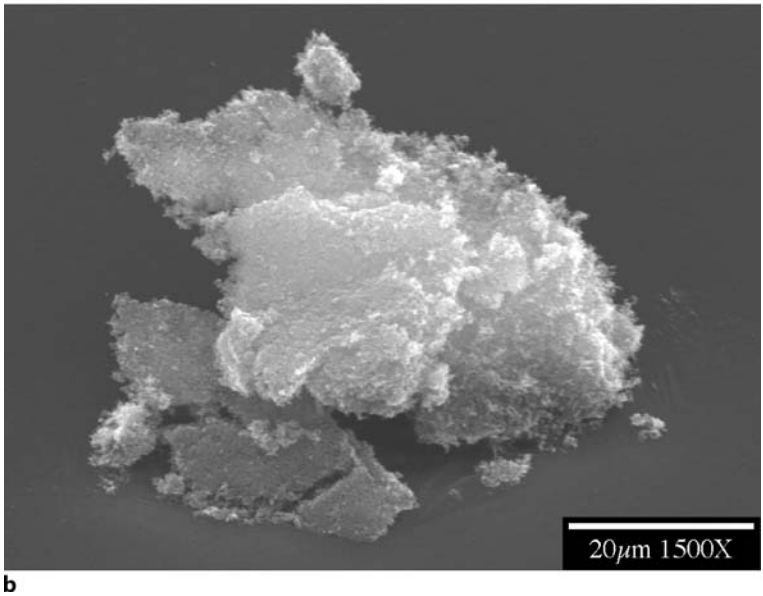

b

Figure 2.7. Carbon black in the form of a porous agglomerate of nanoparticles. **a** Before compression. **b** After compression

Carbon nanofibers commonly have an intertwined morphology (Fig. 2.4) akin to cotton wool. This means that the nanofibers tend to clump together, making it difficult to disperse them. Figure 2.10 illustrates a nonuniform filler distribution due to clumping and a uniform filler distribution in the absence of clumping. A relatively high degree of mechanical agitation, as achieved in high-shear mixing, is typically needed during composite fabrication in order to alleviate the clumping problem.

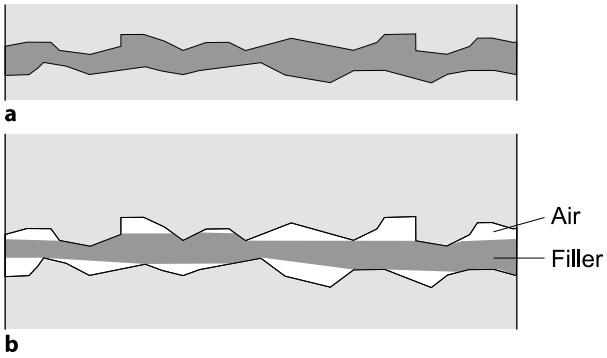

Figure 2.8. Interfacial microstructures for: **a** a conformable interfacial filler; **b** a nonconformable interfacial filler

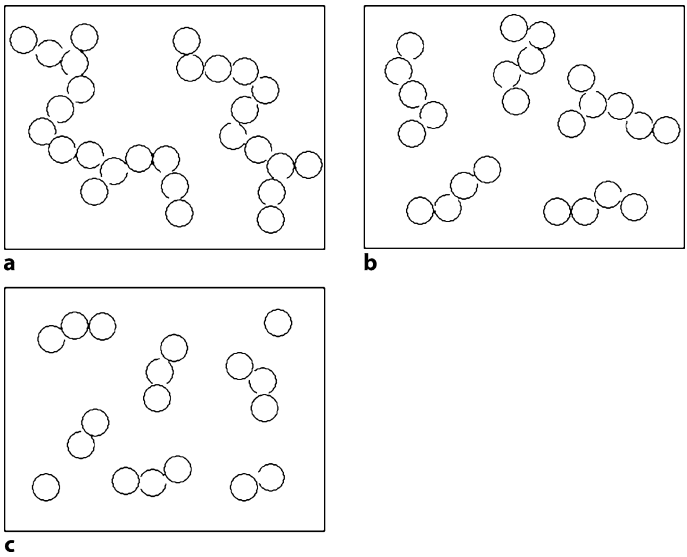

Figure 2.9. Schematic illustration of carbon black structures. **a** High structure (with a large aggregate size). **b** Medium structure (with a medium aggregate size). **c** Low structure (with a small aggregate size)

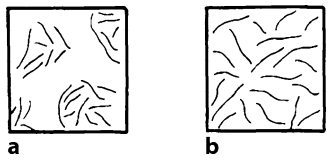

Figure 2.10. The distribution of discontinuous fibers in a composite. **a** Nonuniform distribution due to fiber clumping. **b** Uniform distribution in the absence of clumping

Due to the small thicknesses of composite interfaces, nanofillers are useful for interface modification. For example, silica fume (nanoparticles around 0.1 μm in size) added to a concrete mix aids bonding between the concrete and steel rebars,

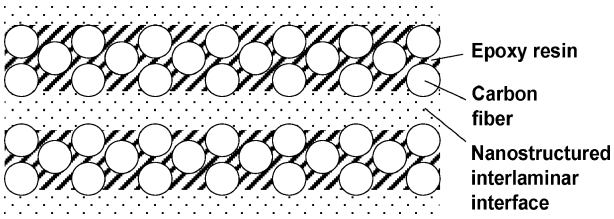

Figure 2.11. Schematic illustration of interlaminar interface nanostructuring

since the nanoparticles cause the pore structure in the concrete to be relatively fine, thereby reducing the porosity at the interface between the concrete and the steel rebars. In another example, the addition of carbon black (nanoparticles around 30 nm in size) to the interlaminar interface of a continuous carbon fiber polymer-matrix composite (Figs. 1.1 and 2.8) improves the through-thickness compressive modulus of the composite. Nanofillers are also useful for surface modification, such as the modification of the surface of a composite material for the purpose of increasing the wear resistance. Figure 2.11 illustrates both surface nanostructuring and interlaminar interface nanostructuring. In surface nanostructuring, the nanofiller is positioned on the surface rather than at the interlaminar interface.

Nanofillers are attractive for use as secondary fillers in composites that contain primary fillers (e.g., continuous carbon fibers) that serve as the load-bearing component in the composite. The secondary filler serves to enhance certain properties other than the load-bearing ability. For example, it may enhance the vibration damping capacity due to the large amount of nanofiller–matrix interface area per unit volume; the slight slippage at these interfaces during vibration causes mechanical energy dissipation. The nanofiller can be mixed with the matrix (e.g., the epoxy resin) prior to using the matrix in composite fabrication, though this approach suffers from increased viscosity of the resin (due to the presence of the nanofiller), which makes it more difficult for the resin to penetrate the small space between adjacent continuous fibers. Alternatively, the nanofiller is positioned at the interlaminar interface between the laminae of continuous fibers (Figs. 1.1 and 2.11).

Review Questions

1. Describe the crystallographic texture of a carbon fiber.
2. From the viewpoint of the chemical bonding, explain why graphite is a good lubricant.
3. From the viewpoint of chemical bonding, explain why diamond is mechanically very hard.
4. What are the three forms of carbon?
5. What is meant by turbostratic carbon?

6. Describe a process for making carbon fiber from pitch.
7. How is graphite nanoplatelet fabricated from graphite flakes?
8. Describe a method for nanostructuring the interlaminar interface of a continuous fiber polymer-matrix composite.
9. How is a carbon nanofiber fabricated?
10. What is the difference in structure between diamond and diamond-like carbon?
11. How is flexible graphite fabricated from graphite flakes?
12. Why is carbon black highly compressible?

Further Reading

D.D.L. Chung, "Flexible Graphite for Gasketing, Adsorption, Electromagnetic Interference Shielding, Vibration Damping, Electrochemical Applications, and Stress Sensing", *J. Mater. Eng. Perf.* 9(2), 161–163 (2000).

D.D.L. Chung, "Graphite Intercalation Compounds", *Encyclopedia of Materials: Science and Technology*, ed. by K.H.J. Buschow, R.W. Cahn, M.C. Flemings, B. Ilschner, E.J. Kramer and S. Mahajan, Elsevier, Oxford, 2001, vol. 4, pp. 3641–3645.

D.D.L. Chung, "Comparison of Submicron Diameter Carbon Filaments and Conventional Carbon Fibers as Fillers in Composite Materials", *Carbon* 39(8), 1119–1125 (2001).

D.D.L. Chung, "Applications of Submicron Diameter Carbon Filaments", Carbon Filaments and Nanotubes: Common Origins, Differing Applications? (Proc. NATO Advanced Study Institute, NATO Science Series, Series E: Applied Sciences, vol. 372), ed. by L.P. Biro, Kluwer, Dordrecht, 2001, pp. 275–288 (also in *Nanostructured Carbon for Advanced Applications*, ed. by G. Benedek et al., Kluwer, Dordrecht, 2001, pp. 331–345).

D.D.L. Chung, "Graphite", *J. Mater. Sci.* 37(8), 1475–1489 (2002).

D.D.L. Chung, "Cement-Matrix Structural Nanocomposites", *Met. Mater. Int.* 10(1), 55–67 (2004).

D.D.L. Chung, "Applications of Nanostructured Carbons in Polymer-Based Materials", *Annu. Tech. Conf. Soc. Plastics Eng.*, 2004, pp. 2314–2318.

C. Lin and D.D.L. Chung, "Effect of Carbon Black Structure on the Effectiveness of Carbon Black Thermal Interface Pastes" *Carbon* 45(15), 2922–2931 (2007).

C. Lin and D.D.L. Chung, "Nanostructured Fumed Metal Oxides for Thermal Interface Pastes", *J. Mater. Sci.* 42(22), 9245–9255 (2007).

C. Lin and D.D.L. Chung, "Nanoclay Paste as Thermal Interface Material for Smooth Surfaces", *J. Electron. Mater.* 37(11), 1698–1709 (2008).

X. Luo, R. Chugh, B.C. Biller, Y.M. Hoi and D.D.L Chung, "Electronic Applications of Flexible Graphite", *J. Electron. Mater.* 31(5), 535–544 (2002).

X. Shui and D.D.L. Chung, "Submicron Diameter Nickel Filaments and Their Polymer-Matrix Composites", *J. Mater. Sci.* 35, 1773–1785 (2000).

Y. Yamada and D.D.L. Chung, "Epoxy-Based Carbon Films with High Electrical Conductivity Attached to an Alumina Substrate", *Carbon* 46(13), 1798–1801 (2008).

3 Mechanical Properties

Composite materials are traditionally designed for use as structural materials; such structures include buildings, bridges, piers, highways, landfill cover, aircraft, automobiles (body, bumper, shaft, window, engine components, brake, etc.), bicycles, wheel chairs, ships, submarines, machinery, satellites, missiles, tennis rackets, fishing rods, skis, pressure vessels, cargo containers, furniture, pipelines, utility poles, armor, utensils, fasteners, etc. This chapter covers the science and applications of structural composites, with emphasis placed on the property requirements, durability, joining and repair.

3.1 Property Requirements

Structural applications are applications that require mechanical performance (e.g., strength, stiffness and vibration damping ability) in the material, which may or may not bear the load in the structure. If the material does bears the load, the mechanical property requirements are particularly stringent. An example is a building in which steel-reinforced concrete columns bear the load of the structure and unreinforced concrete architectural panels cover the face of the building. Both the columns and the panels serve structural purposes and are structural materials, though only the columns bear the load of the structure. Mechanical strength and stiffness are required of the panels, but the requirements are more stringent for the columns.

In addition to mechanical properties, a structural material may be required to have other properties, such as low density (i.e., be lightweight) for to save fuel in the case of aircraft and automobiles, to facilitate high speed in the case of race bicycles, and for easier handling in the case of wheelchairs and armor. Another property that is often required is corrosion resistance, which is desirable for the durability of all structures, particularly automobiles and bridges. Yet another property that may be required is the ability to withstand high temperatures and/or thermal cycling, as heat may be encountered by the structure during operation, maintenance or repair.

A relatively new trend is for a structural material to be able to serve functions other than the structural function, so that the material becomes multifunctional (i.e., killing two or more birds with one stone, thereby saving money and simplifying the design). An example of a nonstructural function is damage sensing. Such sensing, also called structural health monitoring, is valuable for the prevention of hazards. It is particularly important in aging aircraft and bridges. This

sensing function can be attained by embedding sensors (such as optical fibers, in which damage or strain affects the light throughput) in the structure. However, the embedding usually results in the degradation of the mechanical properties of the material, and embedded devices are costly and show poor durability compared to the structural material. Another way to attain the sensing function is to detect changes in a property (e.g., the electrical resistivity) of the structural material due to damage. In this way, the structural material serves as its own sensor and is said to be self-sensing.

Mechanical performance is fundamental to the selection of a structural material. Desirable properties are high strength, high modulus (stiffness), high ductility, high toughness (energy absorbed in fracture), and high capacity for vibration damping. Strength, modulus and ductility can be measured under tension, compression or flexure at various loading rates, as dictated by the type of loading on the structure. A high compressive strength does not imply a high tensile strength. Brittle materials tend to be stronger under compression than tension due to the microcracks in them. High modulus does not imply high strength, as the modulus describes the elastic deformation behavior whereas the strength describes the fracture behavior. Low toughness does not imply a low capacity for vibration damping, as the damping (energy dissipation) may be due to slipping at interfaces in the material, rather than being due to the shear of a viscoelastic phase in the material. Other desirable mechanical properties are fatigue resistance, creep resistance, wear resistance and scratch resistance.

Structural materials are predominantly metal-based, cement-based and polymer-based materials, although they also include carbon-based and ceramic-based materials, which are valuable for high-temperature structures. Among the metal-based structural materials, steel and aluminum alloys are dominant. Steel is advantageous due to its high strength, whereas aluminum is advantageous due to its low density. For high-temperature applications, intermetallic compounds (such as NiAl) have emerged, though they suffer from brittleness. Metal-matrix composites are superior to the corresponding metal matrix due to their high moduli, high creep resistances and low thermal expansion coefficients, but they are expensive due to their processing costs.

Among the cement-based structural materials, concrete is dominant. Although concrete is an old material, improvements in long-term durability are needed, as suggested by the degradation of bridges and highways all over the US. Such improvements include decreasing the drying shrinkage (shrinkage of the concrete during curing or hydration), as this shrinkage can cause cracks. It also includes decreasing the fluid permeability, as water permeating into steel-reinforced concrete can cause corrosion of the reinforcing steel. Moreover, it includes improving the freeze–thaw durability, which is the ability of the concrete to withstand temperature variations between temperatures below 0°C (freezing of water in concrete) and those above 0°C (thawing of water in concrete).

Among the polymer-based structural materials, fiber-reinforced polymers are dominant due to their combination of high strength and low density. All polymer-based materials suffer from an inability to withstand high temperatures. This inability may be due to the degradation of the polymer itself or, in the case of

a polymer-matrix composite, the thermal stress resulting from the thermal expansion mismatch between the polymer matrix and the fibers. (The coefficient of thermal expansion is typically much lower for the fibers than for the matrix.)

3.2 Basic Mechanical Properties

The basic mechanical properties are an important influence on the load-bearing ability and structural performance of the material. Load-bearing ability means that the material has adequately high values of strength, modulus and ductility under a loading condition that is relevant to the application. A particularly common loading condition for a composite panel or slab is bending (flexure). For example, when a wing of an aircraft is hit by a bird during flight, bending is involved; it is also involved when the floor of an aircraft is hit by a heavy falling object (such as a hammer) and when a car is traveling on a bridge (bending of the bridge deck). During flexure, one surface is under tension while the opposite surface is under compression, as illustrated in Fig. 3.1. For a concrete column, the important loading condition is compressive, with the stress occurring along the axis of the column, although flexural loading can also occur, as in the case of a car hitting the column. When mechanical properties are described without indicating the loading condition, they usually refer to the tensile case, with the exception of brittle materials (such as cement-matrix composites), for which the compressive case is dominant due to the fact that the compressive strength is much higher than the tensile strength for a brittle material.

3.2.1 Modulus of Elasticity

The modulus of elasticity describes the resistance to elastic deformation, which is reversible. One common mechanism of elastic deformation under tension is bond stretching. When the load is released, the dimension returns to its original value. The stress–strain curve is linear in the elastic regime. This linear relation constitutes Hooke's Law, which states that stress is proportional to strain, with the proportionality constant being the modulus. The modulus is given by the slope of the linear region; i.e., it is the stress per unit strain in the elastic regime, as illustrated in Fig. 3.2. To emphasize that it is obtained from the slope of the curve, this modulus is also called the tangent modulus. When dynamic strain around an operating point outside the elastic regime is relevant to a particular application,

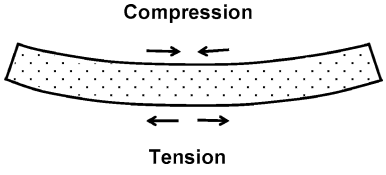

Figure 3.1. Tension and compression on the opposite sides of a beam under flexure

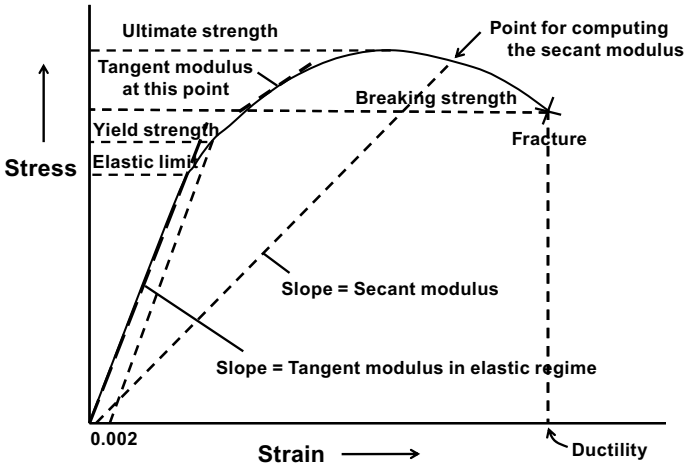

Figure 3.2. Stress–strain curve illustrating the meaning of the tangent modulus, the secant modulus, the elastic limit, the 0.2% offset yield strength, the ultimate strength, and the breaking strength

the relevant tangent modulus is obtained by finding the slope at the operating point, as shown in Fig. 3.2.

In uniaxial loading (whether tension or compression), the tangent modulus is known as the Young's modulus (E). In shear loading, the shear stress (τ) is proportional to the shear strain (γ), with the proportionality constant being the shear modulus (G). The shear stress (τ) is defined as the force divided by the area of the plane on which the force acts. In contrast, the tensile stress is defined as the force divided by the area perpendicular to the stress. The shear strain (γ) is defined as $\tan\alpha$, where α is the shear angle. In contrast, the uniaxial strain is defined as the fractional change in dimension in the stress direction; it is positive for elongation and negative for shrinkage.

The shear modulus is related to the Young's modulus by the equation

$$G = E/[2(1+\upsilon)]\ , \tag{3.1}$$

where υ is the Poisson ratio, which is defined as

$$\upsilon = -(\text{transverse strain})/(\text{axial strain})\ . \tag{3.2}$$

The value of υ typically ranges from 0.2 to 0.5. It is 0.5 if there is no volume change at all. However, due to an increase in volume during uniaxial tension, its value is less than 0.5.

A quantity that is scientifically less meaningful than the tangent modulus is the secant modulus, which is the slope of the line from any particular point on the stress–strain curve to the origin, as illustrated in Fig. 3.2. In other words, the secant modulus at a particular stress or strain is simply given by the stress divided by the strain at that point. The secant modulus can be calculated at any point during mechanical testing, as the stress and strain are con-

tinuously measured during testing. Thus, it is possible to monitor how the secant modulus varies during cycling loading (as in fatigue testing) in real time. Damage tends to cause the secant modulus to decrease. On the other hand, it is difficult to monitor the tangent modulus in real time during such testing since the tangent modulus depends on the curve rather than a particular point on the curve. Unless noted otherwise, the modulus refers to the tangent modulus.

The Young's modulus of a composite material can be calculated from those of the components in the composite. Consider the case where the reinforcement is provided by continuous fibers that are aligned with the applied tensile stress in the fiber direction of the composite, as illustrated in Fig. 3.3. Assume that the fiber–matrix bonding is so strong that there is no slippage at all at the interface during loading. Consider the strain in the stress direction. Due to the strong bond, the strain in the matrix (ε_m) equals that in the fiber (ε_f) and equals that in the composite (ε_c); a situation known as "isostrain." Hence,

$$\varepsilon_c = \sigma_c/E_c = \varepsilon_m = \sigma_m/E_m = \varepsilon_f = \sigma_f/E_f \,, \tag{3.3}$$

where E_c, E_m and E_f are the Young's moduli of the composite, matrix and fiber, respectively, and σ_c, σ_m and σ_f are the stresses experienced by the composite, matrix and fiber, respectively.

Let the load applied to the composite be F_c. This load is shared by the fiber and the matrix according to the fraction of the cross-sectional area (area perpendicular to the stress direction) occupied by these components. Hence,

$$F_c = F_m + F_f \,, \tag{3.4}$$

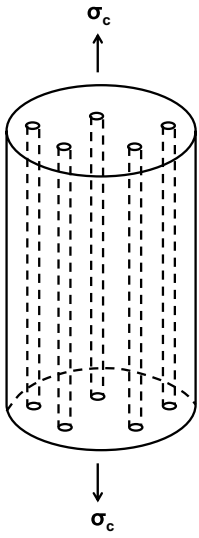

Figure 3.3. Model for calculating the Young's modulus of a composite with continuous fibers oriented in the stress direction

with

$$F_c = \sigma_c A_c \,, \tag{3.5}$$
$$F_m = \sigma_m A_m \,, \tag{3.6}$$

and

$$F_f = \sigma_f A_f \,, \tag{3.7}$$

where A_c, A_m and A_f are the cross-sectional areas of the composite, matrix and fiber (all the fibers together), respectively, such that

$$A_c = A_m + A_f \,. \tag{3.8}$$

Thus, from Eq. 3.4,

$$\sigma_c A_c = \sigma_m A_m + \sigma_f A_f \,. \tag{3.9}$$

However,

$$\sigma_c = E_c \varepsilon_c \,, \tag{3.10}$$
$$\sigma_m = E_m \varepsilon_m \,, \tag{3.11}$$

and

$$\sigma_f = E_f \varepsilon_f \,. \tag{3.12}$$

Thus, Eq. 3.9 becomes

$$E_c \varepsilon_c A_c = E_m \varepsilon_m A_m + E_f \varepsilon_f A_f \,. \tag{3.13}$$

Due to the isostrain situation, the three strains are equal and can be canceled. Hence,

$$E_c A_c = E_m A_m + E_f A_f \,. \tag{3.14}$$

Dividing by A_c gives

$$\begin{aligned} E_c &= E_m (A_m/A_c) + E_f (A_f/A_c) \\ &= E_m v_m + E_f v_f \,, \end{aligned} \tag{3.15}$$

where v_m and v_f are the volume fractions of the matrix and fiber (all the fibers together), respectively. Equation 3.15 implies that the modulus of the composite is the weighted average of the moduli of the matrix and fiber, such that the weighting factors are the volume fractions of the matrix and fiber. It also indicates that the composite modulus is linearly related to the fiber volume fraction, as illustrated in Fig. 3.4. Note that

$$v_m = 1 - v_f \,. \tag{3.16}$$

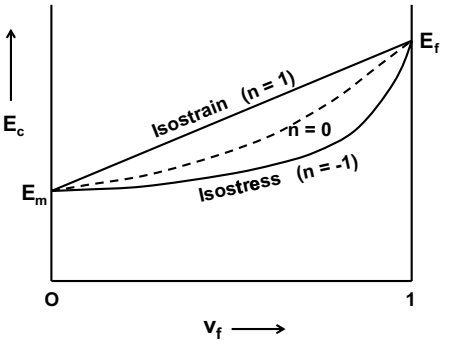

Figure 3.4. Dependence of the Young's modulus (E_c) of a composite on the fiber volume fraction (v_f). The isotrain situation corresponds to Fig. 3.3. The isostress situation corresponds to Fig. 3.5

When $v_f = 0$, $E_c = E_m$; when $v_f = 1$, $E_c = E_f$. This equation is a manifestation of the rule of mixtures (ROM).

The fraction of the load carried by the fiber (all the fibers together) is given by

$$F_f/F_c = (\sigma_f A_f)/(\sigma_c A_c) = (E_f \varepsilon_f A_f)/(E_c \varepsilon_c A_c) = (E_f A_f)/(E_c A_c) = (E_f/E_c)v_f \, . \quad (3.17)$$

This means that the fraction of the load carried by the fiber (all the fibers together) increases with the fiber volume fraction and, for a given fiber volume fraction, it is higher when the modulus of the fiber is larger than that of the composite. Therefore, a high-modulus fiber is a more effective reinforcement than a low-modulus fiber.

Next, consider loading perpendicular to the aligned fibers. For the sake of geometric simplicity, consider that each fiber takes the form of a strip that extends all the way through the thickness of the composite, as illustrated in Fig. 3.5. Thus, the cross-sectional area perpendicular to the stress is the same for the composite, matrix, and each fiber. Hence,

$$\sigma_c = \sigma_m = \sigma_f \, . \quad (3.18)$$

This situation is known as isostress. The elongation in the stress direction is ΔL_c for the composite; the original length is L_c in the stress direction. The elongation

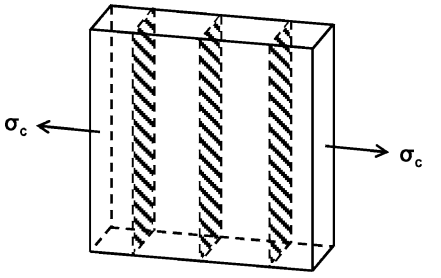

Figure 3.5. Model for calculating the Young's modulus of a composite with continuous fibers (*shaded regions*) oriented in the direction perpendicular to the stress (σ_c)

in the stress direction is ΔL_m for the matrix (all parts of the matrix together); the original length is L_m in the stress direction. The elongation in the stress direction is ΔL_f for the fiber (all fibers together); the original length is L_f in the stress direction. Hence,

$$\Delta L_c = \Delta L_m + \Delta L_f \, . \tag{3.19}$$

Dividing by L_c gives

$$(\Delta L_c/L_c) = (\Delta L_m/L_c) + (\Delta L_f/L_c) \, . \tag{3.20}$$

However,

$$L_m = \nu_m L_c \tag{3.21}$$

and

$$L_f = \nu_f L_c \, , \tag{3.22}$$

where ν_m and ν_f are the volume fractions of the matrix and fiber (all fibers together), respectively. Thus, Eq. 3.20 becomes

$$(\Delta L_c/L_c) = (\nu_m \Delta L_m/L_m) + (\nu_f \Delta L_f/L_f) \, , \tag{3.23}$$

or

$$\varepsilon_c = \nu_m \varepsilon_m + \nu_f \varepsilon_f \, , \tag{3.24}$$

or

$$(\sigma_c/E_c) = \nu_m(\sigma_m/E_m) + \nu_f(\sigma_f/E_f) \, . \tag{3.25}$$

Due to the isostress situation, the stresses are equal and can be canceled. Thus,

$$\begin{aligned} (1/E_c) =& (\nu_m/E_m) + (\nu_f/E_f) \\ =& (\nu_m E_f + \nu_f E_m)/(E_m E_f) \, . \end{aligned} \tag{3.26}$$

Rearranging gives

$$E_c = (E_m E_f)/(\nu_m E_f + \nu_f E_m) \, . \tag{3.27}$$

Equation 3.27 means that the reciprocal of the composite modulus is the weighted average of the reciprocal of the matrix modulus and the reciprocal of the fiber modulus, such that the weighting factors are the volume fractions of the matrix and fiber (all the fibers together). This is a manifestation of the rule of mixtures for the isostress case. Note that, in this case, the composite modulus is not linearly related to the fiber volume fraction, as illustrated in Fig. 3.4.

The equations for the isostrain and isostress cases can be combined into

$$E_c^n = \nu_m E_m^n + \nu_f E_f^n \, , \tag{3.28}$$

where $n = 1$ for the isostrain case and $n = -1$ for the isostress case. For a general case that is between the isostrain and isostress extremes, n can take on various values between -1 and 1, as illustrated in Fig. 3.4.

Table 3.1 shows the Young's moduli and densities of various materials, including polymers, metals, carbons and ceramics. Polymers tend to have low moduli and densities. Metals have higher moduli and densities than polymers. Ceramics and carbons tend to have even higher moduli than metals and their densities tend to be between those of metals and polymers. A high ratio of the modulus to density (also known as the specific modulus) is valuable for lightweight structures. This ratio tends to be high for ceramics and carbons, lower for metals, and even lower for polymers. Due to their high modulus and specific modulus (the ratio of the modulus to the density) values, ceramics and carbons are typically more attractive than polymers and metals for use as reinforcements in composite materials.

The modulus can vary substantially among polymers. In particular, low-density polyethylene (LDPE) has a much lower modulus than high-density polyethylene (HDPE). This is because of the greater degree of branching of the molecules in LPDE and thus the weaker intermolecular forces in LDPE.

Table 3.1. Young's moduli, densities and ratios of modulus to density for various materials under tension (unless stated otherwise)

Material	Young's modulus (GPa)	Density (g/cm^3)	Ratio of modulus to density ($GPa\,cm^3/g$)
Rubber[a] (small strain)	0.01–0.1	0.94–0.98	0.05
Low-density polyethylene[a] (LDPE)	0.2	0.925	0.2
High-density polyethylene[a] (HDPE)	1.379	0.959	1.44
Nylon[a]	2–4	1.14	3
Aluminum alloy[b]	69	2.8	25
Copper[b]	110–130	8.89	13
Steel[b]	190–210	7.85	25
Tungsten[b]	400–410	19.3	21
Carbon fiber (high strength)[c]	231	1.76	130
Carbon fiber (high modulus)[c]	640	2.17	290
Single carbon nanotube[c]	1,000+	1.34	700+
Diamond[c]	1,220	3.51	350
High-strength concrete (under compression)[d]	30–100	2.4	30
E-glass fiber[d]	72.4	2.55	28
S-glass fiber[d]	86.9	2.50	35
Silicon carbide[d]	450	3.3	140
Tungsten carbide[d]	450–650	15.8	35
Yttrium iron garnet[d] (abbreviated YIG, $Y_3Fe_5O_{12}$)	2,000	5.17	390

[a] Polymer; [b] metal; [c] carbon; [d] ceramic

The modulus varies significantly among metals, such that the higher the melting temperature, the higher the modulus tends to be. The melting point as well as the modulus increase in the order: aluminum, copper, steel and tungsten. The correlation between the modulus and the melting temperature occurs because both are governed by the bond strength.

Among the ceramics, concrete has a relatively low modulus due to the incomplete connectivity of the silicate tetrahedra (SiO_4 tetrahedra). The modulus of glass fibers is also relatively low. On the other hand, the moduli of SiC, WC and YIG are very high due to the strong ionic and/or covalent bonding present, which is stronger than the metallic bonding present in metals.

Carbon in the form of a single carbon nanotube (along the nanotube axis) and diamond has a very high modulus due to the high bond strength associated with the covalent bonding between carbon atoms. Carbon fibers are in the graphite family, though they are not ideal graphite in terms of their crystal structure (Fig. 2.1). A carbon fiber has carbon layers that are preferentially oriented along the fiber axis, though each layer does not tend to be flat and limited in size (Fig. 2.2). Between the carbon layers, the bonding is weak (van der Waals forces). As a consequence of the weak interlayer bonding present, graphite and carbon fibers have lower moduli than diamond, which has a crystal structure that consists of a three-dimensional network of strong covalent bonds. For the same reason, carbon fibers have lower moduli than a single carbon nanotube along the tube axis. In spite of the high modulus of a single carbon nanotube, composite materials containing carbon nanotubes exhibit rather low moduli. This is due to the large nanotube–matrix interface area per unit volume of the composite and the weakness of the interface. Diamond, on the other hand, is too expensive for practical use as a filler in composites. Therefore, carbon fibers remain highly attractive fillers.

Carbon fibers can be classified into high-strength (HS) carbon fibers and high-modulus (HM) carbon fibers. A high-modulus carbon fiber has a relatively high degree of orientation of the carbon layers along the fiber axis (i.e., a relatively strong crystallographic texture). However, due to the strong texture in a high-modulus carbon fiber, shear is easy between the carbon layers, resulting in a low ultimate strength. On the other hand, a high-strength carbon fiber has a relatively high ultimate strength due to the low texture and thus the greater shear hindrance. Again, due to its strong texture, a high-modulus carbon fiber has a higher electrical conductivity along the fiber axis than a high-strength carbon fiber. A high-modulus carbon fiber can be obtained by graphitizing a carbon fiber that has gone through the carbonization step, which converts a polymer fiber to a carbon fiber. In contrast, a high-strength carbon fiber is not subjected to the graphitization step after the carbonization step. Thus, a high-modulus carbon tends to be more crystalline than a high-strength carbon fiber. Due to its higher crystallinity, a high-modulus carbon fiber is more resistant to oxidation than a high-strength carbon fiber.

Both high-strength carbon fibers and high-modulus carbon fibers have modulus values that are above those of most metals (e.g., steel, copper and aluminum) and glass fibers, as shown in Table 3.1. Carbon fibers are even more attractive when the ratio of modulus to density is considered (Table 3.1).

3.2.2 Strength

There are a number of strength parameters. The highest stress in a stress–strain curve up to failure is the ultimate strength, which is called the tensile strength in the case of tensile loading. The stress at fracture (failure) is called the breaking strength, which can be lower than the ultimate strength (Fig. 3.2) due to the occurrence of necking during plastic deformation prior to failure. The elastic limit is the stress at which the stress–strain curve starts to deviate from linearity, although this point on the curve cannot be clearly identified in most cases. The stress above which plastic deformation occurs is called the yield strength. A construction is conventionally used to help identify the yield strength. In this construction, a straight line that is parallel to the initial straight line portion of the stress–strain curve and that intersects with the strain axis at 0.002 (or 0.2%) is drawn (Fig. 3.2). The intersection of this straight line with the stress–strain curve defines the yield strength. Upon unloading from the stress equal to this yield strength, a strain of 0.002 is obtained when the stress has returned to zero. Therefore, this yield strength is called the 0.2% offset yield strength. The value of 0.2% is chosen because this value, when applied to metals, usually gives a yield strength value that is close to the minimum stress required for plastic deformation. The yield strength is important for engineering design, as most engineering components are only designed to operate in the elastic regime so that there is no permanent change in dimensions during the use of the component. Plastic deformation may involve not only a permanent change in dimensions but also a change in the microstructure (such as the dislocation density), which affects the strength, modulus and ductility of the material. The ultimate strength is also useful, as it relates to the highest stress that a material can withstand without breaking. When the term "strength" is used without qualification, it usually refers to the ultimate strength.

Table 3.2 gives values of yield strength, ultimate strength and density for various materials, including polymers, metals, carbons and ceramics. The density tends to be the lowest for polymers, the highest for metals, and intermediate for ceramics. Yielding does not tend to occur for ceramics due to their brittleness. The yield strength tends to be lower for polymers than metals. The ultimate strength varies greatly among materials in the same class due to the high sensitivity of the ultimate strength to the microstructure, such as imperfections, molecular length, molecular orientation, degree of crystallinity (i.e., fraction that is crystalline), and crystallographic texture (i.e., preferred orientation of a certain crystallographic plane).

Polyethylene (PE) is a thermoplastic polymer with the mer shown in Fig. 3.6. Because it has no polar chemical groups (such as esters, amides and hydroxyl groups), PE does not absorb water and is chemically and ultraviolet (UV) resistant. Ultrahigh molecular weight polyethylene (UHMWPE), also called high-modulus polyethylene (HMPE) and high-performance polyethylene (HPPE), exhibits a higher ultimate strength than HDPE due to the long molecules associated with its high molecular weight (more than 100,000 mers in a molecule, giving it a molecular weight of 3–6 million amu). Because of its long molecule length, UHMWPE is exceptionally tough and exhibits high impact strength and abra-

Table 3.2. Yield strengths, ultimate strengths, densities and ratios of the ultimate strength to the density for various materials

Material	Yield strength (MPa)	Ultimate strength (MPa)	Density (g/cm^3)	Ratio of ultimate strength to density (MPa cm^3/g)
HDPE[a]	26–33	37	0.94	39
UHMWPE[a]	23	46	0.97	47
UHMWPE fiber[a]	–	2,300–3,500	0.97	2,400–3,600
Polyvinyl chloride[a]	41–45	41–52	1.30–1.58	32
Nylon 6,6 fiber[a]	55–83	95	1.14	83
Kevlar 49 fiber[a]	–	3,600–4,100	1.44	2,700
Aluminum alloy[b] (2014-T6)	400	455	2.7	170
Copper[b], 99.99% Cu	70	220	8.92	25
Brass[b]	≈ 200+	550	5.3	100
Stainless steel[b], AISI 302, cold rolled	520	860	8.00	110
Steel[b], highstrength alloy, ASTM A514	690	760	7.8	97
Steel[b], prestressing strands	1,650	1,860	7.8	240
Tungsten[b]	760	960	19.25	50
Carbon fiber (high strength)[c]	N/A	5,700	1.50	3,800
Carbon fiber (high modulus)[c]	N/A	1,900	1.50	1,300
Single carbon nanotube[c]	N/A	62,000	1.34	46,000
Concrete[d]	N/A	3	2.4	1.3
Bone (limb)[d]	104–121	130	1.6	81
Glass[d]	–	50 (compression)	2.53	20
E-glass fiber[d]	N/A	3,450	2.57	1,340
S-glass fiber[d]	N/A	4,710	2.48	1,900
Silicon carbide fiber[d]	N/A	3,440	3.3	1,040

[a] Polymer; [b] metal;[c] carbon; [d] ceramic
Strengths were obtained under tension unless noted otherwise. N/A, not applicable due to the absence of yielding

sion resistance. However, the long kinked (bent) molecules cannot be packed very densely, so the density of UHMWPE is slightly lower than that of HDPE. UHMWPE has a low coefficient of friction and is self-lubricating. UHMWPE is a biomaterial that is used for total joint replacement (e.g., hip, knee and spine implants). In fiber form, UHMWPE exhibits an even higher strength due to the strong alignment of the molecules along the fiber axis (with 95% of the molecules oriented and consequently a high degree of crystallinity). UHMWPE fiber (produced under the

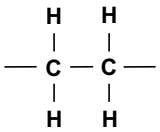

Figure 3.6. The mer of polyethylene (PE)

trade names of Spectra and Dyneema) is used for ballistic vests, ballistic helmets, ballistic vehicle protection, bow strings, climbing equipment, fishing line, high-performance sails, suspension lines on sport parachutes, and rigging on yachts.

Polyvinyl chloride (PVC) is a thermoplastic polymer with the mer shown in Fig. 3.7. It exhibits higher yield strength and ultimate strength than HDPE due to the polar nature (slightly ionic character) of the C–Cl bond (with the Cl end being slightly negative) in PVC, and the resulting strong intermolecular forces in the form of hydrogen bonding, as illustrated in Fig. 3.7. PVC is also inexpensive. It is used as a construction material instead of wood and concrete in some areas. Applications include water and sewage pipes, vinyl siding and flooring.

Nylon (a trade name belonging to DuPont) of the type known as nylon 6,6 (this nomenclature is due to the two monomers that react by condensation polymerization to form a mer with a total of 12 carbon atoms) is a polyamide, meaning that it has the H–N–C=O functional group. Due to the polar nature of the N–H bond (with the hydrogen end of the bond being slightly positive) and C=O bond (with the oxygen end of the bond being slightly negative), there is substantial intermolecular attraction in the form of hydrogen bonding between the hydrogen end of the N–H bond and the oxygen end of the C=O bond (Fig. 3.8), resulting in a yield strength and an ultimate strength that exceed those of UHMWPE. Nylon fibers are used for fabrics, carpets and rope. Solid nylon is used for mechanical parts such as gears that do not experience high stress.

Kevlar (a trade name belonging to DuPont) is an aramid (short for "aromatic polyamide"). Its mer comprises two aromatic rings with amide linkages (that enable intermolecular interactions) attached directly to the rings, which give the

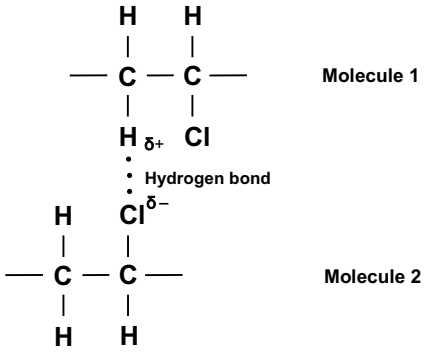

Figure 3.7. The mer of polyvinyl chloride (PVC)

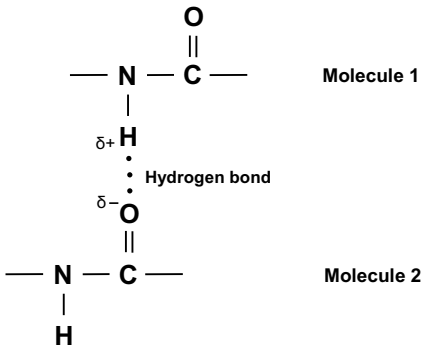

Figure 3.8. The hydrogen bonding between two molecules of a polyamide

molecule a planar covalent structure. This structure causes the ultimate strength of Kevlar to be even higher than that of nylon 6,6. Kevlar is used as a reinforcement in tire rubber, brake linings, body armor, boat hulls, airplanes and bicycles.

Metals tend to have higher yield strengths and higher ultimate strengths than polymers, though there are exceptions, as shown by the high ultimate strengths of UHMWPE fiber and Kevlar fiber. The yield strength and ultimate strength depend much on the microstructure, particularly the imperfections in it. In the case of metals, imperfections in the form of solutes, dislocations and grain boundaries strongly affect these strengths. Therefore, different alloys and different heat treatments of a particular alloy give very different strengths. This is in contrasts with the modulus (Table 3.1), which depends mainly on the bond strength rather than the imperfections.

Due to their brittleness, ceramics do not tend to exhibit yielding. The ultimate strength of a ceramic largely depends on defects such as pores and microcracks. Due to its porosity, concrete has a low ultimate strength. Due to the microcracks that tend to exist in brittle materials, glass in bulk (nonfibrous) form exhibits a low ultimate strength. However, glass fibers are much stronger, since the small diameter of a fiber greatly reduces the chance a microcrack occurring. Microcracks propagate under tension, thus causing a reduction in the tensile strength. E-glass, which was originally intended for electronic applications (hence the "E"), is aluminoborosilicate glass that is alkali-free (less than 2%). S-glass has a high tensile strength (hence the "S").

The ultimate strengths of glass, carbon and silicon carbide fibers are comparable. Glass fibers have a higher density than carbon fibers, and silicon carbide fibers have an even higher density than glass fibers. As a consequence, the ratio of the ultimate strength to the density is lower for glass fibers than for carbon fibers, and is even lower for silicon carbide fibers.

In spite of the high ultimate strength within a single carbon nanotube, composite materials containing carbon nanotubes exhibit low strength. This is due to the large nanotube–matrix interface area per unit volume of the composite, the weakness of the interface, and the high sensitivity of the strength to imperfections.

The ratio of the ultimate strength to the density – also known as the specific strength – is relevant to lightweight structures, as both a high strength and a low density are needed. Table 3.2 shows that this ratio is particularly high for the UHMWPE, Kevlar and carbon fibers. Metals, concrete, bone, glass fibers and silicon carbide fiber have relatively low values of this ratio.

3.2.3 Ductility

The ductility refers to the maximum strain in the stress–strain curve (Fig. 3.2). A brittle material undergoes little or no plastic deformation before failure, whereas a ductile material undergoes considerable plastic deformation before failure. Hence, for a highly brittle material, failure occurs at the end of the elastic regime, with no plastic deformation prior to failure. This also means that, for a brittle material, damage can occur within the elastic regime. Thus, the use of a brittle material should be limited to the low-stress portion of the elastic regime.

Table 3.3 shows the ductilities of representative materials. Carbon fibers are less ductile (more brittle) than polymer or glass fibers. High-modulus carbon fiber is even less ductile than high-strength carbon fiber. Ductility facilitates processing, such as fiber weaving.

Table 3.3. Ductilities of selected materials

Material	Ductility (%)
Polyethylene	2.2
Kevlar	3.8
Carbon fiber (high strength)	2.0
Carbon fiber (high modulus)	0.36
E-glass fiber	4.7
S-glass fiber	5.2

3.3 Effect of Damage on the Mechanical Properties

Figure 3.9 shows the compressive stress–strain curve up to failure for cement reinforced with discontinuous carbon fiber. Curve (a) is that observed before any loading, i.e., in the virgin state. Curve (b) is the state after some loading and subsequent unloading, i.e., a state of minor damage. Both the stress and strain are negative because, by convention, compressive stress is negative (while tensile stress is positive) and strain that involves shrinkage is negative (while strain that involves elongation is positive). A comparison of curves (a) and (b) shows that damage causes the slope of the curve (i.e., the modulus) to decrease and the maximum stress magnitude (i.e., the strength) to decrease. The decreased modulus is known as the residual modulus; the decreased strength is known as the residual strength.

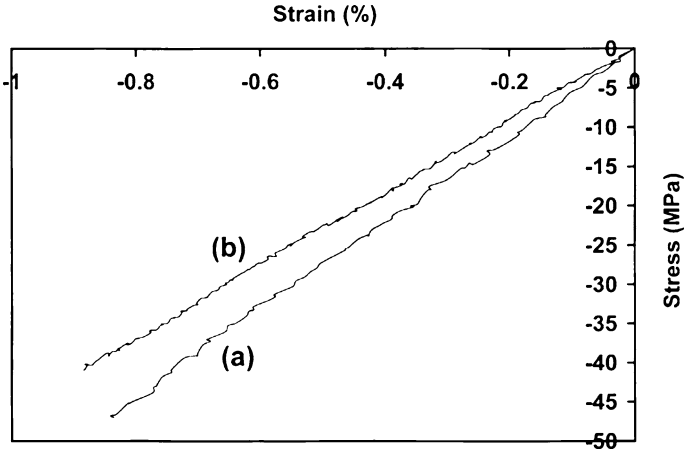

Figure 3.9. Compressive stress–strain curve of cement paste reinforced with discontinuous carbon fiber. **a** Before loading (without damage). **b** After loading and unloading (with minor damage). (From [1])

3.4 Brittle vs. Ductile Materials

A brittle material tends to have microcracks that propagate under tension in the direction perpendicular to the plane of the crack. Under compression in this direction, the crack just closes to a certain degree. As a result, a brittle material breaks much more easily under tension than under compression, so that the tensile strength is lower than the compressive strength and the tensile ductility is lower than the compressive ductility (Fig. 3.10). On the other hand, the compressive and tensile moduli can be comparable, as elastic deformation does not involve crack propagation.

Because of its low tensile strength, a brittle material is preferably used under compression rather than tension, and the part of a brittle material that is expected to encounter a tensile stress needs to be reinforced. This is why the reinforcement of concrete (a brittle material) with embedded steel rebars is widely used, with the rebars positioned at the part of the concrete component that encounters tensile stress. For example, a concrete beam under flexure is reinforced with steel rebars, particularly in the half of the beam that encounters tension (i.e., the lower half of the beam in Fig. 3.1).

3.5 Strengthening

Conventional strengthening methods, such as the use of alloying (e.g., the formation of a solid solution), tend to increase the strength and modulus but decrease the ductility. Thus, a material of high strength and modulus tends to be brittle. However, strengthening through the use of a filler can result in increases in strength, modulus and ductility (all at the same time) when the filler is a fiber that is well bonded to the matrix and when the matrix is brittle. When the matrix is ductile,

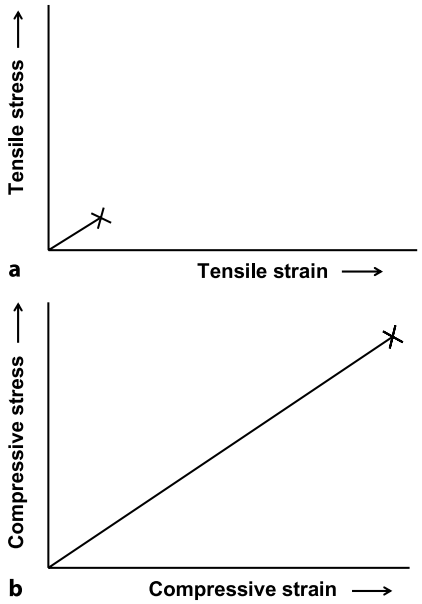

Figure 3.10. Stress–strain curves of a brittle material: **a** under tension; **b** under compression

as is the case for a polymer matrix, filler addition tends to decrease the ductility. However, when the matrix is brittle, as is the case for a cement, carbon or ceramic matrix, filler addition tends to increase the ductility because of the mechanism of fiber pull-out (Fig. 1.13). The increase in modulus due to the use of a filler occurs whenever the filler has a higher modulus than the matrix and the bonding between the filler and the matrix is not too weak. The increase in strength due to the use of a filler requires that the bonding between the filler and the matrix is sufficiently strong, as a weak interface will act as a crack initiation site. Thus, it is much easier to use a filler to increase the modulus than to increase the strength. When the interface is weak, the modulus may increase with increasing filler content, while the strength may decrease with increasing filler content. This is why interface tailoring is critical to composite engineering. When the filler has nanoscale dimensions, the interface area is large and interface tailoring becomes even more important.

Table 3.4 shows that surface treatment of discontinuous carbon fiber using ozone causes increases in the tensile strength, modulus and ductility of the carbon fiber

Table 3.4. Effect of ozone surface treatment of discontinuous carbon fiber (0.51 vol%) on the tensile properties of cement paste (containing silica fume and methylcellulose to aid fiber dispersion) after 28 days of curing (from [2])

	Without treatment	With treatment
Strength (MPa)	1.97 (±5.1%)	2.23 (±2.7%)
Modulus (GPa)	13.8 (±2.6%)	18.2 (±2.1%)
Ductility (%)	0.0167 (±2.6%)	0.0211 (±2.1%)

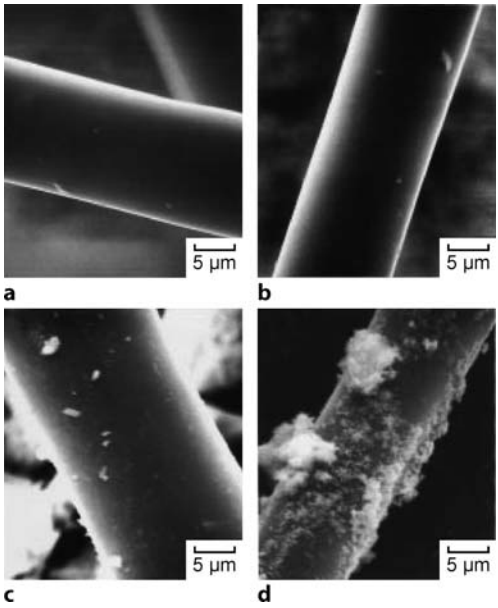

Figure 3.11. Scanning electron micrograph of a single carbon fiber. **a** As-received fiber without prior embedding in cement. **b** Ozone-treated fiber without prior embedding in cement. **c** As-received fiber after pulling out from cement. **d** Ozone-treated fiber after pulling out from cement. (From [2])

cement-matrix composite due to the stronger bonding between the fiber and the matrix. Figure 3.11 shows the surface of a carbon fiber after it has been pulled out of the cement matrix in comparison to the surface of a fiber that has not been embedded in cement at all. The fiber pulled out of the cement matrix has some cement that is adhered to its surface, so it does not look as clean as the fiber that has never been embedded in cement. More important is the comparison between a pulled-out fiber treated with ozone and one that has not been treated. There is more adhered cement on the treated fiber, indicating greater fiber–matrix bonding for the treated fiber.

The mechanical properties of carbon–carbon composites are much better than those of conventional graphite. Three-dimensional carbon–carbon composites are particularly attractive. Their preform structures can be tailored in three directions. The three-dimensional integrated preform structure results in superior damage tolerance and minimum delamination crack growth under interlaminar shearing compared with two-dimensional laminate carbon–carbon composites. Unlike conventional materials, cracks in three-dimensional carbon–carbon composites diffuse in a tortuous manner, probably tracking pre-existing voids or microcracks. Three-dimensional composite failure involves a series of stable crack propagation steps across the matrix and yarn bundles, followed by unstable crack propagation. The dominant damage mechanisms are bundle breakage and matrix cracking.

The tensile and flexural properties of carbon–carbon composites are fiber-dominated, whereas the compression behavior is mainly affected by the density

and matrix morphology. Tensile moduli are sometimes higher than the values calculated based on the fiber content because of the contribution from the sheath matrix morphology (stress graphitization of the matrix). Tensile strength levels are lower than the calculated values due to the residual stresses resulting from thermal processing. A high glass-like carbon fraction in the matrix is associated with enhanced strength and modulus, both in tension and compression.

After carbonization, residual stress remains at the interface between the fibers and the matrix. This is because, during carbonization, fiber–matrix interactions cause the basal crystallite planes to be aligned parallel to the fiber axis. The resulting Poisson effect elongates the fibers along the fiber axis and compresses them in the radial direction. This effect is indicated during carbonization by the transverse shrinkage and the longitudinal expansion of the composite. Its transverse shrinkage is larger than the shrinkage of the resin alone (which is the matrix material), while its longitudinal expansion is larger than the expansion of the fibers alone. This residual stress can cause warpage.

3.6 Vibration Damping Ability

3.6.1 Introduction

Structures tend to encounter vibrations due to live loads during normal usage or natural elements such as earthquakes, wind and ocean waves. Vibrations are detrimental to the function of devices such as optics. They may also cause damage to the structure and its peripheral equipment, such as mechanical and electrical components, piping systems and electrical distribution systems, and HVAC (heating, ventilation and air conditioning) duct systems. For satellites and nuclear reactors, reducing vibrations is important for optimizing operation and safety, respectively. Satellites involve continuous fiber poly-matrix composites, whereas nuclear reactors involve concrete.

Vibration damping involves the dissipation of the mechanical energy associated with the vibration, so that the amplitude of the vibration is diminished. It is a natural phenomenon that occurs due to certain mechanisms within the material that consume the mechanical energy, thereby converting the energy to heat. Since the phenomenon is natural – it does not involve a device for suppressing the vibration, this method of vibration damping is described as passive energy dissipation, which is the focus of this section.

Figure 3.12 illustrates three levels of damping. When the displacement returns to its initial value gradually, such that there is no overshooting, it is termed overdamping. When the displacement overshoots, returns to the initial value, and then overshoots in the opposite direction such that the magnitude of the overshoot decreases oscillation by oscillation, it is termed underdamping. When the displacement just fails to overshoot, it is termed critical damping, which is a scenario between overdamping and underdamping.

The level of damping is mathematically described by the damping ratio ζ, where $\zeta = 1$ for critical damping, $\zeta > 1$ for overdamping, and $\zeta < 1$ for underdamping.

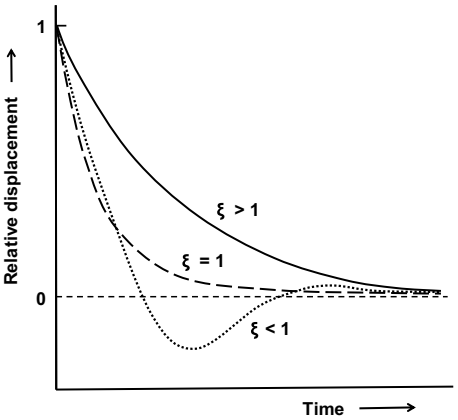

Figure 3.12. Schematic illustration of overdamping ($\zeta > 1$), underdamping ($\zeta < 1$), and critical damping ($\zeta = 1$)

The damping ratio is equal to half of the loss tangent, which will be defined in Eq. 3.37.

On the other hand, damping may be achieved through the use of a device that suppresses the vibration as it occurs. Such a device, termed an actuator, provides a force that is synchronized with the deformation. For example, when a beam bows upward, the force pushes it downward; alternatively, when the beam bows downward, the force pushes it upward. For the force to be synchronized with the deformation, the deformation must be sensed, with the output of the sensor used to activate the actuator. This method of damping is known as active vibration control, which is highly effective for fast vibration suppression, though this is a very expensive approach compared to passive energy dissipation.

Mechanical deformation consumes (i.e., absorbs) mechanical energy by converting the mechanical energy to heat, thus providing a mechanism for passive energy dissipation. The area under a stress–strain curve during loading is the amount of energy absorbed per unit volume due to the deformation. The area under the curve has units of energy per unit volume, since the units of the product of

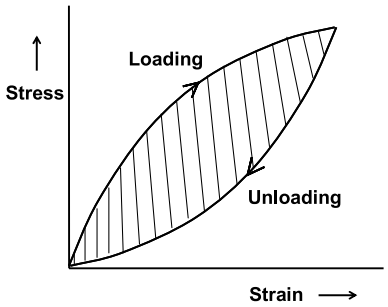

Figure 3.13. Hysteresis in the stress–strain curve because the curves from loading and subsequent unloading do not overlap

stress and strain is the units of stress (since strain is dimensionless), which is N/m^2. Multiplication of both the numerator and denominator of this unit by m (meters, the units of distance) gives $(N\,m)/m^3$, which are the units for energy (N m) per unit volume (m^3). Vibration involves cycles of loading and subsequent unloading. During unloading, energy is released such that this energy per unit volume is the area under the stress–strain curve during unloading. Thus, within a cycle, the net amount of energy absorbed is the difference between the area under the loading curve and the area under the unloading curve. This difference in area is the shaded area in Fig. 3.13. The lack of an overlap between the loading and unloading curves is termed hysteresis. The greater the hysteresis, the greater the energy dissipation. This hysteresis is due to the viscoelastic behavior of the solid, as explained below.

3.6.2 Viscoelastic Behavior

Figure 3.14a illustrates the application of a constant stress for a certain period of time (between the "on" and "off" times). In response to this stress, an ideal elastic solid will instantaneously strain to a constant level (which relates to the modulus and the stress through Hooke's law), and the strain will instantaneously vanish when the applied stress is subsequently removed (Fig. 3.14b). For a solid that deforms both elastically and plastically (Fig. 3.14c), the elastic and plastic strain together will respond instantaneously to the applied stress and stay constant during the period of stress application; upon unloading, the elastic strain is recovered while the plastic strain is permanent.

For a viscous medium (such as a viscous liquid), a degree of viscous (plastic) flow occurs instantaneously, with this viscous flow progressing over time (with the strain increasing linearly with time) during the period of constant stress (Fig 3.14d); upon unloading, a minor degree of elastic recovery occurs. A viscous material is defined as a material that responds to an applied stress by exhibiting the development of strain over a period of time (the strain increases linearly with time), such that the material does not return to its original shape after the stress has been removed.

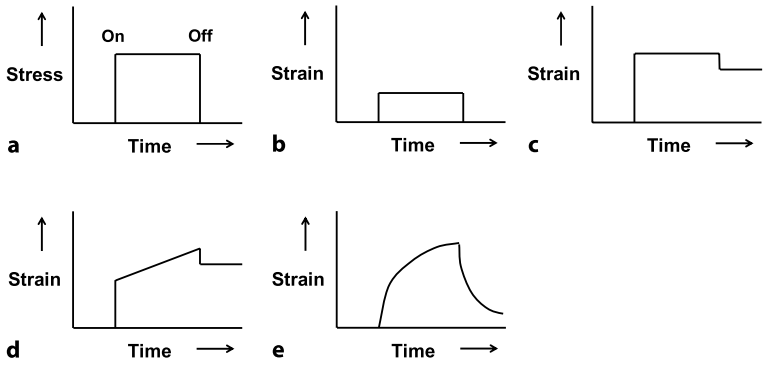

Figure 3.14. Strain response to the application of stress in the time period between "on" and "off." **a** Applied stress. **b** Strain response for an elastic material. **c** Strain response for a material that undergoes both elastic and plastic deformation. **d** Strain response for a viscous material. **e** Strain response for a viscoelastic material

A viscoelastic solid (e.g., rubber) exhibits a behavior that is intermediate between an elastic solid and a viscous medium. As illustrated in Fig. 3.14e, some elastic and viscous deformation occurs instantaneously; this is followed by elastic and viscous deformation that increases over time during the period of stress application. Upon unloading, the elastic strain recovers slowly. In other words, the total strain has both elastic and viscous components.

The viscous component of the deformation is responsible for the flow of a material. The study of the flow behavior of solids and liquids belongs to the field known as rheology.

The behavior in Fig. 3.14e means that the strain response lags behind the stress during both loading and unloading. This lag causes the hysteresis shown in Fig. 3.13, where the strain is higher during unloading than during loading for the same stress. During the application of stress, the change in strain lags behind the change in stress. Similarly, in response to the application of strain, the change in stress lags behind that of the strain. If the solid is purely elastic, the loading and unloading curves will overlap, so that there is no hysteresis and no lag.

Figure 3.15 illustrates the lag of the stress wave resulting from a sinusoidal wave of applied strain. For a purely elastic solid, there is no lag. For a purely viscous material, the lag is 90° (as explained below). For a viscoelastic material, the lag is below 90°.

The viscosity is a material property that describes the resistance to viscous flow. It is defined as the ratio of the shear stress (unit: Pa) to the shear strain rate (also known as the shear rate; unit: s^{-1}). For a purely viscous material (with no elastic behavior) for which the viscosity is independent of the shear strain rate (a behavior that is said to be Newtonian, as in the case of water), the shear stress (τ) is proportional to the shear strain rate ($\dot{\gamma}$, with the dot meaning differentiation with respect to time); the constant of proportionality is known as the viscosity (η). In other words,

$$\tau = \eta\dot{\gamma} \, . \tag{3.29}$$

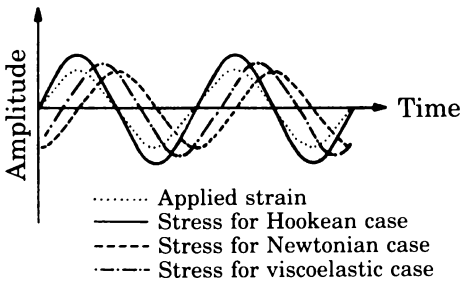

Figure 3.15. The stress changes in response to an applied strain (*dotted curve*). In the Hookean case (i.e., the case of a purely elastic solid), the change in stress does not lag behind the change in strain, so the stress wave and the strain wave are in phase. In the Newtonian case (i.e., the case for a purely viscous and Newtonian medium), the change in stress lags behind that of the strain by a phase angle of 90°. In the viscoelastic case, the behavior lies in-between those of the Hookean and the Newtonian case; i.e., the phase angle that describes the lag is less than 90°

For a viscous material that is non-Newtonian, the viscosity depends on the strain rate, so the proportionality in Eq. 3.29 does not apply. Nevertheless, there is a nonlinear relationship between the stress and the shear rate. Thus, a given stress corresponds to a particular strain rate. Therefore, whether the material is Newtonian or not, the strain rate is constant for a constant stress. In turn, a constant strain rate means that the strain increases linearly with time under a constant stress, as depicted in Fig. 3.14d.

If γ is a sinusoidal function of time (t) such that

$$\gamma = \gamma_o \sin \omega t \ , \tag{3.30}$$

where γ_o is the amplitude of the wave and ω is the angular frequency of the wave in radians per second (with $\omega = 2\pi\upsilon$, where υ is the frequency in Hz, or cycles per second), then

$$\dot{\gamma} = \omega\gamma_o \cos \omega t \ . \tag{3.31}$$

Hence, τ, which is proportional to $\dot{\gamma}$, varies with time as cos ωt. This means the τ is out of phase from γ by 90° (i.e., $\pi/2$ in radians). For a viscoelastic material that has both viscous and elastic components, the phase angle between τ and γ is less than 90°.

Based on the definition of the viscosity, the units of viscosity are Pa s. Alternatively, viscosity can be measured in units of poise (P), where

$$1\,\text{Pa s} = 10\,\text{P} = 1{,}000\,\text{cP} \ . \tag{3.32}$$

cP (centipoise) is more commonly encountered than P itself. Water has a viscosity of 0.0089 P at 25°C, or 1 cP at 20°C.

Figure 3.16 shows the relationship between the shear stress and the shear strain rate. When the curve is linear and passes through the origin (curve a), the behavior is said to be Newtonian and the slope of the curve is the viscosity defined above. Since the slope is independent of the shear strain rate, the viscosity is independent of the shear strain rate. Water is an example of a Newtonian fluid.

When the curve is nonlinear, with the slope (the viscosity) decreasing with increasing shear strain rate (curve b), the behavior is such that flow occurs more easily when the shear strain rate is higher. Examples include polymer melts and paper pulp. Polymer melts tend to be shear thinning, since the long molecules in the polymer melt become more aligned as the shear strain rate increases. Paper pulp is shear thinning because the fibers in the pulp align as the shear strain rate increases. This alignment makes it easier to shear the material. In this case, the material is said to be shear thinning and it is also said to be a pseudoplastic fluid.

When the curve is nonlinear, with the slope (the viscosity) increasing with increasing shear strain rate (curve c), the behavior is such that flow occurs more easily at low strain rates and becomes more difficult as the strain rate increases. Examples include quicksand. In this case, the material is said to be shear thickening and it is also said to be a dilatant substance.

Curves (d) and (a) in Fig. 3.16 are both linear, but curve (d) does not go through the origin whereas curve (a) does. For curve (d), at a shear strain rate of zero, the

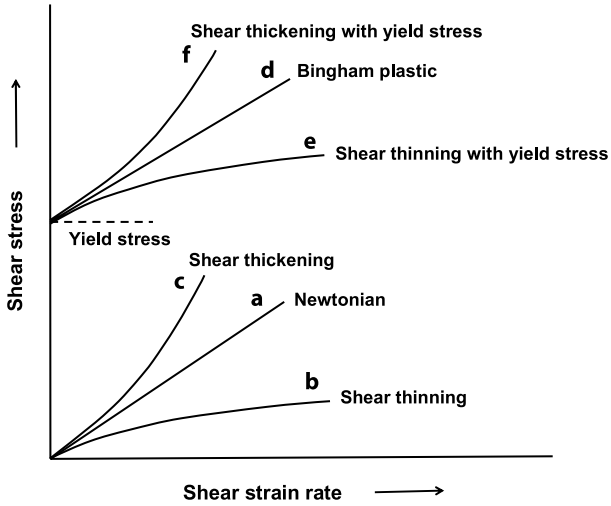

Figure 3.16. Relationship of shear stress to shear strain rate for various types of behavior

shear stress is nonzero; this value is known as the shear yield stress τ_y (or shear yield strength). This means that the shear stress must exceed the shear yield stress in order for viscous deformation to occur for curve (d). A material that exhibits the behavior of curve (d) is said to be a Bingham plastic. An example of a Bingham plastic is chewing gum, which must be chewed with a sufficient stress in order for it to start flowing. Curve (e) describes the behavior of shear thinning with yield stress. Curve (f) describes the behavior of shear thickening with yield stress.

The flow behavior of a substance after the removal of a shear stress is important for numerous applications. For example, a pseudoplastic material flows more easily (with the viscosity decreasing) as the shear strain rate increases (curve b in Fig. 3.16). Upon subsequent removal of the shear stress, the viscosity may or may not completely return to the initial high value. When the viscosity returns fully, the material is said to be thixotropic. Examples of thixotropic materials are paint (which flows easily during brushing but does not sag after brushing) and toothpaste (which flows during squeezing but the shape remains after the squeezing).

Figure 3.17 returns to the curve for a Bingham plastic. The slope of this curve is known as the plastic viscosity, which should be distinguished from the apparent viscosity. The apparent viscosity is the slope of the dashed line in Fig. 3.17; i.e., it is the shear stress divided by the shear strain rate at a particular point in the curve. The apparent viscosity depends on the point chosen.

The field of continuum mechanics includes solid mechanics and fluid mechanics. Solid mechanics includes elasticity and plasticity. Fluid mechanics includes Newtonian and non-Newtonian fluids. Rheology is a branch of continuum mechanics that addresses the flow of materials, so it mainly pertains to plasticity and non-Newtonian fluids. Neither a plastic solid nor a non-Newtonian fluid can support a shear stress in static equilibrium.

Rheological properties can be measured using a rheometer, which commonly utilizes a parallel-plate configuration. In this configuration, the proximate surfaces of the two circular disks (e.g., aluminum disks 40 mm in diameter) are separated by a fixed gap (e.g., 1,000 ± 1 μm) that is filled with the specimen under study. Both the diameter of the disks and the gap between the disks can be varied. The top plate rotates while the bottom plate is stationary, thus providing torsional deformation. The greater the diameter of the disk, the larger the maximum elongation during deformation. The specimen under study is located only in the space between the two plates. Experiments can be conducted under both continuous (steady state, in one direction) shear and oscillatory (dynamic, back and forth) shear.

A viscometer is simpler than a rheometer. It involves continuous rotation at a controlled speed of rotation (which relates to the shear strain rate), such that the rotation is not oscillatory but is continuous in one direction. Because of the continuous rotation, the linear regime (with the shear stress being proportional to the shear strain) cannot be studied and the critical shear strain (the maximum shear strain in the linear regime) cannot be measured. In contrast, a rheometer provides the option of oscillatory rotation at selected shear strain amplitudes, so that the linear regime can be studied (thus allowing measurement of the shear modulus) and the critical shear strain and yield stress can be determined.

Figure 3.18 shows a plot of shear stress vs. shear strain rate for a 2.4 vol% carbon black (CB) paste with a polyolester-based vehicle (liquid), as obtained using a parallel-plate rheometer. The plot is obtained by sweeping the shear stress while the shear rate is monitored. Comparison is made between vehicles with and without dissolved antioxidants. The presence of antioxidants causes the shear rate to decrease for the same shear stress. This means that the ability to flow is diminished by the presence of antioxidants. The yield stress is 16.2 Pa in the absence of antioxidants and 25.0 Pa in the presence of antioxidants. In other words, the yield stress is increased by the presence of antioxidants. Whether antioxidants are present or not, the material is a Bingham plastic with shear thinning, as shown by the continuous decrease in slope as the shear rate increases. The plastic viscosity

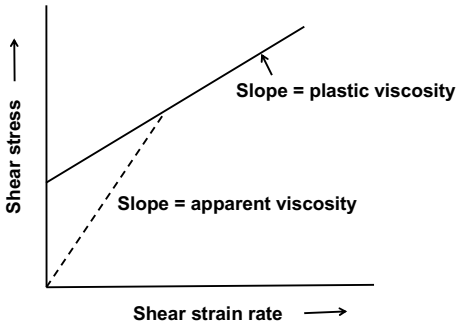

Figure 3.17. Relationship of shear stress to shear strain rate for a Bingham plastic (curve d of Fig. 3.16), illustrating the difference between the plastic viscosity and the apparent viscosity

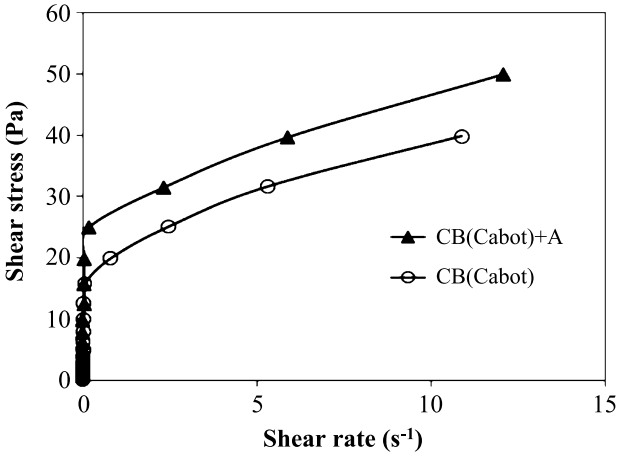

Figure 3.18. Plot of the shear stress versus the shear rate, showing the effect of an applied shear stress on the shear strain rate for a 2.4 vol% carbon black (CB) paste with a polyolester-based vehicle. A, antioxidants

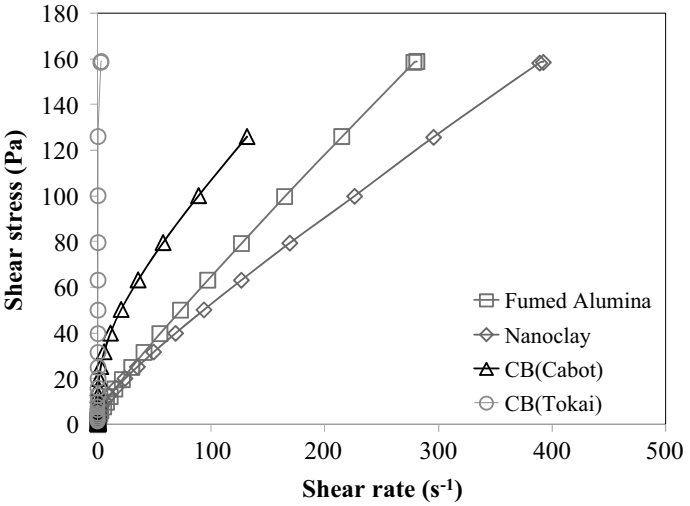

Figure 3.19. Plot of the shear stress versus the shear rate, showing the effect of an applied shear stress on the shear strain rate for various particle pastes that all involve a polyolester-based vehicle in the absence of antioxidants

decreases with increasing shear rate, with values ranging from 3.73 Pa s (at low shear rates) to 0.63 Pa s (at high shear rates).

Figure 3.19 shows corresponding plots for various types of particles in the same polyolester-based vehicle. Among the fumed alumina, nanoclay, carbon black (Cabot) and carbon black (Tokai) pastes, all without antioxidants, the nanoclay paste gives the highest strain rate for the same shear stress, and the carbon black (Tokai) paste gives the lowest shear rate for the same shear stress. The low ability of the carbon black (Tokai) paste to flow is attributed to its high volume fraction (8%)

of the solid component. The high ability of the nanoclay paste to flow is attributed to its low solid volume fraction (1%). Although the fumed alumina paste and the carbon black (Cabot) paste have the same solid volume fraction (2.4%), the ability to flow is greater for the former. The relatively high flow ability of the fumed alumina paste is probably partly due to the silane coating on the fumed alumina and the low specific surface area compared to carbon black (Cabot).

By plotting the shear stress on a logarithmic scale vs. the shear rate on a logarithmic scale (Fig. 3.20), the behavior in the regime of low shear rate can be discerned. For the carbon black pastes (whether Cabot or Tokai), double yielding occurs (i.e., two yield stresses are present); the first yielding is shown in the magnified view in the linear–linear plot in Fig. 3.21 for carbon black (Cabot). Due to the small values of shear stress and shear rate at the first yielding, only the second yielding is shown in the full-scale linear–linear plot in Fig. 3.19. However, in the log–log plot in Fig. 3.20, double yielding is clear. For the nanoclay paste and the fumed alumina paste, only single yielding occurs.

Figure 3.19 shows that the plastic viscosity after second yielding and subsequent shear thinning is lowest for the nanoclay paste (0.34 Pa s), followed by the fumed alumina paste (0.50 Pa s), then the carbon black (Cabot) paste (0.63 Pa s), then the carbon black (Tokai) paste (1 Pa s), and finally the carbon black (Cabot) paste with antioxidants (1.87 Pa s). This trend among the pastes is consistent with the lowest solid volume fraction in the nanoclay paste, the higher solid volume fractions for the alumina and carbon black (Cabot) pastes, and the still higher solid volume fraction for the carbon black (Tokai) paste. The highest plastic viscosity for the carbon black (Cabot) paste with antioxidants shows that there is a significant

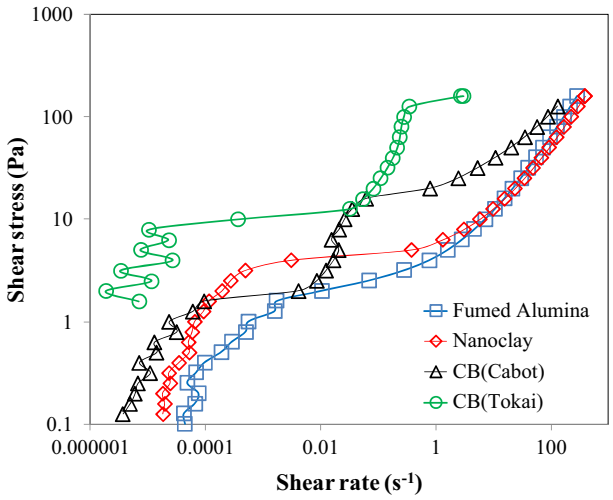

Figure 3.20. Plot of the shear stress versus the shear rate, showing the effect of the applied shear stress on the shear strain rate for various pastes on a log–log scale, in contrast to the linear–linear scale in Figs. 3.18 and 3.19. The pastes are the same as those in Fig. 3.19. The data scatter in the shear rate at low shear rates is due to the low measuring precision for low shear rates (i.e., almost no deformation)

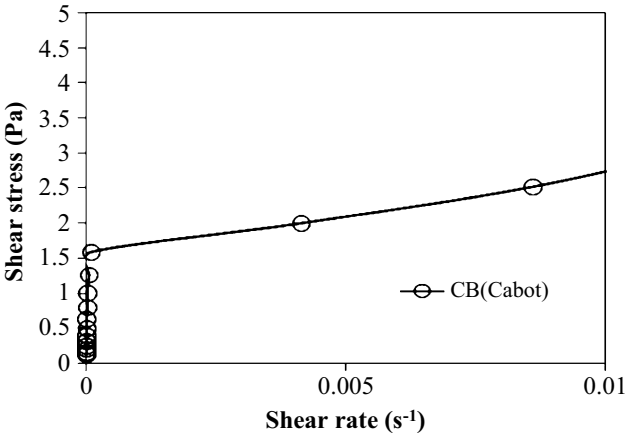

Figure 3.21. Plot of the shear stress versus the shear rate for carbon black (Cabot) paste on a magnified linear–linear scale. The part of the *curve* immediately after the first yielding is magnified

increase in the plastic viscosity due to the antioxidants. The fumed alumina paste has lower plastic viscosity than the carbon black (Cabot) paste in spite of the identical solid volume fractions of these two pastes. This is probably because the fumed alumina has been treated with silane.

The plastic viscosity after second yielding is much lower than the corresponding value after first yielding. The plastic viscosity after first yielding is much higher for the carbon black pastes than the nanoclay or fumed alumina paste. This means that the yielding is not complete after the first yielding.

As shown in Table 3.5, the second yield stress is much higher than the corresponding first yield stress. Among the various pastes, the carbon black (Cabot) paste has the lowest first yield stress, whereas the carbon black (Cabot) paste with antioxidants has the highest first yield stress. The carbon black (Tokai) paste gives the highest second yield stress. Both the first and the second yield stresses are much higher for the carbon black (Tokai) paste than for the carbon black (Cabot) paste. This is consistent with the higher volume fraction of the solid component for the carbon black (Tokai) paste. Both the first and the second yield stresses of the carbon black (Cabot) paste are increased by the addition of antioxidants. The fractional increase in the first yield stress due to the antioxidants is much higher than that of the second yield stress.

The first yield stress of the nanoclay paste is higher than those of the fumed alumina paste and the carbon black (Cabot) paste. This is consistent with the higher value of the critical strain for the nanoclay paste than for the other two pastes. The first yield stress of the nanoclay paste is smaller than that of the carbon black (Tokai) paste and that of the carbon black (Cabot) paste containing antioxidants. This is consistent with the high G' values of the carbon black (Tokai) paste and the carbon black (Cabot) paste with antioxidants.

The double yielding in the carbon black pastes is probably related to the aggregate structure of the carbon black. The first yielding may be due to the shear of

Table 3.5. Shear yield stress and plastic viscosity, as measured by steady-state flow (i.e., continuous strain in one direction, not oscillatory strain) at various shear stresses (from [3])

	First yield stress (Pa)	Second yield stress (Pa)
Nanoclay	4.2	–
Fumed alumina	2.9	–
Carbon black (Cabot)	1.6	16.2
Carbon black (Tokai)	7.7	160[a]
Carbon black (Cabot) + A[b]	10[a]	25.0

[a] Value is not reliable due to the limited number of data points after yielding
[b] A, antioxidants

one aggregate relative to another, whereas the second yielding may be due to the shear of one particle relative to another. Double yielding does not occur for the fumed alumina paste, in spite of the similar aggregate structure of fumed alumina, probably because of the partially polar nature of the bonding in alumina and the consequent greater cohesion among the alumina particles in an aggregate.

The first and the second yield stresses are higher for the carbon black (Tokai) paste than for any of the other pastes. This is attributed to the high solid volume fraction in the carbon black (Tokai) paste. The addition of antioxidants increases both the first and the second yield stresses, as shown for the carbon black (Cabot) paste. This is probably because of the interaction of the antioxidants with the carbon black aggregate surface, making it more difficult for the aggregates to move relative to one another.

The yield stresses shown in Table 3.5 do not show a correlation with the plastic viscosity. Yielding is associated with the stress at the start of flow, and this stress depends on the structure before yielding. However, the plastic viscosity is associated with the ease of flow after flow initiation and does not depend on the structure before yielding.

Yielding is also accompanied by an abrupt drop in the apparent viscosity, which is monitored as the shear stress is swept. The double yielding behaviors of the carbon black pastes are shown in Figs. 3.22 and 3.23 as plots of the apparent viscosity vs. the shear stress. The single yielding behaviors of the nanoclay paste and the fumed alumina paste are shown in Fig. 3.24.

A sinusoidal applied stress wave can be expressed mathematically as

$$\tau = \tau_o e^{i\omega t} = \tau_o(\cos \omega t + i \sin \omega t) \,, \tag{3.33}$$

where τ_o is the amplitude of the shear stress wave, ω is the angular frequency (in radians/second), and t is the time. The frequency, which is in Hz (or cycles/second), is equal to ω divided by 2π, since there are 2π radians in a cycle. Although τ is a complex quantity, the physically meaningful quantity is the real part of τ.

The strain wave (in response to the stress wave) is

$$\gamma = \gamma_o e^{i(\omega t - \delta)} = \gamma_o[\cos(\omega t - \delta) + i \sin(\omega t - \delta)] \,, \tag{3.34}$$

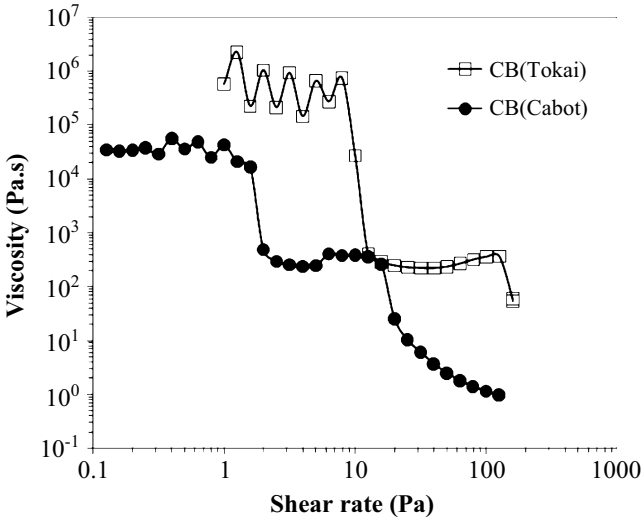

Figure 3.22. Apparent viscosity versus shear stress for the carbon black (CB) (Tokai) paste and the carbon black (CB) (Cabot) paste. Abrupt drops in viscosity occur at the shear yield stresses. There are two yield stresses for each paste

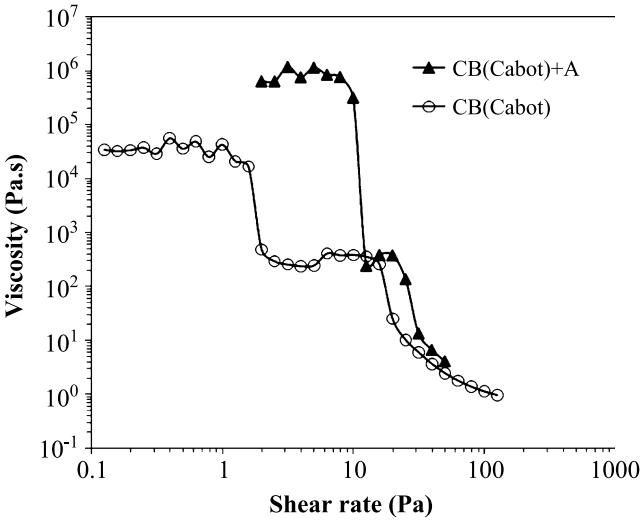

Figure 3.23. Apparent viscosity versus shear stress for the carbon black (CB) (Cabot) paste with and without antioxidants. Abrupt drops in viscosity occur at the shear yield stresses. There are two yield stresses for each paste. A, antioxidants

where γ_o is the amplitude of the shear strain wave and δ is the lag (phase) angle in radians. Although γ is complex, the physically meaningful quantity is the real part of γ.

A plot of the real part of τ versus the real part of γ gives the shear stress–strain curve, as shown in Fig. 3.25a for $\delta = 30^\circ = \pi/6$. The area within the hysteresis loop is the energy loss (dissipated as heat) per unit volume in one cycle. If $\delta = 0$, there

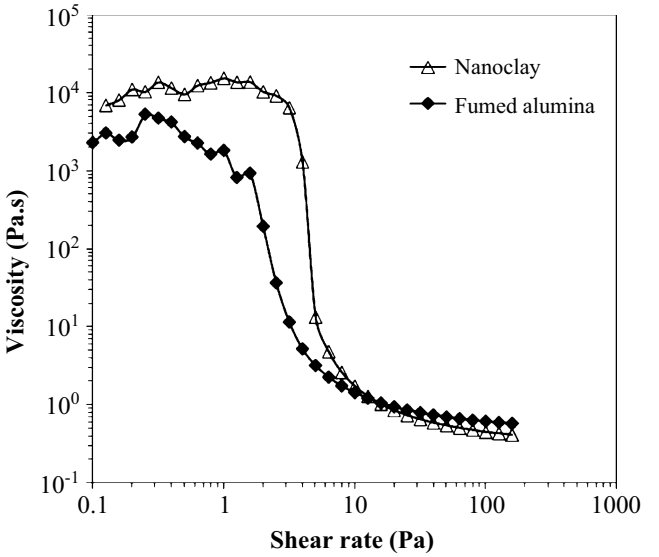

Figure 3.24. Apparent viscosity versus shear stress for the nanoclay paste and the fumed alumina paste. The abrupt drop in apparent viscosity occurs at the shear yield stress

is no hysteresis and the curve is a straight line through the origin (Fig. 3.25b), so there is no energy loss. If $\delta = 90°$, the curve is a circle (Fig. 3.25c), and so the area within the hysteresis loop is the largest and hence the energy loss is the highest.

By definition, the complex shear modulus G is given by

$$G = \tau/\gamma \tag{3.35}$$

and it describes the behavior in the linear regime, where the stress and strain are proportional to one another. The real part of G (abbreviated to G') is called the storage modulus, and it describes the elastic behavior. The imaginary part of G (abbreviated to G'') is called the loss modulus, and it describes the viscous behavior. In the linear regime, G' and G'' are independent of the strain.

The critical shear strain γ_c is the strain at the limit of linear behavior. Above γ_c, linear behavior is lost due to the loss of a certain type of structure in the material. In order to determine the critical strain, the amplitude of the oscillatory strain is progressively increased while G' is monitored. The strain amplitude at which G' drops by, say, 5% may be taken as γ_c.

Figure 3.26 shows the variation of G' and G'' with the strain amplitude for a 2.4 vol% carbon black paste with a polyolester-based vehicle (liquid), as obtained by sweeping the strain amplitude, with the oscillatory strain varying at an angular frequency of 6.28 rad/s (i.e., 1 Hz, or 1 cycle/s). In Fig. 3.26, γ_c is 1.5%, with $G' = 350$ Pa and $G'' = 55$ Pa in the linear regime (i.e., the regime below γ_c).

Using Eqs. 3.33 and 3.34, Eq. 3.35 becomes

$$G = (\tau_o/\gamma_o)e^{i\delta} = (\tau_o/\gamma_o)(\cos\delta + i\sin\delta)\ . \tag{3.36}$$

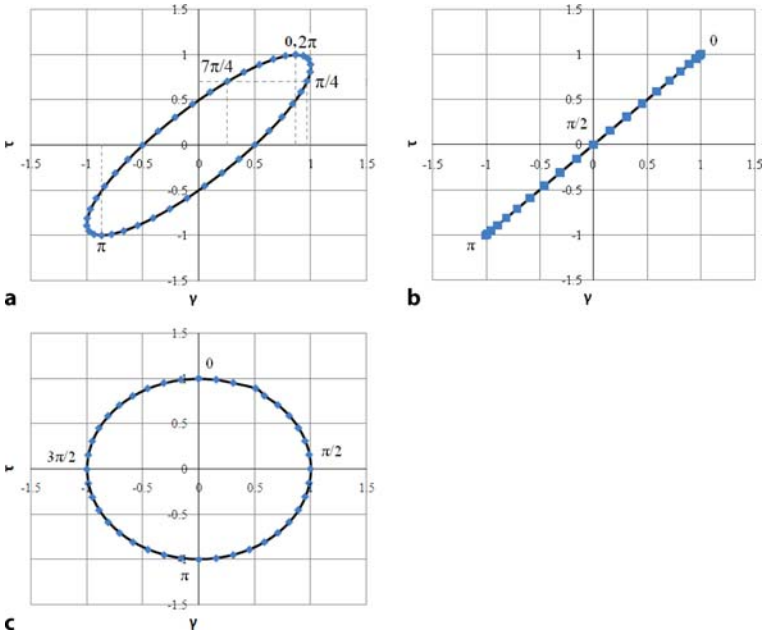

Figure 3.25. The shear stress–strain curve (stress τ vs. strain γ) for one cycle (i.e., ωt increasing from 0 to π and finally to 2π to complete a cycle), with both τ_0 and γ_0 equal to 1. **a** $\delta = \pi/6$ (i.e., 30°), **b** $\delta = 0$, **c** $\delta = \pi/2$ (i.e., 90°)

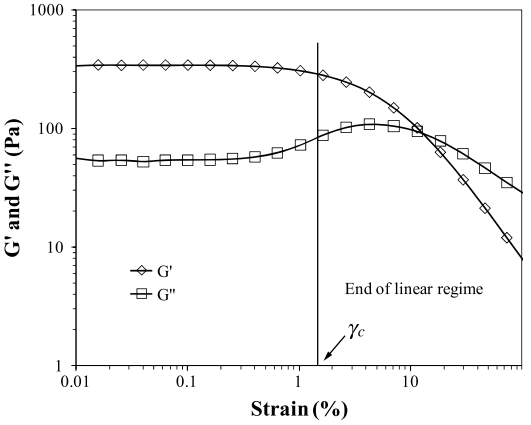

Figure 3.26. Strain sweep for CB (Cabot) thermal paste, showing G' and G'' in the linear regime and beyond

Hence,

$$\tan\delta = (\sin\delta)/(\cos\delta) = (\text{imaginary part of } G)/(\text{real part of } G)\ . \qquad (3.37)$$

The quantity $\tan\delta$ is called the loss tangent, loss factor, or the damping capacity.

The energy dissipation ability of a material is governed by the loss tangent and the stiffness (which is described by the storage modulus). The product of the loss

tangent and the storage modulus is the loss modulus, which is a figure of merit that describes the energy dissipation ability. A high value of loss tangent does not imply good energy dissipation ability, since a high stiffness is also necessary. Thus, the use of the loss tangent as an indicator of the energy dissipation ability is not appropriate.

Equation 3.36 can be written as

$$G = G' + iG'' \,, \tag{3.38}$$

where

$$G' = (\tau_o/\gamma_o)\cos\delta \,, \tag{3.39}$$

and

$$G'' = (\tau_o/\gamma_o)\sin\delta \,. \tag{3.40}$$

According to Eq. 3.36, the magnitude of G, which is a complex quantity, is given by

$$|G| = \tau_o/\gamma_o \,. \tag{3.41}$$

It is customary to describe the real and imaginary parts of G in terms of a plot of G'' versus G', as illustrated in Fig. 3.27. This plot is of the complex plane, which involves the imaginary part on the vertical axis and the real part on the horizontal axis. The lag angle δ is indicated in this plot.

If the material is purely elastic, $\delta = 0$. In this situation, from Eq. 3.39,

$$G' = \tau_o/\gamma_o \,, \tag{3.42}$$

and, from Eq. 3.40,

$$G'' = 0 \,. \tag{3.43}$$

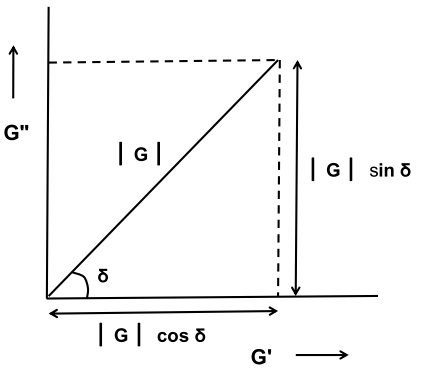

Figure 3.27. The complex plane of G, showing the imaginary part of G vs. the real part of G

If the material is purely viscous, $\delta = \pi/2$. In this situation, from Eq. 3.39,

$$G' = 0 \,, \tag{3.44}$$

and, from Eq. 3.40,

$$G'' = \tau_o/\gamma_o \,, \tag{3.45}$$

Equation 3.37 can be rewritten as

$$\tan\delta = G''/G' \,. \tag{3.46}$$

In Fig. 3.26, in the linear regime (i.e., the regime below γ_c), $G' = 350\,\text{Pa}$, $G'' = 55$ Pa, and $\tan\delta = 55\,\text{Pa}/350\,\text{Pa} = 0.16$.

The angular frequency ω relates to the strain rate, as shown by differentiating Eq. 3.34:

$$\dot{\gamma} = \gamma_o \mathrm{i}\omega \mathrm{e}^{\mathrm{i}(\omega t - \delta)} \,. \tag{3.47}$$

This means that a higher ω is associated with a higher strain rate.

Linear behavior is characterized by a linear relationship between shear stress and shear strain, so that G' and G'' are independent of strain. The critical shear strain γ_c is the strain at the limit of linear behavior. Above γ_c, linear behavior is lost due to the loss of a certain type of structure in the material.

From Eqs. 3.29, 3.33 and 3.47,

$$\eta = \tau_o \mathrm{e}^{\mathrm{i}\omega t}/[\gamma_o \mathrm{i}\omega \mathrm{e}^{\mathrm{i}(\omega t - \delta)}] = -\mathrm{i}(|G|/\omega)\mathrm{e}^{\mathrm{i}\delta} \,. \tag{3.48}$$

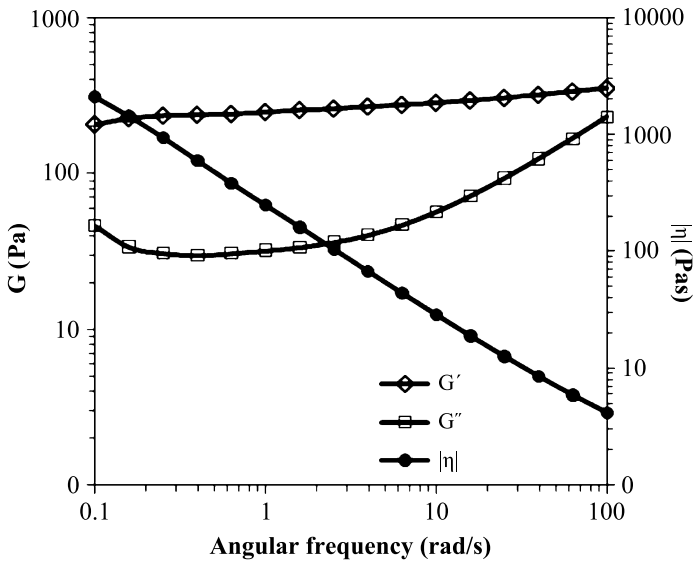

Figure 3.28. Effect of the angular frequency ω on the storage modulus G', loss modulus G'', and the complex apparent viscosity magnitude $|\eta|$ for the carbon black (CB) (Cabot) paste

The magnitude of η is thus given by

$$|\eta| = |G|/\omega \ . \tag{3.49}$$

Equation 3.49 means that $|\eta|$ is inversely related to ω.

Figure 3.28 shows the effect of ω on G', G'' and $|\eta|$ (apparent viscosity) for the carbon black (CB) (Cabot) paste. The apparent viscosity $|\eta|$ decreases with increasing ω, as expected. G' exceeds G'' for all ω values. This means that the paste is solid-like at all frequencies studied. Furthermore, G'' increases and approaches G' as ω increases, meaning that the paste becomes more and more liquid-like as ω increases, though it remains mainly solid-like.

Figure 3.29 shows that, for the carbon black (Cabot) paste, G', G'' and $|\eta|$ are all increased by the addition of antioxidants, such that the frequency dependence is not affected. The increases in G' and $|\eta|$ upon antioxidant addition are consistent with the increases of these parameters upon antioxidant addition in the absence of a solid component (Fig. 3.30). The increase in G'' (Fig. 3.29) contrasts with the negligible increase upon antioxidant addition in the absence of a solid component (Fig. 3.30). This suggests that the antioxidants interact strongly with the carbon black, since the presence of the antioxidants significantly increases G', which relates to the network of carbon black.

Figure 3.31 shows that, for the carbon black (Cabot) paste, the addition of antioxidants increases the viscosity at all temperatures studied. In the absence of antioxidants, the viscosity increases with increasing temperature from 25 to 120°C, probably due to slight phase separation, slight evaporation of the vehicle, and/or the occurrence of crosslinking during heating. However, in the presence of

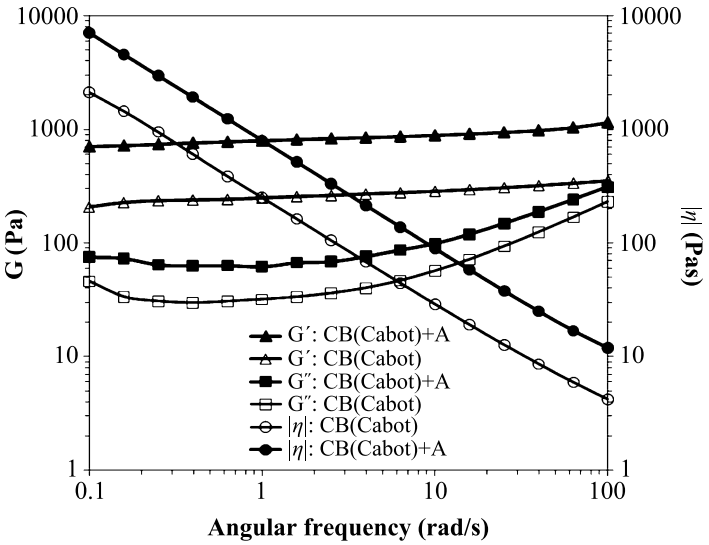

Figure 3.29. Effect of the angular frequency ω on the storage modulus G', loss modulus G'' and complex viscosity magnitude $|\eta|$, showing a comparison of carbon black (CB) (Cabot) pastes with and without antioxidants. A, antioxidants

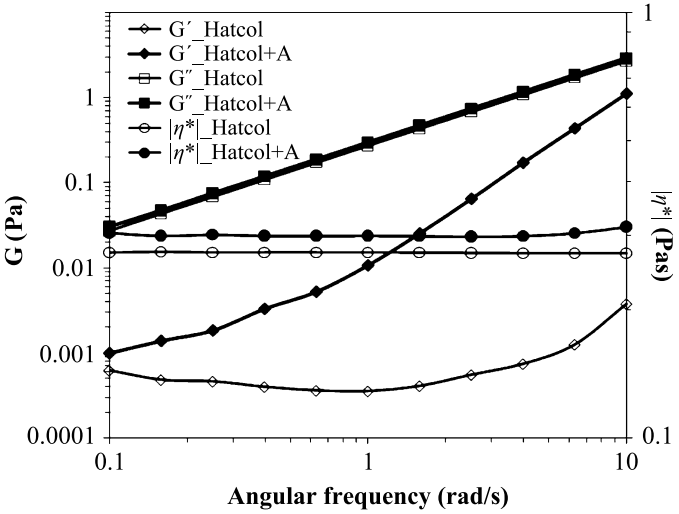

Figure 3.30. Effect of the angular frequency ω on the storage modulus G', loss modulus G'', and the complex viscosity magnitude $|\eta|$ for the vehicle without solid, showing a comparison of the vehicle (polyolesters, produced by Hatcol) with and without antioxidants. A, antioxidants

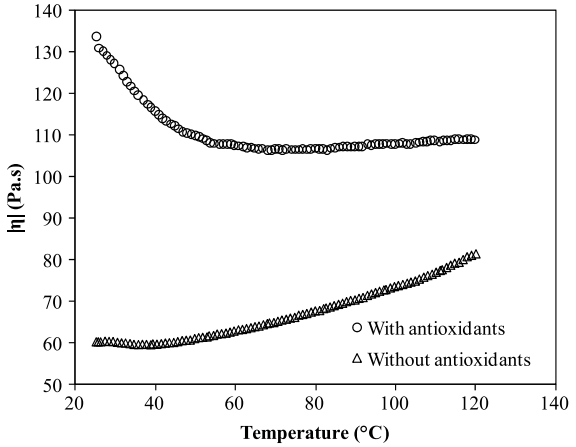

Figure 3.31. Effect of increasing temperature on the complex apparent viscosity magnitude $|\eta|$ for the carbon black (Cabot) paste with and without antioxidants

antioxidants, the viscosity decreases as the temperature increases from 25 to 50°C and remains essentially unchanged as the temperature increases further from 50 to 120°C. As shown in Fig. 3.32, in the presence of antioxidants, G' decreases as the temperature increases from 25 to 50°C and then barely changes as the temperature increases beyond 50°C, while G'' decreases slightly as the temperature increases from 25 to 60°C and then hardly changes as the temperature increases beyond 60°C. These effects in the presence of antioxidants probably occur because heating

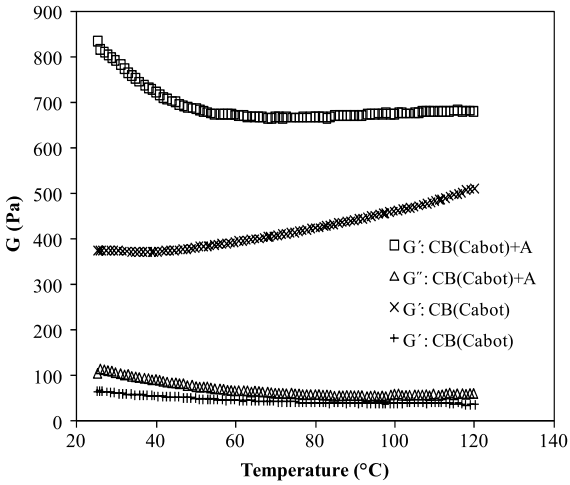

Figure 3.32. Effect of increasing temperature on the storage modulus G' and loss modulus G'' of the carbon black (CB) (Cabot) paste with and without antioxidants. A, antioxidants

below 50°C increases the fluidity of the paste and heating above 50°C reveals the thermal stabilization effect of the antioxidants.

The mechanical energy absorbed per unit volume due to the deformation is given by the area under the stress–strain curve. This corresponds to the mechanical work. Hence, based on Eqs. 3.33 and 3.34, the energy absorbed per unit volume $= \int \tau \mathrm{d}\gamma$,

$$\begin{aligned} &= \tau_o \gamma_o \int e^{i\omega t} d[e^{i(\omega t - \delta)}] \\ &= \tau_o \gamma_o e^{-i\delta} \int e^{i\omega t} de^{i\omega t} \\ &= \tfrac{1}{2} \tau_o \gamma_o e^{-i\delta} e^{i2\omega t} \end{aligned} \tag{3.50}$$

Integrating from $t = 0$ to $t = t$, the energy absorbed per unit volume from $t = 0$ to $t = t$ is given by

$$\tau_o \gamma_o e^{-i\delta} (e^{i2\omega t} - 1)/2 \, . \tag{3.51}$$

The frequency relates to the strain rate, as shown by differentiating Eq. 3.34:

$$= \gamma_o \omega e^{i(\omega t - \delta)} \, . \tag{3.52}$$

This means that a higher ω is associated with a higher strain rate.

Due to their viscoelastic behavior, polymers (particularly thermoplastics) can provide damping. In general, elastomers and other amorphous thermoplastics with a glass transition temperature below room temperature are attractive for damping. Polymer blends and interpenetrating networks are also attractive since the interface between the components in the blend or network provides a mechanism for damping. Rubber is particularly well-known for its damping ability. However, rubber suffers from low stiffness, which results in a rather low value of the loss modulus. Other polymers used for vibration damping include polyurethane, a polypropylene/butyl rubber blend, a polyvinylchloride/chlorinated polyethylene/epoxidized

natural rubber blend, a polyimide/polyimide blend, a polysulfone/polysulfone blend, a nylon-6/polypropylene blend, and a urethane/acrylate interpenetrating polymer network.

3.6.3 Pseudoplasticity and Ferroelasticity

One special class of high-damping materials is known as the shape memory alloys (SMAs), which include Ni-Ti (49–51 at.% Ni, alloy known as Nitinol, which stands for Nickel Titanium Naval Ordinance Laboratory), Ni-Al (36–38 at.% Al), Cu-Zn (38.5–41.5 wt.% Zn), Cu-Sn (about 15 at.% Sn), Fe-Pt (about 25 at.% Pt), Cu-Al-Ni (14.0–14.5 wt.% Al, 3.0–4.5 wt.% Ni), Ag-Cd (44–49 at.% Cd), In-Ti (18–23 at.% Ti), Mn-Cu (5–35 at.% Cu), Fe-Mn-Si, Pt alloys, bone, and human hair. The Ni-Ti alloys are generally more expensive and exhibit superior mechanical properties compared to the copper-based alloys.

Shape memory alloys exhibit pseudoplasticity (Fig. 3.33a), also called superelasticity, which is a phenomenon that gives rise to hysteresis in the stress–strain curve and hence vibration damping ability. The pseudoplasticity is due to the change in the crystal structure A (a phase called austenite) to crystal structure B (a phase called martensite) during loading (i.e., a phase transformation, called the martensitic transformation, that is activated by stress), such that crystal structure B is heavily twinned, thereby allowing a large deformation through twin formation and the growth of favorably oriented twins. The deformation occurs at a temperature where structure A is the thermodynamically stable phase. Upon subsequent unloading, the reverse phase transformation (from structure B to structure A) occurs, since structure A is the stable phase. The resulting stress–strain curve is characterized by much hysteresis, as shown in Fig. 3.33a. The stress has a plateau during loading and another plateau during unloading. The unloading plateau is used to provide a controlled stress to dental brace archwire and to bone plates (which are fastened to fractured bones to help the bones heal). Typically, a strain of 10% can be almost fully recovered; of this, about 8% of the strain is due to the stress-induced martensitic transformation while the rest is due to conventional elasticity. A superelastic material does not follow Hooke's Law but exhibits near-constant stress (a plateau) when strained typically between 1.5 and 7%.

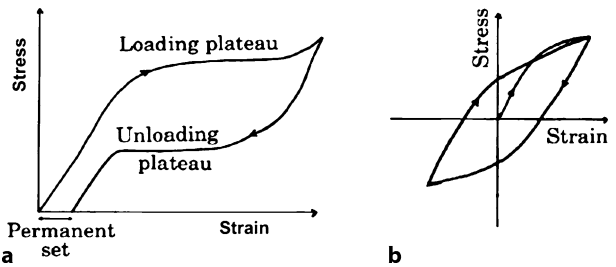

Figure 3.33. **a** The pseudoelastic behavior of a shape memory alloy in the austenite state prior to deformation. **b** The ferroelastic behavior of a shape memory alloy in the martensite state throughout the deformation

A shape memory alloy may also exhibit ferroelasticity, which is illustrated in Fig. 3.33b. In ferroelasticity, the state is martensite in all parts of the stress–strain curve. The martensite deforms quite easily due to its twinned structure, thus providing substantial strain and resulting in a plateau at positive stress values. Subsequent unloading causes partial strain recovery, so that the strain is nonzero when the stress is returned to zero. At this point, the stress crosses the zero line and becomes negative. When the stress is sufficiently negative, the strain returns to zero. With the continued application of stress that is even more negative, the strain becomes negative and results in a plateau at negative stress values. The two plateaux correspond to two directions of twinning. The potential for two directions of twinning is required for the occurrence of ferroelasticity. Subsequent stress cycling follows the hysteresis loop shown in Fig. 3.33b. The large size of the hysteresis loop is attractive for vibration damping.

3.6.4 Interfacial Damping

Another special class of high-damping materials involves the use of nanofillers (e.g., carbon nanofiber) in composites. The nanofiller provides a large filler–matrix interface area. Slight slippage at the interface during vibration absorbs the mechanical energy, thereby resulting in damping. In addition, the difference between the phonon velocities (i.e., the velocity of propagation of lattice vibration waves, akin to the speed of sound) in the components on the two sides of an interface causes phonon scattering at the interface. The scattering provides an additional mechanism of energy dissipation. At the same time, the nanofiller may increase the modulus, thereby stiffening the material. A high stiffness is valuable for vibration reduction. Thus, the nanofiller addition can cause increases in both the damping capacity and the stiffness. In contrast, the use of a viscoelastic component, such as a rubber sheet, to enhance damping suffers from the low stiffness of the viscoelastic component.

3.6.5 Structural Materials for Damping

The use of a structural material (such as a fiber composite) with substantial stiffness for damping should be distinguished from the use of a viscoelastic material (such as rubber) with a low stiffness for damping. Due to the low stiffness, the latter route can only involve a minor amount of the viscoelastic material. However, in the former route, the damping material can constitute the whole of the structure. Even though the damping capacity (loss tangent) of a structural material of high stiffness tends to be small compared to that of a viscoelastic material of low stiffness, the structural material can be highly effective for damping due to the large volume of structural material in the structure. Furthermore, a structural material is advantageous due to its relatively high durability.

The tailoring of a structural material for damping can involve three methods. One method is associated with the attachment (bonding) or embedding of a viscoelastic material of low stiffness to or into the structural material. In the case

of embedding, this method suffers from a decrease in stiffness of the structural material due to the low stiffness of the embedded viscoelastic material. The greater the proportion of the viscoelastic material, the lower the modulus (i.e., the storage modulus) and the higher the damping capacity (i.e., the loss tangent) of the structural material. In the case of attachment, this method suffers from a tendency for detachment and damage of the viscoelastic material.

The second method is associated with a large area of interfaces per unit volume in the structural material. Slight slippage at the interface during vibration provides a mechanism of energy dissipation. In addition, the difference in the phonon velocities in the components on the two sides of an interface causes phonon scattering at the interface, thereby providing an additional mechanism of energy dissipation. The fillers that give rise to the interfaces may or may not strengthen the material. When the filler strengthens the material, both the storage modulus and the loss tangent can be enhanced at the same time. This contrasts with the first method, which results in an increase in loss tangent but a decrease in the storage modulus. An example of a high-damping metal alloy is gray cast iron (named after its gray fracture surface), which is an iron–carbon alloy that naturally contains graphite flakes and has a composition at or near the eutectic composition (4.3 wt.% C) in the iron-carbon binary phase diagram. The carbon content of cast iron is much higher than that of steel. The phonon velocity is much higher in graphite than in iron due to the low mass of the carbon atom compared to that of the iron atom. As a result, phonons are scattered at the interface between graphite and iron, thereby causing cast iron to be effective at damping. Cast iron with coarse graphite flakes is more effective for damping than that with fine graphite flakes. The damping capacity of gray cast iron is around a hundredfold higher than that of eutectoid steel. Due to its high damping capacity, cast iron is widely for machine bases and supports, engine cylinder blocks and brake components.

The third method is associated with the imperfections (such as dislocations, twin boundaries, grain boundaries, phase boundaries, precipitates, cracks, etc.) in the structural material, as slight slippage at these imperfections provides a mechanism of energy dissipation. Imperfections (e.g., dislocations) that enhance both the storage modulus and the loss tangent are more attractive than those (e.g., cracks) that enhance the loss tangent while decreasing the storage modulus. This method is most applicable to metals, which can have a large density of microscopic imperfections.

Alloys for vibration damping include those based on iron (e.g., cast iron, steel, Fe-Ni-Mn, Fe-Al-Si, Fe-Al, Fe-Cr, Fe-Cr-V, Fe-Mn, and Fe-Mn-Co), aluminum (e.g., Al-Ge, Al-Co, Al-Zn, Al-Cu, Al-Si, alloys 6,061, 2,017, 7,022 and 6,082), zinc (e.g., Zn-Al), lead, tin (e.g., Sn-In), titanium (e.g., Ti-Al-V, Ti-Al-Sn-Zr-Mo, and Ti-Al-Nb-V-Mo), nickel (e.g., superalloys, Ni_3Al and NiAl), zirconium (e.g., Zr-Ti-Al-Cu-Ni), copper (e.g., Cu-Al-Zn-Cd), and magnesium (e.g., Mg-Ca). In addition, metal-matrix composites (e.g., Al/SiC_p, Al/graphite$_p$, Mg/carbon$_f$, NiAl/AlN, and Al-Cu/Al_2O_3, where the subscript "p" means particles and the subscript "f" means fibers), and metal laminates (e.g., Fe/Cu) have attractive damping abilities. In general, it is customary to abbreviate a composite with the matrix indicated first,

followed by a slash and then the filler. For example, an aluminum-matrix composite containing SiC is abbreviated to Al/SiC.

The addition of silica fume (nanoparticles) as an admixture in the cement mix results in a large interfacial area and hence a significant increase in the damping capacity. The addition of latex as an admixture also enhances damping due to the viscoelastic nature of latex. The addition of sand or short 15 μm-diameter carbon fibers to the mix does not aid the damping due to the large unit size of these components and the relatively high damping associated with the inherent inhomogeneity within cement paste.

3.6.6 Comparison of Materials Utilized for Damping

Due to the differences between the testing methods and specimen configurations used by different researchers, quantitative comparisons of the damping capacities of the numerous materials mentioned in this section are difficult to perform. Nevertheless, Table 3.6 provides a comparison of representative materials (including polymers, metals, cement-based materials and metal-matrix and polymer-matrix composites) that were all tested in the author's laboratory using the same method and equipment.

Table 3.6 shows a comparison of the dynamic flexural behavior of various engineering materials, all tested at a loading frequency of 0.2 Hz. These materials include polymers, metals, cement-based materials, and metal-matrix and polymer-matrix composites. Among these classes of materials, polymers give the highest

Table 3.6. Dynamic flexural behavior of materials at 0.2 Hz (from [4])

Material	$\tan\delta$	Storage modulus (GPa)	Loss modulus (GPa)
Cement paste (plain)	0.016	13.7	0.22
Mortar (plain)	$< 10^{-4}$	9.43	< 0.001
Mortar with silica fume (treated) (15% by mass of cement)	0.021	13.11	0.28
Aluminum, pure	0.019	51	1.0
Al/AlN_p (58 vol%)	0.025	120	3.0
Zn-Al	0.021	74	1.5
Zn-Al/SiC_w (27 vol%)	0.032	99	3.0
Carbon-fiber epoxy-matrix composite (without interlayer)	0.008	101	0.8
Carbon fiber epoxy-matrix composite (with vibration-damping interlayer)	0.017	92	1.6
Neoprene rubber	0.67	0.0075	0.0067
PTFE	0.189	1.2	0.23
PMMA	0.09	3.6	0.34
PA-66	0.04	4.4	0.19
Acetal	0.03	3.7	0.13
Epoxy	0.03	3.2	0.11

damping capacity ($\tan\delta$), whereas metals give the highest loss modulus. The high damping capacity of polymers is due to the ease of movement of side chains, side groups, functional groups, chain segments, and even entire molecules in the polymers.

Although cement-based materials have less damping capacity than polymers, the loss modulus is comparable (except for plain mortar). Continuous carbon fiber polymer-matrix composites have the worst damping capacities, but their loss moduli are as high as those of metals if a vibration damping interlayer is used in the composite.

Neoprene rubber exhibits an outstandingly high value of $\tan\delta$, but its storage modulus is outstandingly low, so that its loss modulus is almost the lowest of all the materials in Table 3.6. Among the thermoplastics, namely polymethylmethacrylate (PMMA), polytetrafluoroethylene (PTFE), polyamide-66 (PA-66) and acetal, PMMA exhibits the highest loss modulus (partly due to the hydrogen bonding, which restricts movement, thereby decreasing $\tan\delta$ and increasing the storage modulus), while PTFE exhibits the highest loss tangent (due to the presence of fluorine atoms and the helical coil morphology of PTFE molecules). Epoxy (a thermoset) and acetal exhibit the lowest loss tangent among the polymers listed in Table 3.6.

The loss tangent of cement paste (even the plain one, i.e., no admixture at all) is comparable to those of aluminum and carbon fiber epoxy-matrix composites, although the storage modulus is lower. Thus, cement paste itself has a high damping capacity, even without admixtures. The addition of sand to cement paste results in mortar, which exhibits a very low damping capacity. However, the addition of silica fume (nanoparticles) to the mortar greatly increases the damping capacity, due to the increased interface area, thereby bringing the loss tangent back to the level of cement paste.

The carbon fiber epoxy-matrix composite without an interlayer shows poorer damping than pure aluminum. However, the use of a carbon nanofiber (also called carbon filament, of diameter 0.1 μm) interlayer in the composite increases the damping capacity such that it is comparable to that of pure aluminum. On the other hand, the storage modulus is much higher for composites than for pure aluminum. As a result, the loss modulus is higher for a composite with an interlayer than it is for pure aluminum.

A comparison between Al (aluminum), Al/AlN_p (aluminum reinforced with aluminum nitride particles), Zn-Al (zinc-aluminum alloy), and Zn-Al/SiCw (zinc-aluminum alloy reinforced with silicon carbide whiskers) shows that composite formation increases both loss tangent and storage modulus. However, the comparison of Al and Zn-Al shows that alloying also increases both quantities. Alloying is much less expensive than composite formation.

The loss modulus is lower for cement-based materials than for metal-based and polymer-based materials due to the low storage modulus of cement-based materials. Damping enhancement mainly involves microstructural design for metals, interface design for polymers, and admixture use for cement.

In general, the loss tangent, elastic modulus and loss modulus are properties that vary with temperature for a given material. For example, for a thermoplastic

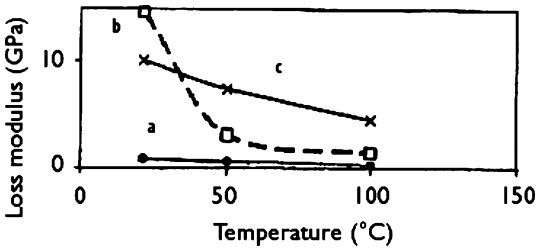

Figure 3.34. Effect of temperature on the loss moduli of continuous carbon fiber thermoplastic-matrix composites (longitudinal configuration) at 0.2 Hz. *a* Composite without interlayer (*solid circles*). *b* Composite with viscoelastic interlayer (*squares*). *c* Composite with treated carbon nanofiber interlayer (*crosses*). (From [5])

polymer, softening upon heating increases the loss tangent but decreases the elastic modulus. Thus, the loss tangent is relatively high, but the elastic modulus is relatively low after softening; whereas the loss modulus is relatively high, but the loss tangent is relatively low before softening.

In relation to fibrous structural composites, viscoelastic polymeric interlayers between the laminae of continuous fibers are often used for damping. However, the presence of the interlayer degrades the stiffness of the composite, particularly when the temperature is high (e.g., 50°C). The use of carbon nanofiber (0.1 μm in diameter; also called carbon filament) in place of the viscoelastic interlayer alleviates this problem and is particularly attractive when the temperature is high. Figure 3.34 shows the loss moduli of continuous carbon fiber polymer-matrix composites. The composite with the viscoelastic interlayer exhibits a higher value of the loss modulus than that with the composite with a nanofiber interlayer at 25°C, but the reverse occurs at 50°C. Both composites are superior to the composite without an interlayer. The large interfacial area between the nanofiber and the polymer matrix contributes to damping.

3.6.7 Emerging Materials for Damping

The damping ability of a Material is described by (i) the loss tangent (two times the damping ratio), which describes the rate of decay of the vibration amplitude and (ii) the loss modulus (the storage modulus times the loss tangent), which describes the energy dissipation ability. Both attributes should be high for effective damping. A figure of merit is the product of the loss tangent and the square root of the elastic modulus.

Damping materials fall into four categories: (i) materials exhibiting high loss modulus but low loss tangent (such as cast iron, metal-matrix composites [6–8], shape-memory alloys [9–12] and acrylic impregnated ceramics [13]), (ii) materials exhibiting high loss tangent but low loss modulus (such as rubber and other polymers [14, 15]), (iii) materials exhibiting low values of both loss tangent and loss modulus (such as quartz particle filled epoxy [16], short carbon fiber filled nylon [17], interpenetrating polymer networks [18], hot-compacted polyethylene/polypropylene [19] and short jute fiber filled polymer blend [20]),

Table 3.7. Emerging damping materials

Material	Storage modulus (GPa)	Loss tangent	Loss modulus (GPa)	Figure of merit ($GPa^{1/2}$)†
Graphite network cement-matrix composite [21]	9.26	0.811	7.502	2.47
Nanoscale Cu-Al-Ni shape-memory alloy [9]	22.06	0.196	4.43	0.93
Tungsten (95%) with In-Sn [9]	161	0.05	8.1	0.63
Acrylic impregnated ceramic [13]	60	0.04	2.4	0.31
Quartz particle filled epoxy [16]	3	0.15	0.45	0.26
Short carbon fiber filled nylon [17]	13	0.05	0.7	0.2
Hot-compacted polyethylene/polypropylene [19]	5.4	0.083	0.45	0.19
Interpenetrating polymer networks [18]	0.13	0.3	0.040	0.11
Short jute fiber filled polymer blend [20]	1	0.1	1	0.1

† Defined as the product of the loss tangent and the square root of the elastic modulus.

and (iv) materials exhibiting high values of both loss tangent and loss modulus (graphite network cement-matrix composite containing 8 vol.% graphite [21]). Table 3.7 lists emerging damping materials that represent the state of the art. The cement-matrix composite that provides the top performance contains a graphite network that is formed by compressing exfoliated graphite. The shear deformation ability (somewhat like rubber) of the graphite network enables the loss tangent to be high, while the stiff cement matrix provides a high storage modulus.

Example Problems

1. Calculate the elastic modulus of a composite material containing unidirectional continuous fiber at a volume fraction of 57%. The modulus of the fiber is 680 GPa. The modulus of the matrix is 1.45 GPa. Assume perfect bonding between the fiber and the matrix.

   Solution:

   $$\text{Modulus} = (0.43)(1.45\,\text{GPa}) + (0.57)(680\,\text{GPa}) = 390\,GPa\ .$$

   Note that the contribution of the matrix to the composite modulus is negligible due to the low modulus of the matrix.

2. A viscoelastic material exhibits a shear storage modulus of 27 kPa and a shear loss modulus of 3.4 kPa. Calculate the value of tan δ.

   Solution:

   $$\tan\delta = 3.4/27 = 0.13\ .$$

3. A viscoelastic material is subjected to a shear stress wave. The magnitude of the shear stress wave is 570 kPa. The magnitude of the resulting shear strain wave is 1.5%. Calculate the magnitude of the shear modulus.

   Solution:
   From Eq. 3.35,

$$\text{Shear modulus} = 570\,\text{kPa}/(1.5\%) = \textit{38 MPa}\ .$$

4. A viscoelastic material exhibits shear modulus of magnitude 350 kPa. The loss tangent is 0.65. Calculate the storage modulus and the loss modulus.

   Solution:

$$\tan\delta = 0.65$$
$$\delta = 33^\circ\ .$$

   From Eq. 3.39,

$$\text{Storage modulus} = (350\,\text{kPa})(\cos 33^\circ) = 290\,\text{kPa}\ .$$

   From Eq. 3.40,

$$\text{Loss modulus} = (350\,\text{kPa})(\sin 33^\circ) = \textit{190 kPa}\ .$$

Review Questions

1. What is meant by damping such that the damping ratio is equal to 1?
2. What is the difference between plastic viscosity and apparent viscosity?
3. What is the cause of double yielding in a carbon black paste?
4. What is the effect of antioxidants on the viscoelastic behavior of a carbon black paste?
5. Why is the addition of carbon nanofiber to the interlaminar interface of a carbon fiber (continuous) polymer-matrix composite able to enhance the vibration damping ability of the composite?
6. Why are the steel rebars used to reinforce concrete typically placed on the tension side of a concrete beam?

References

[1] S. Wen and D.D.L. Chung, "Electrical-Resistance-Based Damage Self-Sensing in Carbon Fiber Reinforced Cement", *Carbon* 45(4), 710–716 (2007).

[2] X. Fu, W. Lu and D.D.L. Chung, "Ozone Treatment of Carbon Fiber for Reinforcing Cement," *Carbon* 36(9), 1337–1345 (1998).

[3] Chuangang Lin and D.D.L. Chung, "Graphite Nanopletelet Pasts versus Carbon Black Pastes as Thermal Interface Materials,"*Carbon* 47(1), 295–305 (2009).

[4] D.D.L. Chung, "Materials for Vibration Damping", *J. Mater. Sci.* 36(24), 5733–5738 (2001).

[5] M. Segiet and D.D.L. Chung, "Discontinuous Surface-Treated Submicron-Diameter Carbon Filaments as an Interlaminar Filler in Carbon Fiber Polymer-Matrix Composites for Vibration Reduction", *Compos. Interfaces* 7(4), 257–276 (2000).

[6] H. Lu, X. Wang, T. Zhang, Z. Cheng and Q. Fang, "Design, fabrication, and Properties of High Damping Metal Matrix Composites – a Review," *Materials* 2(3), 958–977 (2009).

[7] S.C. Sharma, M. Krishn, A. Shashishankar and S.P. Vizhian, "Damping Behavior of Aluminium/Short Glass Fibre Composites," *Mater. Sci. Eng*. A364(1–2), 109–116 (2004).

[8] W.G. Wang, C. Li, Y.L. Li, X.P. Wang and Q.F. Fang, "Damping Properties of $Li_5La_3Ta_2O_{12}$ Particulates Reinforced Aluminum Matrix Composites," *Mater. Sci. Eng*. A518(1–2), 190–193 (2009).

[9] J. San Juan J, M.L. No and C.A. Schuh, "Nanoscale Shape-Memory Alloys for Ultrahigh Mechanical Damping," *Nature Nanotechnology* 4(7), 415–419 (2009).

[10] I. Schmidt and R. Lammering, "The Damping Behavior of Superelastic NiTi Components," *Mater. Sci. Eng*. A378(1–2), 70–75 (2004).

[11] M.L. Corro, S. Kustov, E. Cesari and Y.I. Chumlyakov, "Magnetomechanical Damping in Ni-Fe-Ga Poly and Single Crystals," *Mater. Sci. Eng*. A 521–2, 201–204 (2009).

[12] G.A. Lopez, M. Barrado, J. San Juan and M.L. No, "Mechanical Spectroscopy Measurements on SMA High-Damping Composites," *Mater. Sci. Eng.* A521–2, 359–362 (2009).

[13] T. Shimazu, H. Maeda, E.H. Ishida, M. Miura, N. Isu, A. Ichikawa and K. Ota, "High-Damping and High-Rigidity Composites of Al_2TiO_5-$MgTi_2O_5$ Ceramics and Acrylic resin," *J. Mater. Sci.* 44, 93–101 (2009).

[14] D.D. Andjelkovic, Y. Lu, M.R. Kessler and R.C. Larock, "Novel Rubbers from the Cationic Copolymerization of Soybean Oils and Dicyclopentadiene, 2 – Mechanical and Damping Properties," *Macromolecular Materials and Engineering* 294(8), 472–483 (2009).

[15] Q. Liu, X. Ding, H. Zhang and X. Yan, "Preparation of High-Performance Damping Materials Based on Carboxylated Nitrile Rubbers: Combination of Organic Hybridization and Fiber Reinforcement," *J. Appl. Polymer. Sci*. 114(5), 2655–2661 (2009).

[16] S.N. Goyanes, P.G. Konig and J.D. Marconi, "Dynamic Mechanical Analysis of Particulate-Filled Epoxy Resin," *J. Appl. Polymer. Sci*. 88, 883–892 (2003).

[17] S. Senthilvelan and R.Gnanamoorthy, "Damping Characteristics of Unreinforced, Glass and Carbon Fiber Reinforced Nylon 6/6 Spur Gears," *Polymer Testing* 25:56–62 (2006).

[18] N.V. Babkina, Y.S. Lipatov and T.T. Alekseeva, "Damping Properties of Composites Based on Interpenetrating Polymer Networks Formed in the Presence of Compatibilizing Additives," *Mechanics of Composites Materials* 42(4), 385–392 (2006).

[19] M.J. Jenkins, P.J. Hine, J.N. Hay and I.M. Ward, "Mechanical and Acoustic Frequency Responses in Flat Hot-Compacted Polyethylene and Polypropylene Panels," *J. Appl. Polymer. Sci*. 99:2789–2796 (2006).

[20] G. Sarkhel and A. Choudhury, "Dynamic Mechanical and Thermal Properties of PE-EPDM Based Jute Fiber Composites," *J. Appl. Polymer Sci*. 108, 3442–3453 (2008).

[21] S. Muthusamy, S.Wang and D.D.L. Chung, "Unprecedented Vibration Damping with High Values of Loss Modulus and Loss Tangent, Exhibited by Cement-Matrix Graphite Network Composite," *Carbon* (2010), in press.

Further Reading

D.D.L. Chung, "Structural Composite Materials Tailored for Damping", *J. Alloy. Compd.* 355(1/2), 216–223 (2003).

W. Fu and D.D.L. Chung, "Vibration Reduction Ability of Polymers, Particularly Polymethylmethacrylate and Polytetrafluoroethylene", *Polym. Polym. Compos.* 9(6), 423–426 (2001).

4 Durability and Degradation of Materials

This chapter addresses the durability and degradation of materials, particularly composite materials. The mechanisms of degradation and methods of enhancing durability are covered.

4.1 Corrosion Resistance

Corrosion resistance is important for any structural material, as it tends to degrade the mechanical properties and limit the service life of a component. The most common example of corrosion is the rusting of iron or steel, such as that found in a car body.

Corrosion can involve either direct chemical attack or an electrochemical reaction (a reaction which involves electrons in each of two half-reactions, the sum of which is the overall reaction). Direct chemical attack occurs in the presence of a species that reacts with the structural material. An example is the reaction of copper with molten tin to form a copper-tin compound (e.g., Cu_3Sn). This reaction is of concern to the electronic industry due to the common use of tin-lead solder to make electrical connections, and the common use of copper wires. During soldering, the tin part of the molten solder reacts with the copper, thus causing the soldered joint to become insufficiently reliable. Electrochemical corrosion occurs under the conditions in which an electrochemical reaction can occur, as explained below. In either case, corrosion commonly starts to occur at the surface of the material, so surface modification is a common method of corrosion protection.

This section focuses on corrosion that involves electrochemical reactions. The aim is to understand the cause of corrosion, thus allowing us to control or prevent it.

4.1.1 Introduction to Electrochemical Behavior

Electrochemical behavior pertains to chemical processes brought about by the movement of charged species (ions and electrons) under the influence of an electric field. It occurs when there are ions that can move in a medium (liquid or solid) due to an electric field (i.e., a voltage gradient). The positive ions (cations) move toward the negative end of the voltage gradient, while the negative ions (anions)

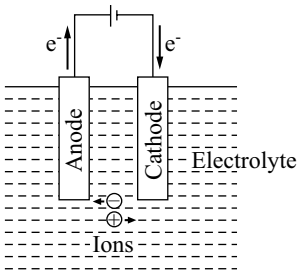

Figure 4.1. Flow of electrons in the outer circuit from the anode to the cathode, and the flows of cations (positive ions) toward the cathode and anions (negative ions) toward the anode in the electrolyte, in response to the applied voltage (which is positive at the anode)

move toward the positive end of the voltage gradient (Fig. 4.1). The medium containing the movable ions is called the electrolyte, which is an ionic conductor. The electrolyte must be an electronic insulator in order to avoid electrically shorting the anode and cathode through the intervening electrolyte. The electrical conductors that are placed in contact with the electrolyte in order to apply the electric field are called the electrodes. The electrode at the positive end of the voltage gradient is called the positive electrode or the anode. The electrode at the negative end of the voltage gradient is called the negative electrode or the cathode. The electrodes must be sufficiently inert so that they do not react with the electrolyte. In order to apply the electric field, the electrodes are connected to a DC power supply (or a battery) such that the cathode is connected to the negative end of the power supply (so that the cathode becomes negative) and the anode is connected to the positive end of the battery (so that the anode becomes positive). In this way, electrons flow in the electrical leads (the outer circuit) from the anode to the cathode, while ions flow in the electrolyte. The electron flow in the outer circuit and the ion flow in the electrolyte constitute loops of charge flow. Note that the anions flow from cathode to anode in the electrolyte while the electrons flow from anode to cathode in the outer circuit, and that both anions and electrons are negatively charged. The electron flow in the outer circuit constitutes an electric current that can be measured using a meter. The current is defined as the amount of charge that flows per unit time (i.e., ampere = coulomb per second).

At the anode, a chemical reaction that gives away one or more electrons occurs. In general, a reaction involving the loss of one or more electrons is known as an oxidation reaction. The electron lost through this reaction supplies the anode with the electron to release to the outer circuit. An example of an oxidation (anodic) reaction is

$$\mathrm{Cu} \rightarrow \mathrm{Cu}^{2+} + 2\mathrm{e}^{-} , \tag{4.1}$$

where Cu is the anode, which is oxidized to Cu^{2+}, thereby becoming corroded and releasing two electrons to the outer circuit. The Cu^{2+} ions formed remain in the electrolyte, while the electrons pass through the anode (which must be electrically conducting) to the outer circuit.

At the cathode, a chemical reaction that takes one or more electrons from the cathode occurs. In general, a reaction involving the gain of one or more electrons is known as a reduction reaction. The electron gained through this reaction is supplied to the cathode (which must be electrically conducting) by the outer circuit. Oxidation always occurs at the anode and reduction always occurs at the cathode.

The product of the reduction reaction at the cathode may be a species coated on the cathode, as in the electroplating of copper, where the reduction (cathodic) reaction is

$$Cu^{2+} + 2e^- \rightarrow Cu\ , \tag{4.2}$$

and Cu^{2+} is the cation in the electrolyte. Cu is the product of the reduction reaction and is the species electroplated on the cathode. The product of the reduction reaction may be OH^- ions, as in the case when oxygen and water are present (a very common situation); i.e.,

$$O_2 + 2H_2O + 4e^- \rightarrow 4OH^-\ . \tag{4.3}$$

The product of the reaction may be H_2 gas, as in the case when H^+ (in an acid) ions are present; i.e.,

$$2H^+ + 2e^- \rightarrow H_2 \uparrow\ . \tag{4.4}$$

The product of the reaction may be H_2 gas together with OH^- ions, as in the case when H_2O is present without O_2 (an anaerobic condition); i.e.,

$$2H_2O + 2e^- \rightarrow H_2 \uparrow + 2OH^-\ . \tag{4.5}$$

The product of the reaction may be water, as in the case when O_2 and H^+ (an acid) are present; i.e.,

$$O_2 + 4H^+ + 4e^- \rightarrow 2H_2O\ . \tag{4.6}$$

Which of the five cathodic reactions described above takes place depends on the chemical species present. The most common of the five reactions is (4.3), as oxygen and water are present in most environments. The variety of cathodic reactions is much greater than that of anodic reactions.

The anodic and cathodic reactions together comprise the overall reaction. For example, anodic reaction 4.1 and cathodic reaction 4.3 together become

$$\begin{aligned} 2Cu &\rightarrow 2Cu^{2+} + 4e^- \\ O_2 + 2H_2O + 4e^- &\rightarrow 4OH^- \\ \hline 2Cu + O_2 + 2H_2O &\rightarrow 2Cu^{2+} + 4OH^- \end{aligned}\ . \tag{4.7}$$

A Cu^{2+} ion and two OH^- ions formed by the overall reaction react to form copper hydroxide [$Cu(OH)_2$], which resides in the electrolyte.

The rusting of iron involves similar reactions; i.e.,

$$Fe \rightarrow Fe^{2+} + 2e^{-} , \tag{4.8}$$

$$O_2 + 2H_2O + 4e^{-} \rightarrow 4OH^{-} . \tag{4.9}$$

The resulting Fe^{2+} and OH^{-}ions react to form ferrous hydroxide [$Fe(OH)_2$], which is water soluble. Subsequent oxidation causes ferrous hydroxide to change to ferric hydroxide [$Fe(OH)_3$] according to the reaction

$$2Fe(OH)_2 + \tfrac{1}{2}O_2 + H_2O \rightarrow 2Fe(OH)_3 . \tag{4.10}$$

Ferric hydroxide is not water soluble and thus forms a precipitate. This precipitate is the rust.

Both the anode and the cathode must be electrically conducting, but they do not have to participate in the anodic or cathodic reactions. In anodic reaction 4.1 the anode (Cu) acts as the reactant, but the cathodic reactions 4.2–4.6 do not involve the cathode. Thus, the cathode is usually a platinum wire or some other electrical conductor that does not react with the electrolyte.

The electrolyte must permit ionic movement within it. It is usually a liquid, although it can be a solid. For the cathodic reaction (4.2) to occur, the electrolyte must contain Cu^{2+} ions (e.g., a copper sulfate or $CuSO_4$ solution). For the cathodic reaction 4.4 to occur, the electrolyte must contain H^{+} ions (e.g., a sulfuric acid or H_2SO_4 solution). The anodic reaction occurs at the interface between the anode and the electrolyte; the cathodic reaction occurs at the interface between the cathode and the electrolyte. The ions that are either reactants (e.g., H^{+} in reaction 4.4) or reaction products (e.g., OH^{-} in reaction 4.3) must move to or from the electrode/electrolyte interface.

Whether an electrode ends up being the anode or the cathode depends on the relative propensity for oxidation and reduction at each electrode. The electrode at which oxidation has a higher propensity than at the other electrode becomes the anode and the other electrode becomes the cathode. This propensity depends on the types and concentrations of the chemical species present.

Different species have different propensities to be oxidized. For example, iron ($Fe \rightarrow Fe^{2+} + 2e^{-}$) has more of a propensity for oxidation than copper ($Cu \rightarrow Cu^{2+} + 2e^{-}$) when the Fe^{2+} and Cu^{2+} ions in the electrolyte are present at the same concentration, so when Fe and Cu are the electrodes and the Fe^{2+} and Cu^{2+} ion concentrations are the same in the electrolyte, Fe will become the anode and Cu will become the cathode (Fig. 4.2). Fe and Cu constitute a galvanic couple, and this setup constitutes a galvanic cell or a composition cell. The anodic reaction will be $Fe \rightarrow Fe^{2+} + 2e^{-}$, while the cathodic reaction will be (4.2), (4.3), (4.4), (4.5) or (4.6), depending on the relative propensity for these competing reduction reactions.

The concentrations of the species also affect the propensity. In general, high concentrations of the reactants increase the propensity for a reaction, and high concentrations of the reaction products decrease the propensity for a reaction. This is known as Le Chatelier's principle. Thus, a high concentration of Cu^{2+} in the electrolyte increases the propensity for reaction 4.2. When both electrodes

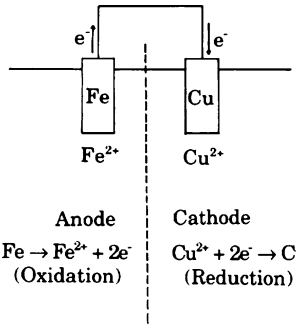

Figure 4.2. Composition cell with Fe acting as the anode and Cu as the cathode. Note that electrons and ions flow without the need for an applied voltage between anode and cathode

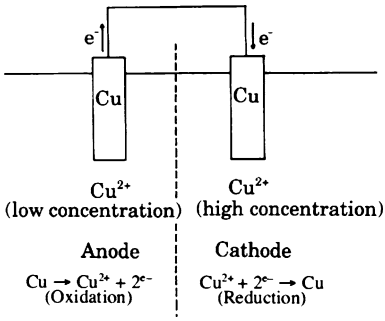

Figure 4.3. Concentration cell with Cu electrodes, a low Cu^{2+} concentration on the anode side and a high Cu^{2+} concentration on the cathode side

are made from copper but the Cu^{2+} concentrations are different in the vicinities of the two electrodes, then the electrode with the higher Cu^{2+} ion concentration will become the cathode (i.e., it has a higher propensity for reaction 4.2, which is the cathodic reaction) and the electrode with the lower Cu^{2+} ion concentration will become the anode (i.e., it has a higher propensity for reaction 4.1, which is the anodic reaction) (Fig. 4.3). This setup involving a difference in concentrations constitutes a concentration cell. Similarly, when both electrodes are copper but the O_2 concentrations are different in the vicinities of the two electrodes (Fig. 4.4), then the electrode with the higher O_2 concentration will become the cathode (i.e., it has a higher propensity for reaction 4.3, which is the cathodic reaction) and the electrode with the lower O_2 concentration will become the anode (i.e., it has a lower propensity for reaction 4.3, forcing the electrode to become the anode, with reaction 4.1 being the anodic reaction). A difference in oxygen concentration is commonly encountered, since oxygen comes from the air and access to the air can vary. Therefore, a concentration cell involving a difference in O_2 concentration is particularly common and is called an oxygen concentration cell. For example, a piece of copper covered with a patch of dirt (Fig. 4.5) is an oxygen concentration cell, because the part of the copper covered by the dirt has restricted access to the air and becomes the anode

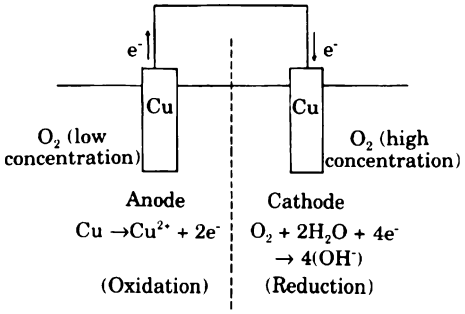

Figure 4.4. Oxygen concentration cell with Cu electrodes, a low O_2 concentration on the anode side and a high O_2 concentration on the cathode side

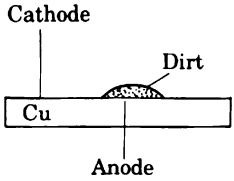

Figure 4.5. A piece of copper partially covered by dirt is an oxygen concentration cell

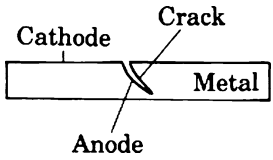

Figure 4.6. A piece of metal with a crack is an oxygen concentration cell

(with anodic reaction 4.1), thus forcing the uncovered part of the copper to be the cathode (with cathodic reaction 4.3). Hence, the covered part becomes corroded. Similarly, a piece of metal (an electrical conductor) that has a crack in it (Fig. 4.6) is an oxygen concentration cell, because the part of the metal at the crack has restricted access to the air and becomes the anode (with anodic reaction 4.1), thus forcing the part of the metal that is exposed to open air to be the cathode.

When the two electrodes are open-circuited at the outer circuit, a voltage (called the open-circuit voltage) exists between the two electrodes. This voltage describes the difference in the propensity for oxidation between the two electrodes, so it is considered the driving force for the cathodic and anodic reactions that occur when the electrodes are short circuited at the outer circuit. The greater the difference in oxidation propensity, the higher the open-circuit voltage. This is the same principle as that used in batteries, which provide a voltage as the output. Because the voltage pertains to the difference between a pair of electrodes, it is customary to describe the voltage of any electrode relative to the same electrode. In this way, each electrode is associated with a voltage, and a scale is established for ranking

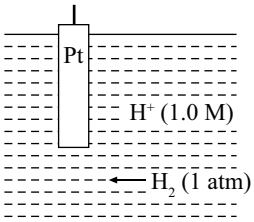

Figure 4.7. The standard hydrogen reference half-cell

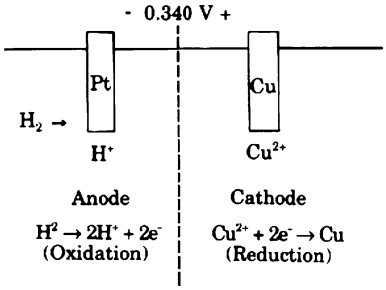

Figure 4.8. A cell with a copper cathode and a hydrogen half-cell anode under open-circuit conditions. The open circuit voltage is 0.340 V – positive at the cathode

various electrodes in terms of their oxidation propensities. The electrode that serves as the reference involves the oxidation reaction

$$H_2 \rightarrow 2H^+ + 2e^- \tag{4.11}$$

such that the H_2 gas is at a pressure of 1 atm, the H^+ ion concentration in the electrolyte is 1.0 M (1 M = 1 molar = 1 mol/l), and the temperature is 25°C. In this reference, the electrode does not participate in the reaction, so it only needs to be an electrical conductor. Therefore, platinum is used. The platinum electrode is immersed in the electrolyte and H_2 gas is bubbled through the electrolyte, as illustrated in Fig. 4.7. The electrode in Fig. 4.7 is called the standard hydrogen reference half-cell (half of a cell). Copper has a lower oxidation propensity (when the Cu^{2+} ion concentration is 1 M and the temperature is 25°C) than this reference half-cell, such that the open-circuit voltage is 0.340 V and the positive end of the voltage occurs at the cathode, which is copper (Fig. 4.8). The positive end of the open-circuit voltage occurs at the cathode because the anode has a higher oxidation propensity than the cathode and it wants to release electrons into the outer circuit, which cannot accept the electrons due to the open circuit situation. The standard electrode potential for copper is thus +0.340 V. Table 4.1 ranks the electrodes in terms of their standard electrode potentials, which is known as the standard electromotive force (emf) series. Note that these rankings are for an ion concentration of 1 M and a temperature of 25°C. If the ion concentration or the temperature is changed, the rankings can differ from those shown in the table. The ion concentrations are fixed in this table in order to allow a fair comparison between the various substances. The higher the rank of the electrode in Table 4.1, the more

Table 4.1. The standard electromotive force (emf) series

	Electrode reaction	Standard electrode
Increasingly inert (cathodic)	$Au^{3+} + 3e^- \rightarrow Au$	+1.420
	$O_2 + 4H^+ + 4e^- \rightarrow 2H_2O$	+1.229
	$Pt^{2+} + 2e^- \rightarrow Pt$	~ +1.2
	$Ag^+ + e^- \rightarrow Ag$	+0.800
	$Fe^{3+} + e^- \rightarrow Fe^{2+}$	+0.771
	$O_2 + 2H_2O + 4e^- \rightarrow 4OH^-$	+0.401
	$Cu^{2+} + 2e^- \rightarrow Cu$	+0.340
	$2H^+ + 2e^- \rightarrow H_2$	0.000
	$Pb^{2+} + 2e^- \rightarrow Pb$	−0.126
	$Sn^{2+} + 2e^- \rightarrow Sn$	−0.136
	$Ni^{2+} + 2e^- \rightarrow Ni$	−0.250
	$Co^{2+} + 2e^- \rightarrow Co$	−0.277
	$Cd^{2+} + 2e^- \rightarrow Cd$	−0.403
	$Fe^{2+} + 2e^- \rightarrow Fe$	−0.440
	$Cr^{3+} + 3e^- \rightarrow Cr$	−0.744
	$Zn^{2+} + 2e^- \rightarrow Zn$	−0.763
	$Al^{3+} + 3e^- \rightarrow Al$	−1.662
	$Mg^{2+} + 2e^- \rightarrow Mg$	−2.363
Increasingly active (anodic)	$Na^+ + e^- \rightarrow Na$	−2.714
	$K^+ + e^- \rightarrow K$	−2.924

cathodic it is. The lower the rank of the electrode in Table 4.1, the more anodic it is. For example, from Table 4.1, Fe is cathodic relative to Zn, and the open-circuit voltage between Fe and Zn electrodes (called the overall cell potential) is

$$[(-0.440) - (-0.763)]\,\mathrm{V} = 0.323\,\mathrm{V}\,,$$

such that the positive end of the voltage is at the Fe electrode (i.e., the negative end of the voltage is at the Zn electrode; Fig. 4.9).

The open-circuit voltage corresponds to the situation where there is zero current in the outer circuit that connects the anode and the cathode. This means that

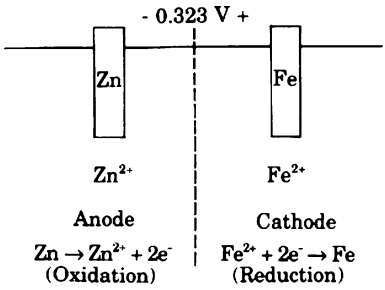

Figure 4.9. A cell with a zinc anode and an iron cathode under open-circuit conditions. The open-circuit voltage is 0.323 V–positive at the cathode

anode current and the cathode current are equal, due to the fact that the anode and cathode reactions are in equilibrium. Under these conditions, the current at either electrode is known as the corrosion current. The corrosion current divided by the area of the interface between the electrode and the electrolyte is called the corrosion current density.

Note from Fig. 4.9 that the electrolyte in the vicinity of the Fe electrode (i.e., the right-hand compartment of the electrolyte) has Fe^{2+} ions at 1.0 M, while the electrolyte in the vicinity of the Zn electrode (i.e., the left-hand compartment of the electrolyte) has Zn^{2+} ions at 1.0 M. The two compartments are separated by a membrane that allows ions to flow through (otherwise it would be open circuited within the electrolyte) but suppresses the mixing of the electrolytes in the two compartments to a sufficient degree. The anode reaction in Fig. 4.9 is

$$Zn \rightarrow Zn^{2+} + 2e^{-} . \tag{4.12}$$

The cathode reaction is

$$Fe^{2+} + 2e^{-} \rightarrow Fe . \tag{4.13}$$

The overall reaction is

$$Zn + Fe^{2+} \rightarrow Zn^{2+} + Fe . \tag{4.14}$$

The cell of Fig. 4.9 is commonly written as

$$Zn|Zn^{2+}||Fe^{2+}|Fe , \tag{4.15}$$

where Zn and Fe^{2+} are the reactants, Zn^{2+} and Fe are the reaction products, and the vertical lines denote phase boundaries.

As another example, consider zinc versus copper. Zinc has relatively high propensity to act as an anode, whereas copper has relatively low propensity to act as an anode (Table 4.1). Therefore, when zinc and copper are electrically connected, zinc will act as the anode and become corroded, while copper will act as the cathode. The standard electrode potential is the open-circuit voltage between the anode and cathode at room temperature when the ion concentration is 1 M at either electrode; i.e., 1 M Zn^{2+} ions in the electrolyte around the zinc anode and 1 M Cu^{2+} ions in the electrolyte around the copper cathode. Under these conditions, the open-circuit voltage between zinc and copper electrodes is the difference between the standard electrode potentials for the two materials; i.e., $[+0.340-(-0.763)]\,V = 1.103\,V$, with the negative end of the open-circuit voltage occurring at the anode. In general, the greater the open-circuit voltage, the greater the driving force for corrosion, which occurs at the anode.

Electrochemistry is a branch of chemistry that addresses chemical reactions that occur in solution at the interface between an electronic conductor and an ionic conductor (the electrolyte), such that the reactions involve electron transfer between the electrode and the electrolyte. Electrochemistry is central to corrosion, batteries and fuel cells.

4.1.2 Corrosion Protection

Based on the concepts covered in Sect. 4.1.1, a number of methods of corrosion protection can be devised, as described in this section. These methods are important for practical engineering design, as corrosion protection is valuable for almost any product.

If the materials in electrical contact have the same composition, the open-circuit voltage is zero and no corrosion occurs. Thus, an effective method of avoiding corrosion is to avoid the electrical contact of dissimilar conductive materials. For example, steel (an iron-based alloy) bolts should be used to fasten steel plates; brass (a copper-based alloy) bolts should be used to fasten brass plates. The fastening of steel plates using brass bolts will lead to corrosion of the steel plates, since the steel acts as the anode while the brass acts as the cathode (Table 4.1), with electrons moving from the steel to the brass during corrosion, and the Fe^{2+} ions generated by the anodic (oxidation) reaction leaving the steel and entering the surrounding medium (e.g., water).

Within a material, there can be multiple phases, such as the tin-rich solid solution and the lead-rich solid solution that coexist in a tin-lead alloy. These phases are different in composition and are in electrical contact, so they form microscopic corrosion cells. Therefore, a multiphase structure is not attractive for corrosion resistance despite such structures commonly possessing advantageous mechanical properties. This means that, from the perspective of corrosion resistance, a single-phase structure is preferred.

If the dissimilar conductive materials are not in electrical contact, the circuit is open and corrosion cannot occur. This means that another method of avoiding corrosion is to electrically insulate the dissimilar conductive materials from one another. Similarly, a material that is electrically nonconductive (e.g., a typical ceramic or a typical polymer) cannot be corroded due to the resulting open circuit. Metals are conductive, so they are prone to corrosion.

Due to the high anodic character of zinc compared to iron (Table 4.1), iron that is coated with zinc is much more corrosion resistant than iron itself. This is because the presence of zinc forces the iron to be the cathode, while zinc acts as the anode. Corrosion only occurs at the anode. Thus, the iron cannot corrode as long as the zinc is still present; in other words, the zinc does not need to cover the iron completely. However, as the zinc corrodes it is gradually consumed. Therefore, the zinc is known as a sacrificial anode. Steel is iron containing a minor amount of interstitial carbon and optionally some other minor alloying elements too. Zinc-coated steel is known as galvanized steel and is widely used.

The propensity for oxidation also depends on the imperfections in the material. Since imperfections (e.g., dislocations and grain boundaries) are sites of high energy (because the atoms are not at their lowest energy positions), they are sites that have relatively high propensities for oxidation. Thus, a polycrystalline metal tends to get corroded at grain boundaries, which act as the anode, while the interior of each grain acts as a cathode. In other words, in the absence of dissimilarity in composition, a corrosion cell may also occur due to dissimilarity in inherent energy. For the same reason, a deformed metal (e.g., a cold-worked

metal) and an annealed metal that are in electrical contact will form a corrosion cell, with the deformed metal acting as the anode and the annealed metal acting as the cathode. An example is a bent wire, which tends to be corroded at the bend due to the greater deformation at the bend than at the region away from the bend. Therefore, for the sake of corrosion prevention, it is advantageous to avoid using a deformed metal and an annealed metal together, and it is advantageous to use a single-crystalline material rather than a polycrystalline material.

A voltage can be applied between the anode and the cathode at the location of the wire such that the positive end of the voltage is on the anodic side and the negative end of the voltage is on the cathodic side. The positive end attracts electrons. If the applied voltage is sufficient, the electrode that is intended to be the cathode will indeed act as the cathode and hence be protected from corrosion, even though it may be more naturally prone to oxidation than the anode material. Similarly, if the applied voltage is sufficient, the electrode that is intended to be the anode will indeed act as the anode, even though it may be naturally less prone to oxidation than the cathode material. By choosing an anode material that is more noble (less active electrochemically) than the cathode material, the oxidation (corrosion) at the anode is limited, while the cathode cannot undergo corrosion. For example, cast iron is more noble (less active) than steel due to the relatively high carbon content in cast iron. Hence, cast iron can be the anode while steel is the cathode, thus resulting in corrosion protection of the steel, while the loss of material from the cast iron through oxidation is sufficiently slow. Graphite is another possible anode material, as it is very noble (more noble than cast iron). However, the use of a highly noble anode makes the voltage needed to achieve cathodic protection rather high, since the applied voltage needs to overcome the inherent potential difference between the anode and the cathode materials. In this way, the overall system is essentially prevented from corrosion. This method of corrosion protection is known as cathodic protection.

Cathodic protection is effective for stopping further corrosion, but it is expensive due to the electricity required. However, energy harvesting (also called energy scavenging, which refers to the conversion of available forms of energy to electricity, such as the conversion of solar energy to electricity using solar cells, or the conversion of mechanical energy to electricity using a piezoelectric device) may be used to provide the electricity. Compared to the corrosion protection method involving a sacrificial anode, cathodic protection is effective over a much longer time frame. This is because the corrosion rate of a sacrificial anode is much higher than that of the anode in cathodic protection.

The corrosion of steel rebars in concrete is an important cause of deterioration in bridges and highways. Figure 4.10 illustrates the use of cathodic protection to provide corrosion protection to steel rebars that are embedded in concrete. The anode material can take the form of wires of a noble metal (e.g., titanium) that are embedded in the cement mortar that coats the concrete. By using cement mortar that contains an electrically conductive admixture, such as short carbon fiber, the electrical conductivity of the mortar is enhanced, thereby reducing the voltage required for cathodic protection. Concrete is slightly conductive electrically, thus allowing the electrons to travel in the concrete from the steel rebars to the anode.

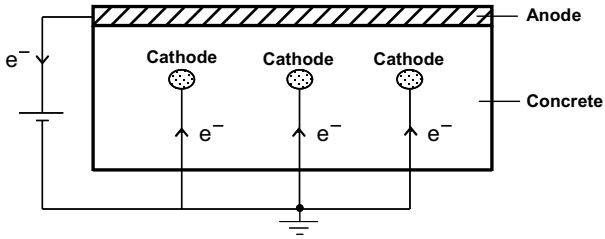

Figure 4.10. Cathodic protection of steel rebars (cathode) embedded in concrete. The surface of the concrete is coated with an anode material. A voltage is applied between the anode and the cathode. The direction of flow of the electrons (e^-) is shown by the *arrows*

The use of concrete that contains an electrically conductive admixture, such as short carbon fiber, reduces the voltage required for cathodic protection.

The oxidation reaction is associated with corrosion of the anode. For example, the oxidation reaction $Fe \rightarrow Fe^{2+} + 2e^-$ causes iron atoms to be corroded away, becoming Fe^{2+} ions that then move into the electrolyte. Thus, the hindering of the oxidation reaction results in corrosion protection. In general, a reaction can be hindered by either increasing the concentration of the reaction product or increasing the concentration of the reactant. Thus, the oxidation of Fe atoms to form Fe^{2+} ions can be hindered by increasing the concentration of Fe^{2+} ions in the electrolyte.

For the same reason, the reduction reaction $O_2 + 2H_2O + 4e^- \rightarrow 4OH^-$ is enhanced by increasing the O_2 concentration. Hence, iron exposed to a high concentration of O_2 gas is more cathodic than iron exposed to a low concentration of O_2 gas. In other words, iron exposed to a low concentration of O_2 gas is more anodic than iron exposed to a high concentration of O_2 gas. As a consequence, iron at a crevice (which is less accessible to oxygen than the iron surface) is more anodic than iron at the surface. This is why a crevice is more prone to corrosion than an open surface. This phenomenon is known as crevice corrosion (Fig. 4.6). Therefore, an absence of crevices aids corrosion resistance.

An example of a crevice is the small gap between two pieces of metal that are fastened together using a bolt. Crevice corrosion tends to occur in a fastened joint and is a significant disadvantage of this type of joining. In contrast, joints formed by welding or soldering do not have gaps and are thus not prone to crevice corrosion. On the other hand, a soldered joint is prone to galvanic corrosion due to the compositional difference between the solder and the two pieces of material that are soldered together. A welded joint where the weld material (called the filler material, which should be distinguished from a filler in a composite material) has the same composition as the pieces of material being joined is not prone to either crevice corrosion or galvanic corrosion. Therefore, welded joints are more corrosion resistant than soldered or fastened joints.

Similarly, the partial coverage of a surface with dirt (or rust, or other substances) causes the covered region to act as an anode, while the uncovered region acts as the cathode (Fig. 4.5). As a consequence, surface cleanliness and surface composition

uniformity aid corrosion resistance. One example pertains to the steel rebars used to reinforce concrete. The steel is carbon steel, not stainless steel. The rebar surface is nonuniform due to the nonuniform rusting that naturally occurs in air. Thus, sand blasting the rebar prior to embedding it in concrete enhances its surface nonuniformity, thereby increasing corrosion resistance [1].

The coating of a material with paint is effective for corrosion protection only if the paint completely covers the material so that the material is isolated from the outside world. If there is a scratch in the paint, the area under the paint next to the scratch (the region without paint) will corrode. This is due to the low oxygen concentration in the area under the paint next to the scratch (and thus the anodic character of this area), compared to the high oxygen concentration (and thus the cathodic character) at the scratch, where the underlying material is exposed.

Water is an electrolyte (an ionic conductor), so its presence tends to promote corrosion. An example relates to steel rebars in concrete. The corrosion resistance of the embedded steel rebars can be improved by making the concrete less porous, so that water cannot readily access the rebars. The addition of silica fume (nanoparticles) to a concrete mix results in concrete with a fine pore structure, thus reducing its porosity to water and improving the corrosion resistance of the embedded steel rebars. Figure 4.11 shows the corrosion resistance of steel rebar in concrete in saturated $Ca(OH)_2$ solution, which simulates the ordinary concrete environment. The corrosion resistance is described in terms of (a) the corro-

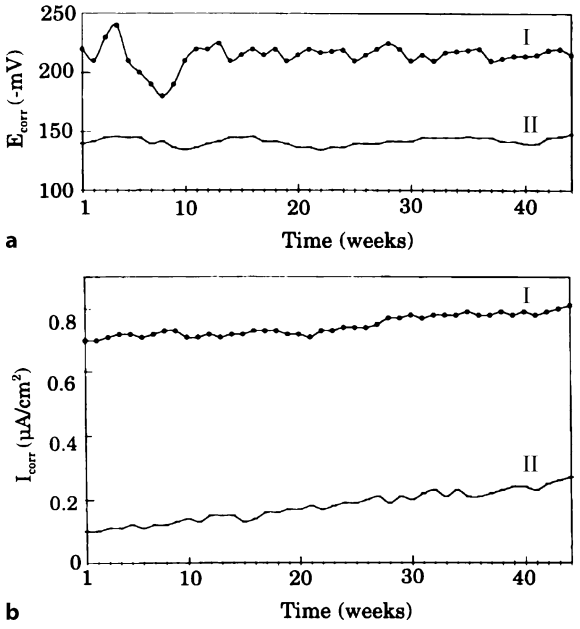

Figure 4.11. Corrosion resistance of a steel rebar in concrete in saturated $Ca(OH)_2$ solution, which simulates the ordinary concrete environment. **a** Corrosion potential (E_{corr}). **b** Corrosion current density (I_{corr}). I Plain concrete. II Concrete with silica fume. (From [2])

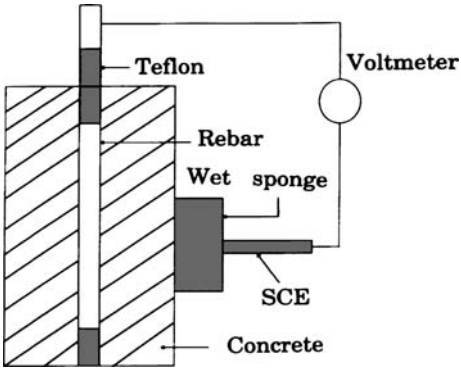

Figure 4.12. Corrosion testing of a steel rebar in concrete. The rebar is sealed with Teflon tape at both ends to control the exact rebar surface area that is exposed to concrete. (From [2])

sion potential (E_{corr}), which describes the propensity for corrosion (a value that is more negative than −270 mV suggests a 90% probability of active corrosion) and is measured using a voltmeter between a reference electrode (the saturated calomel electrode (SCE), in accordance with ASTM C876) and the protruding part of the steel rebar (Fig. 4.12), and (b) the corrosion current density (I_{corr}), which describes the corrosion rate. The SCE is based on the reaction between elemental mercury and mercury chloride (Hg_2Cl_2, known as calomel). The electrolyte in SCE is a saturated aqueous solution of potassium chloride. The SCE is connected to the concrete through a wet sponge that contains water (Fig. 4.12). Figure 4.11 shows that the addition of silica fume addition to concrete makes the corrosion potential less negative and decreases the corrosion current density. Both effects increase the corrosion resistance.

4.2 Elevated Temperature Resistance

4.2.1 Technological Relevance

The ability of a structure to resist elevated temperatures is needed for some applications, such as aircraft with a high thermal load (due to high speed, high engine temperature, low idling time, and onboard devices such as lasers), Space Shuttles (particularly during re-entry into the Earth's atmosphere), heat exchangers (such as that associated with a water heater), friction brakes (which get hot due to the friction that occurs during braking), welded components (due to heat exposure during welding), microelectronic components (which get hot during operation due to the electric current in the circuit and also during soldering), battery components (which get hot during operation due to the to the electric current that passes through the battery), asphalt pavements (which get hot due to both tire friction and the sun), and medical implants (which may get warm due to body heat). In general, elevated temperatures mean temperatures above room temperature, which is

around 25°C. For Space Shuttles, aircraft friction brakes, and welded components, the elevated temperature can be as high as 1,000°C or more. However, for asphalt pavements and medical implants, the elevated temperature is only a little above room temperature. In spite of this large range in elevated temperatures, the issue of elevated temperature resistance is important for all of these applications.

4.2.2 Effects of Thermal Degradation

Effects of thermal degradation include the following:

- Mass loss due to material loss.
- Shrinkage due to material loss, as illustrated in Fig. 4.13 for cement paste containing silica fume as an admixture; here, an irreversible shrinkage occurs around 100°C due to the evaporation of water from the cement, and this dominates over thermal expansion.
- Increased size under constant stress, due to plastic deformation associated with the thermally activated movements of atoms, ions or molecules.
- Decreased stress under constant strain, due to the thermally activated movements of atoms, ions or molecules.
- Shape changes such as warpage.
- Loss of elastic modulus (stiffness), as illustrated in Fig. 4.14 for cement paste containing silica fume as an admixture, where the flexural storage modulus decreases with increasing temperature; although the decrease is largely reversible, there is a slight irreversibility related to the slight shrinkage shown in Fig. 4.13.
- Mechanical strength loss.
- Wear resistance loss.
- Surface property changes due to surface reactions such as surface oxidation
- Increase in paste viscosity, and thus decreased workability.

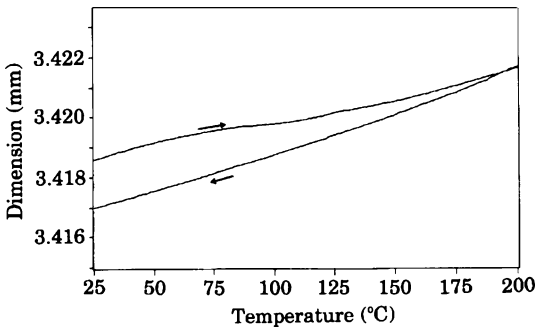

Figure 4.13. Effect of heating and subsequent cooling, both at 2°C/min, on the size of cement paste containing silica fume. (From [3])

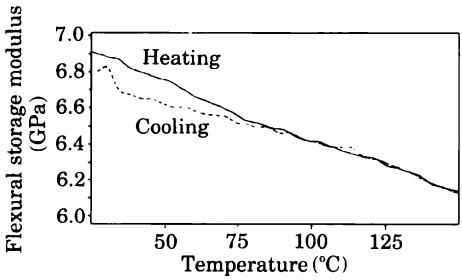

Figure 4.14. Effect of heating (*solid curve*) and subsequent cooling (*dashed curve*) on the flexural storage modulus (1 Hz) of cement paste containing silica fume. The static stress is 1.84 MPa; the dynamic stress is 0.703 MPa; the flexural strength (ASTM C348-80) is 2.75 MPa. (From [3])

4.2.3 Origins of Thermal Degradation

Undesirable thermal effects can have various origins, including the following:

- Cracking (also known as thermal cracking): for example, a relatively volatile component vaporizes and pushes its way out of the solid, or nonuniform heating occurs (i.e., the surface temperature is different from the interior temperature).
- Creep: a crystalline or amorphous solid has enough thermal energy for its atoms, ions or molecules to shift positions significantly in the solid state at temperatures above a temperature equal to one-third of the melting temperature in kelvin; this tends to cause a decrease in modulus.
- Glass transition: the modulus of an amorphous solid (such as an amorphous thermoplastic polymer) decreases as it is heated past the glass transition temperature (abbreviated to T_g: the temperature above which the atoms, ions or molecules in an amorphous or noncrystalline solid have enough thermal energy to move, allowing viscous flow and softening in the solid state; or, the temperature below which the atoms, ions or molecules in an amorphous solid are stuck in their positions because there is insufficient thermal energy to allow them to move).
- Stress relaxation: a gradual decrease in stress occurs at constant strain due to the movement of atoms, ions or molecules in a solid, as in the case of an amorphous thermoplastic polymer above the glass transition temperature or a crystalline solid at a temperature above one-third of the melting temperature in kelvins.
- Grain growth: the grains (or crystallites) in a polycrystalline material grow – a phenomenon that can result in a decrease in strength.
- Oxidation (particularly surface oxidation): results in a loss of surface mechanical properties and a loss of mass. In the case of carbon materials, oxidation causes the conversion of the carbon to a gas, according to reactions such as

$$C + O_2 \rightarrow CO_2 \uparrow , \tag{4.16}$$

thus resulting in mass loss.

- Chemical reactions: for example, the reaction of a material with a fluid present in its surroundings, or the reaction of various components within a material to form a compound. The reaction temperature is the temperature above which the reaction occurs significantly and is governed by the activation energy of the reaction.
- Interdiffusion: for example, the diffusion of two components into one another to form a solid solution.
- Melting: the melting temperature – the temperature at which a solid transforms into a liquid upon heating – and is governed by thermodynamics, though the detrimental effect of melting on the properties of a material can be diminished by using fillers. This is illustrated in Fig. 4.15 for pitch (petroleum pitch) and its particulate composites, in which the particulate fillers (sand and/or silica fume) reduce the change in size upon melting at a fixed pressure of 1,415 Pa, meaning that the softening temperature T_s is decreased.
- Sublimation: the evaporation of a relatively volatile component, such as molecules with a low molecular mass (e.g., water), causes irreversible mass loss (as illustrated in Fig. 4.16 for cement paste containing silica fume during heating and subsequent cooling), and usually shrinkage too (as illustrated in Fig. 4.17 for plain cement paste during heating and subsequent cooling, with the shrinkage superimposed on the thermal expansion; the sluggishness of the shrinkage response due to the viscoelastic behavior of the material is also shown; Fig. 4.18 illustrates severe shrinkage of cement paste containing latex due to the poor thermal stability of latex). The sublimation temperature – the temperature at which a solid transforms into a vapor upon heating without passing through a liquid state – is governed by thermodynamics, and increases with increasing pressure due to the very low density of the vapor compared to the solid.

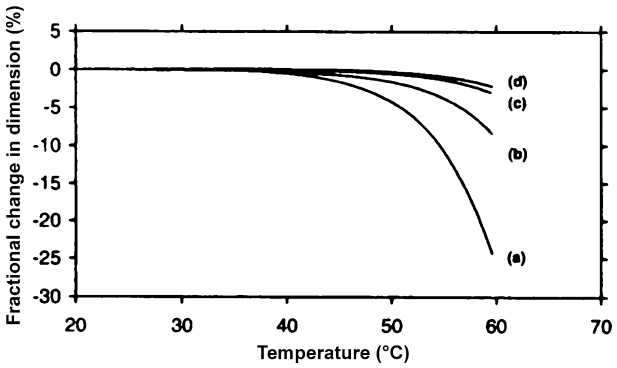

Figure 4.15. Effect of the use of fillers on the change in size of pitch upon melting at a fixed pressure of 1,415 Pa. The softening temperature T_s is taken to be the intersection of the extrapolated baseline with the tangent to the high-temperature portion of the curve. *a* Pitch alone, with $T_s = 40.9$°C, *b* pitch/sand = 1:1, with $T_s = 44.2$°C, *c* pitch/sand/silica fume = 1:1:0.05, with $T_s = 49.9$°C, *d* pitch/sand/silica fume = 1:1:0.15, with $T_s = 51.3$°C. (From [4])

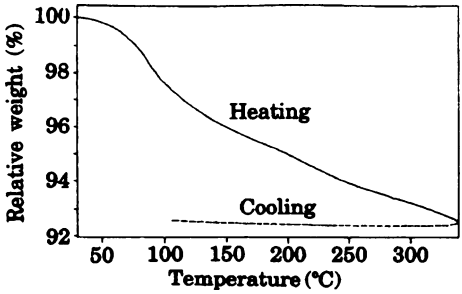

Figure 4.16. Effect of heating and subsequent cooling on the mass of cement paste containing silica fume. The initial specimen mass is 63.966 mg. (From [3])

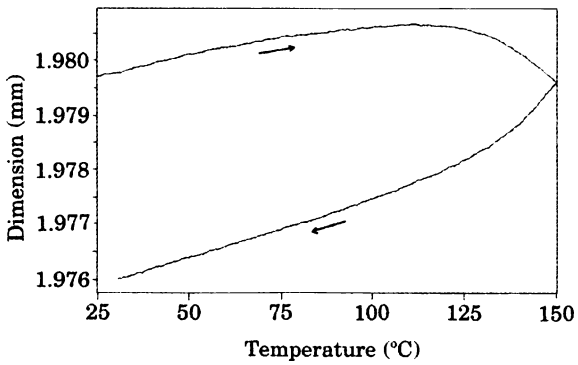

Figure 4.17. Effect of heating and subsequent cooling, both at 2°C/min, on the size of plain cement paste. (From [3])

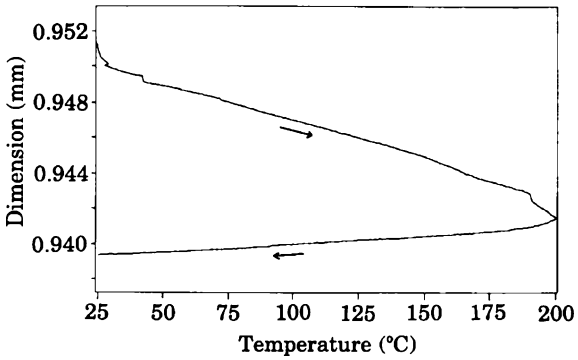

Figure 4.18. Effect of heating and subsequent cooling, both at 2°C/min, on the size of cement paste containing latex. (From [3])

- Decomposition: as in the case of a thermoset polymer losing some of the atoms in each molecule, or a hydrated solid losing a part of its water. The decomposition temperature is the temperature above which a material decomposes significantly, and with mass loss accompanying the decomposition, if the decomposition involves the formation of a gaseous species.

- Crystallization: as in the case of an amorphous solid becoming partially crystalline – a solid–solid phase transformation that tends to make the solid more brittle due to the presence of crystallographic planes in the resulting crystallized portion.
- Weakening of the fiber–matrix interface.
- Fiber–matrix debonding.
- CTE mismatch: two materials with different CTE values are bonded together; one component wants to expand more than the other as the temperature increases, or one component wants to contract more than the other as the temperature decreases, thereby causing warping and even debonding. A continuous fiber composite with fibers of different laminae in different orientations suffers from a CTE mismatch resulting from the anisotropy of each lamina and the different orientations of the fibers in the different laminae. In other words, in the same physical direction in the plane of the laminae, the CTE varies among adjacent laminae that are bonded together. Since the bonding involved in composite formation typically occurs at an elevated temperature, thermal stress arises during the cooling period following this bonding. The presence of this thermal stress weakens the bonds between the laminae.

4.2.4 Effects of Temperature on the Composite Microstructure

Temperature can affect the microstructure of a composite. For example, in a continuous fiber composite, the degree of fiber misalignment ("waviness") can be increased (i.e., the degree of fiber alignment can be diminished) by heating the thermoplastic-matrix composite above the glass transition temperature T_g, due to the flow of the matrix. This microstructural change in turn affects the properties of the composite. The flow of the matrix can be diminished by increasing the crystallinity of the matrix by annealing beforehand if the matrix exhibits a tendency for crystallization.

Since composites are commonly fabricated at elevated temperatures and there is a difference in CTE between the fibers and the matrix, thermal stress is commonly present at room temperature after cooling from the fabrication temperature. In the case of a carbon fiber polymer–matrix composite, the CTE is much lower for the fiber than the matrix. As a result, the thermal stress increases the fiber waviness. Subsequent heating tends to decrease the thermal stress. However, cooling after this would increase the thermal stress again. Hence, the effect of heating on the thermal stress tends to be reversible, and so heating results in reversible changes in the properties of the composite.

For a thermoplastic matrix that has tendency to crystallize (e.g., polyphenylene sulfide, abbreviated to PPS), heating above T_g may cause partial crystallization of the matrix. The tendency to crystallize is particularly high in the part of the matrix next to the fiber if the fiber has atomic layers that are oriented to a certain degree. The order in the fiber enhances the order in the polymer matrix. This is known as transcrystallization. The partial crystallization of the matrix tends to result in

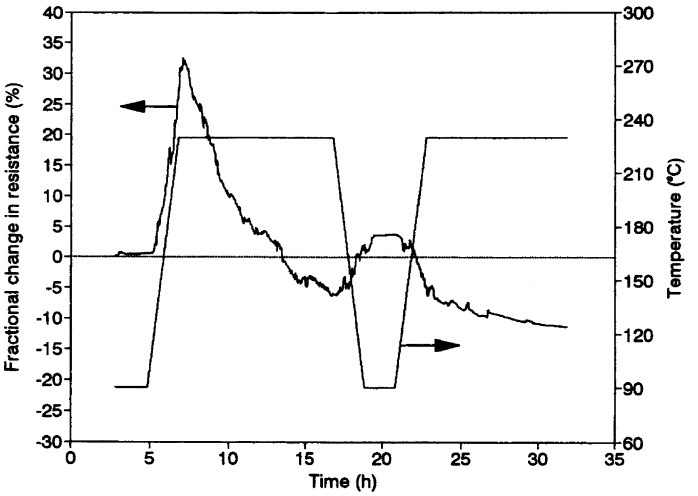

Figure 4.19. Fractional change in electrical resistance in the fiber direction of a unidirectional carbon fiber PPS-matrix composite (as received) during the first two cycles of thermal cycling. (From [5])

decreased fiber waviness. Prior annealing that enhances the crystallinity of the matrix tends to reduce this thermal effect.

Figure 4.19 shows the effect of thermal cycling on the electrical resistance in the fiber direction of a continuous unidirectional carbon fiber (64 wt.%) PPS-matrix composite (as received; i.e., without annealing). The resistance is sensitive to the fiber waviness due to the electrical conductivity of carbon fiber, in contrast to the nonconductivity of the matrix. The PPS matrix has T_g = 90°C and a melting temperature T_m = 280°C. Upon first heating to 235°C (a temperature below T_m), the resistance increases due to the flow of the matrix and the subsequent increase in the fiber waviness. During the subsequent isothermal period of ten hours, the resistance decreases due to matrix crystallization and the consequent decrease in the fiber waviness. Subsequent cooling to 90°C (T_g) causes the resistance to increase due to the build-up of thermal stress and the consequent increase in the fiber waviness. Upon subsequent heating back to 235°C, the resistance decreases due to the decrease in thermal stress and the consequent decrease in the fiber waviness.

Figure 4.20 shows corresponding results for the carbon fiber PPS-matrix composite after annealing at 180°C for 25 h. Due to the attainment of maximum crystallinity after the annealing, the flow and crystallization during heating are essentially absent, leading to an absence of any increase in resistance during the first heating period and an absence of any resistance decrease during the isothermal high-temperature period. Nevertheless, the effect of thermal stress remains, thus causing the observed reversible decrease in resistance upon heating. The resistance after cooling to 90°C is slightly higher after the second heating cycle than after the first heating cycle due to thermal degradation.

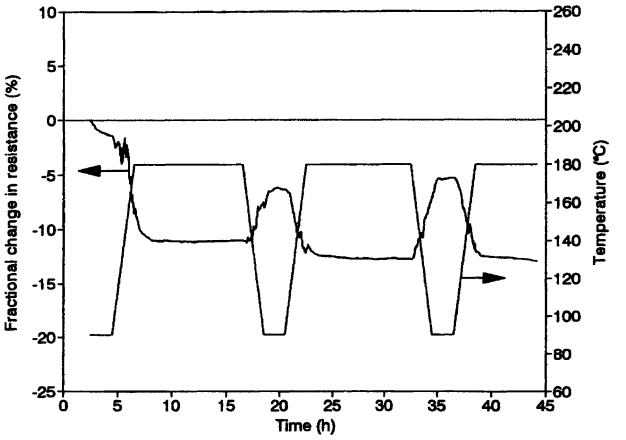

Figure 4.20. Fractional change in electrical resistance in the fiber direction of a unidirectional carbon fiber PPS-matrix composite (after annealing at 180°C for 25 h) during the first three cycles of thermal cycling. (From [5])

4.2.5 Improving the Elevated Temperature Resistance

The elevated temperature resistance may be improved by various methods, including the following:

- Choosing materials with sufficiently high resistance to elevated temperatures, as guided by the melting temperature, the sublimation temperature, the glass transition temperature, the decomposition temperature, and the reaction temperature. An example is the use of aluminum nitride (AlN) particles instead of silicon carbide (SiC) particles to reinforce aluminum, because SiC reacts with aluminum according to the reaction

$$4\mathrm{Al} + 3\mathrm{SiC} \rightarrow \mathrm{Al_4C_3} + 3\mathrm{Si}\,, \tag{4.17}$$

  whereas AlN does not react with Al. Another example is the use of superalloys (such as nickel-base and iron-base superalloys) instead of steel, due to the superior high-temperature strengths and moduli of the superalloys.
- Coating with a material that is able to withstand high temperatures. An example is the coating of a carbon–carbon composite with silicon carbide in order to improve the oxidation resistance at high temperatures.
- Coating the material so that the coating serves as a barrier against the intrusion of a reactant.
- The use of an additive in the form of a sealant when the material is fabricated so that the sealant is incorporated into the material and serves as a barrier against the intrusion of a reactant (e.g., boron as an additive in a carbon–carbon composite to increase the oxidation resistance of the composite, due to the reaction of boron with oxygen and the consequent formation of a borate glass, which undergoes viscous flow and acts as a sealant).

- The use of an additive in the form of an inhibitor for the relevant reaction, so that the propensity for the reaction is reduced (e.g., an additive that reacts with oxygen and acts as an oxygen getter, thus enhancing the oxidation resistance of the host material; an example is boron, as mentioned in the previous point).
- The use of an additive in the form of an antioxidant (which inhibits oxidation), as used for organic materials (such as lubricants) and tailored for each type of organic material in accordance with the corresponding chemistry such that the reactivity of the organic material with oxygen is reduced.
- The use of thermal insulation around the material so that the material encounters a lower temperature than that felt by the insulation.
- The availability of paths for the vapor from the vaporization of the volatile component to move out of the material without cracking it.
- The incorporation of a filler into the material so that the creep resistance is increased (i.e., the filler restrains the matrix from creeping).
- Increasing the degree of crosslinking between molecules in a polymer so that the sliding of its molecules with respect to one another is hindered and so the extent of softening associated with the glass transition is reduced (Fig. 4.21).
- Increasing the degree of crystallinity so that the extent of viscous flow and the consequent softening associated with the amorphous phase above the glass transition temperature is reduced (Fig. 4.22).
- The use of a composition gradient so that the problem of CTE mismatch is reduced. An example is the use of a graded distribution of short carbon fibers in a metal in order to provide a CTE gradient within the resulting metal-matrix composite.
- Increasing the vaporization temperature of the relatively volatile component by modifying the composition of this component.
- Increasing the thermal conductivity through the use of a thermally conductive filler so that the temperature gradient is reduced, thereby lessening the thermal

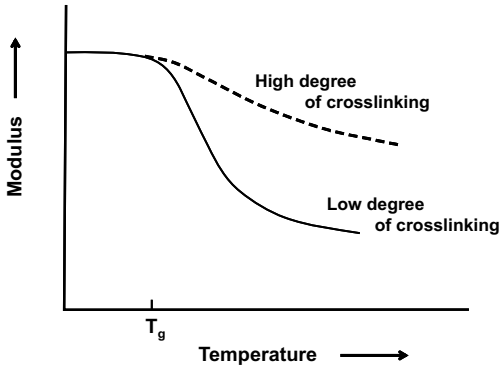

Figure 4.21. Variation in the elastic modulus with the temperature, showing the decrease in modulus at the glass transition temperature T_g upon heating. The effect is diminished by increasing the degree of crosslinking

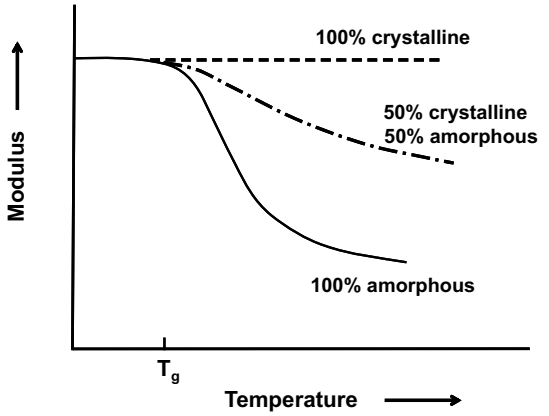

Figure 4.22. Variation in the elastic modulus with the temperature. The decrease in modulus at the glass transition temperature T_g upon heating is diminished by increasing the degree of crystallinity. The effect disappears completely when the material is 100% crystalline

stress associated with the different degrees of thermal expansion that occur in different parts of the material.

- Matching the CTE values of bonded components through the use of an appropriate low-CTE filler in the high-CTE component so that the tendency for warpage or debonding due to the CTE mismatch is reduced.
- Decreasing the modulus by composition modification so that the thermal stress due to a CTE mismatch is reduced (since stress = modulus $\times$ strain).

The carbon matrix significantly enhances the resistance of the carbon fibers to creep deformation, due to the ability of the matrix to distribute loads more evenly and to impose a plastic flow-inhibiting, triaxial stress state in the fibers. The thermally activated process for creep is controlled by vacancy formation and motion.

4.2.6 Investigation of Elevated Temperature Resistance

Elevated temperature resistance requires the material to be able to maintain acceptable properties at elevated temperatures. The relevant properties may be structural and/or functional. Structural and functional properties tend to be related in that they are both sensitive to flaws. However, the minimum temperatures required for the functional and structural properties to degrade may differ in the same material system. This is because the functional and structural properties tend to have different sensitivities to flaws. Consider, for example, soldered joints, which are widely used in microelectronics as electrical interconnections. The degradation of a soldered joint causes the mechanical properties of the joint to degrade and the electrical resistance of the joint to increase. At a certain elevated temperature, the electrical conductivity of a soldered joint may degrade but its mechanical properties may not. This means that studies of the elevated temperature resistance of

a soldered joint for electrical interconnection should include evaluations of both its mechanical and its structural performance at the elevated temperature.

Minor thermal degradation of a material system after exposure to an elevated temperature may be reversible upon cooling, at least to a certain degree. Total reversibility means that the degradation occurs at an elevated temperature but then disappears upon cooling back to room temperature. In contrast, total irreversibility means that the degradation that occurs at an elevated temperature remains upon subsequent cooling. The degree of reversibility depends on the mechanism of degradation. For example, it is possible for degradation in the form of a particular microstructural change at an interface to be reversible upon cooling. A reversible microstructural change tends to be rather subtle, such as the decrease in the extent of contact between adjacent conductive discontinuous fibers in a composite with a nonconductive matrix upon heating. This effect is commonly due to the difference between the coefficients of thermal expansion (CTEs) of the fibers and the matrix. When the matrix has a higher CTE than the fibers, the extent of fiber–fiber contact is diminished upon heating. This microstructural change, which can occur in the absence of debonding between fiber and matrix, causes an increase in the electrical resistivity of the composite upon heating. When the electrical conductivity is important for a functional application, this resistivity increase is considered a functional degradation. However, if the CTE mismatch is so large that debonding occurs at the fiber–matrix interface upon heating, the degradation may not be reversible upon subsequent cooling – the debonded state remains after cooling.

Generally speaking, a thermal effect is partially reversible and partially irreversible. Therefore, studies of any thermal effect should include investigations performed at both room temperature (before and after heating to the elevated temperature) and the elevated temperature. This will allow reversible and irreversible processes to be distinguished, and the degree of reversibility to be determined. An investigation performed in real time during heating and subsequent cooling would be even better, as such a real-time investigation allows the process of degradation, the reverse process (i.e., the process of condition restoration or healing), and the extent of hysteresis (i.e., the difference between the temperatures of the forward and reverse processes) to be studied. The real-time investigation of the degradation process may be conducted by monitoring a certain property (i.e., a relevant performance attribute) while heating at a controlled rate (e.g., 10°C/min), as illustrated in Fig. 4.23. The temperature of the forward process (T_f) may be taken as the temperature at the half-way point during heating, as shown in Fig. 4.23. During subsequent cooling, also at a controlled rate, the reverse process may occur, such that the temperature of the reverse process (T_r) may be taken as the temperature at the half-way point during cooling, as shown in Fig. 4.23. In general, T_f and T_r are not the same. In other words, there is hysteresis, which is due to the difference in kinetics between the forward and reverse processes. When the reverse process is more sluggish than the forward process, T_r is less than T_f. Figure 4.23 also shows that the value of the property after cooling is not the same as that before heating. This means that the process is not completely reversible. In other words, the process is partially reversible and partially irreversible. The degree of reversibility is

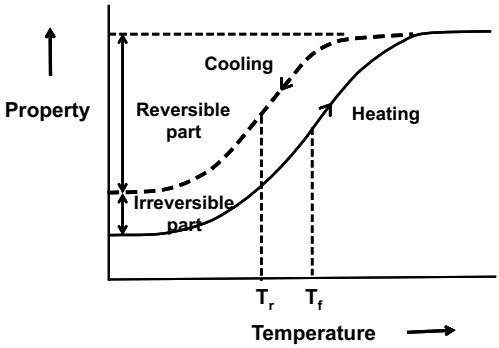

Figure 4.23. Effect of heating and subsequent cooling on a property

described by the reversible part of the property change divided by the sum of the reversible and irreversible parts, as shown in Fig. 4.23.

To obtain rate (kinetic) information on a process, it is better to monitor the process at a constant elevated temperature rather than to monitor it while heating. A number of different constant temperatures are used in separate experiments, as illustrated in Fig. 4.24a, where the temperatures T_1, T_2 and T_3 (with $T_3 > T_2 > T_1$) are used to obtain three experimental curves. The higher the temperature, the faster the process. The rate of the process at a particular temperature may be taken as the inverse of the time at which the process is 50% complete, corresponding to the half-way point in the curve of property versus time, as shown in Fig. 4.24a, where the times of 50% completion are τ_1, τ_2 and τ_3 at temperatures T_1, T_2 and T_3, respectively. Hence, the rates are $1/\tau_1$, $1/\tau_2$ and $1/\tau_3$ at temperatures T_1, T_2 and T_3, respectively.

The rate (r) of a thermally activated process relates to the activation energy of the process according to the equation

$$r = A\mathrm{e}^{-Q/RT}, \tag{4.18}$$

where Q is the activation energy of the process, T is the temperature in K (not in °C), R is the gas constant (a universal constant equal to 8.314 J/(mol K)), and A is a proportionality constant. A plot of r versus T is shown in Fig. 4.25. At $T = 0$, $r = 0$ due to the absence of thermal energy at this temperature. As T increases, r increases exponentially. At $T = \infty$, $r = A$.

The activation energy of any process reflects its kinetics (its rate) rather than its thermodynamics, as it relates to the energy barrier that needs to be overcome in order for the process to proceed. The energy barrier depends on the mechanism of the process. For example, if the process requires the stretching of certain chemical bonds in order for it to proceed, the activation energy is governed by the ease of bond stretching. The activation energy is *not* the difference in energy between the initial state (before the process) and the final state (after the process). This difference in energy is the thermodynamic driving force for the process and is governed by the energies of the initial and final states.

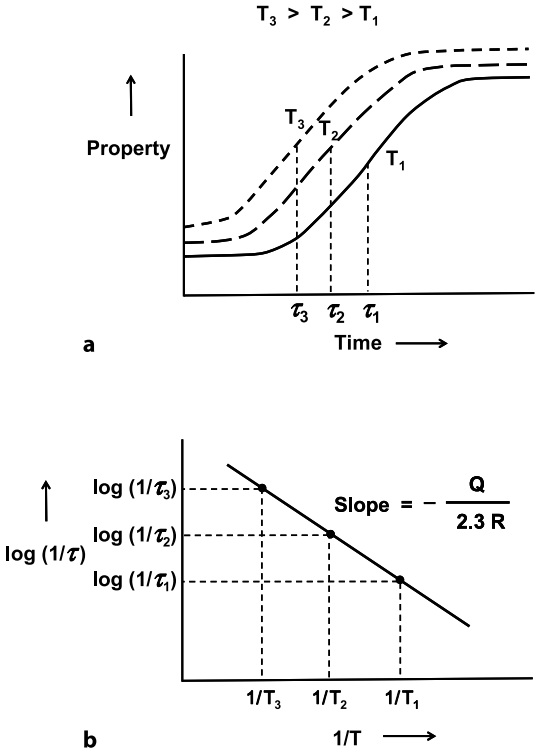

Figure 4.24. Effect of isothermal heating at different constant temperatures on a property. **a** Property vs. time at constant temperatures, **b** log rate vs. 1/*T*, where *T* is the temperature in K and the rate is $1/\tau$, with τ defined in (**a**)

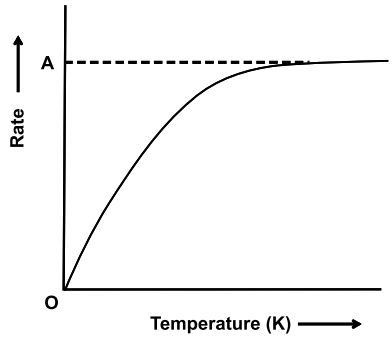

Figure 4.25. Increase in the rate of a thermally activated process with increasing temperature in K

Taking natural logarithms on both sides of Eq. 4.18 gives

$$\ln r = \ln A - Q/(RT) \; . \tag{4.19}$$

Conversion from natural logarithms to logarithms to the base 10 gives

$$\log r = \log A - Q/(2.3RT) \; . \tag{4.20}$$

Equation 4.20 means that the plot of log r versus $1/T$ is a straight line with a negative slope equal to $-Q/(2.3R)$, as illustrated in Fig. 4.24b for a plot of $\log(1/\tau)$ vs. $1/T$. Thus, Q can be determined from the slope of the curve. A semi-logarithmic plot in the form of log rate vs. $1/T$ (with T in K) is generally called an Arrhenius plot, and is commonly used to determine the activation energy of a process.

Similarly, real-time investigations of the reverse process may be conducted either while cooling at a controlled rate or at a constant temperature below the relevant elevated temperature. Again, a number of different constant temperatures can be used to obtain information on the kinetics of the reverse process. In general, the activation energies of the forward and reverse processes are not equal, as explained in Fig. 4.26, where state B (the high-temperature state) is at a higher enthalpy (heat content) than state A (the low-temperature state), and so the activation energy of the process that converts state A to state B is higher than that of the reverse process that converts state B to state A. The higher the activation energy of a process, the slower the kinetics.

The difference in enthalpy between the initial and final states relates to the thermodynamic driving force for the process. When the final state has a lower enthalpy than the initial state, the enthalpy change for the process is negative and the process is spontaneous. In Fig. 4.26, the change from state B to state A involves a negative change in enthalpy, so it is spontaneous and the enthalpy change is the thermodynamic driving force for the process. However, the change from state A to state B involves a positive change in enthalpy.

An example is the process of melting, for which state A is the solid state and state B is the liquid state. The liquid state has a higher enthalpy than the solid state due to the disorder of the atoms or molecules in the liquid state compared to the order in the crystalline solid state. The activation energy for melting is associated with the enthalpy required to achieve the disordering. The activation energy for solidification is associated with the enthalpy required to achieve the ordering.

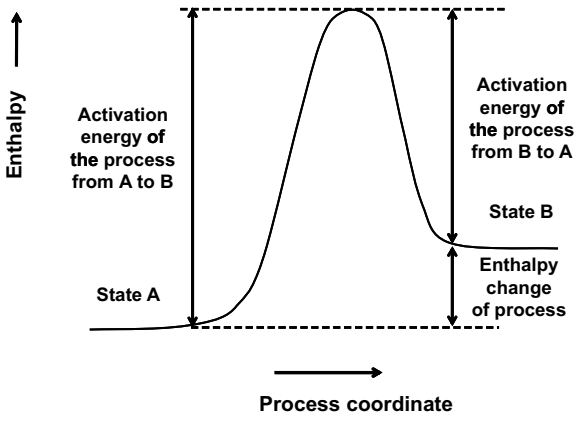

Figure 4.26. Change in enthalpy as a process occurs. The activation energies required to move from state A to state B and from state B to state A (the reverse process) are shown. The enthalpy difference between states A and B is the enthalpy change for the process

During the melting process, latent heat of fusion is absorbed, resulting in the increase in enthalpy from that of state A to that of state B. During solidification, latent heat of solidification is evolved, thus resulting in a decrease in enthalpy from that of state B to that of state A. In other words, the enthalpy change for the process is the same as the latent heat of the process.

As well as the real-time monitoring shown in Figs. 4.23 and 4.24, it is also possible to test at room temperature before and after heating without performing elevated temperature testing. Such testing does not allow observations of a totally reversible process; it can only detect irreversible effects. In addition, it does not provide information on the kinetics of the process. A negative observation obtained using this method only means that there is no irreversible effect. It cannot indicate whether there is a reversible effect or not.

Thermal analysis is a branch of materials science that relates to the study of the effect of temperature on the properties of materials. Conventional methods of thermal analysis include thermogravimetric analysis (also known as thermogravimetry and abbreviated TGA, which involve measuring the weight during heating at either a constant temperature or a constant heating rate), thermomechanical analysis (abbreviated TMA, which involves measuring the sample size while heating at either a constant temperature or a constant heating rate), and differential scanning calorimetry (abbreviated DSC, which involves measuring the heat difference between the specimen and a reference while heating at a constant heating rate).

4.3 Fatigue Resistance

Fatigue refers to degradation due to dynamic stress, which is commonly encountered in moving parts (such as a turbine blade), since each movement cycle corresponds to a stress cycle. It is also encountered in bridges, since each vehicle moving across the bridge imposes a stress cycle unless the vehicles are in a traffic jam. Even though the stress may be below the yield strength, fatigue failure can occur after a sufficient number of loading cycles.

If the stress is due to dynamic mechanical loading, the fatigue is known as mechanical fatigue. If the stress is due to temperature variation (known as thermal stress), the fatigue is known as thermal fatigue.

4.3.1 Mechanical Fatigue

Fatigue commonly starts to occur at an imperfection in the material. An example of an imperfection is a little notch on the surface. As dynamic loading progresses, fatigue propagates from one loading cycle to another, emanating from the initiation point. This cycle-by-cycle propagation progresses until the remaining area (the undamaged part) is too small to support the load. At this point, catastrophic rupture occurs over the remaining area, causing fatigue failure. The portion of the fracture surface associated with the cycle-by-cycle crack propagation is characterized by parallel ridges (called beach marks) around the initiation site, such that

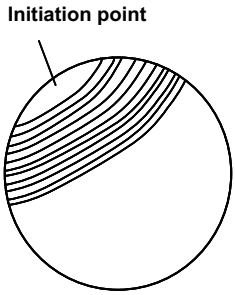

Figure 4.27. A schematic of the fracture surface due to fatigue failure, showing the characteristic beach marks

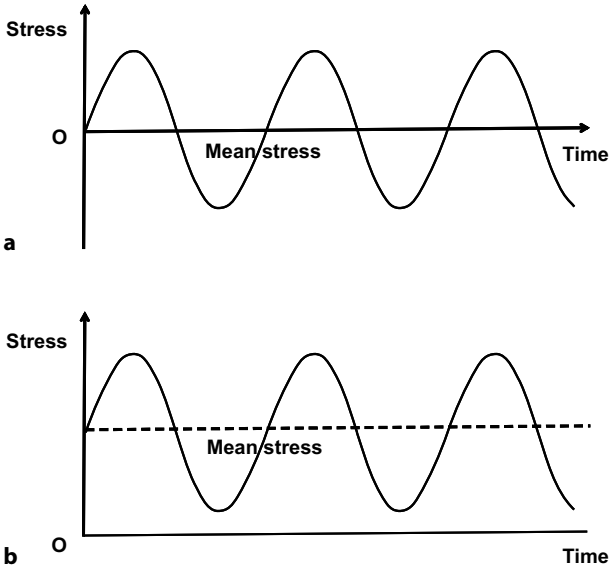

Figure 4.28. Variation of stress with time during fatigue testing. **a** Mean stress = 0, so that the stress is positive for half of each cycle and is negative for the other half of each cycle. **b** Mean stress >0, so that the stress is always positive

each ridge corresponds to one cycle of crack propagation, as illustrated in Fig. 4.27. Beach marks on a fracture surface serve as an indicator of fatigue failure. This is an example of the value of microscopic examinations of fracture surfaces – a technique known as fractography.

Because fatigue crack propagation tends to start at an imperfection, such as a scratch on the surface, an internal crack, a pore, a delamination site in a composite material, and a fiber–matrix debonding site in a composite material, an absence of substantial imperfections aids fatigue resistance. The surface finish tends to affect the fatigue resistance significantly.

High cycle fatigue refers to fatigue with a life of 10^4 cycles or more, whereas low cycle fatigue involves a life of 10^3 cycles or less. High cycle fatigue involves low strains, which are primarily in the elastic regime. Low cycle fatigue involves

high strains that are in the plastic regime. Due to the high strains, low cycle fatigue testing is preferably conducted using a controlled strain wave rather than a controlled stress wave. In contrast, due to the low strains, high cycle fatigue testing is conducted using a controlled stress wave. In order that a high cycle fatigue test can be completed in a reasonable time frame, a high loading frequency (typically 20–50 Hz) is used. In contrast, a low frequency (typically 1–5 Hz) is used for low cycle fatigue testing.

Tensile stress is positive whereas compressive stress is negative. The stress amplitude means the amplitude of the stress wave; the mean stress is not necessarily zero. If the mean stress is zero, the stress is tensile for half of each cycle and is compressive for the other half of each cycle (Fig. 4.28a). When the stress is positive for the entirety of each cycle (Fig. 4.28b), the fatigue is said to be tension–tension fatigue (quite common in experimental work), due to the absence of compression and the tendency of compression to cause a degree of buckling in the specimen.

The dynamic stress encountered in a practical application does not necessarily involve a fixed stress amplitude or a fixed frequency. However, for research purposes, the stress amplitude and frequency are typically fixed in an experiment that is carried out for the entire fatigue life. In more detailed research, the stress amplitude and frequency are varied systematically for the purpose of investigating the effect of these parameters on the fatigue life. The effect of stress amplitude on the fatigue life (i.e., the number of cycles to failure) is typically presented as a plot of the stress amplitude vs. the logarithm to the base 10 of the fatigue life. The logarithmic scale is used to accommodate a large range of fatigue lives. This curve, known as the *S*–*N* curve (with *S* meaning the stress amplitude and *N* meaning the number of cycles to failure) or the Wöhler curve, is illustrated in Fig. 4.29. Unless noted otherwise, the stress amplitude shown in an *S*–*N* curve is for a mean stress of zero. The greater the stress amplitude, the smaller the fatigue life (the number of cycles to failure). The stress amplitude for a fatigue life of one cycle corresponds to the tensile strength. For some materials (such as some steel and titanium alloys), the *S*–*N* curve levels off to give a constant stress amplitude at a sufficiently high fatigue life, as shown in Fig. 4.29. The leveled-off value of the stress amplitude is

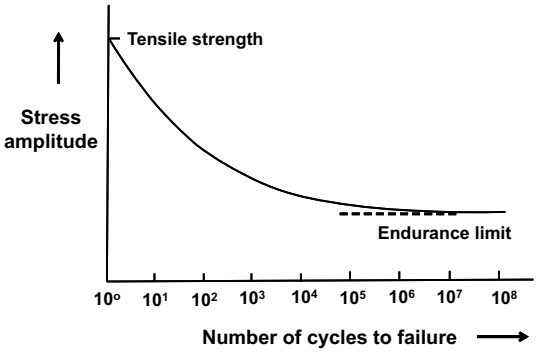

Figure 4.29. The *S*–*N* curve (i.e., plot of the stress amplitude vs. the number of cycles to failure) that describes fatigue performance

known as the endurance limit, which is the stress amplitude below which there is no fatigue failure. The endurance ratio refers to the ratio of the endurance limit to the tensile strength and is typically around 0.5 for ferrous alloys. Thus, the engineer should design the stress amplitude such that it is below the endurance limit if fatigue failure needs to be avoided. Otherwise, the stress amplitude can be chosen according to the *S*–*N* curve so as to give the required fatigue life (i.e., the required number of cycles to failure). The stress amplitude that gives a particular fatigue life is known as the fatigue strength.

4.3.2 Thermal Fatigue

Thermal fatigue occurs due to thermal stress variations, which are in turn due to temperature variations. Because of thermal transients, water boilers tend to suffer from thermal fatigue, which can result in cracking. Similarly, ceramic thermal barrier (thermal insulation) coatings on engine components (e.g., diesel engine components) suffer from thermal fatigue due to the severe thermal cycling conditions they are exposed to. The thermal stress is commonly due to the CTE mismatch between two bonded components that encounter dynamic temperature variations. An example is a copper thin film on a silicon substrate. The copper film takes the form of a line for electrical conduction. The CTE of copper is higher than that of silicon. Due to the electric current in the conduction line, the copper gets hot. This heating is known as the Joule effect. The resulting temperature variations, along with the CTE mismatch, result in damage in the film and even detachment of the film from the substrate. Thermal fatigue is one of the dominant mechanisms for soldered joint failure in microelectronic packages due to the CTE mismatch between the two components (e.g., the semiconductor device and the printed wiring board) joined by the solder. The thermal stress results in deformation in the solder, thus causing the solder to harden (a phenomenon known as work hardening or strain hardening), making it less ductile and more prone to fracture. Thermal fatigue may also be due to the nonuniform composition distribution in a material and the consequent nonuniform CTE distribution. Thermal fatigue has been studied in much less depth than mechanical fatigue.

4.4 Durability

As a structure is intended for use over a long period of time (such as decades), the long-term durability of structural materials is important. However, deterioration due to aging occurs. Causes of deterioration include the following:

- Corrosion
- Fatigue
- Creep (slow and permanent deformation of a material below its yield strength, with the severity of this deformation increasing with temperature)
- Wear (i.e., erosion of a solid surface by the action of another substance, thus causing a decrease in size), reaction with a gas (e.g., reaction with oxygen in

the air to form an oxide film, which may or may not protect the material from further oxidation)

- Heat (e.g., softening of asphalt due to heat, and the hastening of corrosion, creep and other processes by heat)
- Temperature variations (e.g., concrete deterioration caused by freeze–thaw cycling, which refers to temperature cycling between temperatures above and below 0°C and thus the damage arising from the expansion of water in the concrete upon freezing)
- Humidity (e.g., absorption of water by some polymers, which therefore swell)
- Ultraviolet (UV) radiation (e.g., polymer degradation, known as photodegradation, which is caused by exposure to UV rays – more energetic than visible light – such as those from the sun; this results in the breaking of C–C bonds in the polymer molecule chain, with these broken bonds serving as reactive sites that lead to discoloration, chalking and mechanical property loss)
- Salt (e.g., marine salt and deicing salt, which hasten corrosion by providing ions to the electrolyte, thereby increasing the electrical conductivity of the electrolyte)
- Atomic oxygen (e.g., the bombardment of a spacecraft traveling at a high speed by atomic oxygen, which is more reactive than molecular oxygen and is present in the upper regions of the atmosphere – at altitudes of greater than 400 km – such that the bombardment causes surface degradation, erosion and contamination, particularly of polymeric materials) .

Wear processes include surface fatigue (surface weakening by cyclic loading), abrasive wear (material removal by contact with hard particles, as illustrated in Fig. 4.30), fretting wear (repeated cyclical rubbing of two surfaces against one another, causing the removal of material from one or both surfaces), and adhesive wear (the sliding of two surfaces against one another under pressure, thus causing plastic deformation and welding of asperities on the two surfaces, the subsequent breaking of bonds, and the formation of surface cavities and abrasive particles, as illustrated in Fig. 4.31). Wear can be reduced through lubrication, which involves

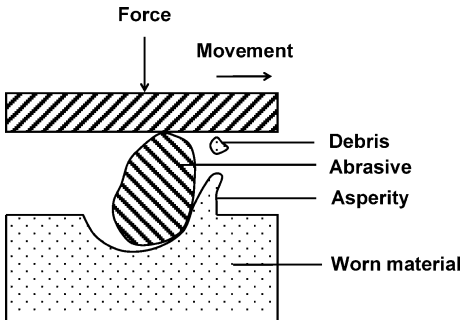

Figure 4.30. Abrasive wear

applying a lubricant between the two surfaces. Lubricants include solids (e.g., graphite and molybdenum disulfide), liquids, and dispersions of solid particles in a liquid. The study of wear and lubrication is a research field known as tribology.

The resistance to sliding wear is commonly assessed using a pin-on-disc geometry. This configuration involves the use of a pin in contact with a rotating disk. Either the pin or the disk can be the material intended for evaluation. The contact surface of the pin may be flat, spherical, or some other shape. The degree of wear can be obtained from either the weight loss of the specimen or the profile of the wear track on the disc. The weight loss relates to the volume loss through the density. The volume loss is a scientifically more meaningful indicator of the degree of wear than the weight loss. The normal load and the velocity are the main variables in this test. A lubricant may be applied at the worn area in order to investigate the effect of the lubricant on the wear resistance.

Abrasion resistance may be tested by rubbing a specimen with one or more abrasive wheels rotating on the surface of the specimen. The weight loss (which relates to the volume loss) of the specimen is used to indicate the degree of wear. The abrasive wheel is commonly made from a silicon carbide particle clay-matrix composite, as used for grinding wheels. The normal load and the velocity are the main variables in the test.

The reaction of a material with a gas in the environment tends to cause deterioration of the material. The most common reaction is that between a metal and oxygen gas, which is present in air. The oxidation reaction results in an oxide film on the metal surface. If the oxide film is porous (Fig. 4.32a), as in the case when magnesium is the metal, it cannot protect the metal from further oxidation, so oxidation continues. If the oxide film is nonporous and adheres to the metal

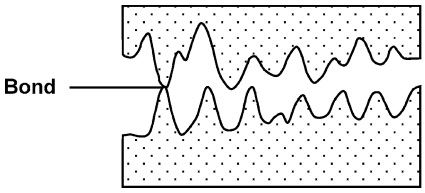

Figure 4.31. Adhesive wear

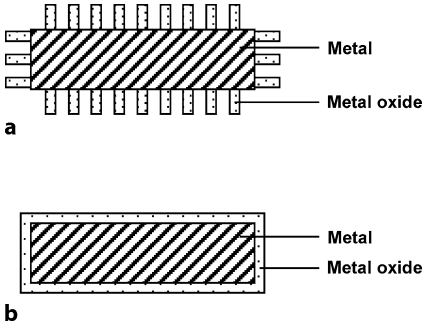

Figure 4.32. Formation of metal oxide due to the reaction of a metal with oxygen. **a** Porous oxide, **b** nonporous oxide

surface (Fig. 4.32b), as in the case when aluminum or titanium is the metal, it can protect the metal from further oxidation. This is why aluminum foil can withstand the temperatures used in cooking. Whether the oxide film is porous or not depends on the volume of the oxide resulting from the oxidation of an atom of the metal. If this volume is close to the volume of a metal atom (not the volume of an isolated atom, but the volume of the unit cell divided by the number of atoms per unit cell), the film is nonporous (Fig. 4.32b). If the volume of the oxide resulting from the oxidation of a metal atom is smaller than the volume of the metal atom, the film is porous (Fig. 4.32a). If the volume of the oxide resulting from the oxidation of a metal atom is larger than the volume of the metal atom (as is the case when iron is the metal), parts of the film flake off due to insufficient room on the surface of the metal. The flaking off of the oxide film is known as spalling, which results in a lack of oxidation protection for the metal.

The ratio of the volume of the oxide resulting from the oxidation of an atom of the metal to the volume of a metal atom is known as the Pilling–Bedworth ratio. The volume of the oxide is related to the density of the oxide. The volume of the metal is related to the density of the metal. In the case of magnesium, one magnesium atom is needed to form one formula unit of MgO, so the volume of one magnesium atom in magnesium metal should be compared to the volume of one formula unit of MgO. In the case of aluminum, two aluminum atoms are needed to form one formula unit of Al_2O_3, so the volume of two aluminum atoms should be compared to the volume of one formula unit of Al_2O_3. The Pilling–Bedworth ratio should be between 1 and 2 in order for the film to be nonporous. When this ratio exceeds 2, spalling occurs. When this ratio is below 1, the film is porous.

The thermodynamic driving force for the oxidation reaction relates to the enthalpy of the final state minus that of the initial state. The more negative this enthalpy change, the greater the driving force and the more stable the oxide. For example, for the oxidation reaction

$$2Mg + 2O_2 \rightarrow MgO\ , \tag{4.21}$$

the final state is MgO and the initial state is $2Mg + 2O_2$. Another example is the reaction

$$4Cu + O_2 \rightarrow 2Cu_2O\ . \tag{4.22}$$

MgO and Al_2O_3 are oxides that are relatively stable (with very negative values for the enthalpy change involved), whereas Cu_2O and NiO are oxides that are relatively unstable (with much less negative values of the enthalpy change involved).

Review Questions

1. Why does corrosion tend to occur mainly at the crack in a piece of steel?
2. What are the anodic and cathodic reactions for the corrosion of steel in air?

3. Why is cathodic protection an expensive method of corrosion protection?
4. Why does sand blasting help to improve the corrosion resistance of steel rebars?
5. Why does the addition of silica fume as an admixture in concrete help to improve the corrosion resistance of steel rebars embedded in the concrete?
6. What is the main advantage of a polymer of high crystallinity compared to one of low crystallinity?
7. Why is aluminum foil quite temperature resistant, meaning that it can be used in cooking?
8. Why is the heat-affected zone in welding a problem?
9. Why does the time spent below the melting temperature prior to bonding affect the quality of the bond for PPS?
10. What is the main advantage of using carbon fiber as a filler in an active brazing alloy?
11. What is the main advantage of using acid phosphate rather than colloidal silica as a binder?
12. Why does corrosion tend to occur in a fastened metal joint?

References

[1] J. Hou, X. Fu, and D.D.L. Chung, "Improving Both Bond Strength and Corrosion Resistance of Steel Rebar in Concrete by Water Immersion or Sand Blasting of Rebar," *Cem. Concr. Res.* 27(5), 679–684 (1997).
[2] J. Hou and D.D.L. Chung, "Effect of Admixtures in Concrete on the Corrosion Resistance of Steel Reinforced Concrete", *Corros. Sci.* 42(9), 1489–1507 (2000).
[3] X. Fu and D.D.L. Chung, "Effect of Admixtures on the Thermal and Thermomechanical Behavior of Cement Paste", *ACI Mater. J.* 96(4), 455–461 (1999).
[4] Z. Mei and D.D.L. Chung, "Improving the Flexural Modulus and Thermal Stability of Pitch by the Addition of Silica Fume", *J. Reinf. Plast. Compos.* 21(1), 91–95 (2002).
[5] Z. Mei and D.D.L. Chung, "Effect of Heating on the Structure of Carbon Fiber Polyphenylenesulfide-Matrix Composite, as Studied by Electrical Resistance Measurement," *Polym. Compos.* 19(6), 709–713 (1998).

Further Reading

Y. Aoyagi and D.D.L. Chung, "Effects of Antioxidants and the Solid Component on the Thermal Stability of Polyol-Ester-Based Thermal Pastes", *J. Mater. Sci.* 42(7), 2358–2375 (2007).
D.D.L. Chung, "Corrosion Control of Steel Reinforced Concrete", *J. Mater. Eng. Perform.* 9(5), 585–588 (2000).

5 Materials for Lightweight Structures, Civil Infrastructure, Joining and Repair

This chapter addresses materials, particularly composite materials, that are important for lightweight structures, the civil infrastructure, joining, and repair. Since the fabrication of a composite material involves the joining of components, an understanding of joining is necessary for the development of composite materials.

5.1 Materials for Lightweight Structures

A low mass is desirable for numerous structures, including aircraft, automobile, bicycles, ships, missiles, satellites, tennis rackets, fishing rods, golf clubs, wheel chairs, helmets, armor, electronics, and concrete precasts. In the cases of aircraft and automobiles, reducing the mass saves on fuel. Steel is a widely used structural material, but it is heavy, with a density of 7.9 g/cm^3.

Composite materials with continuous fiber reinforcement and with lightweight matrices are the most attractive of all lightweight structural materials. Composites with discontinuous fillers tend to be inferior in strength and modulus than those with continuous fibers, but they are amenable to fabrication through the use of a wider variety of techniques.

5.1.1 Composites with Polymer, Carbon, Ceramic and Metal Matrices

Lightweight matrices are those that exhibit a low density. Examples include polymers (with a typical density of less than 1.5 g/cm^3), carbons (with a typical density of 1.8 g/cm^3, which is below the value of 2.26 g/cm^3 for ideal graphite due to incomplete crystallinity), ceramics (e.g., silicon carbide, with a density of 3.3 g/cm^3 if it is made by hot pressing rather than just sintering), and lightweight metals (e.g., aluminum, with density of 2.7 g/cm^3, and titanium, with a density of 4.5 g/cm^3). Among metal matrices, aluminum is the most common, due to its low density, its high processability (associated with its low melting temperature of 660°C), and its high ductility (associated with its face-centered cubic – fcc – crystal structure). Magnesium is even lower in density (1.7 g/cm^3) than aluminum and also has a low melting temperature (650°C), but it suffers from its relatively low ductility, which is a consequence of its hexagonal close-packed (hcp) crystal structure. In general, materials with noncubic unit cells have fewer slip systems and hence lower ductility than materials with cubic unit cells. Ductility is an important factor for the

matrix of a composite material because the reinforcement tends to be strong and brittle, and a brittle matrix causes the composite itself to become very brittle. In contrast, a ductile matrix blunts crack tips upon the emergence of the cracks from the reinforcement, thus making the composite less brittle. Titanium has a relatively high density (4.5 g/cm^3) and is relatively brittle (due to its hcp structure), but it is still attractive due to its high temperature capabilities (melting temperature = 1,668°C).

Due to the wide spectrum of temperature capabilities exhibited by the lightweight matrices mentioned above, the choice of matrix material often depends on the temperature requirement. Composites with carbon and ceramic matrices are the most attractive for high-temperature applications. Composites with polymer matrices are used for applications that do not involve high temperatures. Composites with metal matrices are used for applications that involve moderately high temperatures. However, all of these composites are valuable for some room-temperature applications, as they provide certain special properties. For example, metal-matrix composites are attractive due to their electrical and thermal conductivities, while carbon-matrix composites are attractive due to their corrosion resistance.

The carbon matrix has an even lower density than the silicon carbide matrix or the silicon nitride matrix, though it is inferior to them in terms of elastic modulus and tensile strength. The modulus of graphite (isostatically molded) is 12 GPa, compared to 207–483 GPa for silicon carbide. The high modulus of silicon carbide compared to graphite is due to the partially ionic character of the covalent bonding in silicon carbide, in contrast to the absence of ionic character in the covalent bonding in graphite. The tensile strength of graphite (isostatically molded) is 31–69 MPa, compared to 230–825 MPa for silicon carbide (hot pressed).

There are a wide range of materials within each class of matrix materials, and the various matrix materials can have different temperature capabilities. For example, semicrystalline thermoplastic polymers can withstand higher temperatures than amorphous thermoplastic polymers (Fig. 4.22), and furthermore, heavily crosslinked polymers can withstand higher temperatures than lightly crosslinked polymers (Fig. 4.21), although the temperature capability of any polymer is limited and tends to be inferior to that of a metal.

5.1.2 Cement-Matrix Composites

The density of concrete is typically 2.4 g/cm^3, which is lower than that of aluminum (2.7 g/cm^3). However, this density is still higher than those of polymers. Lightweight concrete refers to concrete that is lower in density than conventional concrete (achieved through the use of lightweight aggregate).

The elastic modulus of concrete is low (25–37 GPa), compared to 380 GPa for aluminum, and 207–483 GPa for silicon carbide. The tensile strength of concrete is also low (37–41 MPa), compared to 90 MPa for annealed aluminum alloy 1,100, and 230–825 MPa for hot-pressed silicon carbide. In spite of its low modulus and strength, concrete is attractive as a structural material due to its processability in the field (outside a factory) – it simply requires mixing and pouring, without any need for heating or the application of pressure.

Concrete is not attractive for lightweight structures because its mechanical properties cannot compete with continuous fiber polymer-matrix composites, even if the cement-matrix composite contains continuous fiber reinforcement. This problem with cement-matrix composites arises because it is difficult for the cement matrix – which is relatively high in viscosity compared to polymer resins – to penetrate the fine space between continuous fibers during composite fabrication (even in the absence of aggregate), in contrast to the relative ease with which a polymer matrix can penetrate this fine space. Inadequate penetration of the fine space means poor bonding between the fibers and the matrix, in addition to high porosity. As a consequence of this inadequate penetration, the fibers are not able to act very effectively as a reinforcement. In other words, the modulus and strength of the resulting composite are lower than the theoretical values obtained by assuming perfect bonding between the fibers and the matrix.

5.2 Materials for Civil Infrastructure

Civil infrastructure refers to structures that support the operation of a society. They include highways, bridges, buildings, water pipes, sewage pipes, oil pipes, and electric power distribution lines. Materials used for highways and bridges include concrete, steel, continuous fiber polymer-matrix composites, asphalt (pitch-matrix composites containing aggregates), aggregates, and soil. Materials used for pipes include concrete, iron, and polymers (such as polyvinyl chloride). Most of these materials are composite materials, including particulate, fibrous and layered composites, as described below.

Concrete is a cement-matrix composite that contains both fine aggregate (sand) and coarse aggregate (gravel). These aggregates make concrete a particulate composite. The use of both fine and coarse aggregates in the same composite allows the total aggregate volume fraction to be higher than what would be obtained if only the fine aggregate or only the coarse aggregate was used. The fine aggregate fills the space between the units of the coarse aggregate, as illustrated in Fig. 1.12. The resulting high total aggregate volume fraction leads to a high compressive strength and modulus, in addition to a low drying shrinkage. Concrete provides an example of a particulate composite with multiple particle sizes.

Mortar is a cement-matrix composite that contains only the fine aggregate. As a result, mortar has a lower aggregate volume fraction than concrete and is thus not as strong as concrete. However, the absence of the coarse aggregate allows mortar to be used as a relatively thin layer, such that the layer of mortar between two bricks can be used to join the bricks by cementitious bonding.

Concrete is much stronger under compression than under tension due to the brittleness of the cement matrix. The aggregates are not sufficient to provide concrete with the required tensile or flexural properties. Therefore, steel reinforcement is necessary. Concrete with steel reinforcing bars (rebars) is widely used for highway pavements and bridge decks (Fig. 5.1). The rebars make the concrete a fibrous composite. Since the rebars are long (e.g., as long as the height of a concrete

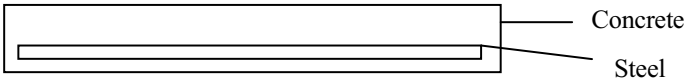

Figure 5.1. Concrete reinforced with an embedded steel rebar. A beam under flexure is under tension on one side and under compression on the other side. The rebar is positioned in the part of the beam that is under tension; it is not positioned in the middle plane

column), they are considered a form of continuous reinforcement. Thus, steel-reinforced concrete is both a fibrous composite and a particulate composite. In this composite, the particulate composite is concrete, which may be considered the matrix, while the steel rebars are the reinforcement.

Cementitious bonding refers to bonding resulting from the adhesiveness of cement. The bonds between aggregate and cement and between a steel rebar and concrete are cementitious. However, this cementitious bonding is weak compared to the bonding resulting from a polymeric adhesive such as epoxy.

A steel rebar exhibits surface deformation such that the surface has undulations like ridges. These ridges allow mechanical interlocking between the rebar and the concrete. This mechanical interlocking makes it difficult to pull the rebar out from the concrete. Since the cementitious bonding between the rebar and concrete is not very strong, the mechanical interlocking is a valuable way of enhancing the bond. This provides an example of a reinforcement with a rough surface.

Only one rebar is shown in Fig. 5.1, but in practice a steel rebar mat is commonly used. A mat is a grid consisting of rebars in two directions that are perpendicular to each other, such that those in one direction are above those in the other direction and are tied (fastened using wires) to those in the other direction. A bridge deck typically has a steel rebar mat in its upper part and another steel rebar mat in its lower part. Vertical concrete beams, called bulb tee beams, with layers of embedded steel strands placed at selected critical positions at the bottom part of the beam (Fig. 5.2) are commonly used for bridges. These are examples of fibrous composites in which the reinforcement is not uniformly distributed but is instead judiciously positioned. For concrete columns, vertical steel rebars and spiral steel wire are commonly used in combination (Fig. 5.3), thus providing an example of a fibrous composite that involves multiple geometries of fibrous reinforcement.

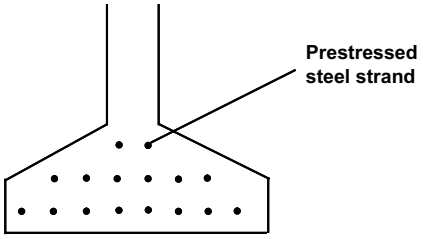

Figure 5.2. The bottom part of a vertical concrete beam, known as a bulb tee beam, with numerous embedded steel strands (indicated by *solid circles*) in the direction perpendicular to the page

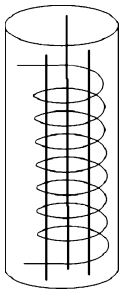

Figure 5.3. A concrete column reinforced with vertical straight steel rebars and a steel spiral

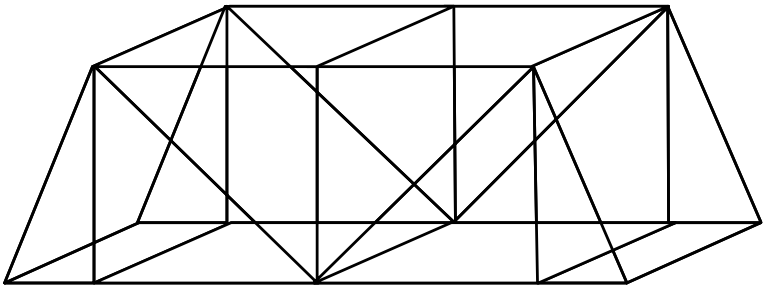

Figure 5.4. A steel truss. Each line represents a steel beam

Steel beams that are fastened together in the absence of concrete are used for trusses, such as that used in a truss bridge (Fig. 5.4). The fastened joints in a truss allow deformation, thereby providing the structure with vibration damping. However, the joints tend to suffer from crevice corrosion.

Immediately beneath a concrete pavement is a layer of aggregate with little or no cement. This layer is called the base (Fig. 5.5), and it provides mechanical stability in addition to drainage. This drainage is enabled by the water permeability of the base and helps to avoid the collection of excess water that can degrade the pavement. Beneath the base is the subgrade (Fig. 5.5), which is soil – the most abundant material on Earth. The base and subgrade are critical to the performance of a pavement. The combination of pavement, base, and subgrade provides an example of a layered composite.

Asphalt is a particulate pitch-matrix composite. Pitch is a thermoplastic polymer that melts upon heating. Thus, the pouring of asphalt requires heating. Like concrete, asphalt has aggregates. It can be used in place of concrete as a pavement material. Compared to concrete, asphalt is not durable and is mechanically soft. However, it is advantageous in terms of its vibration damping ability and the consequent improvement of driving comfort. Therefore, asphalt is also used as an overcoat on a concrete pavement. This provides an example of a layered composite involving concrete as one layer and a polymer-matrix composite as the other layer.

Cast iron, which is known for its corrosion resistance, has historically been used for water and wastewater pipes. Currently, iron with a spheroidal graphite

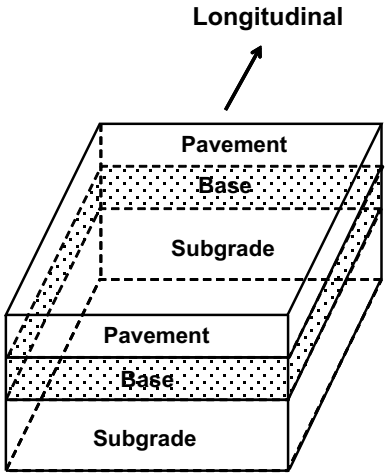

Figure 5.5. A pavement with base (gravel layer) underneath and subgrade (soil layer) underneath the base. The base layer allows water to flow through it in order to avoid the local collection of water. The longitudinal direction refers to the direction of traffic

precipitate – known as ductile iron – is used instead. Ductile iron is akin to but different from cast iron, which has flake graphite precipitate. Due to the spheroidal graphite precipitate, ductile iron is stronger and more ductile than cast iron. This provides an example of a layered composite involving the use of metal as one layer and a cement-based material as the other layer.

A ductile iron pipe has a cement mortar lining inside the pipe for the purpose of corrosion protection. Corrosion is particularly serious when the water is acidic. It causes tuberculation, which refers to the formation of small mounds of corrosion products on the inside surface of a pipe. Due to the centrifugal casting used to manufacture iron pipes, there is variation in the wall thickness along the length of a pipe. As a result, the durability of a pipe varies along its length.

Both unreinforced concrete and steel-reinforced concrete are used for pipes. The unreinforced concrete has no steel reinforcement, but may have asbestos reinforcement. Asbestos fibers are an effective reinforcement, but their carcinogenic character results in health concerns. Due to the water in the pipe and in the soil surrounding the pipe, corrosion is an issue. As a result, the corrosion of the steel rebars and the consequent degradation of the steel-concrete bond are an important consideration for steel-reinforced concrete pipes.

5.3 Materials for Joining

Joining is at the heart of composite fabrication, since the creation of a composite involves the joining of various components, such as the joining of fiber and matrix. The bonding between the reinforcement and the matrix is critical to the mechanical integrity of a composite.

Due to the limited size of a structural component (for example, the size of a panel is limited by the equipment used to fabricate it), most structures involve the joining of components. The structural integrity of the resulting joints is critical to the mechanical integrity of the overall structure.

Joining may be achieved by sintering, welding, brazing, soldering, adhesion, or fastening. This section covers various types of joints.

5.3.1 Sintering or Autohesion

Diffusive adhesion refers to bonding that results from the diffusion of certain species from one party to another. Sintering is one of the forms of diffusive adhesion. It involves solid-state diffusion. Sintering commonly refers to powder metallurgy – the bonding of solid particles due to the solid-state diffusion of atoms between adjacent particles, as illustrated in Fig. 1.7 and shown in Fig. 5.6 for the sintering of silver particles. In the field of thermoplastic polymers, sintering is known as autohesion, which refers to diffusive adhesion at temperatures above the glass transition temperature T_g and below the melting temperature T_m.

In liquid-state sintering, at least one but not all of the elements exist in the liquid state. This means that liquid-state sintering (a rather confusing term) involves solid-state diffusion that is supplemented by the presence of a liquid, the flow of which aids the sintering. For example, the fabrication of a silicon carbide whisker copper-matrix composite may be achieved by sintering a mixture of silicon carbide whiskers and copper particles at a temperature slightly below the melting temperature of copper, so that only solid-state diffusion occurs (i.e., the admixture method). The diffusion involves copper and does not involve silicon carbide, which has a much higher melting temperature than copper. The addition of a minor proportion of zinc particles to the mixture causes the presence of zinc liquid during the sintering, since the melting temperature of zinc is much less than that of

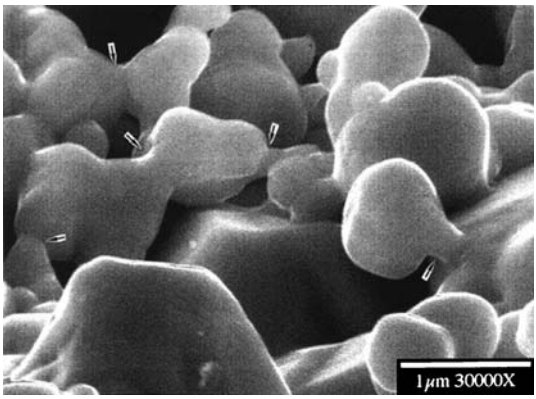

Figure 5.6. Scanning electron microscope photograph of the surface morphology of a silver particle organic-based thick-film paste on an alumina substrate after heating (known as firing) in air at 300°C for 30 min. The heating causes the burning out of the organic vehicle, in addition to the sintering of the silver particles. The *arrows* show the necks between adjacent silver particles. The silver particles are irregularly shaped, with sizes ranging from 1.5 to 2.5 μm. (From [1])

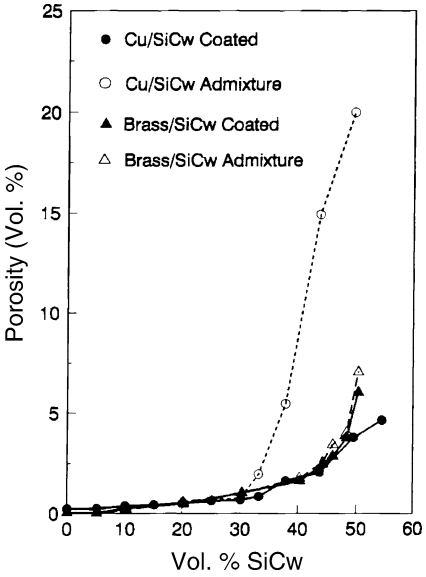

Figure 5.7. Variation of the porosity with the silicon carbide whisker volume fraction in copper-matrix and brass-matrix composites made by the coated filler method and the admixture method. (From [2])

copper. Thus, the presence of zinc results in liquid-state sintering; in other words, the solid-state diffusion of copper that is supplemented by the dissolution of copper in the zinc liquid, which flows, thereby enhancing the mass transport during sintering. Figure 5.7 shows that, for the same filler volume fraction, the presence of zinc results in a composite of lower porosity, whether or not the conventional admixture method of powder metallurgy is used for the composite fabrication (Sect. 1.3.2). If the coated filler method of powder metallurgy is used, the presence of zinc does not make much difference to the porosity of the composite since this method is highly effective at producing composites of low porosity. The presence of zinc in the copper matrix makes the matrix brass.

5.3.2 Welding

A welded joint refers to a joint made by melting parts of the two members involved in the joint at their interface and their subsequent solidification upon cooling. The joining commonly arises from the presence of van der Waals forces – electrostatic interactions between the electric dipoles of one member and those of the other member. These dipoles may be permanent or temporary. Joining based on van der Waals forces is known as dispersive adhesion or adsorption. However, excess material (called the filler metal) that is ideally of the same composition as the members is placed at or around the joint to provide additional mechanical support. The filler metal undergoes melting during welding. Figure 5.8 shows an I-beam (i.e., a beam in the shape of the letter I) obtained by welding a vertical member and two horizontal members together. The filler metal takes the form of a fillet at the

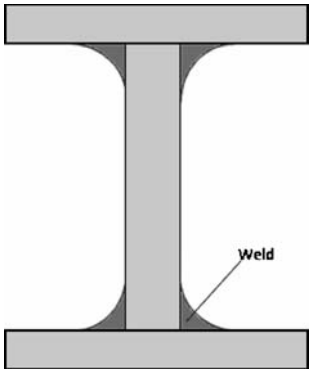

Figure 5.8. A steel I-beam, where the components have been joined by welding

junction between the vertical member and the horizontal member being joined. The molten filler metal penetrates the space between the two members, although this penetration is not shown in Fig. 5.8. This type of weld is called a fillet weld, which is widely used to make lap joints, corner joints, and T-joints.

Because the heat associated with welding affects the microstructure of the members near the joint, the members next to the joint region tend to have a different microstructure than the parts of the members away from the joint region. The zone where the heat has affected the microstructure is known as the heat-affected zone, which is immediately next to the fusion zone (the zone that underwent melting during welding). The change in microstructure is usually undesirable in terms of mechanical properties, as it can take the form of precipitate coalescence (thereby forming larger precipitates), grain growth, and recrystallization. In addition, thermal expansion of the members in the heat-affected zone during welding can cause thermal stress. Therefore, subsequent use of the welded structure under dynamic loading tends to cause fatigue cracks near the toe (tip) of a fillet weld, as illustrated in Fig. 5.9.

A special type of welding involves the joining of members in the form of a thermoplastic polymer, which melts upon heating and subsequently solidifies upon cooling. The joining results from the presence of van der Waals forces, as in the

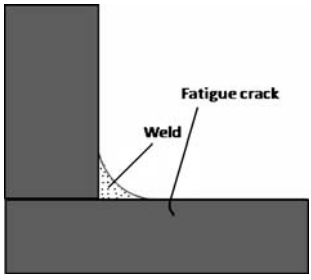

Figure 5.9. A fatigue crack near the toe of the fillet of a weld joining two members that are perpendicular to one another

case of the welding of metals. Although a thermoplastic material softens at the glass transition temperature, it needs to be heated to temperatures close to or beyond the melting temperature in order for it to be sufficiently fluid for a strong bond to form. The required temperature depends on the pressure used to hold the adjoining surfaces together during the joining operation. The higher the pressure, the lower is the required minimum temperature.

Polyphenylene sulfide (PPS) is a high-temperature thermoplastic polymer with a thermosetting/thermoplastic character. Its melting temperature is 280°C and its glass transition temperature is 90°C in the material used to obtain the results given below. Due to the CTE mismatch between crossply laminae of carbon fiber PPS-matrix composite, thermal stress arises during cooling after the bonding has been conducted at an elevated temperature. As a result, debonding can take place during cooling. This debonding can be monitored in real time by measuring the contact electrical resistance of the bonding interface. Upon debonding, the resistance increases abruptly. Figure 5.10 shows the effect of the bonding temperature on the bond between (PPS) surfaces, with the pressure fixed at 4.8×10^3 Pa during the bonding and subsequent cooling. The heating rate up to the bonding temperature is 10°C/min and the temperature is held at the bonding temperature for 5 h. When the bonding temperature is 260, 280, or 285°C (i.e., below the melting temperature, at the melting temperature, or just 5°C above the melting temperature), debonding occurs during the cooling, so that the bonding process fails. However, when the bonding temperature is 290°C (i.e., 10°C above the melting temperature),

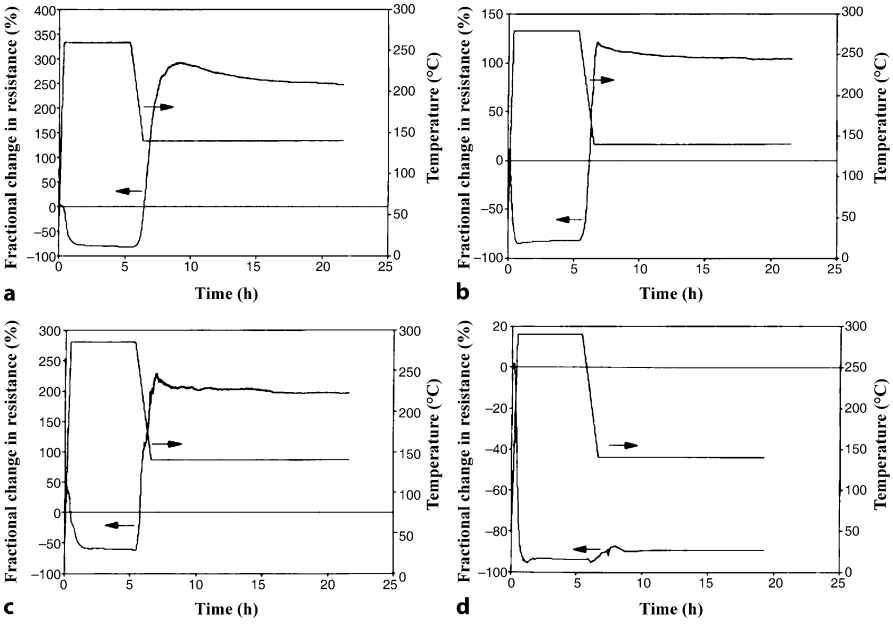

Figure 5.10. Effect of PPS–PPS bonding temperature on the variation in contact electrical resistance at a constant pressure of 4.8×10^3 Pa. **a** 260°C; **b** 280°C; **c** 285°C; **d** 290°C. (From [3])

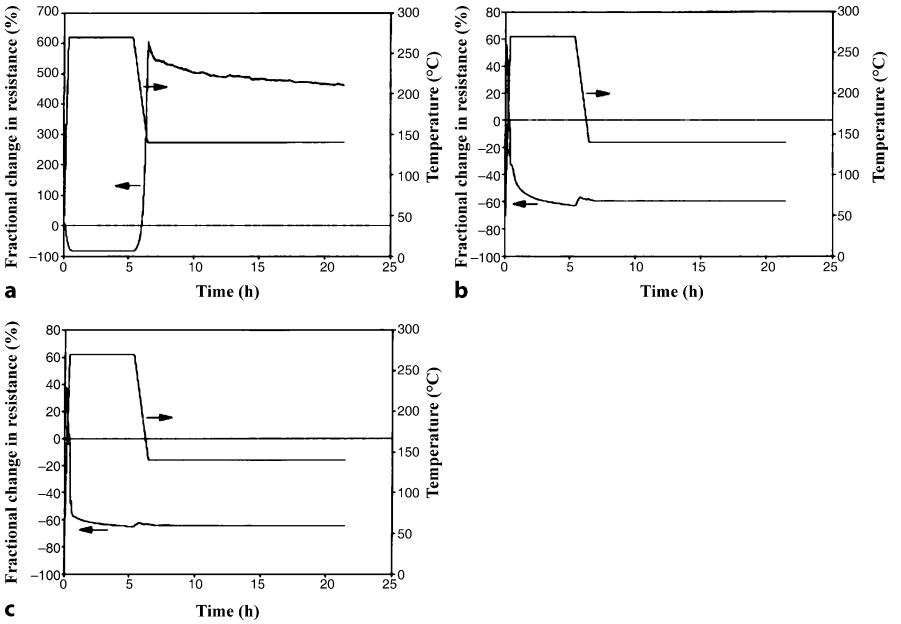

Figure 5.11. Effect of PPS–PPS bonding pressure on the variation in contact electrical resistance at a fixed bonding temperature of 270°C. **a** 4.8×10^3 Pa; **b** 3.0×10^5 Pa; **c** 6.8×10^5 Pa. (From [3])

debonding does not occur, as shown by a slight increase in the resistance during the cooling. This means that, for a bonding pressure of 4.8×10^3 Pa, the minimum bonding temperature is 290°C.

The bonding pressure also affects the PPS–PPS bond. Figure 5.11 shows that, at a fixed bonding temperature of 270°C, with the heating rate up to the bonding temperature being 10°C/min, a bonding pressure of 4.8×10^3 Pa results in debonding during cooling, but a bonding pressure of either 3.0×10^5 Pa or 6.8×10^5 Pa does not cause debonding during cooling. This means that, for a bonding temperature of 270°C, the minimum bonding pressure is 3.0×10^5 Pa.

The time spent below the melting temperature prior to bonding also affects the PPS–PPS bond. The longer the time spent below the melting temperature, the weaker the resulting bond. This is because of the curing reactions that occur below the melting temperature and the consequent reduced mass flow response above the melting temperature. Therefore, a high heating rate (such as 10°C/min) to the bonding temperature gives a stronger bond than a low heating rate (such as 5°C/min).

5.3.3 Brazing and Soldering

A brazed or soldered joint is a joint formed by melting a material (i.e., the brazing or soldering material) that has a melting temperature below that of the members being joined, so that the material melts while the members do not melt during

the brazing or soldering. Upon subsequent solidification of the material, a joint is formed that is at least partly due to van der Waals forces. The joint is stronger if the atoms in the brazing or soldering material diffuse into one or both of the members to be joined. This diffusion is possible if the atoms are mobile enough and are soluble in the member. For example, the diffusion may result in the formation of a solid solution at the joint interface. Joining due to diffusion is known as diffusive adhesion.

Brazing and soldering differ in terms of the temperature range of the operation. Brazing occurs at higher temperatures (above about 450°C) than soldering (below about 450°C), due to the higher melting temperature of the brazing material compared to the soldering material. As a consequence, a brazed joint can withstand higher temperatures than a soldered joint. The fillet geometry used for brazed or soldered joints is similar to that shown in Fig. 5.9.

One problem with a brazed or soldered joint is the possible chemical reaction between the brazing or soldering material and the members to be joined during the brazing or soldering operation. The reaction product tends to line the joint interface, thus making it difficult for the molten brazing or soldering material to wet the surfaces to be joined. Furthermore, the reaction products are often intermetallic compounds that are quite brittle. An example relates to the reaction between copper (commonly used for electrical conduction lines) and the tin in common tin-lead solder. This reaction results in copper-tin intermetallic compounds, such as Cu_3Sn and Cu_6Sn_5.

Brazing or soldering is particularly challenging when one or both of the surfaces being joined is/are not wetted by the molten brazing or soldering material. Poor wetting means the "balling up" of the liquid, rather than the spreading of the liquid on the surface. This results in porosity at the joint interface and hence a poor joint. Metal surfaces are wetted by molten metals, but ceramic surfaces do not tend to be wetted by molten metals. Therefore, the joining of ceramic to ceramic or of ceramic to metal is challenging. This problem can be removed by coating the ceramic surface with a metal. However, the coating process is expensive and may be unsuitable for some applications.

One technique for enhancing the wetting of a molten metal on a ceramic surface involves the addition of a small fraction of an active constituent (such as titanium, which reacts with the ceramic) to form an alloy. Such a soldering or brazing alloy is said to be active. Such an active brazing alloy (ABA) can take the form of a paste or a sheet. An example of an ABA paste is Cusin-1 ABA from WESGO Inc. (Belmont, CA, USA); this contains 63 wt.% Ag, 34.25 wt.% Cu, 1.75 wt.% Ti and 1.0 wt.% Sn; its melting temperature is 780–815°C. Due to the reaction between the active constituent and the ceramic surface and the fact that the reaction requires contact between the species, wetting is enabled by the presence of the active constituent. The use of an active alloy typically requires the use of either an inert atmosphere or a vacuum during the soldering or brazing operation. Otherwise, the active constituent may be oxidized by the oxygen present in air to form an oxide (e.g., titanium dioxide), making it less available to react with the ceramic. The reaction of the active soldering or brazing alloy with the ceramic results in a reaction product that is commonly quite brittle at the interface between the

soldering or brazing material and the ceramic surface. The thicker this reaction product layer, the poorer the joint. To alleviate this problem, a filler (e.g., short carbon fiber, preferably coated with metal to improve the wettability of the fiber by the molten soldering/brazing material) that reacts with the active constituent may be added to the soldering or brazing material. In other words, the soldering or brazing material is a metal-matrix composite containing the filler. The filler acts as a getterer of (trap for) the active constituent, thus diminishing the thickness of the reaction product layer at the interface between the soldering/brazing material and the ceramic surface and hence improving the joint. However, an excessive amount of filler is not desirable, as it may result reduce the reaction at the interface between the soldering/brazing material and the ceramic surface to an insufficient level.

Another problem with joining a metal and a ceramic by soldering or brazing is the CTE difference between the metal and the ceramic. For example, the CTE of alumina is 8.5×10^{-6}/°C, whereas that of stainless steel (No. 304) is 18.4×10^{-6}/°C. The CTE of a soldering or brazing alloy is quite high. For example, the Ag-Cu brazing alloy containing 64 wt.% silver and 36 wt.% copper has a CTE of 19.5×10^{-6}/°C, which is even higher than that of the steel mentioned above. The addition of 8.4 vol% of short carbon fiber to this alloy reduces the CTE from 19.5×10^{-6} to 17.3×10^{-6}/°C, which is between the values of steel and alumina. The CTE mismatch between the metal and ceramic components being joined causes thermal stress, which is particularly severe when the cooling rate after the soldering/brazing is high. As a result, the higher the cooling rate, the lower the shear bond strength of the joint. For example, the shear bond strengths between alumina and steel, as obtained using the configuration of Fig. 5.12a, are 69, 18, and <3 MPa at cooling rates of 4.8, 10.6, and 20°C/min, respectively.

The shear bond strength can be measured using the two specimen configurations shown in Fig. 5.12. The shear stress is the force divided by the joint area. The shear bond strength (also called the shear debonding strength) is the maximum shear stress that the joint can withstand without debonding. Of the two configurations presented in Fig. 5.12, that shown in (a) is less desirable, because a bending moment exists during the shear, as caused by the asymmetry in the geometry

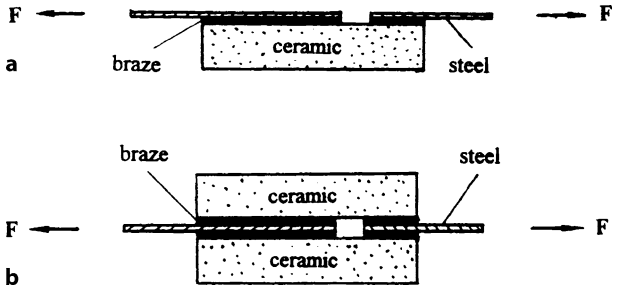

Figure 5.12. Specimen configuration for measuring the shear bond strength between ceramic and metal (e.g., steel). **a** The ceramic is bonded to only one side of the metal. **b** The ceramic is bonded to both sides of the metal. The symmetrical configuration in (**b**) avoids bending moment during testing, so it is preferred to the asymmetrical configuration in (**a**). (From [4])

Table 5.1. Shear bond strength of the brazed joint between stainless steel (No. 304) and alumina (Al_2O_3), obtained using the testing configuration of Fig. 5.12b. The cooling rate after brazing at 950–1,000°C for 15–20 min is 4.8°C/min (from [4])

Carbon fiber content of active brazing alloy	Shear bond strength (MPa)
Without carbon fiber	86.4 ± 3.0
With carbon fiber (uniform distribution)	102.1 ± 3.0
With carbon fiber (graded distribution)	110.7 ± 3.0

(with the ceramic on just one side of the steel). The presence of a bending moment means that the deformation is not pure shear, and this results in an underestimate for the shear bond strength.

The problem associated with the CTE mismatch can be alleviated by adding a low-CTE filler (e.g., short carbon fibers) to the solder/brazing material. A particularly advantageous configuration involves a graded distribution of the low CTE filler, so that the filler concentration is higher in the region near the ceramic surface than in the region near the metal surface. Furthermore, the gettering of the active constituent by the filler results in a low concentration of the active constituent in the matrix of the solder/brazing metal-matrix composite, making the matrix softer and hence reducing the thermal stress. Table 5.1 shows that the shear bond strength of a steel-alumina brazed joint is increased by adding short carbon fibers (8.4 vol%) to the active brazing alloy (63 wt.% Ag, 34.25 wt.% Cu, 1.75 wt.% Ti and 1.0 wt.% Sn), such that the effect is greater when the fiber has a graded distribution than when the fiber is uniformly distributed.

One disadvantage of a brazed or soldered joint compared to a welded joint is that the former involves contact between dissimilar materials, thus allowing galvanic corrosion. In contrast, a welded joint does not involve dissimilar materials. Brazed, soldered, and welded joints are not prone to crevice corrosion, in contrast to fastened joints.

5.3.4 Adhesion

An adhesive joint is a joint formed by using an adhesive, which is a polymeric material. The polymer may be thermoplastic or thermosetting.

If the adhesive is a thermoplastic polymer, it melts upon heating and its melting temperature is below that of the members being joined. Upon subsequent cooling, the polymer solidifies and a joint is formed, partly due to van der Waals forces. The bonding is enhanced if it involves not only van der Waals forces but also the diffusion of some atoms or molecules from one party to the other. This diffusion is possible when the atoms or molecules are mobile enough and are soluble in the other party. For example, a molecule of a thermoplastic polymer adhesive may diffuse into one of the members to be joined such that one end of the molecule enters the member. Bonding resulting from diffusion is known as diffusive adhesion.

If the adhesive is a resin (i.e., the precursor of a thermosetting polymer), it cures after application and a joint is formed when it sets. The bond is partly based on van der Waals forces (i.e., dispersive adhesion). Adhesive bonds that are

mechanically strong tend to involve not only van der Waals forces but also chemical bonding between the adhesive and each of the two members being joined. The chemical bonding may be due to the formation of ionic, covalent or hydrogen bonds. Hydrogen bonding commonly occurs when an electronegative atom, such as oxygen, nitrogen or fluorine, in one molecule interacts with a hydrogen atom in another. Joining resulting from the formation of chemical bonds is known as chemical adhesion. The bond is particularly strong when ionic or covalent bonding is involved. The curing tends to be more complete, resulting in a stronger bond, if it is conducted at an elevated temperature. However, room-temperature curing is possible, particularly if sufficient time is allowed for the curing. The higher the temperature, the shorter the time required. The temperature and time required for the curing process depends on the particular type of resin.

The adhesiveness of the adhesive is obviously important. This depends on the physics and chemistry of the resin, as they govern the nature of the bonding; in other words, the contributions of chemical adhesion, dispersive adhesion, and diffusive adhesion.

In order for an adhesive to be able to penetrate into the small space between the members being joined, it needs to be sufficiently fluid. Thermoplastic polymeric adhesives tend to be low in fluidity compared to resin adhesives. There is a considerable range of fluidity among resin adhesives, and this depends on their chemistry. The use of a solvent in a resin adhesive can increase the fluidity, but it also tends to cause voids in the resulting joint due to the incomplete removal of the solvent.

5.3.5 Cementitious Joining

A cementitious joint is a joint obtained using silicate cement, such as Portland cement. The cement paste is the joining medium. Before curing, the cement paste is fluid enough to enter and conform to the space between the members to be joined, such as the space between two bricks in a brick wall under construction. The ability of the paste to conform to the surface topography of the members to be joined depends on the wettability of the surface by the paste, which contains water. Thus, a surface that is hydrophilic is preferred. Carbon fiber is hydrophobic, but it can be rendered hydrophilic by ozone surface treatment. The iron oxide on steel also helps to improve the hydrophilicity of steel.

After curing (a reaction known as hydration), the cement paste is rigid and a bond has been formed due to van der Waals forces. As the surface of the members being joined is typically rough (as in the case of bricks), the cement paste enters the surface pores of the members, thus allowing mechanical interlocking to take place after the curing of the cement paste. Due to the weakness of van der Waals bonds, mechanical interlocking is an important mechanism for strengthening the joint. The bond between concrete and steel rebars and that between cement and aggregate have similar origins since they both involve van der Waals forces and mechanical interlocking. The bond between carbon fibers and cement also involves van der Waals forces, but the contribution from mechanical interlocking is small due to the smoothness of the fiber surface.

A cementitious bond suffers from the presence of air voids at the joint interface. These voids are due to both the limited fluidity (and hence limited conformability) and the drying shrinkage of the cement paste. The use of silica fume (nanoparticles) as an admixture makes the pores smaller in both the cement matrix and the joint interface. The reduction in air void size at the joint interface helps to strengthen the joint. The use of a polymer admixture (e.g., a latex particle dispersion and methylcellulose aqueous solution) reduces the porosity in the cement matrix and results in a polymer lining at the joint interface. The lining helps to strengthen the joint, because the polymeric lining acts as an adhesive in addition to reducing the porosity at the joint interface.

A cementitious bond also suffers from the drying shrinkage of the cement paste during curing. For example, the cement paste at the interface between two bricks shrinks while the bricks obviously do not shrink. The shrinkage stress encountered by the cement paste is detrimental to the bond between the cement paste and the brick. Although the presence of aggregate lowers the drying shrinkage, the shrinkage remains significant. The use of silica fume and short carbon fiber as admixtures is an effective way of reducing the drying shrinkage due to the small sizes of these admixture units and the consequent ability of these admixtures to restrain the cement matrix from shrinking. As a result, the use of these admixtures results in stronger cementitious joints.

5.3.6 Joining Using Inorganic Binders

Inorganic binders are advantageous compared to adhesives due to their ability to withstand high temperatures. They are commonly glasses, such as silica and alumina in the form of nanoparticles, that are commonly dispersed in a liquid vehicle. Such a dispersion is known as a colloid. The vehicle evaporates during the heating associated with joint formation, thereby leaving just the nanoparticles at the joint. Alternatively, the glass can be used in powder form without a vehicle.

Inorganic binders are commonly used to bind short fibers at their junctions in order to form a porous fibrous article. One application relates to hot gas filtration, in which the article serves as a high-temperature filter membrane. Another application relates to the fibrous preform for metal-matrix composite fabrication by liquid metal infiltration. In such applications, the binder is mixed with the short fibers and subsequently heat treated to allow the binder to join the fibers at their junctions.

Inorganic binders are also used to join metal particles during the formation of thick films (with thicknesses in the micrometer range) that are electrically conductive and used as electrical interconnections in microelectronics. The film is produced on an insulating substrate, such as alumina. In order to achieve high electrical conductivity, the metal particles are commonly silver. In this application, silica glass powder (known as glass frit) with a composition that is chosen according to the desired processing temperature is commonly used as the binder. During the heat treatment, the glass flows, allowing bonding between the film and the substrate in addition to bonding between the metal particles in the film. During the

same heating process, the metal particles sinter, forming necks between adjacent particles and thus resulting in a metal network (Fig. 5.6), which is important for achieving high electrical conductivity. Without the metal network formation, the conductivity is much lower due to the resistance at the interface between the individual metal particles. The resulting composite film consists of two three-dimensional interpenetrating networks – the metal network and the glass network.

An example of an inorganic binder is colloidal silica from Dupont Chemicals (Wilmington, DE, USA), designated Ludox HS40, with a silica particle size of 12 nm and a specific surface area of 220 m^2/g. Another example is colloidal alumina from PQ Corporation (Valley Forge, PA, USA), designated Nyacol AL-20, with an alumina particle size of 50 nm and 20 wt.% solid in the colloid. The glass flows upon heating between the surfaces to be joined and causes bonding upon subsequent cooling.

Another type of inorganic binder is a phosphate liquid solution, such as acid phosphate, which is a solution obtained by dissolving aluminum hydroxide ($Al(OH)_3$) in phosphoric acid (H_3PO_4) by stirring and heating to about 150°C, with the solution preferably having a P/Al atom ratio of 23 [5]. The solution flows between the surfaces to be joined and, upon subsequent heating (e.g., 800°C for 3 h), undergoes a chemical reaction whereby the solution is converted to a solid that acts as a binder. The reaction products are aluminum phosphate solid phases that have been identified by X-ray diffraction (Fig. 5.13).

The phosphate solution binder is advantageous compared to colloidal binders in terms of the high fluidity of the liquid solution and the consequent ability of the binder to enter very small spaces between the surfaces to be joined. As shown in Fig. 5.14, the phosphate binder is only located at the junction of the fibers that need to be bound, so excess binder is not located on the surfaces of the fibers away

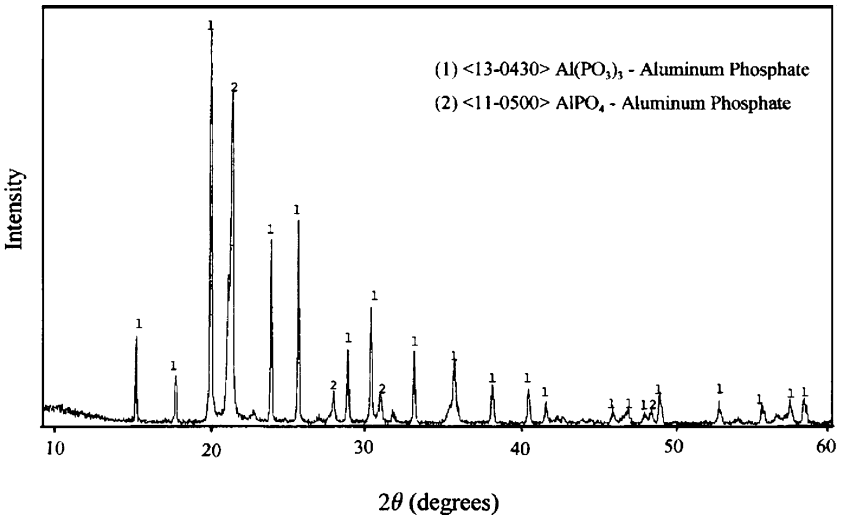

Figure 5.13. X-ray diffraction pattern showing two aluminum phosphate solid phases that result after heating a phosphate liquid solution binder. (From [6])

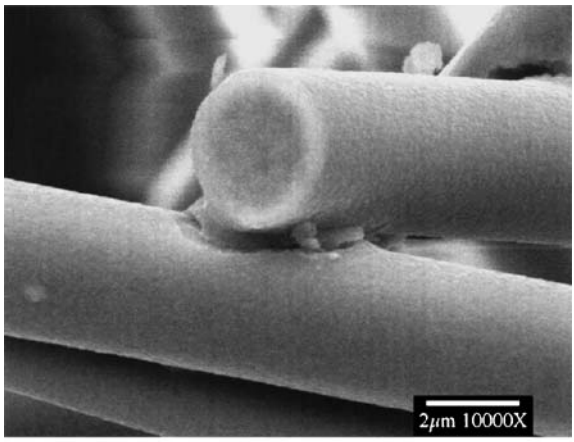

a

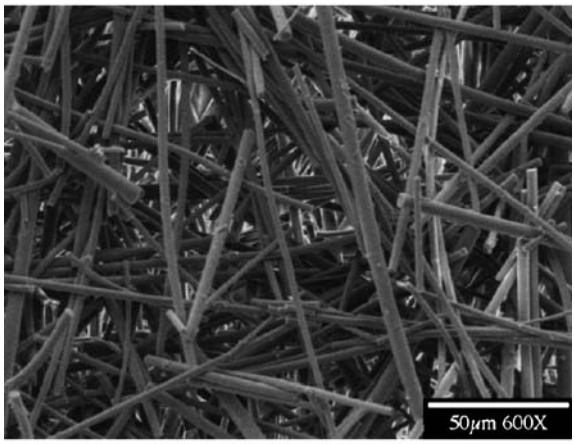

b

Figure 5.14. Scanning electron microscope photographs of alumina fibers bound by a phosphate binder. **a** The phosphate binder at the junction between two alumina fibers. **b** A collection of bound alumina fibers, with the phosphate binder not visible. (From [6])

from the fiber functions. In contrast, the colloidal silica or alumina binder requires a relatively large amount of binder for the binding to be adequate, thus resulting in excess binder being distributed on the surfaces of the fibers (Fig. 5.15). This excess binder is detrimental to the fluid permeability (as needed to filter exhaust gases from coal-fired power stations) of the resulting fiber membrane. As a consequence, the phosphate solution binder provides alumina fiber filter membranes with higher permeability, higher flexural strength, higher compressive strength, and higher modulus than membranes provided by colloidal binders.

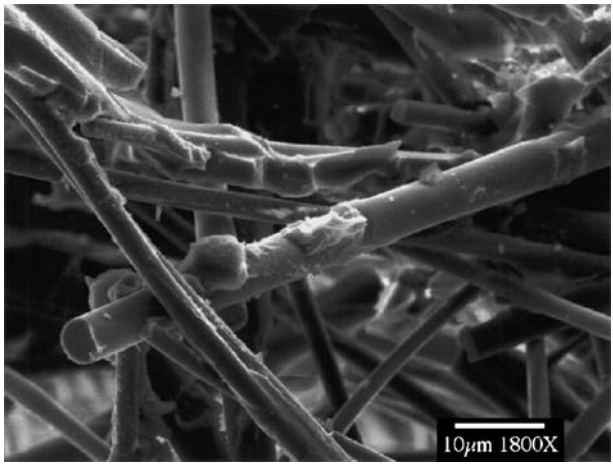

Figure 5.15. Scanning electron microscope photograph showing the colloidal alumina binder distributed on the surfaces of the alumina fibers that it is required to bind. (From [6])

5.3.7 Joining Using Carbon Binders

A carbon binder is used in the form of a carbon precursor (such as pitch). Heating after binder application causes carbonization of the carbon precursor. The resulting carbon is the binder. For ease of penetration into the small space between the adjoining surfaces, the carbon precursor is preferably applied in the form of a liquid, which can be obtained by dissolving pitch in methylene chloride to form a solution, or by heating the pitch to melt it. Carbonization of the carbon precursor can be conducted by heating, for example, in nitrogen at 1,000–1,200°C for 1 h. Advantages of the carbon binder include the high temperature resistance, thermal conductivity, electrical conductivity, and chemical resistance of carbon.

Porous carbons have been made from discontinuous carbon fibers or nanofibers using a pitch-based carbon binder and a solution of pitch in methylene chloride. A porous carbon with a porosity of 56% and mean pore size of 4 μm has been obtained using carbon nanofibers 0.1 μm in diameter. A porous carbon with a porosity of 59% and a mean pore size of 42 μm has been obtained using carbon fibers 10 μm in diameter and 50 μm in length [7]. Such porous carbons are useful for electrodes, catalyst supports, filters, and membranes.

5.3.8 Fastening

A fastened joint is a joint made by mechanically holding two members together. Figure 5.16 shows an example of a joint achieved by fastening. A fastener (e.g., a bolt) is typically kept in place by nuts positioned on both sides of the pair of members being joined. The tightening of the nuts onto the fastener provides the compressive stress (squeezing) needed to achieve the fastening. In order to spread the applied load over a larger area, a washer is used between each nut and the pair of plates.

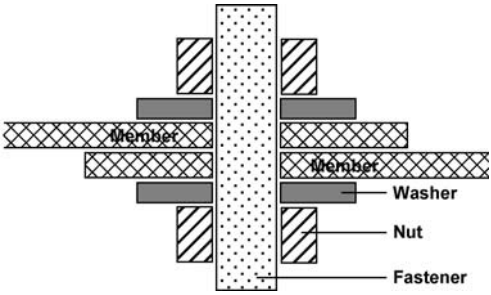

Figure 5.16. A fastened joint. Two member plates are joined by a fastener, such as a bolt

Plastic deformation should not occur in any of the components of a fastened joint during service. Therefore, the stresses encountered should be below the yield stress and all deformations should be elastic. However, the adjoining surfaces are never perfectly flat; there will be some hillocks in the surface topography. Due to the small area of a hillock, the local stress encountered at a hillock may exceed the yield stress, thus resulting in local plastic deformation at the hillock. Upon repeated fastening and unfastening, damage is prone to occur at the adjoining surfaces. When the material is stainless steel, which has a passive film, the damage can involve the passive film, thus resulting in surface oxidation.

Figure 5.17 shows a special type of fastened joint. It is the joint between two sections of a concrete pavement. The joint involves a steel rod with a smooth surface (in contrast to the rough surface of a steel rebar); this rod (called a dowel) is embedded in both sections of the concrete pavement. Due to its smooth surface and the weakness of the resulting cementitious bond, the dowel can slide with respect to the surrounding concrete as the distance between the two concrete pavement sections changes. This provides an example of a joint that is designed for movement.

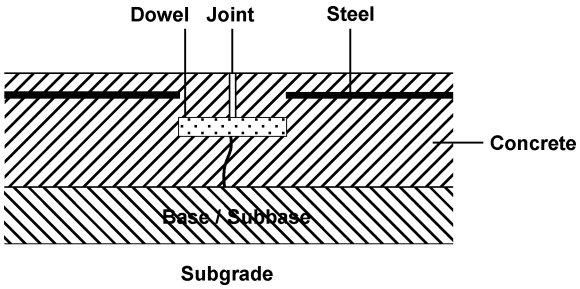

Figure 5.17. A doweled joint in a concrete pavement. This takes the form of a steel dowel embedded in the concrete on both sides of the joint, which is most commonly a construction joint (i.e., a joint included to allow for the pouring of concrete at different sections of a pavement at different times) or an expansion joint (i.e., a joint included to allow room for thermal expansion or contraction of the concrete). The gap between the two sides of the joint above the dowel is typically filled with a flexible board and a sealant

One special type of fastened joint involves the hook-and-loop fastener (commonly known by the brand name Velcro). The fastener involves two surfaces. One surface has tiny hooks, while the other has tiny loops. When the two surfaces are in contact, the hooks get into the loops, thus causing joining. As the hooks and loops are made by polymeric fibers, such as nylon and polyester fibers, they are flexible, thus allowing easy joining and separation, although the joint is not strong mechanically. Upon separation, there is a characteristic ripping sound.

The zipper is another type of fastened joint. It involves a row of teeth (made of metal or polymer) on each of the two members being joined. During zipping, each tooth on one side is inserted into the space between two adjacent teeth on the other side, as facilitated by a slider with a Y-shaped channel, which causes joining when the slider is moved in one direction (the direction from the bottom to the top of the Y), and causes separation when the slider is moved in the opposite direction (the direction from the top to the bottom of the Y).

Sewing (or stitching) is yet another type of fastened joint. It requires threads, which must be so flexible that they can be bent with a small radius of curvature. Due to this requirement for flexibility, polymer fibers are commonly used as threads. Sewing is important not only for clothing and medical sutures but also for the mechanical connection of layers of reinforcing fabrics during the fabrication of a composite material. This connection provides a third dimension of reinforcement in a composite that is otherwise reinforced in only two dimensions. The stitching makes it more difficult for the fabric layers to slide with respect to one another both during and after composite fabrication.

A gasketed joint is a fastened joint that utilizes a gasket at the joint interface to seal the joint. The gasket is a resilient material, not an adhesive, so fastening is necessary. A common configuration involves an elastomer (e.g., rubber) O-ring gasket that is placed on a flange at the joint between two pipe segments (Fig. 5.18). The proximate surfaces of the flanges on the two pipe segments squeeze on the gasket through fastening. The presence of the gasket avoids the leakage of fluid from the pipe.

One disadvantage of elastomers is their limited durability, which is due to the chemical degradation of the elastomer as the material ages. This degradation is

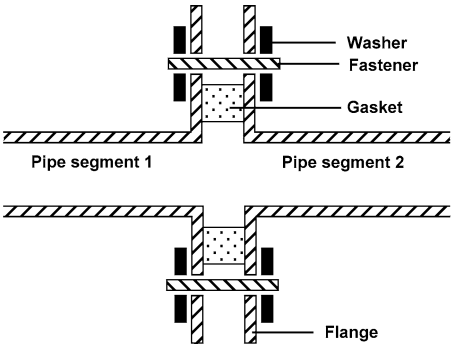

Figure 5.18. A gasketed joint between two pipe segments

akin to rubber bands becoming relatively brittle as they age. Another problem is the gradual occurrence of stress relaxation in the elastomer. Stress relaxation is commonly seen in stretched rubber bands, which gradually become looser. Asbestos is an alternative gasket material that is attractive due to its chemical and high temperature resistance. However, asbestos is carcinogenic. An increasingly important gasket material is "flexible graphite" (made from exfoliated graphite and explained in Sect. 1.1), which is resilient and resistant to chemicals and high temperatures.

5.3.9 Expansion Joints

An expansion joint is a joint that allows the two members to move relative to one another. The two members are separated by a small distance in order to allow room for the thermal expansion of both members as the temperature increases. Expansion joints are most commonly used in concrete pavements and bridge decks in the direction transverse to the traffic direction. An example of such a joint involves a pair of complementary cantilever combs, such each member has a comb, as illustrated in Fig. 5.19. The comb configuration allows the vehicles to travel safely on the pavement in spite of the presence of a gap at the joint. Such a joint is known as a mechanical expansion joint, which should be distinguished from the less effective and less durable expansion joints that simply involve the filling the gap with a caulk. Expansion joint failure is one of the principal causes of bridge substructure and superstructure damage. The failure of a bridge costs hundreds of times more than its material value because of the resulting disruption to traffic and the expensive repairs of piers, abutments, and decks that are required.

The concept of the abovementioned mechanical expansion joint is used in comb sensors in microelectromechanical systems (MEMS). A MEMS involves the integration of mechanical elements, sensors, actuators, and electronics onto a common silicon substrate through microfabrication technology in order to create a complete system on a chip. When the two combs are placed at different potentials and separated from one another, the capacitance of the device is sensitive to the displacement of the combs relative to one another. In other words, the comb sensor is a displacement sensor.

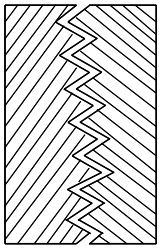

Figure 5.19. A mechanical expansion joint for a bridge, which takes the form of two cantilever steel comb plates that are fastened to the concrete blocks on each side of the joint. The fitted combs move relative to one another as the concrete blocks on both sides of the joint move relative to one another

5.4 Materials Used for Repair

As structures can degrade or be damaged, repair may be needed. Repair often involves the use of a repair material, which may be the same as or different from the original material.

5.4.1 Patching

Due to the tendency for the molecules of a thermoplastic polymer to move upon heating, the joining of two thermoplastic parts can be achieved by thermoplastic welding (Sect. 5.3.2), thereby facilitating the repair of a thermoplastic structure. In contrast, the molecules of a thermosetting polymer do not move readily, and so the repair of a thermoset structure involves other methods, such as the use of adhesives.

A damaged concrete column can be repaired by removing the damaged portion and patching with a fresh concrete mix (Fig. 5.20b). This is akin to repairing the potholes in a road. However, the bond between the patch and the original structure tends to be inadequate, partly because the concrete patch undergoes drying shrinkage whereas the original concrete does not shrink any more. Thus, a loss of patch bonding tends to occur over time, particularly if freeze–thaw cycling occurs, as demonstrated by the frequent need for pothole repair in cold regions.

5.4.2 Wrapping

A superior but much more costly method of repairing a concrete column is to perform the abovementioned patching and then wrap the column with continuous carbon or glass fibers, using epoxy as the adhesive between the fibers and the column (Fig. 5.20a). Although this form of repair is expensive, it is less expensive than tearing down a column and building a new one.

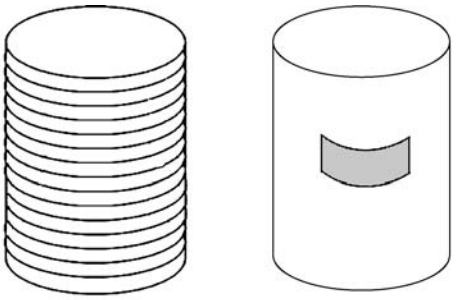

Figure 5.20. Repair of a concrete column by: **a** wrapping the column using carbon fiber epoxy-matrix composite, and; **b** removing the damaged concrete and patching the area with new concrete

5.4.3 Self-healing

Self-healing refers to the ability of a structural material to heal itself upon damage. Preferably, the healing is automatically initiated when damage occurs, akin to a person's wound automatically healing without external means. More established techniques of self-healing involve the automatic filling of cracks with a repair material, which flows into the crack upon damage to the structure.

5.4.3.1 Self-healing Using Microcapsules of a Monomer

One technique involves embedding microcapsules (typically around 100 μm in size, although smaller sizes are possible and are preferred) of a monomer (precursor of a polymer) in a structural material and the incorporation of an appropriate catalyst into the structural material surrounding the microcapsules. When damage that is sufficient to break a microcapsule occurs, the monomer flows out of the microcapsule into a crack, meets the catalyst outside the capsule, and hence polymerizes and fills the crack. By separating the monomer from the catalyst prior to the breaking of the microcapsules, the monomer remains fluid until damage occurs.

The microcapsules need to be small to allow for a large number of microcapsules to be present in a distributed fashion. Upon damage to a given area, only some of the microcapsules break, so that the unbroken microcapsules are still available to provide self-healing during the next round of damage; otherwise the healing can only occur once in a given area. Furthermore, small microcapsules allow the volume fraction of microcapsules in the composite material to be low enough to ensure that the loss of structural material strength resulting from the presence of the microcapsules is acceptably small.

This technique is limited to structural materials that are not porous, since the filling of the pores would then compete with the filling of the cracks; indeed, the filling of the pores overshadows the filling of the cracks in porous materials, resulting no crack healing. An example of a porous structural material for which self-healing is rather ineffective is concrete, which inherently has pores. However, polymer-matrix composites tend to be nonporous and thus suitable for this method of self-healing.

This technique suffers from a restricted selection of monomers and catalysts due to the need for the polymerization to occur without heating. The monomer tends to be toxic and the catalyst is expensive.

5.4.3.2 Self-healing Using Remendable Polymers and Resistance Heating

A remendable polymer is a polymer in which the degree of crosslinking decreases reversibly upon heating. The decrease in crosslinking involves the breaking of certain covalent bonds, which allows the polymer to flow upon heating, providing healing. Such polymers involve certain molecular moieties that are capable of thermally reversible covalent bond formation (i.e., bond breaking upon heating and bond formation upon subsequent cooling). The temperature required for bond

breaking should be low enough to avoid thermal degradation of the polymer-matrix composite. It is typically below 200°C. Such moieties may be incorporated into a monomer or into the backbone of a polymer molecule in order to give the polymer remendability.

The heat required for the remendable polymer to function is preferably provided locally – only in the damaged region of the composite material. This can be achieved by using a composite material that is electrically conductive, with the electrical resistivity increasing upon damage. An electric current is passed through the composite material in order to obtain resistance heating (i.e., the Joule effect, with the electric power given by I^2R, where I is the current and R is the resistance). The higher electrical resistivity of the damaged region causes the heating to be more severe in the damaged region than elsewhere.

An example of a composite material that is suitable for this method is a polymer-matrix composite with continuous carbon fiber reinforcement. Because the fibers are much more conductive than the matrix, the resistivity of the composite in the fiber direction of the composite increases upon fiber breakage. In the usual case that the fibers are oriented in different directions in different composite laminae, the resistivity in the plane of the laminae is increased upon fiber breakage. However, delamination is a more common type of damage than fiber breakage, which tends to occur only when the damage is severe. Delamination causes less contact between fibers of adjacent laminae across the interlaminar interface, thus causing the electrical resistivity in the through-thickness direction of the composite to increase. Even the in-plane resistivity is increased by delamination, because delamination restricts the ability of the current in the plane of a lamina to move into a neighboring lamina. The in-plane resistivity is relevant to resistance heating since the current that leads to resistance heating is typically in-plane. As explained above, the in-plane resistivity is increased upon damage, whether the damage involves delamination or fiber damage.

Review Questions

1. Why do the microcapsules of monomer used in self-healing need to be sufficiently small?
2. What is the advantage of the shear testing configuration of Fig. 5.12b over that of Fig. 5.12a?
3. What is the difference between solid-state sintering and liquid-state sintering?
4. In relation to powder metallurgy, what is the advantage of the coated filler method over the admixture method?
5. What is the difference between diffusive adhesion and dispersive adhesion?
6. What is the advantage of using acid phosphate binder rather than colloidal alumina binder when making a porous article of discontinuous alumina fiber?

References

[1] Z. Liu and D.D.L. Chung, "Burnout of the Organic Vehicle in an Electrically Conductive Thick-Film Paste", *J. Electron. Mater.* 33(11), 1316–1325 (2004).
[2] P. Yih and D.D.L. Chung, "Brass-Matrix Silicon Carbide Whisker Composites," *J. Mater. Sci.* 34, 359–364 (1999).
[3] Z. Mei and D.D.L. Chung, "Thermal Stress Induced Thermoplastic Composite Debonding, Studied by Contact Electrical Resistance Measurement", *Int. J. Adhes. Adhes.* 20, 135–139 (2000).
[4] M. Zhu and D.D.L. Chung, "Active Brazing Alloy Containing Carbon Fibers for Metal-Ceramic Joining", *J. Am. Ceram. Soc.* 77(10), 2712–2720 (1994).
[5] J.-M. Chiou and D.D.L. Chung, "Improving the Temperature Resistance of AluminumMatrix Composites by Using an Acid Phosphate Binder, Part I: Binders", *J. Mater. Sci.* 28, 1435–1446 (1993).
[6] J.A. Fernando and D.D.L. Chung, "Improving an Alumina Fiber Filter Membrane for Hot Gas Filtration using an Acid Phosphate Binder", *J. Mater. Sci.* 36(21), 5079–5085 (2001).
[7] X. Shui and D.D.L. Chung, "High-Strength High-Surface-Area Porous Carbon Made From Submicron-Diameter Carbon Filaments," *Carbon* 34(6), 811–814 (1996); 34(9), 1162 (1996).

Further Reading

D.D.L. Chung, "Joints Obtained by Soldering, Adhesion, Autohesion and Fastening, Studied by Electrical Resistance Measurement", *J. Mater. Sci.* 36(11), 2591–2596 (2001).
X. Luo and D.D.L. Chung, "Material Contacts under Cyclic Compression, Studied in Real Time by Electrical Resistance Measurement", *J. Mater. Sci.* 35(19), 4795–4802 (2000).
X. Luo and D.D.L. Chung "Irreversible Structural Change at the Interface Between Components During Fastening", *Fasten. Technol. Int.* 25(1), 86–87 (2002).
M. Poeller and D.D.L. Chung, "Effect of Heating on the Structure of an Adhesive Joint, as Indicated by Electrical Resistance Measurement", *J. Adhes.* 79(6), 549–558 (2003).

6 Tailoring Composite Materials

The techniques that are used to tailor composite materials in order to achieve improved properties – as needed for a variety of applications – are covered in this chapter. These techniques include the selection and modification of the components and the engineering of the interfaces in the composite. An example of an interface is that between the reinforcement and the matrix. Interfaces can greatly affect the properties of a composite.

6.1 Tailoring by Component Selection

6.1.1 Polymer-Matrix Composites

Epoxy is by far the most widely used polymer matrix for structural composites. This is due to the strong adhesiveness of epoxy, in addition to the long history of its use in composites. Tradenames of epoxy include Epon, Epi-rez, and Araldite. Epoxy displays an excellent combination of mechanical properties and corrosion resistance, is dimensionally stable, exhibits good adhesion, and is relatively inexpensive. Moreover, the low molecular weight of uncured epoxide resin in the liquid state results in exceptionally high molecular mobility during processing. This mobility helps the resin to quickly spread on the surface of carbon fiber, for example.

Epoxy resins are characterized by having two or more epoxide groups per molecule. The chemical structure of an epoxide group is shown in Fig. 6.1.

An epoxy is a thermosetting polymer that cures upon mixing with a catalyst (also known as a hardener). This curing process is a reaction that involves polymerization and crosslinking.

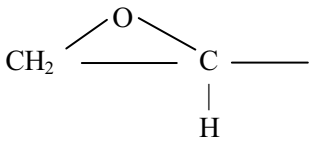

Figure 6.1. Chemical structure of an epoxide group

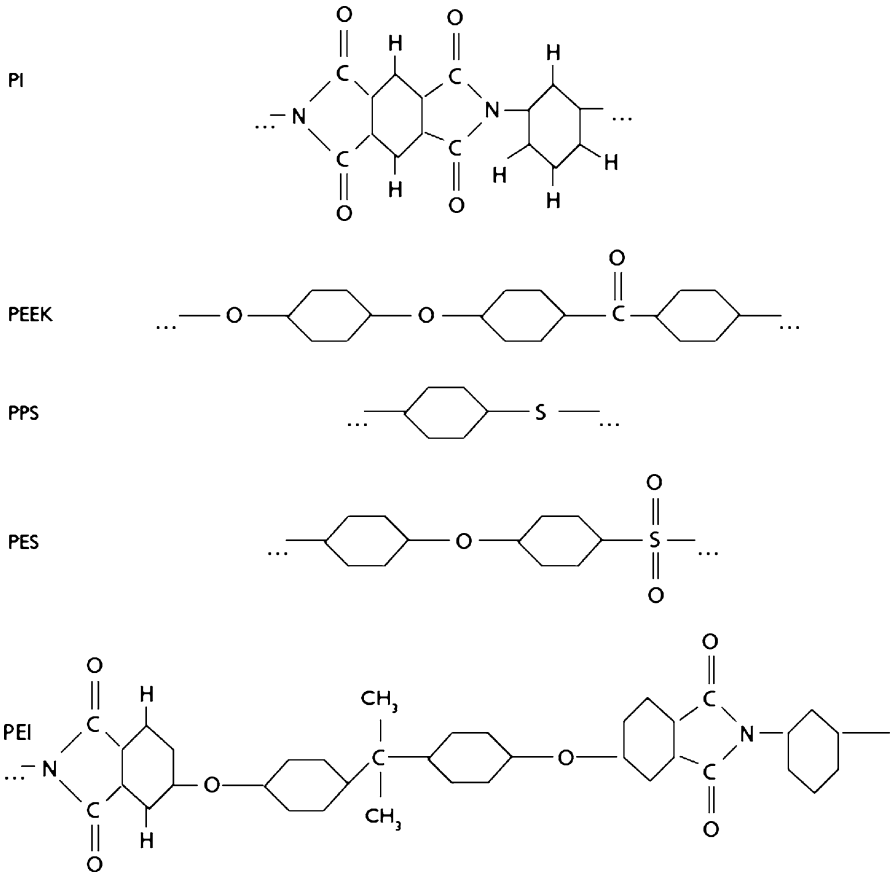

Figure 6.2. The mers (repeating units) of thermoplastic polymers typically used in structural composites

There are many types of epoxy. The most common epoxy resin is produced by a reaction between epichlorohydrin and bisphenol A. The mers (repeating units) of thermoplastic polymers that are typically used in structural composites are shown in Fig. 6.2.

The properties of these thermoplastics are listed in Table 6.1. In contrast, epoxies have a tensile strength of 103 MPa, an elastic modulus of 3.4 GPa, a ductility (elongation at break) of 6%, and a density of 1.25 g/cm^3 [1]. Thus, epoxies are stronger, stiffer and more brittle than most thermoplastic polymers. Another major difference between thermoplastics and epoxies is the higher processing temperatures of thermoplastics (300–400°C).

6.1.2 Cement-Matrix Composites

Component selection for cement-matrix composites involves the use of admixtures, which are additives included in the cement mix. These additives serve various functions, as described below:

Table 6.1. Properties of thermoplastics

	PES	PEEK	PEI	PPS	PI
T_g (°C)	230[a]	170[a]	225[a]	86[a]	256[b]
Decomposition temperature (°C)	550[a]	590[a]	555[a]	527[a]	550[b]
Processing temperature (°C)	350[a]	380[a]	350[a]	316[a]	304[b]
Tensile strength (MPa)	84[d]	70[d]	105[c]	66[d]	117[d]
Modulus of elasticity (GPa)	2.4[d]	3.8[d]	3.0[c]	3.3[d]	2.1[d]
Ductility (% elongation)	80[d]	150[d]	50–65[c]	2[d]	10[d]
Izod impact (ft lb/in.)	1.6[d]	1.6[d]	1[c]	0.5[d]	1.5[d]
Density (g/cm^3)	1.37[d]	1.31[d]	1.27[c]	1.30[d]	1.39[d]

Data from: [a] [2]; [b] [3]; [c] [4]; [d] [5]

- Water reducing agent – a minor additive to increase the workability of the mix
- Polymer (such as latex) – to decrease liquid permeability and bond strength
- Fine particles (such as silica fume) – to decrease liquid permeability, bond strength and drying shrinkage, and to increase the modulus and the abrasion resistance
- Short fiber (such as steel fiber) – to increase the flexural toughness.

Continuous fibers are not suitable for inclusion in a cement mix, although they can be applied prior to cement pouring and can serve as a reinforcement. Both processing and material costs are high. In addition, penetration of the cement mix into the small spaces between microfibers is difficult. On the other hand, macroscopic steel rebars are similar in shape to continuous microfibers and are commonly used to reinforce concrete.

6.1.2.1 Polymers in Cement-Matrix Composites

Polymer particles used as admixtures can take the form of a dry powder or an aqueous dispersion of particles. The latter form is more common. The inclusion of either form as an admixture results in improved joining of the mix constituents (e.g., sand), due to the presence of interweaving polymer films. The improved joining leads to superior mechanical and durability characteristics. Aqueous dispersions of polymer particles are more effective than dry polymer powder for the development and uniform distribution of polymer films. The most common form of polymer in aqueous dispersions is latex, particularly butadiene-styrene copolymer. The dispersions are stabilized by the use of surfactants.

In polymer-modified cement-based material, polymer particles are partitioned between the interiors of hydrates and the surfaces of anhydrous cement grains. The presence of the polymer results in an improved pore structure, thereby decreased porosity. Furthermore, the workability is enhanced and the water absorption is decreased. This enhanced workability allows the use of lower values of the water/cement ratio.

The rate of hydration is reduced by the presence of the polymer. The addition of a polymer tends to increase the flexural strength and toughness, but lower the

compressive strength, modulus of elasticity, and hardness. Furthermore, polymer addition is effective at enhancing the vibration damping capacity, the frost resistance, and the resistance to biogenic sulfuric acid corrosion (relevant to sewer systems). In addition, polymer addition imparts stability and thixotropy to grouts and enables control over the rheology and the stabilization of the cement slurry against segregation. Dry polymer particles used as an admixture can be water-redispersible polymer particles, such as those obtained by spray drying aqueous dispersions. Examples are acrylic and poly(ethylenevinyl acetate). Redispersibility may be attained through the use of functional monomers. The effectiveness of redispersible polymer particles depends on the cement used. One special category of polymer particles is superabsorbent particles (hydrogel), which serve to provide the controlled formation of water-filled macropore inclusions (i.e., water entrainment) in the fresh concrete. The consequence of this is control over self-dessication. Another kind of superabsorbent polymer barely absorbs alkaline water in fresh/hardened concrete, but absorbs a great deal of neutral/acid water and creates a gel. Thus, when neutral water is poured onto the concrete after setting, the concrete is coated with the gel and can thus be kept without drying.

Organic liquid admixtures can be polymer solutions (involving water-soluble polymers such as methylcellulose, polyvinyl alcohol and polyacrylamide) or resins (such as epoxy and unsaturated polyester resin). The liquid form is attractive due to the ease with which it can be uniformly spatially distributed, and hence its effectiveness in even small proportions. In contrast to polymer solutions, particles (including particle dispersions) tend to require a higher proportion in order to be comparably effective. Polymer solutions used as admixtures can serve to optimize the air void distribution and rheology of the wet mix, thereby improving workability with low air contents.

Short fibers rather than continuous ones are used because they can be incorporated in the cement mix, thereby facilitating processing in the field. Furthermore, short fibers are less expensive than continuous ones. Polypropylene, polyethylene and acrylic fibers are particularly common due to the requirements of low cost and resistance to the alkaline environment in cement-based materials. Compared to carbon, glass and steel fibers, polymer fibers are attractive due to their high ductility, which results in high flexural toughness in the cement-based material. The combined use of short polymer fibers and a polymer particle dispersion (e.g., latex) results in superior strength (tensile, compressive, and flexural) and flexural toughness compared to the use of fibers without a polymer particle dispersion.

6.1.2.2 Silica Fume in Cement-Matrix Composites

Silica fume is very fine noncrystalline silica produced by electric arc furnaces as a by-product of the production of metallic silicon or ferrosilicon alloys. It is a powder with particles that have diameters that a hundredfold smaller than those of anhydrous Portland cement particles (i.e., the mean particle size is between 0.1 and 0.2 μm). The SiO_2 content ranges from 85 to 98%. Silica fume is pozzolanic – it has a limited ability to serve as a cementitious binder.

Silica fume used as an admixture in a concrete mix has significant positive effects on the properties of the resulting material. These effects pertain to the strength, modulus, ductility, vibration damping capacity, sound absorption, abrasion resistance, air void content, shrinkage, bonding strength with reinforcing steel, permeability, chemical attack resistance, alkali-silica reactivity reduction, corrosion resistance of embedded steel reinforcement, freeze–thaw durability, creep rate, coefficient of thermal expansion (CTE), specific heat, thermal conductivity, defect dynamics, dielectric constant, and degree of fiber dispersion in mixes containing short microfibers. However, silica fume addition degrades the workability of the mix. This problem can be alleviated by using more water-reducing agent or by treating the surfaces of the silica fume particles with silane.

6.1.2.3 Short Fibers in Cement-Matrix Composites

Short fibers are used as admixtures in cement-based materials in order to decrease the drying shrinkage, increase the flexural toughness, and in some cases to increase the flexural strength too. When the fibers are electrically conductive, they may also provide nonstructural functions, such as self-sensing (sensing the strain, damage, or temperature), self-heating (for deicing), and electromagnetic reflection (for electromagnetic interference shielding; i.e., EMI shielding).

Although continuous fibers are more effective than short fibers when used as a reinforcement, they are not amenable to incorporation in a concrete mix and they are relatively expensive. Low cost is critical to the practical viability of cement-based materials.

Although macroscopic steel fibers that are around 1 mm in diameter are used, the most effective fibers are usually microfibers with diameters ranging from 5 to 100 μm. For example, carbon fibers are typically around 10 μm in diameter. Nanofibers with diameters that are typically around 0.1 μm are less effective than microfibers as a reinforcement, although they are more effective than microfibers at providing EMI shielding (due to their small diameters and the skin effect, which refers to the phenomenon in which high-frequency electromagnetic radiation only interacts with the near-surface region of an electrical conductor). In general, the smaller the fiber diameter (and thus the higher the aspect ratio), the more difficult it is to disperse the fibers. Similarly, the smaller the fiber length (which relates to a lower aspect ratio), the easier it is to disperse the fibers. This is due to the tendency for fibers with small diameters or long lengths to cling to one another. The effectiveness of a fiber admixture at improving the structural or functional properties of cement-based materials is greatly affected by the degree of fiber dispersion. The attainment of a high degree of fiber dispersion is particularly critical when the fiber volume fraction is low. A low fiber volume fraction is usually preferred because the material cost increases, the workability decreases, the air void content increases, and the compressive strength decreases as the fiber content increases. The fiber dispersion is enhanced by improving the hydrophilicity (i.e., the wettability by water) of the fibers, as the cement mix is water-based. The hydrophilicity can be controlled by treating the surfaces of the fibers prior to incorporating the fibers into the cement mix. Furthermore, the fiber dispersion is affected by the admixtures that may

be used along with the fibers. These admixtures may be fine particles (such as silica fume, which has a typical particle size of around 0.1 μm), the presence of which helps the fibers to break loose from one another as mixing occurs. Other admixtures may be polymers such as latex particle dispersions, which help fiber–cement bonding as well as fiber dispersion.

6.1.3 Metal-Matrix Composites

Aluminum is the most common matrix material used in metal-matrix composites because of (i) its low melting temperature, which allows casting to be conducted at relatively low temperatures, and (ii) its low density. Copper's high density makes it unattractive for lightweight composites, but its high thermal conductivity and low electrical resistivity make it attractive for electronic applications (Table 6.2).

Metals and ceramics tend to have very different in their properties, as shown in Table 6.2. Metals are electrically and thermally conductive. The thermal conductivities of aluminum and copper (Table 6.2) are higher than those of any of the ceramics listed, while the electrical resistivities of aluminum and copper are much lower (by many orders of magnitude) than those of any of the ceramics listed. However, most metals exhibit a high coefficient of thermal expansion (CTE) and a low elastic modulus compared to ceramics. The CTE values of aluminum and copper are higher than those of any of the ceramics listed, and the elastic moduli of aluminum and copper are lower than those of any of the ceramics listed. The density of aluminum is comparable to those of ceramics, but the density of copper is higher than those of ceramics.

Among the metals, molybdenum, tungsten, Kovar (Fe-Ni29-Co17) and Invar (Fe-Ni36) have exceptionally low CTE values (Table 6.2). Their CTE values are comparable to those of ceramics; indeed, the CTE of Invar is even lower than those of ceramics. Thus, Invar is used for precision instruments, such as clocks, physical laboratory devices, seismic creep gauges, and valves in motors. Guillaume received the Nobel Prize in Physics in 1920 for discovering Invar (which means "invariability in relation to the essential absence of thermal expansion"). However, all of these metals/alloys have low values of thermal conductivity. In addition, their densities are high. Furthermore, molybdenum and tungsten are refractory metals (i.e., metals that are extraordinarily resistant to heat and wear; a group that also includes niobium, tantalum, and rhenium). For example, the melting point of tungsten is 3,410°C. Such high melting temperatures make metal processing that involves casting (melting and subsequent solidification) difficult.

Carbon fibers exhibit slightly negative CTE values, so they are highly effective CTE-reducing fillers. The electrical resistivities of carbon fibers (all grades) are lower than those of metals, but their thermal conductivities can be lower or higher than those of metals, depending on the fiber grade. High-modulus carbon fiber can be more thermally conductive than metals (and even more thermally conductive than copper for the grade of high-modulus carbon fiber shown in Table 6.2), whereas high-strength carbon fiber is less thermally conductive than metals.

The incorporation of a carbon or ceramic filler into a metal to form a metal-matrix composite is attractive for attaining a low CTE (although not as low as that

Table 6.2. Properties of metals, carbons and ceramics

Material	Density (g/cm^3)	Thermal conductivity (W/(m K))	Electrical resistivity (Ωcm)	Elastic modulus (GPa)	CTE (10^{-6}/K)
Aluminum[a]	2.70	237	2.65×10^{-6}	70	23.1
Copper[a]	8.96	401	1.68×10^{-6}	110–128	16.5
Molybdenum[a]	10.22	142	5.2×10^{-6}	320	4.9
Tungsten[a]	19.3	155	5.3×10^{-6}	400	4.5
Kovar[a] (Fe-Ni29-Co17)	8.35	17	4.9×10^{-5}	159	5.2
Invar[a] (Fe-Ni36)	8.05	10.5	8.2×10^{-5}	141	1.2
Carbon fiber[b] (high strength)	1.76	8	1.8×10^{-3}	231	−0.60
Carbon fiber[b] (high modulus)	2.17	640	2.2×10^{-4}	827	−1.45
Silicon carbide (SiC)[c]	3.1	120	10^2–10^6	410	4.0
Silicon nitride (Si_3N_4)[c]	3.29	30	/	310	3.3
Aluminum nitride (AlN)[c]	3.26	140–180	$> 10^{14}$	330	4.5
Aluminum oxide (Al_2O_3)[c]	3.89	35	$> 10^{14}$	375	8.4
Boron nitride[c] (hexagonal)	1.9	121	$> 10^{14}$	/	−0.46
Titanium diboride (TiB_2)[c]	4.50	96	10^{-5}	565	6.4
Zirconium oxide (ZrO_2)[c], Y_2O_3 stabilized	6	2	$> 10^{10}$	200	10.3

[a] Metal; [b] carbon; [c] ceramic

of the carbon or ceramic filler) and a high elastic modulus (although not as high as that of the carbon or ceramic filler), in addition to high thermal and electrical conductivities (although not as high as those of the metal matrix). When copper is used as the matrix, the composite also allows a reduction in density (although the density does not become as low as that of the carbon or ceramic filler).

The combination of low CTE and high thermal conductivity is particularly attractive for electronic packaging, such as heat sinks, housings, substrates, lids, etc. The combination of high electrical and thermal conductivity and hardness is particularly attractive for welding electrodes, motor brushes, and sliding contacts.

Among the ceramic fillers listed in Table 6.2, titanium diboride and silicon carbide are most attractive due to their high elastic moduli. This is an important factor for strengthening the composite. Among the ceramic fillers listed, aluminum nitride is most attractive due to its high thermal conductivity, although silicon carbide and hexagonal boron nitride have quite high thermal conductivities. One

drawback of aluminum nitride is its reactivity with water to form aluminum oxynitride, which has a much lower thermal conductivity than aluminum nitride. Aluminum oxide and zirconium oxide have particularly low thermal conductivities.

Among the ceramic fillers, titanium diboride is most attractive because of its low electrical resistivity, which allows it to be used as an anode material for aluminum smelting (the extraction of aluminum from its oxide, alumina) and to be machined by electrical discharge machining (abbreviated to EDM, and also called spark machining; this refers to the removal of material using electric arcing discharges between an electrode, which is the cutting tool, and the workpiece in the presence of an energetic electric field). EDM requires that the workpiece is electrically conductive.

Due to its low cost and high elastic modulus, silicon carbide is the filler most commonly used to reinforce metals. SiC is also used as an abrasive (e.g., in sandpaper). There are numerous polymorphs of SiC, but the most common polymorph is α-SiC, which has a hexagonal crystal structure (similar to wurtzite). A less common polymorph is β-SiC, which exhibits the zinc blende crystal structure.

Silicon carbide is available in particle and whisker forms. A whisker is a short fiber that can be essentially a single crystal. The SiC particle is typically α-SiC, with a size of 1–10 μm. The SiC whisker is typically β-SiC, with a diameter of about 1 μm and a length of about 20 μm. Figure 6.3 shows an SEM photograph of β-SiC whiskers of diameter 1.4 μm and length 18.6 μm. Figure 6.4 shows SEM photographs of an aluminum-matrix composite containing 10 vol% SiC whiskers of the type shown in Fig. 6.3. The composite is fabricated by liquid metal infiltration at an infiltration pressure of 13.8 MPa. The porosity in the composite is $< 0.5\%$.

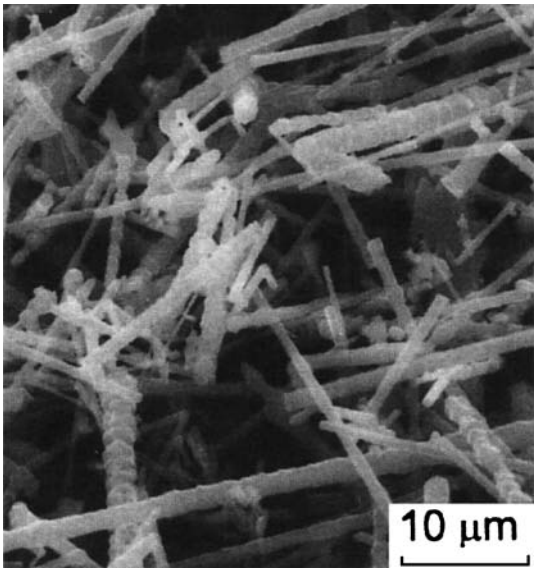

Figure 6.3. SEM photograph of silicon carbide whiskers without a matrix (from [6])

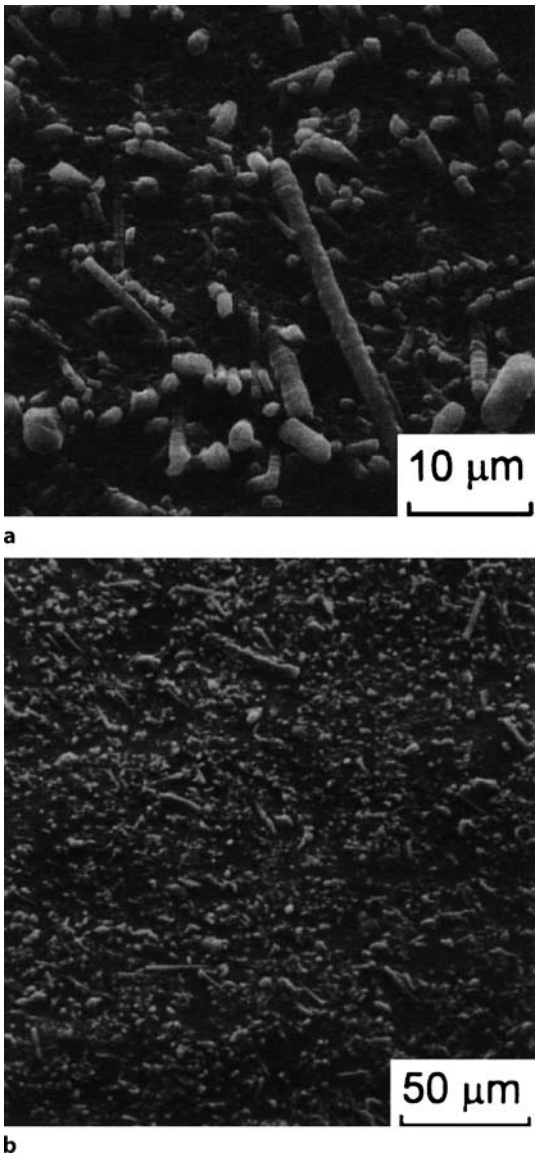

Figure 6.4. SEM photographs of mechanically polished sections of aluminum-matrix composites containing 10 vol% silicon carbide whiskers. **a** High-magnification view, **b** low-magnification view. The whiskers are essentially randomly oriented; the whisker diameter is 1.4 µm and the whisker length is 18.6 µm. (From [6])

Compared to silicon carbide, titanium diboride has a higher modulus but a lower thermal conductivity (Table 6.2). The high modulus makes titanium diboride a highly effective reinforcing material. The addition of TiB_2 to a metal greatly increases the stiffness, hardness and wear resistance and decreases the CTE, while it reduces the electrical and thermal conductivity much less than the addition of

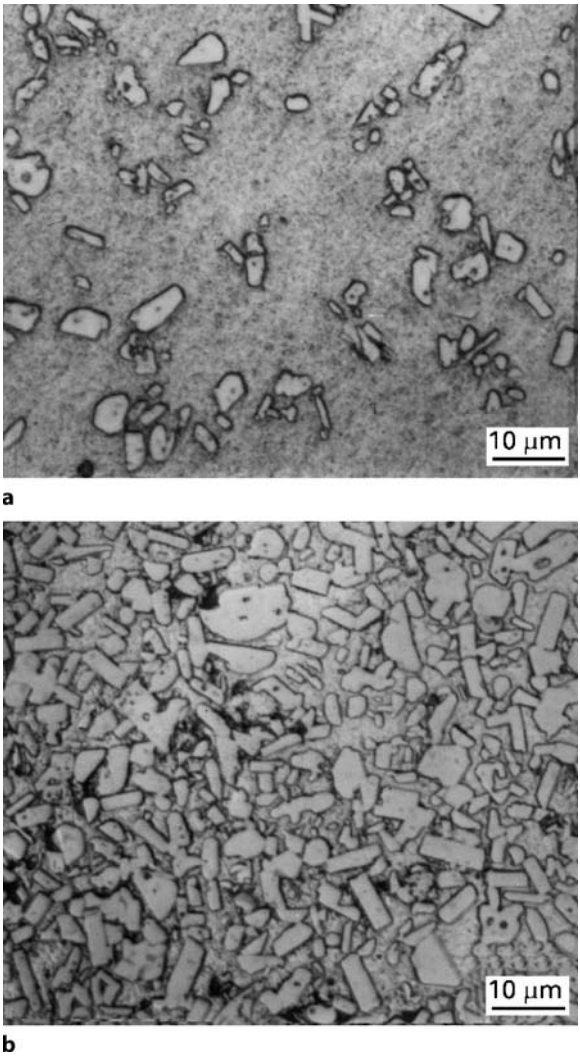

Figure 6.5. Optical microscope photographs of a copper-matrix composite containing: **a** 15 vol% TiB_2 platelets; **b** 60 vol% TiB_2 platelets. (From [7])

most other ceramic fillers. Figure 6.5 shows optical microscope photographs of copper-matrix composites containing TiB_2 platelets with diameters 3–5 μm and aspect ratios of about 3. The composites are made by the coated filler method (Fig. 1.9) of powder metallurgy. The CTE decreases monotonically with increasing TiB_2 volume fraction (Fig. 6.6) such that the coated filler method gives slightly lower CTE than the admixture method (Fig. 1.7) for the same TiB_2 volume fraction. However, even for the coated filler method, a high TiB_2 volume fraction of 60% is needed in order to reduce the CTE of copper from 17×10^{-6} to 8.5×10^{-6}/°C (Fig. 6.6). The thermal conductivity decreases monotonically with increasing TiB_2

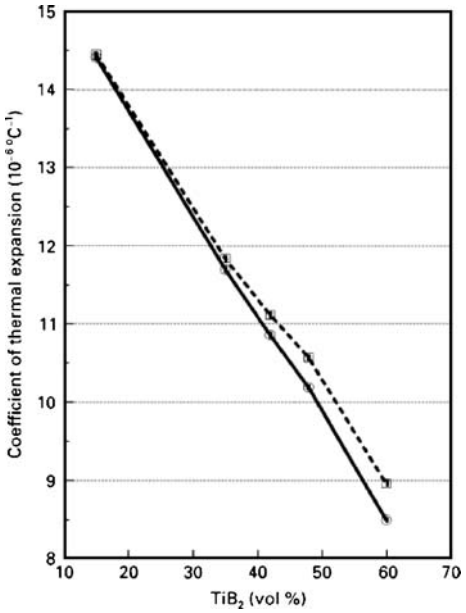

Figure 6.6. Effect of TiB_2 volume fraction on the coefficient of thermal expansion (CTE) of copper-matrix composites. *Circles* – coated filler method of powder metallurgy; *squares* – admixture method of powder metallurgy. (From [7])

volume fraction (Fig. 6.7). The electrical resistivity increases monotonically with increasing TiB_2 volume fraction (Fig. 6.8). Both the compressive yield strength (Fig. 6.9) and the hardness (Fig. 6.10) increase with increasing TiB_2 volume fraction up to a certain TiB_2 volume fraction, beyond which they decrease with increasing TiB_2 volume fraction. This behavior of the compressive yield strength and hardness is due to the porosity (Fig. 6.11), which increases abruptly with increasing TiB_2 volume fraction when this volume fraction exceeds a certain value. The coated filler method gives a slightly lower CTE, a higher thermal conductivity, a lower electrical resistivity, a higher compressive yield strength, a higher hardness, and a lower porosity than the admixture method for the same TiB_2 volume fraction.

In general, the difficulty involved in getting molten metal to wet the surface of a ceramic or carbon reinforcement complicates the fabrication of metal-matrix composites. This difficulty is particularly severe for high-modulus carbon fibers (e.g., Amoco's Thornel P-100) which have graphite planes that are mostly aligned parallel to the fiber surface. The edges of the graphite planes are more reactive with the molten metal than the graphite planes themselves, so low-modulus carbon fibers are more reactive and are thus wetted more easily by the molten metals. Although this reaction between the fibers and the metal aids the wetting, it produces a brittle carbide and degrades the strength of the fibers.

The wetting of a reinforcement by molten metal can be improved by adding alloying elements to the molten metal. When aluminum is used as the matrix and carbon fiber as the reinforcement, effective alloying elements include Mg, Cu, and Fe.

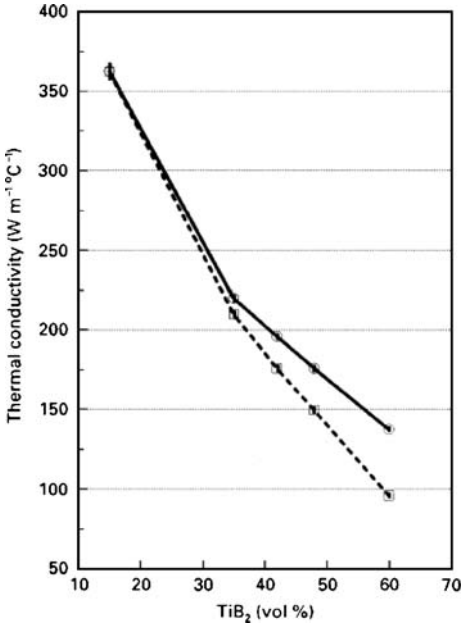

Figure 6.7. Effect of TiB_2 volume fraction on the thermal conductivity of copper-matrix composites. *Circles* – coated filler method of powder metallurgy; *squares* – admixture method of powder metallurgy. (From [7])

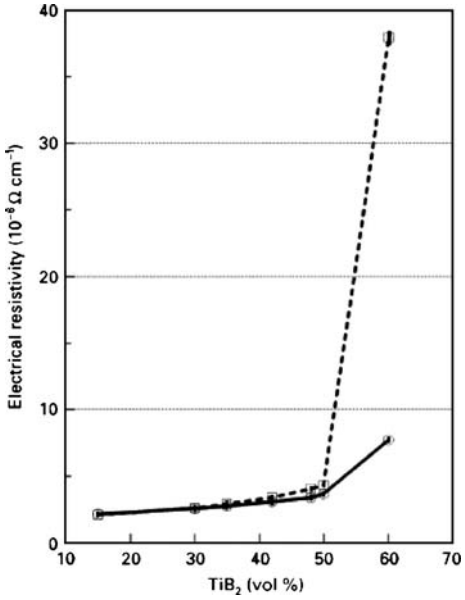

Figure 6.8. Effect of TiB_2 volume fraction on the electrical resistivity of copper-matrix composites. *Circles* – coated filler method of powder metallurgy; *squares* – admixture method of powder metallurgy. (From [7])

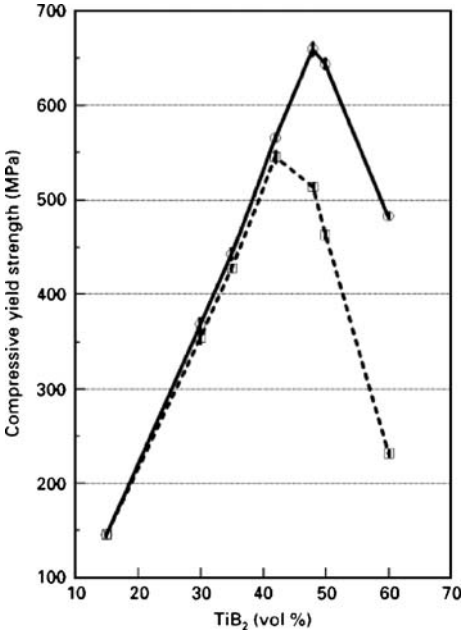

Figure 6.9. Effect of TiB_2 volume fraction on the compressive yield strength of copper-matrix composites. *Circles* – coated filler method of powder metallurgy; *squares* – admixture method of powder metallurgy. (From [7])

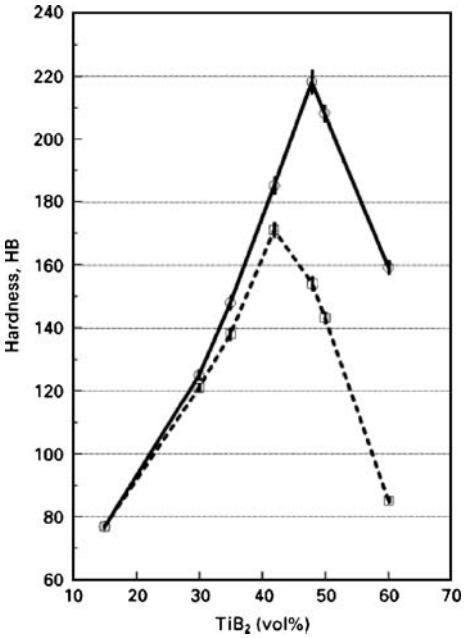

Figure 6.10. Effect of TiB_2 volume fraction on the hardness of copper-matrix composites. *Circles* – coated filler method of powder metallurgy; *squares* – admixture method of powder metallurgy. (From [7])

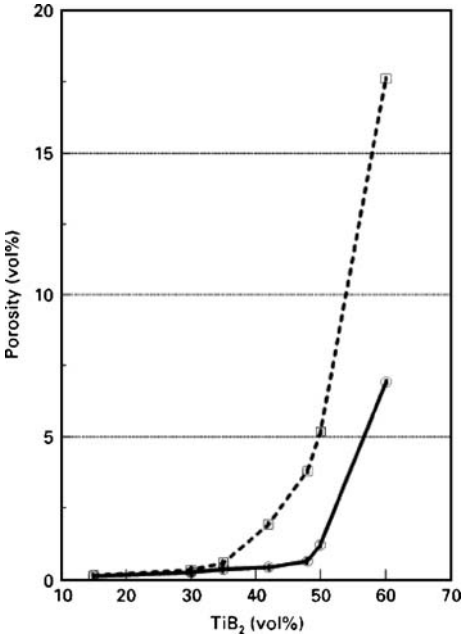

Figure 6.11. Effect of TiB_2 volume fraction on the porosity of copper-matrix composites. *Circles* – coated filler method of powder metallurgy; *squares* – admixture method of powder metallurgy. (From [7])

6.2 Tailoring by Interface Modification

6.2.1 Interface Bond Modification

6.2.1.1 General Concepts

Effective reinforcement requires good bonding between the filler and the matrix, especially for short fibers. For an ideally unidirectional composite (i.e., one containing continuous fibers all aligned in the same direction) containing fibers with a modulus that is much higher than that of the matrix, the longitudinal tensile strength is quite independent of the fiber–matrix bonding, but the transverse tensile strength and the flexural strength (for bending in the longitudinal or transverse directions) increase with increasing fiber–matrix bonding. On the other hand, excessive fiber–matrix bonding can cause a composite with a brittle matrix (e.g., carbon and ceramics) to become more brittle, as the strong fiber–matrix bonding causes cracks to propagate linearly in the direction perpendicular to the fiber–matrix interface without being deflected to propagate along this interface. In the case of a composite with a ductile matrix (e.g., metals and polymers), a crack initiating in the brittle fiber tends to be blunted when it reaches the ductile matrix, even when the fiber–matrix bonding is strong. Therefore, an optimum degree of fiber–matrix bonding (i.e., not too strong and not too weak) is needed for brittle-matrix composites, whereas a high degree of fiber–matrix bonding is preferred

for ductile-matrix composites. In particular, the fiber–matrix bond strength in carbon–carbon composites must be optimal. If the bond strength is too high, the resulting composite may be extremely brittle, exhibiting catastrophic failure and poor strength. If it is too low, the composites fail in pure shear, with poor transfer of the load to the fiber.

The mechanisms involved in filler–matrix bonding include chemical bonding, interdiffusion, van der Waals bonding, and mechanical interlocking. Chemical bonding gives a relatively large bonding force provided that the density of chemical bonds across the filler–matrix interface is sufficiently high and that a brittle reaction product is absent from the filler–matrix interface. The density of chemical bonds can be increased by (i) chemically treating the filler, (ii) using a suitable sizing (coating) on the filler, and (iii) using a molecular coupling agent. Interdiffusion at the filler–matrix interface also results in bonding, though its occurrence requires the interface to be rather clean. Mechanical interlocking between the fibers and the matrix is an important contribution to the bonding if the fibers form a three-dimensional network. Otherwise, the filler should have a rough surface in order to allow a small degree of mechanical interlocking to take place.

Chemical bonding, interdiffusion and van der Waals bonding require the filler to be in intimate contact with the matrix. For intimate contact to take place, the matrix or matrix precursor must be able to wet the surfaces of the filler during the infiltration of the matrix or matrix precursor into the filler preform. Wetting is governed by the surface energies. Chemical treatments and coatings can be applied to the fibers to enhance wetting through their effects on the surface energies. The choice of treatment or coating depends on the matrix. A related method involves adding a wetting agent to the matrix or matrix precursor before infiltration. As the wettability may vary with temperature, the infiltration temperature can be chosen to enhance wetting. Although wetting is governed by thermodynamics, it is strongly affected by kinetics. Thus, yet another way to enhance wetting is to use a high pressure during infiltration.

The occurrence of a reaction between the filler and the matrix aids the wetting and bonding between the filler and the matrix. However, an excessive reaction degrades the filler, and the reaction product(s) may have an undesirable effect on the mechanical, thermal, or moisture resistance properties of the composite. Therefore, an optimum amount of reaction is preferred.

An example relates to the reaction between silicon carbide and aluminum during the fabrication of a silicon carbide aluminum-matrix composite by infiltrating molten aluminum into a heated SiC preform. The reaction is

$$4\mathrm{Al} + 3\mathrm{SiC} \rightarrow \mathrm{Al_4C_3} + 3\mathrm{Si}\,, \tag{6.1}$$

which consumes a part of the SiC, produces silicon (Si) that dissolves in the molten aluminum, and also produces the Al_4C_3 compound at the interface between the SiC and the aluminum matrix. The fraction of SiC consumed increases with decreasing SiC volume fraction in the composite. The amount of silicon produced by the reaction increases with increasing SiC volume fraction. The extent of the reaction increases with increasing infiltration temperature. The fraction of SiC whiskers

consumed is inversely proportional to the volume fraction of SiC whiskers in the composite. The product of these two fractions provides a scale (called the reactivity index) that describes the Al-SiC reactivity. The index decreases with decreasing infiltration temperature and is higher for SiC whiskers than SiC particles. At an infiltration temperature of 670°C, the fraction of SiC whiskers consumed is 26% for a SiC volume fraction of 0.10. In contrast, the fraction of SiC consumed is only 8.4% for a 55 vol% SiC particle composite made at an infiltration temperature of 800°C [6].

6.2.1.2 Filler Surface Treatment

The surface treatment of a filler is usually a valuable method of improving the bonding between the filler and the matrix. If the filler is carbon fiber, surface treatments involve oxidation treatments and the use of coupling agents, wetting agents, and/or sizings (coatings). Carbon fibers need treatment for both thermosetting and thermoplastic polymers. As the processing temperature is usually higher for thermoplastic polymers than for thermosetting polymers, the treatment must be stable to a higher temperature (300–400°C) when a thermoplastic polymer is used.

Oxidation treatments can be applied by gaseous, solution, electrochemical, and plasma methods. Oxidizing plasmas include those involving oxygen, CO_2 and air. The resulting oxygen-containing functional groups on the fiber surface cause improvements in the wettability of the fiber and the fiber–matrix adhesion. The result of this is enhanced interlaminar shear strength (ILSS) and flexural strength. Other plasmas (not necessarily oxidizing) that are also effective involve nitrogen, acrylonitrile, and trimethyl silane. Ion beam treatment is somewhat similar to plasma treatment, but it involves oxygen or nitrogen ions. Plasma treatments are useful for epoxy as well as thermoplastic matrices. Oxidation by gaseous methods includes the use of oxygen gas containing ozone. Oxidation by solution methods involves wet oxidation, such as acid treatments. Oxidation by electrochemical methods (i.e., anodic treatment) includes the use of ammonium sulfate solutions, a diammonium hydrogen phosphate solution containing ammonium rhodanide, ammonium bicarbonate solutions, a phosphoric acid solution, and other aqueous electrolytes. In general, the various treatments chemically modify the fiber surface and remove a loosely adhering surface layer. More severe oxidation treatments also serve to roughen the fiber surface, thereby enhancing the mechanical interlocking between the fibers and the matrix.

In the case of cement-matrix composites, it is important for the filler to be wettable by water, which is an important component of the cement mix. Inadequate wettability makes fiber dispersion more difficult and increases the amount of fiber–matrix interfacial voids in the resulting composite. The interfacial voids reduce the fiber–matrix bond strength. Thus, surface treatment of the filler is conducted to improve the wettability, whether the filler is fibrous (e.g., carbon fiber) or particulate (e.g., silica fume). Examples of surface treatment include ozone treatment of carbon fibers and silane treatment of carbon fibers and silica fume. Figure 6.12 shows that the drying shrinkage of cement paste containing silica fume is reduced by using silane-treated silica fume in place of as-received silica

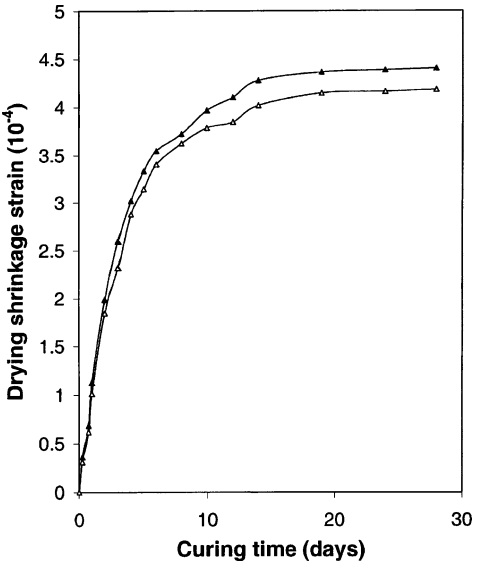

Figure 6.12. Drying shrinkage strain versus curing time for cement paste containing silica fume. *Filled triangles* – as-received silica fume; *unfilled triangles* – silane-treated silica fume. (From [8])

fume. This effect of silane treatment is due to the improved bonding between the silica fume and the cement matrix, facilitated by the improved wettability of the silica fume by water.

The surface treatment of the carbon fibers has a significant effect on the mechanical properties of the resulting carbon–carbon composites. Surface-treated fibers that bond strongly with the polymer exhibit high flexural strength in polymer composites, but result in carbonized composites of poor flexural strength. For graphitized composites, the flexural strength increases monotonically with increasing treatment time. Graphitization causes composites with surface-treated fibers to increase in flexural strength and interlaminar shear strength and those with untreated fibers to decrease in flexural strength and interlaminar shear strength. Hence, the fiber–matrix bonding is very poor in graphitized composites containing untreated fibers and is stronger in graphitized composites containing treated fibers.

6.2.1.3 Use of an Organic Coupling Agent

6.2.1.3.1 Organic Coupling of Inorganic Components

The use of an organic molecule (known as a coupling agent; also known as a molecular tether) to covalently link an inorganic particle and an inorganic matrix enhances the bonding between the inorganic particle and the matrix, thus resulting in a nanocomposite of increased strength. The chosen molecule must have functional groups at its two ends that are able to react with the surface of the inorganic

particle and the matrix material. Silane coupling agents are most commonly used as the organic molecules.

An example is a nanocomposite with cement as the matrix and silica fume as the inorganic particles. The effectiveness of silane for cement is due to the reactivity of its molecular ends with –OH groups and the presence of –OH groups on the surfaces of both the silica and the cement.

One method of introducing the silane coupling agent involves coating the silica fume particles with the silane prior to incorporating the particles into the cement mix. An effective silane coupling agent for this situation is a 1:1 (by mass) mixture of $H_2NCH_2CH_2NHCH_2CH_2CH_2Si(OCH_3)_3$ (referred to as S_1, available as product Z-6020 from Dow Corning, Midland, MI, USA) and $OCH_2CHCH_2OCH_2CH_2CH_2Si(OCH_3)_3$ (referred to as S_2, available as product Z-6040 from Dow Corning). The amine (NH_2) group in S_1 serves as a catalyst for the curing of epoxy and consequently allows the S_1 molecule to attach to the epoxy (OCH_2) end of the S_2 molecule. The trimethylsiloxy (OCH_3) ends of the S_1 and S_2 molecules then connect to the –OH functional group on the surface of silica fume. The silane can be dissolved in ethylacetate. The introduction of the silane can involve immersion of the silica fume in the silane solution, heating to 75°C while stirring, and holding at 75°C for 1 h, followed by filtration, washing with ethylacetate, and drying. After this, the silica fume can be heated in a furnace at 110°C for 12 h for the purpose of drying. Table 6.3 shows that silane coupling results in increases in the strength, modulus, and ductility of cement mortar both under tension and in compression, and also slightly increases the density. In particular, the tensile strength is increased by 31% and the compressive strength is increased by 27%. Moreover, the hydrophilic nature of silane improves the workability of the mixture and also probably enhances the dispersion of silica fume in the cement mix.

Another method of introducing a silane coupling agent into silica fume cement involves adding the silane to the cement mix rather than coating the silica fume with silane. In this situation, the silane must be stable in water. An effective silane in this situation is aqueous amino vinyl silane (Hydrosil 2781, Sivento, Piscataway, NJ, USA). In contrast, the silane used to coat silica fume that was

Table 6.3. Effect of silane coupling of silica fume particles on the mechanical properties of cement mortar containing silica fume (from [9])

Property	Without silane coupling	With silane coupling
Tensile strength (MPa)	2.35 ± 0.11	3.09 ± 0.13
Tensile modulus (GPa)	10.2 ± 0.07	14.57 ± 0.08
Tensile ductility (%)	0.0141 ± 0.0003	0.0150 ± 0.0004
Compressive strength (MPa)	61.95 ± 2.3	78.4 ± 3.2
Compressive modulus (GPa)	21.1 ± 0.54	28.7 ± 0.46
Compressive ductility (%)	0.138 ± 0.002	0.145 ± 0.003
Density (g/cm^3)	2.13	2.20

mentioned in the last paragraph is not sufficiently stable in aqueous systems. The silane admixture is added at levels of 0, 0.20, 0.50, 0.75, 1.0, 1.5, and 2.0% by mass of cement. The corresponding amount of water-reducing agent is 1.0, 0.10, 0.10, 0.05, 0.05, 0.025, and 0.025% by mass of cement, respectively. Adding more silane means that less water-reducing agent is needed to maintain workability. The surfactant, added at the level of 1% by mass of cement to help distribute the silane, can be polyoxyethylene lauryl ether, $C_{12}H_{25}(OCH_2CH_2)_nOH$, (Aldrich Chemicals, Milwaukee, WI, USA). The defoamer can be Rhodoline 1010 (Rhodia, Cranbury, NJ, USA), added at the level of 0.13 vol%.

The use of silane as an admixture that is added directly to the cement mix involves slightly more silane material but less processing cost than the use of silane in the form of a coating on silica fume. Both methods of introducing silane result in increases in the tensile and compressive strengths. The network produced by the admixture method of silane introduction is not achieved with the silane coating method due to the localization of the silane in the coating, which nevertheless provides chemical coupling between the silica fume and cement. This network, which is formed by the hydrolysis and polymerization (condensation) reactions of silane during the hydration of cement, also causes the ductility to decrease.

6.2.1.3.2 Organic Coupling of an Inorganic filler and a Polymer Matrix

An organic coupling agent can be used to improve the bond between an inorganic filler and a polymer matrix. For example, a silane coupling agent is effective at enhancing the bond between boron nitride particles and an epoxy matrix. Boron nitride (BN) is a ceramic material, with some ionic character in the covalent bond between boron and nitrogen. Its thermal conductivity is one of the highest among electrical insulators. Polymer-matrix composites that exhibit high thermal conductivity are valuable for electronic packaging due to the importance of heat dissipation from microelectronics.

Two materials are said to be isoelectronic if they have the same number of valence electrons per unit cell and the same structure (i.e., the same number and connectivity of atoms), even though the two materials may be different in composition. Boron nitride is isoelectronic with carbon. Boron nitride with a cubic crystal structure and boron nitride with a hexagonal crystal structure are different polymorphs (also called allotropes – two different crystal forms with the same composition) of boron nitride. Diamond and graphite are different polymorphs of carbon. The cubic form of boron nitride is analogous to diamond, whereas the hexagonal form of boron nitride is analogous to graphite. The hexagonal form is made up of layers of hexagonal sheets, with the boron atom directly above the nitrogen atoms in the crystal structure. Cubic boron nitride, like diamond, is one of the hardest materials known. Hexagonal boron nitride, like graphite, is a lubricant.

Equiaxed hexagonal boron nitride particles of size 5–11 μm and thermal conductivity 280 W/m K (Product Polartherm 180, Advanced Ceramic Corporation, Cleveland, OH, USA) can be surface treated with silane (O CH_2 CH CH_2O $CH_2CH_2CH_2$ Si $(OCH_3)_3$, Product Z-6040, Dow Corning Corp.). The epoxy structure at one end

of the silane molecule allows coupling to the epoxy matrix in the composite. The silane treatment process can involve (i) making a silane–water solution at a selected concentration, (ii) adding BN to the solution and stirring with a magnetic stirrer, (iii) heating at 60–70°C for 20 min, (iv) rinsing with water by filtration, and (v) drying at 110°C for 12 h.

The effects of the silane surface treatment of boron nitride have been compared with those of acid treatment. The acid treatment process involves (i) immersing the BN in acid in a beaker, (ii) stirring for 2 h with a magnetic stirrer, (iii) adding water and stirring for 2 min, (iv) rinsing with water by filtration until the water is neutral, and (v) drying at 110°C for 12 h.

The effects of the silane surface treatment of boron nitride have also been compared with those of acetone treatment. The surface treatment of BN particles using acetone involves (i) immersing BN in acetone, (ii) stirring for 2 h, (iii) filtering, and (iv) drying at 110°C for 12 h.

The polymer used in this example is epoxy, namely Epon (R) Resin 813 and EPI-Cure (R) 3234 Curing Agent from Shell Chemical Co. (Houston, TX, USA). The BN epoxy-matrix composites are fabricated by (i) mixing the epoxy resin and curing agent in the mass ratio 100:13, (ii) adding BN and mixing, (iii) pressing at room temperature and 10.5 MPa for 2 h, and (iv) heating at 45°C and 10.5 MPa for 1 h to complete polymerization.

Since the organic coupling is volatile compared to BN, the fractional loss in weight of the silane-treated BN particles after heating to a high temperature relates to the amount of silane present. Thus, BN particles with and without surface treatment are tested by measuring the weight loss upon heating to 600°C at 20°C/min under nitrogen gas flow (30 ml/min) protection, using a thermogravimetric analyzer (abbreviated TGA).

The fractional loss in weight of treated BN upon heating to 600°C is shown in Table 6.4. The amounts of volatile or decomposable material on the as-received, acetone-treated and acid (HNO_3 or H_2SO_4)-treated BN particles are negligible, indicating that treatments involving acetone and acid do not result in a coating on the BN particle. However, the weight losses for the silane-treated BN particles are much higher, indicating that the silane treatment results in a coating on the BN particle, since the weight loss results from the decomposition of the coating

Table 6.4. Fractional loss of mass from BN particles upon heating to 600°C (from [10])

Treatment	Fractional loss of mass (%)
As received	0.15
Acetone treated	0.14
Nitric acid (HNO_3) treated	0.10
Sulfuric acid (H_2SO_4) treated	< 0.10
Silane (low concentration) treated	0.7
Silane (medium concentration) treated	0.8
Silane (high concentration) treated	2.4

Table 6.5. Specific surface area of BN particles (from [10])

Treatment	Specific surface area (m^2/g)
As received	10.8
Acetone treated	16.4
Nitric acid (HNO_3) treated	14.9
Sulfuric acid (H_2SO_4) treated	12.5
Silane (high concentration) treated	10.5

at high temperature. Silane-water solutions of three different concentrations yield different amounts of coating. The higher the silane concentration in the solution, the greater the amount of coating.

Surface roughening that causes an increase in the surface area may result from acid treatment, due to the reaction between the acid and BN. Thus, the specific surface area (surface area per unit mass) of the BN particles with and without surface treatment is determined by nitrogen adsorption at 77 K and by measuring the pressure of the gas during adsorption using a surface area analyzer, such as the Micromeritics ASAP 2010 instrument. Nitrogen gas is commonly used for adsorption on the surface, due to its low reactivity and low cost. Adsorption of nitrogen gas on the BN surface causes a decrease in the pressure of the nitrogen gas in the chamber, so measuring the pressure allows the amount of nitrogen adsorbed to be determined. The surface area relates to the amount of nitrogen required to cover completely the surface with a monolayer of nitrogen.

Table 6.5 shows the specific (BET) surface areas of BN particles with and without surface treatment. Acetone treatment increases the specific surface area from 10.8 to 16.4 m^2/g due to its cleansing function and the consequent exposure of the true surface of the particle. Treatment with either acid also increases the specific surface area, but only by small amounts. Nitric acid treatment results in a slightly higher specific surface area than sulfuric acid treatment. However, both acid treatments result in lower specific surface areas than acetone treatment. The acid treatments also have a cleansing function, but acids are reactive and can change the surface morphology. On the other hand, the acid treatments do not have much effect on the surface, as shown by the fact that low specific surface areas are retained after the acid treatments. Silane (high concentration) treatment results in essentially no change in the specific surface area compared to the as-received case. However, the specific surface area is decreased compared to the acetone-washed case, since acetone washing allows the true surface to be exposed and the silane treatment coats the surface.

The composition of a surface tends to be affected by surface treatment. Thus, the surface elemental compositions of BN particles with and without surface treatment were analyzed by electron spectroscopy (electron spectroscopy for chemical analysis, abbreviated to ESCA).

The surface carbon, oxygen, and silicon concentrations were much higher after silane (high concentration) treatment than for the as-received, acetone-treated or H_2SO_4-treated particles (Table 6.6). This is because of the presence of these three elements in silane. The silane-treated BN particle surface has less

Table 6.6. Surface elemental compositions (in at.%) of as-received and treated BN particles (from [10])

Element	As received	Acetone treated	Sulfuric acid (H_2SO_4) treated	Silane (high concentration) treated
B	44.2	44.6	42.7	34.8
N	41.5	40.2	38.2	31.2
C	11.1	12.5	13.6	19.8
O	3.2	2.8	4.4	11.0
Si	–	–	1.1	3.2

boron and nitrogen compared to the as-received, acid-treated, and acetone-treated BN particles (Table 6.6), because the treated particles are partially covered by silane.

Table 6.7 shows the fractional increases in thermal conductivity following various treatments of epoxy-matrix composites with two BN volume fractions. At either volume fraction of BN, silane (high concentration) treatment gives the greatest fractional increase in thermal conductivity; the lower the silane content, the lower the fractional increase in thermal conductivity, except for the silane treatment with an extra high concentration, which corresponds to a weight loss of 3.2% upon heating to 600°C. At 57 vol% BN, silane (medium concentration) is more effective than H_2SO_4, whereas at 44 vol% BN, silane (medium concentration) is less effective than H_2SO_4. H_2SO_4 is more effective than HNO_3 at either volume fraction of BN, though the difference is small at 57 vol% BN. Silane (low concentration) is less effective than HNO_3 or H_2SO_4. Silane (extra high concentration) is less effective than silane (high concentration) or silane (medium concentration) at either volume fraction of BN, though this is not shown in Table 6.7. Acetone treatment is less effective than most of the other treatments at either volume fraction of BN.

The fractional increase in thermal conductivity due to surface treatment is much higher at 57 vol% BN than at 44 vol% BN for any BN condition. As shown in Table 6.7, at a low BN volume fraction, none of the treatments have a significant effect. However, their effects do become important at a high BN volume fraction, probably because of the increased tendency for adjacent particles to touch one

Table 6.7. Fractional increases in the thermal conductivity of a BN epoxy-matrix composite due to various BN particle surface treatments (from [10])

	44 vol% BN	57 vol% BN
Acetone treated	4.9%	48%
Nitric acid (HNO_3) treated	5.6%	62%
Sulfuric acid (H_2SO_4) treated	12%	63%
Silane (low concentration) treated	−5.6%	46%
Silane (medium concentration) treated	8.0%	72%
Silane (high concentration) treated	13%	96%

another at the higher BN volume fraction and the positive effect of the treatments on the filler–filler interface quality. HNO_3 treatment results in a higher specific surface area than H_2SO_4 treatment (Table 6.5), but it results in a lower fractional increase in thermal conductivity. This indicates that a high specific surface area is not needed to attain a high thermal conductivity. The effectiveness of the acid treatments at enhancing the thermal conductivity is probably due to certain surface functional groups that result from the treatments.

All silane treatments are effective at increasing the thermal conductivity. As the amount of silane coating on the particles increases, the thermal conductivity is enhanced until the silane concentration reaches the high concentration corresponding to a weight loss of 2.4% at 600°C. Further increasing the silane concentration to the extra high concentration corresponding to a weight loss of 3.2% at 600°C causes the thermal conductivity to decrease. Silane (high concentration) treatment is therefore the most effective. This means that the coating resulting from the silane treatment must be sufficiently thick in order for the treatment to be fully effective. The coating serves as an interlayer at the filler–matrix interface, thereby improving the quality of the interface. However, if the coating is too thick, the interlayer will become less effective or even a thermal barrier, thereby decreasing the thermal conductivity. Acetone treatment is effective due to its cleansing function. However, it is only moderately effective.

6.2.2 Interface Composition Modification

6.2.2.1 Filler–Matrix Interface Composition Modification

6.2.2.1.1 Ceramic–Metal and Carbon–Metal Interface Composition Modification

Due to the low CTEs of ceramics compared to metals, ceramic fillers are commonly used in metal-matrix composites in order to achieve a composite with a low CTE. However, liquid metals tend not to wet ceramic surfaces well (i.e., a liquid metal tends to ball up on a ceramic surface), thus making the liquid metal infiltration process difficult. To alleviate this problem, the ceramic surface may be modified by applying a coating that the liquid metal can wet sufficiently well.

In order to enhance the wetting of a reinforcement by a molten metal, the reinforcement can be coated by a metal or a ceramic. The metals used as coatings may be formed by plating and include Ni, Cu, and Ag; these generally result in lower strength composites than those predicted by the rule of mixtures (ROM). In the case of nickel-coated and copper-coated carbon fibers in an aluminum matrix, metal aluminides (Al_3M) form and embrittle the composites. In the case of nickel-coated carbon fibers in a magnesium matrix, nickel reacts with magnesium to form Ni-Mg compounds and a low-melting (508°C) eutectic. On the other hand, copper-coated fibers are suitable for matrices of copper, tin, or other metals. A metal coating that is particularly successful involves sodium, which wets carbon fibers and coats them with a protective intermetallic compound by reacting with one or more other molten metals (e.g., tin). This is called the sodium process. A related process immerses the fibers in liquid NaK. However, these processes involving sodium

suffer from sodium contamination of the fibers, probably due to the intercalation of sodium into graphite. Nevertheless, aluminum-matrix composites containing unidirectional carbon fibers treated by the sodium process exhibit tensile strengths close to those calculated using the rule of mixtures, indicating that the fibers are not degraded by the sodium process.

Examples of ceramics used as coatings on carbon fibers include TiC, SiC, B_4C, TiB_2, TiN, K_2ZrF_6, and ZrO_2. Methods used to deposit the ceramics include (i) reaction of the carbon fibers with a molten metal alloy, called the liquid metal transfer agent (LMTA) technique, (ii) chemical vapor deposition (CVD), and (iii) solution coating.

The LMTA technique involves immersing the fibers in a melt of copper or tin (called a liquid metal transfer agent, which must not react with carbon) in which a refractory element (e.g., W, Cr, Ti) is dissolved, and subsequent removal of the transfer agent from the fiber surface by immersion in liquid aluminum (suitable for fabricating an aluminum-matrix composite). For example, to form a TiC coating, the alloy can be Cu-10% Ti at 1,050°C or Sn-1% Ti at 900–1,055°C. In particular, by immersing the fibers in Sn-1% Ti at 900–1,055°C for 0.25–10 min, a 0.1 μm layer of TiC is formed on the fibers, although they are also surrounded by the tin alloy. Subsequent immersion for 1 min in liquid aluminum causes the tin alloy to dissolve in the liquid aluminum. The result of this is a wire preform suitable for fabricating aluminum-matrix composites. Other than titanium carbide, tungsten carbide and chromium carbide have been formed on carbon fibers by the LMTA technique.

The CVD technique has been used to form coatings of TiB_2, TiC, SiC, B_4C, and TiN. The B_4C coating is formed by reactive CVD on carbon fibers, using a BCl_3/H_2 mixture as the reactant. The TiB_2 deposition uses $TiCl_4$ and BCl_3 gases, which are reduced by Zn vapor. The TiB_2 coating is particularly attractive because of the exceptionally good wetting between TiB_2 and molten aluminum. During composite fabrication, the TiB_2 coating is displaced and dissolved in the matrix, while an oxide (γ-Al_2O_3 for a pure aluminum matrix, $MgAl_2O_4$ spinel for a 6,061 aluminum matrix) is formed between the fiber and the matrix. The oxygen for the oxide formation comes from the sizing on the fibers; the sizing is not completely removed from the fibers before processing. The oxide layer serves as a diffusion barrier to aluminum, but allows the diffusion of carbon, thereby limiting Al_4C_3 growth to the oxide–matrix interface. Moreover, the oxide provides bonding between the fiber and the matrix. Because of the reaction at the interface between the coating and the fiber, the fiber strength is degraded after coating. To alleviate this problem, a layer of pyrolytic carbon is deposited between the fiber and the ceramic layer. The CVD process involves high temperatures (e.g., 1,200°C for SiC deposition using CH_3SiCl_4); this high temperature degrades the carbon fibers. Another problem with the CVD process is the difficulty involved in obtaining a uniform coating around the circumference of each fiber. Moreover, it is expensive and requires the scrubbing and disposal of most of the corrosive starting material, as most of it does not react at all. The most serious problem with the TiB_2 coating is that it is not air stable; it cannot be exposed to air before immersion in the molten metal or wetting will not take place. This problem limits the shapes of the

materials that can be fabricated, especially since the wire preforms are not very flexible.

A high compliance (or a low modulus) is preferred for the coating in order to increase the interface strength. An increase in the interface (or interphase) strength results in an increase in the transverse strength. The modulus of SiC coatings can be varied by controlling the plasma voltage in plasma-assisted chemical vapor deposition (PACVD). Modulus values in the range from 19 to 285 GPa have been obtained in PACVD SiC, which should be compared to a value of 448 GPa for CVD SiC. Unidirectional carbon fiber (Thornel P-55) aluminum-matrix composites in which the fibers are coated with SiC exhibit interface and transverse strengths that increase with decreasing modulus of the SiC coating.

The most attractive coating technique developed to date is the solution coating method. When using an organometallic solution, fibers are passed through a toluene solution containing an organometallic compound, followed by hydrolysis or pyrolysis of the organometallic compounds to form the coating. Thus, the fibers are passed sequentially through a furnace in which the sizing on the fibers is vaporized, followed by an ultrasonic bath containing an organometallic solution. The coated fibers are then passed through a chamber containing flowing steam in which the organometallic compound on the fiber surface is hydrolyzed to oxide, and finally through an argon atmosphere drying furnace in which any excess solvent or water is vaporized and any unhydrolyzed organometallic is pyrolyzed. In contrast to the TiB_2 coatings, the SiO_2 coatings formed by organometallic solution coating are air stable.

The organometallic compounds used are alkoxides in which metal atoms are bound to hydrocarbon groups by oxygen atoms. The general formula is $M(OR)_x$, where R is any hydrocarbon group (e.g., methyl, ethyl, propyl) and x is the oxidation state of the metal atom M. When exposed to water vapor, these alkoxides hydrolyze:

$$M(OR)_x + \tfrac{x}{2}H_2O \rightarrow MO_{x/2} + xROH \tag{6.2}$$

For example, the alkoxide tetraethoxysilane (also called tetraethylorthosilicate) is hydrolyzed by water as follows:

$$Si(OC_2H_5)_4 + 2H_2O \rightarrow SiO_2 + 4C_2H_5OH\,. \tag{6.3}$$

Alkoxides can also be pyrolyzed to yield oxides; for example:

$$Si(OC_2H_5)_4 \rightarrow SiO_2 + 2C_2H_5OH + 2C_2H_4\,. \tag{6.4}$$

Most alkoxides can be dissolved in toluene. By controlling the solution concentration and the time and temperature of immersion, it is possible to control the uniformity and thickness of the resulting oxide coating. The thickness of the oxide coatings on the fibers varies from 700 to 1,500 Å. The oxide is amorphous and contains carbon, which originates in the carbon fiber.

Liquid magnesium wets SiO_2-coated low-modulus carbon fibers (e.g., T-300) and infiltrates the fiber bundles due to reactions between the molten magnesium

and the SiO_2 coating. The reactions include the following:

$$2Mg + SiO_2 \rightarrow 2MgO + Si \qquad \Delta G^{\circ}_{670^{\circ}C} = -76\,\text{kcal} \tag{6.5}$$

$$MgO + SiO_2 \rightarrow MgSiO_3 \qquad \Delta G^{\circ}_{670^{\circ}C} = -23\,\text{kcal} \tag{6.6}$$

$$2Mg + 3SiO_2 \rightarrow 2MgSiO_3 + Si \qquad \Delta G^{\circ}_{670^{\circ}C} = -122\,\text{kcal} \tag{6.7}$$

$$2MgO + SiO_2 \rightarrow Mg_2SiO_4 \qquad \Delta G^{\circ}_{670^{\circ}C} = -28\,\text{kcal} \tag{6.8}$$

$$2Mg + 2SiO_2 \rightarrow Mg_2SiO_4 + Si \qquad \Delta G^{\circ}_{670^{\circ}C} = -104\,\text{kcal}\,. \tag{6.9}$$

The interfacial layer between the fiber and the Mg matrix contains MgO and magnesium silicates. However, immersion of SiO_2-coated high-modulus fibers (e.g., P-100) in liquid magnesium causes the oxide coating to separate from the fibers due to the poor adherence of the oxide coating to the high-modulus fibers. This problem with the high-modulus fibers can be solved by first depositing a thin amorphous carbon coating onto the fibers by passing the fiber bundles through a toluene solution of petroleum pitch, and then evaporating the solvent and pyrolyzing the pitch.

The most effective air-stable coating for carbon fibers used in aluminum-matrix composites is a mixed boron-silicon oxide applied from organometallic solutions.

Instead of SiO_2, TiO_2 can be deposited onto carbon fibers by the organometallic solution method. For TiO_2, the alkoxide can be titanium isopropoxide.

SiC coatings can be formed by using polycarbosilane (dissolved in toluene) as the precursor, which is pyrolyzed to SiC. These coatings are wetted by molten copper containing a small amount of titanium due to a reaction between SiC and Ti to form TiC.

Instead of using an organometallic solution, another kind of solution coating method uses an aqueous solution of a salt. For example, the salts potassium zirconium hexafluoride (K_2ZrF_6) or potassium titanium hexafluoride (K_2TiF_6) are used to deposit microcrystals of K_2ZrF_6 or K_2TiF_6 on the fiber surface. These fluoride coatings are stable in air. The following reactions supposedly take place between K_2ZrF_6 and the aluminum matrix:

$$3K_2ZrF_6 + 4Al \rightarrow 6KF + 4AlF_3 + 3Zr \tag{6.10}$$

$$3Zr + 9Al \rightarrow 3Al_3Zr \tag{6.11}$$

$$Zr + O_2 \rightarrow ZrO_2\,. \tag{6.12}$$

When an Al-12 wt.% Si alloy (rather than pure Al) is used as the matrix, the following reaction may also occur:

$$Zr + 2Si \rightarrow ZrSi_2\,. \tag{6.13}$$

The fluorides KF and AlF_3 are thought to dissolve the thin layer of Al_2O_3 on the liquid aluminum surface, thus helping the liquid aluminum to wet the carbon fibers. Furthermore, reactions 6.10 and 6.11 are strongly exothermic and may therefore cause a local temperature increase near the fiber–matrix interface. The increased temperature probably gives rise to a liquid phase at the fiber–matrix interface.

Although the K_2ZrF_6 treatment causes the contact angle between carbon and liquid aluminum at 700–800°C to decrease from 160° to 60–75°, it causes the fiber tensile strength to degrade during aluminum infiltration.

Another example of a salt solution coating method involves the use of the salt zirconium oxychloride ($ZrOCl_2$). Dip coating the carbon fibers in the salt solution and then heating to 330°C causes the formation of a ZrO_2 coating less than 1 μm thick. The ZrO_2 coating serves to improve fiber–matrix wetting and reduce the fiber–matrix reaction in aluminum-matrix composites.

6.2.2.1.2 Reinforcement-Cement Interface Composition Modification

Due to the poor adhesiveness of cement compared to polymeric adhesives, the reinforcement–cement bond strength is low in cement-matrix composites. This problem exists whether the reinforcement is microscopic (such as with carbon, glass and polymer fibers) or macroscopic (such as for a steel rebar and an aggregate). The bond strength can be enhanced by adding polymeric admixtures such as latex (in the form of an aqueous particulate dispersion) and methylcellulose (in the form of an aqueous solution, since methylcellulose is water soluble) to the cement or concrete mix. The polymer not only resides in the cement matrix but it also lines the fiber–cement interface, thereby enhancing the fiber–matrix bond. The bond strength can also be enhanced by adding a fine particulate to the mix, such as silica fume, which is around 0.1 μm in particle size. The fine particles reduce the pore size in the cement matrix and at the reinforcement–cement interface. The pore size reduction at the interface results in the strengthening of the interface.

The bonding between carbon fiber and the cement matrix, as well as the wettability of the fiber by the cement matrix (water based), can be improved by ozone treatment of the carbon fiber prior to incorporation into the cement. The treatment involves surface oxidation, which results in surface oxygen-containing functional groups, thus increasing the surface oxygen concentration, and it changes the surface oxygen from C–O to C=O, as shown in Table 6.8. The improved bonding is shown in Fig. 3.11 by the adhesion of the cement matrix to a pulled-out fiber that has been ozone treated.

6.2.2.2 Interlaminar Interface Composition Modification

For continuous fiber polymer-matrix composites, the interface between adjacent laminae of fibers is a polymer-rich region. It is the weak link in the composite, as shown by the fact that delamination is a common type of damage in these composites. The composition of this interface can be modified by filling this region with

Table 6.8. Fractions of surface carbon atoms bonded as C–H, C–O and C=O (from [11])

Treatment	C–H	C–O	C=O
As received	86.5	13.5	0
After ozone exposure	76.0	0	24.0

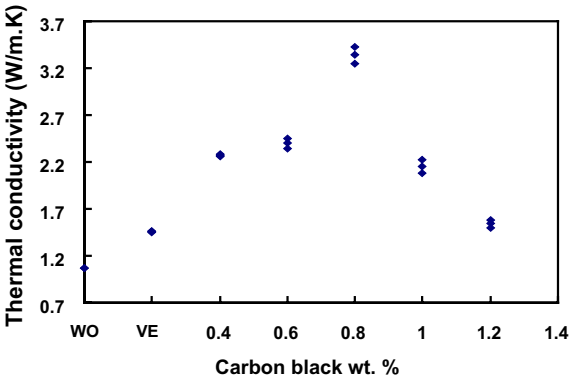

Figure 6.13. Thermal conductivity of crossply carbon fiber polymer-matrix composites with and without various interlaminar interface modifications. WO – without carbon black and without vehicle. VE – with vehicle and without carbon black. The vehicle is ethylene glycol monoethyl ether. The carbon black wt.% refers to the concentration of carbon black in the dispersion involving the vehicle. The dispersion is applied onto the fiber epoxy prepreg surface prior to consolidation of the laminae to form a composite. Three specimens of each composition are tested

a nanofiller, as illustrated in Fig. 6.13. Through such a modification, the through-thickness thermal conductivity and the compressive and flexural properties can be improved [12]. This improvement is due to the removal of some of the excess polymer at the interlaminar interface through the use of a solvent (the vehicle, namely ethylene glycol monoethyl ether, in the nanofiller dispersion), in addition to the filling of the interface region with the nanofiller, namely carbon black, which is introduced in the form of nanoparticles (30 nm).

The through-thickness thermal conductivity is enhanced by using the vehicle without carbon black for interlaminar interface modification and is further increased by using the vehicle with carbon black (Fig. 6.13). The optimum carbon black content for attaining the highest thermal conductivity is 0.8 wt.% (with respect to the dispersion). At the optimum carbon black content, the thermal conductivity increase (relative to the case of no interlaminar interface modification) is 212%. In contrast, the fractional increase attained by using aligned carbon nanotubes grown on continuous silicon carbide fibers is only 50% [13]. The increase in the thermal conductivity due to the use of the vehicle without carbon black is consistent with the fact that the vehicle dissolves away a part of the resin at the interface, thereby allowing greater proximity between the fibers of the adjacent laminae. The further increase in the thermal conductivity due to the use of the vehicle with carbon black is consistent with the fact that the carbon black is a conformable and conductive filler that improves the thermal contact across the interlaminar interface. An excessive content of carbon black decreases the thermal conductivity relative to the value at the optimum carbon black content because of the separation of the fibers of adjacent laminae when the carbon black content is excessive.

Nanoclay is a more effective interlaminar filler than carbon black when used to increase the flexural properties. It increases the flexural modulus by 30%, while carbon black increases it by only 10%. Nanoclay is more effective because of its

nanoplatelet morphology, which contrasts with the particulate morphology of carbon black.

6.2.3 Interface Microstructure Modification

Mechanical interlocking is valuable for enhancing the cohesion between the reinforcement and the matrix, particularly when chemical bonding (whether covalent, van der Waals or other forces) is weak. Roughening an interface, typically by roughening the surface of the reinforcement, is commonly used to enhance the mechanical interlocking between the reinforcement and the matrix. The roughening can be achieved by mechanical or chemical methods. An example of a mechanical method is mechanical deformation of the surface region of the reinforcement by threading, like forming threads on a screw. An example of a chemical method is the use of an etchant (e.g., an acid) to react with the surface of the reinforcement. Chemical methods tend to provide microscopic roughness (low roughness, with a high density of hillocks in the resulting topography), whereas mechanical methods tend to provide macroscopic roughness (high roughness, with a low density of hillocks in the resulting topography). Both a high roughness and a high density of hillocks promote mechanical interlocking. Thus, both types of methods have their advantages and disadvantages. Chemical methods are usually used for microscopic reinforcements (e.g., carbon fiber), whereas mechanical methods are usually used for macroscopic reinforcements (e.g., steel rebars). Nonmechanical physical methods such as ion bombardment are costly and characterized by low productivity.

Due to the poor adhesiveness of cement compared to polymeric adhesives in addition to the high viscosity of the cement mix, voids tend to occur at the interface between a fiber and the cement matrix. One method of reducing the interfacial void content is to add silica fume to the cement mix. Due to the small size (around 0.1 μm) of the particles in silica fume, the void structure of the cement matrix becomes much finer and the fiber–matrix interfacial void content is lessened. As a consequence, the fiber–matrix bond strength is increased.

6.3 Tailoring by Surface Modification

The coating of carbon materials to protect them from oxidation is used in this section to illustrate methods of surface composition modification. In the absence of oxygen, carbon materials have excellent high-temperature resistance. For example, the carbon–carbon composites used for the nose cap of a Space Shuttle can withstand 1,600°C, whereas more advanced carbon–carbon composites can withstand 2,200°C. In contrast, superalloys can only withstand 1,200°C and also have high densities.

Carbon materials are highly susceptible to oxidation at temperatures above 320°C. The predominant reaction that occurs in air is

$$C + O_2 \rightarrow CO_2 \uparrow \tag{6.14}$$

This reaction converts carbon to a gas, thus causing carbon mass loss. The reaction is associated with a very large negative value of the Gibbs free energy change, so it proceeds with a large driving force, even at very low O_2 partial pressures. Thus, the rate of oxidation is controlled not by the chemical reaction itself, but by the transport of the gaseous species to and from the reaction front.

The oxidation of carbon–carbon composites preferentially occurs at the fiber–matrix interface and weakens the fiber bundles. The unoxidized material fails catastrophically by delamination cracking between plies and at bundle–bundle interfaces within plies. As oxidation progresses, failure becomes a multistep process with less delamination cracking and more cross-bundle cracking. This change of failure mode with oxidation is attributed to greater attack within bundles than at bundle–bundle interfaces. For a weight loss on oxidation of 10%, the reductions in elastic modulus and flexural strength are 30 and 50%, respectively.

Protecting carbon–carbon composites from oxidation up to 1,700°C involves the application of various combinations of the following methods:

1. SiC coating applied by pack cementation, reaction sintering, silicone resin impregnation/pyrolysis, or chemical vapor deposition (CVD) to the outer surface of the composite.
2. Oxidation inhibitors (oxygen getters and glass formers) introduced into the carbon matrix during lay-up and densification cycles, which provide additional oxidation protection from within by migrating to the outer surface and sealing cracks and voids during oxidation.
3. Application of a glassy sealant on top of the SiC conversion coating, mainly by brushing a slurry on, so that the sealants melt, fill voids and stop oxygen diffusion, and in some cases act as oxygen getters.
4. Dense SiC or Si_3N_4 overlayer applied by chemical vapor deposition (CVD) on top of the glassy sealant (if used) or the SiC conversion coating; this overlayer controls and inhibits the transfer of oxygen to the substrate, and controls the venting of reaction products to the outside.
5. Application of an aluminum metaphosphate coating by ozone treatment, followed by the impregnation of a liquid solution of aluminum hydroxide dissolved in phosphoric acid, and then heating in nitrogen gas at 800°C for 20 min. Without the ozone treatment, which increases the surface oxygen concentration, the impregnation is not effective for coating or for oxidation protection. Figure 6.14 shows the decrease in weight loss upon heating in air due to the coating.

The SiC coating in the first method described above, known as SiC conversion coating, is gradated in composition so that it changes gradually from pure silicon compounds on the outside surface to pure carbon on the inside. This gradation minimizes spallation resulting from the thermal expansion mismatch between SiC and the carbon–carbon composite. The conversion coating can also be made to be gradated in porosity so that it is denser near the outside surface. The coating is applied by pack cementation, which involves packing the composite into a mixture

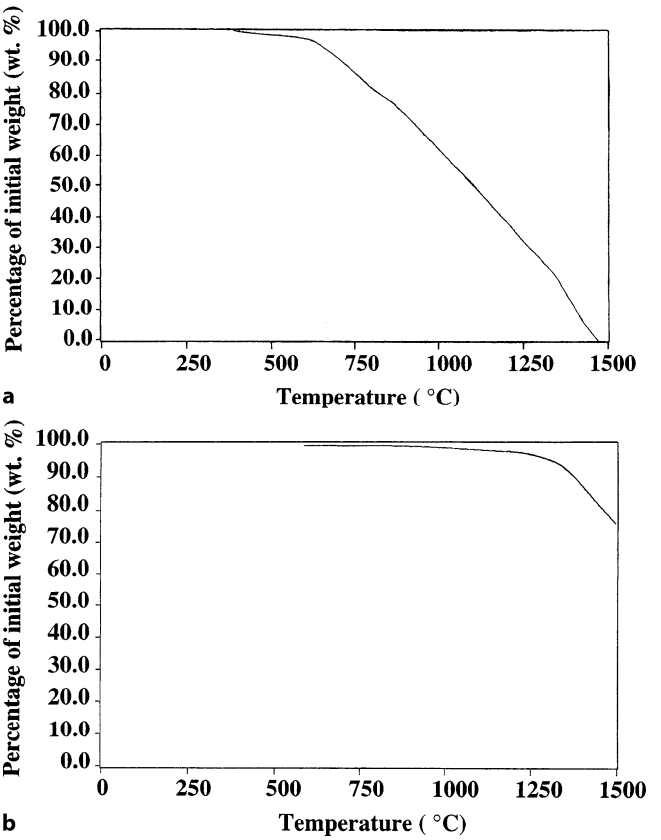

Figure 6.14. Percentage of initial weight versus temperature for graphite heated in air to 1,500°C at a heating rate of 10°C/min. **a** Untreated graphite, with 10% weight loss at 750°C. **b** Graphite coated with aluminum metaphosphate (weighing 20% of that of the graphite before coating), with 10% weight loss at 1,375°C. (From [14])

of silicon carbide and silicon powders and then heating this assembly up to 1,600°C. During this process, the following are the main reactions that take place:

$$Si_{(l)} + C \rightarrow SiC \tag{6.15}$$

$$Si_{(g)} + C \rightarrow SiC \tag{6.16}$$

$$SiO_{(g)} + 2C \rightarrow SiC + CO_{(g)} \, . \tag{6.17}$$

The net result is the chemical conversion of the outermost surfaces of the composite to silicon carbide. Typical thicknesses of pack cementation coatings range from 0.3 to 0.7 mm. One disadvantage of this process is that elemental silicon may be trapped in the carbon matrix under the conversion coating. The entrapped silicon tends to vaporize at elevated temperatures and erupt through the coating, leaving pathways for oxygen to migrate to the carbon–carbon substrate.

A second method of forming a SiC coating is reaction sintering, which involves dipping a carbon–carbon composite into a suspension of silicon powder (average 10 μm size) in an alcohol solution and then sintering at 1,600°C for 4 h in argon.

A third method of forming a SiC coating involves vacuum impregnation and cold isostatic pressing (30,000 psi or 200 MPa) of a silicone resin into the matrix of a carbon–carbon composite, with subsequent pyrolysis at 1,600°C for 2 h in argon.

The SiC overlayer described in method 4 above is denser (less porous) than the SiC conversion coating described in method1. It serves as the primary oxygen barrier. It is prepared by CVD, which involves the thermal decomposition/reduction of a volatile silicon compound (e.g., CH_3SiCl, CH_3SiCl_3) to SiC. The reaction takes the form:

$$CH_3SiCl_{3(g)} \xrightarrow{Heat/H_2} SiC + 3HCl_{(g)} \tag{6.18}$$

The decomposition occurs in the presence of hydrogen and heat (e.g., 1,125°C). If desired, the overlayer can be deposited so that it contains a small percentage of unreacted silicon that is homogeneously dispersed in the SiC. Upon oxidation, the excess silicon becomes SiO_2, which has a very low oxygen diffusion coefficient. This silicon-rich SiC is termed SiSiC. Instead of SiC, Si_3N_4 may be used as the overlayer; Si_3N_4 can also be deposited by CVD.

Among all high-temperature ceramics, silicon-based ceramics (SiC and Si_3N_4) have the best thermal expansion compatibilities with carbon–carbon composites and exhibit the lowest oxidation rates. Moreover, the thin amorphous SiO_2 scales that grow have low oxygen diffusion coefficients and can be modified with other oxides to control the viscosity. Above 1,800°C, these silicon-based ceramic coatings cannot be used because of the reactions at the interface between the SiO_2 scale and the underlying ceramic. Furthermore, the reduction of SiO_2 by carbon produces $CO_{(g)}$.

The glass sealants in method 3 take the form of glazes that usually contain silicates and borates. If desired, the glaze can be filled with SiC particles. The sealant is particularly important if the SiC conversion coating is porous. Moreover, when microcracks develop in the dense overlayer, the sealant fills the microcracks. Borate (B_2O_3) glazes wet C and SiC quite well, but they are useful up to 1,200°C due to volatilization. Moreover, B_2O_3 has poor moisture resistance at ambient temperatures, as it undergoes hydrolysis, which results in swelling and crumbling. In addition, B_2O_3 has a tendency to galvanically corrode SiC coatings at high temperatures. However, these problems with B_2O_3 can be alleviated by using multicomponent systems, such as $10TiO_2 \cdot 20SiO_2 \cdot 70B_2O_3$. TiO_2 has a high solubility in B_2O_3; it is used to prevent the volatilization of B_2O_3 and to increase the viscosity over a wide temperature range. The SiO_2 component acts to increase the moisture resistance at ambient temperatures, reduce the B_2O_3 volatility at high temperatures, increase the overall viscosity of the sealant, and prevent galvanic corrosion of the SiC at high temperatures by the B_2O_3.

The inhibitors used in method 2 are added to the carbon matrix by incorporating them as particulate fillers into the resin or pitch prior to prepregging. They function as oxygen getters and glass formers. These fillers can take the form of elemental

silicon, titanium, and boron. Oxidation of these particles within the carbon matrix forms a viscous glass, which serves as a sealant that flows into the microcracks of the SiC coating, covering the normally exposed carbon–carbon surface to prevent oxygen ingress into the carbon–carbon. The mechanism of oxidation inhibition by boron-based inhibitors may involve B_2O_2, a volatile suboxide that condenses to B_2O_3 upon encountering a locally high oxygen partial pressure in coating cracks. Instead of using elemental Ti and Si, a combination of SiC, Ti_5Si_3, and TiB_2 may be used. For a more uniform distribution of the glass sealant, the filler ingredients can be prereacted to form alloys such as Si_2TiB_{14} prior to their addition to the resin or pitch. Yet another way to obtain the sealant is to use an organoborosilazane polymer solution.

The addition of glass-forming additives such as boron, silicon carbide and zirconium boride to the carbon matrix can markedly reduce the reactivity of the composite with air, but the spread of the glassy phase throughout the composite is slow and substantial fractions of the composite are gasified before the inhibitors become effective. Thus, in the absence of an exterior impermeable coating, the oxidation protection afforded at temperatures above 1,000°C by inhibitor particles in the carbon matrix is strictly limited.

The inhibition mechanism of B_2O_3 involves the blockage of active sites (such as the edge carbon atoms) for small inhibitor contents and the formation of a mobile diffusion barrier for oxygen when the B_2O_3 amount is increased. The inhibiting effect of B_2O_3 is most pronounced at the beginning of oxidation, as shown by the shallow slopes of the weight loss curves near time zero. Thereafter, a pseudolinear oxidation regime takes hold, just as for the untreated composite. The inhibition factor is defined as the ratio of the oxidation rate of the untreated carbon to that of the treated carbon.

For oxidation protection above 1,700°C, a four-layer coating scheme is available. This scheme consists of a refractory oxide (e.g., ZrO_2, HfO_2, Y_2O_3, ThO_2) used as the outer layer of erosion protection, an SiO_2 glass inner layer used as an oxygen barrier and sealant for cracks in the outer coating, followed by another refractory oxide layer for isolating the SiO_2 from the carbide layer underneath, and finally a refractory carbide layer (e.g., TaC, TiC, HfC, ZrC) to interface with the carbon–carbon substrate and to provide a carbon diffusion barrier to the oxide in order to prevent carbothermic reduction. The four-layer system is thus refractory oxide/SiO_2 glass/refractory oxide/refractory carbide. It should be noted that ZrO_2, HfO_2, Y_2O_3 and ThO_2 all have the required thermal stability for long-term use at $> 2{,}000$°C, but they have very high oxygen permeabilities; silica exhibits the lowest oxygen permeability and is the best candidate for use as an oxygen barrier other than iridium at $> 1{,}800$°C; however, iridium suffers from a relatively high thermal expansion coefficient, a high cost, and limited availability.

A ternary HfC-SiC-$HfSi_2$ system deposited by CVD has been reported to provide good oxidation protection up to 1,900°C. The HfC component is chemically compatible with carbon. Furthermore, HfO_2 is generated from HfC by the reaction:

$$HfC + \tfrac{3}{2}O_2 \rightarrow HfO_2 + CO \tag{6.19}$$

Also, HfO_2 is a very stable oxide at high temperatures. However, HfO_2 undergoes a phase change from monoclinic to tetragonal at 1,700°C, with a volume change of 3.4%. To avoid catastrophic failure due to the volume change, HfO_2 is stabilized through the addition of $HfSi_2$. The SiC component acts as a diffusion barrier.

Pack cementation is a relatively inexpensive technique for coating carbon–carbon composites in large quantities. The quality of SiC coatings prepared by pack cementation can be improved by first depositing a 10 μm carbon film by CVD onto the surface of the carbon–carbon composite, because the carbon film improves the homogeneity of the carbon–carbon surface and eases the reaction with Si. Similarly, carbon CVD can be used to improve SiC films deposited by reaction sintering or resin impregnation. Carbon CVD involves the pyrolysis of methane in a tube furnace at 1,300°C.

Pack cementation has been used to form chromium carbide coatings in addition to SiC coatings for the oxidation protection of carbon–carbon composites. For chromium carbide coatings, the carbon–carbon composite sample is packed into a mixture of chromium powder, alumina powder, and a small quantity of NH_4Cl (an activator) and reacted at 1,000°C in argon. The chromium powder produces chromium carbide by reacting with the carbon–carbon composite. At the same time, HCl dissociated from NH_4Cl reacts with the chromium powder to form chromous halide liquid, which reacts with the carbon–carbon composite to form chromium carbide. This latter type of chromium carbide permeates into the openings in the former kind of chromium carbide. Upon oxidation of the chromium carbide coating, a dense layer of Cr_2O_3 is formed that serves to prevent the oxidation of the carbon–carbon composite.

Another form of oxidation protection can be provided by treating the carbon–carbon composites with various acids and bromine.

The fundamental approaches to the oxidation protection of carbons can be categorized into four groups: (i) preventing catalysis; (ii) blocking the access of gas to the carbon; (iii) inhibiting carbon–gas reactions, and; (iv) improving the carbon crystallite structure. Approach (ii) is the main one applied to carbon–carbon composites, as it provides the greatest degree of oxidation protection. However, the other approaches need to be exploited as well. In particular, Approach (iv) means that pitch and CVI carbon are preferred to resins as precursors for carbon–carbon matrices, as pitch and CVI carbon are more graphitizable than resins. Nevertheless, the stress applied to the matrix by the adjacent fibers during carbonization causes the alignment of the matrix molecules near the fibers. Furthermore, the microstructure of the carbon fibers strongly affects the microstructure of the carbon matrix, even when the fiber fraction is only about 50 wt.%, and the microstructure of the carbon matrix affects the amount of accessible porosity, thereby affecting the oxidation behavior.

The application of coatings to carbon–carbon composites can deteriorate their room-temperature mechanical properties. For example, after the application of a 0.25–0.50 mm thick SiC conversion coating, the flexural strength decreases by 29%. On the other hand, the oxidation of a carbon–carbon composite to a burn-off of 20% causes the flexural strength to decrease by 64%.

6.4 Tailoring by Microstructure Control

6.4.1 Crystallinity Control

6.4.1.1 Polymer-Matrix Composites

The ductility of a semicrystalline thermoplastic decreases with increasing crystallinity, though the ability to resist elevated temperatures increases with increasing crystallinity.

For thermoplastic-matrix composites, increasing the cooling rate after lamination decreases the crystallinity of the polymer matrix. Because the fibers act as nucleation sites for polymer crystallization when the polymer melt is sheared, the presence of fibers enhances the polymer crystallinity to a level above that of the neat polymer. Greater crystallinity is associated with a higher level of fiber–matrix interaction. The crystallinity can be increased by annealing; the presence of carbon fibers accelerates the annealing effect.

6.4.1.2 Carbon-Matrix Composites

The carbon matrix is derived from a pitch, a resin, or a carbonaceous gas. Depending on the carbonization/graphitization temperature, the resulting carbon matrix can range from being amorphous to being graphitic. The higher the degree of graphitization of the carbon matrix, the greater the oxidation resistance and the thermal conductivity, but the more brittle the material. As the carbon fibers used can be highly graphitic, it is usually the carbon matrix that limits the oxidation resistance of the composite.

The heat treatment temperature has a significant effect on the mechanical properties of carbon–carbon composites. Composites that are carbonized at 1,000°C before being graphitized at 2,700°C show a 54% increase in the flexural strength, a 40% decrease in the interlaminar shear strength, and a 93% increase in the flexural modulus. This suggests that the fiber–matrix interaction is different before and after graphitization. The increase in the flexural modulus is probably due to the further graphitization of the carbon fibers under the influence of the carbon matrix around them, even though the fibers have been graphitized prior to this. The choice of the graphitization temperature affects the toughness of the composite. For a pitch-based matrix, the optimum graphitization temperature is 2,400°C, since this is the temperature at which the microstructure is sufficiently ordered to accommodate some slip from shear forces but is disordered enough to prevent long-range slip. A similar graphitization temperature may be used for a polymer-based matrix.

The crystallinity of carbon fibers affects the quality of the resulting carbon–carbon composites. The use of graphitized fibers (fired at 2,200–3,000°C) with a carbon content in excess of 99% is preferred because their thermal stability reduces the part warpage during later high-temperature processing to form a carbon–carbon composite. Moreover, graphitized fibers lead to better densified carbon–carbon composites than carbon fibers that have not been graphitized. This

is because the adhesion of the fibers to the polymer resin is weaker for graphitized fibers, so that the matrix can easily shrink away from the fibers during carbonization, leaving a gap which can be filled in during subsequent impregnation. In contrast, the polar surface groups on carbonized fibers make strong bonds with the resin, thus inhibiting the shrinking of the charred matrix away from the fibers and leading to the formation of fine microcracks in the carbon matrix.

The high-temperature resistance of carbon–carbon composites containing boron or zirconium diboride glass-forming oxidation inhibitors can be impaired by the reactions between the inhibitors and the carbonaceous components of the composite. These reactions, which probably form carbides, affect both fibers and matrix. They result in almost complete crystallization of the composite components. This crystallization transforms the microstructure of the composite, weakening it and producing brittle failure behavior. For boron, the reaction occurs at temperatures of between 2,320 and 2,330°C; for zirconium diboride, it occurs at temperatures of between 2,330 and 2,350°C.

6.4.2 Porosity Control

Porosity is detrimental to the strength of a material. The increase in the filler content may cause an increase in the porosity, especially when the filler–matrix bond is not strong or when the filler volume fraction is so high that the matrix is insufficient.

For carbon fiber reinforced cement paste, as shown in Fig. 6.15, the air void content (i.e., the porosity) increases significantly with increasing fiber content, even though the fiber volume fraction is less than 5%. This is due to the poor bonding between carbon fiber and the cement matrix, in addition to the decrease in workability (i.e., the paste gets thicker) with increasing fiber content.

For copper-matrix silicon carbide whisker composites fabricated by powder metallurgy, the porosity increases when the whisker volume fraction exceeds 30%, as shown in Fig. 1.10. Microscope photographs of the porosity are shown in Fig. 1.11 for copper-matrix titanium diboride platelet (60 vol%) composites made by powder metallurgy. The detrimental effect of the porosity on the mechanical properties is also shown in Fig. 1.10.

The porosity can be reduced by tailoring the process and composition. For silicon carbide whisker copper-matrix composites, the use of the coated filler method of powder metallurgy in place of the admixture method of powder metallurgy for composite fabrication reduces the porosity at a given filler volume fraction, as shown in Fig. 1.10.

In the case of carbon fiber cement-matrix composites, the use of appropriate admixtures can reduce the porosity. The use of a combination of methylcellulose (a water-soluble polymer that helps fiber dispersion, at the level of 0.4% by mass of cement) and silica fume (size about 0.1 μm, at the level of 15% by mass of cement) as admixtures gives lower porosity than the use of methylcellulose (0.4% by mass of cement) at the same fiber volume fraction, as shown in Fig. 6.15. This is because the silica fume (nanoparticles) causes a finer microstructure and enhances the

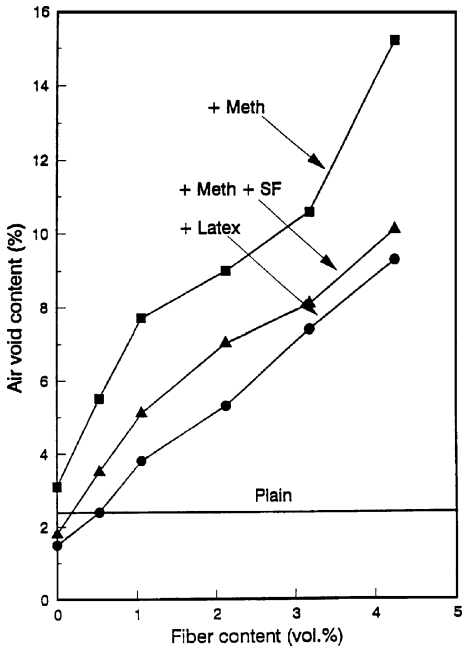

Figure 6.15. Dependence of the air void content on the fiber content in a carbon fiber cement-matrix composite. Meth – methylcellulose (0.4% by mass of cement); SF – silica fume (15% by mass of cement); Latex – aqueous latex particle dispersion (20% by mass of cement). (From [15])

dispersion of the fiber in the cement matrix. Since fiber clumping gives rise to porosity within the clump, improved fiber dispersion reduces the porosity. The use of latex (an aqueous dispersion of latex particles; the amount of dispersion used is 20% by mass of cement) as an admixture gives even lower porosity than the use of methylcellulose and silica fume, as also shown in Fig. 6.15, due to the ability of the fine latex particles in the dispersion to fill the voids (at least the relatively large ones). Figure 6.16 shows that the average air void size is diminished by using the abovementioned admixtures. A lower air void content and a smaller average air void size are associated with a higher tensile strength, as shown in Fig. 6.17.

Figure 6.18 shows that the air void content decreases monotonically with increasing latex content in the absence of fiber, but, in the presence of fiber, it decreases with increasing latex content up to a latex content of 15% by mass of cement, and increases with further increase in the latex content. This means that an excess amount of latex is not desirable in the presence of fiber. This is because the degree of fiber dispersion is reduced as the latex content increases, as shown by electrical resistivity measurements (Sect. 6.5.1). At any latex content, the addition of fiber increases the air void content, as shown in Fig. 6.18.

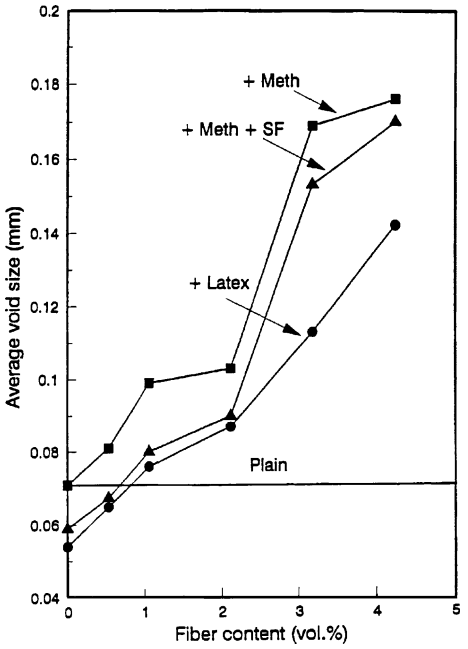

Figure 6.16. Dependence of the average air void size on the fiber content in a carbon fiber cement-matrix composite. Meth – methylcellulose (0.4% by mass of cement); SF – silica fume (15% by mass of cement); Latex – aqueous latex particle dispersion (20% by mass of cement). (From [15])

6.5 Tailoring by Organic–Inorganic Nanoscale Hybridization

Due to the large difference in properties between organic and inorganic materials, the combined use of these materials in a composite is often attractive for composite tailoring. The use of glass fiber (not a nanofiber) in a polymer matrix is an example of such a combined use. In general, neither the organic component nor the inorganic component needs to have a particular shape. Another example of such a combined use is a nanoscale organic–inorganic hybrid. The nanoscale allows the hybrid to serve as the matrix of a composite that contains a filler, such as a fiber. This section covers nanoscale organic–inorganic hybrids; i.e., nanocomposites involving organic and inorganic components.

6.5.1 Nanocomposites with Organic Solid Nanoparticles Dispersed in an Inorganic Matrix

Nanocomposites with dispersed organic nanoparticles in an inorganic matrix can be attractive for toughening and porosity reduction, since the organic component is relatively tough and its nanosize may allow it to fill the pores that tend to be present in an inorganic material.

An example of such a nanocomposite is cement with dispersed polymer particles that are used as an admixture. An example of the polymer is latex (styrene-

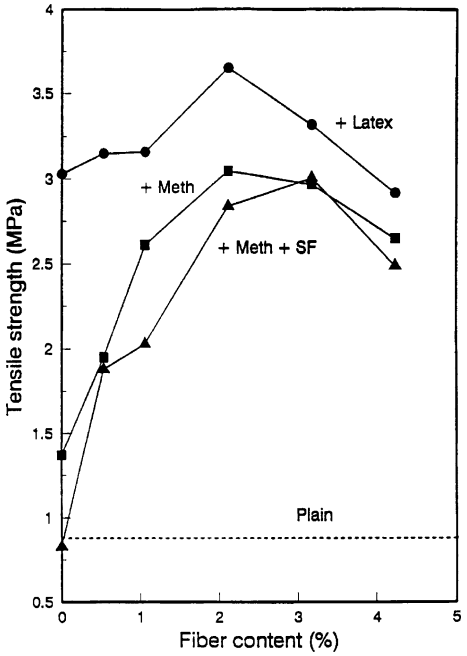

Figure 6.17. Dependence of the tensile strength on the fiber content in a carbon fiber cement-matrix composite. Meth – methylcellulose (0.4% by mass of cement); SF – silica fume (15% by mass of cement); Latex – aqueous latex particle dispersion (20% by mass of cement). (From [15])

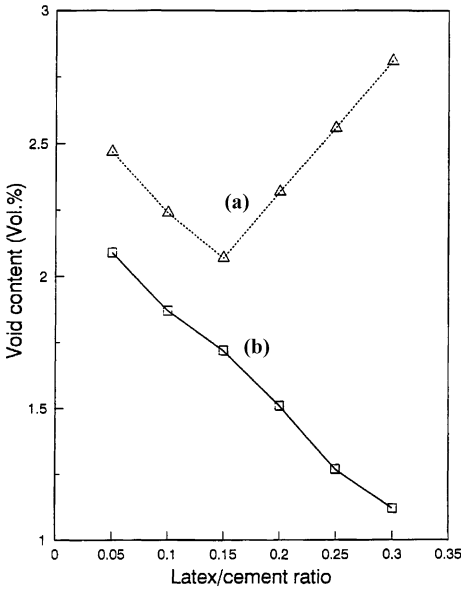

Figure 6.18. Effect of latex/cement ratio on the air void content of cement paste. *a* With 0.53 vol% carbon fibers, *b* without fibers. (From [15])

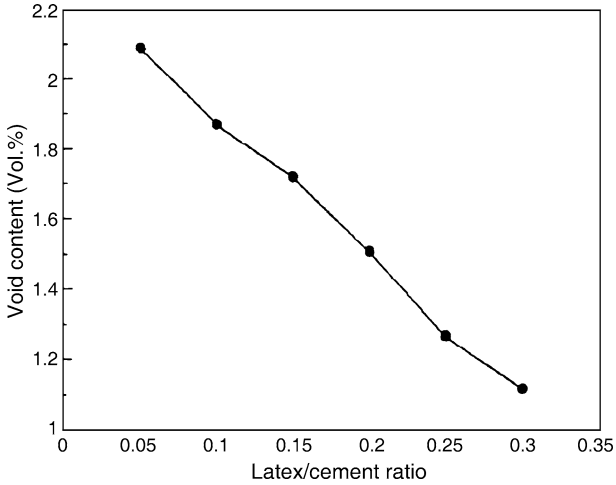

Figure 6.19. Decrease in the air void content with increasing latex/cement ratio (from [16])

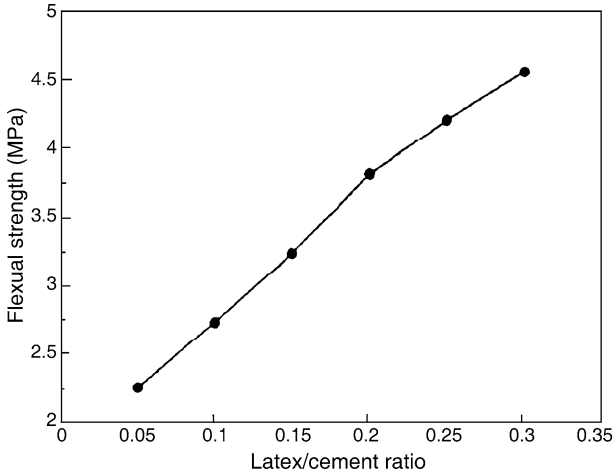

Figure 6.20. Increase in the flexural strength with increasing latex/cement ratio (from [16])

butadiene copolymer) particles of size 0.2 μm (e.g., Latex 460NA of Dow Chemical Corp., Midland, MI, USA, where the styrene:butadiene mass ratio is 66:34 and the copolymer solid amounts to 48 wt.% of the product, which is a water-based dispersion). This means that a latex dispersion proportion of 0.05 by mass of cement is equivalent to a latex solid proportion of 0.024 (i.e., 0.05×0.48) by mass of cement. Figure 6.19 shows the monotonic decrease in the air void content (porosity) with increasing latex content in the nanocomposite. The decrease in porosity results in an increase in the flexural strength, as shown in Fig. 6.20. Due to the toughness of the polymer compared to cement, the flexural toughness increases with increasing latex content in the nanocomposite (Fig. 6.21). Due to the high

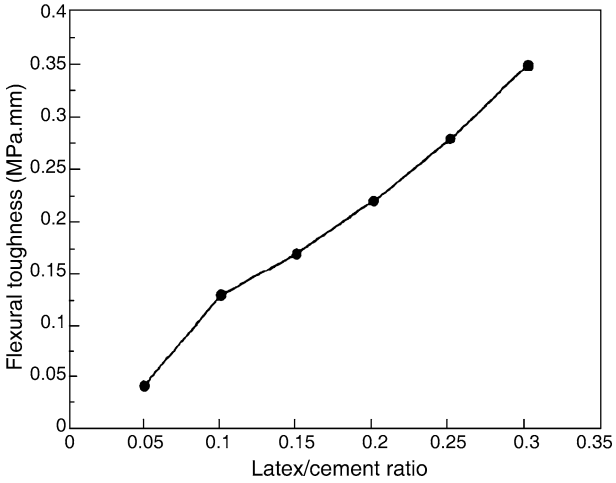

Figure 6.21. Increase in the flexural toughness with increasing latex/cement ratio (from [16])

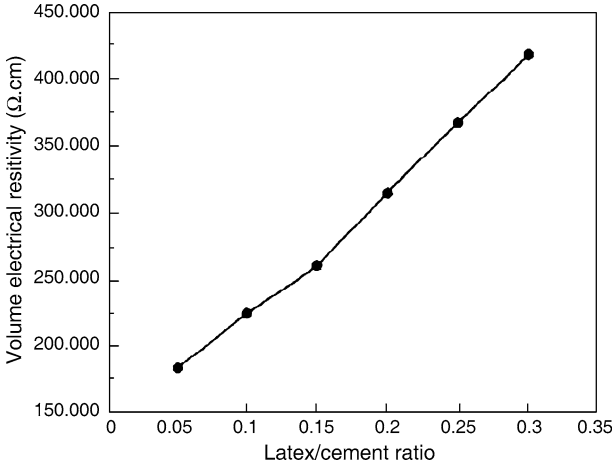

Figure 6.22. Increase in the volume electrical resistivity with increasing latex/cement ratio (from [16])

electrical resistivity of the polymer compared to cement, the electrical resistivity increases with increasing latex content in the nanocomposite (Fig. 6.22).

6.5.2 Nanocomposites with an Organic Component Dispersed in an Inorganic Matrix Where the Organic Component is Added as a Liquid

Instead of using an organic component in the form of particles, one can use an organic component in the form of a liquid solution obtained by dissolving the organic component in a solvent. The dispersion of a liquid solution is usually easier than that of solid particles, due to the greater fluidity of a liquid than a solid particle dispersion. Furthermore, the spatial distribution of the organic component

Table 6.9. Effect of organic component (methylcellulose) on the tensile properties of cement paste (from [17])

Methylcellulose (% by mass of cement)	Strength (MPa)	Modulus (GPa)	Ductility (%)
0	0.89 (±3.1%)	11.13 (±2.9%)	0.0052 (±0.9%)
0.4	1.38 (±3.2%)	6.89 (±1.9%)	0.0213 (±0.8%)
0.6	1.42 (±2.3%)	5.95 (±2.5%)	0.0254 (±1.1%)
0.8	1.53 (±2.4%)	4.74 (±2.3%)	0.0375 (±1.2%)

tends to be more uniform when the component takes the form of a solution rather than solid particles, especially when the proportion of organic component is low. The greater spatial uniformity allows a relatively small proportion of the organic component to be needed to achieve a similar level of property enhancement.

Methylcellulose is a water-soluble polymer and water is needed for a cement mix anyway. Thus, the water used to dissolve the methylcellulose can be counted as some or all of the water in the cement mix. The addition of a methylcellulose solution to cement paste results in a slight increase in the tensile strength (due to the decreased porosity), a decrease in the tensile modulus (due to the low modulus of the methylcellulose compared to cement), and a significant increase in the tensile ductility (due to the high ductility of the methylcellulose compared to cement), as shown in Table 6.9. The highest methylcellulose (solid) proportion of 0.008 by mass of cement in Table 6.9 is much lower than the lowest latex solid proportion of 0.024 by mass of cement in Figs. 6.19–6.22. Due to the low methylcellulose proportion, the tensile strength is increased only slightly by methylcellulose addition (Table 6.9), whereas it is increased substantially by latex addition (Fig. 6.17). However, due to the uniform distribution of the methylcellulose (because the methylcellulose is introduced in the form of a solution) and the consequent high degree of continuity of the organic component, the small proportion of methylcellulose (0.8% by mass of cement) results in increases in ductility and shear bond strength (between steel rebars and concrete) that are as large as those due to 20% latex solid dispersion by mass of cement (i.e., 9.5% latex solid by mass of cement). The increase in bond strength is due to the presence of a layer of the polymer component at the bond interface. However, due to the uniform distribution and the consequent continuity of the methylcellulose in the nanocomposite, the modulus is decreased by the addition of methylcellulose much more severely than that of latex at a much higher proportion.

6.5.3 Nanocomposites Made by Inorganic Component Exfoliation and Subsequent Organic Component Adsorption

Inorganic components (e.g., clay) that form loosely bonded layers in the crystal structure may be exfoliated. Exfoliation is a chemical and/or physical process that results in the separation of the material into platelets, such that each platelet consists of a small number of atomic layers. The resulting platelets are known as nanoplatelets. Subsequent adsorption of an organic component onto the surface

of the nanoplatelets results in a nanocomposite with the organic component as the matrix and the inorganic nanoplatelets as the filler. [In general, adsorption is a process that occurs when a gas or liquid accumulates on the surface of a solid (adsorbent), forming a film of molecules or atoms (the adsorbate).] The overall process is known as exfoliation–adsorption. When clay (such as montmorillonite) is used as the inorganic component, the platelets are known as nanoclay, and each nanoplatelet tends to consist of a silicate monolayer. The exfoliation of clay is preceded by the intercalation of the clay with an organic modifier (such as a quaternary ammonium salt) that contains ions. [In general, intercalation refers to the chemical process of inserting a foreign species, typically in the form of a monolayer of atoms, ions or molecules, between the layers of a host material.] The modified clay is known as organoclay, which is then immersed in a liquid solution of the organic component (or its resin) that serves as the matrix for the resulting composite. Interaction of the solution with the salt in the modified clay, along with sonication (e.g., using an ultrasonic cleaner for, say, 2 h, perhaps supplemented by minor heating to, say, 35–45°C), results in exfoliation of the clay and adsorption of the solution onto the exfoliated silicate platelets. Subsequent evaporation of the solvent in the solution allows the organic component to adsorb onto the exfoliated silicate platelets, thus rendering a nanocomposite. The evaporation can be hastened by heating (at, say, 100°C for 4 h) and/or evacuation.

Review Questions

1. What is special about the behavior of the alloy known as Invar?
2. What is the difference between the admixture method and the coatedfiller method of power metallurgy?
3. Why is it undesirable to have an excessively strong bond between the fiber and the matrix in a composite with a brittle matrix?
4. Describe a method of improving the thermal conductivity of a boron nitride particle epoxy-matrix composite.
5. Describe a method for coating a carbon–carbon composite with silicon carbide.
6. What is the advantage of having silica fume, which is used as an admixture in cement, coated with silane?
7. What is the advantage of adding methylcellulose to cement?
8. What is attractive about having a high degree of graphitization in the carbon matrix of a carbon-matrix composite?

References

[1] D.R. Askeland and P.P. Phule, *The Science and Engineering of Materials*, 5th edn., PWS-Kent, Boston, 2006, p. 597.
[2] W.-T. Whang and W.-L. Liu, *SAMPE Q.* 22(1), 3–9 (1990).
[3] D.C. Sherman, C.-Y. Chen and J.L. Cercena, *Proc. Int. SAMPE Symp. and Exhib., 33, Materials: Pathway to the Future*, ed. by G. Carrillo, E.D. Newell, W.D. Brown, and P. Phelan, 1988, pp. 538–539.
[4] D.R. Askeland, *The Science and Engineering of Materials*, 2nd edn., PWS-Kent, Boston, 1989, pp. 538–539.
[5] D.R. Askeland and P.P. Phule, *The Science and Engineering of Materials*, 5th edn., PWS-Kent, Boston, 2006, p. 574.
[6] S.-W. Lai and D.D.L. Chung, "Consumption of SiC Whiskers by the Al-SiC Reaction in Aluminum-Matrix SiC Whisker Composites", *J. Mater. Chem.* 6(3), 469–477 (1996).
[7] P. Yih and D.D.L. Chung, "Titanium Diboride Copper-Matrix Composites," *J. Mater. Sci.* 32(7), 1703–1709 (1997).
[8] Y. Xu and D.D.L. Chung, "Silane-Treated Carbon Fiber for Reinforcing Cement", *Carbon* 39 (ER13), 1995–2001 (2001).
[9] Y. Xu and D.D.L. Chung, "Cement-Based Materials Improved by Surface Treated Admixtures", *ACI Mater. J.* 97(3), 333–342 (2000).
[10] Y. Xu and D.D.L. Chung, "Increasing the Thermal Conductivity of Boron Nitride and Aluminum Nitride Particle Epoxy-Matrix Composites by Particle Surface Treatment", *Compos. Interfaces* 7(4), 243–256 (2000).
[11] X. Fu, W. Lu and D.D.L. Chung, "Ozone Treatment of Carbon Fiber for Reinforcing Cement," *Carbon* 36(9), 1337–1345 (1998).
[12] S. Han, J.T. Lin, Y. Aoyagi and D.D.L. Chung, "Enhancing the Thermal Conductivity and Compressive Modulus of Carbon Fiber Polymer-Matrix Composites in the Through-Thickness Direction by Nanostructuring the Interlaminar Interface with Carbon Black", *Carbon* 46(7), 1060–1071 (2008).
[13] V.P. Veedu, A. Cao, X. Li, K. Ma, C. Soldano, S. Kar, P.M. Ajayan and M.N. Ghasemi-Nejhad. Multifunctional Composites Using Reinforced Laminae with Carbon-Nanotube Forests. *Nat. Mater.* 5(6), 457–462 (2006).
[14] W. Lu and D.D.L. Chung, "Oxidation Protection of Carbon Materials by Acid Phosphate Impregnation", *Carbon* 40(8), 1249–1254 (2002).
[15] P.-W. Chen, X. Fu, and D.D.L. Chung, "Microstructural and Mechanical Effects of Latex, Methylcellulose and Silica Fume on Carbon Fiber Reinforced Cement", *ACI Mater. J.* 94(2), 147–155 (1997).
[16] X. Fu and D.D.L. Chung, "Degree of Dispersion of Latex Particles in Cement Paste, as Assessed by Electrical Resistivity Measurement," *Cem. Concr. Res.* 26(7), 985–991 (1996).
[17] X. Fu, and D.D.L. Chung, "Improving the Bond Strength of Concrete to Reinforcement by Adding Methylcellulose to Concrete," *ACI Mater. J.* 95(5), 601–608 (1998).

Further Reading

D.D.L. Chung, "Interface Engineering for Cement-Matrix Composites", *Compos. Interfaces* 8(1), 67–82 (2001).
D.D.L. Chung, "Applications of Polymers in Cement-Based Structural Materials", *Annu. Tech. Conf. Soc. Plast. Eng.*, 2004, pp. 3845–3858.
C.-K. Leong and D.D.L. Chung, "Improving the Electrical and Mechanical Behavior of Electrically Conductive Paint by Partial Replacement of Silver by Carbon Black", *J. Electron. Mater.* 35(1), 118–122 (2006).
C. Lin, Timothy A. Howe and D.D.L. Chung, "Electrically Nonconductive Thermal Pastes with Carbon as the Thermally Conductive Component", *J. Electron. Mater.* 36(6), 659–668 (2007).

W. Lu and D.D.L. Chung, "Preparation of Conductive Carbons with High Surface Area", *Carbon* 39(1), 39–44 (2000).
W. Lu and D.D.L. Chung, "A Comparative Study of Carbons for Use as an Electrically Conducting Additive in the Manganese Dioxide Cathode of an Electrochemical Cell", *Carbon* 40 (ER3), 447–449 (2002).
W. Lu and D.D.L. Chung, "Oxidation Protection of Carbon Materials by Acid Phosphate Impregnation", *Carbon* 40(8), 1249–1254 (2002).
W. Lu and D.D.L. Chung, "A Comparative Study of Carbons for Use as an Electrically Conducting Additive in the Manganese Dioxide Cathode of an Electrochemical Cell", *Carbon* 40 (ER3), 447–449 (2002).
S. Wen and D.D.L. Chung, "Pitch-Matrix Composites for Electrical, Electromagnetic and Strain-Sensing Applications", *J. Mater. Sci.* 40(15), 3897–3903 (2005).

7 Electrical Properties

This chapter covers the principles and applications of electrical behavior, emphasizing those related to composite materials. This includes thermoelectric behavior and the effects of temperature and stress on electrical resistivity, as well as applications such as thermoelectric energy generation, thermocouples, thermistors, heating (such as deicing), and electrical resistance-based sensing of strain, stress and damage. The materials used to make electrical connections are also covered.

7.1 Origin of Electrical Conduction

Unless noted otherwise, an electrically conductive material utilizes electrons and/or holes as the charge carriers (mobile charged particles) for electrical conduction. A hole is an electron-deficient site.

In the presence of an electric field (i.e., a voltage gradient), a hole drifts toward the negative end of the voltage gradient due to electrostatic attraction, thus resulting in a current (defined as the charge per unit time) in the same direction. In the presence of an electric field, an electron drifts toward the positive end of the voltage gradient, thus resulting in a current (defined as the charge per unit time – not the magnitude of the charge per unit time) in the opposite direction. Hence, the currents resulting from electron drift and hole drift occur in the same direction, even though electrons and holes drift in opposite directions. This means that in a material with both holes and electrons, the total current is the sum of the current due to the holes and that due to the electrons. Drift is actually a term that refers to the movement of charge in response to an applied electric field.

The drift velocity (v) is the velocity of the drift. It is actually the net velocity, since electrons or holes are quantum particles that obey the Heisenberg Uncertainty Principle, and so they constantly move, even in the absence of an applied electric field. The drift velocity is proportional to the applied electric field E, with the constant of proportionality being the mobility (μ), which describes the ease of movement of the carrier in the medium under consideration. Hence,

$$v = \mu E \,. \tag{7.1}$$

Since the units of E are V/m and the units of v are m/s, the units of μ are $m^2/(V\,s)$. For a given combination of carrier and medium, v depends on the temperature.

7.2 Volume Electrical Resistivity

The electric current (or simply "current," I, with units of ampere, or A) is defined as the charge (in coulomb, or C) flowing through the cross-section per unit time. It is the charge, not the magnitude of charge. Thus, the direction of the current is the same as the direction of positive charge flow and is opposite to the direction of negative charge flow.

The current density is the charge flow per unit cross-sectional area per unit time. The units of current density are A/m^2.

The presence of a current in a material requires the presence of charges that can move in response to the applied voltage. These mobile charges are called carriers (i.e., carriers of electricity). The carrier concentration (with units of m^{-3}) is defined as the number of carriers per unit volume.

An electrical conductor may be an electronic conductor (electrons are the main carriers), an ionic conductor (ions are the main carriers), or a mixed conductor (both ions and electrons are the main carriers). In this context, electrons constitute a class of carriers that include both electrons and holes. Holes are electron-deficient sites that are present in semiconductors and semimetals, but not in conventional metals. Holes are positively charged, since the removal of a (negatively charged) electron leaves something that is positively charged.

The current due to mobile charges with a charge q per carrier is given by

$$I = nqvA \ , \tag{7.2}$$

where n is the carrier concentration. When the carriers are electrons, $q = -1.6 \times 10^{-19}$ C. Equation 7.2 derives from the simple argument that each electron drifts by a distance v in one second, and that nvA electrons (the number of electrons in a volume of vA) move through a particular cross-section in one second, as illustrated in Fig. 7.1. Dividing Eq. 7.2 by A gives

$$I/A = nqv \ . \tag{7.3}$$

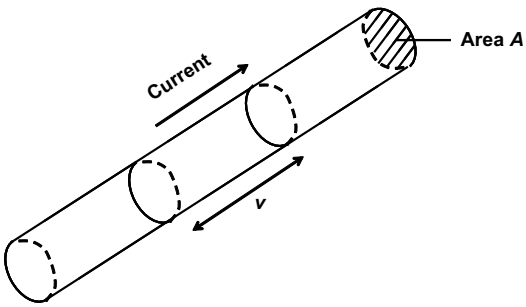

Figure 7.1. An electric current in a wire of cross-sectional area A. The current results from the drift of a type of charge carrier with a charge q per carrier at a drift velocity of v

The current density (J, with units of A/m^2) is defined as the current (I) per unit cross-sectional area (A):

$$J = I/A \ . \tag{7.4}$$

Hence, Eq. 7.3 can be written as

$$J = nqv \ . \tag{7.5}$$

Dividing Eq. 7.5 by the electric field E and using Eq. 7.1, we get

$$J/E = nq\mu \ . \tag{7.6}$$

The electrical conductivity (σ) is defined as J/E. In other words, it is defined as the current density per unit electric field. Hence, Eq. 7.6 becomes

$$\sigma = nq\mu \ . \tag{7.7}$$

From Eq. 7.7, the units of σ are $1/(\Omega\,\mathrm{m})$, i.e., $\Omega^{-1}\,\mathrm{m}^{-1}$, since the units of n are m^{-3}, the units of q are C (coulomb), and the units of μ are $\mathrm{m}^2/(\mathrm{V\,s})$. Alternate units for σ are $\mathrm{S\,m}^{-1}$, where S (short for siemens) equals Ω^{-1}. Note that, by definition,

$$\text{ampere} = \text{coulomb/second} \tag{7.8}$$

and, from Ohm's law,

$$\Omega = \text{volt/ampere} \ . \tag{7.9}$$

The electrical resistivity (ϱ) is defined as $1/\sigma$. Hence, the units of ϱ are $\Omega\,\mathrm{m}$. The electrical resistivity is also known as the volume electrical resistivity in order to emphasize that it relates to the property of a volume of the material. It is also known as the specific resistance.

The electrical resistivity ϱ is related to the electrical resistance (R) by the equation

$$R = \varrho l/A \ , \tag{7.10}$$

where l is the length of the material in the direction of the current. This length is perpendicular to the cross-sectional area A. Equation 7.10 means that the resistance R depends on the geometry such that it is proportional to l and inversely proportional to A. On the other hand, the resistivity ϱ is independent of the geometry and is thus a material property. Similarly, σ is a material property. Equation 7.7 allows the calculation of σ from n, q and μ.

The rearrangement of Eq. 7.10 gives

$$\varrho = RA/l \ . \tag{7.11}$$

Hence,

$$\sigma = l/RA \ . \tag{7.12}$$

Since, by definition, $\sigma = J/E$,

$$J/E = l/RA \ . \tag{7.13}$$

Based on Eq. 7.4, Eq. 7.13 becomes

$$I/E = l/R \ . \tag{7.14}$$

Since, by definition, $E = V/l$, Eq. 7.14 becomes

$$V = IR \ , \tag{7.15}$$

which is known as Ohm's law. Thus, the equation $\sigma = J/E$ is the same as Ohm's law.

7.3 Calculating the Volume Electrical Resistivity of a Composite Material

The volume electrical resistivity of a composite material can be calculated from the resistivities and volume fractions of all of the components. Various mathematical models are available for this calculation. The simplest model is known as the rule of mixtures (ROM), as described below for two configurations: the parallel configuration (each component is continuous and oriented in the direction of the current) and the series configuration (each component is continuous and oriented in the direction perpendicular to the current).

7.3.1 Parallel Configuration

Consider an electric current I flowing in a composite material under a voltage difference of V over a distance of l, such that the composite material consists of two components, labeled 1 and 2, as illustrated in Fig. 5.16a. The cross-sectional areas are A_1 and A_2 for Component 1 (all the strips of Component 1 together) and Component 2 (all the strips of Component 2 together), respectively. The electrical resistivities are ϱ_1 and ϱ_2 for Components 1 and 2, respectively. The current (i.e., the charge per unit time) I through the composite is given by

$$I = I_1 + I_2 \ , \tag{7.16}$$

where I_1 is the current in Component 1 (all the strips of Component 1 together) and I_2 is the current in Component 2 (all the strips of Component 2 together). Using Ohm's law,

$$I_1 = V/R_1 \tag{7.17}$$

and

$$I_2 = V/R_2 \,, \tag{7.18}$$

where R_1 is the resistance of Component 1 (all the strips of Component 1 together) and R_2 is the resistance of Component 2 (all the strips of Component 2 together). Hence, Eq. 7.16 becomes

$$I = V\left[(1/R_1) + (1/R_2)\right] \,. \tag{7.19}$$

Based on Eq. 7.10,

$$R_1 = \varrho_1 l/A_1 \,, \tag{7.20}$$

and

$$R_2 = \varrho_2 l/A_2 \,. \tag{7.21}$$

Based on Eqs. 7.20 and 7.21, Eq. 7.19 becomes

$$I = (V/l)\left[(A_1/\varrho_1) + (A_2/\varrho_2)\right] \,. \tag{7.22}$$

On the other hand, from Ohm's law,

$$I = V/R \,, \tag{7.23}$$

where R is the resistance of the composite. Based on Eq. 7.10, R is given by

$$R = \varrho l/A \,, \tag{7.24}$$

where ϱ is the resistivity of the composite and A is the total cross-sectional area of the composite. Combining Eqs. 7.23 and 7.24 gives

$$I = VA/\varrho l \,. \tag{7.25}$$

Combining Eqs. 7.22 and 7.25 gives

$$VA/\varrho l = (V/l)\left[(A_1/\varrho_1) + (A_2/\varrho_2)\right] \,, \tag{7.26}$$

or

$$A/\varrho = \left[(A_1/\varrho_1) + (A_2/\varrho_2)\right] \,. \tag{7.27}$$

Dividing by A gives

$$1/\varrho = (A_1/A)(1/\varrho_1) + (A_2/A)(1/\varrho_2) = v_1/\varrho_1 + v_2/\varrho_2 \,, \tag{7.28}$$

where v_1 and v_2 are the volume fractions of Components 1 and 2, respectively. Equation 7.28 implies that, for the parallel configuration, the reciprocal of the resistivity of the composite is the weighted average of the reciprocal of the resistivities of the two components, where the weighting factors are the volume fractions of the two components. In other words,

$$\sigma = v_1\sigma_1 + v_2\sigma_2 \,, \tag{7.29}$$

where σ is the electrical conductivity of the composite material, and σ_1 and σ_2 are the conductivities of Components 1 and 2, respectively. Equation 7.29 is a manifestation of the rule of mixtures.

Example Problem

1. Calculate the volume electrical resistivity of a composite material consisting of three components that are in parallel electrically. The resistivity required is the resistivity in the direction in which the components are parallel. Component 1 has a volume electrical resistivity of $1.4 \times 10^{-3}\,\Omega\,\text{cm}$ and a volume fraction of 0.35. Component 2 has a volume electrical resistivity of $4.4 \times 10^{-4}\,\Omega\,\text{cm}$ and a volume fraction of 0.25. Component 3 has a volume electrical resistivity of $9.5 \times 10^{-4}\,\Omega\,\text{cm}$ and a volume fraction of 0.40.

Solution:
From Eq. 7.28,

$$\begin{aligned}
1/\text{resistivity } T &= 0.35/(1.4 \times 10^{-3}\,\Omega\,\text{cm}) + 0.25/(4.4 \times 10{-}4\,\Omega\,\text{cm}) \\
&\quad + 0.40/(9.5 \times 10^{-4}\,\Omega\,\text{cm}) \\
&= 1.24 \times 10^{3}\,(\Omega\,\text{cm})^{-1}, \\
\text{Resistivity} &= 8.1 \times 10^{-4}\,\Omega\,\text{cm}\,.
\end{aligned}$$

7.3.2 Series Configuration

Consider an electric current I flowing in a composite material under a voltage difference of V over a distance of l, such that the composite material consists of two components, labeled 1 and 2, as illustrated in Fig. 7.2b. The lengths are l_1 and l_2 for Component 1 (all the strips of Component 1 together) and Component 2 (all

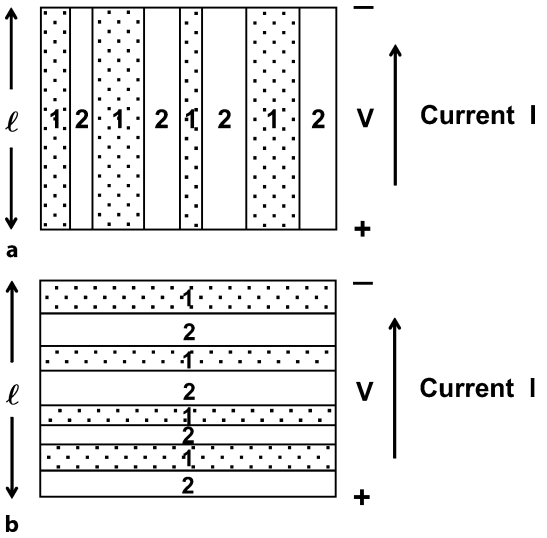

Figure 7.2. An electrically conducting composite material. The composite consists of Component 1 (*dotted regions*) and Component 2 (*white regions*). **a** Components 1 and 2 of the composite in parallel, **b** components 1 and 2 of the composite in series

the strips of Component 2 together), respectively. The electrical resistivities are ρ_1 and ρ_2 for Components 1 and 2, respectively.

The voltage drop V is given by

$$V = V_1 + V_2 \,, \tag{7.30}$$

where V_1 is the voltage drop in Component 1 (all the strips of Component 1 together) and V_2 is the voltage drop in Component 2 (all the strips of Component 2 together). From Ohm's law, and using the fact that the two components have the same cross-sectional area A and the same current I,

$$V = IR = I\rho l/A \,, \tag{7.31}$$

$$V_1 = IR_1 = I\rho_1 l_1/A \,, \tag{7.32}$$

and

$$V_2 = IR_2 = I\rho_2 l_2/A \,. \tag{7.33}$$

Combining Eqs. 7.30, 7.31, 7.32 and 7.33 gives

$$I\rho l/A = I\rho_1 l_1/A + I\rho_2 l_2/A \,, \tag{7.34}$$

or

$$\rho l = \rho_1 l_1 + \rho_2 l_2 \,. \tag{7.35}$$

Dividing by l gives

$$\rho = \rho_1(l_1/l) + \rho_2(l_2/l) = \rho_1 v_1 + \rho_2 v_2 \,, \tag{7.36}$$

where v_1 and v_2 are the volume fractions of Components 1 and 2, respectively. Equation 7.36 implies that, for the series configuration, the resistivity of the composite material is the weighted average of the resistivities of the two components, where the weighting factors are the volume fractions of the two components. Equation 7.36 is a manifestation of the rule of mixtures.

7.4 Contact Electrical Resistivity

An interface is associated with an electrical resistance in the direction perpendicular to the interface. The contact electrical resistance refers to the resistance of an interface between two objects (or between two components in a composite material) when a current is passed across the interface in the direction perpendicular to the interface. When the interface has air voids, for example, the contact resistance will be relatively high. This is because air is an electrical insulator and the objects themselves are more conductive than air. When the interface has an impurity that is less conductive than the objects themselves, the contact resistance will also be

relatively high. Thus, the contact resistance is highly sensitive to the condition of the interface.

The contact resistance also depends on the area of the interface. The larger the area, the lower the contact resistance. Hence, the contact resistance R_c is inversely proportional to the interface area A, and the relationship between these two quantities can be written as

$$R_c = \rho_c / A \ , \tag{7.37}$$

where the proportionality constant ρ_c is known as the contact electrical resistivity. This quantity does not depend on the area of the interface; it only reflects the condition of the interface. The units of ρ_c are $\Omega\,\mathrm{cm}^2$, which are different from those of the volume resistivity ρ, $\Omega\,\mathrm{cm}$.

7.5 Electric Power and Resistance Heating

7.5.1 Scientific Basis

The electric power P associated with the flow of a current I under a voltage difference V is given by

$$P = VI \ . \tag{7.38}$$

This power is dissipated as heat, thus allowing a form of heating known as resistance heating. Applications of this include the deicing of aircraft and bridges. This effect, in which electrical energy is converted to thermal energy, is known as the Joule effect. The units of P are watts (W), with watt = volt $\times$ ampere. Based on Eq. 7.15, Eq. 7.38 can be expressed as

$$P = I^2 R \tag{7.39}$$

and as

$$P = V^2 / R \ . \tag{7.40}$$

Therefore, in order to obtain a high value for the power, both V and I should not be too small (Eq. 7.38). The values of V and I depend on the resistance R. When R is small, V is small since $V = IR$. When R is large, I is small since $I = V/R$. Thus, an intermediate value of R is optimal for obtaining a high power. It is R rather ρ that governs P. Therefore, for a given material (i.e., a given value of ρ), the dimensions can be chosen to obtain a particular value of R (Eq. 7.10). Since the current direction does not affect the resistance heating, the heating can be carried out using DC or AC electricity.

Consider an example in which $R = 1\,\mathrm{M}\Omega$ (i.e., $10^6\,\Omega$) and $V = 120\,\mathrm{V}$ (which is a common voltage from an electrical outlet). Hence,

$$I = V/R = (120\,\mathrm{V})/(1 \times 10^6\,\Omega) = 1.2 \times 10^{-4}\,\mathrm{A} = 0.12\,\mathrm{mA} \ , \tag{7.41}$$

and

$$P = VI = (120\,\mathrm{V})(1.2 \times 10^{-4}\,\mathrm{A}) = 1.4 \times 10^{-2}\,\mathrm{W} = 14\,\mathrm{mW}\,. \tag{7.42}$$

Consider another example in which $R = 1\,\mathrm{k}\Omega$ (i.e., $1 \times 10^3\,\Omega$) and $V = 120\,\mathrm{V}$. Hence,

$$I = V/R = (120\,\mathrm{V})/(1 \times 10^3\,\Omega) = 0.12\,\mathrm{A}\,, \tag{7.43}$$

and

$$P = VI = (120\,\mathrm{V})(0.12\,\mathrm{A}) = 14\,\mathrm{W}\,. \tag{7.44}$$

Now consider another example in which $R = 1\,\Omega$ and $V = 120\,\mathrm{V}$. Hence,

$$I = V/R = (120\,\mathrm{V})/(1\,\Omega) = 120\,\mathrm{A}\,, \tag{7.45}$$

which is a current that is too high to be provided by conventional power sources, which often limit the current to, say, 1 A. Thus, in spite of the high V that the power source can provide, the actual V across the heating element is just

$$V = IR = (1\,\mathrm{A})(1\,\Omega) = 1\,\mathrm{V}\,, \tag{7.46}$$

and the power is thus merely

$$P = VI = (1\,\mathrm{V})(1\,\mathrm{A}) = 1\,\mathrm{W}\,. \tag{7.47}$$

Therefore, among the three examples mentioned above, the intermediate R of $1\,\mathrm{k}\Omega$ gives the highest P.

Nichrome (Ni-20Cr alloy), with $\rho = 1 \times 10^{-4}\,\Omega\,\mathrm{cm}$, is a material that is commonly used for resistance heating because it has a relatively high resistivity for a metal. We can calculate the length of the wire required for a nichrome wire of diameter 1 mm to provide a resistance of $1\,\mathrm{k}\Omega$ using Eq. 7.10:

$$l = RA/\rho = (1\,\mathrm{k}\Omega)\left[\pi(0.5\,\mathrm{mm})^2\right]/(1 \times 10^{-4}\,\Omega\,\mathrm{cm}) = 7.9 \times 10^4\,\mathrm{cm} = 790\,\mathrm{m}\,. \tag{7.48}$$

This length of 790 m is quite long, so the wire cannot be packaged linearly; it needs to be coiled. This is why heating elements commonly take the form of coils.

In order to pass current to a heating element, two electrical contacts are required, as illustrated in Fig. 7.3. An electrical contact may, for example, be a soldered joint

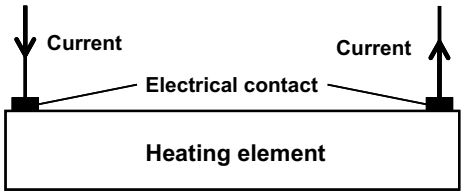

Figure 7.3. Electrical contacts that are used to pass current to a heating element contribute to the electrical resistance

between the heating element and a wire. Each electrical contact is associated with a resistance, which is the sum of (i) the resistance of the joining medium (e.g., solder), (ii) the resistance of the interface between the joining medium and the heating element, and (iii) the resistance of the interface between the joining medium and the wire. Since the joining medium is typically a highly conductive material, the resistance of the joining medium is usually negligible compared to the two interfacial resistances. The interfacial resistance can be substantial due to air voids, impurities, reaction products or other species at the interface. The resistances of both of the contacts contribute to the resistance R encountered by the current I. Therefore, the design of a heating element must consider the contribution to R from the electrical contacts. In particular, the resistance from the two contacts must not be so large that it overshadows the resistance within the heating element material. If it is too large, the electrical contacts become the main heating elements, while the actual heating element contributes little to heat generation, resulting in nonuniform heating as it is concentrated at the electrical contacts.

7.5.2 Self-Heating Structural Materials

7.5.2.1 Introduction

Resistance heating (or Joule heating) involves the conversion of electricity into heat. It requires a heating element through which electric current is passed. Heating elements are commonly used in toasters and hair dryers. Other applications include deicing, home improvement, ovens, space heating, warming vests, heating pads, electric blankets, and seat heating.

The materials most commonly used for heating elements are metal alloys, such as nichrome (an alloy with a common composition of 80% nickel and 20% chromium), which is attractive due to its low cost, high resistivity (compared to many other metals), and its resistance to oxidation or degradation in air at elevated temperatures. In spite of its high resistivity compared to many metals, its resistivity is low compared to carbon or ceramics. Because of this low resistivity (typically $10^{-5}\,\Omega\,\text{cm}$), sufficient resistance in the metallic heating element is commonly attained by using a long length of the metal, which may be coiled or take the form of an etched foil or a patterned thick film. The thick film is made from a paste that contains the metal in powder form.

Compared to metals, carbon is attractive due to its higher resistivity (typically $10^{-3}\,\Omega\,\text{cm}$), high temperature resistance, ability to radiate heat, and its availability in the form of fibers. Carbon heating elements take the form of continuous carbon fiber, unwoven carbon fiber mats/felts, woven carbon fiber fabrics, and flexible graphite. Flexible graphite (also known as Grafoil) is a graphite sheet that is formed by compressing exfoliated graphite in the absence of a binder.

Heating elements that are also structural components are attractive, particularly when the heating is needed for purposes such as deicing in aeronautical and automotive systems, transportation infrastructures (e.g., aircraft, driveways, airport runways, highways and bridges), and industrial systems. This can be achieved by

incorporating a nonstructural heating element into the structural component. For example, the nonstructural heating element can take the form of a sheet that is at or near the surface of the structural component. Examples of nonstructural heating elements include flexible graphite and carbon fiber mats, which are mechanically inadequate for load bearing. An alternate method involves using the load-bearing structural material as the heating element, so that the structural material becomes multifunctional and the need to combine a structural element with a nonstructural element is eliminated. Attractions of this alternative method include higher durability (no need to worry about the detachment of the nonstructural element from the structural element, or about the possible mechanical degradation of the nonstructural element), lower fabrication cost, greater implementation convenience, higher spatial uniformity of the heating, and greater volume of the heating element. Structural materials that also function as heating elements are said to be self-heating.

The dominant structural materials in this context are cement-matrix composites (for buildings) and continuous fiber polymer–matrix composites (for lightweight structures such as aircraft). These materials cannot withstand high temperatures. However, heating to temperatures that are not far from room temperature is needed for deicing, comfortable living, and hazard mitigation. For example, in deicing, the relevant temperature is around 0°C. This section addresses self-heating in both types of structural composites.

The materials used in heating elements cannot have electrical resistivities that are too low, as this would result in the resistance of the heating element being too low and so a high current would be needed to achieve a specific power. The materials of heating elements cannot be too resistive either, as this would result in a current in the heating element that is too low (unless the voltage is very high). Materials used in heating elements include metal alloys, ceramics (such as silicon carbide), graphite, polymer–matrix composites, carbon–carbon composites, asphalt, and concrete.

Resistance heating is useful for heating buildings, for deicing bridge decks, driveways and aircraft, for plastic welding, and for the demolition of concrete structures. On the other hand, electrical self-heating is undesirable for optimizing the performance and reliability of electrical interconnections, bolometers, superconductors, transistors, diodes, and other semiconductor devices.

7.5.2.2 Self-heating Cement-Matrix Composites

Conventional concrete is electrically conductive but its resistivity is too high for resistance heating to be effective. The resistivity of concrete can be diminished by the use of electrically conductive admixtures or aggregates, such as discontinuous carbon fibers, discontinuous steel fibers or shavings, and graphite or carbon particles. It can also be diminished by using an alkaline slag binder. However, the most effective method of decreasing the resistivity is to use a conductive admixture at a volume fraction beyond the percolation threshold. Percolation means the attainment of a continuous conductive path due to contact between adjacent conductive fibers or particles. The objective of this section is to compare various conductive

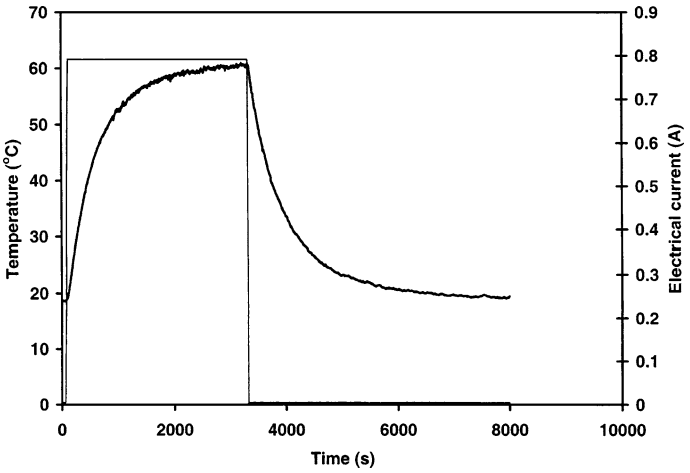

Figure 7.4. Temperature variation during heating (current on) and subsequent cooling (current off) when using steel fiber (8 µm diameter) cement as the resistance heating element. *Thick curve*: temperature, *thin curve*: current. (From [1])

cement-matrix composites in terms of resistance heating effectiveness. These composites have lower resistivities than cement itself (by orders of magnitude) due to the percolation of the conductive admixtures.

Due to the exceptionally low electrical resistivity (0.85 Ω cm) attained by ising 8 µm diameter steel fibers in cement, cement with the steel fibers is a highly effective material for heating, as described below. A DC electrical power input of 5.6 W (7.1 V, 0.79 A) results in a maximum temperature of 60°C (initial temperature = 19°C) and a time of 6 min to achieve half of the maximum temperature rise (Fig. 7.4). The efficiency of energy conversion increases with the duration of heating, reaching 100% after 50 min (Fig. 7.5). The heat power output per unit area provided by steel fiber cement is 750 W/m^2, compared to 340 W/m^2 for a metal wire with the same

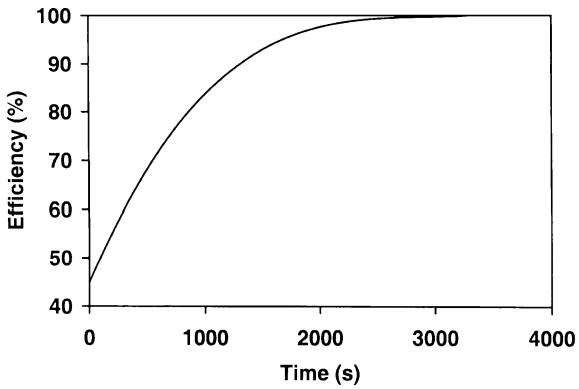

Figure 7.5. Efficiency vs. time for the heating of steel fiber (8 µm diameter) cement at a current of 0.48 A (from [1])

resistance. Due to the presence of steel fibers, the structural properties are superior to those of conventional cement-based materials.

In contrast, for carbon fiber (1.0 vol%) cement of electrical resistivity 104 Ω cm, an electrical power input of 1.8 W (28 V, 0.065 A) results in a maximum temperature of 56°C (initial temperature = 19°C) and a time of 256 s to achieve half of the maximum temperature rise. The high voltage (28 V, compared to 7 V in the case of steel fiber cement) is undesirable due to the voltage limitations of typical power supplies. The performance is even worse for graphite particle (37 vol%) cement paste of resistivity 407 Ω cm.

The steel fibers mentioned above are only 8 μm in diameter. Steel fibers of larger diameter (e.g., 60 μm) are much less effective at reducing the electrical resistivities of cement-based materials and are therefore less effective for self-heating. For example, cement paste with 8 μm diameter steel fibers at 0.54 vol% gave a resistivity of 23 Ω cm, whereas steel fibers of 60 μm diameter at 0.50 vol% led to resistivity 1.4×10^3 Ω cm, steel fibers of 8 μm diameter at 0.36 vol% gave a resistivity of 57 Ω cm, and steel fibers of 60 μm diameter at 0.40 vol% gave a resistivity of 1.7×10^3 Ω cm.

An alternative concrete technology involves using steel shavings (0.15–4.75 mm in particle size) as the conductive aggregate in conjunction with low-carbon steel fibers as the conductive admixture. The use of 20 vol% steel shavings together with 1.5 vol% steel fibers resulted in an electrical resistivity of 75–100 Ω cm. The resistivity increased over time, reaching 350 Ω cm in six months, presumably due to the corrosion of the steel shavings and fibers. The high resistivity and the increase in resistivity with time are undesirable. In contrast, cement with stainless steel fibers (8 μm diameter, 0.7 vol%) has a low resistivity of 0.85 Ω cm and the resistivity is stable over time. Furthermore, it does not require any special mixing equipment or procedure and does not require any special aggregate.

7.5.2.3 Self-heating Polymer-Matrix Composites

Self-heating in continuous fiber polymer-matrix composites can be attained using the following methods: (a) by embedding a low-resistivity interlayer (e.g., a carbon fiber mat) between adjacent laminae during composite fabrication and using the interlayer as a heating element, (b) by using conductive reinforcing fibers (e.g., continuous carbon fibers) to make the composite conductive and using the overall composite as a heating element, and (c) by using the interlaminar interface between adjacent laminae of conductive reinforcing fibers (e.g., continuous carbon fibers) as a heating element.

Method (a) is the one most commonly employed, as it is applicable to a broad range of composites, whether the reinforcing fibers are conductive or not. Method (b) is also feasible, but suffers from difficulties in attaining localized heating. Method (c) involves an innovative concept in which the contact resistance associated with the interlaminar interface between laminae of conductive fibers allows the interface to serve as a heating element. The interface between two crossply laminae can be subdivided to provide a two-dimensional array of heating elements, in addition to an x–y grid of electrical interconnections, thereby allowing spatially distributed heating (Fig. 7.6) and a very small thermal mass for each

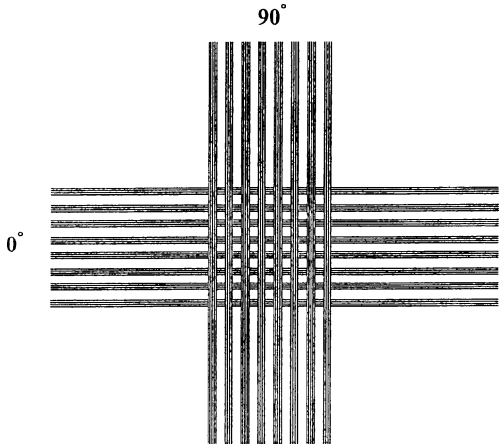

Figure 7.6. Sensor array in the form of a carbon fiber polymer-matrix composite comprising two crossply laminae (from [2])

heating element. Figure 7.7 shows the ability of the interlaminar interface to serve as a resistance heating element. The area of the interface is 5×5 mm and there is a resistance of 0.067 Ω in the direction perpendicular to the area. The heat power output is up to 4×10^4 W/m^2.

An example of the application of method (a) involves the use of a porous mat comprising short carbon fibers and a small proportion of an organic binder as the interlayer. The fibers in a mat are randomly oriented in two dimensions. The mats are made by wet-forming, as in papermaking. A mat comprising bare short carbon fibers and exhibiting a volume electrical resistivity of 0.11 Ω cm and a thermal stability of up to 205°C has been shown to be effective as a resistive heating element. It provides temperatures of up to 134°C (initial temperature = 19°C) at a power of up to 6.5 , with a time of up to 106 s required to achieve half of the

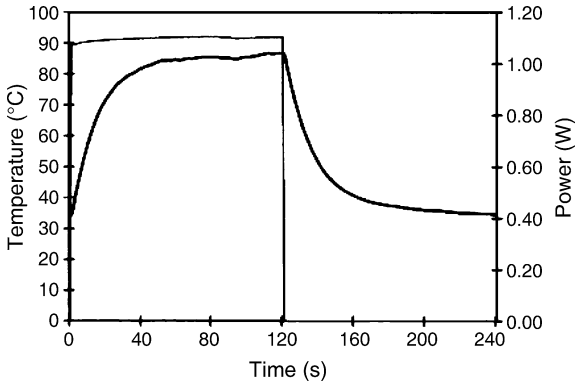

Figure 7.7. The interlaminar interface of a crossply two-lamina carbon fiber epoxy-matrix composite serving as a resistance heating element. The temperature rises while the power is applied and drops during the subsequent period when it is not. *Thick curve*: temperature, *thin curve*: power. (From [2])

maximum temperature rise. The electrical energy used to increase the temperature by 1°C during the initial rapid temperature rise (5 s) is up to 3.8 J. The efficiency is nearly 1.00, even in the first 5 s of heating. A mat comprising metal (Ni/Cu/Ni trilayer)-coated short carbon fibers and exhibiting a volume electrical resistivity of 0.07 Ω cm provides lower temperatures (up to 79°C) but a faster response (up to 14 s to achieve half of the maximum temperature rise).

An example of the application of method (c) involves the use of the interface between two crossply laminae of a continuous carbon fiber epoxy-matrix composite. For an interface of area 5 × 5 mm and a resistance of 0.067 Ω, a DC electrical power input of 0.59 W (3.0 A, 0.20 V) results in a maximum temperature of 89°C (initial temperature = 19°C). The time needed to reach half of the maximum temperature rise is up to 16 s. The efficiency of energy conversion reaches 100% after about 55 s of heating, when the heat power output is up to 4×10^4 W/m^2 of the interlaminar interface.

7.5.2.4 Comparison of Self-heating Structural Materials

Table 7.1 shows a comparison of various materials in terms of their self-heating effectiveness, as evaluated in the laboratory of the author. The carbon fiber epoxy-matrix interlaminar interface (No. 6 in Table 7.1) and the Ni/Cu/Ni-coated carbon fiber mat (No. 5 in Table7.1) have exceptional abilities to provide fast and significant temperature responses, though they have low power capacities. Carbon fiber mat (No. 4 in Table 7.1) has an exceptional ability to deliver high power and significant temperature rises; it is superior to cement-matrix composites (Nos. 1–3 in Table 7.1) in terms of power capacity, temperature capacity, and fast response. On the other hand, it is much inferior to flexible graphite (not a structural material; No. 7 in Table 7.1) in terms of all three attributes.

A comparison of the volume electrical resistivities of the various materials in Table 7.1 shows that a low resistivity tends to be associated with good self-heating performance, although there are exceptions. The outstanding performance of flexible graphite is attributed to its outstandingly low resistivity.

The maximum temperature is limited by the ability of the material to withstand high temperatures. Flexible graphite is outstanding in this ability. However, the maximum temperature is also determined by the ability of the material to sustain current. A low resistivity greatly helps this ability, as shown by comparing the performances of the three cement-based materials (Nos. 1–3 in Table 7.1).

The time to reach half of the maximum temperature rise increases with the maximum temperature rise, as shown by comparing the response times at different input powers for the same material. This time is expected to be reduced by a decrease in thermal mass (which relates to the mass and the specific heat) or an increase in thermal conductivity. The fast response of the carbon fiber epoxy-matrix interlaminar interface is attributed mainly to its low thermal mass, which is due to the microscopic thickness of the interface. The fast responses of the Ni/Cu/Ni-coated carbon fiber mat and the flexible graphite are attributed mainly to the high thermal conductivity.

Table 7.1. Effectiveness of self-heating from a temperature of 19°C

Material	Maximum temperature (°C)	Time to reach half of the maximum temperature rise	Power (W)	Volume resistivity (Ω cm)
1. Steel fiber (0.7 vol%) cement	60	6 min	5.6	0.85
2. Carbon fiber (1.0 vol%) cement	56	4 min	1.8	100
3. Graphite particle (37 vol%) cement	24	4 min	0.27	410
4. Carbon fiber (uncoated) mat	134	2 min	6.5	0.11
5. Ni/Cu/Ni-coated carbon fiber mat	79	14 s	3.0	0.07
6. Carbon fiber epoxy-matrix interlaminar interface	89	16 s	0.59	–[b]
7. Flexible graphite[a]	980	4 s	94	7.5×10^{-4}

[a] Not a structural material
[b] The relevant quantity is the contact resistivity rather than the volume resistivity

The power in Table 7.1 is the electrical power input, which is essentially equal to the heat power output after an initial period in which the material itself is being heated. The power is governed by the ability of the material to sustain current and voltage. This ability is enhanced by a decrease in resistivity.

Although the resistivity is not the only criterion that governs the effectiveness of a material for self-heating, it is the dominant criterion, particularly in relation to the power and the maximum temperature. In general, the selection of a self-heating structural material depends on the requirements in terms of the maximum temperature, the power response time, and the mechanical properties. For cement-based structures, steel fiber cement (No. 1 in Table 7.1) is recommended. For a continuous fiber polymer–matrix composite, carbon fiber mat (No. 4 in Table 7.1) is recommended for use as an interlayer. For spatially distributed heating, the carbon fiber epoxy-matrix interlaminar interface is recommended.

Flexible graphite cannot be incorporated into a structural composite due to its mechanical weakness and impermeability to resin. However, it can be placed on a structural material, and its flexibility allows it to conform to the topography of the structural material.

7.5.2.5 Summary of Self-heating Structural Materials

Self-heating structural materials in the form of cement-matrix and polymer–matrix composites have been engineered by using electrically conductive fibers (continuous or discontinuous) and interlayers. Both the volume of the composite and the interlaminar interface can be used as heating elements. The interlaminar

interface between continuous carbon fiber laminae is attractive since it is amenable to providing a two-dimensional array of heating elements. A cement-matrix composite containing 0.7 vol% steel fibers (8 μm diameter) and a mat of discontinuous uncoated carbon fibers for use as an interlayer are effective for self-heating. However, the effectiveness of such a system is low compared to flexible graphite, which is not a structural material.

7.6 Effect of Temperature on the Electrical Resistivity

7.6.1 Scientific Basis

For a given material, the volume electrical resistivity depends on the temperature. This dependence means that the resistivity can be employed as an indicator of the temperature; in other words, by measuring the resistance, one can obtain the temperature. This type of temperature sensor is known as a thermistor.

The dependence of the volume electrical resistivity on temperature is expressed by the temperature coefficient of electrical resistivity (α), which is defined as

$$(\Delta\rho)/\rho_o = \alpha\Delta T \,, \tag{7.49}$$

where ρ_o is the resistivity at 20°C and $\Delta\rho$ is the change in resistivity relative to ρ_o when the temperature is increased or decreased from 20°C by ΔT. The units of α are $°C^{-1}$. Since

$$\Delta\rho = \rho - \rho_o \,, \tag{7.50}$$

Equation 7.49 can be rewritten as

$$\rho = \rho_o(1 + \alpha\Delta T) \,. \tag{7.51}$$

Thus, the plot of ρ vs. ΔT gives a line with a slope of $\rho_o\alpha$. This line tends to be straight only for metals. However, temperature sensing based on this phenomenon does not require the curve to be a straight line. The greater the magnitude of α, the more sensitive the thermistor.

For metals, α is positive; in other words, the resistivity increases with increasing temperature. This is because the amplitudes of the thermal vibrations of the atoms in the metal increase with increasing temperature, thereby decreasing the mobility μ (as defined in Eq. 7.1). A decrease in mobility in turn results in a decrease in the conductivity (Eq. 7.7); in other words, an increase in the resistivity. The carrier concentration n of a metal does not change with temperature, due to the availability of the valence electrons as mobile charges without any need to excite them. When the temperature is 0 K, there is no thermal energy to provide thermal vibrations, so the resistivity at this temperature is not due to thermal vibrations but rather the scattering of the electrons (carriers) at any defects present in the material. The resistivity at 0 K is known as the residual resistivity (Fig. 7.8). The greater the defect concentration, the higher the residual resistivity.

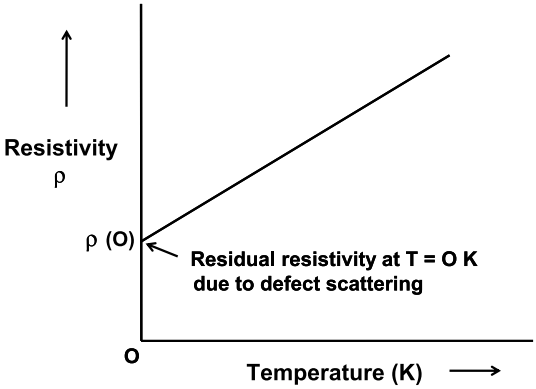

Figure 7.8. Dependence of the volume electrical resistivity on the temperature near 0 K, showing the residual resistivity at 0 K

Semiconductors (e.g., silicon and germanium) and semimetals (e.g., graphite) together constitute a class of materials known as metalloids (or semimetals). For metalloids, α is negative. This is because, for these materials, n increases significantly with increasing temperature. This trend in n is due to the thermal excitation of electrons to form mobile carriers. For a semiconductor, the valence electrons need to be excited across the energy band gap in order for them to become mobile. The larger the energy band gap, the greater the effect of temperature on the resistivity. For a semimetal there is no energy band gap, only a small band overlap, thus resulting in a small effect of temperature on the resistivity. The increase in n with increasing temperature predominates over the decrease in mobility μ with increasing temperature (Eq. 7.7), thus resulting in an overall effect in which the conductivity increases with increasing temperature (i.e., the resistivity decreases with increasing temperature).

For metals, the value of α is typically around +0.004/°C. For semiconductors and semimetals, α is negative, but its magnitude is higher for semiconductors than for semimetals due to the energy band gap present in a semiconductor. Thus, the magnitude of α is smaller for carbon (a semimetal) than for silicon or germanium (semiconductors). The magnitude of α is larger for silicon than germanium due to the larger energy band gap for silicon (1.12 eV, compared to 0.68 eV for germanium). The energy band gap (also known as the energy gap) is the energy between the top of the valance band and the bottom of the conduction band above the valence band, and describes the energy needed to excite an electron from the valence band to the conduction band so that the electron becomes free to respond to an applied electric field.

For a composite with an electrically nonconductive matrix and a conductive discontinuous filler (particles or fibers) where the CTE of the matrix is higher than that of the filler, increasing the temperature causes more thermal expansion of the matrix than the filler. As a consequence, the degree of contact between adjacent filler units (i.e., adjacent particles or adjacent fibers) is reduced, causing the volume resistivity of the composite to increase. The resistivity typically increases abruptly

when the increase in temperature has reached a sufficiently large value. This means that the curve of resistivity vs. temperature is not linear. When the filler volume fraction is around the percolation threshold, the increase in resistivity is particularly large. This is because the resistivity is particularly sensitive to the degree of contact between adjacent filler units when the filler volume fraction is around the percolation threshold. This phenomenon is useful for temperature-activated switching – the deactivation of a circuit (due to the high resistivity of the composite used in series in the circuit) when the temperature is higher than a critical value. The composite therefore serves as a fuse that protects the electronics from excessive temperatures.

7.6.2 Structural Materials Used as Thermistors

7.6.2.1 Polymer-Matrix Structural Composites Used as Thermistors and Thermal Damage Sensors

Continuous fiber polymer-matrix composites are structural composites, in contrast to the relative weaknesses of short-fiber polymer-matrix composites. The interlaminar interface of a continuous carbon fiber polymer-matrix composite is associated with a contact (two-dimensional) resistivity that decreases quite reversibly upon heating, as shown in Fig. 7.9, thereby allowing it to be a thermistor. The contact resistivity of the interface decreases with increasing temperature because of the energy needed for electrons to jump from one lamina to the next through the interlaminar interface. The higher the temperature, the greater the thermal energy available, and the larger the proportion of electrons that manage to jump across the interface. By using the configuration shown in Fig. 7.6, one can

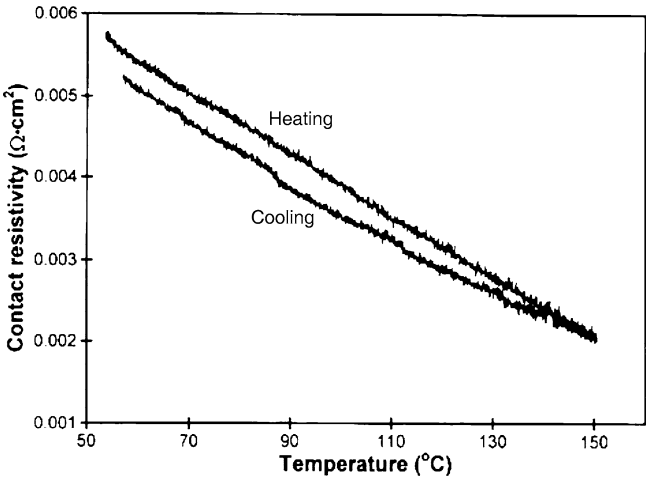

Figure 7.9. Variation in the contact electrical resistivity with temperature during heating and cooling at 0.15°C/min of the crossply interlaminar interface of a continuous carbon fiber epoxy-matrix composite made with a curing pressure of 0.33 MPa (from [3])

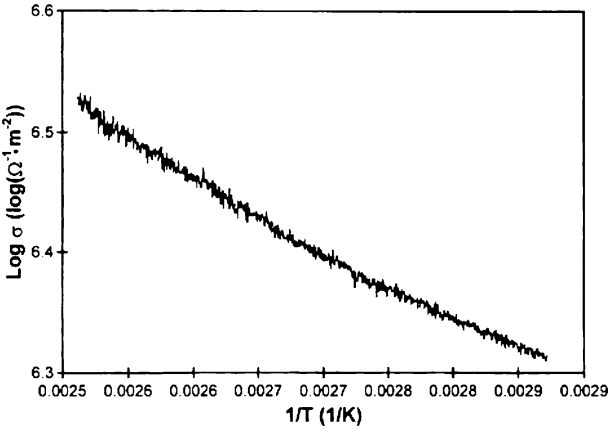

Figure 7.10. Arrhenius plot of log contact conductivity versus inverse absolute temperature during heating at 0.15°C/min for the crossply interlaminar interface of a continuous carbon fiber epoxy-matrix composite made with a curing pressure of 0.33 MPa (from [3])

obtain a two-dimensional array of thermistors, thereby enabling spatially resolved temperature sensing.

Corresponding Arrhenius plots of log contact conductivity (inverse of contact resistivity) versus inverse absolute temperature during heating are shown in Fig. 7.10. From the slope (negative) of the Arrhenius plot, which is quite linear, the activation energy can be calculated by using the equation

$$\text{Slope} = -E/(2.3\,k_B)\,, \tag{7.52}$$

where k_B is the Boltzmann constant, T is the absolute temperature (in K) and E is the activation energy, which is thus found to be 0.118 eV. This activation energy is the energy needed for an electron to jump from one lamina to the next. Exciting electrons to this energy enables conduction in the through-thickness direction.

Figure 7.11 shows the sensing of both temperature and thermal damage through the measurement of the contact electrical resistivity (the geometry-independent quantity equal to the product of the contact resistance and the contact area) of the interlaminar interface. The resistivity decreases upon heating during each heating cycle due to the activation energy associated with the movement of electrons across the interface. This is the thermistor effect, which allows temperature sensing. Minor thermal damage at the maximum temperature of the hottest cycle causes a spike in the resistivity, allowing damage sensing.

Polymer-matrix composites with conductive short fibers or particles can also function as thermistors, due to the increase in spacing between adjacent filler units as the polymer matrix (which has a high CTE compared to the filler) expands upon heating. The increase in spacing means that the chance of filler units touching one another to form a continuous conductive path is decreased, thereby causing the resistivity of the composite to increase. Instead of increasing smoothly with increasing temperature, the resistivity tends to increase abruptly as the temperature

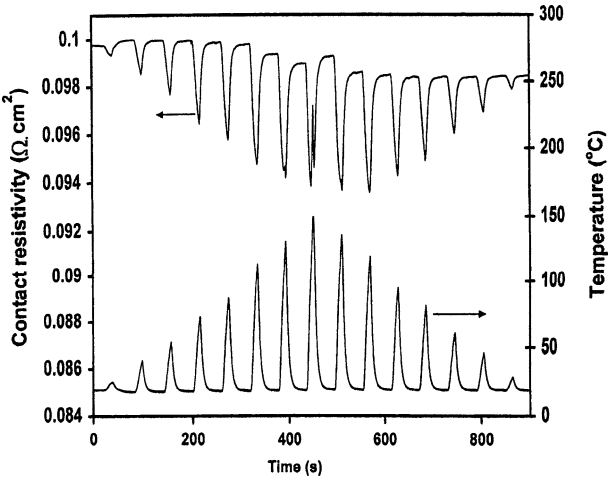

Figure 7.11. The contact electrical resistivity of the interlaminar interface of a crossply continuous carbon fiber epoxy-matrix composite during temperature variation (from [3])

increases beyond a certain level. As a result, the resistance of such a composite is not a very good indicator of the temperature.

7.6.2.2 Cement-Matrix Structural Composites Used as Thermistors and Freeze–Thaw Damage Sensors

Cement is a material that is slightly conductive, with both ions and electrons involved in the conduction. The volume electrical resistivity of cement paste is around $10^5\,\Omega\,\text{cm}$, as compared to $10^{-3}\,\Omega\,\text{cm}$ for carbon and $10^{-6}\,\Omega\,\text{cm}$ for copper. This resistivity decreases with increasing temperature because of the inhomogeneity of cement paste and the thermally activated jumping of carriers across the diffuse interfaces associated with this inhomogeneity. The inhomogeneity stems from the incomplete curing of some of the cement particles and the partial setting or curing of some of the cement particles prior to their incorporation in the cement mix. The sensitivity of a cement-based thermistor is enhanced by the addition of short carbon fiber, which introduces fiber–cement interfaces and decreases the resistivity of the composite. Figure 7.12 shows the decrease in the volume electrical resistivity of carbon-fiber (short) silica-fume cement paste with increasing temperature. The fiber volume fraction is below the percolation threshold (i.e., the fibers do not touch one another sufficiently to form a continuous conductive path in the composite). The resistivity is $2 \times 10^4\,\Omega\,\text{cm}$, compared to $6 \times 10^5\,\Omega\,\text{cm}$ for silica-fume cement (without fiber) and $5 \times 10^5\,\Omega\,\text{cm}$ for plain cement paste (without silica fume or fiber). Figure 7.13 shows the corresponding Arrhenius plot, the slope of which gives the activation energy of the conduction. The activation energy is 0.390 eV, compared to 0.035 eV for silica-fume cement paste and 0.040 eV for plain cement paste. The activation energy is much higher in the presence of carbon fiber.

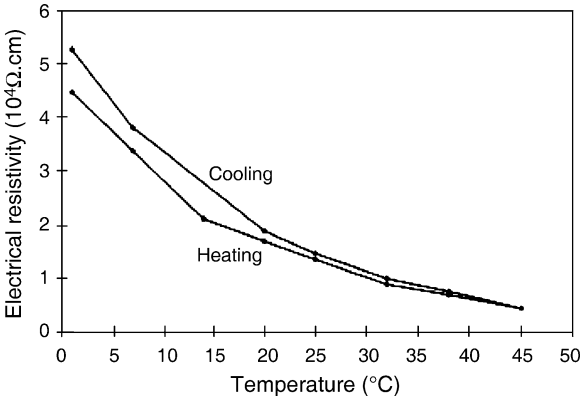

Figure 7.12. Plot of electrical resistivity vs. temperature during heating and subsequent cooling for carbon fiber silica fume cement paste (from [4])

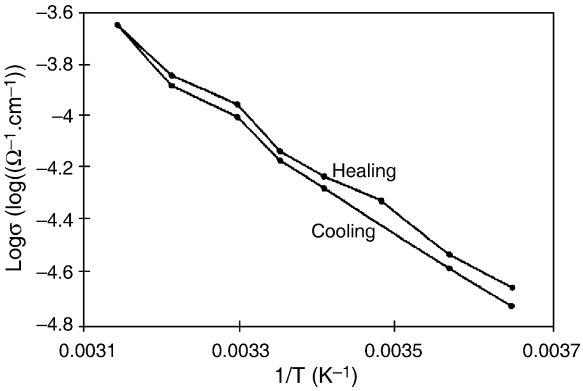

Figure 7.13. Arrhenius plot of log electrical conductivity vs. reciprocal absolute temperature for carbon-fiber silica-fume cement paste (from [4])

Damage causes the volume resistivity to increase irreversibly, while increasing the temperature in the absence of damage causes the resistivity to decrease reversibly. A common cause of damage in cement-based materials is freeze–thaw cycling, which is detrimental to the integrity of the material. The mechanism of the damage involves the expansion of the water present in the pores of a cement-based material upon freezing. The progression of freeze–thaw damage can be monitored by measuring the volume resistivity of the cement-based material while the temperature is simultaneously monitored. This monitoring is feasible even in the absence of a conductive admixture such as carbon fibers. As shown in Fig. 7.14 for cement mortar, the resistivity decreases upon cooling during each temperature cycle due to the activation energy associated with charge carrier movement in the cement-based material. This effect of temperature allows the cement-based material to function as a thermistor for temperature sensing. At the end of each freeze–thaw cycle, the resistivity is slightly higher than the value at the beginning

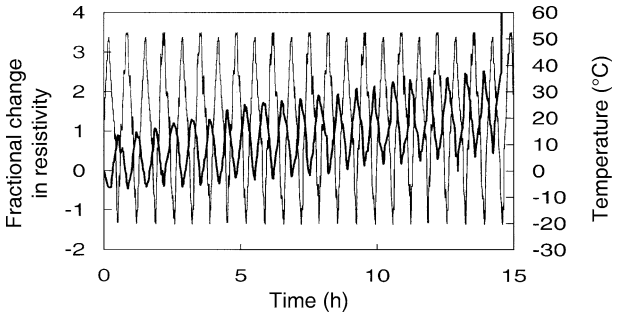

Figure 7.14. Variation in the volume electrical resistivity (fractional change) with time, and of the temperature with time, during freeze–thaw cycling of cement mortar (with fine aggregate, but without any conductive admixture). *Thick curve*: fractional change in resistivity, *thin curve*: temperature. (From [5])

of the cycle. This is due to the occurrence of minor damage during each cycle, including the first cycle. The damage accumulates cycle by cycle, as shown by the irreversible increase in the resistivity with each cycle. Failure occurs at the coldest point of the last cycle, as shown by the abrupt increase in resistance.

7.7 Effect of Strain on the Electrical Resistivity (Piezoresistivity)

7.7.1 Scientific Basis

Piezoresistivity is a phenomenon in which the electrical resistivity of a material changes with strain. It is useful from a practical point of view since it enables strain sensing through electrical resistance measurement. Strain sensing should be distinguished from damage sensing. Strain causes reversible effects, whereas damage causes irreversible effects.

The resistance R is related to the resistivity ϱ, the length ℓ in the direction of resistance measurement, and the cross-sectional area A perpendicular to the direction of resistance measurement:

$$R = \varrho\ell/A \; . \tag{7.53}$$

The fractional change in resistance is given by the equation

$$\delta R/R = \delta\varrho/\varrho + (\delta\ell/\ell)(1 - \nu_{12} - \nu_{13}) \; , \tag{7.54}$$

where ν_{12} and ν_{13} are values of the Poisson ratio for the transverse and through-thickness strains, respectively. If the material is isotropic, so that $\nu_{12} = \nu_{13} = \nu$, Eq. 7.54 becomes

$$\delta R/R = \delta\varrho/\varrho + (\delta\ell/\ell)(1 - 2\nu) \; . \tag{7.55}$$

Positive piezoresistivity refers to behavior where the resistivity increases with increasing strain, i.e., $(\delta\varrho/\varrho)/(\delta\ell/\ell) > 0$. Negative piezoresistivity refers to behavior where the resistivity decreases with increasing strain, i.e., $(\delta\varrho/\varrho)/(\delta\ell/\ell) < 0$. Piezoresistivity is usually positive, because elongation tends to change the microstructure in such a way that the resistivity increases in the direction of elongation. For example, a composite with an electrically nonconductive polymer matrix and a filler in the form of electrically conductive particles or short fibers tends to exhibit positive piezoresistivity, because the distance between adjacent particles increases upon elongation of the composite, thereby decreasing the chance of contact between the adjacent particles. However, negative piezoresistivity has been reported in polymer-matrix composites with continuous carbon fibers and with carbon nanofiber, as well as in semiconductors.

To achieve effective strain sensing, a large fractional change in resistance per unit strain is desirable. Thus, the severity of piezoresistivity is commonly described in terms of the gage factor, which is defined as the fractional change in resistance per unit strain. Equation 7.54 shows that the gage factor depends on both the fractional change in resistivity per unit strain and the Poisson ratio. A positive value of the gage factor does not necessarily mean that the piezoresistivity is positive, but a negative value of the gage factor necessarily means that the piezoresistivity is negative.

In order to attain a large fractional change in resistance at a particular strain, positive piezoresistivity is more desirable than negative piezoresistivity for the same fractional change in resistivity. When the strain is small, which is the case for example when the piezoresistive material is a stiff structural material, the fractional change in resistance is essentially equal to the fractional change in resistivity. In this case, positive and negative piezoresistivities are equally desirable for achieving a large fractional change in resistance. Note that, in terms of its scientific origin, negative piezoresistivity is more intriguing than positive piezoresistivity.

7.7.2 Effects of Strain and Strain-Induced Damage on the Electrical Resistivity of Polymer-Matrix Structural Composites

Polymer-matrix composites containing continuous carbon fibers are important for aircraft, missiles, satellites and other lightweight strategic structures. In order to enhance safety and its operation, such a structure needs to sense its condition, such as any damage to it and the strain that it is under. Damage sensing is used in structural health monitoring. Strain sensing is used in structural vibration control, stress monitoring, and weighing.

This section addresses the attainment of sensing without the need to use of embedded or attached sensors, as the structural material itself is the sensor. The ability of a structural material to sense itself is known as self-sensing. The advantages of self-sensing include low cost, high durability, large sensing volume, and an absence of mechanical properties (which tend to occur in the case of embedded sensors). Examples of embedded or attached sensors include optical fibers and piezoelectric sensors.

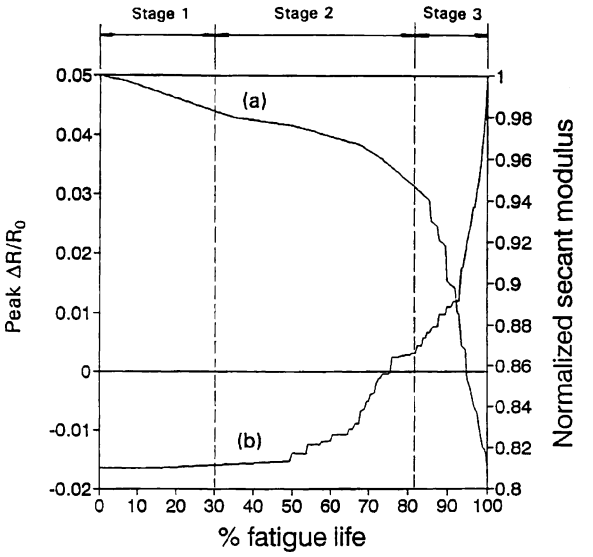

Figure 7.15. Evolution of damage in the form of fiber breakage during tension–tension fatigue, as shown by the longitudinal volume resistance. *a* Normalized secant modulus, *b* the peak value of the fractional change in resistance (relative to the initial resistance) in a stress cycle. The variation in resistance within a cycle (not shown) is due to the effect of strain rather than that of damage. (From [6])

Self-sensing is made possible by the effects of strain and damage on the electrical resistivity, which can be the volume/surface resistivity of the composite or the contact resistivity of the interlaminar interface (interface between the laminae of a continuous fiber in a composite). This ability has been shown for composites that involve carbon fibers, which are electrically conductive, in contrast to the insulating character of the polymer matrix, thereby allowing the resistivity of the composite to vary with damage or strain.

Damage in the form of fiber breakage causes the electrical conductivity in the fiber direction of the composite to decrease. In other words, the resistance increases, as shown in Fig. 7.15 for damage during tension–tension fatigue, with the stress occurring in the fiber direction of the composite. The resistance increase correlates with a decrease in the secant modulus.

Damage in the form of delamination causes the electrical conductivity in the through-thickness direction of the composite to decrease, as explained below. Although the polymer matrix is electrically nonconductive, the through-thickness conductivity of a composite is never zero due to the flow of the resin during composite fabrication and the waviness of the fiber, and the consequent direct contact between fibers that belong to adjacent laminae. The contact occurs at certain random points of the interlaminar interface. When delamination occurs, a crack occurs at this interface. This crack diminishes the extent of fiber–fiber contact, thereby causing the through-thickness conductivity of the composite to decrease. Figure 7.16 shows the increase in through-thickness resistance during tension-tension fatigue, with the stress occurring in the fiber direction of the composite.

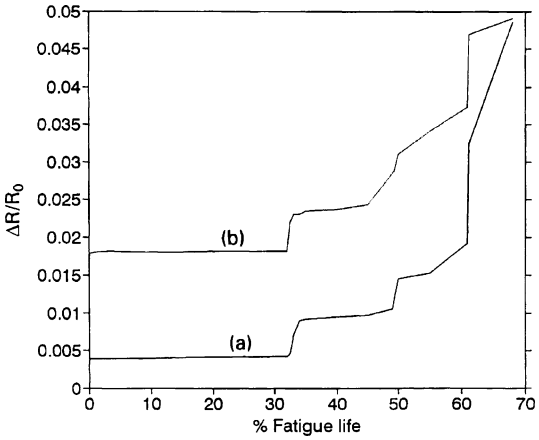

Figure 7.16. Evolution of damage in the form of delamination during tension–tension fatigue, as shown by the through-thickness volume resistance. *a* The minimum value of the fractional change in resistance (relative to the initial resistance) in a stress cycle. *b* The maximum value of the fractional change in resistance in a stress cycle. The variation in resistance within a cycle (not shown) is due to the effect of strain rather than that of damage. (From [6])

As a consequence of the effects mentioned above, the electrical conductivity (the reciprocal of the electrical resistivity) provides an indicator of the damage. By selecting the direction of conductivity measurement, different types of damage can be selectively detected.

Yet another direction of resistance measurement is the oblique direction, which is a direction between the longitudinal and through-thickness direction. The oblique resistance increases upon damage, as shown in Fig. 7.17 for the case of impact damage.

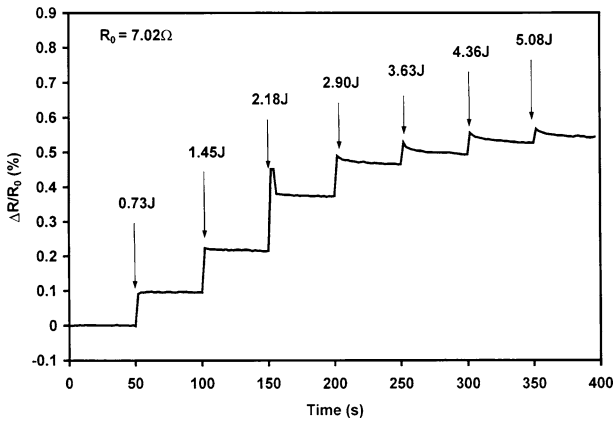

Figure 7.17. Fractional change in oblique resistance (relative to the initial resistance) vs. time during impact at progressively increasing energy. The *arrows* indicate the impact times. (From [7])

Strain sensing is particularly effective under flexure, which is one of the most common forms of loading in composite structures. Upon flexure, one side is under tension while the opposite side is under compression. The surface resistance of the side under compression decreases reversibly upon flexure due to the increase in the degree of current penetration in the through-thickness direction (Fig. 7.18a); the surface resistance of the side under tension increases reversibly upon flexure due to the decrease in the degree of current penetration in the through-thickness direction (Fig. 7.18b).

Sensing is also effective under through-thickness compression (which is relevant to fastening), as indicated by either the contact resistance of the interlaminar interface or the longitudinal resistance of the composite. Upon compression, the contact

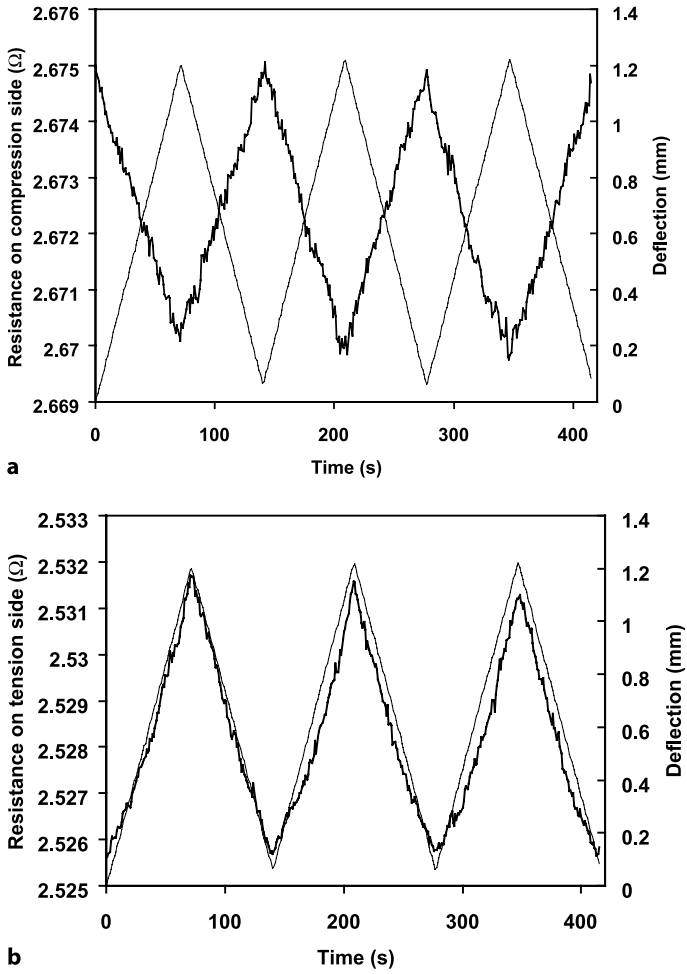

Figure 7.18. Resistance (*thick curve*) during deflection (*thin curve*) cycling at a maximum deflection of 1.199 mm (stress amplitude of 218.5 MPa). **a** Compression surface resistance, **b** tension surface resistance. (From [8])

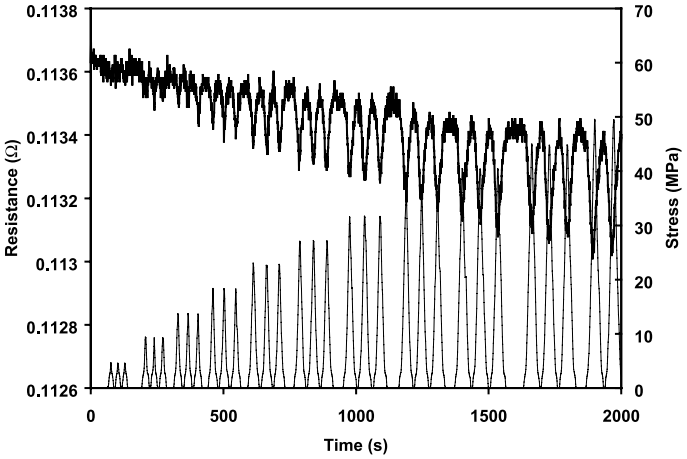

Figure 7.19. Variation in the longitudinal volume resistance (*thick curve*) with time, and of the through-thickness compressive stress (*thin curve*) with time, during through-thickness compressive stress cycling at progressively increasing stress amplitudes (three cycles for each amplitude). (From [9])

resistance of the interlaminar interface decreases (Fig. 7.19) due to increased proximity between the fibers of adjacent laminae, while the longitudinal resistance also decreases due to the decrease in through-thickness resistivity, which enables the longitudinal current to take detours around defects.

The interlaminar interface is itself a damage sensor, as the contact electrical resistivity of this interface is sensitive to minor damage, as inflicted by impact at low energy. Figure 7.20 shows the irreversible decrease in this resistivity upon

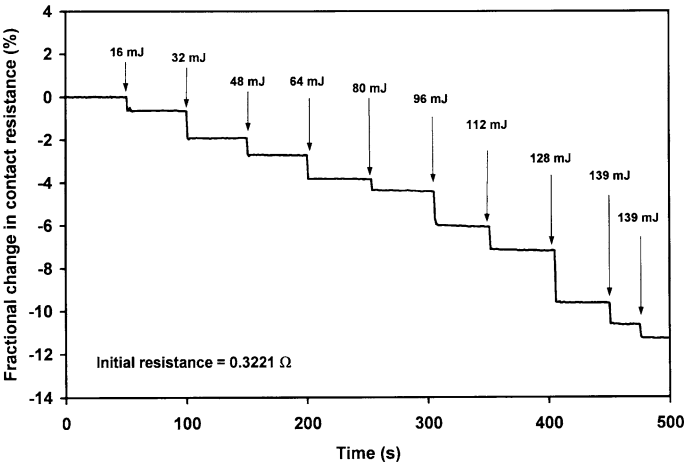

Figure 7.20. Contact resistance vs. time during impact for progressively increasing impact energies from 16 to 139 mJ, as directed onto the exterior composite surface above the interlaminar interface, which is monitored in terms of the contact electrical resistance. (From [10])

impact. The decrease in resistivity occurs at impact energies as low as 0.8 mJ. The greater the damage, the lower the resistivity. Damage causes a decrease in resistivity due to the irreversible increase in the extent of fiber–fiber contact between fibers of adjacent laminae.

In resistance measurement, the voltage and current contacts are placed along a straight line, which is the direction of resistance measurement. In contrast, in potential measurement, the voltage contacts are placed along a line that does not overlap with the line formed by the current contacts. Sensing by resistance measurement is more effective than sensing by potential measurement, although the latter is more amenable to spatially resolved sensing.

For resistance measurement, the four-probe method (with four electrical contacts, the outer two of which are for passing current and the inner two of which are for measuring the voltage) is more effective than the two-probe method (with two electrical contacts, each of which are for both current and voltage) due to the inclusion of the resistance of the electrical contacts in the resistance obtained using the two-probe method. Damage to the electrical contacts affects the two-probe resistance more than the four-probe resistance.

An analytical model is available for the piezoresistance of a continuous carbon fiber polymer-matrix composite under flexure. This phenomenon allows strain sensing and entails a reversible increase in the tension surface resistance and a reversible decrease in the compression surface resistance during flexure. The model considers that the change in surface resistance is due to the change in the degree of current penetration. The longitudinal strain resulting from the flexure affects the through-thickness resistivity (which relates to the contact resistivity of the interlaminar interface).

In summary, the self-sensing abilities of carbon fiber polymer-matrix structural composites are due to the effects of strain and damage on the electrical resistivity, which can be the volume resistivity of the composite or the contact resistivity of the interlaminar interface. Sensing is particularly effective under flexure, as indicated by the surface resistance of the side under compression or that under tension. It is also effective under through-thickness compression (which is relevant to fastening), as indicated by the longitudinal resistance of the composite. In addition, it is effective under impact, as indicated by the contact resistance of the interlaminar interface. Sensing by resistance measurement is more effective than sensing by potential measurement, although the latter is more amenable to spatially resolved sensing. For resistance measurement, the four-probe method is more effective than the two-probe method.

7.7.2.1 Effects of Strain and Strain-Induced Damage on the Electrical Resistivities of Cement-Matrix Structural Composites

Functional behavior similar to that described in Sect. 7.7.2 is exhibited by cement-matrix composites containing discontinuous and electrically conductive fibers as an admixture. Continuous fiber is not attractive due to its high cost and its unsuitability for incorporation into a cement mix.

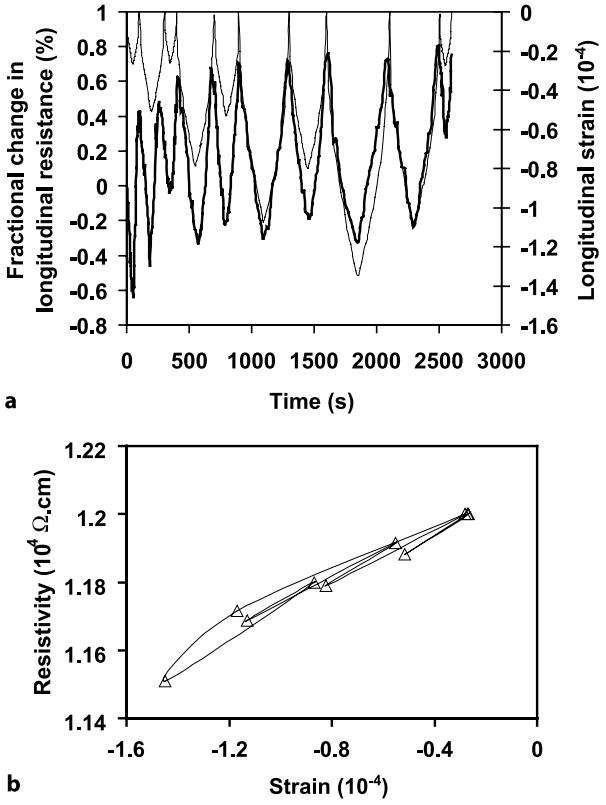

Figure 7.21. **a** Curves of fractional change in longitudinal resistance (*thick curve*) versus time and of longitudinal strain (*thin curve*) versus time using repeated compression of carbon fiber reinforced cement at various strain amplitudes. The resistance is measured using the four-probe method. **b** Variation in the resistivity at the peak strain versus the strain amplitude for the data in (**a**). The data points are connected with a *line* drawn to indicate the order in which the various strain amplitudes were imposed. The order is as shown in (**a**). (From [11])

By using carbon fiber (isotropic-pitch-based, about 5 mm long, 0.5 vol%, just below the percolation threshold, which is between 0.5 and 1.0 vol%) in cement paste (without aggregate), piezoresistivity-based strain sensing has been achieved, as shown upon repeated uniaxial compression by using the four-probe method in Fig. 7.21. The gage factor (fractional change in volume resistance per unit strain) is around 280 and the volume resistivity is around $1.2 \times 10^4\,\Omega\,\mathrm{cm}$. There is little, if any, hysteresis, as shown in Fig. 7.21b. However, when the two-probe method is used instead of the four-probe method, the strain sensing is not feasible due to poor repeatability, as shown in Fig. 7.22. In spite of the presence of piezoresistivity, with a gage factor of around 200 and a resistivity of $1.3 \times 10^4\,\Omega\,\mathrm{cm}$, the poor repeatability makes the sensing infeasible. The poor repeatability is due to the variation in the contact resistance during loading and unloading. The contact resistance is included in the measured resistance in the two-probe method.

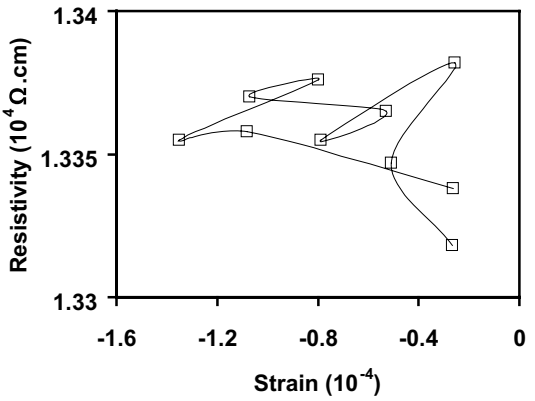

Figure 7.22. Variation in the resistivity at the peak strain versus the strain amplitude for carbon fiber reinforced cement. The resistance is measured using the two-probe method. The data points are connected with a *line* drawn to indicate the order in which the various strain amplitudes were imposed. The order is as shown in Fig. 7.21a. (From [11])

Upon flexure (three-point bending), the surface electrical resistance on the compression side decreases reversibly, while that on the tension side increases reversibly, thus allowing strain sensing (Fig. 7.23). Damage, which occurs when the deflection is sufficiently large, causes the resistance to increase irreversibly, as shown clearly for the surface resistance on the tension side. At failure, either resistance increases abruptly.

An analytical model is available to describe the piezoresistivity in carbon fiber reinforced cement (with and without embedded steel reinforcing bars) under flexure (three-point bending) [12]. The phenomenon involves the reversible increase in the tension surface electrical resistance and the reversible decrease in the compression surface electrical resistance upon flexure. The piezoresistivity is enhanced by the presence of steel rebars. The theory is based on the concept that the piezoresistivity is due to the slight pulling out of crack-bridging fibers during crack opening and the consequent increase in the contact electrical resistivity of the fiber–matrix interface.

The strain sensing ability of carbon fiber reinforced cement, as based on piezoresistivity, remains in the presence of damage. However, the gage factor is affected by strain and damage. The gage factor under uniaxial compression is diminished by compressive strain by up to 70% and is diminished by damage by up to 25%. This means that the sensing is best at low strains.

7.8 Seebeck Effect

7.8.1 Scientific Basis

When an electrical conductor is subjected to a temperature gradient, charge carriers move. The movement is typically in the direction from the hot point to the cold point of the temperature gradient, due to the higher kinetic energies of the carriers

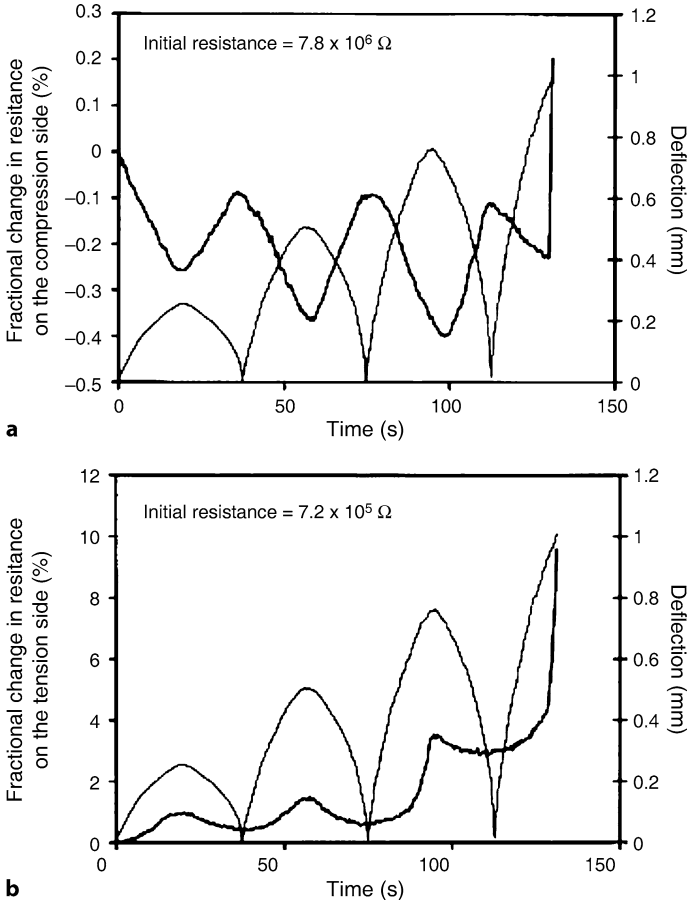

Figure 7.23. Variation in the surface resistance (*thick curve*) with time, and of the mid-span deflection (*thin curve*) with time, during three-point bending at progressively increasing deflection amplitude (up to failure) for a carbon fiber (about 5 mm long, 0.5 vol%) reinforced cement paste. **a** Resistance on the compression side, **b** resistance on the tension side. (From [13])

at the hot point. The carrier flow results in a voltage difference (called the Seebeck voltage) between the hot and cold ends of the conductor. This phenomenon is known as the Seebeck effect, which is a type of thermoelectric effect.

The Seebeck effect allows the conversion of thermal energy (associated with the temperature gradient) to electrical energy, and is the basis for thermoelectric energy generators, which are devices for generating electricity from temperature gradients. This type of electricity generation is attractive due to the absence of pollution and the fact that temperature gradients are commonplace (e.g., that between a water heater and its surroundings, that between an engine and its surroundings, etc). In other words, using the Seebeck effect, waste heat can be utilized to generate electricity.

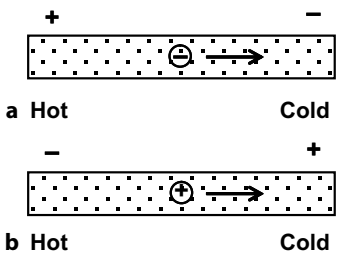

Figure 7.24. Seebeck effect due to carriers moving from a hot point to a cold point. **a** Negative carrier, **b** positive carrier

If the dominant carrier is negatively charged (as in the case of electrons), the movement results in a Seebeck voltage that has its negative end at the cold end of the specimen, as illustrated in Fig. 7.24a. If the dominant carrier is positively charged (as in the case of holes, which refer to electron vacancies), the movement results in a Seebeck voltage that has its negative end at the hot end of the specimen, as illustrated in Fig. 7.24b. It is possible for a conductor to have both electrons and holes, as in the case of a semiconductor.

The Seebeck coefficient (S; also known as the thermoelectric power or the thermopower) is defined as the negative of the Seebeck voltage divided by the temperature difference between the hot and cold ends. In other words,

$$S = -\Delta V/\Delta T \,, \tag{7.56}$$

where ΔV is the voltage difference and ΔT is the corresponding temperature difference. The units of S are V/K.

In Fig 7.24b, which shows the situation where the carrier is positive, the Seebeck coefficient is positive since ΔV and ΔT have opposite signs. In the case of Fig. 7.24a, which shows the situation where the carrier is negative, the Seebeck coefficient is negative since ΔV and ΔT have the same sign.

Carriers tend to be scattered when they collide with the thermally vibrating atoms in the solid. The extent of carrier scattering depends on the relationship of the carrier energy with the carrier momentum (i.e., the energy band structure) near the Fermi energy (the highest occupied energy level in the absence of any thermal agitation; i.e., at the temperature of 0 K). As a result of the scattering, the carriers do not necessarily move in the direction illustrated in Fig. 7.24. In other words, it is possible for a material containing negative carriers to have a positive Seebeck coefficient.

The Seebeck effect also allows the sensing of temperature, since the voltage output relates to the temperature difference. Thus, the Seebeck voltage can be used to find the temperature of one end of the conductor if the temperature of the other end is known. To measure the temperature of a hot point, it is more convenient to measure the voltage difference between two cold points rather than that between the hot point and the cold point. Therefore, two conductors that have different values of the Seebeck coefficient are used in the configuration shown in Fig. 7.25. This configuration constitutes a thermocouple, which is a device for temperature

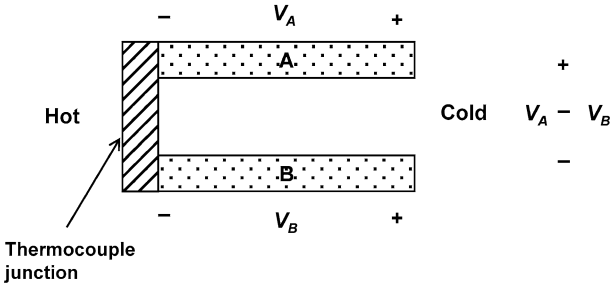

Figure 7.25. A thermocouple consisting of dissimilar conductors A and B (*dotted regions*) that are electrically connected at one end. The *shaded region* at the hot end is the conductor that electrically connects A and B

measurement. The two conductors, labeled A and B, are electrically connected at one end to form a thermocouple junction, which corresponds to the hot point (in the case where the temperature to be measured is above room temperature). The cold ends of A and B are at the same temperature (typically room temperature). The voltage difference between the hot and cold points of A is given by

$$V_{\mathrm{A}} = S_{\mathrm{A}} \Delta T \,, \tag{7.57}$$

where S_{A} is the Seebeck coefficient of A. The voltage difference between the hot and cold points of B is given by

$$V_{\mathrm{B}} = S_{\mathrm{B}} \Delta T \,, \tag{7.58}$$

where S_{B} is the Seebeck coefficient of B. The voltage difference between the cold ends of A and B is given by

$$V_{\mathrm{A}} - V_{\mathrm{B}} = (S_{\mathrm{A}} - S_{\mathrm{B}}) \Delta T \,, \tag{7.59}$$

where Eqs. 7.57 and 7.58 have been used. Equation 7.59 means that $V_{\mathrm{A}} - V_{\mathrm{B}}$ is proportional to ΔT. The greater $(S_{\mathrm{A}} - S_{\mathrm{B}})$, the more sensitive the thermocouple. Thus, A and B should be chosen to be as dissimilar as possible.

Particularly strong dissimilarity occurs when A and B contain carriers of opposite signs. In other words, S_{A} and S_{B} are opposite in sign, so that $S_{\mathrm{A}} - S_{\mathrm{B}}$ is equal to the sum of the magnitudes of S_{A} and S_{B}. Due to the resulting large voltage output, the configuration involving A and B with Seebeck coefficients of opposite sign is commonly used for thermoelectric power generation. In order to obtain an even larger voltage output, multiple junctions are used, as illustrated in Fig. 7.26, so that the A and B legs are in series and the output voltage is the sum of the voltages from all of the legs.

The Seebeck coefficient is measured using electrical leads (wires) that are made of a certain conductor (e.g., copper). The leads are attached to the hot and cold ends of the conductor under investigation, as illustrated in Fig. 7.27. The lead attached to the hot end has a temperature gradient along its length, while that attached to the cold end does not. Thus, a Seebeck voltage V_{w} occurs between the hot and cold

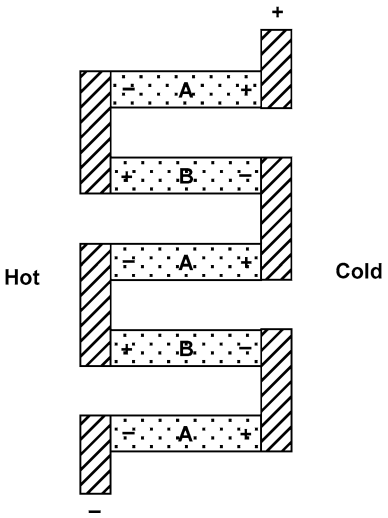

Figure 7.26. A thermoelectric energy generator consisting of a series of alternately positioned conductors A and B (*dotted regions*). The *shaded regions* are conductors that electrically connect A and B. The temperature to the left of the device is different from that to the right of the device

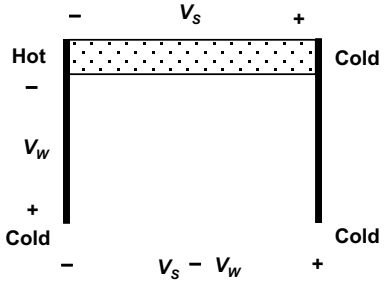

Figure 7.27. A conductor (*dotted region*) subjected to a temperature gradient, with electrical leads attached in order to measure the Seebeck voltage

ends of the wire attached to the hot end of the conductor under investigation, while a Seebeck voltage V_s occurs between the hot and cold ends of the conductor under investigation (i.e., the specimen). Thus, the measured voltage difference between the cold ends of the two leads equals $V_s - V_w$. This means that V_w must be added to this measured voltage difference in order to obtain V_s.

Based on Eq. 7.40, the electric power provided by the Seebeck effect is given by S^2/ρ, where S is the Seebeck coefficient and ρ is the electrical resistivity. Thus, S^2/ρ is known as the power factor. This means that a high value of S and a low value of ρ are preferred.

In order for a material to sustain a substantial temperature gradient, its thermal conductivity must be sufficiently low. Therefore, both a high power factor and a low thermal conductivity are necessary for a thermoelectric material used in

a thermoelectric energy generator. As a consequence, the figure of merit (Z) of a thermoelectric material is given by

$$Z = S^2/(\varrho k) \,, \tag{7.60}$$

where k is the thermal conductivity. The units of Z are K^{-1}. The dimensionless figure of merit (ZT) of a thermoelectric material is given by the product of Z and the temperature in K, where the temperature is the average temperature of the temperature gradient. A higher value of T helps to provide a higher value of ZT. Thus, a material (e.g., a ceramic material) that can withstand high temperatures is preferred. The quantity ZT relates to the thermodynamic efficiency of the energy conversion and is commonly used to describe the performance of a thermoelectric material. However, the area perpendicular to the thermoelectric direction is also important, since a larger area gives a lower resistance and hence a higher power output. Thermoelectric research has focused on raising ZT, with little attention paid to increasing the area.

The need for a low thermal conductivity and a low electrical resistivity represents a challenge. Metals do not satisfy this requirement, since they have high thermal conductivities, although their electrical resistivities are low. Electrical insulators do not satisfy this requirement, since they have high electrical resistivities. Semiconductors, on the other hand, can have reasonably low thermal conductivities and reasonably low electrical resistivities. Thus, thermoelectric materials are commonly semiconductors in the form of alloys or compounds that have been tailored for the abovementioned combination of properties. Examples are bismuth telluride (Bi_2Te_3) and lead telluride (PbTe). Another advantage of semiconductors is that they can be doped (typically through the use of a solute to form a dilute solid solution) to be n-type (i.e., a situation in which electrons are the dominant carrier) or p-type (i.e., a situation in which holes are the dominant carrier), thus providing widely dissimilar materials. However, disadvantages of the semiconductors include their high material cost and their mechanical brittleness.

A ZT value of 1 is considered to be very good. The highest ZT values reported are in the range from 2 to 3. However, a ZT value above 3 is necessary for a thermoelectric energy generator to compete with mechanical methods of electricity generation. This is why thermoelectric energy generation is currently not playing a substantial role in the energy sector. Nevertheless, due to the severity of the energy crisis, much research is being conducted to develop thermoelectric materials with higher ZT values.

As an example, a state-of-the-art Bi_2Te_3 thermoelectric thin-film material has $S = -287\,\mu V/K$ at 54°C, an electrical resistivity of $9.1 \times 10^{-6}\,\Omega\,m$, and a thermal conductivity of $1.20\,W/(m\,K)$. These values give $Z = 7.5 \times 10^{-3}\,K^{-1}$ or $ZT = 2.5$.

Due to their high thermal conductivities, metals are low in ZT. As an example of a metal, consider copper, with $S = +3.98\,\mu V/K$, electrical resistivity = $1.678 \times 10^{-8}\,\Omega\,m$ and thermal conductivity = $401\,W/(m\,K)$ at room temperature. These values correspond to $Z = 2.4 \times 10^{-6}\,K^{-1}$ or $ZT = 7.0 \times 10^{-4}$, which is tiny. Even if T is 1,000 K, ZT remains low.

A ZT value of around 2–3 is needed to provided an energy conversion efficiency of 15–20% [14]. State-of-the-art bulk thermoelectric materials have $ZT = 1.2$ at

300 K [14–16]. Thin-film thermoelectric materials can reach higher *ZT* values; e.g., 2.4 in the case of a p-type Bi_2Te_3/Sb_2Te_3 superlattice at 300 K [17]. Thin films can allow quantum confinement of the carrier, thereby obtaining an enhanced density of states near the Fermi energy. In addition, thin films can allow structures in the form of superlattices with interfaces that block phonons but transmit electrons. Due to the barrier layers needed for quantum confinement, the *ZT* value of a device with an electron gas as the active region is much higher than that of the electron gas itself [18]. For example, in the case of strontium titanate, *ZT* is 2.4 for the electron gas and 0.24 for the device [18]. Bulk thermoelectric materials are needed for practical applications. However, state-of-the-art thermoelectric materials tend to suffer from problems associated with one or more of the following: high cost of materials and processing, thermoelectric material size limitations, production scale-up difficulties, insufficiently high *ZT*, inadequate mechanical performance, and implementation difficulties.

A different thermoelectric approach involves modifying a structural material that is not thermoelectric but is widely available on a large scale. The modification gives the material thermoelectric properties. This approach results in a multifunctional structural material that can provide both structural and thermoelectric functions. Such a multifunctional material enables self-powered structures (i.e., structures that generate electric power). Self-powering is attractive for structures for which the use of batteries is not desirable, structures that power transmission lines cannot reach, and strategic structures that require back-up energy. In the case of structural materials in the form of composites with continuous fiber reinforcement, the volume fraction of the continuous fibers in the composite must be sufficiently high after the modification, since the fibers are the load-bearing component.

Imparting energy-harvesting properties to a structure through the use of a structural material that already has such properties should be distinguished from an approach that involves the use of embedded or attached devices. The latter method suffers from high cost, poor durability, mechanical property loss, and limited functional volume.

7.8.2 Thermoelectric Composites

Binary alloys such as Si-Ge and ternary alloys such as Bi-Sb-Te, all in a single-phase crystalline form, have long been investigated due to their thermoelectric behaviors. Recently, such alloys with nanoscale grain sizes have been shown to be particularly effective, since the grain boundaries inhibit heat transport but allow electron transport. Due to the combination of low thermal conductivity and high electrical conductivity, the *ZT* value is quite high. Although the term "composites" is used in the physics community for such nanostructured alloys, these materials are not composites, regardless of whether these alloys are single-phase or multiphase. This is because the structure is not formed by artificially blending the components of the structure; it is formed by high-temperature heat treatment after mixing the ingredients. The high-temperature heat treatment results in one or more phases

that are in accordance with the thermodynamics and kinetics of the material system. For example, steel is formed from its ingredients through high-temperature heat treatment and is an alloy rather than a composite. In contrast, a carbon fiber epoxy-matrix composite is indeed a composite, as it is formed by artificially blending the components. This section discusses thermoelectric composites but not thermoelectric alloys, although the development of thermoelectric composites is still in its infancy.

By sandwiching (bringing the polished surfaces into contact without bonding them) a Bi-Te compound of thickness 100 μm between 300 μm thick copper electrodes, a ZT of 8.81 at 298 K (compared to 1.04 for the Bi-Te compound itself) and a thermoelectric power of 711 μV/K (compared to 245 μV/K for the Bi-Te compound itself) were obtained in the direction perpendicular to the plane of the sandwich [19]. The ZT value in the presence of the copper electrodes decreases rapidly with increasing thickness of either the Bi-Te compound or the copper electrodes, thus leading to the conclusion that the high ZT of 8.81 is due to the large barrier thermo-emf generated in the Bi-Te region $< 50\,\mu m$ from the boundary [19]. By sandwiching (by welding) a Bi-Sb alloy of thickness 14 mm between 3 mm thick metal (either copper or nickel) electrodes, a ZT of 0.44 at 298 K (compared to 0.26 for the Bi–Sb alloy itself) and a thermoelectric power of −110 μV/K (compared to −85 μV/K for the Bi–Sb alloy itself) were obtained [20]. This means that the sandwiching [18, 19] causes significant increases in both ZT and the thermoelectric power.

A more practical example of the composite route to thermoelectric material development relates to the incorporation of a mixture of tellurium and bismuth telluride thermoelectric nanoparticles at the interface between adjacent laminae of continuous carbon fibers (fiber diameter 7 μm) in an epoxy-matrix structural composite. The use of particles that are sufficiently small is helpful, as the use of large particles would result in substantial distances between the carbon fiber laminae, thus decreasing the fiber volume fraction and hence reducing the mechanical properties. The thermoelectric particle incorporation has been shown to increase the thermoelectric power of the overall composite in the through-thickness direction (i.e., the direction perpendicular to the interlaminar interface) from 8 to 128 μV/K [21, 22]. After the thermoelectric particle incorporation, the through-thickness electrical resistivity is 0.0022 Ω cm (compared to 7.41 Ω cm for the unmodified composite; the interlaminar interface modification decreases the resistivity by three orders of magnitude) and the through-thickness thermal conductivity is 0.69 W/(m K) (compared to 0.96 W/(m K) for the unmodified composite; the thermal conductivity is decreased by the modification) [22]. Thus, for the modified composite, Z is calculated to be $0.00108\,K^{-1}$, based on Eq. 7.60, and ZT is calculated to be 0.38 at 70°C (compared to 2.8×10^{-7} for the unmodified composite) [22]. The effect of the thermoelectric particle incorporation depends on the prepreg type. In general, it is much smaller for the thermoelectric power in the longitudinal (fiber) direction of the composite [21], since the carbon fibers are the dominant influence on the longitudinal effect.

The electric power output is equal to V^2/R, where V is the voltage output and R is the resistance. The results described in the last paragraph [22] thus indicate that

the electric power output from the composite specimen (area 23 × 23 mm) is 0.46 W if the temperature difference is 70°K, and 1.3 W if the temperature difference is 120°C. Since the resistance is inversely proportional to the area, the power output is proportional to the area. In practice, the area of the composite structure can be many times larger than 23 × 23 mm, resulting in much higher power output. For example, if the area of the relevant part of a composite structure is 100 times the abovementioned area (i.e., 2.3 × 2.3 m), the power is 46 W when the temperature difference is 70°K.

A negative value for the thermoelectric power is obtained by using bismuth telluride as the main interlaminar filler. Composites that have thermoelectric power values with opposite signs can be connected in series electrically in order to obtain a large output voltage/power.

Although a polymer matrix was used in this work, alternative matrices include carbons, ceramics, and metals. These other matrices are attractive due to their abilities to withstand relatively high temperatures, hence enhancing *ZT*. A zirconia-matrix composite containing 10 vol% single-walled carbon nanotubes exhibits a *ZT* of 0.006 at 350 K and 0.017 at 850 K [23].

While thermoelectric composite engineering involving thin films is possible, it is not practical. This is because of the difficulties involved in using a thermoelectric material in the form of a thin sandwich (e.g., with a total thickness of 300 + 100 + 300 = 700 μm) [19]) in an energy conversion device.

The development of thermoelectric nonstructural composites centers on increasing *ZT* by decreasing the thermal conductivity and increasing the electrical conductivity. These composites are mainly ceramic–ceramic composites, such as B_4C-SiB_{14}-Si, B_4C-YB_6, SiB_6-TiB_2, B_4C-TiB_2, B_4C-SiC, SiB_n-SiB_4, B_4C-W_2B_5, $AgBiTe_2$-Ag_2Te, $Bi_{92.5}Sb_{7.5}$-BN-ZrO_2, $CoSb_3$-$FeSb_2$, $CoSb_3$-oxide, Ni_3B-B_2O_3 and $Ca_2CoO_{3.34}$-CoO_2. Boron carbide is particularly attractive for high-temperature thermoelectric conversion, since it has a high melting temperature. Thermoelectric nonstructural composites also include ceramic–metalloid composites, such as Bi_2Te_3-C, SiC-Si, SiB_{14}-Si and PbTe-SiGe.

Thermoelectric composites involving metals are not common, as a metal tends to increase the thermal conductivity. However, intermetallic compounds involving rare earth atoms (e.g., $CePd_3$ and $YbAl_3$) are attractive.

Thermoelectric composites are mainly designed by considering the electrical and thermal properties of the components, as a high electrical conductivity tends to be accompanied by a high thermoelectric power. For example, the addition of TiB_2 to B_4C to form the B_4C-TiB_2 composite causes *ZT* to increase due to the increase in the electrical conductivity, the slight decrease in the thermal conductivity, and the increase in the thermoelectric power. Less commonly, composites are designed by considering the interface between the components, as the interface contributes to the scattering of the carriers.

The thermal stress between a thermoelectric cell and the wall of a heat exchanger in a thermoelectric energy conversion system affects the thermal coupling as well as the durability. To reduce the thermal stress, compliant pads are used at the interface, although the pad acts as a barrier against thermal conduction. If the thermoelectric material is itself compliant, a compliant pad will not be necessary.

Metals are generally more compliant than semiconductors, but their Seebeck effects are relatively weak and they tend to suffer from corrosion. Polymers can be more compliant than metals, but they are usually electrically insulating and do not exhibit the Seebeck effect. On the other hand, a polymer containing an electrically conductive discontinuous filler (e.g., carbon black) above the percolation threshold is conductive. The use of a polymer that is an elastomer (e.g., silicone) leads to a composite that is resilient and compliant.

Electrically conductive polymer-matrix composites such as carbon black filled silicone are used for electromagnetic interference (EMI) shielding and for electrostatic discharge protection. Resilience is important when they are used as EMI gaskets. Due to the heating associated with the operation of microelectronics, which require shielding, the shielding material (particularly that associated with a mixed signal module such as one that involves both data and voice) may encounter a temperature gradient. The thermoelectric effect of the shielding material results in a voltage that may affect the performance of the microelectronics. For example, the electrical grounding may be affected. Therefore, the thermoelectric behavior of shielding materials is of concern.

An unconventional approach involves taking structural composites as a starting point and modifying these composites for the purpose of enhancing the thermoelectric properties. These structural composites are preferably ones that provide a framework that exhibits low thermal conductivity and low electrical resistivity. The modified composites are multifunctional (i.e., both structural and thermoelectric). Because structural composites are used in large volumes, imparting thermoelectric properties to these materials means that large volumes of thermoelectric materials are available for use in, say, electrical energy generation. Moreover, temperature sensing is useful for structures used in thermal control, to save energy, and in hazard mitigation. Imparting thermoelectric properties to a structural material also means that the structure can sense its own temperature without the need for embedded or attached thermometric devices, which suffer from high cost and poor durability. Embedded devices, in particular, degrade the mechanical properties of the structure.

In general, techniques for thermoelectric composite tailoring include the following. These techniques can be used in combination but they have not received adequate attention. There is much room for further research

- *Use of interfaces in a high-ZT component in the composite to decrease the thermal conductivity.* This method typically involves using the high-*ZT* component as the dominant component, so it tends to involve high material costs and to have limited design flexibility. It is commonly used to develop thermoelectric materials from semiconductors. The interfaces must hinder thermal transport but allow charge transport. In order to get a large interface area per unit volume, nanostructuring is an attractive approach.
- *Use of interfaces in a low-ZT component in the composite to decrease the thermal conductivity.* This technique does not necessarily involve a high-*ZT* component, so it tends to involve very low material costs. However, the absence of a high-*ZT*

component tends to result in a composite that does not have a particularly high *ZT*.

- *Use of a high-ZT component as the composite matrix, such that the filler is low in ZT and serves mainly to decrease the thermal conductivity and/or decrease the electrical resistivity.* This method typically involves the use of the high-*ZT* component as the dominant component in the composite, so it tends to involve high material costs and to have limited design flexibility. The *ZT* of the composite is governed by that of the high-*ZT* component.

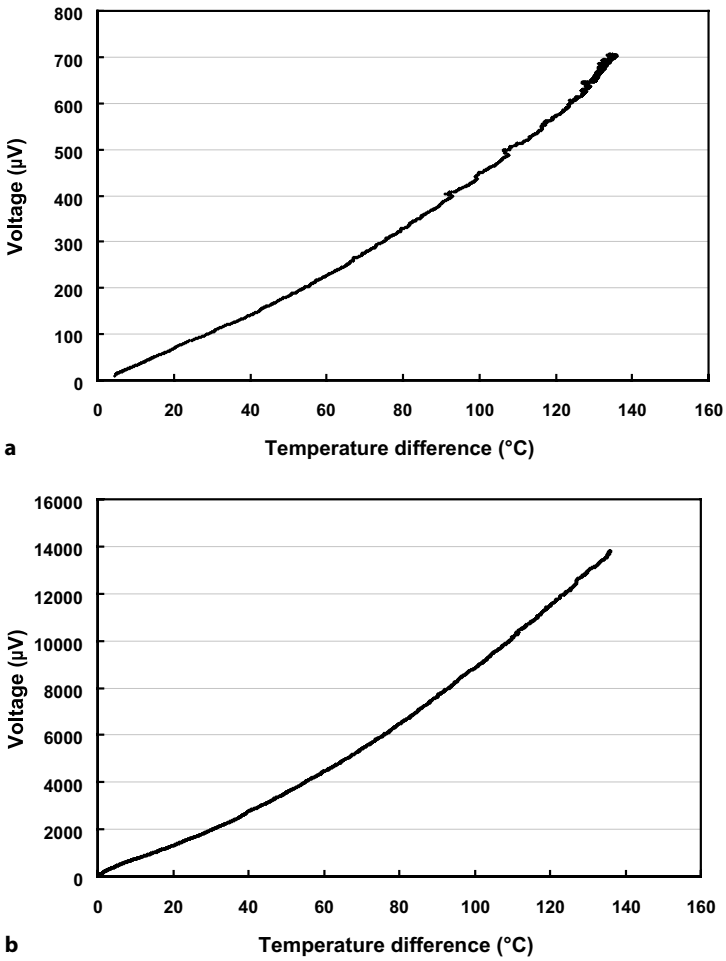

Figure 7.28. Seebeck voltage (without correction for the copper leads) vs. the temperature difference for carbon fiber epoxy-matrix composites in the through-thickness direction. **a** Without an interlaminar interface modification, **b** with tellurium and bismuth telluride particles as the interlaminar fillers, where the interlaminar interface thickness is about 33 μm. (From [22])

- *Use of a high-ZT component as a filler in the composite, such that the matrix serves to provide a framework that exhibits low thermal conductivity and low electrical resistivity.* The high-*ZT* component serves mainly to enhance the Seebeck coefficient. When the framework is a structural material, this method provides a thermoelectric structural material. It involves using the high-*ZT* component as a minor component, so it tends to have low material costs. The design of the framework is central to this technique. An example of such a framework is a continuous carbon fiber polymer-matrix composite, which exhibits a combination of low thermal conductivity and low electrical resistivity in the through-thickness direction. The waviness of the fibers causes fiber–fiber contact points between fibers of adjacent laminae across the interlaminar interface, resulting in a low through-thickness electrical resistivity, while the polymer-rich regions between the contact points at the interlaminar interface lead to a low through-thickness thermal conductivity. Fig. 7.28 shows the measured Seebeck voltage (without correction for the copper leads) vs. the temperature difference (between the hot and cold ends) for carbon fiber epoxy-matrix composites without and with tellurium (thermoelectric) particles at the interlaminar interface. The presence of tellurium and bismuth telluride nanoparticles greatly enhances the through-thickness Seebeck effect.

7.9 Applications of Conductive Materials

7.9.1 Overview of Applications

Composites for electrical conduction exhibit various levels of electrical conductivity, as needed for various applications. The highest possible level of electrical conductivity is needed for electrical interconnections in microelectronics. Less demanding levels of conductivity are needed for electrochemical electrodes, lightning protection, and electrical grounding. Still lower levels of conductivity are required for electromagnetic interference (EMI) shielding and electrostatic charge dissipation. For some applications, such as heating elements (as explained below), only an intermediate level of conductivity is required. Thus, various levels of conductivity have specific applications, and such conduction is known as controlled electrical conduction. Such materials are known as controlled resistivity materials.

By controlling the volume fraction of the conductive filler, composites with a nonconductive (or less conductive) matrix can exhibit a wide range of electrical conductivities (Fig. 7.29), as needed for various applications. Therefore, composite materials are ideally suited for use as controlled resistivity materials.

A heating element works because of the resistance (Joule or I^2R) heating that occurs when a current flows through the heating element. When the resistance is too high, there is not enough current to provide the resistance heating unless the voltage is huge. When the resistance is too low, there is not enough resistance to provide the resistance heating, even though the current is rather high. Therefore, an intermediate level of resistivity is optimum for heating elements.

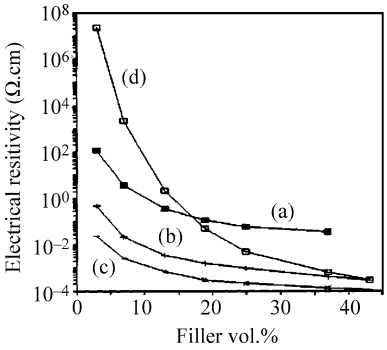

Figure 7.29. Effect of filler volume fraction on the electrical resistivity of polyethersulfone-matrix composites. *a* 0.1 μm diameter carbon nanofiber, *b* 0.4 μm diameter nickel nanofiber, *c* 2 μm diameter nickel fiber, *d* 20 μm diameter nickel fiber. (From [24])

A conductive composite commonly consists of a conductive filler in a nonconductive (or less conductive) matrix. This design is due to the fact that the matrix has the desired processability in spite of its low conductivity. For example, a polymer matrix that is nonconductive (as is the case for all conventional polymers) is attractive due to its processability (moldability) at temperatures that are not high (typically under 200°C). Processability is necessary to form articles of various shapes and sizes. Metals are highly conductive, but their processabilities are relatively low. Therefore, polymer-matrix composites are an important class of conductive materials.

For a particular conductive filler and filler volume fraction, the use of a matrix that is more conductive will result in greater electrical connectivity and hence higher conductivity for the composite. In other words, the percolation threshold is lower when the matrix is more conductive.

Polymers that are inherently conductive in the absence of conductive fillers are also available, though they are expensive and tend to be limited in terms of processability and conductivity. They utilize sp^2 hybridized carbon atoms in addition to doping (oxidation or reduction of the polymer) to increase the conductivity. Examples are polyaniline (PANI) and polypyrrole.

Carbon and cement are matrices that are conductive. Though the conductivity of cement is low, cement is attractive due to its low cost and importance in civil engineering. Depending on the heat treatment temperature, which affects the crystallinity, carbon can exhibit a wide range of conductivities.

For some applications, such as heating elements, the material needs to be able to withstand high temperatures. Polymer-matrix composites are not suitable for these applications, but carbon-matrix composites are. Unlike polymer matrices, the carbon matrix is conductive, though it is much less conductive than metals. The carbon matrix is also attractive due to its chemical resistance and low CTE. A low CTE is particularly valuable when the conductive material takes the form of a coating on a substrate (e.g., a ceramic substrate) of low CTE.

7.9.2 Microelectronic Applications

An electrical interconnection in microelectronics is a conducting line for signal transmission, supplying power, or for electrically grounding the system. It usually takes the form of a thick film of thickness > 1 μm. It can be placed on a chip, a substrate, or a printed circuit board. The thick film is created by either screen printing or plating. Thick film conducting pastes containing silver particles (the conductor) and glass frit (a binder that functions due to the viscous flow of glass upon heating) are widely used to form thick film conducting lines (interconnections) on substrates by screen printing and subsequent firing. These films suffer from a reduction in the electrical conductivity due to the presence of the glass and the porosity of the film after firing. The choice of a metal in a thick film paste depends on the need to withstand oxidation from the air during the heating process encountered upon subsequent processing, which can be the firing of the green (i.e., not sintered) thick film together with the green ceramic substrate (a process known as cofiring). It is during cofiring that bonding and sintering take place. Copper is an excellent conductor, but it oxidizes readily when heated in air. The choice of metal also depends on the temperature encountered during subsequent processing. Refractory metals, such as tungsten and molybdenum, are suitable for use in interconnections subjected to high temperatures (> 1,000°C), for example during Al_2O_3 substrate processing.

A substrate, also called a chip carrier, is a sheet on which one or more chips are attached and interconnections are drawn. In the case of a multilayer substrate, interconnections are also drawn on each layer inside the substrate, such that interconnections in different layers are connected, if desired, by electrical paths. A substrate is usually an electrical insulator. Substrate materials include ceramics (e.g., Al_2O_3, AlN, mullite, glass ceramics), polymers (e.g., polyimide), semiconductors (e.g., silicon), and metals (e.g., aluminum). The most common substrate material is Al_2O_3. As the sintering of Al_2O_3 requires temperatures of > 1,000°C, the metal interconnections need to be refractory, and thus made of materials such as tungsten or molybdenum. The disadvantage of using tungsten or molybdenum lies in their higher electrical resistivities than copper. In order to make use of more conductive metals (e.g., Cu, Au, Ag-Pd) as the interconnections, ceramics that sinter at temperatures below 1,000°C ("low temperature") can be used in place of Al_2O_3. The competition between ceramics and polymers for use as substrates is becoming fiercer. Ceramics and polymers are both electrically insulating; ceramics are advantageous in that they tend to have a higher thermal conductivity than polymers; polymers are advantageous in that they tend to have a lower dielectric constant than ceramics. A high thermal conductivity is attractive for heat dissipation; a low dielectric constant is attractive due to the reduced capacitive effect that results, reducing the signal delay. Metals are attractive due to their very high thermal conductivities compared to ceramics and polymers.

Conductive materials commonly take the form of films. There are two types of film, namely standalone films and films on substrates. Standalone films tend to be thick compared to films on substrates. Substrates are commonly electrically insulating, such as ceramics and polymers. Ceramic substrates are advantageous

compared to polymeric substrates because of their abilities to withstand high temperatures, their low CTEs, and their typically high thermal conductivities.

A *z*-axis anisotropic electrical conductor is a standalone film or an adhesive film that is electrically conducting only along the *z*-axis (in the direction perpendicular to the plane of the film). As one *z*-axis film can replace a whole array of solder joints, *z*-axis films are valuable for replacing solder, reducing processing costs, and improving repairability in surface mount technology.

Conductive films on substrates are commonly used as electrical interconnections and electrical contact pads in microelectronics. In this case, a common substrate is a printed wiring board (also called a printed circuit board), which is a polymer-matrix composite with continuous glass fiber (in the plane of the substrate), which serves to reduce the CTE. Carbon fiber is not usually used for printed wiring boards because it is conductive.

Electrically conductive joints, such as that between a wire and an electrical contact pad on a substrate, are commonly involved in microelectronics. Materials used to make such joints include solder and conductive adhesives.

7.9.3 Electrochemical Applications

Electrochemical electrodes need to be electronically conductive. In contrast, electrolytes need to be ionically conductive (i.e., ions, which can be cations and/or anions, are the charge carriers for electrical conduction). An electrochemical electrode contains an active component that participates in the electrochemical reaction. The reaction is responsible for the operation of the electrochemical device. As a result, the active component must be in contact with the electrolyte.

Since electrolytes are most commonly liquids, an electrode is commonly porous so that the electrolyte can flow into the porous electrode and thus make contact with a substantial area of the electrode. Therefore, instead of using a matrix, a small amount of binder (e.g., thermoplastic polymer particles) is used. The amount of binder used should not be excessive. There should be just enough to hold the electrode together; it should not hinder the flow of the electrolyte into the electrode. Since the electrolyte needs to make contact with the active component in the electrode, the binder should not block the active component. Therefore, the design of an electrode is quite different from that of a conventional conductor.

The active component in the electrode is not necessarily conductive, though the electrode must be conductive. For example, manganese dioxide, a common active material for cathodes, is not conductive. When the active component is not conductive, a conductive additive (e.g., carbon black) is needed to make the electrode conductive.

A current collector is an electronic conductor that is inserted into an electrochemical device (e.g., a battery) in order to allow the electric current to flow out of the device. In a common configuration, a current collector is also used as a carrier to hold the active component of the electrode. Thus, the active component of the anode releases electrons in the electrochemical reaction, and the released electrons flow to the current collector. For example, the active component takes the

form of particles that are attached to the current collector using a small amount of a binder. The amount of binder must not be excessive, as the active component and the current collector must be in electrical contact. In the less common case that the active component is a liquid, the current collector does not need to serve as a carrier; it just needs to be porous and conductive.

7.10 Conductive Phase Distribution and Connectivity

The spatial distribution of the phases can greatly affect the properties of a material. In a fibrous composite, the distribution of the fiber is important. It is particularly important when the fibers are discontinuous and present in a volume fraction below the percolation threshold. The percolation threshold is the filler volume fraction above which the filler units touch one another, forming a continuous path. When the fiber is much more conductive electrically than the matrix, percolation results in a continuous conductive path, so that the conductivity of the composite is much higher than the value below the percolation threshold.

7.10.1 Effect of the Conductive Filler Aspect Ratio

For a conductive filler in a considerably less conductive matrix, the percolation threshold decreases with increasing aspect ratio (ratio of length to width; i.e., the ratio of the length to the diameter in the case of a fiber) of the filler. This is expected from geometry, since a larger aspect ratio will make it easier for the filler units to touch one another and form a continuous path. Due to its small diameter, a nanofiber tends to have a high aspect ratio. As a consequence, a nanofiber tends to give a low percolation threshold value. A low threshold is advantageous for processability, since the processability of a composite (e.g., the ability to form it by injection molding) tends to decrease with increasing filler volume fraction. In addition, a low threshold is advantageous due to the associated cost savings and, in case of a filler of high density, weight savings too.

Although the percolation threshold tends to be low for a nanofiber compared to a microfiber, the electrical conductivity attained above percolation is relatively low for a nanofiber. This is because of the abundance of nanofiber–nanofiber contact points in a nanofiber composite and the electrical resistance associated with each contact point. Therefore, nanofibers are typically not effective at providing composites of high electrical conductivity. For example, among nickel fibers with diameters of 20 and 2 μm and nickel nanofibers with diameters of 0.4 μm, all used in the same thermoplastic polymer matrix, the nickel fibers of diameter 2 μm gave composites with the highest conductivity, whether the percolation threshold was exceeded or not (Fig. 7.29). In this context, a "nanofiber" has a diameter of less than 1 μm, whereas a "fiber" has a diameter of more than 1 μm. In Fig. 7.29, the electrical resistivity decreases with increasing filler volume fraction for each type of filler. For all other fillers than the 20 μm diameter nickel fibers, the resistivity levels off as the filler concentration increases. However, for the 20 μm diameter

nickel fiber, the resistivity does not level off, even at the highest filler volume fraction of 43%. Not leveling off means not achieving percolation. In other words, percolation is relatively difficult for the 20 μm diameter nickel fiber. Thus, there is an optimum diameter for reaching a low resistivity. This is because a diameter that is too large means that percolation becomes difficult, whereas a diameter that is too small causes a large density of high-resistance contact points between adjacent filler units.

7.10.2 Effect of the Nonconductive Thermoplastic Particle Viscosity

Figure 7.30 shows the abrupt drop in resistivity by orders of magnitude at the percolation threshold in the case of nickel particles (1–5 μm) in a thermoplastic matrix that is made from thermoplastic particles by compression molding above T_g. Two kinds of thermoplastics are used, namely polyethersulfone (PES) of particle size 100–150 μm and T_g = 220–222°C, and polyimidesiloxane (PISO) of particle size 50–100 μm and T_g = 220°C. The percolation threshold is 5 vol% for the PISO-matrix composite. For PES, the drop in resistivity is not as sharp and occurs over 4–10 vol% Ni.

When the composite is fabricated from a mixture of a conductive filler and a nonconductive matrix that takes the form of thermoplastic particles, the viscosity of the thermoplastic particles above T_g and the size of the thermoplastic particles relative to that of the filler affect the conductivity of the resulting composite. When the thermoplastic particles are considerably larger than the filler particles, small filler particles surround each thermoplastic particle in the mixture, as illustrated in Fig. 7.31a. This means that the presence of the thermoplastic particles results in the segregation of the filler particles, thereby promoting percolation. During subsequent fabrication of the composite under heat and pressure, the thermoplastic particles deform. The viscosity of a thermoplastic decreases with increasing

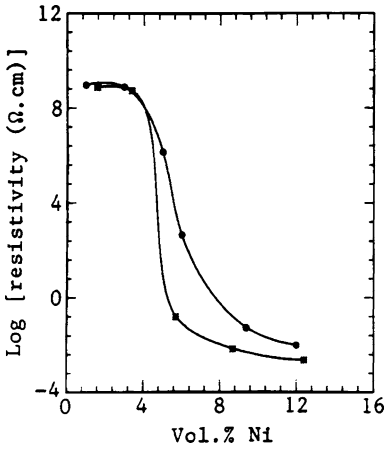

Figure 7.30. Effect of nickel particle volume fraction on the electrical resistivity of nickel particle thermoplastic-matrix composites. *Upper curve*: PES-matrix composites, *lower curve*: PISO-matrix composites. (From [25])

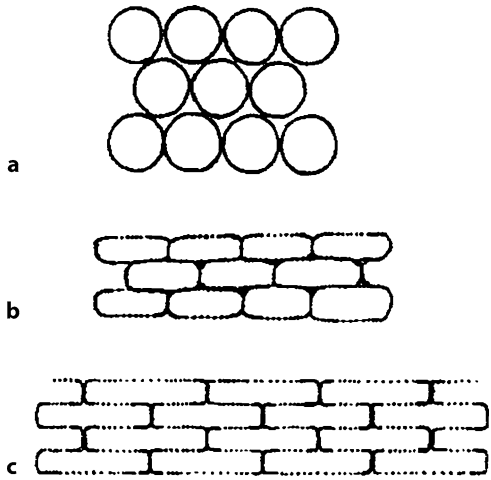

Figure 7.31. Segregation of conductive filler particles on the surfaces of larger thermoplastic particles. **a** Before compression molding, **b** after compression molding for a thermoplastic with a high viscosity, **c** after compression molding for a thermoplastic with a low viscosity. (From [25])

temperature. The lower the viscosity of the thermoplastic at the processing temperature above T_g, the greater the deformation at a given pressure, the greater the separations of some of the adjacent conductive particles, and hence the higher the resistivity of the composite after cooling to room temperature. In other words, the flow of the thermoplastic at the fabrication temperature of the composite tends to

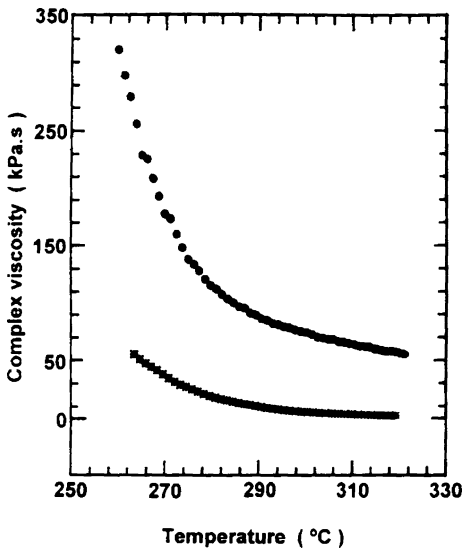

Figure 7.32. Effect of temperature on the viscosity of a thermoplastic polymer in the absence of a filler, *lower curve*: PES, *upper curve*: PISO. (From [25])

disturb the connectivity of the conductive filler particles achieved prior to heating. Figure 7.31b illustrates the structure of a composite with a high-viscosity thermoplastic, whereas Fig. 7.31c illustrates the structure of a composite with a low-viscosity thermoplastic.

At the same temperature, the viscosity is higher for PISO than PES, as shown in Fig. 7.32. As a consequence, the resistivity is lower for the PISO-matrix composite than the PES-matrix composite, as shown in Fig. 7.30.

7.10.3 Effect of Conductive Particle Size

The ratio of the size of the thermoplastic particles used to make the matrix to that of the conductive particles affects the resistivity of the composite. The higher the ratio, the lower the resistivity. This is due to the segregation of the conductive particles, as illustrated in Fig. 7.31a. A greater local concentration of the conductive particles occurs when the ratio is higher. Figure 7.33 shows the resistivities of polyimidesiloxane (PISO) matrix composites made from PISO particles of size 50–100 μm using conductive particles of various sizes. The resistivity is relatively low for composites with silver particles (0.8–1.35 μm) or nickel particles (1–5 μm) due to the high values (30 or more) of this ratio. However, it is relatively high for composites with nickel particles (78–127 μm) or graphite flakes (25 μm) due to the low values (much below 30) of this ratio. The graphite flakes give a relatively low resistivity due to their large aspect ratio.

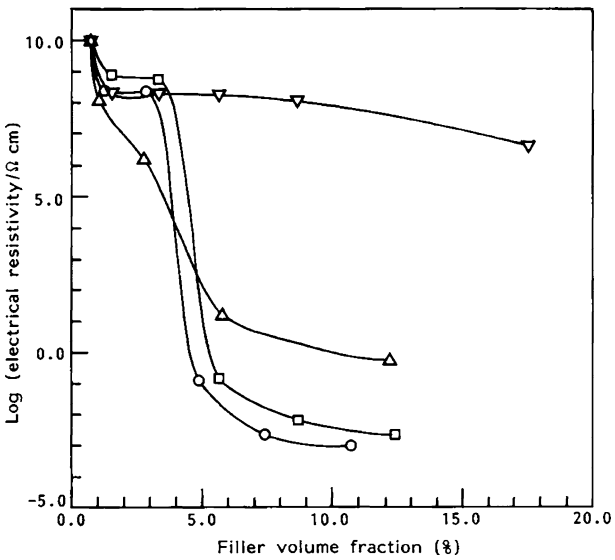

Figure 7.33. Effect of the conductive particle volume fraction on the electrical conductivities (log scale) of polyimidesiloxane-matrix composites. *Circles* – silver (0.8–1.35 μm); *squares* – nickel (1–5 μm); *inverted triangles* – nickel (78–127 μm); *triangles* – graphite flakes (25 μm). The polyimidesiloxane particle size was 50–100 μm. (From [26])

7.10.4 Effect of Additives

The additives present in a composite can affect the phase distribution, as illustrated below for the distribution of short fibers in cement. The distribution of short fibers in cement is greatly affected by the admixture (the additives present in the cement mix). Due to the high electrical conductivity of carbon fiber compared to cement, the electrical conductivity of carbon fiber reinforced cement reflects the degree of fiber dispersion. At a given fiber volume fraction, the conductivity increases with increasing degree of fiber dispersion. The lower the degree of fiber dispersion, the more severe the fiber clumping (Fig. 2.10) and, as a consequence, the less effective the fibers are at increasing the conductivity of the cement.

Figure 7.34 shows the effects of the fiber volume fraction and the admixture on the conductivity ratio, which is defined as the ratio of the measured conductivity to a calculated idealized conductivity. For the sake of simplicity, the calculated idealized conductivity is obtained using the rule of mixtures (ROM), with the fibers taken to be continuous and unidirectional in the direction of conductivity measurement and the matrix conductivity taken to be the measured conductivity of the matrix with the corresponding admixture(s) in the absence of fiber. ROM refers to weighted averaging using the volume fraction of the components as weights in

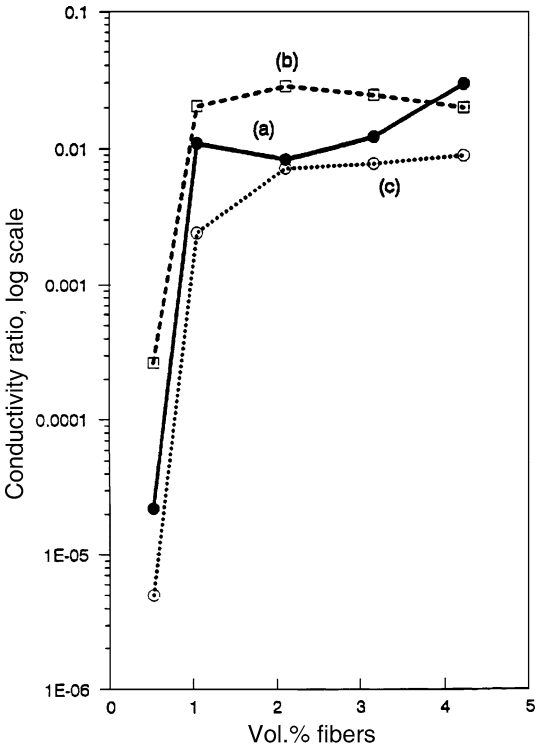

Figure 7.34. Effect of carbon fiber volume fraction on the conductivity ratio of carbon fiber cement paste. *a* With methylcellulose, *b* with methylcellulose and silica fume, *c* with latex (20% by mass of cement) . (From [27])

the averaging. In other words,

$$\begin{aligned}&\text{Calculated idealized conductivity}\\&= (\text{conductivity of fiber}) \times (\text{volume fraction of fiber})\\&= +(\text{conductivity of matrix}) \times (\text{volume fraction of matrix}) ,\end{aligned} \tag{7.61}$$

where

$$(\text{volume fraction of fiber}) + (\text{volume fraction of matrix}) = 1 . \tag{7.62}$$

The greater the conductivity ratio, the higher the degree of fiber dispersion. Microscopic examinations are not capable of discerning small differences in the degree of fiber dispersion. In contrast, the conductivity ratio approach is highly sensitive to small differences in the degree of fiber dispersion, as illustrated below.

Figure 7.34 shows that, for the same fiber volume fraction, the conductivity ratio is highest for methylcellulose with silica fume, lower for methylcellulose, and lowest for latex. Figure 7.35 shows that, for a fixed fiber volume fraction, the conductivity ratio decreases with increasing latex content. This means that the combined use of methylcellulose and silica fume gives the highest degree of fiber dispersion, whereas the use of latex gives the lowest degree of fiber dispersion, and that the degree of fiber dispersion decreases with increasing latex content. Figure 7.34 also shows that the percolation threshold is between 0.5 and 1.0 vol% carbon fiber, whichever admixture is used.

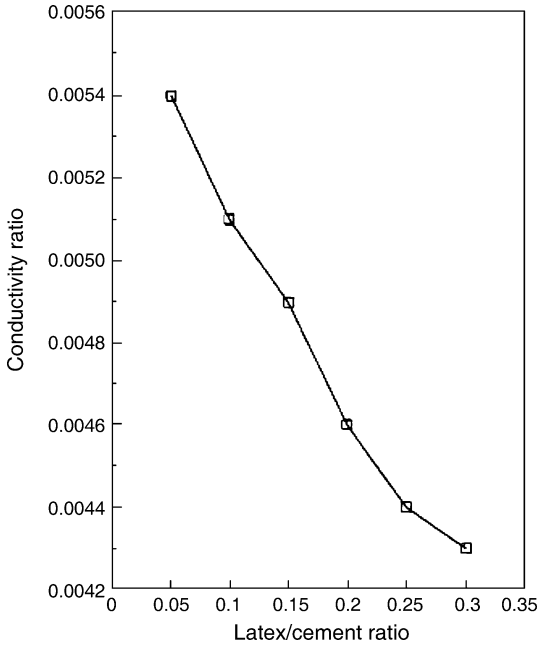

Figure 7.35. Effect of latex/cement ratio (by mass) on the conductivity ratio of carbon fiber (0.53 vol%) cement paste (from [27])

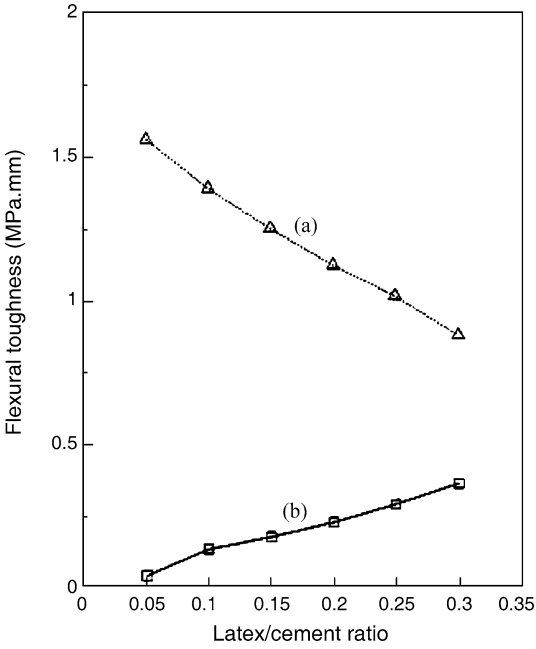

Figure 7.36. Effect of latex/cement ratio (by mass) on the flexural toughness of cement paste. *a* With carbon fiber (0.53 vol%), *b* without fiber. (From [27])

For a given fiber volume fraction, the higher the degree of fiber dispersion, the greater the flexural toughness, which is the area under the curve of flexural stress vs. midspan deflection up to failure. This is because fiber pull-out during deformation provides a mechanism for energy dissipation, and toughness is a measure of the amount of energy absorbed prior to failure. As shown in Fig. 7.36, for a fixed fiber volume fraction (0.53%), the flexural toughness decreases monotonically with increasing latex content. This is because of the decrease in the degree of fiber dispersion with increasing latex content (Fig. 7.35). On the other hand, in the absence of fiber, the flexural toughness increases monotonically with increasing latex content (Fig. 7.35) due to the viscoelastic mechanism of damping provided by latex.

At a fixed carbon fiber volume fraction of 0.53%, the flexural strength increases with increasing latex/cement ratio up to 0.15 and decreases upon increasing the latex/cement ratio further, as shown in Fig. 7.37. This is because of the effect of the latex/cement ratio on the air void content (Fig. 6.18). The air void content is lowest at the intermediate latex/cement ratio of 0.15, thus causing the flexural strength to be greatest at this latex/cement ratio. The flexural strength is sensitive to voids since voids tend to facilitate failure and the strength reflects the stress needed to cause failure. On the other hand, in the absence of fiber, the flexural strength increases monotonically with increasing latex/cement ratio (Fig. 7.37) due to the monotonic decrease in the air void content with increasing latex/cement ratio (Fig. 6.18).

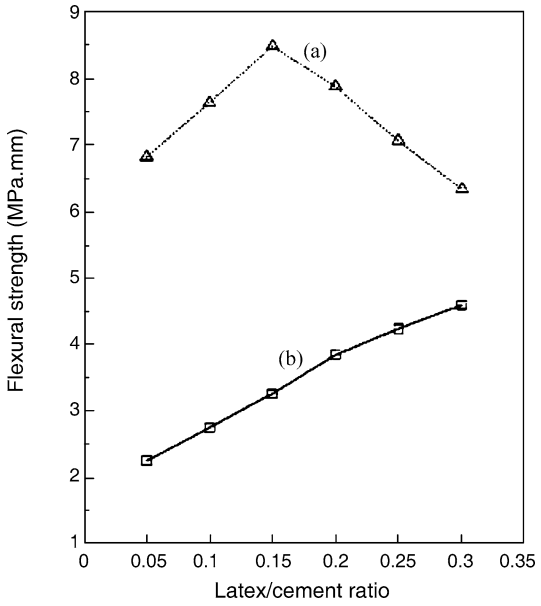

Figure 7.37. Effect of the latex/cement ratio (by mass) on the flexural strength of cement paste. *a* With carbon fiber (0.53 vol%), *b* no fiber. (From [27])

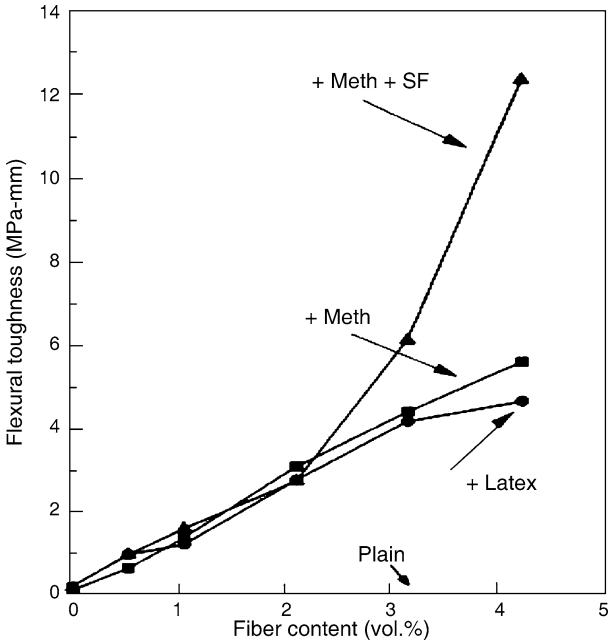

Figure 7.38. Effect of carbon fiber volume fraction on the flexural toughness of cement paste. Meth – methylcellulose (0.4% by mass of cement). SF – silica fume (15% by mass of cement). Latex – aqueous latex particle dispersion (20% by mass of cement). (From [27])

Figure 7.38 shows that, for a given fiber volume fraction, the flexural toughness is highest for methylcellulose with silica fume and lowest for latex. This is consistent with Fig. 7.34, which shows that methylcellulose with silica fume gives the highest degree of fiber dispersion, while latex gives the lowest degree of fiber dispersion. As mentioned above, the toughness is sensitive to the degree of fiber dispersion due to the mechanism of fiber pull-out for energy dissipation.

7.10.5 Levels of Percolation

In a cement-matrix composite containing a fine aggregate (typically sand) – a composite known as mortar – the cement paste (including fibers or other admixtures that may be present) can be considered to be the matrix, while the aggregate is the filler. The connectivity of the matrix is important if the matrix is conductive (as is the case when carbon fiber is present) and mortar conductivity is desired. When the conductive fibers in the cement matrix percolate (i.e., become connected due to the fiber volume fraction exceeding the percolation threshold) and the cement matrix in the mortar also percolates (since the fine aggregate volume fraction is sufficiently high), high mortar conductivity is possible and double percolation is said to occur. However, when conductivity is not needed, connectivity of the cement matrix in the mortar is usually not desirable, because the continuity promotes liquid permeability.

In a cement-matrix composite containing a fine aggregate (typically sand) and a coarse aggregate (typically gravel) – a composite known as concrete – the mortar can be considered the matrix, while the coarse aggregate is the filler. The conductivity of the mortar is important if the mortar is conductive and conductivity in the concrete is desired. When the conductive fibers in the cement matrix percolate (due to the fiber volume fraction being sufficiently high), the cement matrix in the mortar percolates (due to the fine aggregate volume fraction being sufficiently high), and the mortar in the concrete also percolates (due to the coarse aggregate volume fraction being sufficiently high), high concrete conductivity is possible and triple percolation is said to occur.

Various levels of percolation can also occur in polymer-matrix composites. For example, double percolation can occur when the composite is created from two kinds of pellets, one of which is nonconductive (due to the absence of a conductive filler), while the other is conductive (due to the presence of a conductive filler beyond the percolation threshold). If the conductive pellets form a continuous path in the composite, double percolation occurs. In this case, double percolation is advantageous since it reduces the amount of conductive raw material needed.

7.11 Electrically Conductive Joints

Electrically conductive joints, also known as electrical connections, are needed in electronics. They are mechanical joints with low electrical resistance. An electrical connection must have a resistance that is below a certain value in order for it

to be acceptable. The electrical resistance is sensitive to minor changes in the microstructure, such as the microstructure of the joint interface. Even when the mechanical aspects of the joint are acceptable, its electrical performance may not be. Electrical failure and mechanical failure may not occur simultaneously. A drop in stress due to mechanical debonding is not necessarily accompanied by an increase in the electrical resistance, particularly when the joining medium is ductile (e.g., in the case of solder). When the joining medium is relatively brittle, as in a silver-epoxy conductive adhesive, there is a greater tendency for an abrupt increase in resistance to accompany mechanical debonding. Due to the large number of electrical connections in a microelectronic package, the reliability of the connections is of great importance.

7.11.1 Mechanically Strong Joints for Electrical Conduction

With the exception of joints obtained by thermoplastic welding, soldered, brazed and welded joints are all conductive. Among these, soldered joints involve the lowest processing temperatures, so they are the joints most commonly used in electronics, since circuitry can be harmed by elevated temperature processing.

Soldering is commonly conducted by applying a flux that removes metal oxides, thereby promoting the wetting of the working metal surface by the molten solder during soldering. An example of a flux is aluminum chloride (rosin) for soldering tin.

In order to increase the density of an electronic package, a two-dimensional array of soldered joints between the contact pads on two surfaces is needed. Most commonly, one surface is the chip (i.e., the semiconductor device), while the other surface is the substrate. The chip is flipped, so that its contact pads are facing the top surface of the substrate, with the contact pads of the chip aligned with those on the substrate, as illustrated in Fig. 7.39. Each soldered joint in the array (known as a ball grid array) contains a solder sphere (called a solder bump or a solder ball), which can be applied by evaporation, electroplating, printing, direct placement, or other methods. The joints are formed by heating each solder bump to melt it, such that the molten solder remains on each contact pad. After joint formation, a nonconductive adhesive such as an epoxy is used to fill the region between the bumps in order to improve the thermal fatigue resistance of the joint. The thermal fatigue stems from the CTE mismatch between the chip and the substrate. The adhesive is known as an underfill.

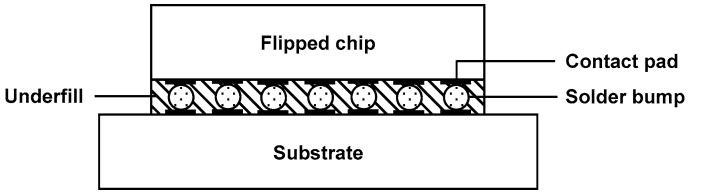

Figure 7.39. Flip chip electronic assembly involving an array of solder bumps

Solder used for printing (such as screen printing to form a two-dimensional pattern) is applied in the form of a paste called a solder paste. The paste is a slurry of solder particles in a vehicle that is a flux as well as an adhesive that provides temporary joining prior to soldering. During subsequent soldering (known as reflow soldering), every solder particle in the paste melts.

There are numerous problems with soldered joints. One problem stems from the usual presence of lead in the solder. The most common solders are tin-lead alloys near the eutectic composition. Lead is poisonous, though it aids the rheology of the solder. Therefore, lead-free solders (e.g., SnAgCu alloys) are rapidly gaining in importance, although the higher processing temperature required for them causes complications during the associated manufacturing processes.

Soldered joints also suffer from their tendency to degrade due to thermal fatigue and creep. Thermal fatigue is associated with temperature variations between the on and off states of the electronics, and stems from the difference between the thermal expansion coefficients of the two members joined by the solder.

Creep arises due to the viscoelastic behavior of solder in the solid state. Due to the low melting temperature of solder, this creep is substantial when the electronics is at its operating temperature. The creep resistance of solder can be increased by incorporating nanoparticles into the solder (i.e., by forming a particulate metal-matrix composite). The particles also serve as reinforcement besides restraining the solder from creep. The particles are nanosized in order to reduce the tendency for the particles to become nonuniformly distributed (due to the difference in density between the metal and the particles) when the solder is molten. In order for the molten solder to remain sufficiently fluid, the volume fraction of the particles must be low.

Another method of increasing the creep resistance is to use a metal-matrix composite with a solder alloy as the matrix and a continuous fiber as the reinforcement. The composite takes the form of a sheet (called a solder preform), with the fiber in the plane of the sheet. The solder preform is also attractive because of its low CTE, which is due to the low CTE of the fiber. However, the application of solder preforms is limited to planar joints.

A further issue is the reaction between the solder and a member (e.g., copper) and the formation of intermetallic compounds at the joint interface. The intermetallic compounds hinder the wetting of the member by the molten solder.

Furthermore, solder produces a large footprint on the circuit board to which the solder is applied. This large footprint is a consequence of the high fluidity of the molten solder, and is undesirable for the miniaturization of microelectronics, as it makes the fine-pitch patterning of interconnection lines difficult.

Yet another complication with soldering is the need to use flux, which is necessary to reduce the copper oxide on the copper to which the solder is bonded. Although tin-lead solder attaches well to copper, it does not attach well to copper oxide, which forms readily on copper at the soldering temperature. Flux also acts as a wetting agent during soldering; in other words, it reduces the surface tension of the molten solder so that the molten solder can wet the surfaces of the members to be joined. Due to the chemical reactivity of the flux, the flux needs to be

removed after soldering. Some fluxes require volatile organic compounds (VOCs, which contribute to air pollution) for their removal.

Due to the numerous problems associated with soldering, the replacement of soldered joints by conductive adhesive joints is being actively pursued. Conductive adhesives are polymeric adhesives (e.g., epoxy resin) that contain conductive fillers (e.g., silver particles). The conductive filler units (e.g., the silver particles) must touch one another in order to form a continuous conductive path. To achieve this, the conductive filler volume fraction needs to exceed the percolation threshold. Even when the percolation threshold is exceeded, the electrical conductivity is considerably below that of a metal, due to the contact resistance at the interface between contacting filler units. Therefore, the use of fillers that melt during the processing (the melting enables the bonding of the filler units with one another) is a method that is being investigated to achieve electrical conductivity that approaches that of a metal.

The most common conductive epoxy on the market is silver epoxy, which contains a high proportion of silver particles in an epoxy resin. For example, the silver epoxy Circuitworks CW2400 of Chemtronics contains 60–90 wt.% silver, 10–25 wt.% epoxy resin, and 1–3 wt.% modified epoxy ester. An epoxy ester is epoxy resin that has been partially esterified with fatty acids, which react with both the epoxide and the hydroxyl groups of the epoxy resin to form the ester. The epoxy ester enhances the chemical resistance. This product comes in two parts, one of them being the epoxy and the other the hardener. Curing conducted at room temperature takes 8 h, though it can be hastened by heating. The volume electrical resistivity of the product after curing is 0.001 Ω cm, which is higher than that of solders by orders of magnitude. For example, the electrical resistivity of the eutectic tin-lead solder is $1.4 \times 10^{-5}\,\Omega\,\mathrm{cm}$.

The electrical resistance of an electrical connection is the sum of the volume resistance within the joining medium (e.g., solder) and the resistance of the interface between the joining medium and each of the two surfaces to be joined. The volume resistance R_v of the joining medium is governed by the volume resistivity ϱ_v of the medium:

$$R_\mathrm{v} = \varrho_\mathrm{v} l/A \,, \tag{7.63}$$

where A is the geometric area of the electrical connection and l is the length of the joining medium in the direction perpendicular to the joint area.

The interfacial resistance R_i is governed by the interfacial resistivity ϱ_i, which depends on the microstructure of the interface, i.e.,

$$R_\mathrm{i} = \varrho_\mathrm{i}/A \,. \tag{7.64}$$

The overall resistance R of the connection is given by

$$R = R_\mathrm{v} + 2R_\mathrm{i} \,. \tag{7.65}$$

The contact resistivity of the electrical connection is given by

$$\varrho = RA \,. \tag{7.66}$$

In the case of an eutectic tin-lead electrical connection between copper surfaces, with $A = 4.2 \times 3.0\,\text{mm}^2$ and $l = 125 \pm 75\,\mu\text{m}$, the contact resistivity $\rho = 2.5 \times 10^{-4}\,\Omega\,\text{cm}$ [28]. Using Eq. 7.66,

$$R = \rho/A = 2.0 \times 10^{-3}\,\Omega\,. \tag{7.67}$$

Using Eq. 7.63, with $\rho_v = 1.4 \times 10^{-5}\,\Omega\,\text{cm}$ and $l = 125\,\mu\text{m}$,

$$R_v = \rho_v l/A = 1.4 \times 10^{-6}\,\Omega\,, \tag{7.68}$$

which is negligible compared to R. Hence, using Eq. 7.65,

$$R_i = (R - R_v)/2 \approx R/2 = 1.0 \times 10^{-3}\,\Omega\,, \tag{7.69}$$

And, using Eq. 7.64,

$$\rho_i = R_i A = 1.3 \times 10^{-4}\,\Omega\,\text{cm}\,. \tag{7.70}$$

In case of a CW 2400 silver epoxy electrical connection between copper surfaces, with $A = 5.1 \times 4.9\,\text{mm}^2$ and $l = 152 \pm 76\,\mu\text{m}$, the contact resistivity $\rho = 6.7 \times 10^{-4}\,\Omega\,\text{cm}$ [28]. Thus,

$$R = \rho/A = 2.7 \times 10^{-3}\,\Omega\,. \tag{7.71}$$

With $\rho_v = 1 \times 10^{-3}\,\Omega\,\text{cm}$ and $l = 152\,\mu\text{m}$,

$$R_v = \rho_v l/A = 6.1 \times 10^{-5}\,\Omega\,, \tag{7.72}$$

which is negligible compared to R. Hence,

$$R_i = (R - R_v)/2 \approx R/2 = 1.4 \times 10^{-3}\,\Omega\,, \tag{7.73}$$

and

$$\rho_i = R_i A = 3.4 \times 10^{-4}\,\Omega\,\text{cm}\,. \tag{7.74}$$

In spite of the much higher ρ_v of silver epoxy compared to solder, ρ and ρ_i are comparable for these two types of electrical connections. This means that ρ_i rather than ρ_v governs the electrical resistance of the overall connection. Therefore, studying the interface between the joining medium and each of the two surfaces to be joined is critical to understanding the science of the overall connection. However, research in this area has focused on ρ_v, with relatively little attention paid to ρ_i.

Figure 7.40 shows that the contact electrical resistivity of an eutectic tin-lead (63 wt.% tin, 37 wt.% lead) soldered joint (i.e., the resistance of the joint multiplied by the geometric area of the joint) between copper surfaces increases reversibly by 15% upon compression of the joint (with a stress of only 0.12 MPa) in the direction perpendicular to the joint interface. Mechanical deformation due to the compression would have caused dimensional changes that increased the resistance. Thus,

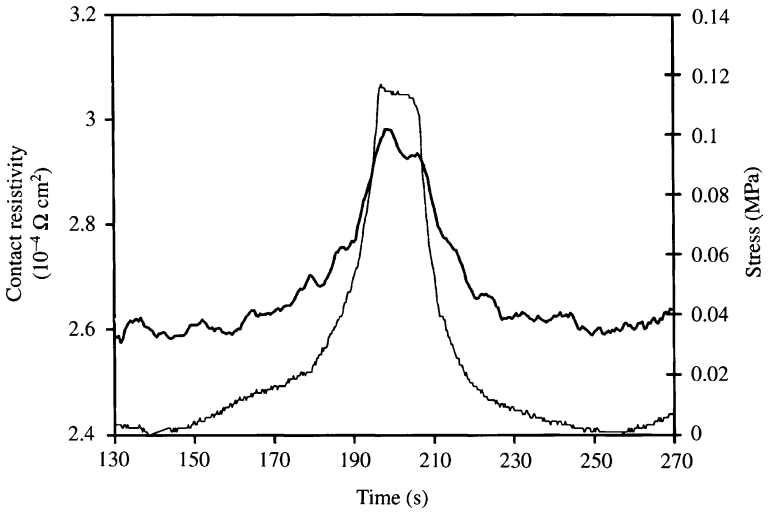

Figure 7.40. Soldered joint as an electrical connection between copper surfaces. The contact electrical resistivity of the joint increases reversibly upon compression of the joint in the direction perpendicular to the joint interface, due to a subtle reversible microstructural change at the solder–copper interface. *Thick curve*: resistivity, *thin curve*: stress. (From [28])

the observed resistance increase cannot be due to the mechanical deformation of the solder. After all, the volume resistance of the solder barely contributes to the overall resistance of the connection. The observed resistance increase is believed to be due to a subtle reversible microstructural change at the solder–copper interface. This microstructural change has not yet been identified, but it may be related to a decrease in the true contact area at the solder–copper interface (i.e., a decrease in the number of contact points across the interface) upon compression. This true contact area decrease may be related to the effect of compression on the brittle intermetallic compound (formed during soldering due to the reaction between the molten solder and the copper) at the interface.

Figure 7.41 shows that the contact electrical resistivity of a silver epoxy (room temperature cured, without postcuring) joint between copper surfaces increases reversibly by 4.5% upon compression of the joint (with a stress of only 0.04 MPa) in the direction perpendicular to the joint interface. The observed resistance increase cannot be due to the mechanical deformation of the silver epoxy. It is believed to be due to a subtle reversible microstructural change at the adhesive–copper interface.

Figure 7.42 shows that the contact resistivity ϱ of the soldered joint mentioned above increases quite reversibly by up to 6% with increasing temperature up to 50°C. For the adhesive joint mentioned above, the contact resistivity increases by up to 48% with increasing temperature up to 50°C. Thus, the thermal reliability of the soldered joint is superior to that of the adhesive joint.

The abovementioned experimental results show that the performance of an electrical connection depends on both temperature and pressure. Figure 7.43 shows the combined effects of temperature and compression on the contact electrical resistivity ϱ for an adhesive joint (silver epoxy without postcuring, between cop-

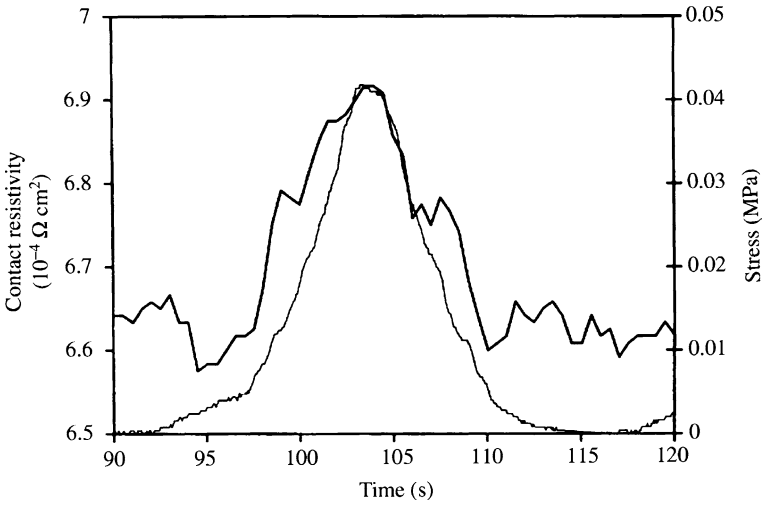

Figure 7.41. Conductive adhesive (silver epoxy without postcuring) joint as an electrical connection between copper surfaces. The contact electrical resistivity of the joint increases reversibly upon compression of the joint in the direction perpendicular to the joint interface, due to a subtle reversible microstructural change at the adhesive–copper interface. *Thick curve*: resistivity, *thin curve*: stress. (From [28])

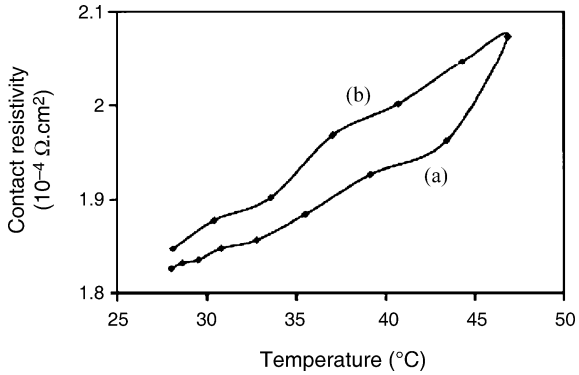

Figure 7.42. Variation in the contact resistivity ρ of a soldered joint with temperature: *a* during heating; *b* during subsequent cooling (from [29])

per surfaces). The resistivity increases upon heating quite reversibly, although it decreases cycle by cycle, as shown by the results for three cycles of heating shown in Fig. 7.43. This change in resistivity relates to a change in thickness of the sandwich, as shown in Fig. 7.44. The thickness increases upon heating quite reversibly, decreasing cycle by cycle.

The thermal stability of the adhesive joint mentioned above can be improved by postcuring; i.e., by heating at an elevated temperature (e.g., 80°C for 4 h) after curing at room temperature (e.g., for 24 h). The postcuring removes the cycle-by-cycle decreases in resistivity (Fig. 7.43) and thickness (Fig. 7.44), meaning that the curves for various cycles essentially overlap.

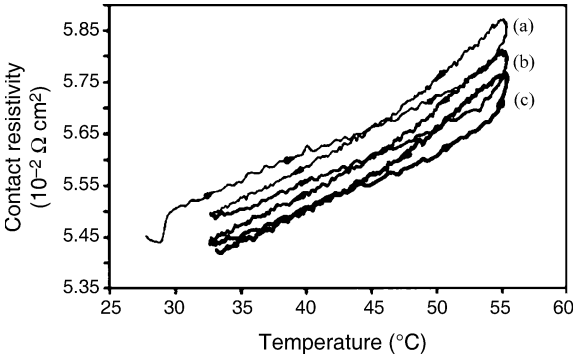

Figure 7.43. Contact electrical resistivity ϱ of an adhesive joint (silver epoxy between copper surfaces, without postcuring) during three cycles of heating at a constant compressive stress of 0.33 MPa. *a* First cycle, *b* second cycle, *c* third cycle. (From [30])

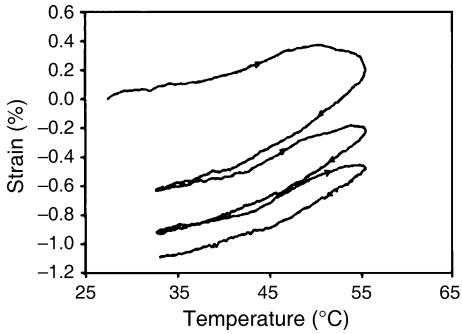

Figure 7.44. Strain (fractional change in sandwich thickness) of an adhesive joint (silver epoxy between copper surfaces, without postcuring) during three cycles of heating at a constant compressive stress of 0.33 MPa (from [30])

In some applications, the conductive adhesive needs to penetrate into a small space. Figure 7.45 shows the inability of silver epoxy (Product GPC-251, Creative Materials Inc., Tyngsboro, MA, USA, with 70–75 wt.% silver and bisphenol A epoxy resin, and a resistivity of 0.005 Ω cm after curing at 25°C) to penetrate into the small space between the 130 μm diameter strands of a seven-strand tin-coated copper wire. The electrical connection is between the wire and a substrate. This inadequate penetration is due to the high viscosity and hence low conformability of the silver epoxy. It causes a small area of contact between the silver epoxy and the wire, thus resulting in a high resistance at the interface between the silver epoxy and the wire. Figure 7.45 also shows that the silver flakes in the epoxy are about 15 μm in size and are preferentially oriented in the plane of the surfaces that are joined by the silver epoxy. The large dimensions of the silver flakes lead to the difficulties with the penetration of the silver epoxy into small spaces. In Fig. 7.45, one of the surfaces is the copper wire, the surface of which is curved. This preferred orientation of the silver flakes is not desirable, since it causes high resistance of the silver epoxy in the

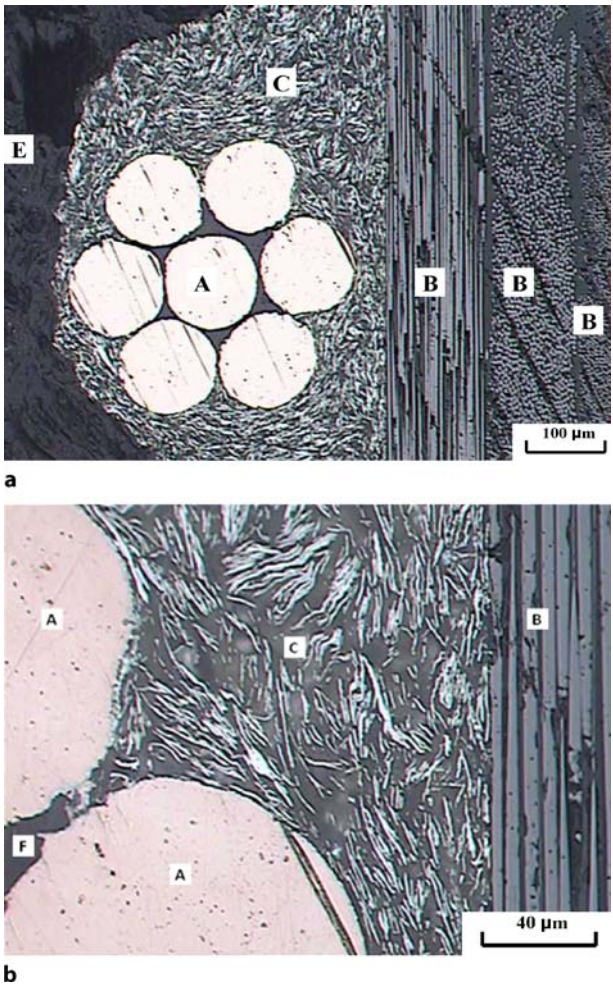

Figure 7.45. Optical microscope photographs of the cross-section of an electrical contact involving silver epoxy (a conductive adhesive). A – copper wire with seven strands; B – substrate in the form of a carbon fiber epoxy-matrix composite; C – silver epoxy, with the curved edges of the silver flakes shown; E – phenolic molding compound; *F*, void. **a** Low-magnification view, **b** high-magnification view. (From [31])

direction perpendicular to the plane of the joint, thereby increasing the resistance of the joint.

7.11.2 Mechanically Weak Joints for Electrical Conduction

An electrical connection does not have to be a strong mechanical joint, since the mechanical integrity can be derived from peripheral devices, such as clips and adhesive tape. By allowing the mechanical strength of the joint to be relatively weak, the choice of materials available is widened, thus allowing the electrical

resistance of the joint to minimized. For example, instead of an adhesive type of polymer (such as epoxy), numerous other organic vehicles can be used. Such conductive media are often known as conductive paints. A paint is a dispersion of fine conductive particles in a liquid, known as a vehicle. A common class of conductive paints uses volatile vehicles. A volatile vehicle evaporates from the joint interface after application, thereby allowing adjacent conductive particles in the paint to touch one another. In contrast, the polymer in a conductive adhesive is not volatile and remains at the interface between adjacent conductive particles, thus increasing the resistance of the particle–particle interface. In order to increase the ability of the paint to bond to a surface, a small proportion of a binder is typically used. The greater the proportion of binder, the stronger the bond mechanically, but the higher the electrical resistance of the bond. Therefore, it is necessary to make a compromise between the mechanical and electrical properties in the design of a conductive paint.

An example of a conductive paint is colloidal graphite, which is a dispersion of fine graphite particles in water (a volatile vehicle). Polyvinyl alcohol (PVA), which dissolves in water, is a commonly used binder for water-based dispersions. Another example is silver paint, which is a dispersion of silver particles in a volatile vehicle, such as propanol (an alcohol). Ethyl cellulose (the ethyl ether of cellulose) is a commonly used binder for organic-based dispersions, as it is soluble in some organic solvents (e.g., ethanol), though it is insoluble in water. The solubility in organics depends on the ethoxyl ($-OC_2H_5$) content in the particular ethyl cellulose.

Figure 7.46 shows that silver paint (Product Electrodag 416, from Acheson Colloids Co., Port Huron, MI, USA, consisting of 45 wt.% silver particles, 1–5 wt.% ethyl cellulose, which is a binder, and 48 wt.% ethanol, which is the volatile vehicle, with a resistivity of 0.003 Ω cm) is able to penetrate into small spaces due to its low viscosity. The silver particles in the paint are so small that they are not individually observed in the optical micrograph, in contrast to the large size of the silver flakes in the silver epoxy of Fig. 7.45.

Figure 7.47 shows that graphite colloid (LUBRODAL EC 1204 B, from Fuchs Lubricant Co., Emlenton, PA, USA, a water-based dispersion containing less than 20 wt.% graphite particles of size $< 0.75\,\mu m$, less than 1 wt.% sodium salt of cellulose, which is a binder, and less than 1 wt.% dispersants, with a resistivity of 0.03–0.10 Ω cm, which is much higher than that of the silver paint mentioned above) is able to penetrate into small spaces due to its low viscosity. The graphite particles in the paint are so small that they are not individually observed in the optical micrograph. Graphite colloid is much less expensive than silver paint.

Comparing the silver epoxy (Fig. 7.45), silver paint (Fig. 7.46) and graphite colloid (Fig. 7.47) mentioned above shows that the resistance of the electrical contact between the copper wire and the substrate is lowest for silver paint and is relatively high for graphite colloid and silver epoxy. The silver epoxy joint degrades under hydrothermal conditions (40°C in water for 60 min), meaning that the resistance increases further. This is because of the low hygrothermal stability of epoxy. In contrast, silver paint degrades only slightly under the same conditions. Graphite colloid degrades even more significantly than silver epoxy due to the fact that it is water based.

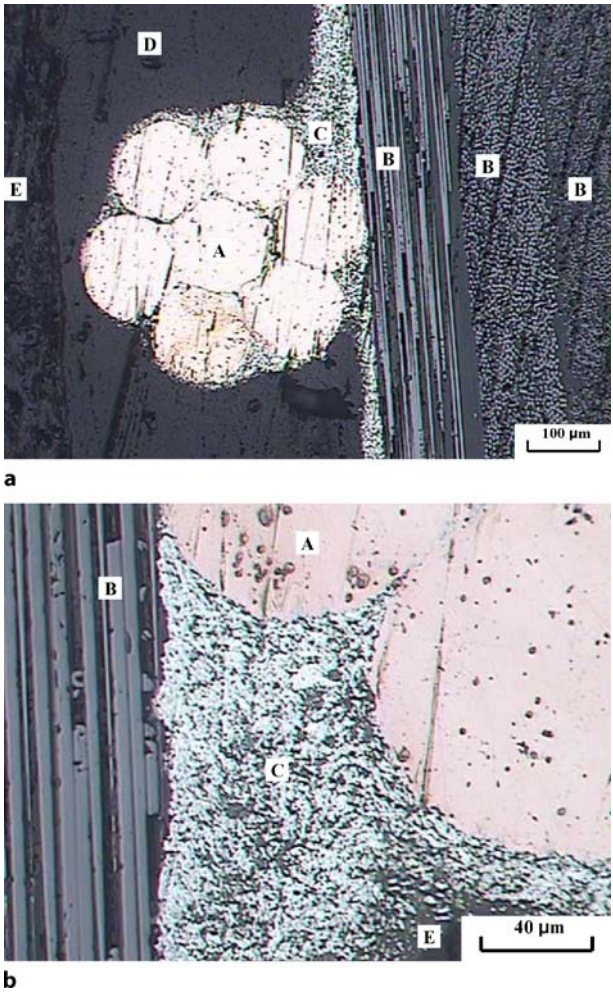

Figure 7.46. Optical microscope photographs of the cross-section of an electrical contact involving silver paint. A – copper wire with seven strands; B – substrate in the form of a carbon fiber epoxy-matrix composite; C – silver paint; D – epoxy overcoat; E – phenolic molding compound. **a** Low-magnification view, **b** high-magnification view. (From [31])

The combined use of silver particles and a low proportion of carbon black (0.055 of the total filler volume) provides a paint that performs well both electrically and mechanically [32]. Carbon black is less conductive than silver by a few orders of magnitude. However, it is inexpensive and is used in the form of porous agglomerates of nanoparticles. This morphology allows carbon black to be highly compressible (squishable), meaning that it is highly conformable. Because of this conformability, the carbon black fills the space among the silver particles, thereby improving both the electrical conductivity and the scratch resistance of the resulting conductive film. The scratch resistance relates to the shear strength of the film. With a total solid volume fraction of 0.1969 and a silane-propanol (1:1 by weight)

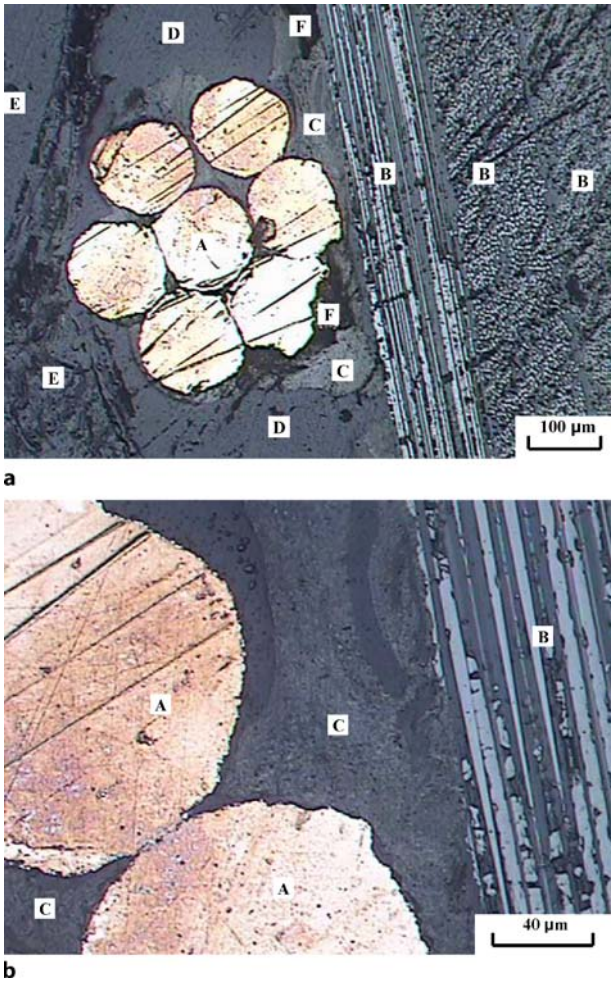

Figure 7.47. Optical microscope photographs of the cross-section of an electrical contact involving graphite colloid. A – copper wire with seven strands; B – substrate in the form of a carbon fiber epoxy-matrix composite; C – graphite colloid; D – epoxy overcoat; E – phenolic molding compound; F – void. **a** Low-magnification view, **b** high-magnification view. (From [31])

solution vehicle, a conductive film of resistivity $2 \times 10^{-3}\,\Omega\,\mathrm{cm}$ (in the plane of the film) and thickness 50 µm is obtained. The combined use of silane and propanol in the vehicle is due to the hydrolysis of silane with the aqueous propanol solution and the mechanical strengths of the resulting reaction products.

7.11.3 Electrical Connection Through Pressure Application

An electrical connection that requires continuous pressure application in order for it to function is known as a pressure contact. Although the requirement for pressure is a disadvantage, pressure contacts are attractive since they are separable

connections. A connection involving a clip is an example of a pressure contact; here, connecting and disconnecting simply involve clipping and unclipping. In contrast, disconnection is not as simple for a joint involving solder or adhesive. A pressure contact should be distinguished from conductive adhesive, conductive paint and solder connections, which tend to degrade upon the application of pressure.

Positioning a material at the pressure contact interface can help to improve the contact, particularly if it is conformable to the surface topography of the adjoining surfaces. Surfaces are never perfectly smooth; they have microscopic hillocks. The valley between two hillocks contains air, which is an insulator. Therefore, the conformability of the material enables the displacement of air from the contact interface, thereby decreasing the electrical resistance of the interface.

Due to the conformability of carbon black, carbon black paste makes a particularly effective pressure contact interface material [33]. It yields a contact resistivity of $2 \times 10^{-5}\,\Omega\,\mathrm{cm}^2$ in the direction perpendicular to the plane of the contact when the contact pressure is 0.92 MPa, compared to the higher value of $1 \times 10^{-4}\,\Omega\,\mathrm{cm}^2$ for a pressure contact without an interface material.

7.11.4 Electrical Connection Through a *Z*-Axis Electrical Conductor

A *z*-axis anisotropic electrical conductor is a conducting sheet that conducts only in the *z*-direction, which is the direction perpendicular to the sheet. It is insulating in all other directions. Such a conductor is a composite material involving an insulating matrix and conductive columns that are perpendicular to the plane of the sheet, as illustrated in Fig. 7.48. Since the columns do not touch one another, the sheet is insulating in the plane of the sheet. The columns do not need to be regularly spaced.

The presence of a polymer matrix film, which is insulating, on the conductive column surface in the plane of the sheet must be avoided. To ensure this, each column protrudes slightly from each of the two outer surfaces of the sheet in one of the designs.

Z-axis conductors are used for electrically connecting corresponding contact pads on the two proximate surfaces that sandwich the *z*-axis conductor. One or more conductive columns can link a pair of contact pads on each surface, as shown in Fig. 7.48. If the column density is high enough that there is at least one conductive column per pair of opposite contact pads, there is no need to align

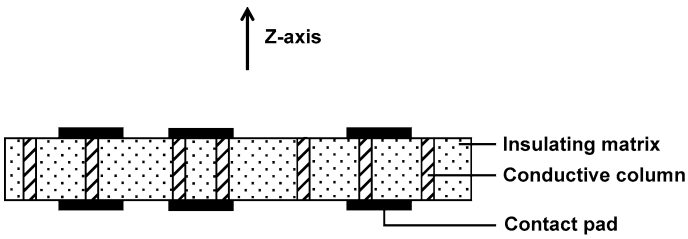

Figure 7.48. A *z*-axis anisotropic electrical conductor

the *z*-axis conductor sheet relative to the two proximate surfaces. However, if the column density is low and/or the contact pad size is small, alignment is necessary and, in this case, the columns are regularly spaced.

A single sheet of a *z*-axis conductor can replace a two-dimensional array of soldered joints. It is thus attractive for replacing solder and reducing processing costs. The *z*-axis conductor can take the form of a standalone sheet or an adhesive. The standalone sheet needs to be squeezed between the proximate surfaces by fastening. The adhesive becomes a *z*-axis conductor sheet after application and does not require fastening.

Each conductive column can take the form of a single conductive particle (which is not necessarily columnar in shape, but must be large enough to extend for the entire thickness of the sheet), a cluster (or column) of conductive particles, or a single wire that is oriented along the *z*-axis. A single particle is advantageous compared to a cluster of particles, due to the presence of contact resistance at the interface between particles in a cluster. For a standalone sheet, all of these options are possible, due to the variety of methods available for introducing and orienting the conductive component in a composite sheet. For example, the orientation of a particle column or a wire can be achieved through the use of an electric or magnetic field. For an adhesive, the single particle option is typically used, since orientation is difficult after the application of the particle-filled adhesive at the joint interface. In other words, the single particles are randomly distributed in the adhesive after application to the joint interface, with the particles not in contact with one another.

The conductive particles in a *z*-axis conductor involving a single particle per conductive column must have a narrow size distribution. Otherwise, the particles that are small cannot extend for the entire thickness of the sheet and thus cannot serve as a conductive column. Ideally, all of the particles are slightly larger than the thickness of the sheet.

The conductive particles used in a *z*-axis conductor can be metal particles or metal-coated polymer particles. The latter is attractive due to the ease with which the particles can be deformed in response to the fastening stress. A limited degree of erosion of the metal coating on a polymer particle is acceptable, although, in the case of a single particle per column, the fragmented coating must extend for the entire thickness of the sheet. However, the latter is disadvantageous due to the small volume of metal in a metal-coated polymer particle and the consequent high resistance of a conductive column compared to a metal particle.

7.12 Porous Conductors

Porous conductors are important for electrodes and current collectors in electrochemical devices such as batteries, in addition to applications related to filters and catalyst supports. For the abovementioned applications (other than catalyst supports), the pores need to be continuous and accessible from the outer surface so that fluids can flow in the porous conductor. The porosity (i.e., the fraction of

the volume occupied by pores) is typically high, exceeding 50%. Pores are generally detrimental to mechanical properties. The larger the pore size, the lower the strength. However, mechanical strength and modulus are typically not needed for electrochemical applications.

A porous conductor can take the form of a collection of conductive particles or fibers. In order to provide some mechanical integrity, a small amount of binder may be used with the conductive particles or fibers. In some electrochemical electrodes, the active component is not conductive, as in the case of manganese dioxide particles used as a cathode material, so conductivity is achieved by using a conductive additive, which can be conductive particles or fibers that are mixed with the active component.

One method of making porous conductors involves dry compaction of a collection of conductive particles or short fibers, optionally in the presence of a small amount of a binder, which is typically a thermoplastic polymer powder. The binder flows upon heating, thereby providing binding. Examples of thermoplastic binders are polytetrafluoroethylene (Teflon) and polyvinylidene fluoride (PVDF). By varying the pressure used for compacting, different volume fractions of the filler may be obtained.

Another method of making porous conductors involves (i) making a slurry of the conductive particles or short fibers dispersed in a liquid, (ii) casting the slurry and then baking to remove the liquid, thereby forming a preform, (iii) infiltrating the preform with a binder, and (iv) heating to cause the binder to bind.

A binder may be conductive or nonconductive. A polymer binder is nonconductive. A conductive binder is obviously attractive for making a porous conductor. An example of a conductive binder is carbon, which is made from a carbon precursor, such as pitch, by carbonization (heating). The pitch may be used in the molten state. Alternatively, it may be used at room temperature by dissolving it in a solvent, such as methylene chloride. With carbon fiber used as the conductive filler and a carbon binder, the resulting porous conductor is all carbon and is thus attractive due to its chemical resistance, high temperature resistance, thermal conductivity, and low CTE.

7.12.1 Porous Conductors Without a Nonconductive Filler

A low resistivity of the filler is obviously advantageous for providing a low resistivity in the resulting porous conductor. Thus, graphitized carbon nanofiber is more effective than carbon nanofiber that has not been graphitized. The resistivities of a carbon nanofiber (0.1 μm diameter) compact without a binder are 0.053 and 0.0095 Ω cm for nongraphitized and graphitized carbon nanofibers, respectively, where the density of the porous carbon is 0.47 g/cm^3 in both cases (compared to a density of 2 g/cm^3 for the nanofiber itself) [34].

The contact resistance at a filler–filler contact point in a porous conductor is comparable to that in a polymer-matrix composite with the same filler at a similar volume fraction. This is indicated by the similarity in the volume resistivity. For example, the volume resistivity is 4.1×10^{-2} Ω cm for a carbon nanofiber (0.1

μm diameter, not graphitized) compact without a binder and with a nanofiber content of 28%, compared to a resistivity of $6.2 \times 10^{-2}\,\Omega\,\mathrm{cm}$ for a dense carbon nanofiber (0.1 μm diameter, not graphitized) polyethersulfone-matrix composite with a nanofiber content of 25% [35].

A high aspect ratio of the filler is also advantageous because of the smaller number of filler–filler contact points. The resistivity of a carbon nanofiber (0.05 μm diameter, with aspect ratio 20–50) compact without a binder is $0.21\,\Omega\,\mathrm{cm}$ at a density of $0.49\,\mathrm{g/cm^3}$, compared to a low value of $0.053\,\Omega\,\mathrm{cm}$ at a density of $0.47\,\mathrm{g/cm^3}$ for the carbon nanofiber (0.1 μm diameter, with aspect ratio 50–200) mentioned above [34]. Furthermore, a conductive filler in the form of particles (e.g., carbon black) is less effective than one in the form of fibers (e.g., carbon nanofiber) at providing a porous material of low resistivity.

In the case of a porous carbon with a discontinuous carbon fiber, the length of the fiber matters greatly. As shown for a carbon matrix (with pitch as the precursor), the longer the fiber, the higher (i) the mean pore size, (ii) the specific geometric surface area (surface area per unit volume), (iii) the porosity, and (iv) the resistivity of the resulting porous carbon [36].

7.12.2 Porous Conductors With a Nonconductive Filler and a Conductive Additive

In the presence of a nonconductive filler, which provides the necessary function for the porous conductor, a conductive additive is necessary. Only a small amount of the conductive additive is applied, but it needs to provide a continuous conductive path. Carbon black is even more effective than carbon nanofiber as a conductive additive because of its squishability, which stems from its presence in the form of porous agglomerates of nanoparticles, and which facilitates the formation of a continuous conductive path. The carbon black is squished between adjacent nonconductive filler particles (60 μm manganese dioxide particles) during the compaction. This contrasts sharply with the case where the nonconductive filler is absent (Sect. 7.11.1). In the absence of a nonconductive filler, the squishability of the conductive filler is much less important.

An increase in the amount of binder can increase or decrease the resistivity of a porous conductor, depending on the particular conductive filler used. This has been shown when manganese dioxide particles (60 μm) were used as the nonconductive filler and PVDF (5 μm particles) as the binder [37]. When carbon black (0.05 μm particles), which is squishable, is used as the conductive additive, decreasing the amount of binder from 10 to 6 wt.% decreases the resistivity slightly. However, when the conductive additive is natural graphite powder (27 μm particles), the resistivity increases greatly when the binder amount is decreased. This is attributed to the positive influence of the binder on the conductive additive dispersion when the filler is not squishable. The lower the degree of conductive additive dispersion, the higher the resistivity of the porous conductor. In other words, a particulate filler that is not squishable needs the binder to aid its dispersion. When the conductive additive is carbon nanofibers (0.1 μm diameter), which

are not squishable but have high aspect ratios, decreasing the amount of binder results in a moderate increase in the resistivity.

Review Questions

1. Why is graphite a good electrical conductor in the planes of the carbon layers, but a poor electrical conductor perpendicular to the layers?
2. Why does the electrical resistivity of a metal increase with increasing temperature?
3. Why does the contact electrical resistivity of the interlaminar interface of a carbon fiber (continuous) epoxy-matrix composite decrease with increasing temperature?
4. Why is a conductor with an electrical resistance that is too high ineffective for resistance heating?
5. Why is a metal typically a poor thermoelectric material (i.e., one with a low value of ZT)?
6. Why is a polymer typically a poor thermoelectric material (i.e., one with a low value of ZT)?
7. Which parts of an electronic package can benefit from using a metal-matrix composite with a low thermal expansion and high thermal conductivity?
8. What is the function of glass frit (i.e., glass particles) in a thick-film electrical conductor paste?
9. Describe a process for making a multilayer ceramic chip carrier.
10. What is the main application of a z-axis conductor film?
11. Thermally conducting but electrically insulating polymer-matrix composites are useful for which aspects of electronic packaging?
12. Give an example of each of the following:
    a. A z-axis conductor
    b. An electrically conductive thick-film paste.
13. The following materials are used in electronic packaging. For each material, describe the properties that make it useful for electronic packaging.
    a. Kovar
    b. Silver-epoxy
    c. BN-epoxy.
14. What is the main advantage of a surface-mounting type of electronic package compared to a pin-inserting type of package?
15. What are the three main ingredients of a printed circuit board?

16. What are the two attractive properties of metal-matrix composites that make them useful for electronic packaging applications?
17. Why are ceramics that can be sintered at temperatures of below 1,000°C attractive for electronic packaging?
18. What are the two main problems with soldered joints in an electronic package?
19. What are the two main criteria that govern the effectiveness of a *z*-axis conductor?

References

[1] S. Wang, S. Wen and D.D.L. Chung, "Resistance Heating Using Electrically Conductive Cements", *Adv. Cem. Res.* 16(4), 161–166 (2004).

[2] A. Fosbury, S. Wang, Y.F. Pin and D.D.L. Chung, "The Interlaminar Interface of a Carbon Fiber Polymer-Matrix Composite as a Resistance Heating Element", *Compos. Part A* 34, 933–940 (2003).

[3] S. Wang, D.P. Kowalik and D.D.L. Chung, "Self-Sensing Attained in Carbon Fiber Polymer-Matrix Structural Composites by Using the Interlaminar Interface as a Sensor", *Smart Mater. Struct.* 13(3), 570–592 (2004).

[4] S. Wen and D.D.L. Chung, "Carbon Fiber-Reinforced Cement as a Thermistor," *Cem. Concr. Res.* 29(6), 961–965 (1999).

[5] J. Cao and D.D.L. Chung, "Damage Evolution During Freeze-Thaw Cycling of Cement Mortar, Studied by Electrical Resistivity Measurement", *Cem. Concr. Res.* 32(10), 1657–1661 (2002).

[6] X. Wang and D.D.L. Chung, "Self-Monitoring of Fatigue Damage and Dynamic Strain in Carbon Fiber Polymer-Matrix Composite," *Compos. Part B* 29(1), 63–73 (1998).

[7] S. Wang, D.D.L. Chung and J.H. Chung, "Impact Damage of Carbon Fiber Polymer-Matrix Composites, Monitored by Electrical Resistance Measurement", *Compos. Part A* 36, 1707–1715 (2005).

[8] S. Wang and D.D.L. Chung, "Self-Sensing of Flexural Strain and Damage in Carbon Fiber Polymer-Matrix Composite by Electrical Resistance Measurement", *Carbon* 44(13), 2739–2751 (2006).

[9] D. Wang and D.D.L. Chung, "Through-Thickness Stress Sensing of Carbon Fiber Polymer-Matrix Composite by Electrical Resistance Measurement", *Smart Mater. Struct.* 16, 1320–1330 (2007).

[10] S. Wang and D.D.L. Chung, "The Interlaminar Interface of a Carbon Fiber Epoxy-Matrix Composite as an Impact Sensor", *J. Mater. Sci.* 40, 1863–1867 (2005).

[11] S. Wen and D.D.L. Chung, "Strain Sensing Characteristics of Carbon Fiber Reinforced Cement", *ACI Mater. J.* 102(4), 244–248 (2005).

[12] S. Zhu and D.D.L. Chung, "Theory of Piezoresistivity for Strain Sensing in Carbon Fiber Reinforced Cement Under Flexure", *J. Mater. Sci.* 42(15), 6222–6233 (2007).

[13] S. Wen and D.D.L Chung, "Self-Sensing of Flexural Damage and Strain in Carbon Fiber Reinforced Cement and Effect of Embedded Steel Reinforcing Bars", *Carbon* 44(8), 1496–1502 (2006).

[14] G.J. Snyder, E.C. Toberer, "Complex Thermoelectric Materials", *Nature Mater.* 7, 105 (2008).

[15] T.M. Tritt, H. Boettner, L. Chen, "Thermodynamics: Direct Solar Thermal Energy Conversion", *MRS Bull.* 33, 366 (2008).

[16] B. Poudel, Q. Hao, Y. Ma, Y. Lan, A. Minnich, B. Yu, X. Yan, D. Wang, A. Muto, D. Yashaee, X. Chen, J. Liu, M.S. Dresselhaus, G. Chen, Z. Ren, "High-Thermoelectric Performance of Nanostructured Bismuth Antimony Telluride Bulk Alloys", *Science* 320, 634 (2008).

[17] R. Venkatasubramanian, E. Siivola, T. Colpitts, B. O'Quinn, "Thin-Film Thermoelectric Devices with High Room-Temperature Figure of Merit", *Nature* 413, 597 (2001).

[18] H. Ohta, S. Kim, Y. Mune, T. Mizoguchi, K. Nomura, S. Ohta, T. Nomura, Y. Nakanishi, Y. Ikuhara, M. Hirano, H. Hosono, K. Koumoto, "Giant Thermoelectric Seebeck Coefficient of a Two-Dimensional Electron Gas in $SrTiO_3$", *Nat. Mater.* 6, 129 (2007).

[19] O. Yamashita, H. Odahara, "Effect of the Thickness of Bi-Te Compound and Cu Electrode on the Resultant Seebeck Coefficient in Touching Cu/Bi-Te/Cu Composites", *J. Mater. Sci.* 42, 5057 (2007).

[20] O. Yamashita, K. Satou, H. Odahara, S. Tomiyoshi, "Enhancement of the Thermoelectric Figure of Merit in $M/T/M$ (M = Cu or Ni and $T = Bi_{0.88}Sb_{0.12}$) Composite Materials" *J. Appl. Phys.* 98, 073707 (2005).
[21] V. H. Guerrero, S. Wang, S. Wen, D.D.L. Chung, "Thermoelectric Property Tailoring by Composite Engineering", *J. Mater. Sci.* 37(19), 4127–4136 (2002).
[22] S. Han, S. Wang, D.D.L. Chung, *SAMPE Fall Tech. Conf.*, 2009. [9]
[23] G.-D. Zhan, J.D. Kuntz, A.K. Mukherjee, P. Zhu, K. Koumoto, "Thermoelectric Properties of Carbon Nanotube/Ceramic Nanocomposites", *Scr. Mater.* 54, 77 (2006).
[24] X. Shui and D.D.L. Chung, "Submicron Diameter Nickel Filaments and Their Polymer-Matrix Composites", *J. Mater. Sci.* 35, 1773–1785 (2000).
[25] L. Li and D.D.L. Chung, "Effect of Viscosity on the Electrical Properties of Conducting Thermoplastic Composites Made by Compression Molding of a Powder Mixture", *Polym. Compos.* 14(6), 467–472 (1993).
[26] L. Li and D.D.L. Chung, "Electrically Conducting Powder Filled Polyimidesiloxane", *Composites* 22(3), 211–218 (1991).
[27] P.-W. Chen, X. Fu, and D.D.L. Chung, "Microstructural and Mechanical Effects of Latex, Methylcellulose and Silica Fume on Carbon Fiber Reinforced Cement", *ACI Mater. J.* 94(2), 147–155 (1997).
[28] K.-D. Kim and D.D.L. Chung, "Electrically Conductive Adhesive and Soldered Joints under Compression", *J. Sci. Tech.* 19(11), 1003–1023 (2005).
[29] K.-D. Kim and D.D.L. Chung, "Effect of Heating on the Electrical Resistivity of Conductive Adhesive and Soldered Joints", *J. Electron. Mater.* 31(9), 933–939 (2002).
[30] J. Xiao and D.D.L. Chung, "Thermal and Mechanical Stability of Electrical Conductive Adhesive Joints", *J. Electron. Mater.* 34(5), 625–629 (2005).
[31] S. Wang, D.S. Pang and D.D.L. Chung, "Hygrothermal Stability of Electrical Contacts Made from Silver and Graphite Electrically Conductive Pastes", *J. Electron. Mater.* 36(1), 65–74 (2007).
[32] C.-K. Leong and D.D.L. Chung, "Improving the Electrical and Mechanical Behavior of Electrically Conductive Paint by Partial Replacement of Silver by Carbon Black", *J. Electron. Mater.* 35(1), 118–122 (2006).
[33] C.-K. Leong and D.D.L. Chung, "Pressure Electrical Contact Improved by Carbon Black Paste", *J. Electron. Mater.* 33(3), 203–206 (2004).
[34] X. Shui and D.D.L. Chung, "Electrical Resistivity of Submicron-Diameter Carbon-Filament Compacts", *Carbon* 39 (ER11), 1717–1722 (2001).
[35] D.D.L. Chung, "Comparison of Submicron Diameter Carbon Filaments and Conventional Carbon Fibers as Fillers in Composite Materials", *Carbon* 39(8), 1119–1125 (2001).
[36] X. Shui and D.D.L. Chung, "High-Strength High-Surface-Area Porous Carbon Made From Submicron-Diameter Carbon Filaments," *Carbon* 34(6), 811–814 (1996); 34(9), 1162 (1996).
[37] W. Lu and D.D.L. Chung, "A Comparative Study of Carbons for Use as an Electrically Conducting Additive in the Manganese Dioxide Cathode of an Electrochemical Cell", *Carbon* 40 (ER3), 447–449 (2002).

Further Reading

J. Cao and D.D.L. Chung, "Microstructural Effect of the Shrinkage of Cement-Based Materials During Hydration, as Indicated by Electrical Resistivity Measurement", *Cem. Concr. Res.* 34(10), 1893–1897 (2004).
D.D.L. Chung, "Electrical Behavior of Solids," *J. Educ. Mod. Mat. Sci. Eng.* 2, 747 (1980).
D.D.L. Chung, "Thermal Analysis of Carbon Fiber Polymer-Matrix Composites by Electrical Resistance Measurement", *Thermochim. Acta* 364, 121–132 (2000).
D.D.L. Chung, "Continuous Carbon Fiber Polymer-Matrix Composites and Their Joints, Studied by Electrical Measurements", *Polym. Compos.* 22(2), 250–270 (2001).
D.D.L. Chung, "Thermal Analysis by Electrical Resistivity Measurement", *J. Therm. Anal. Calorim.* 65, 153–165 (2001).

D.D.L. Chung, "Piezoresistive Cement-Based Materials for Strain Sensing", *J. Intell. Mater Syst. Struct.* 13(9), 599–609 (2002).
D.D.L. Chung, "Damage in Cement-Based Materials, Studied by Electrical Resistance Measurement", *Mater. Sci. Eng. R* 42(1), 1–40 (2003).
D.D.L. Chung, "Self-Heating Structural Materials", *Smart Mater. Struct.* 13(3), 562–565 (2004).
D.D.L. Chung, "Electrically Conductive Cement-Based Materials", Adv. Cem. Res. 16(4), 167–176 (2004).
D.D.L. Chung, "Electrical Applications of Carbon Materials", *J. Mater. Sci.* 39(8), 2645–2661 (2004).
D.D.L. Chung, "Dispersion of Short Fibers in Cement", *J. Mater. Civil Eng.* 17(4), 379–383 (2005).
D.D.L. Chung, "Damage Detection Using Self-Sensing Concepts" (Invited Review), *J. Aerosp. Eng. (Proc. Inst. Mech. Eng., Part G)* 221(G4), 509–520 (2007).
V.H. Guerrero, S. Wang, S. Wen and D.D.L. Chung, "Thermoelectric Property Tailoring by Composite Engineering", *J. Mater. Sci.* 37(19), 4127–4136 (2002).
D. Wang and D.D.L. Chung, "Through-Thickness Stress Sensing of Carbon Fiber Polymer-Matrix Composite by Electrical Resistance Measurement", *Smart Mater. Struct.* 16, 1320–1330 (2007).
S. Wang and D.D.L. Chung, "The Interlaminar Interface of a Carbon Fiber Epoxy-Matrix Composite as an Impact Sensor", *J. Mater. Sci.* 40, 1863–1867 (2005).
S. Wang and D.D.L. Chung, "Negative Piezoresistivity in Continuous Carbon Fiber Epoxy-Matrix Composite", *J. Mater. Sci.* 42(13), 4987–4995 (2007).
S. Wen and D.D.L. Chung, "Strain Sensing Characteristics of Carbon Fiber Reinforced Cement", *ACI Mater. J.* 102(4), 244–248 (2005).
S. Wen and D.D.L. Chung, "Spatially Resolved Self-Sensing of Strain and Damage in Carbon Fiber Cement", *J. Mater. Sci.* 41(15), 4823–4831 (2006).
S. Wen and D.D.L. Chung, "Model of Piezoresistivity in Carbon Fiber Cement", *Cem. Concr. Res.* 36(10), 1879–1885 (2006).
S. Wen and D.D.L. Chung, "Double Percolation in the Electrical Conduction in Carbon Fiber Reinforced Cement-Based Materials", *Carbon* 45(2), 263–267 (2007).
S. Wen and D.D.L. Chung, "Electrical-Resistance-Based Damage Self-Sensing in Carbon Fiber Reinforced Cement", *Carbon* 45(4), 710–716 (2007).
S. Wen and D.D.L. Chung, "Piezoresistivity-Based Strain Sensing in Carbon Fiber Reinforced Cement", *ACI Mater. J.* 104(2), 171–179 (2007).
D.C. Wobschall and D.D.L. Chung, "Ohmmeters", *The Encyclopedia of Electrical and Electronics Engineering*, Wiley, New York, 1999, vol. 15, pp. 122–123.
S. Zhu and D.D.L. Chung, "Analytical Model of Piezoresistivity for Strain Sensing in Carbon Fiber Polymer-Matrix Structural Composite under Flexure", *Carbon* 45(8), 1606–1613 (2007).
S. Zhu and D.D.L. Chung, "Theory of Piezoresistivity for Strain Sensing in Carbon Fiber Reinforced Cement Under Flexure", *J. Mater. Sci.* 42(15), 6222–6233 (2007).
S. Zhu and D.D.L. Chung, "Numerical Assessment of the Methods of Measurement of the Electrical Resistance in Carbon Fiber Reinforced Cement", *Smart Mater. Struct.* 16, 1164–1170 (2007).

8 Thermal Properties

This chapter considers composites for thermal applications, including the basic principles related to the thermal behavior of materials. The applications include thermal conduction, heat dissipation, thermal insulation, heat retention, heat storage, rewritable optical discs, and shape-memory actuation.

8.1 Thermal Expansion

Upon heating, the length of a solid typically increases. Upon cooling, its length typically decreases. This phenomenon is known as thermal expansion.

The coefficient of thermal expansion (CTE, also abbreviated to α) is defined as

$$\alpha = (1/L_o)(\Delta L/\Delta T) , \tag{8.1}$$

where L_o is the original length and L is the length at temperature T. In other words, α is the fractional change in length per unit change in temperature (i.e., strain per unit change in temperature). Equation 8.1 can be rewritten as

$$\Delta L/L_o = \alpha \Delta T . \tag{8.2}$$

Thermal expansion is reversible, so thermal contraction occurs upon cooling, and the extent of thermal contraction is also governed by α.

The change in dimensions that occurs upon changing the temperature may be undesirable when the dimensional change results in thermal stress; i.e., internal stress associated with the fact that the dimensions are not the same as those the component should have when it is not constrained. An example concerns a joint between two components that exhibit different thermal expansion coefficients. The joint is created at a given temperature. Subsequent to the bonding, the joint is heated or cooled. Upon heating or cooling, the bonding constrains the dimensions of both components, thus causing both components to be unable to attain the dimensions that they would do if they were not bonded. When the thermal stress is too high, deformation such as warpage may occur. Debonding can even occur. If thermal cycling occurs, the thermal stress is cycled, thus resulting in thermal fatigue when the number of thermal cycles is sufficiently high.

Thermal expansion can be advantageously used to obtain a tight fit between two components. For example, a pipe (preferably one with a rather high coefficient of

thermal expansion) is cooled and then, in the cold state, inserted into a larger pipe. Upon subsequent warming of the inner pipe, thermal expansion causes a tight fit between the two pipes.

The energy associated with a bond depends on the bond distance (i.e., the bond length), as shown in Fig. 8.1a. The energy is lowest at the equilibrium bond distance. The curve of energy vs. bond distance takes the shape of a trough that is asymmetric. The higher the temperature, the higher is the energy, and the average bond distance (the midpoint of the horizontal line cutting across the energy trough) increases. Thermal expansion stems from the increasing amplitude of thermal vibrations with increasing temperature and the greater ease of outward vibration (bond lengthening) than inward vibration (bond shortening), reflecting the asymmetry in the energy versus bond length curve. This asymmetry causes the distance QR to be greater than the distance QP in Fig. 8.1b, so that the outward vibration travels a greater distance than the inward vibration at a given temperature. The depth of the energy trough below the energy of zero is the bond energy. At the energy minimum, the bond length is the equilibrium value. A weaker bond has a lower bond energy and corresponds to greater asymmetry in the energy trough. Greater asymmetry means a higher value of the CTE. Hence, weaker bonding tends to give a higher CTE.

Table 8.1 shows that the CTE tends to be high for polymers, medium for metals, and low for ceramics. This reflects the weak intermolecular bonding in polymers,

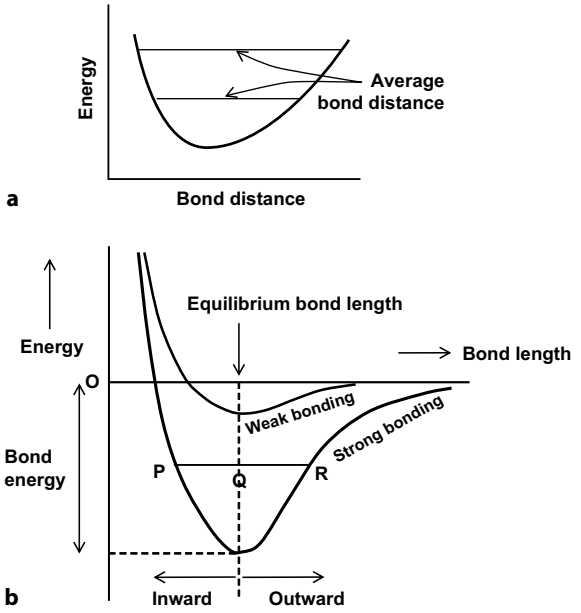

Figure 8.1. Dependence of the energy between two atoms on the distance between the atoms. **a** The average bond distance, which occurs at the midpoint of the horizontal line across the energy trough at a given energy, increases with increasing energy. **b** Comparison of a solid with strong bonding and one with weak bonding. The equilibrium bond length occurs at the minimum energy

Table 8.1. Coefficients of thermal expansion (CTEs) of various materials at 20°C

Material	CTE (10^{-6}/K)
Rubber[a]	77
Polyvinyl chloride[a]	52
Lead[b]	29
Magnesium[b]	26
Aluminum[b]	23
Brass[b]	19
Silver[b]	18
Stainless steel[b]	17.3
Copper[b]	17
Gold[b]	14
Nickel[b]	13
Steel[b]	11.0–13.0
Iron[b]	11.1
Carbon steel[b]	10.8
Platinum[b]	9
Tungsten[b]	4.5
Invar (Fe-Ni36)[b]	1.2
Concrete[c]	12
Glass[c]	8.5
Gallium arsenide[c]	5.8
Indium phosphide[c]	4.6
Glass, borosilicate[c]	3.3
Quartz (fused)[c]	0.59
Silicon	3
Diamond	1

[a] Polymer; [b] metal; [c] ceramic

the moderately strong metallic bonding in metals, and the strong ionic/covalent bonding in ceramics. Silicon and diamond are not ceramics, but their CTE values are low because they are covalent network solids. Because stronger bonding tends to give a higher melting temperature, a lower CTE tends to correlate with a higher melting temperature. This is why tungsten, with a very high melting temperature of 3,410°C, has a low CTE of 4.5×10^{-6}/K. In contrast, magnesium, with a low melting temperature of 660°C, has a high CTE of 23. Invar (Fe-Ni36) has an exceptionally low CTE among metals because of its magnetic character (due to the iron part of the alloy) and the effect of the magnetic moment on the volume. Among ceramics, quartz has a particularly low CTE due to its three-dimensional network of covalent/ionic bonding. Glass has a higher CTE than quartz due to its lower degree of networking.

The CTE of a composite can be calculated from those of its components. When the components are placed in series, as illustrated in Fig. 8.2a, the change in length ΔL_c of the composite is given by the sum of the changes in the lengths of the components:

$$\Delta L_c = \Delta L_1 + \Delta L_2 \,, \tag{8.3}$$

where ΔL_1 and ΔL_2 are the changes in the lengths of the components. Only two components are shown in the summation in Eq. 8.3 for the sake of simplicity. Dividing by the original length L_{co} of the composite gives

$$\Delta L_c/L_{co} = \Delta L_1/L_{co} + \Delta L_2/L_{co} = \nu_1 \Delta L_1/L_{1o} + \nu_2 \Delta L_2/L_{2o} \,, \tag{8.4}$$

where L_{1o} and L_{2o} are, respectively, the original lengths of component 1 (all of the strips of component 1 together) and component 2 (all the strips of component 2 together), and ν_1 and ν_2 are the volume fractions of components 1 and 2, respectively. In Eq. 8.4, the relations

$$L_{1o} = \nu_1 L_{co} \,, \tag{8.5}$$

and

$$L_{2o} = \nu_2 L_{co} \tag{8.6}$$

have been used. Using Eq. 8.2, Eq. 8.4 becomes

$$\alpha_c \Delta T = \nu_1 \alpha_1 \Delta T + \nu_2 \alpha_2 \Delta T \,, \tag{8.7}$$

where α_c is the CTE of the composite and α_1 and α_2 are the CTEs of components 1 and 2, respectively. Division by ΔT gives

$$\alpha_c = \nu_1 \alpha_1 + \nu_2 \alpha_2 \,. \tag{8.8}$$

Equation 8.8 is the rule of mixtures expression for the CTE of the composite in the case of the series configuration shown in Fig. 8.2a.

For the parallel configuration of Fig. 8.2b, when the component strips are perfectly bonded to one another, the two components are constrained so that their lengths are the same at any temperature. This constraint causes each component

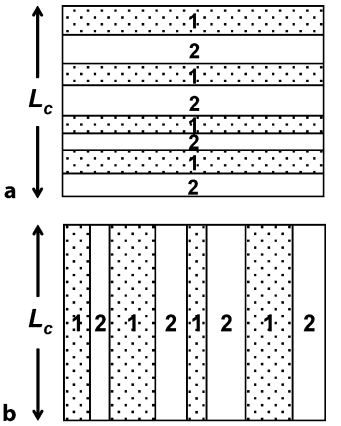

Figure 8.2. Calculation of the CTE of a composite with two components, labeled 1 and 2. **a** Series configuration, **b** parallel configuration

to be unable to change its length by the amount dictated by its CTE (Eq. 8.2). As a result, each component experiences a thermal stress. The component that expands more than the amount indicated by its CTE experiences thermal stress that is tensile, whereas the component that expands less than the amount indicated by its CTE experiences thermal stress that is compressive. The thermal stress is equal to the thermal force divided by the cross-sectional area. In the absence of an applied force,

$$F_1 + F_2 = 0 \,, \tag{8.9}$$

where F_1 and $F_2$are the thermal forces in component 1 (all of the strips of component 1 together) and component 2 (all of the strips of component 2 together), respectively. Hence,

$$F_1 = -F_2 \,. \tag{8.10}$$

Since force is the product of stress and cross-sectional area, Eq. 8.10 can be written as

$$U_1 v_1 A = U_2 v_2 A \,, \tag{8.11}$$

where U_1 and U_2 are the stresses in components 1 and 2, respectively, and A is the area of the overall composite. Dividing by A gives

$$U_1 v_1 = U_2 v_2 \,. \tag{8.12}$$

Using Eq. 8.2, the strain in component 1 is given by $(\alpha_c - \alpha_1)\Delta T$ and the strain in component 2 is given by $(\alpha_c - \alpha_2)\Delta T$. Since stress is the product of the strain and the modulus, Eq. 7.12 becomes

$$(\alpha_c - \alpha_1)\Delta T M_1 v_1 = -(\alpha_c - \alpha_2)\Delta T M_2 v_2 \,, \tag{8.13}$$

where M_1 and M_2 are the elastic moduli of components 1 and 2, respectively. Dividing Eq. 8.13 by ΔT gives

$$(\alpha_c - \alpha_1) M_1 v_1 = -(\alpha_c - \alpha_2) M_2 v_2 \,. \tag{8.14}$$

Rearrangement gives

$$\alpha_c = (\alpha_1 M_1 v_1 + \alpha_2 M_2 v_2)/(M_1 v_1 + M_2 v_2) \,. \tag{8.15}$$

Equation 8.15 is the rule of mixtures expression for the CTE of a composite in the parallel configuration.

In the case that $M_1 = M_2$, Eq. 8.15 becomes

$$\alpha_c = (\alpha_1 v_1 + \alpha_2 v_2)/(v_1 + v_2) = \alpha_1 v_1 + \alpha_2 v_2 \,, \tag{8.16}$$

since

$$v_1 + v_2 = 1 \,. \tag{8.17}$$

If there are three components instead of two components in the composite, Eq. 8.9 becomes

$$F_1 + F_2 + F_3 = 0 \,, \tag{8.18}$$

and Eq. 8.17 becomes

$$v_1 + v_2 + v_3 = 1 \,, \tag{8.19}$$

but the method of deriving the rule of mixtures expression is the same.

8.2 Specific Heat

The heat capacity of a material is defined as the heat energy required to increase the temperature of the entire material by 1°C. The units of specific heat are commonly $\mathrm{J\,K^{-1}}$. The specific heat (also known as the specific heat capacity) is defined as the heat energy required to increase the temperature of a unit mass of the material by 1°C. The units of specific heat are commonly $\mathrm{J\,g^{-1}\,K^{-1}}$. Hence, the specific heat is the heat capacity divided by the mass of the material. However, this distinction between heat capacity and specific heat is not strictly followed by many authors.

The specific heat of a composite can be calculated from those of the components of the composite. Consider that the composite has a component 1 of specific heat c_1 and mass fraction f_1, and a component 2 of specific heat c_2 and mass fraction f_2. Let M be the total mass of the composite. Hence, the mass of component 1 is $f_1 M$, and the mass of component 2 is $f_2 M$. The heat absorbed per K rise in temperature is $c_1 f_1 M$ for component 1, and is $c_2 f_2 M$ for component 2.

The specific heat c_c of the composite is the total heat absorbed per °C rise in temperature divided by the total mass. Hence,

$$c_\mathrm{c} = (c_1 f_1 M + c_2 f_2 M)/M = c_1 f_1 + c_2 f_2 \,. \tag{8.20}$$

Equation 8.20 implies that the specific heat of the composite is the weighted average of the specific heats of the components, where the weighting factors are the mass fractions of the components. This equation is a manifestation of the rule of mixtures. Note that the derivation of this equation does not require any particular distribution of the two components.

Kinetic energy is stored in a material through the vibrations of the crystal lattice and molecules and the rotations of molecules. Each way of vibrating or rotating is said to be a degree of freedom. Heat is needed to increase the temperature of a material because the kinetic energy per degree of freedom needs to increase as the temperature increases. The more degrees of freedom, the greater the specific heat of the material. Figure 8.3 shows the various vibrational modes in graphite.

For solids, the specific heat refers to that at a constant pressure (abbreviated c_p), unless noted otherwise. This is because the pressure is usually fixed when using solid materials.

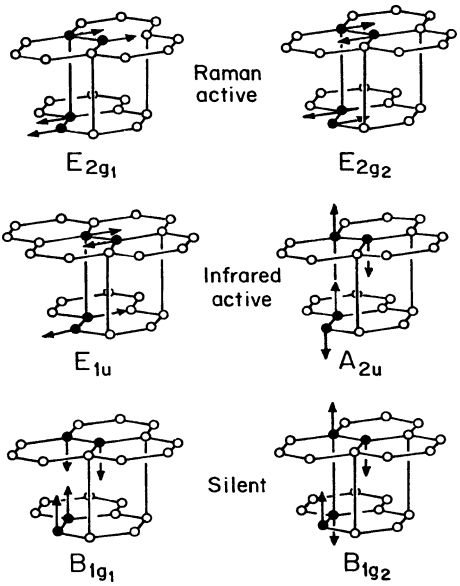

Figure 8.3. Various modes of vibration in graphite

Table 8.2. Specific heat values (c_p) of various materials

Material	c_p ($J\,g^{-1}\,K^{-1}$)
Water (25°C)	4.1813
Ice (−10°C)	2.050
Paraffin wax	2.5
Magnesium	1.02
Aluminum	0.897
Graphite	0.710
Diamond	0.5091
Glass	0.84
Silica (fused)	0.703

Table 8.2 shows a comparison of the c_p values for various materials. c_p is higher for water than ice. This is because there are more degrees of freedom for vibrations/rotations in the liquid, which has a disordered structure, than in the ordered structure of ice. c_p of paraffin wax is higher than that of ice, due to the disordered structure of solid wax, which is a molecular solid. Magnesium has a higher c_p than aluminum (which is next to magnesium in the periodic table of the elements), because it has a hexagonal crystal structure. In contrast, aluminum has a cubic (fcc) crystal structure. A hexagonal structure is less symmetrical than a cubic structure, resulting in more modes of lattice vibration. Similarly, graphite (hexagonal) has a higher c_p than diamond (cubic), even though graphite and diamond are both 100% carbon. Glass has a higher c_p than fused silica due to the lower degree of

three-dimensional networking in glass, meaning that there are more degrees of freedom for vibrations.

A material with a high specific heat may be used for thermal energy storage. An increase in temperature causes the storage of energy (which is the energy needed to raise the temperature of the material), while a decrease in temperature causes the release of this stored energy. A building should be designed to have a high heat capacity (known as the thermal mass in this context, so as to be distinguished from the specific heat) so that the temperature of the building does not change readily as the outdoor temperature changes. Thus, building materials of high specific heat are valuable. They include gypsum ($1.09, \mathrm{J\,g^{-1}\,K^{-1}}$), asphalt ($0.92, \mathrm{J\,g^{-1}\,K^{-1}}$), concrete ($0.88, \mathrm{J\,g^{-1}\,K^{-1}}$) and brick ($0.84, \mathrm{J\,g^{-1}\,K^{-1}}$).

8.3 Phase Transformations

8.3.1 Scientific Basis

A phase is a physically homogeneous region of matter. Different phases differ in structure. For example, ice and liquid water are different phases due to their different structures. A phase transformation, also known as a phase transition, refers to the change in phase upon changing the temperature/pressure. For example, the melting of ice to form liquid water is a phase transition. A phase transition is usually reversible. Indeed, liquid water freezes upon cooling.

The melting temperature limits the applicable temperature range of a solid material. However, below the melting temperature, there can be other limits. In the case of a solid that is at least partially amorphous (i.e., not completely crystalline) and an application in which high stiffness is required, the glass transition temperature (T_g) is a temperature limit. Upon heating, a solid that is at least partially amorphous softens (i.e., the modulus reduces) at T_g, because the amorphous part in it softens. The softening at T_g is due to the movements of the constituent molecules, ions or atoms above T_g. Below T_g, there is not enough thermal energy for such movements to occur. This phase transition is reversible. Upon cooling, the modulus increases at T_g because the molecules, ions or atoms cannot move below T_g. T_g is below the melting temperature.

Amorphous materials (also known as glassy materials and noncrystalline materials) are commonly polymers and ceramics. Metals can be amorphous, but they are usually 100% crystalline. To make an amorphous metal it is necessary to cool the liquid metal at an extremely fast cooling rate so that there is insufficient time for the atoms to order and form a crystalline phase. On the other hand, polymers and ceramics involve ionic/covalent units that are much larger than atoms, and the ordering of these units to form a crystalline phase is relatively difficult. As a result, polymers and ceramics are commonly partially amorphous, if not completely amorphous.

Table 8.3. Glass transition temperatures T_g of various materials

Material	T_g (°C)
Polyethylene (low-density)[a]	−105
Polypropylene (atactic)[a]	−20
Polypropylene (isotactic)[a]	0
Polyvinyl chloride[a]	81
Polystyrene[a]	95
Chalcogenide AsGeSeTe[b]	245
Soda lime glass[b]	520–600
Fused quartz[b]	1,175

[a]Polymer; [b] ceramic

Although the glass transition and melting are distinct phase transitions, both involve the movements of atoms, ions or molecules in the solid. These movements are more extensive during melting than during the glass transition. Therefore, a material that has a high melting temperature tends to have a high T_g.

Table 8.3 lists the T_g values of various polymers and ceramics. The T_g values are higher for ceramics than for polymers. This is consistent with the higher melting temperatures of ceramics.

Among the polymers, polyethylene has a very low T_g because of an absence of functional groups that cause intermolecular interactions, and an absence of bulky side groups. The bulky side groups as well as the intermolecular interactions hinder the sliding of molecules relative to one another. Polyvinyl chloride has a higher T_g because of the chloride functional group in its structure, which promotes intermolecular interactions. Polystyrene has an even higher T_g because of its bulky benzene side group. Isotactic polypropylene (with the $-CH_3$ side groups of different mers on the same side of the polymer molecular chain) has a higher T_g than atactic polypropylene (with the $-CH_3$ side groups of different mers positioned randomly on both sides of the polymer molecular chain) because the former is associated with more order and hence better packing of the molecular chains relative to one another. The better packing hinders the sliding of molecules relative to one another, thus causing a higher T_g.

Isotactic polypropylene is a commonly used thermoplastic polymer. The addition of rubber to it results in a composite that is tough and flexible. Polypropylene–polyethylene copolymers (with two types of mer in the same molecule) are attractive because the presence of the polyethylene component increases the low temperature impact. A shortcoming of polypropylene is its tendency to degrade upon exposure to ultraviolet (UV) radiation. In order to increase the UV resistance, carbon black can be added as a filler that absorbs the UV radiation.

Among ceramics, fused quartz has a higher T_g than soda lime glass. This is consistent with the higher melting temperature of fused quartz.

A chalcogenide is a compound with at least one chalcogen ion (sulfur, selenium or tellurium: all elements in Group IV of the periodic table) and at least one element that is more electropositive. For example, AsGeSeTe is a chalcogenide that has Se

and Te as chalcogens and As and Ge as electropositive elements. Another example is AgInSbTe, where Te is the chalcogen and Ag, In and Sb are the electropositive elements.

The T_g values of chalcogenides make these materials suitable for use in phase-change memory (abbreviated PCM, PRAM, PCRAM, chalcogenide RAM or C-RAM), which is a non-volatile computer memory that functions by switching between crystalline and amorphous states upon heating. Heating can change an amorphous material to a crystalline material because the amorphous state is a metastable state (a state that is not the lowest energy state, though it is not unstable), whereas the crystalline state is the thermodynamically stable state (the state with the lowest energy). On the other hand, the change of a crystalline state to an amorphous state requires melting and then rapid cooling. The cooling must be quick enough to avoid the formation of the crystalline state from the melt.

AgInSbTe is commonly used for rewritable optical discs (CDs). The writing process involves switching from the crystalline state to the amorphous state, which has low reflectivity, thereby storing the information optically. This involves (i) initially erasing the disc by switching the surface to the crystalline state through long, low-intensity laser irradiation (avoiding melting), (ii) heating the spot with short (less than 10 ns) high-intensity laser pulses to achieve local melting, and (iii) rapidly cooling the molten spot to transform it to the amorphous state.

A phase transition is known as a first-order phase transition if it involves the absorption or release of latent heat during the transition. The units of latent heat are joules (J). Latent heat is also known as the heat of transformation. The specific latent heat (often loosely called the latent heat) is the latent heat per unit mass, so its units are J/g. During the transformation, the temperature stays constant as the latent heat is absorbed or released. For example, latent heat of fusion is absorbed during melting and latent heat of solidification is released during freezing. A process that absorbs latent heat is said to be endothermic, while a process that evolves latent heat is said to be exothermic. All spontaneous reactions are exothermic.

The latent heat is due to the difference in heat content (also known as the enthalpy) between the initial and final states of the phase transition. The heat content is higher for the liquid state than for the solid state because the atoms, ions or molecules are slightly more separated in the liquid state than in the solid state, and energy is needed to cause this separation. The greater the energy required to cause the separation, the higher the latent heat of fusion. For the same material, the latent heat of vaporization is much higher than that of fusion. For example, the specific latent heat of fusion of lead is 24.5 J/g, whereas the specific latent heat of vaporization of lead is 871 J/g. This difference is due to the much greater change in the degree of separation required for a liquid to boil (i.e., to change from liquid to vapor, where the vapor has a much lower density than the liquid) than that required for a solid to melt (i.e., to change from solid to liquid; in other words, the density difference between the solid and the liquid is small compared to the density difference between the liquid and the vapor). Latent heat is absorbed when a solid melts and latent heat is released when a solid freezes. The specific latent heat of fusion of carbon dioxide is high (184 J/g), whereas it is low for nitrogen

(25.7 J/g). This is because of the stronger intermolecular attractions in carbon dioxide compared to nitrogen.

A phase transition that does not involve a latent heat is known as a second-order phase transition or a continuous phase transition. The glass transition is an example of such a transition. The glass transition involves no latent heat because there is no difference in heat content between the initial state (the amorphous solid state) and the final state (the softened state). The transition between ferromagnetic and paramagnetic states is another example of a second-order phase transition.

The latent heat associated with a first-order phase transition provides a mechanism for the storage of thermal energy. For example, energy is stored during melting (when the ambient temperature is above the melting temperature) and released during freezing (when the ambient temperature is below the freezing temperature). A material with a melting temperature that is near room temperature and placed outdoors can be used to store energy during the day (when the outside temperature is above room temperature) and release energy during the night (when the outside temperature is below room temperature). Such a material is known as a phase-change material (abbreviated to PCM; note that this should not be confused with phase-change memory, which has the same abbreviation). Wax is an example of a phase-change material.

Due to the difference in kinetics between the melting and freezing transitions, the melting temperature and the freezing temperature may not be equal. Freezing changes a liquid to a crystalline solid, the formation of which requires the ordering of atoms, ions or molecules. The ordering process can be hastened if freezing is allowed to occur on a crystalline solid surface, which serves as a seed for crystallization. Hence, the freezing of a liquid is facilitated by the presence of seed crystals (called nuclei) around which the liquid freezes. Thus, in the absence of nuclei, a liquid can remain a liquid (called a supercooled liquid) below the equilibrium freezing temperature (the freezing temperature in the case of infinitely slow cooling, which provides plenty of time for freezing to take place, and where kinetics do not affect the outcome). For example, droplets of supercooled water in the clouds may change to ice upon being hit by the wings of a passing airplane. The ice formed on the wings can cause problems with lift. Freezing rain is also supercooled water droplets, which become ice upon hitting a solid surface.

The supercooling ΔT is defined as

$$\Delta T = \text{melting temperature} - \text{freezing temperature} . \tag{8.21}$$

When the supercooling is positive, the freezing temperature is below the melting temperature. This is usually due to the sluggishness of the freezing. When the supercooling is negative, the freezing temperature is above the melting temperature. Negative supercooling occurs, but it is not well understood.

8.3.2 Shape Memory Effect

The shape memory effect (Sect. 3.6.3) involves a phase transformation (called a martensitic transformation) that changes the material from the austenite phase

(cubic) to the martensite phase (typically tetragonal). Due to the change in crystal structure, the martensitic transformation is accompanied by twinning, meaning that the martensite that forms from the austenite is heavily twinned, as illustrated in Figs. 8.4 and 8.5.

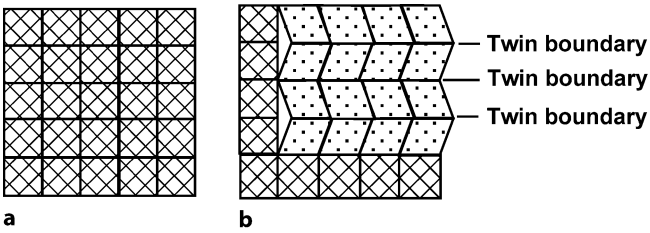

Figure 8.4. **a** Austenite, **b** austenite (*cross-hatched region*) coexisting with martensite (*dotted region*), which is twinned. The change in lattice parameters upon changing from austenite to martensite is exaggerated in (**b**) for the sake of clarity

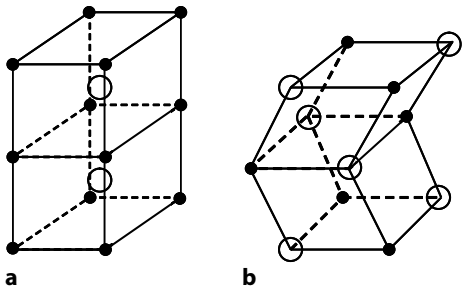

Figure 8.5. Typical crystal structures of a shape memory alloy in the form of an AB compound, with A atoms shown by *solid circles* and B atoms shown by *open circles*. **a** Austenite, **b** twinned martensite, with the twin boundary being the horizontal plane

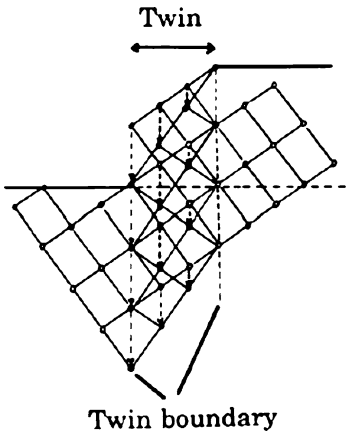

Figure 8.6. The formation of a twin

Twinning refers to the existence of a mirror plane in a material such that the parts of the material adjacent to the mirror plane are mirror images in terms of the positions of the atoms in them, as illustrated in Fig. 8.6, which shows two mirror planes (each of which is called a twin boundary). The region between the two twin boundaries is called the twin, and it differs in structure from the regions outside the twin. The arrows in Fig. 8.6 show the movements of the atoms during the twin formation. The atom movement means deformation (i.e., strain).

The martensite phase is special in that it is highly twinned, thus allowing it to undergo reversible strain that is beyond the elastic limit. This phenomenon is known as pseudoplasticity or superplasticity. If the strain is restrained, stress is provided. Thus, the shape memory effect can be used to provide strain and/or stress; i.e., it serves as an actuator. Upon the subsequent return from the martensite phase to the austenite phase (i.e., the reverse of the martensitic transformation), the original shape (i.e., nearly zero strain) returns.

Figure 3.33a shows pseudoplastic behavior. It involves the use of stress to induce the change from the austenite phase to the martensite phase. Applications include orthodontal braces, bone plates, eyeglass frames, medical tools, cellular phone antennae, and bra underwiring. In case of an orthodontal brace, the brace is installed in a patient in the state corresponding to the upper (loading) plateau in Fig. 3.33a. The lower (unloading) plateau then allows the stress to be maintained at a roughly constant value as the strain is gradually decreased (i.e., as the teeth are gradually pulled together by the brace). It is important for the stress to be maintained during the course of this dental treatment. Similarly, for a bone plate that is used to fasten pieces of broken bones, it is important for the stress to be maintained as the fracture gradually heals.

The martensitic transformation can be induced by cooling instead of the application of stress. After cooling, the martensite phase is deformed to a new shape. The deformation is easy due to the twinned structure of the martensite. Subsequent heating returns the martensite phase to the austenite phase. This change in phase means a return to the shape associated with the original austenite.

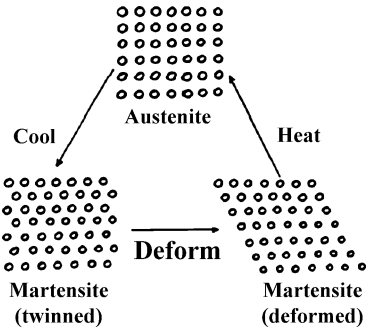

Figure 8.7. The shape memory effect that involves cooling from austenite to form martensite, deformation of the martensite, and then heating to change the martensite back to austenite. The return to the austenite phase brings a return to the shape of the austenite (i.e., the shape prior to the deformation)

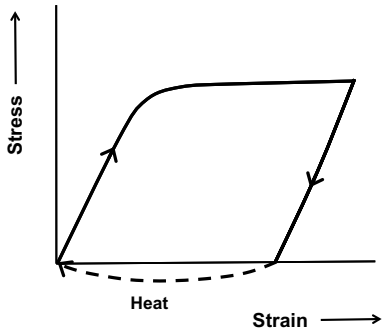

Figure 8.8. The stress–strain curve during the deformation of a shape memory alloy in the form of martensite (below A_s). Heating subsequent to the deformation returns the strain to zero (i.e., the original shape)

The shape memory effect is illustrated in Fig. 8.7, which shows that austenite (the initial phase) transforms to a martensite upon cooling, which is heavily twinned. The martensite is then mechanically deformed to a particular shape. After this, the deformed martensite is heated so that it transforms back to austenite. The reverse transformation is accompanied by a return to the original shape of the austenite (i.e., the shape prior to the deformation). This effect is further illustrated in Fig. 8.8, where the starting point is martensite. The loading part of the stress–strain curve shows the deformation of the martensite. After subsequent unloading, heat is applied to change the martensite back to austenite. This change of phase results in the restoration of the shape of the austenite; i.e., the state prior to deformation (or strain = 0).

As shown in Fig. 8.9, the temperature at which the transformation from austenite to martensite begins upon cooling is denoted M_s. The temperature at which the martensitic transformation is completed upon cooling is denoted M_f. Obviously, M_f is below M_s. The temperature at which the transformation from martensite to austenite begins upon heating is denoted A_s. The temperature at which the transformation from martensite to austenite finishes upon heating is denoted A_f. Again, obviously A_f is above A_s. Due to hysteresis, M_s tends to be less than A_s, though it is usually close to A_s.

Figure 8.8 is the behavior belowA_s, since it describes the deformation of the martensite. If the stress after unloading is continued into the negative regime without heating, ferroelasticity (Fig. 3.33b) results, provided that there are two states of twinning that allow the positive stress plateau and the negative stress plateau.

The values of these four temperatures defined in Fig. 8.9 depend on the stress, as illustrated in Fig. 8.10. Due to the dependence on the stress, at a fixed temperature austenite changes to martensite upon increasing the stress. The pseudoplastic behavior shown in Fig. 3.33a is based on this stress-induced martensitic transformation; it occurs at temperatures above A_f, so that applying stress causes the change from austenite to martensite.

The values of these four temperatures defined in Fig. 8.9 may shift upon repeated use of the shape memory effect. This shift is known as functional fatigue and is due to microstructural changes upon multiple cycles of the effect.

The various manifestations of the shape memory effect are illustrated in Fig. 8.11. These manifestations depend on the temperature. The effect in Fig. 8.11a is the same as that in Fig. 8.8 and occurs at temperatures below A_s, with the deformation shown in the stress–strain curve being that of martensite. The effect shown in Fig. 8.11b occurs at temperatures above A_f (i.e., when the phase is austenite prior to deformation) and relates to pseudoelasticity; it is the same as the effect shown in Fig. 3.33a, except that, for the sake of simplicity, it does not show any degree of strain irreversibility after unloading. The effect in Fig. 8.11c occurs at temperatures between A_s and A_f and shows characteristics that are intermediate between those shown in Fig. 8.11a and b. In this intermediate temperature range, austenite and martensite coexist, with the martensite portion undergoing the effect shown in Fig. 8.11a and the austenite portion undergoing the effect depicted in Fig. 8.11b.

The shape memory effect shown in Fig. 8.8 (i.e., Fig. 8.11a) is valuable for numerous applications. Examples of its application are self-expandable cardiovascular stents, blood clot filters, engines, actuators, flaps that change the direction of air flow depending on the temperature (for air conditioners and aircraft), and couplings. Some of these applications are described below. However, applications to robotics have problems due to energy inefficiency, slow response, and large hysteresis.

A stent is used to reinforce weak vein walls and to widen narrow veins. It can be introduced in a chilled deformed shape; i.e., a scaffold with a relatively small diameter. During deployment, the stent travels through the arteries. After deployment, due to the warmth from the body, the stent expands to the appropriate diameter with sufficient force to open the vessel lumen and reinstate blood flow. Such a stent replaces similar stainless steel stents that are expanded with a little balloon.

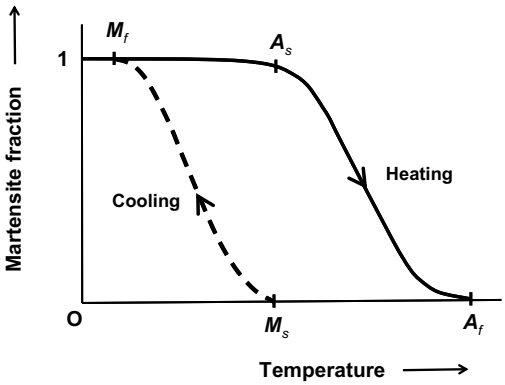

Figure 8.9. Decrease in the martensite fraction during heating, and the increase in this fraction during subsequent cooling

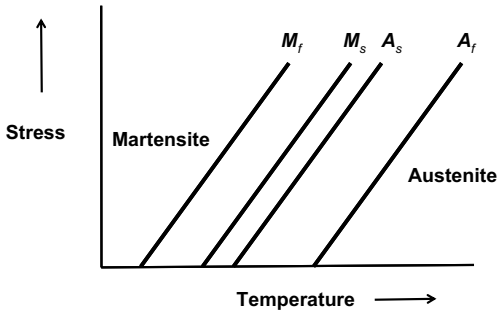

Figure 8.10. Effect of stress on the start and finish temperatures of the change from austenite to martensite (M_s and M_f) and the start and finish temperatures of the change from martensite to austenite (A_s and A_f)

A shape memory coupling for connecting two tubes is placed over the joint area in an expanded state, so that it fits over the tubing (Fig. 8.12a and b). Upon subsequent heating, it shrinks back to its original diameter, thereby squeezing the tubing and providing a tight fit (Fig. 8.12c).

Examples of shape memory alloys (abbreviated to SMAs) are copper-zinc-aluminum, copper-aluminum-nickel and nickel-titanium alloys. NiTi with 50 at.% Ti is known as nitinol, which stands for nickel titanium Naval Ordnance Laboratory (the place where it was discovered). NiTi alloys are generally more expensive and exhibit better mechanical properties than copper-based SMAs. Disadvantages

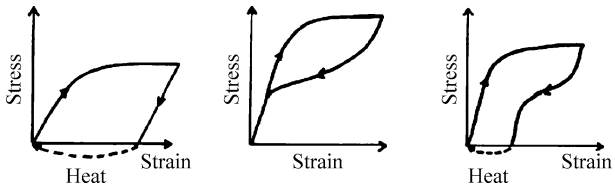

Figure 8.11. Manifestations of the shape memory effect, depending on the temperature. **a** Temperatures below A_s, as shown in Fig. 8.7, **b** temperatures above A_f, as shown in Fig. 3.33a, **c** temperatures between A_s and A_f, showing behavior intermediate between those shown in (**a**) and (**b**)

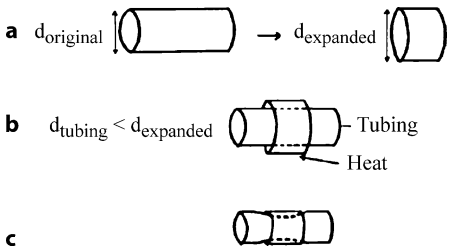

Figure 8.12. The use of the shape memory effect (Fig. 8.7) to achieve a coupling that fits tightly around tubing. **a** Deformation of the martensite to cause expansion of the coupling, **b** fitting the expanded coupling around the tubing, **c** heating to change the martensite back to austenite, thereby restoring the coupling its original, undeformed shape with a smaller diameter

of shape memory alloys include high cost, poor machinability and poor fatigue resistance compared to steel.

8.3.3 Calorimetry

Investigations of phase transitions are commonly conducted by calorimetry, which allows the transition temperature to be measured during heating and cooling, and the latent heat of the transformation during heating and cooling. A first-order transition gives a peak in the heat flow vs. temperature plot such that the area under the peak is the latent heat of the transformation. In contrast, a second-order transition does not give a peak, just a change in slope in this plot, due to the absence of latent heat.

One widely used form of calorimetry is differential scanning calorimetry (DSC), which involves scanning the temperature at a controlled heating/cooling rate, while the temperature of the specimen is kept the same as a reference (typically an empty pan). At a first-order phase transition, the absorption or release of latent heat from the specimen means that the calorimeter must add heat to or remove heat from the specimen in order to maintain the specimen and the reference at the same temperature as the temperature is scanned. The amount of heat applied or removed is the latent heat, which is therefore measured.

An alternative form of DSC involves measuring the temperature difference between the specimen and the reference when the two are subjected to the same constant heating/cooling rate. The higher the heat capacity of the specimen compared to that of the reference, the greater the amount of heat that needs to be applied to the specimen in order to maintain the specimen and reference at the same constant heating/cooling rate. The application of heat gives rise to a small temperature difference between the specimen and the reference.

8.4 Thermal Conductivity

The thermal conductivity (k) is a material property that describes the ability of the material to conduct heat. It is defined as

$$\Delta Q/\Delta t = kA(\Delta T/x) \,, \tag{8.22}$$

where Q is the heat (with units of J), t is the time, $\Delta Q/\Delta t$ is the heat flow (i.e., the amount of heat flowing per unit time), A is the cross-sectional area of the material perpendicular to the direction of heat flow, and ΔT is the temperature difference between the two ends of the material of length x in the direction of heat flow, as illustrated in Fig. 8.13, where one-dimensional heat flow is assumed (i.e., there is no loss of heat to the surrounding). The temperature gradient is $\Delta T/x$. Equation 8.22 means that the thermal conductivity is the heat flow per unit cross-sectional area per unit temperature gradient; i.e., the heat flux per unit temperature gradient. The heat flow per unit cross-sectional area is also called the heat flux. Since W = J/s, the units of k are W/(m K), which are the same as W/(m °C).

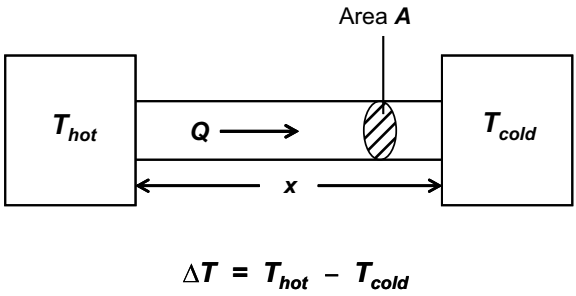

Figure 8.13. Heat flowing from the hot end to the cold end of a material of cross-sectional area *A* and length *x*

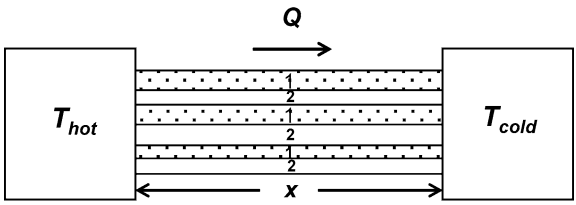

Figure 8.14. A thermal conductor in the form of a composite with components labeled 1 (*dotted regions*) and 2 (*white regions*) in the form of strips that are parallel and oriented in the direction of heat flow

The thermal conductivity of a composite (k_c) can be calculated from the thermal conductivities and volume fractions of each of the components (labeled 1 and 2) in the composite. Consider the case where the components are positioned in parallel, as shown in Fig. 8.14. The heat flow in component 1 (all the strips of component 1 together) plus that in component 2 (all the strips of component 2 together) equals the heat flow in the overall composite. Hence, based on Eq. 8.22,

$$k_1 A_1(\Delta T/x) + k_2 A_2(\Delta T/x) = k_c A(\Delta T/x) \,, \tag{8.23}$$

where k_1 and k_2 are the thermal conductivities of components 1 and 2 respectively, A_1 and A_2 are the cross-sectional areas (all the strips of each component considered together) of components 1 and 2, respectively, and A is the cross-sectional area of the overall composite. Obviously,

$$A = A_1 + A_2 \,. \tag{8.24}$$

Eq. 8.23 can be rewritten as

$$k_c = (k_1 A_1/A) + (k_2 A_2/A) = v_1 k_1 + v_2 k_2 \,, \tag{8.25}$$

where $v_1 = A_1/A$ and is the volume fraction of component 1, and $v_2 = A_2/A$and is the volume fraction of component 2. Equation 8.25 is the rule of mixtures for the parallel configuration.

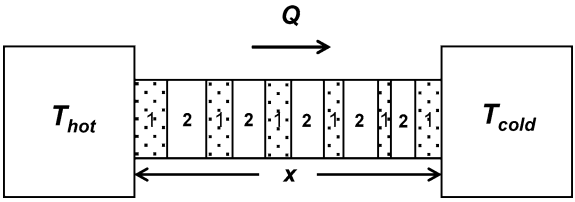

Figure 8.15. A thermal conductor in the form of a composite with components labeled 1 (*dotted regions*) and 2 (*white regions*) in the series configuration; i.e., the components are in the form of strips that are parallel and oriented perpendicular to the direction of heat flow

Next, consider the case where the components are in series, as shown in Fig. 8.15. The temperature difference between the two ends of the composite is given by

$$\Delta T = \Delta T_1 + \Delta T_2 \ , \tag{8.26}$$

where ΔT_1 is the contribution to the temperature difference from component 1 (all the strips of component 1 together) and ΔT_2 is the contribution to the temperature difference from component 2 (all the strips of component 2 together). Based on Eq. 8.22, Eq. 8.26 becomes

$$(\Delta Q/\Delta t)\,[x_1/(k_1 A)] + (\Delta Q/\Delta t)\,[x_2/(k_2 A)] = (\Delta Q/\Delta t)\,[x/(k_c A)] \ , \tag{8.27}$$

assuming that both components have the same cross-sectional area A. Simplification of Eq. 8.27 gives

$$x_1/k_1 + x_2/k_2 = x/k_c \ . \tag{8.28}$$

Dividing by x gives

$$v_1/k_1 + v_2/k_2 = 1/k_c \ , \tag{8.29}$$

where $v_1 = x_1/x$ is the volume fraction of component 1, and $v_2 = x_2/x$ is the volume fraction of component 2. Equation 8.29 is the rule of mixtures for the series configuration.

The thermal resistivity is defined as the reciprocal of the thermal conductivity. Thus, the units of thermal resistivity are m K/W. From Eq. 8.22, the thermal resistivity $1/k$ is given by

$$1/k = [A(\Delta T/x)]/(\Delta Q/\Delta t) \ . \tag{8.30}$$

In other words, the thermal resistivity is the temperature gradient divided by the heat flux.

The thermal resistance is defined as the temperature gradient divided by the heat flow (not flux). Hence, it is given by the thermal resistivity divided by the cross-sectional area A:

$$\text{Thermal resistance} = 1/(kA) = (\Delta T/x)/(\Delta Q/\Delta t) \ . \tag{8.31}$$

The units of thermal resistance are K/(m W). In the series configuration (Fig. 8.14), the thermal resistance of the composite is the weighted sum of the thermal resistances of the two components:

$$v_1/(k_1A) + v_2/(k_2A) = 1/(k_cA) \,, \tag{8.32}$$

which, upon canceling A, is the same as Eq. 8.29.

The conduction of heat can involve the movement of electrons and/or phonons (vibrational waves) from the hot point to the cold point, since electrons and phonons are both associated with kinetic energy. Due to the abundance of mobile electrons in them, metals are good thermal conductors. Diamond and cubic boron nitride are even more thermally conductive than metals in spite of their absence of mobile electrons, as evidenced by the fact that they are electrical insulators. The high thermal conductivities of diamond and cubic boron nitride are due to the high mobility of the phonons in them, which is in turn due to the low masses of the atoms in these materials (carbon in the case of diamond).

The thermal conductivity values of various materials, including both thermal conductors and thermal insulators, are listed in Table 8.4. The best thermal conductors are diamond and cubic boron nitride, but these materials are very expensive. Other than these exceptional materials, the best thermal conductors are metals, particularly silver and copper. Brass (Cu-Zn alloy) has a much lower thermal conductivity than copper due to the zinc alloying element, which causes electron scattering. Similarly, the thermal conductivity is lower for carbon steel than iron due to the carbon alloying element in the steel. Beryllium oxide and aluminum nitride are comparable in terms of thermal conductivity to metals, though their values are much lower than those of cubic boron nitride and diamond. Hexagonal boron nitride is less thermally conductive than aluminum nitride or beryllium oxide. Other than cubic/hexagonal boron nitride, beryllium oxide and aluminum nitride, ceramics are typically thermal insulators rather than thermal conductors because of the inadequate numbers of mobile electrons and phonons in them, as shown by the low thermal conductivities of fused silica, mica, fiberglass, vermiculite (a clay mineral), and perlite (a volcanic glass, mainly comprising SiO_2).

The thermal conductivity of a material varies with the temperature. The values in Table 8.4 are at or near room temperature. For a metal, the free (mobile) electrons govern both the thermal conductivity (k) and the electrical conductivity (σ), which are thus proportional to one another. The relationship, known as the Wiedemann–Franz Law, is

$$k/\sigma = LT \,, \tag{8.33}$$

where T is the temperature in K (Kelvin) and L is a constant equal to 2.44×10^{-8} W·Ω/K^2. Equation 8.33 means that, as the temperature increases, k increases and σ decreases. The increase in k with increasing temperature occurs because the average particle (electron) velocity increases with temperature, and this increase in velocity enhances the forward transport of energy. The decrease in σ with increasing temperature arises because an increase in temperature causes more scattering of the electrons. At low temperatures, a metal tends to be a poor thermal conductor but a good electrical conductor.

For copper at room temperature (25°C = 298 K), $\sigma = 0.596 \times 10^8 \Omega^{-1}\,m^{-1}$ (Table 6.2) and $k = 401\,W/(m\,K)$ (Table 8.4). Substitution of these values into Eq. 8.33 gives $L = 2.26 \times 10^{-8}\,W\,\Omega/K^2$. The theoretical value of L is $2.44 \times 10^{-8}\,W\,\Omega/K^2$.

Metals and graphite are thermally and electrically conductive. Thermal conductors that are electrically insulating are needed for heat dissipation from microelectronics. For example, the encapsulation of an integrated circuit component needs to be electrically insulating, but thermal conductivity will help to dissipate the heat from the electronic package. A combination of high thermal conductivity and high electrical resistivity is provided by diamond, cubic boron nitride, beryllium oxide and aluminum nitride, and to a lesser extent in terms of the thermal conductivity, hexagonal boron nitride.

Table 8.4. Thermal conductivities of various materials, including thermal conductors and thermal insulators

Material	Thermal conductivity (W/(m K))
Diamond	2,000
Boron nitride (cubic)	1,700
Silver	429
Copper	401
Beryllium oxide (BeO)	325
Aluminum	250
Aluminum nitride	140–180
Molybdenum	138
Brass	109
Nickel	91
Iron	80
Cast iron	55
Carbon steel	54
Boron nitride (hexagonal)	33
Monel (Cu-Ni alloy)	26
Alumina	18
Zirconia (yttria stabilized)	2
Carbon	1.7
Fused silica	1.38
Window glass	0.96
Mica	0.71
Nylon 6	0.25
Paraffin wax	0.25
Machine oil	0.15
Straw insulation	0.09
Vermiculite	0.058
Paper	0.05
Rock wool insulation	0.045
Fiberglass	0.04
Styrofoam	0.033
Perlite (1 atm)	0.031
Air	0.024
Perlite (vacuum)	0.00137

8.5 Thermal Conductance of an Interface

An interface is associated with a thermal resistance in the direction perpendicular to the interface. This thermal resistance relates to the temperature difference across the interface per unit heat flow. Its units are K/W. The greater the thermal resistance of the interface, the higher the temperature difference across the interface for the same heat flow. It should be distinguished from the thermal resistance of a volume (which has different units of K/(m W); see Sect. 8.4).

The thermal resistance of an interface is inversely proportional to the area of the interface. Thus, a more scientifically meaningful quantity that is independent of the area of the interface is the thermal resistivity of the interface, defined as

$$\text{Thermal resistivity of interface} = (\text{thermal resistance of interface}) \times (\text{area of interface}) \,. \tag{8.34}$$

In other words, the thermal resistivity of an interface is the temperature difference across the interface per unit heat flux. The units of thermal resistivity are m^2 K/W.

The thermal conductance of an interface is defined as the reciprocal of the thermal resistivity of the interface. Hence, the units of conductance are W/(m^2 K), which are different from the units of W/(m K) for the thermal conductivity of a volume of material (Sect. 8.4).

Consider an interface that consists of two components, labeled 1 and 2, that have interfacial thermal resistivities of ϱ_1 and ϱ_2, respectively, and interfacial areas of A_1 (all the regions of component 1 together) and A_2 (all the regions of component 2 together), respectively, as illustrated in Fig. 8.16. Since the thermal resistance R is the temperature difference ΔT across the interface divided by the heat flow,

$$\text{Heat flow} = \Delta T/R \,. \tag{8.35}$$

The heat flow in component 1 plus that in component 2 equals that in the overall interface. Hence,

$$(\Delta T/R_c) = (\Delta T/R_1) + (\Delta T/R_2) \,, \tag{8.36}$$

where R_1, R_2 and R_c are the thermal resistances of component 1, component 2, and the overall interface respectively. Note that the temperature difference across the interface is the same for components 1 and 2. Simplifying Eq. 8.36 gives

$$1/R_c = (1/R_1) + (1/R_2) \,. \tag{8.37}$$

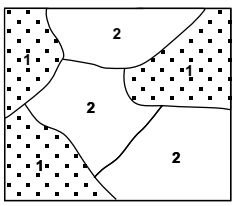

Figure 8.16. An interface in the form of a composite consisting of components labeled 1 (*dotted regions*) and 2 (*white regions*)

Since the thermal resistivity is the thermal resistance multiplied by the area, Eq. 8.37 can be written as

$$A_c/\varrho_c = A_1/\varrho_1 + A_2/\varrho_2 \ , \tag{8.38}$$

where A_1, A_2, and A_c are the areas of component 1, component 2, and the overall interface, respectively. Dividing by A_c gives

$$1/\varrho_c = a_1/\varrho_1 + a_2/\varrho_2 \ , \tag{8.39}$$

where a_1 and a_2 are the area fractions of components 1 and 2, respectively. Equation 8.39 is the rule of mixtures expression for calculating the thermal resistivity of an interface that is a two-dimensional composite. The thermal conductance σ_c of the overall interface is given by

$$\sigma_c = 1/\varrho_c \ . \tag{8.40}$$

Combining Eq. 8.39 and 8.40 gives

$$\sigma_c = a_1/\varrho_1 + a_2/\varrho_2 = a_1\sigma_1 + a_2\sigma_2 \ , \tag{8.41}$$

where $\sigma_1 (= 1/\varrho_1)$ and $\sigma_2 (= 1/\varrho_2)$ are the thermal conductances of components 1 and 2, respectively. Equation 8.41 is the rule of mixtures expression for calculating the thermal conductance of an interface that is a two-dimensional composite.

8.6 Evaluating the Thermal Conduction

The most commonly used methods of evaluating the thermal conduction are the guarded hot plate method (a steady-state method) and the laser flash method (a transient method), as described below.

8.6.1 Guarded Hot Plate Method

Thermal conduction is most commonly evaluated using the guarded hot plate method (ASTM D5470), which involves measuring under a steady-state heat flux. The heat flux is provided by a heated block (e.g., a copper block with heating wires inside) and a cooled block (e.g., a copper block with running water inside). The heat flows from the heated block to the cooled block, as shown in Fig. 8.17. Between the heated block and the cooled block are two smaller conductor blocks made of a thermal conductor such as copper, and labeled conductor I and conductor II in Fig. 8.17. The specimen is sandwiched between conductors I and II. Each conductor has at least two drilled holes for inserting a thermocouple into each hole. In Fig. 8.17, the temperatures T_1 and T_2 are measured in conductor I and the temperatures T_3 and T_4 are measured in conductor II. Due to the thermal insulation surrounding the specimen and conductors I and II, the heat flow is assumed to be one-dimensional, with no loss of heat to the surroundings.

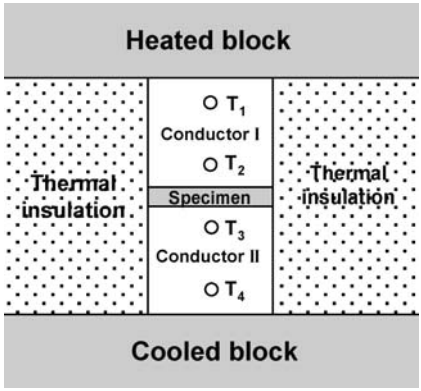

Figure 8.17. Guarded hot plate method of evaluating thermal conduction. The specimen is sandwiched between conductors I and II. Heat flows from the heated block to the cooled block

In an experiment, the equilibrium (state state) is assumed to have been obtained when $T_1 - T_2$ and $T_3 - T_4$ are essentially equal. The heat flow $\Delta Q/\Delta t$ is given by

$$\Delta Q/\Delta t = kA\Delta T/d_A \,, \tag{8.42}$$

where d_A is the distance between thermocouples T_1 and T_2, A is the cross-sectional area of conductor I, and k is the thermal conductivity of conductor I.

The temperature at the bottom of conductor I (i.e., the temperature at the top surface of the specimen) is T_A, which is given by

$$T_A = T_2 - \frac{d_B}{d_A}(T_1 - T_2) \,, \tag{8.43}$$

where d_B is the distance between thermocouple T_2 and the top surface of the specimen. Similarly, the temperature at the bottom surface of the specimen is T_D, which is given by

$$T_D = T_3 + \frac{d_D}{d_C}(T_3 - T_4) \,, \tag{8.44}$$

where d_D is the distance between thermocouple T_3 and the bottom surface of the specimen, and d_C is the distance between thermocouples T_3 and T_4.

The temperature difference between the top and bottom surfaces of the specimen is thus

$$\Delta T = T_A - T_D \,. \tag{8.45}$$

If the thermal resistance of the interface between the specimen and each of conductors I and II is ignored, the thermal resistance R of the specimen is given by

$$R = 1/(kA) = (\Delta T/x)/(\Delta Q/\Delta t) \,, \tag{8.46}$$

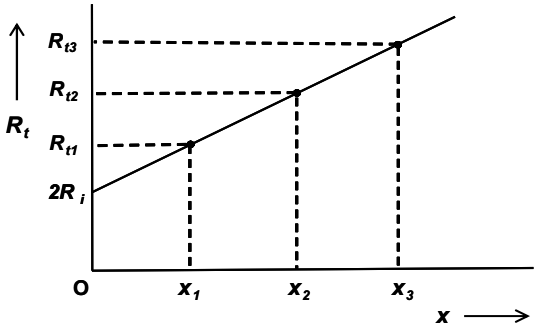

Figure 8.18. Variation of the total thermal resistance R_t with the thickness x

where x is the specimen thickness, ΔT is given by Eq. 8.45, $\Delta Q/\Delta t$ is given by Eq. 8.42, and Eq. 8.31 has been used. The thermal conductivity k can be calculated from R and A.

However, the thermal resistance of the interface between the specimen and each of the conductors I and II cannot be ignored. Thus, the total thermal resistance R_t (i.e., the measured thermal resistance) is given by

$$R_t = R_s + 2R_i \,, \tag{8.47}$$

where R_s is the thermal resistance of the specimen and R_i is the thermal resistance of each interface. In order to determine R_s, specimens of at least three different known thicknesses should be measured. Figure 8.18 shows the plot of R_t vs. x. It is a straight line, with the R_t intercept being $2R_i$ and the slope being the thermal resistance of the specimen material (of area A) per unit thickness. The thermal resistance of the specimen material per unit thickness, multiplied by the specimen thickness under consideration, gives the thermal resistance of the specimen, which is equal to $1/(kA)$, where k is the thermal conductivity of the specimen. Thus, k can be determined from the slope of the plot of Fig. 8.18.

The plot in Fig. 8.18 also allows the determination of R_i, which depends on the roughness of the proximate surfaces of conductors I and II. The greater their roughness, the greater the volume of air voids at the interface, and the higher R_i. In addition, R_i depends on the ability of the specimen to conform to the surface topography of conductor I or II. The greater the conformability, the smaller the volume of air voids at the interface and the lower R_i.

Whether a thin interface material is placed at the interface between the proximate surfaces of conductors I and II or not, the two-dimensional thermal resistivity of the interface can be evaluated. If an interface material is present, the overall interface consists of (i) the interface material and (ii) the interfaces between the interface material and each of the two proximate surfaces. From Eq. 8.35, the two-dimensional thermal resistance R of this overall interface is given by

$$R = \Delta T/(\Delta Q/\Delta t) \,, \tag{8.48}$$

where ΔT is experimentally obtained using the method of Fig. 8.17 and Eq. 8.45, and $\Delta Q/\Delta t$ is experimentally obtained using the method of Fig. 8.17 and Eq. 8.42. From R, the two-dimensional thermal resistivity can be calculated using Eq. 8.34. The reciprocal of the thermal resistivity is the thermal conductance of the interface.

8.6.2 Laser Flash Method

The laser flash method is a transient (not steady-state) method of evaluating thermal conduction. It involves applying a flash of laser radiation to the surface of the specimen and then measuring the rate of temperature rise at the back surface of the specimen using a sensitive temperature measurement device (e.g., a thermocouple that is small enough to respond rapidly, or an infrared sensor) (Fig. 8.19). The laser flash provides a heat pulse. This heat is then conducted through the specimen from the front surface to the back surface. The higher the thermal diffusivity (defined below), the steeper the temperature rise at the back surface.

The thermal diffusivity (α, not to be confused with CTE, which is also denoted by α) is defined as the ratio of the thermal conductivity (k) to the volumetric specific heat (ϱc_p). The volumetric specific heat is defined as the product of the specific heat (c_p, at constant pressure) and the density (ϱ). Since the specific heat is defined as the amount of heat required to increase the temperature by 1 K for a unit mass of a material, the multiplication of the specific heat by the density (which is the mass per unit volume) gives the amount of heat required to increase the temperature by 1°C for a unit volume of the material. Because the heat travels through a volume, it is more meaningful to consider the volumetric specific heat rather than the specific heat.

By definition, the thermal diffusivity is given by

$$\alpha = k/(\varrho c_\mathrm{p}) \,. \tag{8.49}$$

The units α of are m^2/s, since the units of k are $\mathrm{W/(m\,K)}$; the units of ϱ are $\mathrm{g/m}^3$; and the units of c_p are $\mathrm{J/(g\,K)}$. The laser flash method gives α, which allows k to be calculated using Eq. 8.49 provided that ϱ and c_p are known.

Compared to the guarded hot plate method (Sect. 8.6.1), the laser flash method has the advantage that the specimen under investigation does not need to be sandwiched between two surfaces. As a result, the interface between the specimen and an external surface is not involved in the laser flash method, but it is involved in the guarded hot plate method. This means that the work needed in the setup shown in Fig. 8.17 to decouple the contribution of the specimen to the thermal resistance from the contribution of the interface is not required when the laser flash method is used.

The thermal diffusivity describes the ease with which heat is transported by conduction in a material (i.e., the heat moves from one point to another within the material). Along the path of heat transport, the material is heated, thereby consuming heat; the amount consumed is governed by the volumetric specific heat. The higher the volumetric specific heat, the greater the heat consumed. The

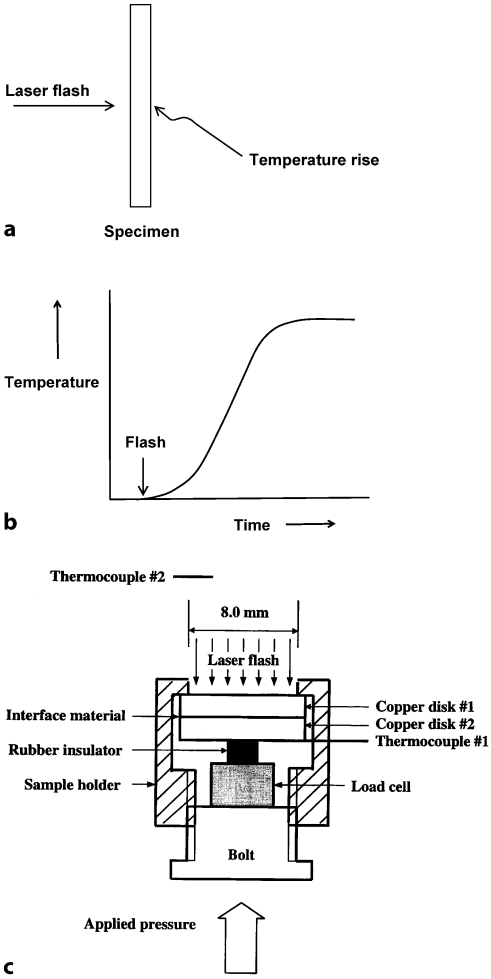

Figure 8.19. The laser flash method of evaluating thermal conduction. **a** Testing geometry, with the laser flash originating from the left. **b** Temperature rise at the back side of the specimen. **c** An example of a detailed experimental setup, with the laser flash originating from the top, thermocouple 2 for sensing the laser flash, and thermocouple 1 for measuring the temperature rise at the back of the specimen. The sample holder in this particular setup involves the use of a load cell to apply pressure to the specimen during testing. This particular configuration is used to evaluate thermal interface materials (Sect. 8.7)

more heat consumed, the less remains to reach the destination, and hence the lower the temperature rise at the destination and the lower the thermal diffusivity.

Table 8.5 lists the thermal diffusivity values of various materials. Pyrolytic graphite is a form of polycrystalline graphite that has a strong crystallographic texture, so the carbon layers are preferentially oriented in a plane. Due to the low density of pyrolytic graphite and its high thermal conductivity parallel to the carbon layers, pyrolytic graphite exhibits a very high thermal diffusivity parallel to the carbon layers. Its thermal diffusivity is even higher than those of silver and

Table 8.5. Thermal diffusivities of various materials

Material	Thermal diffusivity (m^2/s)
Pyrolytic graphite (parallel to the carbon layers)	1.22×10^{-3}
Silver	1.6563×10^{-4}
Copper	1.1234×10^{-4}
Air (1 atm, 300 K)	2.2160×10^{-5}
Alumina	1.20×10^{-5}
Pyrolytic graphite (perpendicular to the carbon layers)	3.6×10^{-6}
Common brick	5.2×10^{-7}
Window glass	3.4×10^{-7}
Nylon	9×10^{-8}

copper, which have higher thermal conductivities but also higher densities. The thermal diffusivity of air is higher than those of alumina and pyrolytic graphite (perpendicular to the carbon layers) because of the low density of air. Nylon has a very low thermal diffusivity because of its low thermal conductivity.

An example of a laser flash testing system is described below and illustrated in Fig. 8.19c. A Coherent General Everpulse Model 11 Nd (neodymium) glass laser (a solid-state laser) with a pulse duration of 0.4 ms, a wavelength of 1.06 μm (near-infrared) and a pulse energy of up to 15 J is used for impulse heating. The laser power is adjusted to allow the temperature rise of the specimen to be between 0.5 and 1.0°C. The upper surface of disk #1, on which the laser beam impacts, is coated with carbon in order to increase the extent of laser energy absorption relative to the extent of reflection. An E-type thermocouple (#1) is attached to the back surface of disk #2 to monitor the temperature rise. Another thermocouple (#2) of the same type is put ~30 cm above the specimen holder to detect the initial time when the laser beam is emitted. A plexiglass holder is used to facilitate the application of pressure, which is used to tighten the interface (between the proximate copper surfaces) under investigation. A load cell is used to measure the pressure. Calibration using a standard NBS 8426 graphite disc (thickness = 2.62 mm) is performed before testing each specimen in order to ensure measurement accuracy. The data acquisition rate used for each test is adjusted so that there are at least 100 temperature data points during the temperature rise.

The experimental error in these transient thermal contact conductance measurements consists of (i) random error due to experimental data scatter and (ii) systematic error that is mainly due to the lag in the thermocouple response and partly due to the method used to calculate the conductance from the temperature data. The higher the thermal contact conductance, the greater the error.

8.7 Thermal Interface Materials

Due to the miniaturization of microelectronics, the amount of heat generated per unit area has been increasing year by year. In order to dissipate this heat efficiently,

it is necessary to improve the thermal contacts within the microelectronic package. Without adequate thermal contacts, heat dissipation is hampered, in spite of the possible presence of heat sinks of high thermal conductivity.

A thermal interface material (TIM) is a material positioned at the interface between two surfaces for the purpose of enhancing the flow of heat from one surface to the other. For example, one surface is the heat spreader and the other surface is the heat sink (Fig. 8.20). As another example, one surface is the heat spreader and the other surface is the CPU of a computer (Fig. 8.20). Surfaces are never perfectly flat (Fig. 8.20), so air pockets are associated with the valleys in the surface topography. As air is thermally insulating, the displacement of the air by a TIM is crucial to improving the thermal interface. Thus, the conformability of the TIM is critical (Fig. 8.21).

TIMs are needed to improve thermal contacts. By placing a thermal interface material at the interface between two components across which heat must flow, the thermal contact between the two components is improved. An important market

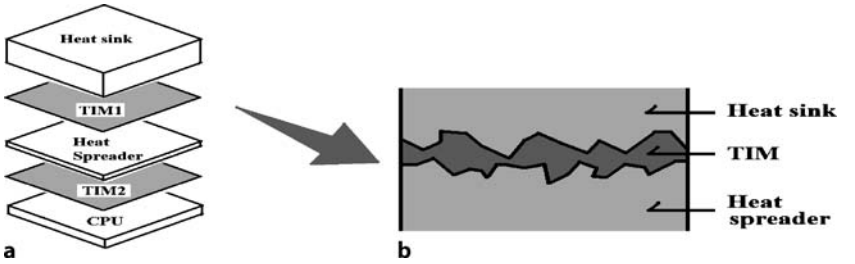

Figure 8.20. Schematic illustration of thermal interface materials (TIMs) sandwiched between two solid surfaces. **a** TIM1 at the interface between the heat sink and the heat spreader; TIM2 at the interface between the heat spreader and the CPU. **b** TIM filling the gap between two solid surfaces and conforming to the topography of the two surfaces

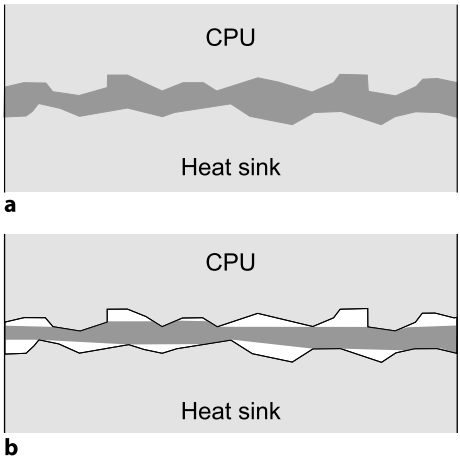

Figure 8.21. Schematic illustrations of thermal interface materials (TIMs, *dark regions*) with: **a** good conformability; **b** poor conformability. Poor conformability results in air pockets (*white regions*) at the thermal interface

for TIMs is the electronic industry, as heat dissipation is critical to the performance, reliability, and further miniaturization of microelectronics. For example, a TIM is used to improve the thermal contact between a heat sink and a printed circuit board, or between a heat sink and a chip carrier.

A TIM can be a thermal fluid, a thermal grease (paste), a resilient thermal conductor, or a solder applied in the molten state. The thermal fluid, thermal grease, or molten solder is spread on the mating surfaces. A resilient thermal conductor is sandwiched between the mating surfaces and held in place by pressure. The most commonly used thermal fluid is mineral oil, while the most commonly used thermal greases (pastes) are conducting particle (usually metal or metal oxide)-filled silicones. Conducting particle-filled elastomers are most commonly used as resilient thermal conductors. Among these four types of thermal interface materials, thermal greases (based on polymers, particularly silicone) and solder are by far the most commonly used. Resilient thermal conductors are not as well developed as thermal fluids or greases.

As the materials to be interfaced are good thermal conductors (such as copper), the effectiveness of a thermal interface material is enhanced if it has a high thermal conductivity and low thickness and if there is a low thermal contact resistance between the interface material and each mating surface. The rougher the mating surfaces, the larger the thickness required for the thermal interface material (Fig. 8.22). As the mating surfaces are not perfectly smooth, the interface material must be able to flow or deform in order to conform to the topographies of the mating surfaces. If the interface material is a fluid, grease, or paste, it should have a high fluidity (workability) in order to conform and to have a small thickness

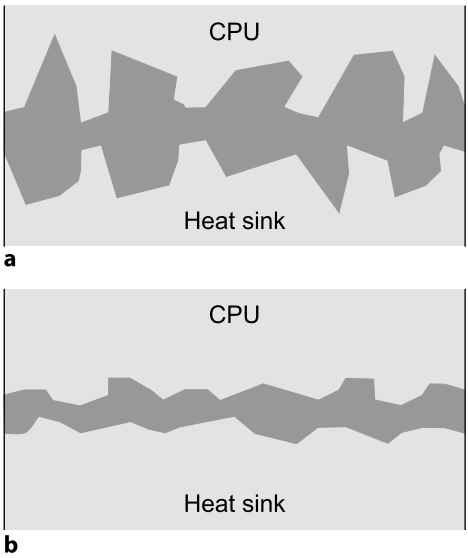

Figure 8.22. Thermal interface materials between: **a** rough surfaces; **b** smooth surfaces. Rough surfaces result in the need for large thicknesses of thermal interface material

after mating. On the other hand, the thermal conductivity of the grease or paste increases with increasing filler content, and this is accompanied by a decrease in the workability. Without a filler, as in the case of an oil, the thermal conductivity is poor. A thermal interface material in the form of a resilient thermal conductor sheet (e.g., a felt consisting of conducting fibers bound together without a binder, a resilient polymer-matrix composite containing a thermally conducting filler, and a form of graphite known as flexible graphite) cannot usually be as thin or conformable as one that takes the form of a fluid, grease, or paste, so it needs to have a very high thermal conductivity for it to be effective.

Solder is commonly used as a thermal interface material to enhance the thermal contact between two surfaces. This is because solder can melt at rather low temperatures and the molten solder can flow and spread itself thinly on the adjoining surfaces, thus resulting in high thermal contact conductance at the interface between the solder and each of the adjoining surfaces. Furthermore, solder in the metallic solid state is a good thermal conductor. In spite of the high thermal conductivity of solder, the thickness of the solder greatly affects the effectiveness of the solder as a thermal interface material; a small thickness is desirable. Moreover, the tendency for solder to react with copper to form intermetallic compounds reduces the thermal contact conductance of the solder–copper interface.

Thermal pastes are predominantly based on polymers, particularly silicone, although thermal pastes based on sodium silicate have been reported to be better at providing high thermal contact conductance. The superiority of sodium-silicate-based pastes over silicone-based pastes is primarily due to the low viscosity of sodium silicate compared to silicone, and the importance of high fluidity in the paste so that the paste can conform to the topography of the surfaces that it interfaces.

A TIM is generally prepared by combining an organic vehicle (liquid) or matrix (solid) with a thermally conductive filler, which typically takes the form of particles dispersed in the vehicle or matrix. When a vehicle is used, the TIM takes the form of a paste known as a thermal paste. A special type of matrix is a solid that melts upon heating at the operating temperature of the microelectronics. Such a matrix is known as a phase-change material, which is attractive due its lack of a tendency to seep during transportation, which occurs below the operating temperature. The vehicle or matrix should be able to conform to the topography of the proximate solid surfaces. In addition, it should be able to withstand the elevated temperatures present in the microelectronics package. Commonly used fillers are silver, boron nitride and zinc oxide particles, since they each exhibit high thermal conductivity and, in the case of boron nitride and zinc oxide, electrical nonconductivity, which is attractive for avoiding electrical short-circuiting in the microelectronic package upon the seepage of the thermal interface material.

Previously, the development of thermal interface materials has focused on maximizing the thermal conductivity of the interface material, with relatively little attention paid to the conformability. Thus, the volume fraction of the thermally conductive filler tends to be high in thermal interface materials, and the choice of filler has been governed by the thermal conductivity rather than the conformability of the filler.

Recent work by Chung et al. [1, 2] has shown that carbon black is a highly effective thermally conductive filler in thermal pastes, in spite of its moderate thermal conductivity. The effectiveness of carbon black is due to its conformability, which stems from the fact that carbon black takes the form of porous agglomerates of nanoparticles. Furthermore, Chung et al. [3] have shown that there is an optimum volume fraction of a filler, due to the increase in thermal conductivity and the decrease in conformability that occurs as the filler content increases. In addition, Chung et al. have shown that the performance of a TIM depends on the roughness of the proximate surfaces, with increasing demands being placed on the conformability as the roughness decreases and on the thermal conductivity as the roughness increases. Carbon black thermal paste, which shows excellent conformability, is particularly effective when the roughness is low.

The findings mentioned above have led to a paradigm shift in the design of TIMs [4]. The new criteria for designing a TIM are high conformability, low thickness (known as the bond line thickness, abbreviated to BLT, Fig. 8.23), and high thermal conductivity. A low thickness is important because the thermal resistance increases with increasing thickness. In order to achieve a low thickness, a TIM should be highly spreadable. Due to its conformability and spreadability, carbon black paste exhibits superior performance to both a single-walled carbon nanotube paste [5] and a carbon nanotube array [6]. The carbon nanotubes in the paste tend to lie down along the plane of the thermal interface and are also limited in terms of conformability. The carbon nanotube array has the nanotubes aligned in the direction of heat transfer, but it has a large thickness and the thermal conductivity of the array is limited.

This paradigm shift also means that the performance of a TIM cannot be described by the thermal conductivity of the TIM, but should instead be described by the thermal contact conductance between the two proximate surfaces. The thermal resistance of the overall thermal contact is the sum of the thermal resistance within the TIM and that of the interface between the TIM and each of the two proximate surfaces. The overall thermal resistance divided by the geometric area of the thermal contact gives the overall thermal resistivity. The reciprocal of the thermal resistivity is the thermal contact conductance (in $W/(m^2\,K)$). Performance comparisons for various TIMs must be conducted for the same composition and roughness of the proximate surfaces and for the same pressure that squeezes the two surfaces together. The guarded hot plate method (a steady-state method) can be used for this evaluation (Fig. 8.17). It is more reliable than the method of TIM

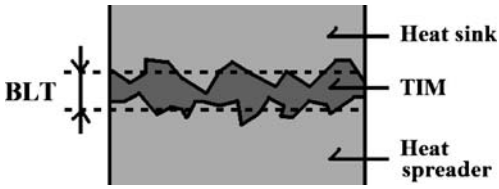

Figure 8.23. Schematic illustration of the bond line thickness (BLT) of a thermal interface material

performance evaluation that involves the measuring the temperature rise of an operating computer [7].

In the thermal pastes described below, unless noted otherwise, the vehicle consists of polyol esters. This is attractive due to its high workability and its ability to resist elevated temperatures. The polyol esters in the vehicle are a pentaerythritol ester of linear and branched fatty acids and a dipentaerythritol ester of linear and branched fatty acids. The polyol ester mixture is provided by Hatco Corp. (Fords, NJ, USA). The specific gravity is 0.97.

Carbon nanofillers that make effective thermal pastes have been studied comparatively [8]. These include carbon black (CB) and graphite nanoplatelets (GNPs, obtained by the sonication of exfoliated graphite). Figure 2.6 shows the nanoplatelet morphology of the GNPs. The GNPs have dimensions of around 3–8 μm in the plane of the platelet. The platelet thickness is on the nanoscale. There are numerous types of carbon black that differ in terms of agglomerate size and particle size. Tokaiblack #3800 (graphitized carbon black from Tokai Carbon Co., Ltd., Tokyo, Japan) has a smaller structure (i.e., smaller agglomerates) and a smaller particle size than Vulcan XC72R carbon black (Cabot Corp., Billerica, MA, USA).

Table 8.6 and Fig. 8.24 show the thermal contact conductances of graphite nanoplatelet (GNP) pastes and carbon black (CB) pastes for both rough (15 μm) and smooth (0.01 μm) surfaces. For the rough surfaces, GNP is slightly more effective than CB (Tokai), which is in turn more effective than CB (Cabot). For the smooth surfaces, CB (Tokai) is more effective than CB (Cabot), which is in turn more effective than GNP. This comparison is based on testing various filler

Table 8.6. Thermal contact conductances of thermal contacts with graphite nanoplatelet (GNP) pastes and carbon black (CB) pastes. The bond line thicknesses of various pastes are shown in Fig. 8.24. (From [8])

Thermal paste		Thermal conductance (10^4 W/(m^2 K))				
		Rough surfaces			Smooth surfaces	
Filler	Vol.%	0.46 MPa	0.69 MPa	0.92 MPa	0.46 MPa	0.69 MPa
GNP	0.6	–	–	–	23.81 ± 0.34	25.18 ± 0.21
	1.2	10.66 ± 0.04	11.38 ± 0.05	11.66 ± 0.06	24.26 ± 0.66	25.66 ± 0.06
	2.4	11.72 ± 0.28	11.98 ± 0.18	12.36 ± 0.10	22.07 ± 1.18	24.47 ± 0.37
	3.6	10.32 ± 0.15	10.71 ± 0.05	11.17 ± 0.09	21.17 ± 0.07	22.16 ± 0.28
	4.8	9.35 ± 0.34	10.74 ± 0.32	9.68 ± 0.34	17.40 ± 0.37	19.14 ± 0.21
CB	1.2	9.45 ± 0.02	9.59 ± 0.09	9.89 ± 0.02	–	–
(Tokai)	2.4	10.20 ± 0.20	11.01 ± 0.05	11.87 ± 0.08	24.23 ± 0.17	27.75 ± 0.11
	4.8	10.12 ± 0.16	11.10 ± 0.10	11.59 ± 0.15	–	–
	8.0	10.85 ± 0.20	11.39 ± 0.10	11.64 ± 0.12	30.41 ± 0.47	32.75 ± 0.19
	12.0	11.06 ± 0.27	11.71 ± 0.12	12.57 ± 0.28	–	–
	15.0	11.27 ± 0.34	12.41 ± 0.22	13.18 ± 0.11	25.58 ± 0.35	27.86 ± 0.10
	20.0	9.34 ± 0.21	9.86 ± 0.11	11.11 ± 0.13	17.48 ± 0.17	22.33 ± 0.29
CB	1.2	8.50 ± 0.16	9.39 ± 0.11	10.36 ± 0.20	–	–
(Cabot)	2.4	8.72 ± 0.07	10.18 ± 0.20	11.12 ± 0.12	25.91 ± 0.16	27.75 ± 0.14
	4.8	8.45 ± 011	9.39 ± 0.15	10.58 ± 0.11	19.10 ± 0.20	21.33 ± 0.32
	8.0	7.96 ± 0.08	8.71 ± 0.10	8.78 ± 0.09	16.52 ± 0.61	18.17 ± 0.22
	12.0	2.05 ± 0.02	2.28 ± 0.03	2.49 ± 0.02	–	–

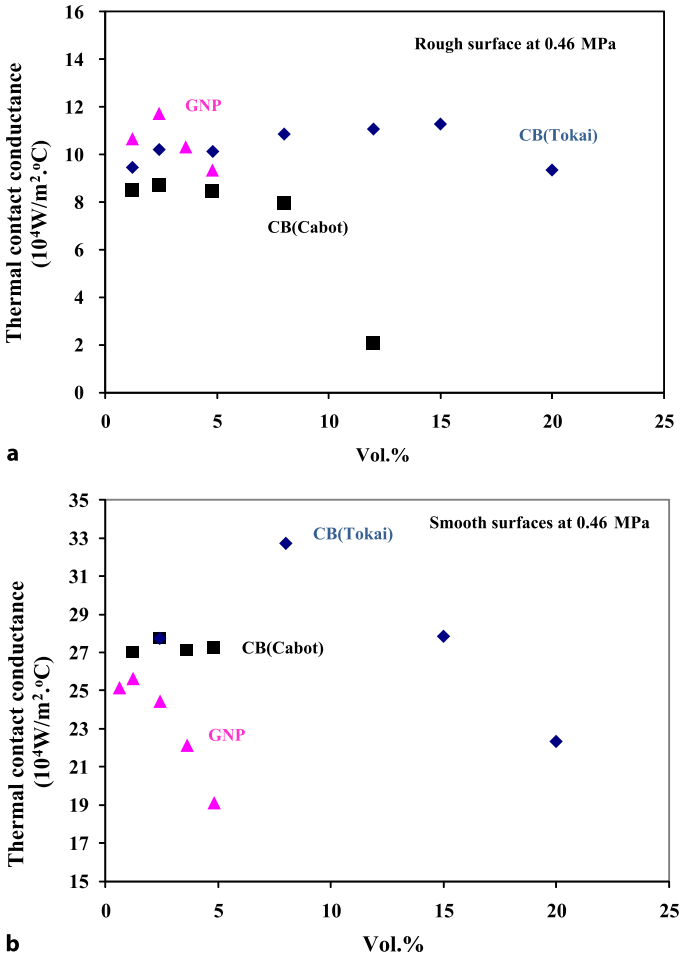

Figure 8.24. Thermal contact conductance measured for: **a** rough surfaces; **b** smooth surfaces. *Triangles*, GNP; *diamonds*, carbon black (Tokai); *squares*, carbon black (Cabot). A *vertical bar with a horizontal line at each end* indicating the data scatter is shown for each data point, though the bar is very short and thus covered by the data symbol for most data points

volume fractions for each type of filler and selecting the best performance. The highest value of thermal contact conductance attained for the rough surfaces is 12×10^4 W/m^2 K (as attained by GNP); the highest value of conductance attained for the smooth sufaces is 33×10^4 W/m^2 K (as attained by CB (Tokai)).

The high effectiveness of GNP for the rough surfaces is attributed to the high thermal conductivity of GNP. The high effectiveness of CB (Tokai) for the smooth surfaces is attributed to the high conformability, as suggested by its low viscosity [9]. Thermal conductivity is more important for rough surfaces than smooth surfaces, whereas conformability is more important for smooth surfaces than rough surfaces.

The optimum filler volume fraction differs among the three filler types. For the rough surfaces, the optimal fractions are 2.4, 15 and 2.4 vol% for GNP, CB (Tokai) and CB (Cabot), respectively. For the smooth surfaces, the optimal fractions are 1.2, 8 and 2.4 vol% for GNP, CB (Tokai) and CB (Cabot), respectively. Thus, the optimum filler volume fraction decreases as the proximate surfaces become smoother for GNP and CB (Tokai), but it is not affected by the surface smoothness for CB (Cabot). For GNP beyond the optimum volume fraction, the conductance decreases significantly with increasing GNP volume fraction (Fig. 8.24). Due to the low value of the optimum filler volume fraction for GNP compared to CB (Tokai), GNP is less effective than CB (Tokai) when the filler volume fraction exceeds about 5 vol% for rough surfaces. An optimum occurs because the thermal conductivity of the paste increases with increasing filler content while the conformability and spreadability of the paste decrease with increasing filler content. The optimal volume fraction is higher for rough surfaces than for smooth surfaces for the same filler type, as shown for both GNP and CB (Tokai), because of the relatively high importance of the thermal conductivity for rough surfaces and the relatively high importance of the conformability for smooth surfaces. The optimal volume fraction is higher for CB (Tokai) than for CB (Cabot) for both rough and smooth surfaces, and CB (Tokai) is more effective than CB (Cabot) for rough surfaces, because of the lower DBP value (i.e., the smaller structure) of CB (Tokai). Although the GNPs have nanoscale thicknesses, their other dimensions (in the plane of the platelet) are on the micron scale. The large in-plane dimensions and the expected tendency for the flakes to lie down in the plane of the thermal interface probably lead to the low optimum filler volume fraction of GNPs, akin to CB (Cabot), in the rough case.

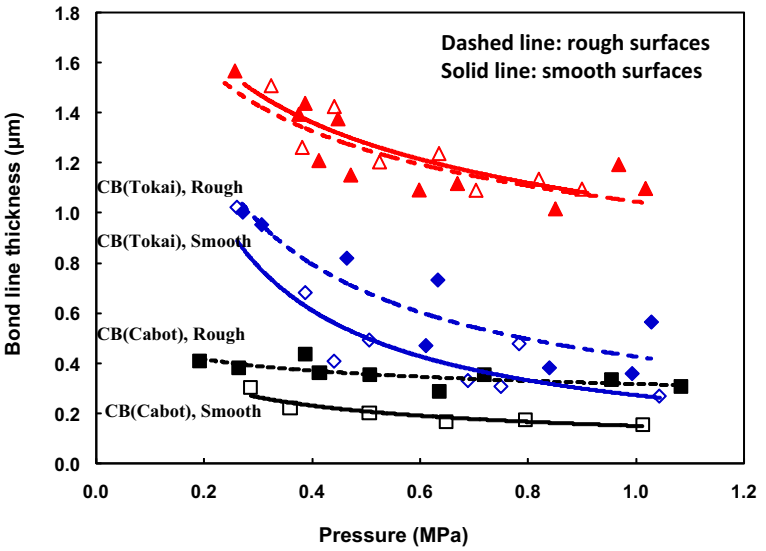

Figure 8.25. Bond line thicknesses for rough (15 μm, *solid symbols*) and smooth (0.01 μm, *open symbols*) proximate copper surfaces. *Triangles* – 2.4 vol% GNP pastes; *diamonds* – 15 vol% CB (Tokai); *squares* – 2.4 vol% CB (Cabot)

Figure 8.25 shows the dependence of the bond line thickness on the pressure for various thermal pastes and for rough (15 μm) and smooth (0.01 μm) proximate copper surfaces, respectively. For any paste, the bond line thickness decreases with increasing pressure, whether the proximate surfaces are rough or smooth. This trend is consistent with the increase in thermal contact conductance with increasing pressure, as observed for all of the pastes investigated, whether the proximate surfaces are rough or smooth (Table 8.6). This implies that the thermal contact conductance correlates with the bond line thickness for all of the pastes investigated.

As shown in Fig. 8.25, at the same pressure, 2.4 vol% GNP gives the highest bond line thickness, 2.4 vol % CB (Cabot) gives the lowest thickness, and 15 vol% CB (Tokai) gives an intermediate value, whether the proximate surfaces are rough or smooth. In particular, at a pressure of 0.46 MPa, which is one of the pressures used in the thermal contact conductance measurements, the bond line thicknesses are, respectively, 1.3, 0.72 and 0.36 μm for 2.4 vol% GNP, 15 vol% CB (Tokai) and 2.4 vol% CB (Cabot) pastes in the case of rough surfaces.

Phase-change materials, which are solid at room temperature but melt at temperatures around the operating temperature, are attractive as thermal interface materials. This is because the phase change (melting) provides a mechanism of heat absorption and the molten state is associated with high fluidity. An example of a phase-change material is paraffin wax, which melts at 48°C. The addition of boron nitride particles to the wax makes the material effective as a thermal interface material; the thermal contact conductance (between copper, as in Table 8.6) reaches 17×10^4 W/(m^2 K) at 22°C and 0.3 MPa.

Flexible graphite (a flexible foil that is all graphite) is effective as a thermal interface material if its thickness is low (0.13 mm), its density is low (1.1 g/cm^3) and the contact pressure used is high (11.1 MPa). It is much less effective than solder and thermal pastes, but flexible graphite is advantageous due to its thermal stability.

8.8 Composites Used for Microelectronic Heat Sinks

Materials of high thermal conductivity are needed to conduct heat for heating or cooling purposes, especially by the electronic industry. Due to the miniaturization and increasing power of microelectronics, heat dissipation is key to the reliability, performance, and further miniaturization of microelectronics. The heat dissipation problem is so severe that even expensive thermal conductors such as diamond, metal-matrix composites and carbon-matrix composites are being used in high-end microelectronics. Due to the low coefficients of thermal expansion (CTEs) of semiconductor chips and their substrates, heat sinks also need to have low CTEs. Thus, the thermal conductor material needs to have not just high thermal conductivity but low CTE too. For example, copper is a good thermal conductor but its CTE is high, as shown in Table 8.7. Therefore, copper-matrix composites containing low CTE fillers such as carbon fibers or molybdenum particles are used. For lightweight electronics, such as laptop computers and avionics, an additional requirement for

Table 8.7. Thermal properties and densities of various materials

Material	Thermal conductivity (W/(m K))	Coefficient of thermal expansion (10^{-6}°C^{-1})	Density (g/cm^3)
Aluminum	247	23	2.7
Gold	315	14	19.32
Copper	398	17	8.9
Lead	30	39	11
Molybdenum	142	4.9	10.22
Tungsten	155	4.5	19.3
Invar	10	1.6	8.05
Kovar	17	5.1	8.36
Diamond	2,000	0.9	3.51
Beryllium oxide	260	6	3
Aluminum nitride	320	4.5	3.3
Silicon carbide	270	3.7	3.3

the thermal conductor material is low density. As aluminum and carbon are light compared to copper, aluminum, carbon, and their composites are used for this purpose. Compared to aluminum, carbon has the additional advantage of being corrosion resistant.

8.8.1 Metals, Diamond, and Ceramics

Table 8.7 gives the thermal conductivities of various metals. Copper is most commonly used when materials of high thermal conductivity are required. However, copper suffers from a high coefficient of thermal expansion (CTE). A low CTE is needed when the adjoining component has a low CTE. When the CTEs of the two adjoining materials are sufficiently different and the temperature is varied, thermal stress occurs and may even cause warpage. This is the case when copper is used as heat sink for a printed wiring board, which is a continuous fiber polymer-matrix composite that has a lower CTE than copper. Molybdenum and tungsten are metals that have low CTEs, but their thermal conductivities are poor compared to copper. The alloy Invar (64Fe-36Ni) has an outstandingly low CTE among metals, but has a very poor thermal conductivity. Diamond is most attractive, as it has a very high thermal conductivity and a low CTE, but it is expensive. Aluminum is not as conductive as copper, but it has a low density, which is attractive for aircraft electronics and applications (e.g., laptop computers) that need to be light. Aluminum nitride is not as conductive as copper, but it is attractive due to its low CTE. Diamond and most ceramic materials are very different from metals in terms of their electrical insulation abilities. In contrast, metals conduct both thermally and electrically. For applications that require thermal conductivity and electrical insulation, diamond and appropriate ceramic materials can be used but metals cannot.

8.8.2 Metal-Matrix Composites

One way to lower the CTE of a metal is to form a metal-matrix composite using a low CTE filler. Ceramic particles such as AlN and SiC are used for this purpose, due to their combination of high thermal conductivity and low CTE. As the filler usually has a lower CTE and a lower thermal conductivity than the metal matrix, the higher the filler volume fraction in the c omposite, the lower the CTE and the lower the thermal conductivity.

Metal-matrix composites with discontinuous fillers (commonly particles) are attractive due to their high processability into various shapes. However, layered composites in the form of a matrix–filler–matrix sandwich are useful for planar components. Discontinuous fillers are most commonly ceramic particles. The filler sheets are most commonly low-CTE metal alloy sheets (e.g., Invar or 64Fe-36Ni, and Kovar or 54Fe-29Ni-17Co). Aluminum and copper are commonly used as metal matrices due to their high conductivities.

8.8.2.1 Aluminum-Matrix Composites

Aluminum is the most dominant matrix used in metal-matrix composites intended for both structural and electronic applications. This is because of the low cost of aluminum and its low melting point (660°C), which allows the composite to be fabricated by methods that involve melting the metal.

Liquid-phase methods used for the fabrication of metal-matrix composites include liquid metal infiltration, which usually involves the use of pressure (from a piston or compressed gas) to push the molten metal into the pores of a porous preform comprising the filler (commonly particles that are not sintered) and a small amount of a binder. Pressureless infiltration is less common but is possible. The binder prevents the filler particles from moving during the infiltration, and also provides sufficient compressive strength to the preform, so that the preform will not be deformed during the infiltration. This method thus provides near-net-shape fabrication; i.e., the shape and size of the composite product are the same as those of the preform. Since the composite is far more difficult to machine than the preform, near-net-shape fabrication is desirable.

In addition to the ability to perform near-net-shape fabrication, liquid metal fabrication is advantageous since it is able to provide composites with high filler volume fractions (up to 70%). A high filler volume fraction is necessary to attain a sufficiently low CTE ($< 10 \times 10^{-6}$/°C) in the composite, even if the filler is a low-CTE ceramic (e.g., SiC), since the aluminum matrix has a relatively high CTE. However, to attain a high volume fraction using liquid metal infiltration, the binder used must be present in only a small amount (to avoid clogging the pores in the preform) but still be effective. Hence, the binder technology used is critical.

The ductility of a composite decreases as the filler volume fraction increases, so a composite with a low enough CTE is also quite brittle. Although this brittleness is not acceptable for structural applications, it is acceptable for electronic applications.

Another liquid-phase technique is stir casting, which involves stirring the filler in the molten metal and then casting. This method suffers from the nonuniform distribution of the filler in the composite due to the difference in density between the filler and the molten metal and the consequent tendency for the filler to either float or sink in the molten metal prior to solidification. Stir casting also suffers from an inability to produce composites with a high filler volume fraction.

Yet another liquid-phase technique is plasma spraying, which involves spraying a mixture of molten metal and filler onto a substrate. This method suffers from a relatively high porosity of the resulting composite and the consequent need for densification by hot isostatic pressing or other methods, which tend to be expensive.

One solid-phase technique is powder metallurgy, which involves mixing the matrix metal powder and filler and subsequent sintering under heat and pressure. This method is relatively difficult to use for an aluminum matrix because aluminum has a layer of protective oxide on it, and this oxide layer on the surface of each aluminum particle hinders sintering. Furthermore, this method is usually limited to low volume fractions of the filler.

The most common filler used is silicon carbide (SiC) particles, due to their low cost and the low CTE of SiC. However, SiC reacts with aluminum. The reaction is:

$$3SiC + 4Al \rightarrow 3Si + Al_4C_3 \, . \tag{8.50}$$

This reaction becomes more severe as the composite is heated. The aluminum carbide is a brittle reaction product that lines the filler–matrix interface of the composite, thus weakening the interface. Silicon, the other reaction product, dissolves in the aluminum matrix, lowering the melting temperature of the matrix, and causing nonuniform phase and mechanical property distributions. Furthermore, the reaction consumes some of the SiC filler.

One way to diminish this reaction is to use an Al-Si alloy matrix, since the silicon in the alloy matrix promotes the opposite reaction and thus counters this reaction. However, the Al-Si matrix is less ductile than the Al matrix, thus causing the mechanical properties of the Al-Si matrix composite to be far inferior to those of the corresponding Al-matrix composite. Thus, using an Al-Si alloy matrix is not a solution to the problem.

An effective solution is to replace SiC by aluminum nitride (AlN) particles, which do not react with aluminum, thus resulting in superior mechanical properties in the composite. The fact that AlN tends to have a higher thermal conductivity than SiC aids the thermal conductivity of the composite. Since the cost of the composite fabrication process is the biggest influence on the cost of composite production, the higher material cost of AlN compared to SiC does not matter, especially for electronic packaging. Aluminum oxide (Al_2O_3) also does not react with aluminum, but it does have a low thermal conductivity and it tends to suffer from particle agglomeration.

Other than ceramics such as SiC and AlN, another filler used in aluminum-matrix composites is carbon in the form of fibers with diameters of around 10 μm, and (less commonly) filaments (also known as nanofibers) with diameters of less than 1 μm.

Carbon also reacts with aluminum to form aluminum carbide. However, fibers are more effective than particles for reducing the CTE of the composite. Carbon fibers can even have continuous lengths. Moreover, carbon, especially when graphitized, is much more thermally conductive than ceramics. In fact, carbon fibers that are sufficiently graphitic are even more thermally conductive than the metal matrix, so the thermal conductivity of the composite increases with increasing fiber volume fraction. However, these fibers are expensive. The mesophase-pitch-based carbon fiber K-1100 (discontinued) from Amoco Performance Products (Alpharetta, GA, USA) exhibits a longitudinal thermal conductivity of 1,000 W/(m K).

Both carbon and SiC form galvanic couples with aluminum, which is the anode (the component in the composite that is corroded). The corrosion becomes more severe in the presence of heat and/or moisture.

The thermal conductivity of an aluminum-matrix composite depends on the filler and its volume fraction, the alloy matrix heat treatment condition, as well as the filler–matrix interface.

To increase the thermal conductivity of a SiC aluminum-matrix composite, diamond film can be deposited on the composite. The thermal conductivity of single-crystal diamond is 2,000–2,500 W/(m K), though diamond film is not single crystalline.

8.8.2.2 Copper-Matrix Composites

Because copper is heavy anyway, the filler does not have to be lightweight. Thus, low-CTE but heavy metals such as tungsten, molybdenum and Invar are used as fillers. These metals (except Invar) have the advantage that they are quite conductive thermally and are available in particle and sheet forms, so that they are suitable for particulate as well as layered composites. Yet another advantage of the metal fillers is the better wettability of the molten matrix metal with metal fillers than with ceramic fillers when the composite is fabricated by a liquid phase method.

An advantage of copper over aluminum is its nonreactivity with carbon, so carbon is a highly suitable filler for copper. Additional advantages are that carbon is lightweight and carbon fibers are available in a continuous form. Furthermore, copper is a rather noble metal, as shown by its position in the electromotive series, so it does not suffer from the corrosion which plagues aluminum. Carbon is used as a filler in copper in the form of fibers with diameters of around 10 μm. As carbon fibers that are sufficiently graphitic are even more thermally conductive than copper, the thermal conductivity of a copper-matrix composite can exceed that of copper. Less common fillers for copper are ceramics such as silicon carbide, titanium diboride (TiB_2) and alumina.

The melting point of copper is much higher than that of aluminum, so copper-matrix composites are commonly fabricated by powder metallurgy, although liquid metal infiltration is also used. In the case of liquid metal infiltration, the metal matrix is often a copper alloy (e.g., Cu-Ag) chosen for its reduced melting temperature and good castability.

Powder metallurgy conventionally involves mixing the metal matrix powder and the filler, and then pressing and sintering under either heat or both heat and

pressure. The problem with this method is that it is limited to low volume fractions of the filler. In order to attain high volume fractions, a less conventional method of powder metallurgy is recommended. This method involves coating the matrix metal on the filler units, followed by pressing and sintering. The mixing of matrix metal powder with the coated filler is not necessary, although it can be done to decrease the filler volume fraction in the composite. The metal coating on the filler forces the distribution of matrix metal to be uniform even when the metal volume fraction is low (i.e., when the filler volume fraction is high). On the other hand, with the conventional method, the matrix metal distribution is not uniform when the filler volume fraction is high, thus causing porosity and the presence of filler agglomerates. In each of these agglomerates, the filler units touch one another directly. This microstructure results in low thermal conductivity and poor mechanical properties.

Continuous carbon fiber copper-matrix composites can be made by coating the fibers with copper and then diffusion bonding (i.e., sintering). This method is akin to the abovementioned less conventional method of powder metallurgy.

Less common fillers used in copper include diamond powder, aluminosilicate fibers and Ni-Ti alloy rod. The Ni-Ti alloy is attractive due to its negative CTE of -21×10^{-6}/°C.

Coatings can be used to further improve the thermal conductivity. This is particularly valuable when the substrate to be coated is prone to surface oxidation. The surface oxide tends to act as a thermal barrier. For example, a carbon fiber copper-matrix composite has been coated with a diamond film to enhance the thermal conductivity.

8.8.2.3 Beryllium-Matrix Composites

Beryllium oxide (BeO) has a high thermal conductivity (Table 8.4). Beryllium-matrix BeO-platelet composites with 20–60 vol% BeO exhibit low density (2.30 g/cm^3 at 40 vol% BeO, compared to 2.9 g/cm^3 for Al/SiC at 40 vol% SiC), high thermal conductivity (232 W/(m K) at 40 vol% BeO, compared to 130 W/(m K) for Al/SiC at 40 vol% SiC), low CTE (7.5×10^{-6}/°C at 40 vol% BeO, compared to 12.1×10^{-6}/°C at 40 vol% SiC), and high modulus (317 GPa at 40 vol% BeO, compared to 134 GPa for Al/SiC at 40 vol% SiC).

8.8.3 Carbon-Matrix Composites

Carbon is an attractive matrix for composites used for thermal conduction because of its high thermal conductivity (though not as high as those of metals) and low CTE (lower than those of metals). Furthermore, carbon is corrosion resistant (more corrosion resistant than metals) and lightweight (lighter than metals). Yet another advantage of the carbon matrix is its compatibility with carbon fibers, in contrast to the common reactivity between a metal matrix and its fillers. Hence, carbon fibers are the dominant filler for carbon-matrix composites. Composites where both the filler and the matrix are carbon are called carbon–carbon composites. Their

primary applications in relation to thermal conduction are heat sinks, thermal planes and substrates. There is considerable competition between carbon–carbon composites and metal-matrix composites for the same applications.

The main drawback of carbon-matrix composites is their high cost of fabrication, which typically involves making a pitch-matrix or resin-matrix composite and subsequent carbonization (by heating at 1,000–1,500°C in an inert atmosphere) of the pitch or resin to form a carbon-matrix composite. After carbonization, the carbon matrix is relatively porous, so pitch or resin is impregnated into the composite and then carbonization is carried out again. Quite a few impregnation–carbonization cycles are needed in order to reduce the porosity to an acceptable level, thus resulting in a high cost of fabrication. Graphitization (by heating at 2,000–3,000°C in an inert atmosphere) may follow carbonization (typically in the last cycle) in order to increase the thermal conductivity, which increases with the degree of graphitization. However, graphitization is an expensive step. Some or all of the impregnation–carbonization cycles may be replaced by chemical vapor infiltration (CVI), in which a carbonaceous gas infiltrates the composite and decomposes to form carbon.

Carbon–carbon composites have been made using conventional carbon fibers with diameters of around 10 μm, as well as carbon filaments (also known as carbon nanofibers) grown catalytically from carbonaceous gases and with diameters of less than 1 μm. Using graphitized carbon fibers, thermal conductivities exceeding that of copper can be reached.

Carbon–carbon composites are typically less conductive than copper. To increase the thermal conductivity, carbon–carbon composites can be impregnated with copper and can also be coated with a diamond film.

8.8.4 Carbon and Graphite

An all-carbon material (called ThermalGraph, a tradename of Amoco Performance Products, Alpharetta, GA, USA), made by consolidating oriented precursor carbon fibers without a binder and subsequent carbonization and optional graphitization, exhibits thermal conductivities ranging from 390 to 750 W/(m K) in the fiber direction of the material.

Another material is pyrolytic graphite (called TPG) encased in a structural shell. The graphite (highly textured with the *c*-axes of the grains preferentially perpendicular to the plane of the graphite), has an in-plane thermal conductivity of 1,700 W/(m K) (four times that of copper), but it is mechanically weak due to the tendency to shear in the plane of the graphite. The structural shell serves to strengthen by hindering shear.

Pitch-derived carbon foams with thermal conductivities of up to 150 W/(m K) after graphitization are attractive due to their high specific thermal conductivities (thermal conductivity divided by the density).

8.8.5 Ceramic-Matrix Composites

The SiC matrix is attractive due to its high CTE compared to the carbon matrix, though it is not as thermally conductive as carbon. The CTE of carbon–carbon composites is too low (0.25×10^{-6}/°C), thus resulting in reduced fatigue life in chip-on-board (COB) applications with silica chips (CTE = 2.6×10^{-6}/°C). The SiC-matrix carbon fiber composite is made from a carbon–carbon composite by converting the matrix from carbon to SiC. To improve the thermal conductivity of the SiC-matrix composite, coatings in the form of chemical vapor deposited AlN or Si have been used. The SiC-matrix metal (Al or Al-Si) composite, as made by a liquid-exchange process, also exhibits relatively high thermal conductivity.

The borosilicate glass matrix is attractive due to its low dielectric constant (4.1 at 1 MHz for B_2O_3-SiO_2-Al_2O_3-Na_2O glass), compared to 8.9 for AlN, 9.4 for alumina (90%), 42 for SiC, 6.8 for BeO, 7.1 for cubic boron nitride, 5.6 for diamond and 5.0 for glass-ceramic. A low value of the dielectric constant is desirable for electronic packaging applications. On the other hand, glass has a low thermal conductivity. Hence, fillers with relatively high thermal conductivity are used with the glass matrix. An example is continuous SiC fibers, the glass-matrix composites of which are made by tape casting followed by sintering. Another example is aluminum nitride with interconnected pores (about 28 vol%), the composites of which are obtained by glass infiltration to a depth of about 100 μm.

8.8.6 Polymer-Matrix Composites

Polymer-matrix composites with continuous or discontinuous fillers are used for thermal management. Composites with continuous fillers (fibers, whether woven or not) are used as substrates, heat sinks, and enclosures. Composites with discontinuous fillers (particle or fibers) are used for die (semiconductor chip) attachment, electrically/thermally conducting adhesives, encapsulations, and thermal interface materials. Composites with discontinuous fillers can be in a paste form during processing, thus allowing their application by printing (screen printing or jet printing) and injection molding. Composites with continuous fillers cannot undergo paste processing, but the continuous fillers provide lower thermal expansion and higher conductivity than discontinuous fillers.

Composites can have thermoplastic or thermosetting matrices. Thermoplastic matrices have the advantage that a connection can be reworked by heating for repair purposes, whereas thermosetting matrices do not allow reworking. On the other hand, controlled-order thermosets are attractive for their thermal stability and dielectric properties. Polymers exhibiting a low dielectric constant, low dissipation factor, low coefficient of thermal expansion, and compliance are preferred.

Composites can be electrically conducting or electrically insulating; the electrical conductivity is provided by a conductive filler. The composites can made be both electrically and thermally conducting through the use of metal or graphite fillers; they can also be made electrically insulating but thermally conducting through the use of diamond, aluminum nitride, boron nitride, or alumina fillers. An electrically

conducting composite can be isotropically conducting or anisotropically conducting. A *z*-axis conductor is an example of an anisotropic conductor; it is a film that is electrically conducting only along the *z*-axis (i.e., in the direction perpendicular to the plane of the film). As one *z*-axis film can replace a whole array of solder joints, *z*-axis films are valuable for solder replacement, reducing processing costs, and improving repairability.

Epoxy-matrix composites that have continuous glass fibers and are made by lamination are most commonly used for printed wiring boards, due to the electrically insulating nature of glass fibers and the good adhesive behavior and established industrial usage of epoxy. Aramid (Kevlar) fibers can be used instead of glass fibers to provide a lower dielectric constant. Alumina (Al_2O_3) fibers can be used to increase the thermal conductivity. By selecting the fiber orientation and loading in the composite, the dielectric constant can be decreased and the thermal conductivity can be increased. By impregnating the yarns or fabrics with a silica-based sol and subsequent firing, the thermal expansion can be reduced. Matrices other than epoxy can be used. Examples are polyimide and cyanate ester.

For heat sinks and enclosures, conducting fibers are used, since the conducting fibers enhance the thermal conductivity and the ability to shield electromagnetic interference (EMI); i.e., to block electromagnetic radiation that is mainly in the radio wave frequency range. EMI shielding is particularly important for enclosures. Carbon fibers are most commonly used for these applications due to their conductivity, low thermal expansion, and wide availability as a structural reinforcement. For high thermal conductivity, carbon fibers made from mesophase pitch or copper-plated carbon fibers are preferred.

8.9 Carbon Fiber Polymer-Matrix Composites for Aircraft Heat Dissipation

Heat dissipation from aircraft systems is increasingly important due to the rapid increase in thermal load, which is expected to reach 10,000 kW. The increased thermal load is a consequence of the limited aircraft idling time, the heating of the fuel by electronics, increased engine performance, increased flight speed, and the heat generated by high-energy lasers. Furthermore, low temperatures are required for the reliability of electron field emitters (cold cathodes).

Polymer-matrix composites with continuous and aligned carbon fiber reinforcement are widely used for lightweight structures, due to their high strength-to-weight ratio, good fatigue resistance, and corrosion resistance. They are increasingly used in both commercial and military aircraft. Although the polymer matrix is not conductive, the carbon fibers in the composite give it a high in-plane thermal conductivity. Carbon fibers that are even more conductive thermally than copper are commercially available. The high in-plane thermal conductivity promotes heat spreading. However, a drawback of these composites is the low through-thickness thermal conductivity, which hinders heat removal in the through-thickness direction (the direction perpendicular to the laminae). Both in-plane heat spreading and through-thickness heat removal are important for effective heat dissipation.

Methods for increasing the through-thickness thermal conductivity of polymer-matrix composites include the use of continuous carbon fiber with carbon nanofibers grown on its surface and the use of continuous silicon carbide fiber with aligned carbon nanotubes grown perpendicular to its surface. The nanofibers or nanotubes promote heat conduction in the through-thickness direction. In the case of silicon carbide fibers, the carbon nanotubes grown on the fibers increase the through-thickness thermal conductivity of the epoxy-matrix composite by 50% and increase the flexural modulus by 5%. However, the presence of nanofibers or nanotubes results in a low fiber volume fraction in the composite, thus limiting the reinforcing ability. In addition, such modified continuous fibers make composite fabrication difficult and costly.

A particularly effective and practical method for increasing the thermal conductivity of a carbon fiber polymer-matrix composite in the through-thickness direction involves interlaminar interface nanostructuring. As this interface is the polymer-rich region between adjacent laminae, it contributes significantly to the thermal resistance of the composite in the through-thickness direction. Improving the thermal contact across the interlaminar interface allows the through-thickness thermal conductivity of the composite to be increased.

Although polymer-matrix composites with continuous carbon fiber exhibit excellent tensile properties in the fiber direction (in the plane of the laminae in the case of a multidirectional composite), the weak link at the interlaminar interface causes the through-thickness compressive properties to be poor. The poor through-thickness compressive properties are of concern to the quality and durability of composite joints made by fastening, which involves the application of a through-thickness compressive stress. This concern is relevant to aircraft safety, as indicated by the 2001 Airbus accident in New York. The accident involved detachment of the tail section from the body of the aircraft (Investigation of the Crash of American Airlines Flight 587; http://www.airsafe.com/events/aa587.htm). Increasing the through-thickness compressive modulus can also be achieved by nanostructuring the interlaminar interface.

A composite panel commonly encounters flexural loading. The weak link at the interlaminar interface is a disadvantage with respect to the flexural properties. The flexural modulus can also be increased by nanostructuring the interlaminar interface.

8.9.1 Interlaminar Interface Nanostructuring

The interlaminar interface nanostructuring involves the application of conductive nanoparticles between the laminae during the fabrication of the composite, such that the nanoparticles fit between the fibers of the adjacent laminae without causing the fibers of the adjacent laminae to move farther away from one another. Carbon nanoparticles in the form of carbon black are inexpensive and ineffective. The vehicle (liquid carrier) used to disperse the carbon black is chosen so as to remove part of the resin on the surface of the carbon fiber epoxy prepreg. Both the removal of the partial resin and the addition of the carbon black contribute to improving the thermal contact across the interlaminar interface.

The effect of the interlaminar interface nanostructuring depends on the relative orientations of the fibers on the two sides of the interlaminar interface. When the fibers of the two laminae are not parallel, the fibers of one lamina tend to press against those of the adjacent lamina, thus resulting in substantial fiber–fiber contact across the interlaminar interface (as indicated by a relatively low value of the electrical contact resistivity of the interface). On the other hand, when the fibers of the two laminae are parallel, the fibers of one lamina tend to sink into the adjacent laminae to a certain degree, thus resulting in relatively little fiber–fiber contact across the interlaminar interface (as indicated by a relatively high value of the contact resistivity of the interface). In practice, structural composites are not unidirectional but involve fibers of different orientations in the various laminae in the composite. The crossply configuration may be used to represent the general situation in which the fibers of the two adjacent laminae are not parallel.

8.9.2 Through-Thickness Thermal Conductivity

As shown in Figs. 8.28 and 6.13 for unidirectional and crossply composites, respectively, the thermal conductivity is enhanced by using the vehicle ethylene glycol monoethyl ether (EGME) without carbon black for interlaminar interface modification and is further increased by using the vehicle with carbon black. The optimal carbon black content for attaining the highest thermal conductivity is 0.8 wt.% (with respect to the vehicle). The trend is the same for unidirectional and crossply configurations, but the thermal conductivity is higher for the crossply configuration than for the unidirectional configuration in every case except for the highest carbon black content of 1.2 wt.%. At the optimal carbon black content of 0.8 wt.%, the thermal conductivity increases (relative to the case of no interlaminar interface modification) are 115 and 212% for unidirectional and crossply

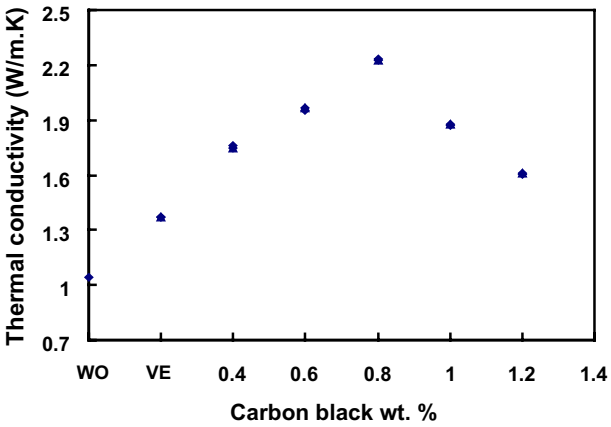

Figure 8.26. Thermal conductivities of unidirectional carbon fiber polymer-matrix composites with and without various interlaminar interface modifications. WO – without carbon black and without vehicle. VE – with vehicle and without carbon black. Three specimens of each composition were tested

configurations, respectively. In contrast, the fractional increase attained by using aligned carbon nanotubes grown on continuous silicon carbide fibers is only 50%.

Although both the vehicle and the carbon black are useful for improving the through-thickness thermal conductivity, the effect of carbon black is greater than that of EGME, as shown by the much larger fractional increase in thermal conductivity relative to the unmodified composite when both carbon black and vehicle are used than when only EGME is used, whether the configuration is unidirectional or crossply.

The observation that the thermal conductivity is increased by the use of EGME without carbon black is consistent with the fact that the vehicle dissolves away part of the resin at the interface, thereby allowing greater proximity between the fibers of the adjacent laminae. The observation that the thermal conductivity is further increased by the use of EGME with carbon black is consistent with the fact that the carbon black is a conformable and conductive filler that improves the thermal contact across the interlaminar interface. The fact that an excessive content of carbon black decreases the thermal conductivity relative to the value at the optimal carbon black content is due to the separation of the fibers of the adjacent laminae when the carbon black content is excessive. The thermal conductivity is higher for the crossply configuration than the unidirectional configuration because of the larger number of fiber–fiber contacts across the interlaminar interface for the crossply configuration.

8.9.3 Through-Thickness Compressive Properties

Figures 8.27 and 8.28 show the through-thickness compressive moduli, as determined from the slope of the compressive stress–strain curve in the elastic regime, for unidirectional and crossply composites, respectively. The modulus is decreased

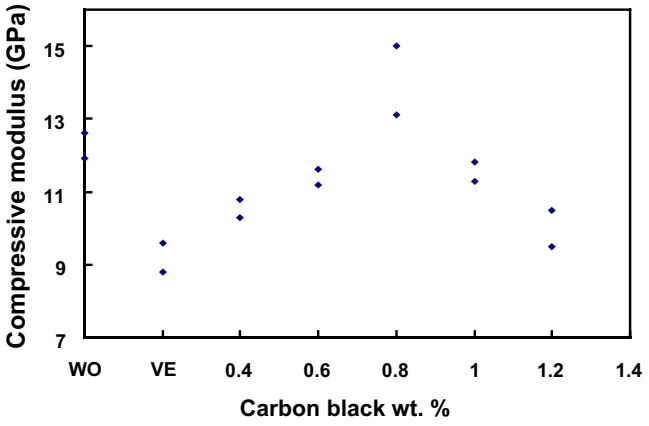

Figure 8.27. Through-thickness compressive moduli of unidirectional carbon fiber polymer-matrix composites with and without various interlaminar interface modifications. WO – without carbon black and without vehicle. VE – with vehicle and without carbon black. Two specimens of each composition were tested

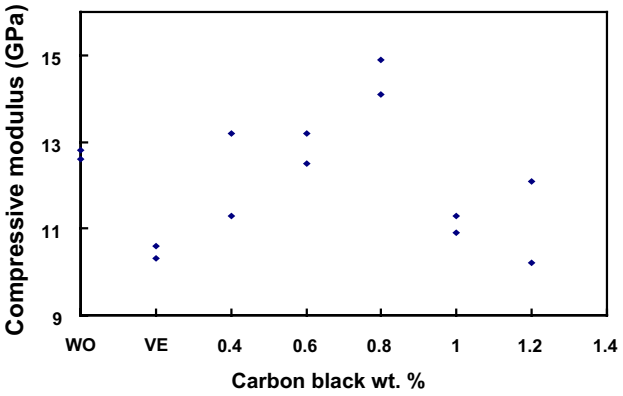

Figure 8.28. Through-thickness compressive moduli of crossply carbon fiber polymer-matrix composites with and without various interlaminar interface modifications. WO – without carbon black + without vehicle. VE – with vehicle + without carbon black. Two specimens of each composition were tested

by the use of the vehicle in the absence of carbon black, such that the decrease is more significant for the unidirectional composite than the crossply composite. This difference between unidirectional and crossply composites is attributed to the negligible thickness of the interlaminar interface for the unidirectional composite and the observable thickness of the interface for the crossply composite. However, the combined use of EGME and carbon black causes the modulus to increase from the value for modification with EGME alone. The optimal carbon black content in EGME that achieves the highest value of the modulus is 0.8 wt.% , whether the composite is unidirectional or crossply. Beyond this optimal value, the modulus decreases, due to the excessive thickness of the interlaminar interface. When EGME contains the optimal amount of carbon black, the modulus exceeds that of the unmodified composite by up to 14% and exceeds that of the composite modified with the vehicle alone by up to 52%. The fractional increase of the modulus relative to the corresponding unmodified composite is similar for the unidirectional and crossply composites.

The nanostructuring improves the through-thickness compressive strength (data not included here) for the crossply composites, and has a negligible effect on the unidirectional composites. This observation supports the quality of the nanostructured composites.

8.9.4 Flexural Properties

Figures 8.29 and 8.30 show values of the flexural modulus (three-point bending) for unidirectional and crossply composites, respectively. For each formulation, the flexural modulus is higher for the unidirectional composite than the crossply composite. This is because the 90° fiber of the crossply composite does not contribute to the flexural stiffness. The modulus is essentially unaffected by the use of EGME in the absence of carbon black. However, the combined use of EGME and carbon black

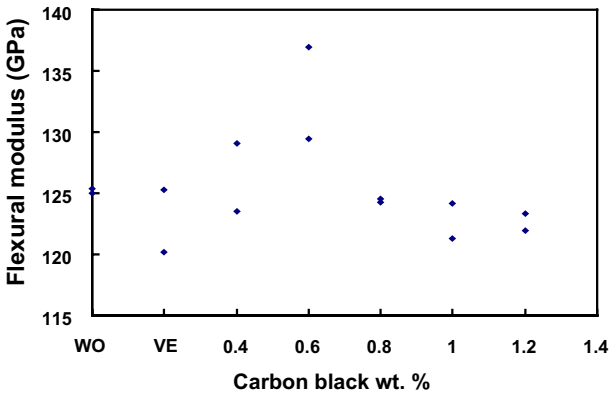

Figure 8.29. Flexural moduli of unidirectional carbon fiber polymer-matrix composites with and without various interlaminar interface modifications. WO – without carbon black + without vehicle. VE – with vehicle + without carbon black. Two specimens of each composition were tested

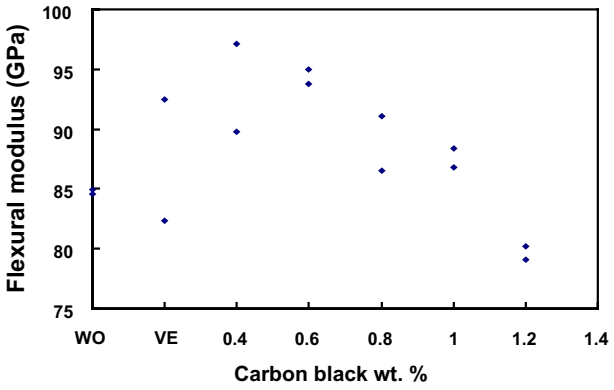

Figure 8.30. Flexural moduli of crossply carbon fiber polymer-matrix composites with and without various interlaminar interface modifications. WO – without carbon black + without vehicle. VE – with vehicle + without carbon black. Two specimens of each composition were tested

causes the modulus to increase from the value for modification with the vehicle alone. The optimal carbon black content in EGME that achieves the highest value of the modulus is 0.6 wt.%, whether the composite is unidirectional or crossply. (In the crossply case, the optimum is either 0.4 or 0.6 wt.%.) Beyond the optimal value, the modulus decreases due to the excessive thickness of the interlaminar interface. When the vehicle contains the optimal amount of carbon black, the modulus exceeds that of the corresponding unmodified composite by up to 6 and 11% for the unidirectional and crossply composites, respectively, and exceeds that of the corresponding composite modified with the vehicle alone by up to 9 and 8% for unidirectional and crossply composites, respectively. The fractional increase in the modulus, whether it is relative to the corresponding unmodified composite or relative to the composite modified by using the vehicle alone, is comparable for

the crossply and unidirectional composites. This occurs in spite of the fact that the 90° fiber of the crossply composite does not contribute to the flexural stiffness and the interlaminar interface is between 0 and 90° laminae. It is probably partly due to the tendency for the 0 and 90° fibers in the crossply composite to press onto one another during flexure, thus increasing the importance of the interlaminar interface.

The effect of the interlaminar interface modification on the flexural modulus is less than that on the through-thickness compressive modulus, particularly when the composite is unidirectional. For example, for the unidirectional configuration, the fractional increase in through-thickness compressive modulus relative to the unmodified composite is up to 14%, whereas the fractional increase in flexural modulus relative to the unmodified composite is up to 6%. Although the improvement in the flexural modulus is small, it is important that the optimum interlaminar interface modification does not degrade the flexural modulus. In contrast, the fractional increase attained by using aligned carbon nanotubes grown on continuous silicon carbide fibers is only 5%.

The effect of the nanostructuring on the flexural strength (data not included here) is negligible for both crossply and unidirectional composites. This observation supports the quality of the nanostructured composites.

8.10 Composites Used for Thermal Insulation

Materials used for thermal insulation are characterized by a low thermal conductivity (Table 8.4), which is most commonly attained by the use of air (a thermal insulator), as in the case of polymer foams (e.g., Styrofoam, which is a trademark of the Dow Chemical Company for extruded polystyrene foam), glass fiber felts, and porous ceramics (e.g., perlite and vermiculite). Perlite is an amorphous volcanic glass that expands upon heating, due to the vaporization of the trapped water. Vermiculite is a natural clay mineral that expands upon heating. Foaming agents may be used in the fabrication of polymer and cement materials in order to provide a large number of small air cells that are uniformly distributed. Silica fiber tiles are used as a high-temperature thermal insulation for the Space Shuttles, which face very high temperatures during re-entry through the atmosphere. Multiple glass panes that are hermetically sealed (airtight) so that the environment inside the unit is isolated from that outside the unit are commonly used for insulated glass windows.

Composite materials for thermal insulation are designed to obtain a low thermal conductivity while the mechanical properties remain acceptable. They are mainly polymer-matrix and cement-matrix composites. Either type of composite typically contains a foamy or porous phase, which can be the matrix or the filler. However, such a phase is detrimental to the mechanical properties. For example, perlite and vermiculite are used as admixtures to decrease the thermal conductivity of concrete, although they decrease the strength of the concrete.

The use of a structural material that is itself a thermal insulator contrasts with the combined use of a structural material (which is not a thermal insulator) and

Table 8.8. Thermal conductivities and specific heats of cement-matrix composites in the form of cement pastes (from [10])

Cement paste	Thermal conductivity (W/(m K)) (± 0.03)	Specific heat (J/(g K)) (± 0.001)
Plain	0.52	0.703
+ latex (20% by mass of cement)	0.38	0.712
+ latex (25% by mass of cement	0.32	0.723
+ latex (30% by mass of cement)	0.28	0.736
+ methylcellulose (0.4% by mass of cement)	0.42	0.732
+ methylcellulose (0.6% by mass of cement)	0.38	0.737
+ methylcellulose (0.8% by mass of cement)	0.32	0.742
+ silica fume	0.36	0.765
+ silica fume + methylcellulose[a]	0.33	0.771
+ methylcellulose[a] + fibers[b] (0.5% by mass of cement)	0.44	0.761
+ methylcellulose[a] + fibers[b] (1.0% by mass of cement)	0.34	0.792
+ silica fume + methylcellulose[a] + fibers[b] (0.5% by mass of cement)	0.28	0.789

[a] 0.4% by mass of cement; [b] carbon fibers

a thermal insulator (which is not a structural material). The former is attractive due to the space saved and the durability of the structural material. However, the development of a structural material that is also a thermal insulator is scientifically challenging. One route is to use the interfaces rather than pores in the structural composite (such as the filler–matrix interface, with the filler being either particles or fibers) to provide thermal barriers.

In the case of a cement-matrix composite, methods of decreasing the thermal conductivity involve (i) the addition of a polymer (e.g., latex particles) admixture, since the thermal conductivity of a polymer is lower than that of cement, and (ii) the use of interfaces as thermal barriers. Table 8.8 lists the thermal conductivities of various cement pastes that utilize silica fume (fine particles), latex (a polymer), methylcellulose (molecules) and short carbon fibers as admixtures. Although carbon fibers are thermally conducting, the addition of carbon fibers to cement lowers the thermal conductivity, thus allowing applications related to thermal insulation. This effect of carbon fiber addition occurs due to the increase in air void content. The electrical conductivity of carbon fibers is higher than that of the cement matrix by about eight orders of magnitude, whereas the thermal conductivity of carbon fibers is higher than that of the cement matrix by only one or two orders of magnitude. As a result, the electrical conductivity increases upon carbon fiber addition in spite of the increase in air void content, but the thermal conductivity decreases upon fiber addition.

Example Problems

1. Calculate the thermal expansion coefficient of a composite material that consists of three components in series (Fig. 8.2a). Component 1 has a CTE of 4.1×10^{-6}/°C and a volume fraction of 0.29. Component 2 has a CTE of 6.7×10^{-5}/°C and a volume fraction of 0.21. Component 3 has a CTE of 7.8×10^{-6}/°C and a volume fraction of 0.50.

   Solution:

   From Eq. 8.8,
   CTE of composite

   $$= [(0.29)(4.1 \times 10^{-6}) + (0.21)(6.7 \times 10^{-5}) + (0.50)(7.8 \times 10^{-6})]/°C$$
   $$= 1.9 \times 10^{-5}/°C$$

2. Derive an expression for the thermal expansion coefficient of a composite material that consists of three components in parallel (Fig. 8.2b). Assume perfect bonding between the components. Component 1 has a CTE of α_1 and a volume fraction of v_1. Component 2 has a CTE of α_2 and a volume fraction of v_2. Component 3 has a CTE of α_2 and a volume fraction of v_3.

   Solution:

   Since there is no applied force,

   $$F_1 + F_2 + F_3 = 0 ,$$

   where F_1, F_2, and F_3 are the thermal forces in components 1, 2, and 3 respectively. Hence,

   $$(\alpha_c - \alpha_1)M_1 v_1 + (\alpha_c - \alpha_2)M_2 v_2 + (\alpha_c - \alpha_3)M_3 v_3 = 0 .$$

   Rearrangement gives

   $$\alpha_c = (\alpha_1 M_1 v_1 + \alpha_2 M_2 v_2 + \alpha_3 M_3 v_3)/(M_1 v_1 + M_2 v_2 + M_3 v_3) .$$

3. Calculate the thermal conductivity of a composite material that consists of three components in parallel. The conductivity is in the parallel direction. Component 1 has a thermal conductivity of 3.8 W/(m K) and a volume fraction of 0.33. Component 2 has a thermal conductivity of 2.1 W/(m K) and a volume fraction of 0.19. Component 3 has a thermal conductivity of 4.1 W/(m K) and a volume fraction of 0.48.

   Solution:

   From Eq. 8.25,

   $$\text{Thermal conductivity} = [(0.33)(3.8) + (0.19)(2.1) + (0.48)(4.1)]\,\text{W/(m K)}$$
   $$= 3.6\,\text{W/(m K)} .$$

4. Calculate the thermal conductance of an interface that consists of three components that are two-dimensionally distributed. The conductance is in the direction perpendicular to the interface. Component 1 has a thermal conductance of $2.7 \times 10^4\,\mathrm{W/(m^2\,K)}$ and an area fraction of 0.61. Component 2 has a thermal conductance of $8.9 \times 10^4\,\mathrm{W/(m^2\,K)}$ and an area fraction of 0.22. Component 3 has a thermal conductance of $1.3 \times 10^4\,\mathrm{W/(m^2\,K)}$ and an area fraction of 0.39.

   Solution: From Eq. 8.41,

$$\begin{aligned}\text{Thermal conductance} &= [(0.61)(2.7) + (0.22)(8.9) + (0.39)(1.3)] \\ &\quad \times 10^4\,\mathrm{W/(m^2\,K)} \\ &= 4.1 \times 10^4\,\mathrm{W/(m^2\,K)}\,.\end{aligned}$$

5. Calculate the specific heat of a composite material that consists of three components. Component 1 has a specific heat of $1.52\,\mathrm{J\,g^{-1}\,K^{-1}}$ and a volume fraction of 0.68. Component 2 has a specific heat of $0.34\,\mathrm{J\,g^{-1}\,K^{-1}}$ and a volume fraction of 0.21. Component 1 has a specific heat of $3.81\,\mathrm{J\,g^{-1}\,K^{-1}}$ and a volume fraction of 0.11.

   Solution: From Eq. 8.20,

$$\begin{aligned}\text{Specific heat} &= [(0.68)(1.52) + (0.21)(0.34) + (0.11)(3.81)]\ \mathrm{J\,g^{-1}\,K^{-1}} \\ &= 1.5\,\mathrm{J\,g^{-1}\,K^{-1}}\,.\end{aligned}$$

6. Calculate the thermal conductivity of a metal that exhibits an electrical resistivity of $1.5 \times 10^{-5}\,\Omega\,\mathrm{cm}$ at a temperature of 450°C.

   Solution: From Eq. 8.33,

$$\begin{aligned}\text{Thermal conductivity} &= LT(\text{electrical conductivity}) \\ &= LT/(\text{electrical resistivity}) \\ &= (2.44 \times 10^{-8}\,\mathrm{W\,\Omega/K^2})(450 + 273)\mathrm{K}/(1.5 \times 10^{-5}\,\omega\,\mathrm{cm}) \\ &= 1.2 \times 10^2\,\mathrm{W/(m\,K)}\,.\end{aligned}$$

7. Calculate the heat flow in a material that exhibits a thermal conductivity of $46\,\mathrm{W/(m\,K)}$ under a temperature gradient of 125°C/cm. The cross-sectional area of the material is $158\,\mathrm{mm^2}$.

   Solution: From Eq. 8.22,

$$\text{Heat flow} = (46\,W/(\mathrm{m\,K}))(158\,\mathrm{mm^2})(125°\mathrm{C/cm}) = 91\,\mathrm{W}\,.$$

Review Questions

1. Why is diamond a good thermal conductor?
2. Why do polymers tend to have high values of coefficient of thermal expansion?
3. Define the glass transition temperature.
4. Why does a thermal interface material need to be conformable?
5. What is the difference between a first-order phase transition and a second-order phase transition?
6. Why is the martensite phase of a shape memory alloy able to sustain a large reversible strain?
7. Describe the procedure for using a shape memory alloy as a temperature-sensitive actuator.
8. Describe a method of modifying a carbon fiber (continuous) epoxy-matrix composite in order to increase the through-thickness thermal conductivity.
9. Why are metal-matrix composites attractive for use in microelectric heat sinks?

References

[1] C.-K. Leong, Y. Aoyagi and D.D.L. Chung, "Carbon-Black Thixotropic Thermal Pastes for Improving Thermal Contacts", *J. Electron. Mater.* 34(10), 1336–1341 (2005).
[2] C.-K. Leong, Y. Aoyagi and D.D.L. Chung, "Carbon Black Pastes as Coatings for Improving Thermal Gap-Filling Materials", *Carbon* 44(3), 435–440 (2006).
[3] C.-K. Leong and D.D.L. Chung, "Carbon Black Dispersions as Thermal Pastes That Surpass Solder in Providing High Thermal Contact Conductance", *Carbon* 41(13), 2459–2469 (2003).
[4] D.D.L. Chung, "Advances in Thermal Interface Materials", *Adv. Microelectron.* 33(4), 8–11 (2006).
[5] Y. Xu, C.-K. Leong and D.D.L. Chung, "Carbon Nanotube Dispersions as Thermal Pastes", *J. Electron. Mater.* 36(9), 1181–1187 (2007).
[6] H. Huang, C. Liu, Y. Wu and S. Fan, "Aligned Carbon Nanotube Composite Films for Thermal Management", *Adv. Mater.* 17, 1652–56 (2005).
[7] T.A. Howe, C.-K. Leong and D.D.L. Chung, "Comparative Evaluation of Thermal Interface Materials for Improving the Thermal Contact Between an Operating Computer Microprocessor and its Heat Sink. *J. Electron. Mater.* 35(8):1628–1635 (2006).
[8] C. Lin and D.D.L. Chung, "Graphite Nanopletelet Pastes versus Carbon Black Pastes as Thermal Interface Materials", *Carbon* 47(1), 295–305 (2009).
[9] C. Lin and D.D.L. Chung, "Effect of Carbon Black Structure on the Effectiveness of Carbon Black Thermal Interface Pastes", *Carbon* 45(15), 2922–31 (2007).
[10] X. Fu and D.D.L. Chung, "Effect of Admixtures on the Thermal and Thermomechanical Behavior of Cement Paste," *ACI Mater. J.* 96(4), 455–461 (1999).

Further Reading

P.P.S.S. Abadi, C.-K. Leong and D.D.L. Chung, "Factors that Govern the Performance of Thermal Interface Materials", *J. Electron. Mater*. 38(1), 175–192 (2009).

Y. Aoyagi and D.D.L. Chung, "Antioxidant-based phase-change thermal interface materials with high thermal stability", *J. Electron. Mater.* 37(4), 448–461 (2008).
Y. Aoyagi, C.-K. Leong and D.D.L. Chung, "Polyol-Based Phase-Change Thermal Interface Materials", *J. Electron. Mater.* 35(3), 416–424 (2006).
D.D.L. Chung, "Materials for Thermal Conduction", *Appl. Therm. Eng.* 21 (ER16), 1593–1605 (2001).
D.D.L. Chung, "Cement-Matrix Composites for Thermal Engineering", *Appl. Therm. Eng.* 21(ER16), 1607–1619 (2001).
D.D.L. Chung, "Advances in Thermal Interface Materials", *Adv. Microelectron.* 33(4), 8–11 (2006).
D.D.L. Chung and C. Zweben, "Composites for Electronic Packaging and Thermal Management", *Comprehensive Composite Materials*, Pergamon, Oxford, 2000, vol. 6, pp. 701–725.
Z. Liu and D.D.L. Chung, "Calorimetric Evaluation of Phase Change Materials for Use as Thermal Interface Materials", *Thermochim. Acta* 366(2), 135–147 (2001).
Z. Liu and D.D.L. Chung, "Boron Nitride Particle Filled Paraffin Wax as a Phase-Change Thermal Interface Material", *J. Electron. Packag.* 128(4), 319–323 (2006).
Z. Mei and D.D.L. Chung, "Thermoplastic Matrix Phase Transitions in a Carbon Fiber Composite, Studied by Contact Electrical Resistivity Measurement of the Interface between Two Unbonded Laminae", *Polym. Compos.* 23(5), 824–827 (2002).

Appendix: Test

Test Questions

This test consists of two parts covering a total of 6 pages. Part I consists of 16 multiple-choice questions. Part II consists of 17 questions in the conventional style.

Part I (32%)

Choose the best answer for each question.

1. (2%) In relation to structural vibration control, what is meant by active control?
   a) Use of a viscoelastic material.
   b) Use of a sensor.
   c) Use of an actuator.
   d) Combined use of a sensor and an actuator.
   e) Energy dissipation.
2. (2%) Flexible graphite is a flexible sheet that is all graphite. The fabrication of flexible graphite involves the following procedure:
   a) Intercalation.
   b) Exfoliation.
   c) Intercalation and exfoliation.
   d) Compression.
   e) Intercalation, exfoliation, and compression.
3. (2%) The fabrication of high-strength carbon fiber from pitch fiber involves the following procedure:
   a) Carbonization.
   b) Carbonization and graphitization.
   c) Stabilization and carbonization.
   d) Stabilization, carbonization, and graphitization.

4. (2%) What is the main advantage of pultrusion compared to compression molding for fabricating a continuous fiber polymer-matrix composite?
   a) Higher fiber volume fraction.
   b) Lower fiber volume fraction.
   c) Long length of the resulting composite.
   d) Composite has a constant cross-section.
   e) Unidirectional configuration.
5. (2%) The rule of mixtures expression for the modulus of a unidirectional continuous fiber composite is:
   a) $n = 0$ for the isostrain situation and $n = -1$ for the isostress situation.
   b) $n = -1$ for the isostrain situation and $n = 1$ for the isostress situation.
   c) $n = 1$ for the isostrain situation and $n = 0$ for the isostress situation.
   d) $n = 0$ for the isostrain situation and $n = 1$ for the isostress situation.
   e) $n = 1$ for the isostrain situation and $n = -1$ for the isostress situation.
6. (2%) Give an example of a glassy sealant that is used to improve the oxidation resistance of carbon–carbon composites.
   a) HfC
   b) B_2O_3
   c) Ni
   d) Si_3N_4
   e) SiC
7. (2%) Describe the process of liquid metal infiltration involved in the creation of a SiC particle aluminum-matrix composite.
   a) Mixing SiC particles with molten aluminum and subsequent casting.
   b) Mixing SiC particles with molten aluminum and subsequent spraying.
   c) A SiC particle preform is created and molten aluminum is forced into the preform.
   d) Mixing SiC particles and aluminum particles and subsequent hot pressing above the melting temperature of aluminum.
   e) Mixing SiC particles and aluminum particles and subsequent hot pressing below the melting temperature of aluminum.
8. (2%) Describe the coated filler method of power metallurgy that is used to create a SiC particle copper-matrix composite.
   a) Mixing SiC particles with molten copper and subsequent casting.
   b) Mixing SiC particles with molten copper and subsequent spraying.
   c) Mixing SiC particles and copper particles and subsequent hot pressing below the melting temperature of copper.

d) Hot pressing copper-coated SiC particles below the melting temperature of copper.

e) A SiC particle preform is created and molten copper is forced into the preform.

9. (2%) The rusting of iron in air involves the following anodic and cathodic reactions:

a) $Fe \rightarrow Fe^{2+} + 2e^{-}$; $O_2 + 2\,H_2O + 4e^{-} \rightarrow 4OH^{-}$

b) $Fe \rightarrow Fe^{2+} + 2e^{-}$; $O_2 + 4H^{+} + 4e^{-} \rightarrow 2\,H_2O$

c) $Fe \rightarrow Fe^{2+} + 2e^{-}$; $2H_2O + 2e^{-} \rightarrow H_2 \uparrow + 2OH^{-}$

d) $Fe^{2+} \rightarrow Fe^{3+} + e^{-}$; $O_2 + 2\,H_2O + 4e^{-} \rightarrow 4OH^{-}$

e) $Fe^{2+} \rightarrow Fe^{3+} + e^{-}$; $O_2 + 4H^{+} + 4e^{-} \rightarrow 2H_2O$

10. (2%) Figure A.1 shows specimen configurations for measuring the shear bond strength between a ceramic and a metal (e.g., steel). In Fig. A.1a, the ceramic is bonded to only one side of the metal. In Fig. A.1b, the ceramic is bonded to both sides of the metal. The configuration in Fig. A.1b is advantageous compared to that in Fig. A.1a. Give the main reason.

a) Larger joint interface area.

b) Larger amount of ceramic.

c) More brazing material.

d) The steel is better protected.

e) No bending moment during shear.

11. (2%) Why are both fine and coarse aggregates used in concrete?

a) To attain a low total aggregate volume fraction.

b) To attain a high total aggregate volume fraction.

c) To decrease the fluidity of the mix.

d) To increase the fluidity of the mix.

e) To increase the rate of curing.

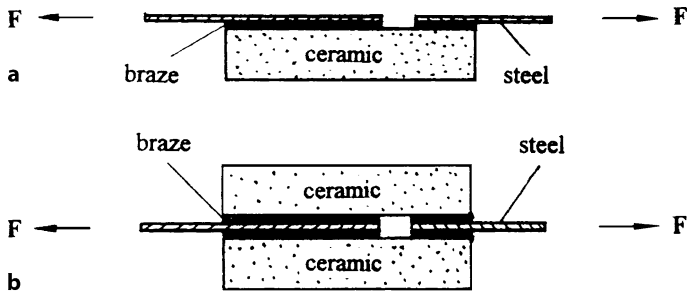

Figure A.1. Specimen configurations for measuring the shear bond strength between a ceramic and a metal (e.g., steel). **a** Ceramic is bonded to one side of the metal only. **b** Ceramic is bonded to both sides of the metal

12. (2%) What is the main advantage of using activated carbon fiber rather than activated carbon particles for water purification?
    a) Faster water flow.
    b) Greater surface area.
    c) Larger pores.
    d) Higher strength.
    e) More flexibility.
13. (2%) Why are polymers typically advantageous compared to ceramics when used as electrically insulating layers in microelectronics?
    a) Higher thermal conductivity.
    b) Higher coefficient of thermal expansion.
    c) Lower coefficient of thermal expansion.
    d) Lower value of the relative dielectric constant.
    e) Higher value of the relative dielectric constant.
14. (2%) A Bingham plastic refers to the following:
    a) A material that exhibits Newtonian behavior.
    b) A material that exhibits elastic behavior.
    c) A material that exhibits shear yielding.
    d) A material that exhibits shear thinning.
    e) A material that exhibits shear thickening.
15. (2%) In relation to viscoelastic behavior, the quantity $\tan\delta$ refers to the following:
    a) The ratio of the storage modulus to the loss modulus.
    b) The ratio of the loss modulus to the storage modulus.
    c) The magnitude of the shear modulus.
    d) The product of the magnitude of the shear modulus and $\sin\delta$.
    e) The product of the magnitude of the shear modulus and $\cos\delta$.
16. (2%) A remendable polymer is:
    a) A thermoplastic polymer.
    b) A thermosetting polymer.
    c) A polymer that melts upon heating.
    d) A polymer that decomposes upon heating.
    e) A polymer for which the degree of crosslinking decreases reversibly upon heating.

Part II (68%)

1. (4%) Name two main advantages of high-modulus carbon fiber compared to high-strength carbon fiber.
2. (4%) A piezoresistive material exhibits a gage factor of 22. The gage factor is defined as the fractional change in resistance per unit strain. A piece of this material has a resistance of 46 Ω. What is its resistance when the strain is 4.5%?
3. (4%) A unidirectional continuous fiber composite contains fibers of modulus 3.4 GPa. The fiber volume fraction is 57%. The modulus of the matrix is 0.12 GPa. Assuming that the bonding between the fiber and the matrix is perfect, calculate the modulus of the composite in the longitudinal direction (i.e., in the fiber direction).
4. (4%) In relation to carbon materials, the inhibition factor of a treated carbon is defined as the ratio of the oxidation rate of untreated carbon to the oxidation rate of the treated carbon. The oxidation rates are 9.9%/min for the untreated carbon and 2.8%/min for the treated carbon. Calculate the inhibition factor.
5. (4%) The rate r of a thermally activated process relates to the activation energy Q of the process by the equation

$$r = A\mathrm{e}^{-Q/RT}$$

   where T is the temperature in K (not in °C), R is the gas constant (a universal constant equal to 8.314 J/(mol K)) and A is just a proportionality constant. The rate at temperature T_1 is r_1 and the rate at temperature T_2 is r_2. Derive an expression for Q in terms of T_1, T_2, r_1 and r_2.
6. (4%) Using a graph, define the plastic viscosity and the apparent viscosity.
7. (4%)

$$\tau = \eta\,,$$
$$\tau = \tau_\mathrm{o}\mathrm{e}^{\mathrm{i}\omega t}\,,$$
$$\gamma = \gamma_\mathrm{o}\mathrm{e}^{\mathrm{i}(\omega t-\delta)}$$

   In the above equations that pertain to viscoelastic behavior, τ is the shear stress, γ is the shear strain, and η is the viscosity. Derive the equation

$$|\eta| = |G|/\omega\,,$$

   where G is the shear modulus.
8. (4%) Using a graph of stress versus strain, explain the phenomenon of pseudoplasticity.
9. (4%) A brittle material is much stronger under compression than under tension. Explain the scientific origin of this phenomenon.

10. (4%) Polyvinyl chloride is stiffer than polyethylene. Explain the scientific origin of this observation. Note that the mer of polyethylene is

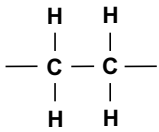

while the mer of polyvinyl chloride is the same as this except that one for the four hydrogen atoms has been replaced with a chlorine atom.

11. (4%) What are the main problems with the method of self-healing involving microcapsules of a monomer?
12. (4%) Describe an effective method of improving the vibration damping ability of a continuous carbon fiber polymer-matrix composite.
13. (4%) Why does the time spent below the melting temperature prior to bonding affect the quality of the bond for polyphenylene sulfide (PPS)?
14. (4%) Why is aluminum foil sufficiently temperature resistant that it can be used in cooking?
15. (4%) Why does corrosion tend to occur in a fastened metal joint?
16. (4%) Why does sand blasting help to improve the corrosion resistance of steel rebars?

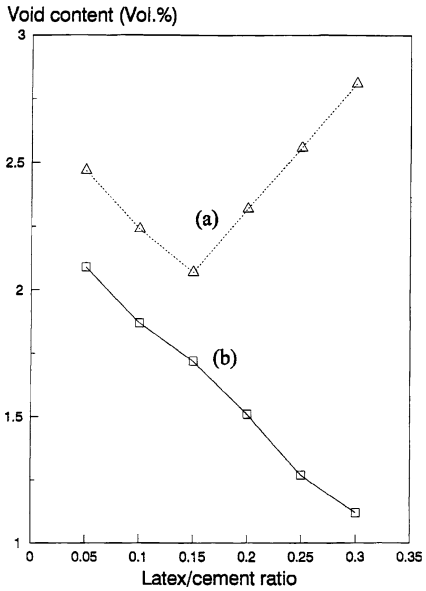

Figure A.2. Effect of the latex/cement ratio on the air void content of cement paste: **a** with 0.53 vol% carbon fibers; **b** with no fibers

17. (4%) Figure A.2 shows the effect of the latex/cement ratio on the air void content of cement paste. Curve (a) is for the case with 0.53 vol% carbon fibers. Curve (b) is for the case without fiber. Explain the features of curve (a) in terms of their scientific origin.

Test Solutions

Part I (32%)

The correct answers are:

1. d
2. e
3. c
4. c
5. e
6. b
7. c
8. d
9. a
10. e
11. b
12. a
13. d
14. c
15. b
16. e

Part II (68%)

1. Any two of the following answers are acceptable: higher modulus; higher thermal conductivity; higher electrical conductivity; higher oxidation resistance.
2. $[(R - 46)/46]/4.5\% = 22$
   $(R - 46)/46 = 0.99$
   $R - 46 = 45.54$
   $R = 91.5\Omega$.
3. Modulus = (0.57) (3.4 GPa) + (0.43) (0.12 GPa) = 2.0 GPa.
4. Inhibition factor = 9.9%/2.8% = 3.5.

5. $r_1 = A\,\mathrm{e}^{-Q/RT1}$
   $r_2 = A\,\mathrm{e}^{-Q/RT2}$
   $r_1/r_2 = \mathrm{e}^{-Q/RT1}/\mathrm{e}^{-Q/RT2} = \mathrm{e}^{-Q/RT1+Q/RT2}$
   $\ln(r_1/r_2) = -Q/RT_1 + Q/RT_2 = -(Q/R)[(1/T_1) - (1/T_2)]$
   $Q = -R\ln(r_1/r_2)/[(1/T_1) - (1/T_2)]$.
6. The graph defining the plastic viscosity and the apparent viscosity should look like this:

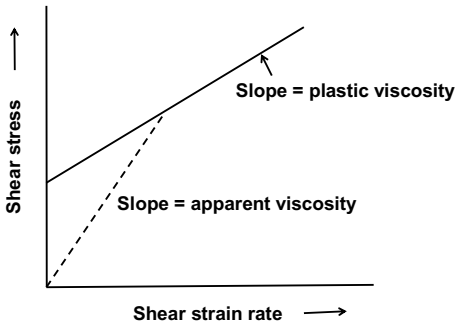

7. $\dot{\gamma} = \gamma_o \mathrm{i}\omega \mathrm{e}^{\mathrm{i}(\omega t-\delta)}$
   $\eta = \tau_o \mathrm{e}^{\mathrm{i}\omega t}/\left[\gamma_o \mathrm{i}\omega \mathrm{e}^{\mathrm{i}(\omega t-\delta)}\right] = -\mathrm{i}(|G|/\omega)\mathrm{e}^{\mathrm{i}\delta}$
   $|\eta| = |G|/\omega$.
8. A graph of stress versus strain that explains the phenomenon of pseudoplasticity should look like this:

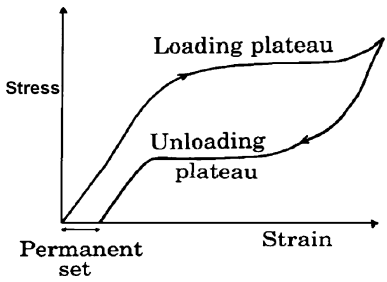

9. The microcracks that tend to be present in a brittle material propagate much more under tension than under compression.

10. In PVC, there is hydrogen bonding (secondary bonding) between a hydrogen of one molecule and the chlorine of another molecule (the following diagram is not required):

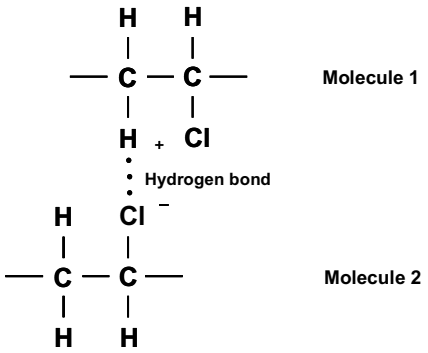

11. Toxicity of the monomer; high cost of the catalyst.
12. Add either a viscoelastic material or a nanofiber material to the composite at the interlaminar interface (mentioning either material is sufficient).
13. PPS is a thermoplastic that has thermosetting character, so it cures to a limited degree as it spends time below the melting temperature prior to bonding.
14. It is covered with a nonporous protective layer of aluminum oxide.
15. The reduced availability of oxygen at the crevice in the fastened joint results in an oxygen concentration cell, meaning that the crevice region becomes the anode.
16. Sand blasting removes the impurities on the surface of the rebar, thus resulting in a more uniform surface composition.
17. The decrease in void content as the latex/cement ratio increases up to about 0.15 is due to the latex. The increase in void content as the latex/cement ratio increases beyond about 0.15 is due to the decreasing degree of fiber dispersion. (Fiber clumping increases the void content.)

Index